Valve-regulated Lead–Acid Batteries

This page intentionally left blank

Valve-regulated Lead–Acid Batteries

Editors

D.A.J. Rand

CSIRO Energy Technology
Victoria, Australia

P.T. Moseley

International Lead Zinc Research Organisation Inc.
North Carolina, USA

J. Garche

Ulm, Germany

C.D. Parker

North Carolina, USA

2004

ELSEVIER

Amsterdam – Boston – Heidelberg – London – New York – Oxford
Paris – San Diego – San Francisco – Singapore – Sydney – Tokyo

ELSEVIER B.V.	ELSEVIER Inc.	ELSEVIER Ltd	ELSEVIER Ltd
Sara Burgerhartstraat 25	525 B Street, Suite 1900	The Boulevard, Langford Lane	84 Theobalds Road
P.O. Box 211	San Diego	Kidlington,	London
1000 AE Amsterdam	CA 92101-4495	Oxford OX5 1GB	WC1X 8RR
The Netherlands	USA	UK	UK

First edition 2004

Library of Congress Cataloging in Publication Data
A catalog record is available from the Library of Congress.

British Library Cataloguing in Publication Data
Valve-regulated lead-acid batteries
1. Lead-acid batteries
I. Rand, D. A. J. (David Anthony James), 1942-
621.3′1242

ISBN: 0-444-50746-9

♾ The paper used in this publication meets the requirements of ANSI/NISO Z39.48-1992 (Permanence of Paper).
Printed in The Netherlands.

Preface

For over a hundred years from its conception, the lead–acid cell was normally operated with unrestricted access between the surface of its electrolyte and the external atmosphere so that, during periods of overcharge, hydrogen and oxygen were lost from the cell via electrolysis. As a result, periodic additions of distilled water were necessary. Since about 1970, an alternative to the traditional 'flooded' cell has been available — one that avoids the need for water maintenance. Moreover, acid is immobilized in the new design and this endows the cell with the additional advantages of being 'spill-proof' and able to operate in any orientation (upright, on its side, or even upside down).

The change to the so-called 'valve-regulated lead–acid' (VRLA) technology has not, however, been accomplished without some difficulty. Experience has demonstrated forcibly the fundamental differences between the two systems, and the lead–acid battery manufacturing industry has faced major challenges in investing the VRLA version with a performance to match that of its flooded predecessor. Nevertheless, research into understanding the electrochemisty, producing improved cell components and optimizing charge strategies has resulted in VRLA batteries becoming well-established and reliable devices. Operators now take advantage of the particular properties of these batteries for the storage of electrical energy in a wide variety of stationary applications.

Much of the recent advancement of VRLA technology has been achieved through a co-operative research effort under the auspices of the Advanced Lead-Acid Battery Consortium (ALABC). The main effort has been directed towards the development of VRLA battery systems for new-generation road transportation — electric and hybrid electric vehicles — that will reduce fuel consumption and lower emissions. The progress gained in this endeavour will ultimately also benefit the enormously important markets in telecommunications and remote-area power supplies.

This volume presents a detailed account of recent advances in the science and technology of VRLA batteries. The expert contributors are from organizations which have either been members of, or contractors to, the ALABC. In editing the contributions, we have aimed to unify the style of the volume as far as possible, but have allowed a little overlap between those chapters where there is a natural interaction between topics. It is hoped that this work will constitute a sound exposition of the present status of VRLA batteries, and will provide a resource that will enable technologists to deliver products with performances that surpass the requirements of the major markets.

We wish to express our special appreciation of the dedication and expert skills of Ms. Rita Spiteri (CSIRO) for producing the complete text for publication and redrafting most of the illustrations.

D.A.J. Rand J. Garche
P.T. Moseley C.D. Parker

This page intentionally left blank

List of Contributors

W. Böhnstedt
Daramic, Inc.
Erlengang 31
D-22844 Norderstedt, Germany
E-mail: WBoehnstedt@Daramic.com

C.J. Boreiko
International Lead Zinc Research Organization, Inc.
PO Box 12036
Research Triangle Park
NC 27709-2036, USA
E-mail: cboreiko@ilzro.org

R.D. Brost
Ford Motor Company
Sustainable Mobility Technologies
15050 Commerce Drive North
Dearborn, MI 48120, USA
E-mail: rbrost@ford.com

K.R. Bullock
980 Clover Court
Blue Bell, PA 19422, USA
E-mail: coolohm@earthlink.net

A. Cooper
Lead Development Association International
42 Weymouth Street
London, W1G 6NP, UK
E-mail: ACatCorfe@aol.com

T.C. Dayton
Wilson Greatbatch Technologies, Inc.
10,000 Wehrle Drive
Clarence, NY 14031, USA
E-mail: tdayton@greatbatch.com

J. Garche
Center for Solar Energy and Hydrogen Research (ZSW)
Electrochemical Energy Storage and Energy Conversion Division
Baden-Württemberg
Helmholtzstr. 8
D-89081 Ulm, Germany
E-mail: Jugarche@aol.com
juergen.garche@zsw-bw.de

K. Ihmels
Daramic, Inc.
Erlengang 31
D-22844 Norderstedt, Germany
E-mail: Klhmels@Daramic.com

A. Jossen
Center for Solar Energy and Hydrogen Research (ZSW)
Electrochemical Energy Storage and Energy Conversion Division
Baden-Württemberg
Helmholtzstr. 8
D-89081 Ulm, Germany
E-mail: andreas.jossen@zsw-bw.de

L.T. Lam
CSIRO Energy Technology
Novel Battery Technologies Group
Bayview Avenue
Clayton South
Victoria 3169, Australia
E-mail: Lan.Lam@csiro.au

E. Meissner
VARTA Automotive
Am Leineufer 51
30419 Hannover, Germany
E-mail: eberhard.meissner@jci.com

P.T. Moseley
International Lead Zinc Research Organization, Inc.
2525 Meridian Parkway
Suite 100
Durham, NC 27713, USA
E-mail: pmoseley@ilzro.org

R.F. Nelson
Recombination Technologies
909 Santa Fe Drive
Denver, CO 80204, USA
E-mail: Nelson909SantaFe@aol.com

R.H. Newnham
CSIRO Energy Technology
Novel Battery Technologies Group
Bayview Avenue
Clayton South
Victoria 3169, Australia
E-mail: Russell.Newnham@csiro.au

C.D. Parker
International Lead Zinc Research Organization, Inc.
PO Box 12036
Research Triangle Park
NC 27709-2036, USA
E-mail: cparker@ilzro.org

D. Pavlov
Central Laboratory of Electrochemical Power Sources
Bulgarian Academy of Sciences
Acad. G. Bonchev Str., Bl. 10
Sofia 1113, Bulgaria
E-mail: dpavlov@mbox.cit.bg

K. Peters
Battery Design & Manufacturing Services
Glen Bank
Broadoak Park
Worsley
Manchester M28 2GG, UK
E-mail: PetersGlenbank@aol.com

R.D. Prengaman
RSR Technologies, Inc.
2777 Stemmons Freeway
Suite 1800
Dallas, TX 75207, USA
E-mail: rdprengaman@rsrtechnologies.com

D.A.J. Rand
CSIRO Energy Technology
Bayview Avenue
Clayton South
Victoria 3169, Australia
E-mail: David.Rand@csiro.au

G. Richter
VARTA Automotive
Am Leineufer 51
30419 Hannover, Germany
E-mail: gerolf.richter@jci.com

M.W. Stevenson
Pasminco
Level 7, Royal Domain Centre
380 St. Kilda Road
Melbourne
Victoria 3001, Australia
E-mail: StevensM@Pasminco.com.au

R. Wagner
EXIDE Technologies
Network Power R&D Centre
D-63654 Büdingen, Germany
E-mail: rainer.wagner@exide.de

M.J. Weighall
12 Low Stobhill
Morpeth
Northumberland, NE61 2SG, UK
E-mail: mjweighall@battery1.demon.co.uk

B. Wilson
International Lead Management Center, Inc.
P.O. Box 14189
Research Triangle Park
NC 27709-4189, USA
E-mail: bwilson@ilmc.org

Contents

Chapter 7

Chapter 8

ABBREVIATIONS, SYMBOLS AND UNITS USED REPEATEDLY IN TEXT

Abbreviations

a.c.	alternating current
AGM	absorptive glass mat
AGV	automatically guided vehicle
AJS	acid jellying separator
ALABC	Advanced Lead-Acid Battery Consortium
AM	active mass
AMCL	active-mass collecting layer
ANN	artificial neural network
BCI	Battery Council International
BESS	battery energy-storage system
BET	Brunauer, Emmett, Teller method of measuring surface area (*J. Am. Chem. Soc.*, **60**, (1938) 309)
BJT	bipolar junction transistor
BMM	battery management module
BMS	battery management system
BoP	balance-of-plant
1BS	monobasic lead sulfate, $PbO \cdot PbSO_4$
3BS	tribasic lead sulfate, $3PbO \cdot PbSO_4 \cdot H_2O$
4BS	tetrabasic lead sulfate, $4PbO \cdot PbSO_4$
CAES	compressed-air energy storage
CAFE	corporate average fuel economy
CAN	controller area network
CBEMA	Computer and Business Equipment Manufacturers' Association
CC	constant current
CCA	cold-cranking amps
CFMEA	Concept Failure Modes and Effects Analysis
CI	current interrupt
CMC	carboxymethyl cellulose
CoP	Conference of the Parties
COS	cast-on-strap
CSIRO	Commonwealth Scientific and Industrial Research Organisation
CSM	copper-stretch-metal
CV	constant voltage

d.c.	direct current
DFMEA	Design Failure Modes and Effects Analysis
DLC	double layer capacitor
DoD	depth-of-discharge
DST	dynamic stress test
DVP	design verification plan — plan to verify component/system design to functional intent
DVPR	design verification plan and report — program/product oriented structured system to determine verification test requirements for a new or modified part, component, or system
ECE	Economic Commission for Europe
ECU	engine control unit
EDI	electronic data interchange — a protocol for the electronic exchange of data and documents
EDS	electrical distribution system
EMC	Electric Membership Corporation
EMI	electromagnetic interference
EN	European Norm. (a standard)
EPA	Environmental Protection Authority
EPRI	Electric Power Research Institute
EOL	end-of-life
EV	electric vehicle
FM	failure mechanism
FMEA	failure modes and effects analysis
FUDS	Federal Urban Drive Schedule
GE	General Electric Company
GTO	gate-turn-off (thyristor)
HEPA	high efficiency particulate air
HEV	hybrid electric vehicle
HMW	high molecular weight
HRPSoC	high-rate partial-state-of-charge
HVAC	high-voltage alternating current
HVDC	high-voltage direct current
HWFET	Highway Fuel Economy Test
IC	intermittent charging
ICE	internal-combustion engine
IEC	International Electrotechnical Commission
IGBT	insulated gate bipolar transistor
IPTV	incidents per thousand vehicles
ISA	integrated starter alternator
ISG	integrated starter generator
ISO	International Standards Organization
IU	current-limited constant voltage (charging)

IUI	current-limited constant voltage (charging) with constant-current finishing step
JIS	Japanese Industrial Standard
JEVs	Japan Electric Vehicle Society
KST	Kochis Stress Test
LMT	Lead Metal Technologies (Mexico)
LMW	low average molecular weight
MCE	mixed cellulose ester
MP&L	Metlakatla Power and Light
MOSFET	metal-oxide-semiconductor field effect transistor
MSDS	material safety data sheet
NAM	negative active mass
NERC	National Energy Reliability Council
NVH	noise, vibration, and harshness — the acoustic and tactile stimuli generated by the vehicle that are perceived by the customer as indicators of product quality
OCV	open-circuit voltage
OCSM	CSM (copper-stretch-metal)-technology battery
OEM	original equipment manufacturer
OSHA	Occupational Safety & Health Administration
PAM	positive active mass
PCL	premature capacity loss
PCM	phase-change material
PCS	power-conditioning system
PFMEA	process failure modes and effects analysis
PG&E	Pacific Gas & Electric
POB	power-optimized battery
PowerNet	vehicle electrical system
PREPA	Puerto Rico Electric Power Authority
PSoC	partial-state-of-charge
PSoR	partial-state-of-recharge
PTFE	polytetrafluoroethene
PV	photovoltaic *also:* process validation — production validation (PV) — program of engineering tests and evaluations conducted to assure that initial production parts meet the design intent
PVC	polyvinyl chloride
PWM	pulse-width modulation
RAPS	remote-area power supply
RBSM	recombinant-battery separator mat (same as AGM)
RC	reserve capacity
rel. dens	relative density

RFI	radio frequency interference
RFQ	request for quotation
RFV	resistance-free voltage
RIMU	relaxable insufficient mass utilization
RMS	root mean square
rpm	revolutions per minute
SAE	Society of Automotive Engineers
SCE	Southern California Edison
SCR	silicon controlled rectifier
SDG&E	San Diego Gas & Electric
SDS	system design specification
SEM	scanning electron microscopy
SHE	standard hydrogen electrode
SLGM	silica-loaded glass mat
SLI	starting, lighting and ignition
SMES	superconducting magnetic energy storage
SNL	Sandia National Laboratory
SoC	state-of-charge
SoH	state-of-health
SPC	statistical process control — the process which uses statistical techniques such as control charts to analyze a process output
SGTP	strap-grid tubular plate
SWP	synthetic wood pulp
T&D	transmission and distribution
TC	taper current
TCLP	toxic characteristic leaching procedure
TGR	things gone right
TGW	things gone wrong
ToCV	top-of-charge voltage
UL	Underwriters Laboratory
ULAB	used lead–acid batteries
UPS	uninterruptible power supply
USDOE	US Department of Energy
VAR	volt-ampere reactive
VC	vehicle controller
VPC	volts per cell
VRLA	valve-regulated lead–acid (battery)
VS-A	Vanisperse A (negative-plate expander)
XRD	X-ray diffraction

Symbols and units — Roman letters

a	activity of species which is usually specified as a subscript (e.g., HSO_4^-)

A	ampere
Ah	ampere hour (= 3600 coulombs)
°C	degree Celsius
C	capacity (symbol also used for capacitance)
C_b	heat capacity of materials in battery
$C_p(i)$	heat capacity of component i
C_X/t	discharge rate (current) of a battery, where C is the rated capacity; X is the hour rate; t is the specified discharge time, usually in hours
cm	centimeter
d	interplanar spacing in crystal
D_{H_2}	diffusion constant for hydrogen
D_{O_2}	diffusion constant for oxygen
$\triangle G$	Gibbs free energy of reaction
e^-	electron
E	electrode potential under load
E_a	activation energy
E_M	mixed potential
E^0	standard electrode potential
E_r	reversible electrode potential
F	faraday (96,485 coulombs per mole) *also:* farad (1 coulomb per volt)
g	gram
GW	gigawatt
h	hour
H	henry (1 volt second per ampere)
$\triangle H$	enthalpy of reaction
Hz	hertz (= 1 cycle per second)
i	current density
I	current
I_{ch}	current on charge
I_{corr}	grid corrosion current
I_d	current on discharge
I_{float}	float current
I_{H_2}	hydrogen evolution current
I_{O_2}	oxygen evolution current
$I_{O_2\text{-red}}$	oxygen reduction current
in	inch
J	joule
kg	kilogram
kJ	kilojoule (= 238.85 calories)
km	kilometer

kPa	kilopascal
kW	kilowatt
kWh	kilowatt hour
l	litre
m	metre
$m(i)$	mass of component i
M	molar
mA	milliampere
mAh	milliampere hour
min	minute
mm	millimeter
MPa	megapascal
mol	mole
mV	millivolt
MV	megavolt
mW	milliwatt
MW	megawatt
mWh	milliwatt hour
MWh	megawatt hour
μm	micrometer
pH	negative value of logarithm of hydrogen ion concentration
Q_g	heat generated
Q_d	heat dissipated
r	Sn:Ca ratio in lead alloys
R	gas constant (8.3145 joules per degree per mole)
s	second
$\triangle S$	entropy of reaction
t	time
T	temperature
U	voltage (see also V)
UTS	ultimate tensile strength
V	volt
$\triangle$V	shift in voltage
V_p	total pore volume
$V_{\mu p}$	volume of micropores
W	watt
Wh	watt hour
wt.%	percentage by weight
x	distance variable
YS	yield strength

Symbols and units — Greek letters

ε	Stefan-Boltzmann constant
η	overpotential (symbol also used for viscosity)
λ	thermal conductivity
θ	phase angle
ρ	density
σ	emissivity (with respect to an ideal emitter)
Ω	ohm

This page intentionally left blank

Valve-Regulated Lead–Acid Batteries
D.A.J. Rand et al., editors

—CHAPTER 1—

THE VALVE-REGULATED BATTERY — A PARADIGM SHIFT IN LEAD–ACID TECHNOLOGY

P.T. Moseley and D.A.J. Rand

1.1. Lead–Acid Batteries — A Key Technology for Energy Sustainability

A ready and affordable supply of energy is essential for maintaining the standard-of-living of the developed world and for markedly improving that of the less-developed countries. Coal, mineral oil, and natural gas (the 'fossil fuels'), together with uranium ('nuclear energy'), have long been exploited as major sources of primary energy. The most important, versatile, and useful means of distributing such energy to where it is needed is through conversion to electricity. Unfortunately, the cumulative environmental effects of burning fossil fuels, the profligate consumption of these fuels, and concerns over the safety of nuclear power and radioactive wastes, have placed Planet Earth in jeopardy.

One strategy for safeguarding the future is to move away from the traditional fuels towards so-called 'renewable' sources of energy which are of a non-polluting nature and are sustainable. The harnessing of renewable energies — hydro, solar, wind, geothermal, wave, tidal, biomass — presents, however, a further set of technical and economic problems. Unlike fossil and nuclear fuels, which are concentrated sources of energy that can be easily stored and transported, renewable forms of energy are, for the most part, highly dilute and diffuse. Moreover, their supply can be extremely intermittent and unreliable. It is therefore not surprising that, except for hydro-electric power, renewable energy sources have made little contribution to world electricity supplies. In 1999, for example, renewables provided only 1.6% of the energy required for world electricity generation; the remainder came from: coal, 38.1%; hydroelectric power, 17.5%; nuclear power, 17.2%; natural gas, 17.1%; oil, 8.5% [1].

Irrespective of the source, an effective storage system is critical for the efficient use of the energy, and for the good stewardship of its supply. The development of effective and affordable means to store electrical energy for an ever-increasing number of applications of great variety continues to present a major challenge to scientists, technologists, and engineers.

The scale of energy-storage systems ranges from minuscule elements on integrated circuits to pumped hydroelectric reservoirs that store the equivalent of giga watt-hours of electrical energy. The needs of small electrical appliances can be supplied by primary (single-use and discard) batteries, or by a rapidly developing range of

rechargeable types which are principally based on the use of lithium or nickel. To date, however, batteries based on these two metals have failed to become economically viable for larger energy-storage applications. Examples of this category include systems designed to cope with diurnal fluctuations in electricity demand. In small communities remote from a grid supply, electricity generated during the day by photovoltaic ('solar') installations must be stored for use during the hours of darkness. In electricity utility systems, there is often a need to store surplus energy generated during the night for use at peak periods on the following day. When electric power is used for transport, it is often necessary for a vehicle to move free from the source of power and for the electricity to be stored 'in a box'. In most medium- and large-scale energy-storage functions, lead–acid batteries, in one form or another, have been the technology of choice.

Lead–acid batteries are employed in a wide variety of different tasks, each with its own distinctive duty cycle. In internal-combustion engined vehicles, the battery provides a quick pulse of high current for starting and a lower, sustained current for other purposes; the battery remains at a high state-of-charge for most of the time. The same is true of batteries used for back-up power in telecommunications and in other uninterruptible power supplies, although in such service (so-called 'float duty') the battery should seldom be called upon to discharge. Electric vehicle (EV) batteries, on the other hand, are expected to undergo deep discharges and recharges over periods of a few hours repeatedly (so-called 'deep-discharge duty'). In between the extreme cases of float duty and deep discharge, the batteries in hybrid electric vehicles (HEVs) and in storage units for remote-area power supply (RAPS) systems spend most of the time cycling about an intermediate state-of-charge, often near 50% (so-called 'partial-state-of-discharge duty').

In all cases, the battery must be able to provide adequate power for the task in hand. This may be a more severe requirement for batteries in EVs and HEVs than for batteries in solar-based RAPS systems. For mobile applications, the energy-storage capability should be provided with a minimum weight penalty. In essence, the battery should have a high 'specific energy', i.e., a high energy output per unit weight, $\mathrm{Wh\,kg^{-1}}$. Generally, a high coulombic efficiency (charge out : charge in) is also an asset as this preserves primary energy.

Finally, a *sine qua non* is acceptable cost. The factors to be considered are the initial price of the battery, the operational life of the battery, and the associated maintenance costs. Lead–acid batteries are eminently suitable for medium- and large-scale energy-storage operations because they offer an acceptable combination of performance parameters at a cost which is substantially below that of alternative systems.

1.2. The Lead–Acid Battery

The fundamental elements of the lead–acid battery were set in place over 100 years ago. Gaston Planté [2] was the first to report that a useful discharge current could be drawn from a pair of lead plates that had been immersed in sulfuric acid and subjected to a charging current. Later, Camille Fauré [3] proposed the concept of

the pasted plate. In the subsequent hundred yeasrs or so, the principal elements of the battery have not undergone any further radical change. The most commonly employed design has 'flat plates'. These are prepared by coating pastes of lead oxides and sulfuric acid on to conductive lead or lead-alloy 'grids', which act as current-collectors. The plates are then 'formed' electrolytically into 'active' materials. One alternative cell design uses positive plates in which the active material is contained in tubes, each fitted with a coaxial current-collector. Such 'tubular plates' serve to prevent shedding of the material during battery service (*v.i.*). A more recent cell design, aimed at high-power applications, has a single pair of positive and negative plates which are interleaved with microfibre-glass mat separators and wound together in a cylindrical can (the 'spirally wound' or 'jellyroll' design). Ironically, this arrangement mimics that invented originally by Planté. Schematics of the various plate types are given in Fig. 1.1.

The discharge reactions of the lead–acid cell are as follows:

$$\text{Positive plate: } PbO_2 + 3H^+ + HSO_4^- + 2e^- \rightarrow PbSO_4 + 2H_2O \tag{1.1}$$

$$\text{Negative plate: } Pb + HSO_4^- \rightarrow PbSO_4 + H^+ + 2e^- \tag{1.2}$$

In both cases, a solid conductor of electrons (semi-conducting lead dioxide, PbO_2, in the positive plate; metallic lead, Pb, in the negative) reacts with sulfuric acid to form a non-conductive, solid product of lead sulfate, $PbSO_4$. Both discharge reactions are accompanied by an increase in volume of the solid phase. The volume increase for the transformation of PbO_2 to $PbSO_4$ (shown in Fig. 1.2) is 92%, while that for Pb to $PbSO_4$ is 164%.

The key technical challenge to be met in maximizing battery performance involves facilitating continuity of supply, contact and interaction of reactants. In principal, this requires an adequate supply of acid, solid reactants of high surface-area, maintenance of good contact between the particles of the active material (particularly in positive plates that show a tendency to expand during charge–discharge service, *v.i.*), and minimization of the insulating effects of $PbSO_4$.

After each discharge, the above set of optimum conditions is to be restored by charge reactions, which are the reverse of those expressed by eqns. (1.1) and (1.2). In the ideal case, the discharge capacity would be constant during cycling of the cell (or during time on float). For even the most advanced design of commercial battery, however, the practical utilization of the active materials is generally limited to considerably less than 50% when discharge is performed at a rate of five hours, or less. As cycling (or life) proceeds, a number of processes ('failure mechanisms') can degrade further this limited performance. Conventional batteries (i.e., those with free electrolyte, so-called 'flooded' designs) commonly suffer from one or more of the following five failure mechanisms.

FM1. Positive-plate expansion. This can occur both in the plane of the plate (if the grid is stretched by a growing corrosion layer) and in the direction normal to the plate (through expansion of the active material itself). Repetitive discharge and

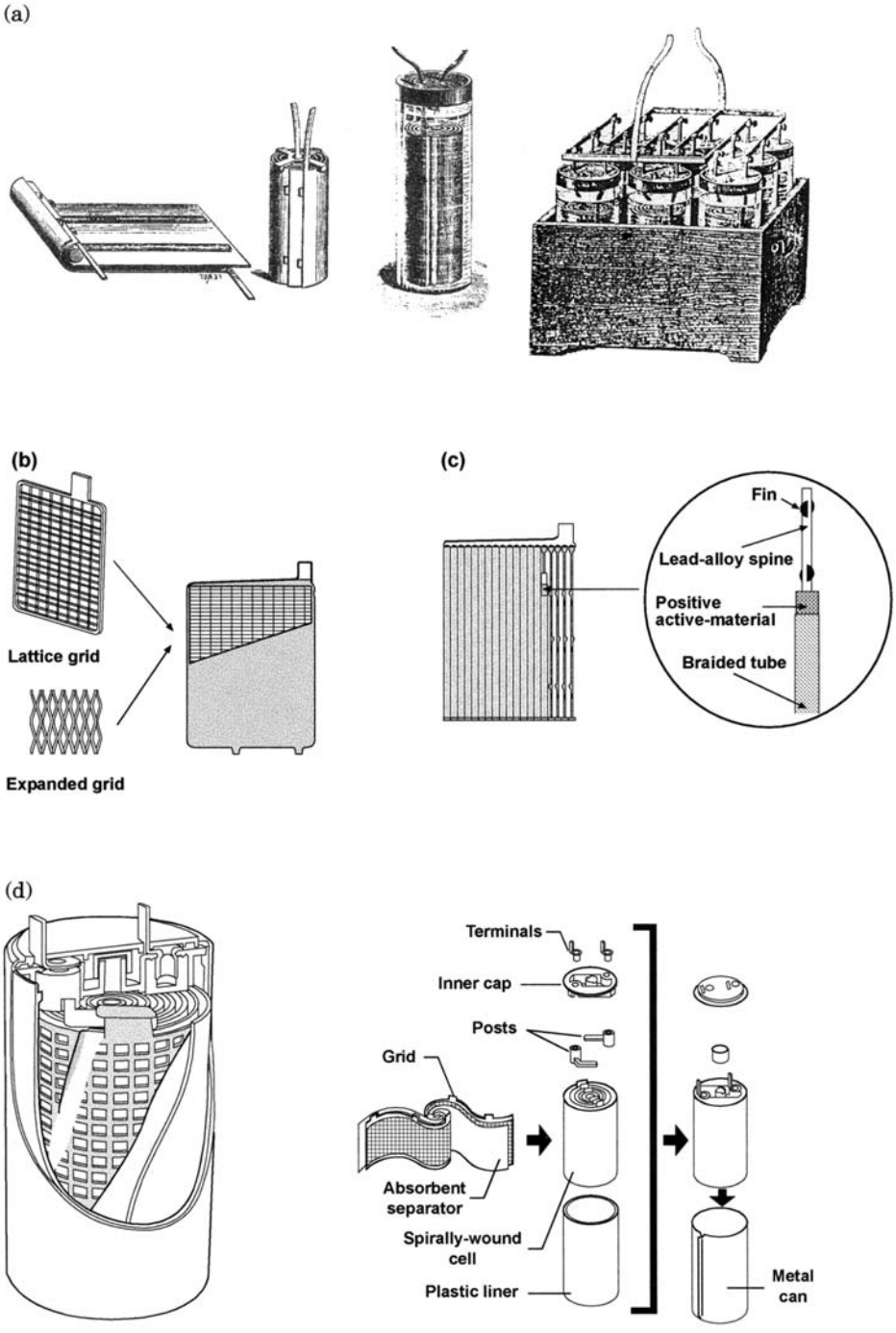

Fig. 1.1. (a) Gaston Planté's cell and battery; (b) flat plate; (c) tubular positive plate; (d) spiral-wound cell.

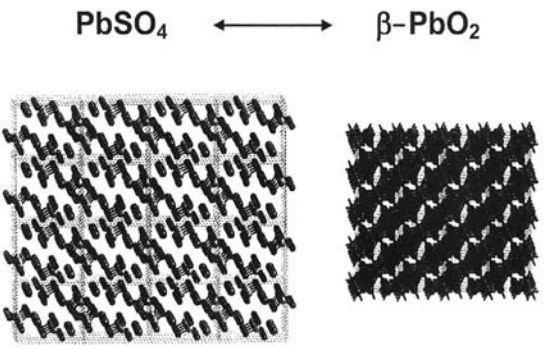

Fig. 1.2. Projections of crystal structures of $PbSO_4$ and β-PbO_2. Each contains the same number of lead atoms and thus a comparison illustrates the volume change that accompanies the interconversion of the two compounds.

recharge causes expansion of the positive active-material because, as shown in Fig. 1.2, the solid product of the discharge reaction ($PbSO_4$) occupies a substantially greater formula volume than the reactant material (PbO_2). Recharge of the cell restores most of the PbO_2, but not within the original volume. By contrast, the negative plate does not show the same tendency to expand, perhaps because lead is softer than lead dioxide and therefore the active material is more easily compressed as the conversion to the more voluminous lead sulfate proceeds. Progressive expansion of the positive plate with cycling service causes an increasing fraction of the active material to become electrically disconnected from the current-collection process [4].

FM2. Water loss. Production of hydrogen and oxygen during overcharge can reduce the volume of electrolyte to a degree that some of the active material loses contact with the liquid phase. This process can be auto-accelerating in that dry-out increases the internal resistance of the battery which, in turn, can cause excessive heating during charging and consequently an increased rate of water loss through evaporation. It should also be noted that the propensity of a battery to gas can be strongly influenced by the presence of impurities [5,6].

FM3. Acid stratification. On recharge, sulfuric acid is produced in and between the plates and there is a tendency for acid of higher concentration, which has a greater relative density, to collect at the bottom of the cell, see Fig. 1.3 [7].

The development of a vertical concentration gradient of acid can give rise to non-uniform utilization of active material and, consequently, shortened service life through the irreversible formation of $PbSO_4$ [8].

FM4. Incomplete charging. If either of the electrodes is persistently undercharged, either because of a defective charge regime or as a result of physical changes which prevent the electrode from reaching an adequate potential, then a rapid decline in available battery capacity may occur.

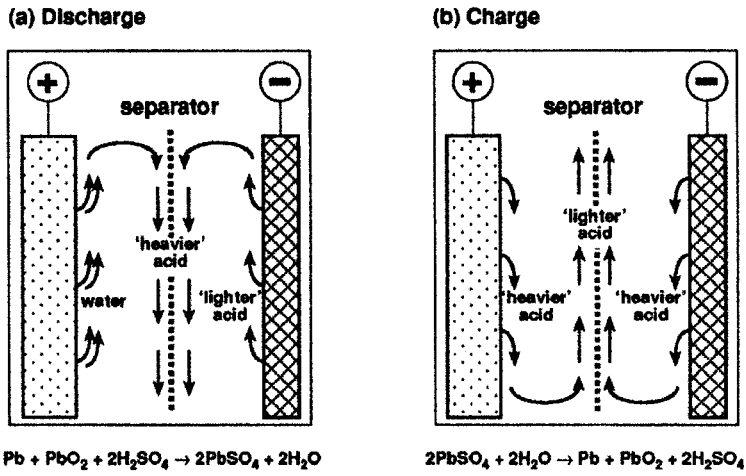

Fig. 1.3. Schematic representation of processes and electrolyte flow that contribute to acid stratification during (a) discharge and (b) charge [7].

FM5. Corrosion. The positive grid is subject to corrosion. The rate of this debilitating process is influenced by: grid composition and microstructure, plate potential, electrolyte composition, temperature. The corrosion product is generally more electrically resistive than the grid and thus diminishes the output of the battery. In extreme cases, corrosion results in disintegration of the grid and collapse of the plate.

Most of the above modes of failure can be suppressed to an acceptable level in conventional lead–acid batteries, as follows.

FM1. Positive-plate expansion. The use of lead–antimony alloy enhances the creep strength of the positive grid and thus retards growth in the plane of the plate. For the flat design of positive plate, expansion normal to the plate can be moderated by applying a compressive force to the plate group. Tubular positive plates have gauntlets that constrain the active material and reduce its tendency to expand, disconnect, and shed.

FM2. Water loss. Water loss can be made good by the process of 'topping up'.

FM3. Acid stratification. Acid concentration gradients can be removed through agitation of the acid by setting the battery to deliberate gassing during extended overcharge.

FM4. Incomplete charging. Batteries operated under partial-state-of-charge duty (as experienced in remote-area power supplies and hybrid electric vehicles) require a periodic full charge in order to maintain capacity.

With the aid of these several measures, substantial service lives can be obtained from flooded batteries in their various applications. The drive towards increased

convenience through eliminating the need for water maintenance and avoiding the release of acid-carrying gases has led, however, to the widespread adoption of the 'valve-regulated' form of the lead–acid battery. This paradigm shift in battery design has brought about a new set of scientific and technological challenges.

1.3. The Valve-regulated Battery

Towards the end of the twentieth century, the lead–acid battery underwent a significant functional revision. For most of its long history, the battery had operated with its plates immersed in a mobile electrolyte and provision had been made for the hydrogen and the oxygen produced during overcharge to be released freely into the atmosphere. The dissipated gases represented a loss of water from the electrolyte, but, as mentioned above, this could be replaced in a regular maintenance operation.

For many years, scientists attempted to develop 'sealed' batteries. At first, efforts focused on the catalytic recombination of the gases within the battery; this approach has proven to be impractical. Success came, however, with the invention of the valve-regulated lead–acid (VRLA) battery. The first commercial units were devised by Sonnenschein GmbH in the 1960s [9] and by Gates Energy Products, Inc. [10] during the 1970s. These were, respectively, the 'gel' and the 'absorptive glass mat' (AGM) technologies (*v.i.*).

The VRLA battery is designed to operate by means of an 'internal oxygen cycle' (or 'oxygen-recombination cycle'), see Fig. 1.4 [11]. Oxygen evolved during the latter stages of charging, and during overcharging, of the positive electrode, i.e.,

$$H_2O \rightarrow 2H^+ + \tfrac{1}{2}O_2\uparrow + 2e^- \tag{1.3}$$

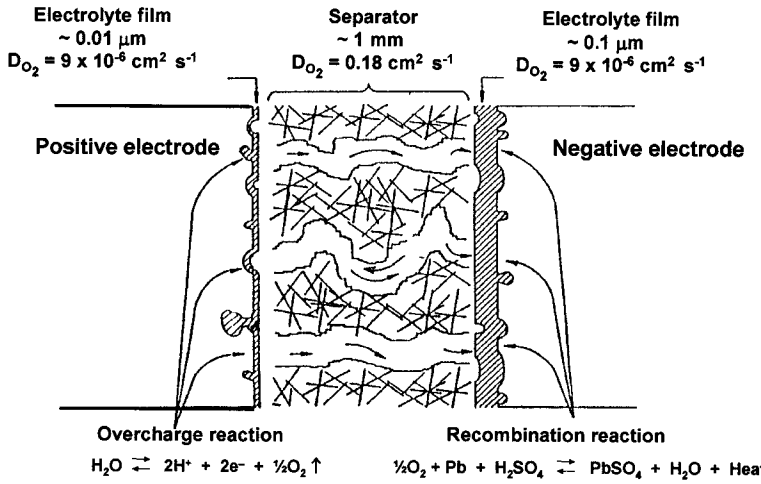

Fig. 1.4. Conceptual view of internal oxygen cycle in a valve-regulated lead–acid cell (Nelson, 1999) [11].

transfers through a gas space to the negative electrode where it is reduced ('recombined') to water:

$$Pb + \tfrac{1}{2}O_2 + H_2SO_4 \rightarrow PbSO_4 + H_2O + \text{Heat} \tag{1.4}$$

Two other reactions must be taken into account during the charging of a VRLA cell. These are, the evolution of hydrogen at the negative plate:

$$2H^+ + 2e^- \rightarrow H_2 \tag{1.5}$$

and the corrosion of the positive grid:

$$Pb + 2H_2O \rightarrow PbO_2 + 4H^+ + 4e^- \tag{1.6}$$

Thus, the charging of a VRLA cell is potentially more complex than the charging of its flooded counterpart. During the charging of a VRLA cell, thermodynamic/kinetic conditions allow the progress of six separate reactions at significant rates: two charge reactions (the reverse of reactions (1.1) and (1.2)) and four secondary reactions (1.3) to (1.6).

The oxygen cycle, defined by reactions (1.3) and (1.4), shifts the potential of the negative electrode to a less negative value and thus decreases the rate of hydrogen evolution to a much lower level (i.e., much less than in the older, flooded design of battery). A one-way, pressure-relief valve is provided to ensure that even the small amounts of hydrogen produced do not generate a high pressure within the battery — hence, the term: 'valve-regulated'. Since the plate is simultaneously on charge, the lead sulfate produced is immediately reduced to lead via the reverse of reaction (1.2). This restores the chemical balance of the cell, i.e., in stoichiometric terms, the net sum of reactions (1.3), (1.4) and the reverse of reaction (1.2) is zero. Thus, part of the electrical energy delivered to the cell is consumed by the oxygen-recombination cycle and is converted into heat rather than into chemical energy [11].

As long as the overcharge current remains moderate, the charge and recombination reactions can remain in equilibrium and little net gas is generated. For example, consider a flooded cell charged to a constant voltage, e.g., 2.45 V as in Fig. 1.5 [12]. The current at the positive electrode is consumed principally by oxygen evolution (I_{O_2}) and by grid corrosion (I_c), and is balanced by that consumed by hydrogen evolution at the negative electrode (I_{H_2}). With a valve-regulated cell, however, oxygen reduction ($I_{O_2\text{-red}}$) shifts the potential of the negative electrode ($\triangle V$) and the rate of hydrogen evolution (I_{H_2}) becomes much reduced, but is not eliminated completely, compared with that experienced in the flooded system. With a high recombination efficiency and with no loss of oxygen from the cell, the rate of hydrogen evolution is balanced by the rate of positive-grid corrosion. In general, the rate at which oxygen recombines at the negative plate is a complex function of the cell design, the operating conditions, and the overcharge regime. By contrast, the recharge of a battery which performs deep-discharge cycling service is more complicated because the relative kinetics of the several competing reactions alter as

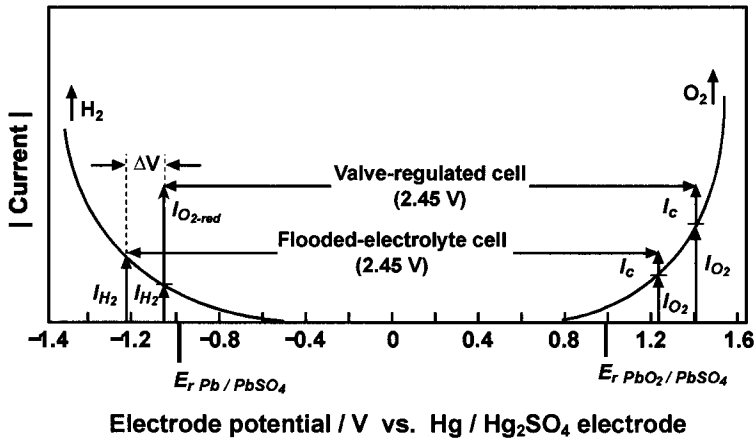

Fig. 1.5. Current distribution in flooded and valve-regulated cells during constant-voltage charging at 2.45 V (Note, anodic and cathodic currents are opposite in sign but, for convenience, are both presented on the same side of the potential axis.) [12].

the battery approaches top-of-charge. If recharging is not managed correctly, current may be continually consumed by the internal oxygen cycle such that the negative plate never reaches a full state-of-charge.

There are two alternative designs which provide the gas space in VRLA cells. One design has the electrolyte immobilized as a gel, the other has the electrolyte held in an AGM separator. Gas passes through fissures in the gel, or through channels in the AGM (Fig. 1.4).

Antimony is no longer included in the grid alloys for VRLA cells because this element lowers the hydrogen overpotential and therefore encourages gassing at the negative electrode. Care needs to be taken against the introduction of other elements that might act similarly [5,6]. Excessive gassing at either the negative or the positive electrode can result in selective discharge of the respective electrode [13]. Lead–calcium–tin alloys are preferred by manufacturers of VRLA batteries for float duties, and lead–tin alloys for cycling applications.

If the cell is over-filled with acid initially, the oxygen cycle cannot function because oxygen diffuses through the aqueous phase at a rate which is approximately four orders of magnitude slower than through the gas space, see Fig. 1.4 [11]. The cell then behaves as if it were of a conventional, flooded design. Towards top-of-charge, first oxygen (from the positive), and then oxygen (from the positive) and hydrogen (from the negative), are evolved and may be released through the valve. This loss of water eventually opens gas spaces (due to drying out of the gel or a decrease in the volume of electrolyte held by the AGM) and allows the transfer of oxygen to proceed. Gas release from the cell then falls to a very low level.

If the oxygen cycle is worked too hard then substantial heat is generated, charging of the negative plate becomes difficult, and progressive sulfation begins from the bottom of the plate where the acid concentration tends to be highest. The function of the oxygen cycle is subtly linked to the microstructure of the separator material

(for AGM designs) and to the nature of the charge algorithm applied, especially near top-of-charge.

As a result of the move from the flooded to the valve-regulated design it is possible that several of the failure mechanisms discussed above may reappear.

FM1. Replacement of lead–antimony alloys with lead–calcium alternatives, as a means to discourage hydrogen evolution, reduces the creep strength of grids so that expansion in the plane of the plate may again become a concern. Use of a separator with insufficient rigidity (i.e., too much 'compressibility') may allow expansion normal to the plane of the plate.

FM2. Water loss is reduced to the extent that periodic replenishment, as required by flooded cells, is no longer necessary. Nevertheless, both hydrogen evolution at the negative electrode and grid corrosion at the positive electrode do cause some water loss.

FM3. Any acid stratification which occurs cannot be overcome by overcharging because there is little free electrolyte and, hence, ineffective mixing. Moreover, water lost cannot be replaced because the battery is expected to remain sealed for life.

FM4. The operation of the oxygen cycle may cause incomplete charging of either the negative or the positive plate [13].

1.4. Heat Management in Lead–Acid Batteries

1.4.1 Heat generation

Batteries generate heat during charge–discharge cycling and this must be dissipated to the environment to prevent the battery temperature from rising continuously. The heat effects originate from the change in entropy of the cell reaction ('reversible heat effect'), and from energy losses caused by overpotential factors and ohmic resistance ('Joule heating'). The former effect is small and gives rise to heat generation during charging and corresponding cooling on discharging. By contrast, Joule heating occurs during both charging and discharging. Proper heat management will ensure that the battery temperature does not exceed a safe level and will maintain all the cells within as small a range of temperatures as possible. The penalty for allowing the development of temperature gradients is non-uniform states-of-charge and states-of-health between cells, which can result in premature failure.

Overcharging causes greater temperature increases in VRLA batteries than in flooded types; in the latter designs, much of the heat generated escapes with the gases evolved during charging. Moreover, the heat that arises from the internal oxygen cycle in VRLA batteries (reaction (1.4)) can be substantial [14], especially in aged batteries where separator dry-out allows oxygen recombination to proceed at a high rate. Thus, closer attention has to be paid to the generation and management of heat in VRLA batteries than in flooded counterparts.

The rate of change in temperature, dT/dt ($K\,s^{-1}$), of a battery during charging or discharging is given by [14]:

$$dT/dt = (dQ_g/dt - dQ_d/dt)/C_b \tag{1.7}$$

where: dQ_g/dt is the heat generated per unit time ($J\,s^{-1}$ or W); dQ_d/dt is the heat dissipated per unit time ($J\,s^{-1}$ or W); C_b is the heat capacity of the materials that comprise the battery ($J\,K^{-1}$). The heat capacity is defined by:

$$C_b = \sum m(i)C_p(i) \tag{1.8}$$

where: $m(i)$ is the mass of component i (g); $C_p(i)$ is the specific heat of component (i) ($J\,g^{-1}\,K^{-1}$). The specific heat C_p of VRLA batteries is in the range 0.7 to $0.9\,Jg^{-1}\,K^{-1}$, while the corresponding value for flooded batteries is slightly above $1\,J\,g^{-1}\,K^{-1}$. The difference is due mainly to the additional electrolyte in flooded designs.

A battery reaches a stable temperature when heat generation balances heat dissipation, i.e., when $dQ_g/dt = dQ_d/dt$. When heat generation exceeds heat dissipation, 'thermal runaway' may result.

1.4.2 Heat dissipation

The dissipation of heat from a battery to its surroundings normally proceeds via three mechanisms: (i) heat flow through the components of the battery and the container walls; (ii) heat radiation; (iii) free convection of air. In practice, the cooling of a battery takes place mainly through the side walls of the container. The bottom surface is usually in contact with a solid surface, which attains the same temperature as the battery and then ceases to be an effective heat sink. The upper surface plays little part in heat exchange; the lid has no direct contact with the electrolyte, and the intermediate layer of gas, which has low thermal conductivity, hinders heat exchange.

The quantity of heat per unit area ($W\,m^{-2}$) that can be conducted through the battery wall per unit time is given by

$$dQ/dt = \lambda(\Delta T/x) \tag{1.9}$$

where λ is the thermal conductivity ($W\,m^{-1}\,K^{-1}$); x is the thickness of the medium, e.g., the container wall (m); $\triangle T$ is the temperature difference across the battery wall (K). For plastic materials, λ is of the order of $0.2\,W\,m^{-1}\,K^{-1}$. Thus, for example, the heat conduction through a container wall of thickness 3 mm is $67\,W\,m^{-2}\,K^{-1}$.

The thermal conductivity of the battery electrolyte solution is higher than that of plastic, and that of lead is higher again. Accordingly, the internal heat flux is fast compared with that through the container wall, mainly due to the thermal conductivity of the electrodes, and the temperature measured at the side wall usually represents a good approximation of the average cell temperature. This approximation does not hold good, however, at high rates of charge.

The quantity of the heat lost per unit area ($W\,m^{-2}$) per unit time by the radiation process is governed by the Stefan-Boltzmann law:

$$dQ/dt = \varepsilon\sigma T^4 \tag{1.10}$$

where ε is the Stefan-Boltzmann constant ($5.67 \times 10^{-8}\,W\,m^{-2}\,K^{-4}$); σ is the emissivity of the material with respect to an ideal emitter ($\sim$0.95 for plastic materials normally used for battery containers); T is the absolute temperature (K). For comparatively small differences in temperature between the battery and the environment, the heat dissipated for each unit temperature difference (K) is [14]:

$$dQ/dt = 5 \text{ to } 6\,Wm^{-2}K^{-1} \tag{1.11}$$

For small differences in temperature between the battery and the environment, and a minimum spacing of about 1 cm between facing walls, the rate of removal of heat from the battery wall by the free convection of air for each unit temperature difference (K) is [14]:

$$dQ/dt = 2 \text{ to } 4\,Wm^{-2}K^{-1}. \tag{1.12}$$

For a free-standing battery, the total dissipation of heat is given by

$$dQ_d/dt = dQ/dt \text{ (radiation)} + dQ/dt \text{ (conduction)} \tag{1.13}$$

with the second factor limited by the rate of removal by air convection. Thus, the total heat dissipation for each unit temperature difference is the sum of eqns. (1.11) and (1.12), i.e.,

$$dQ_d/dt = 7 \text{ to } 10\,Wm^{-2}K^{-1} \tag{1.14}$$

Clearly, the combined processes of radiation and free convection of air are inadequate to remove all of the heat that is conducted through the battery container (e.g., $67\,W\,m^{-2}\,K^{-1}$ for the example given above). Far greater rates of heat removal can be achieved by means of forced flow of liquid coolants over the outer surface of the battery.

1.5. The Challenges Ahead

The changes made to the construction of the battery in the move to the valve-regulated design (summarized in Fig. 1.6) have brought new challenges for battery scientists and technologists in terms of overcoming the various life-limiting mechanisms of the lead–acid battery. The reward for a complete resolution of these issues will be a battery that requires no maintenance, presents no threat of acid spill,

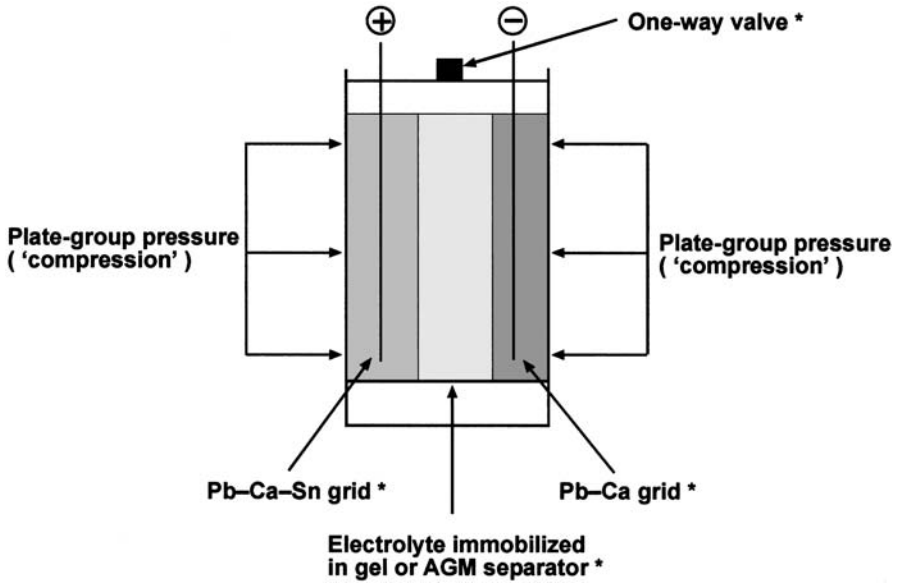

Fig. 1.6. Schematic of section through a VRLA cell. Components modified in the change from the flooded design are denoted by asterisks.

can be deployed with a minimal footprint, and can deliver high-rate performance combined with higher specific energy.

As the new millennium begins, there are clear signs that the demands placed on lead–acid batteries, in all existing and prospective applications, are about to undergo a dramatic change. The rapidly expanding use of electronics within automobiles, for example, is leading to the adoption of 42-V PowerNets. These will require batteries with higher power, good ability to withstand extensive periods of operation at a partial state-of-charge (PSoC), and long service-life. The same qualities will be expected from batteries used to power HEVs. Partial-state-of-charge duty brings both an advantage and a disadvantage compared with float and cycling duties. On the credit side, it has been found that VRLA batteries operated under PSoC regimes at modest rates of charge and discharge enjoy a significant increase in life-time storage capability (i.e., an increase in the total amount of energy that can be stored and delivered during the life of the battery) compared with regular cycling. On the debit side, at the higher charge–discharge rates required for 42-V PowerNet and HEV duties, VRLA batteries (still in a PSoC mode) suffer from rapid and irreversible formation of lead sulfate on the negative plates that curtails operating life. Thus, significant modifications in VRLA design will be required for new-generation transportation applications (see Chapter 17). Likewise, consumers are insisting on improvements in VRLA batteries used for stationary energy-storage in telecommunications and remote-area power-supply systems.

A summary of the new demands that are being placed on medium- and large-scale VRLA batteries in all their applications is given in Table 1.1. The necessary

Table 1.1. New demands imposed on VRLA battery performance by present and future markets.

Application	Battery requirements
Automobiles (42-V PowerNets)	• PSoC duty, 2 kWh, 20 kW • 5000 kWh throughput/life
Hybrid electric vehicles	• PSoC duty, 1–3 kWh, 30 kW • 600 W kg^{-1} • 5000 kWh throughput per kWh of capacity
Electric vehicles	• 40 Wh kg^{-1} • fast charge • 1000 deep-discharge cycles
Telecommunications systems	• reliable float life of 10 years at all foreseeable operating temperatures
Remote-area power-supplies	• PSoC duty • reliable life of 10 years

transition from the flooded to the valve-regulated version must also be accompanied by a step-function advance in performance. It is the purpose of this book to set forth the way this transition in technology is being successfully accomplished.

References

1. *Key World Energy Statistics from the IEA*, 2001 Edition, International Energy Agency, Paris, France, 2001.
2. G. Planté, *C.R. Acad. Sci. Paris*, **50** (1860) 640–642.
3. C.A. Fauré, *C.R. Acad. Sci. Paris*, **92** (1881) 951–953.
4. A.F. Hollenkamp, *J. Power Sources*, **59** (1996) 87–98.
5. B. Culpin, M.W. Pilling, F.A. Fleming, *J. Power Sources*, **24** (1988) 127–136.
6. D.M. Rice, J.E. Manders, *J. Power Sources*, **67** (1997) 251–255.
7. D.A.J. Rand, R. Woods, R.M. Dell, *Batteries for Electric Vehicles*, Research Studies Press Ltd., Taunton, England, 1998, p. 203.
8. M. Shinpo, H. Nakashima, S. Sasabe, Y. Kasai, *Yuasa Jiho*, **68** (1990) 26–34.
9. O. Jache, U.S. Patent 3,257,237 (1966).
10. D.H. McClelland, J.L Devitt, U.S. Patent 3,862,861 (1975).
11. R.F. Nelson, *Proceedings of the 4th International Lead–Acid Battery Seminar*, 25–27 April, 1990, San Francisco, USA, International Lead Zinc Research Organization, Inc., 1990, pp. 31–60.
12. Ref. [7], p. 154.
13. L.T. Lam, N.P. Haigh, C.G. Phyland, N.C. Wilson, D.G. Vella, L.H. Vu, D.A.J. Rand, J.E. Manders, C.S. Lakshmi, *Proceedings of the 20th International Telecommunications Energy Conference*, San Francisco, CA, USA, IEEE, 1998, pp. 452–460.
14. D. Berndt, *J. Power Sources*, **100** (2001) 29–46.

Valve-Regulated Lead–Acid Batteries
D.A.J. Rand et al., editors

—CHAPTER 2—

LEAD ALLOYS FOR VALVE-REGULATED LEAD–ACID BATTERIES

R.D. Prengaman

2.1. Antimony-free Grid Alloys

Early grid materials for valve-regulated lead–acid (VRLA) batteries consisted of pure lead or lead–calcium alloys for both the positive and negative plates. Although batteries made with plates using these grid materials were usually found to be acceptable for float applications, a rapid decline in capacity was observed in cycling duties, often within the first 50 cycles. This phenomenon was first termed the 'antimony-free effect', but later became known as 'premature capacity loss' (PCL). Two theories were proposed to account for this loss of capacity. According to the first, the cause was thought to be the formation of electrically resistive $PbSO_4$/α-PbO layers at the grid|active-material interface in the absence of sufficient antimony in the positive grid. The second theory asserted that capacity loss was due to excessive corrosion, and particularly growth, of the positive grid that resulted in inadequate attachment of the active material (lead dioxide).

The addition of tin to pure lead and lead–calcium alloys was found to improve the mechanical properties, increase the rechargeability, reduce corrosion, and increase the conductivity at the grid|active-material interface. Sufficient tin also modified the grain structure of the grid materials, changed the method of precipitation of the alloys, and dramatically decreased the amount of $PbSO_4$ or α-PbO formed at the interface. Silver additions to lead–calcium–tin alloys enhanced the corrosion resistance and reduced markedly the creep rate or growth rate of the alloys, which resulted in grid materials of much greater stability.

2.2. Pure-lead Positive Grids

Pure lead has been used for many years in Planté cells for float service in flooded batteries. The spiral-wound VRLA batteries produced by Gates incorporate chill-cast, high purity, lead sheet for grid manufacturing [1]. The lead is very soft and facilitates the manufacturing process. Moreover, pure lead is excellent in terms of good corrosion resistance in the positive plate, and of suppressing gassing rates at the negative due to the high overpotential for hydrogen evolution. Batteries produced from pure lead have produced exceptional performance in float applications.

One area of performance of pure-lead batteries has been unsatisfactory, namely, the failure to recover from deep discharge in cycling applications. The phenomenon is thought to be caused by a passive layer at the grid|active-material interface. This raises the impedance of the cell and thus impairs rechargeability. The phenomenon was first noted in 1941 [2]. Subsequently, it was proposed [3–6] that the passivation layer was due to the formation of $PbSO_4$, α-PbO, and basic lead sulfates at the grid|active-material interface. The occurrence of α-PbO is quite remarkable given that it cannot be formed on a lead surface in an acid environment [7]. To explain its presence, it was postulated [7] that the grid surface is separated from the electrolyte by a semi-permeable membrane that enables the pH in the vicinity of the corroded surface to be much higher than that in the bulk electrolyte solution. Pavlov and his colleagues [8–11] developed a detailed model of the corrosion process. It was demonstrated that α-PbO can indeed be generated in the corrosion layer when the overlaying $PbSO_4$ layer functions as a semi-permeable membrane and blocks the ingress of HSO_4^- and SO_4^{2-}, but allows the migration of H^+ ions away from the grid surface. This model was verified experimentally by Ruetschi [12]. The high pH associated with the deficiency of H^+ ions results in the creation of a Pb|PbO corrosion couple. Since α-PbO is an insulator, the grid becomes passivated (formation of an electrically insulating surface layer) by the corrosion film. The passivation has also been attributed [13,14] to cracking of the corrosion layers due to stresses at the grid|corrosion-layer interface that result from the growth of the grid and the extra volume occupied by the corrosion products. Accommodation of these products causes the corrosion layer to lose contact with non-antimonial grids.

It has been shown [15] that the insulating α-PbO layer forms on lead-sheet electrodes at high positive potentials via an oxidation process which is the equivalent of overcharge. Furthermore, α-PbO can be produced at the grid interface during self-discharge of an acid-starved battery at low states-of-charge [16]. There is evidence [17] for a galvanic coupling between PbO_2 and lead (grid metal) on open-circuit stand. This causes a local increase in pH and results in the growth of $PbSO_4$ which acts as a semi-permeable membrane and hinders ionic migration. The reaction depends on the structure formed by the self-discharge and the size of the $PbSO_4$ particles [18]. The $PbSO_4$ layer gives rise to passivation as α-PbO can now form in a solid-state process beneath the $PbSO_4$ layer. Poorly conducting α-PbO films were shown to be produced in dry-charged plates through a process called 'thermopassivation', which involves a solid-state reaction between lead and PbO_2, particularly at low pH [19,20].

The passivation layer that forms on pure-lead grids in spiral-wound cells can lead to a premature drop in capacity during the first few cycles [21]. The passive film completely covers the surface of the pure-lead grid.

2.3. Lead–Calcium Alloys

Lead–calcium alloys were introduced into standby and telephone systems in the 1930s [22,23]. The alloys were primarily binary compositions with very low calcium

contents, viz., 0.03 wt.%. Similar alloys were also used in batteries for submarines. The corrosion rates of the alloys were very low and battery lives of over 30 years were attained. The positive grids also performed very well in float service. The calcium content must be controlled precisely because excess calcium causes rapid growth of the grids [24], while too little calcium results in inferior mechanical properties [22]. The casting conditions also influence the grain structure and the eventual degree of corrosion [25]. Because lead–calcium alloys had been used in flooded standby-power and telephone batteries, they became the first alloys of choice for VRLA batteries and had the same binary lead–calcium compositions.

When batteries with lead–calcium alloys were cycled, difficulties in recharge emerged and rapid capacity loss often occurred in the first few dozen cycles [26–28], particularly when using constant-voltage charging. As mentioned above, this phenomenon was called the antimony-free effect by early researchers [29] because it did not occur when batteries with antimonial grids were cycled. During the following years, the antimony content in positive grids was progressively reduced and it was found that batteries with low-antimony grids could also exhibit poor cycle-life. Thus, the phenomenon was afforded the general term: 'premature capacity loss — PCL' [30]. The cycling difficulties experienced with lead–calcium alloys were initially believed to be due to the formation of a barrier layer of an insulating compound, which was formed during discharge. Early studies [13,31,32] reported that the compound was $PbSO_4$. A layer of α-PbO was then found below the $PbSO_4$ layer [33]. The phenomenon was believed to be similar to that seen with pure-lead grids. It was proposed [34] that, in lead–calcium grids, the calcium present at the grid|active-material corrosion surface, whether as Pb_3Ca or CaO, might be a contributor to the alkaline condition. A loss of conductivity in certain areas of the grid was also thought to be a contributory factor [35]. Extensive task groups were commissioned [36–38] to attack the problem of severe capacity decline during cycling of batteries which employed lead–calcium alloys (Fig. 2.1). This phenomenon was found to be associated with processes at the grid|AM interface and was termed PCL-1. A second, less severe, loss in capacity was attributed to degradation of the positive-active material itself and was termed PCL-2 (see Chapter 9).

Hardening mechanism in lead–calcium alloys. Lead–calcium alloys harden extremely rapidly; 80% of the ultimate strength is reached in one day, and virtually full ageing in seven days. Such rapid hardening enhances grid handling and battery production. The rapid hardening was a benefit to VRLA batteries.

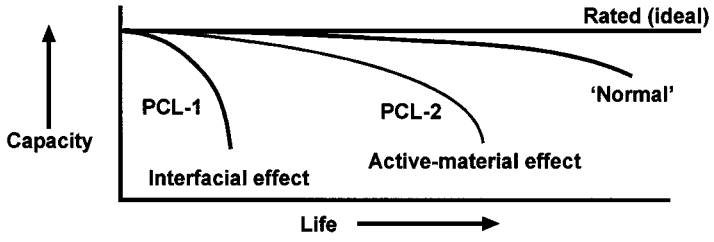

Fig. 2.1. Schematic representation of premature capacity loss (PCL).

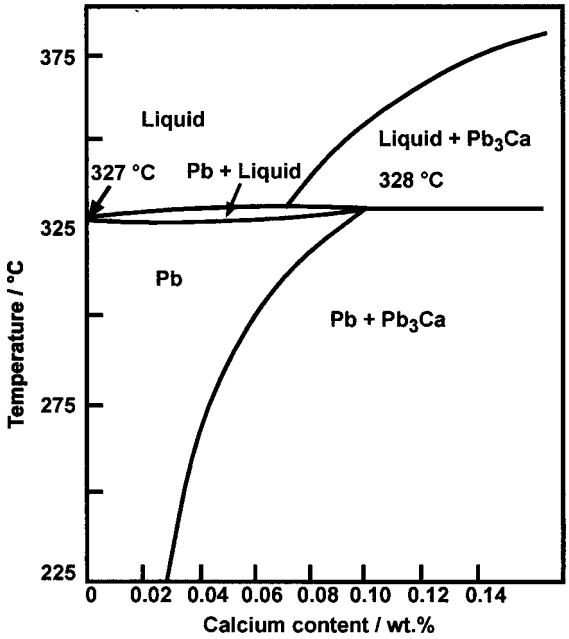

Fig. 2.2. Lead–calcium phase diagram.

The lead–calcium phase diagram [39] is shown in Fig. 2.2. The method of strengthening lead–calcium grid alloys is very complex. A small amount of calcium (of the order of a few hundredths of one percent) is sufficient, after cooling, to produce a supersaturated matrix. At room temperatures, precipitation of the calcium produces very rapid hardening to relatively high mechanical property levels in rather short holding times. Below 0.07 wt.% Ca, the alloys solidify into a cellular dendritic grain structure with large columnar crystals [40,41]. The primary method of strengthening is a discontinuous precipitation or cellular precipitation reaction, which entails movement of grain boundaries into the supersaturated matrix with subsequent precipitation of Pb_3Ca particles in the matrix behind the moving boundaries. This precipitation mechanism has been thoroughly described [42–47].

The boundaries move with a very low activation energy of 11–20 kJ mol^{-1} [48] due to the ease of precipitation of the Pb_3Ca particles. The discontinuous precipitation reaction is responsible for the irregular ('jagged' or 'puzzle-like') grain boundaries seen in the microstructures of these alloys. The grain structure is related to the calcium content, the cooling rate, and the manner in which the alloy is worked [49]. Low calcium contents and slow cooling produce large grains [50], as seen in Fig. 2.3. In all cases, the lead–calcium binary alloys are strengthened by the discontinuous precipitation reaction. Fine grains are created by the simultaneous movement of many boundaries through a supersaturated solution of high calcium content, as seen in Fig. 2.4. Bismuth accelerates the discontinuous precipitation reaction, while silver delays it [48]. In most cases, the reactions take a few days to

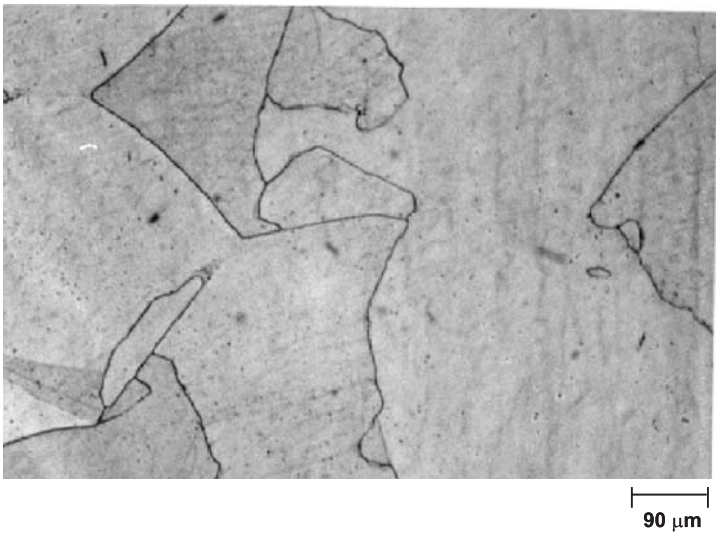

Fig. 2.3. Coarse-grained lead–calcium alloy, 0.03 wt.% Ca.

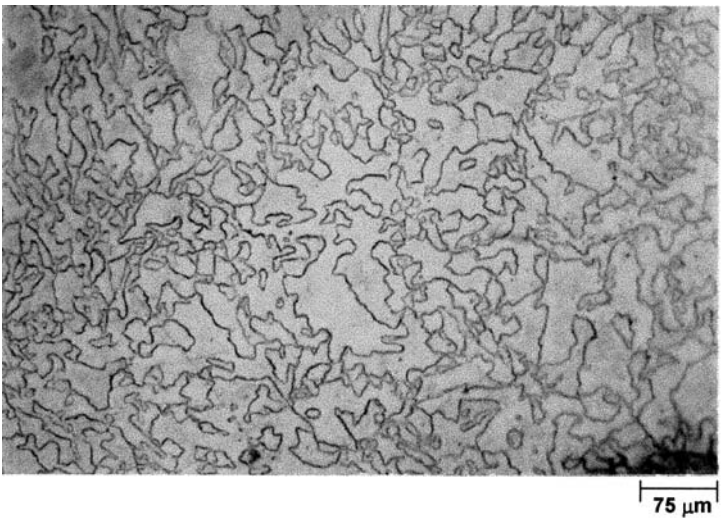

Fig. 2.4. Fine-grained lead–calcium alloy, 0.09 wt.% Ca.

complete, but this time can be shortened to a few hours by the application of elevated temperature.

As the grain boundaries move through the casting, they are trapped on defects and impurities. This can result in boundaries that are more prone to corrosion. It has been suggested [25] that heat treatment of the alloy can redissolve the Pb_3Ca particles near the boundary and, thereby, reduce the rate of corrosion of the alloy. Certainly, the mechanical properties, creep rate, and corrosion rates of lead–calcium alloys are

Table 2.1. Mechanical properties of binary lead–calcium alloys.

Calcium (wt.%)	Yield strength (MPa)	Tensile strength (MPa)	YS:UTS[a]	Creep to failure at 20.7 MPa (h)	Corrosion rate (mm per year)
0.025	17.7	25.1	0.71	1	0.279
0.050	29.0	37.2	0.78	30	0.345
0.065	31.8	42.5	0.75	50	0.348
0.075	35.3	46.4	0.78	40	0.358
0.090	32.9	47.0	0.70	20	0.392
0.100	32.5	47.8	0.68	10	0.411
0.110	30.5	46.3	0.66	7	0.429
0.120	27.6	43.2	0.64	5	0.480
0.140	24.7	39.2	0.63	2	0.513

[a]YS = yield strength; UTS = ultimate tensile strength.

dependent on the calcium content [51]. These properties are listed in Table 2.1. The maximum values of the yield strength, the ultimate tensile strength, and the creep resistance are reached at 0.075, 0.10, and 0.065 wt.% Ca, respectively. The corrosion rate increases continuously with calcium content. The creep rate is increased markedly at calcium contents above 0.09 wt.% Ca, due to the very fine nature of the grain structure of these alloys. Part of the problem of PCL with lead–calcium alloys was believed to be the low mechanical properties, particularly creep resistance, which permitted significant growth of the positive grids [52].

2.4. Tin Additions to Pure Lead and Lead–Calcium Alloys

Tin additions to pure lead have greatly diminished the problems experienced on cycling batteries with grids made from this metal. Small amounts of tin (0.3–0.6 wt.%) increase dramatically the charge-acceptance of pure lead [53]. The beneficial effects of tin on passivation were demonstrated quite early. Tin additions to lead and lead alloys reduce the rate of bare-metal corrosion of grids to a significant degree [54]. Pavlov demonstrated [55] that tin doping of the PbO layer resulted in an increased photoelectric current, and therefore concluded that tin-containing corrosion layers were more conductive than those formed on pure lead. It has been suggested [56,57] that complex semiconductor structures of SnO- or SnO_2-doped PbO account for the increased conductivity of the corrosion layer.

The addition of 0.6–0.7 wt.% Sn to a pure-lead positive grid can virtually eliminate the rapid loss in capacity displayed by VRLA batteries within the first 50 cycles [21]. The results also show that the corrosion process changes from the formation of a continuous and uniform layer to a much more selective attack which penetrates into the grain boundaries. Despite the penetration, the corrosion rates are lower than that for pure lead. When tin is present at 0.6–0.7 wt.% in the alloy, doping of the corrosion layer at the grid|active-material interface with SnO_2 inhibits, but does not eliminate, the formation of a passivation layer of $PbSO_4$ and/or α-PbO on the surface of the grid.

Several workers [54,55,57] have investigated the effect of tin as an alloying element in lead. In addition to conventional bulk alloying, tin-rich surface layers have been added to grids by lamination [58–60], and lead–tin has been co-extruded over wires to form grids [61]. Tin has also been added to the surface of lead grids by electroplating [62,63].

Recently, there has been more definitive work on the addition of tin to lead and its effect on corrosion and passivation [64,65]. In a series of experiments with 0.5–3.5 wt.% Sn added to lead, it was found that the passive layer which impedes electrical conduction through the grid|active-material interface could be reduced or eliminated by the addition of sufficient tin. Below 0.8 wt.% Sn, the passive films have only ionic conductivity. The electrical conductivity increases rapidly beyond 0.8 wt.% Sn and reaches a plateau at 1.5 wt.% Sn. The work shows that the corrosion resistance of the alloy increases sharply as the tin content of the alloy increases. A minimum tin content of about 1.5 wt.% is required to ensure high conductivity of the corrosion layer and a minimum corrosion rate. It was found that tin inhibits the oxidation of Pb to Pb^{+2}, as predicted by an earlier model [57].

Alloying lead with tin has the effect of inhibiting the oxidation of lead to PbO, but intermediate compounds, PbO_x, can be formed. The corrosion product on pure lead is a semiconductor. Tin additions to the lead grid alloy transform the semiconducting corrosion layer of lead oxide into a lead–tin oxide layer, which is highly conductive. The tin content of the passive film is greatly increased i.e., from 3 wt.% for an alloy of 0.5 wt.% Sn to 44 wt.% for an alloy of 3.5 wt.% Sn [65]. Measurement of the resistance of the grid|active-material interface upon cycling in actual cells [66] has shown that antimony or tin additions to grids improve the conductivity of the corrosion layer.

At high pH values, lead is oxidized to $Pb(OH)_2$ in a first step, and tin is oxidized, first to SnO, and subsequently to SnO_2. The $Pb(OH)_2$ may be reduced by SnO back to lead with consequent formation of SnO_2, in a simple redox procedure [67]. In this reaction, the PbO layer becomes thinner and more enriched with SnO_2. Significant conductivity of the grid|active-material interface requires a concentration of tin of 10 wt.% or higher in the corrosion product [65].

2.5. Lead–Calcium–Tin Alloys

2.5.1 Grain structure

Tin additions to lead–calcium alloys change dramatically the method of precipitation and age-hardening from discontinuous precipitation of Pb_3Ca to a mixed discontinuous and continuous precipitation of Pb_3Ca and $(PbSn)_3Ca$ and, finally, to a continuous precipitation of Sn_3Ca. Such precipitation reactions have been described for alloys that contain low tin contents [45,48,68–70]. The reactions are not influenced or modified by impurities in the lead alloys [71,72]. A ternary phase diagram has been proposed [41], which sets the areas of stability of Pb_3Ca, Sn_3Ca, and mixed $(PbSn)_3Ca$ precipitates, and this is shown in Fig. 2.5. The phase diagram has been confirmed [73].

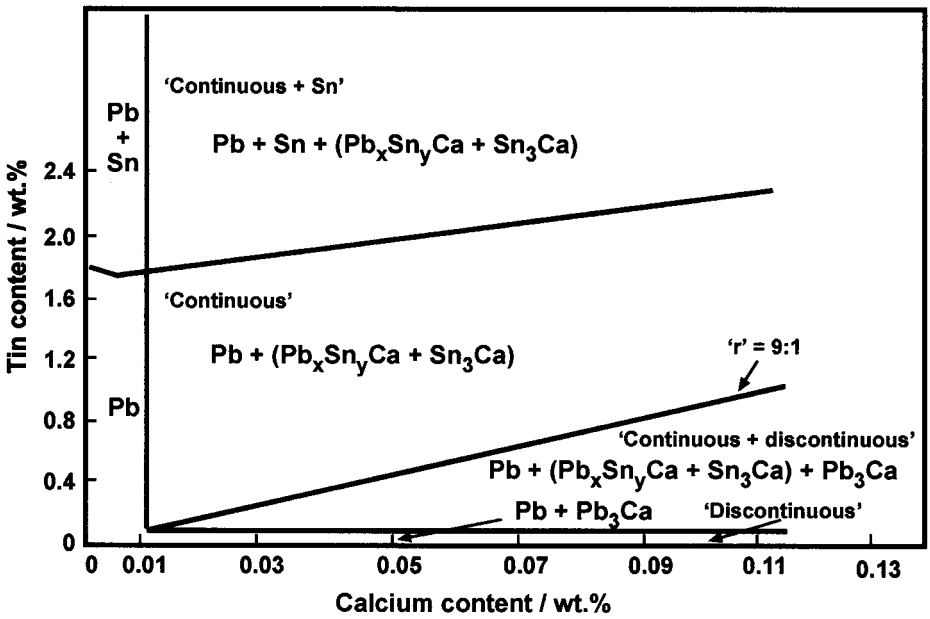

Fig. 2.5. Lead-rich region of lead–calcium–tin phase diagram.

At low tin contents, the calcium initially precipitates rapidly as Pb_3Ca in the same manner as in binary lead–calcium alloys. These alloys have a fine grain structure and quickly reach high hardness as discontinuous precipitation predominates. At higher tin contents, the mode of precipitation changes to a mixed discontinuous precipitation of Pb_3Ca followed by a continuous precipitation reaction of Pb_xSn_yCa. These reactions lead to overageing of the precipitates and a decrease in mechanical properties.

Below a calcium content of 0.08 wt.% and above a Sn:Ca ratio ('*r*' value) of 9:1 (the value corresponding to stoichiometric Sn_3Ca), the reaction changes to a continuous precipitation. In the continuous precipitation mode, the original cast grain structure is maintained.

2.5.2 Mechanical properties of cast lead–calcium–tin alloys

The mechanical properties and ageing response of cast lead–calcium–tin alloys have been described by several authors [44,74,75]. The effect of calcium at 0.5 and 1.5 wt.% Sn on the yield strength, ultimate tensile strength, creep resistance, and corrosion rates of fully aged cast materials is shown in Tables 2.2 and 2.3, respectively [51]. Alloys with low calcium contents have low mechanical properties which can be increased with additional tin. Tin additions above an '*r*' value of 9:1 are believed to drive the precipitation reaction to completion. Higher calcium contents do not produce higher mechanical properties unless accompanied by higher tin contents. Sn_3Ca occupies a larger volume and has a higher misfit with the lead lattice than Pb_3Ca. The increase in second phase volume and greater stability of Sn_3Ca

Table 2.2. Mechanical properties of lead–calcium–tin alloys with 0.5 wt.% Sn.

Calcium (wt.%) Silver (wt.%)	Yield strength (MPa)	UTS (MPa)	YS:UTS	Creep to failure at 20.7 MPa (h)
0.025	19.3	25.5	0.75	10
0.050	38.5	48.2	0.80	70
0.050 + 0.035 Ag	42.6	50.7	0.84	300
0.065	40.0	48.9	0.82	200
0.075	40.2	50.3	0.80	300
0.090	40.0	51.3	0.78	100
0.100	38.7	51.7	0.75	70
0.120	31.1	45.8	0.68	20
0.140	31.2	46.5	0.67	15

Table 2.3. Mechanical properties of lead–calcium–tin alloys with 1.5 wt.% Sn.

Calcium (wt.%) Silver (wt.%)	Yield strength (MPa)	UTS (MPa)	YS:UTS	Creep to failure at 20.7 MPa (h)
0.025	34.3	45.8	0.75	30
0.050	46.8	55.1	0.84	100
0.050 + 0.05 Ag	49.1	57.7	0.85	700
0.065	49.1	58.6	0.84	750
0.075	50.2	60.1	0.84	1000
0.090	46.9	58.6	0.80	600
0.100	43.7	57.9	0.75	250
0.120	41.7	57.2	0.73	140
0.140	39.5	56.5	0.70	120

compared with Pb_3Ca cannot, however, explain fully the higher mechanical properties. These properties must be due to the change in morphology of the precipitate from the larger Pb_3Ca formed in discontinuous precipitation to the smaller continuous Sn_3Ca. Higher tin contents accelerate the change from mixed Pb_3Ca-$(PbSn)_3Ca$ to the more stable Sn_3Ca.

For many years, alloys with '*r*' values above 9:1 were not utilized for VRLA batteries. Large battery grids and tubular grids required alloys which would harden rapidly. Alloys of 0.08–0.12 wt.% Ca and 0.3–0.6 wt.% Sn were most commonly utilized for VRLA batteries for standby and telecommunications service. These alloys harden rapidly and the alloys can be handled and pasted after a short ageing time at room temperature compared with weeks for materials with high '*r*' values.

Alloys with '*r*' values of 3:1 to 6:1 have much lower yield strength, significantly lower creep resistance and lower corrosion resistance than alloys with '*r*' values above 9:1 and particularly those with '*r*' values of 12:1 or higher. It has been suggested that the poor mechanical properties of calcium alloys with low tin contents are also the cause of the poor cycling performance of these alloys. The grids are prone to growth [52] and this may result in cracking of the corrosion layer [13].

2.5.3 *Aluminium addition*

Aluminium has been added to lead–calcium and lead–calcium–tin alloys to protect the alloy from loss of calcium and variations in calcium content [76–78]. The oxidation of calcium — and, if present, tin — is prevented by the formation of a thin, tough skin of aluminium oxide which denies access of oxygen to the surface of the molten alloy. Aluminium additions greatly decrease the amount of calcium oxide suspended in the cast grid and increase the mechanical properties due to higher utilization of metallic calcium. The reduced oxidation of calcium when aluminium is present in the castings reduces the rate of penetrating corrosion into the grain boundaries of positive grids. It has been confirmed [78] that aluminium renders more calcium available in metallic form in lead–calcium–tin alloys. The effective '*r*' values of lead–calcium–tin alloys in more recent applications may have decreased compared with those reported years ago when aluminium was not included in grid alloys.

Corrosion of lead–calcium–tin alloys. Tin not only increases the mechanical properties of all lead–calcium alloys, but also has a dramatic effect on the yield strength and creep resistance of alloys with an '*r*' value above 9:1. Perhaps more importantly than its influence on mechanical properties, tin addition to lead–calcium alloys reduces dramatically the rate of corrosion of lead–calcium alloys. For cast lead–calcium–tin alloys, the rate of corrosion is a function of both calcium and tin composition [79]. High tin contents can offset the higher rates of corrosion experienced by alloys with high calcium contents, as shown in Table 2.4. Higher tin contents in rolled expanded grids result in improved tensile strength, greatly improved corrosion resistance, and significantly reduced grid growth [80]. An appreciable decrease in the corrosion weight loss of lead–calcium–tin alloys occurs when tin is increased above 0.6 wt.% [81]. Corrosion rates also decrease as the calcium content is decreased, as demonstrated in Table 2.5. Alloys with low '*r*' values show higher corrosion weight loss and growth [82] and confirm the results of earlier studies [52,83]. The discontinuous precipitation reactions at low '*r*' values are

Table 2.4. Corrosion behaviour of cast lead–calcium alloys with various amounts of tin. (Corrosion rate: mils per year at 0.84 mA cm^{-2}.)

Calcium (wt.%)	Tin (wt.%)					
	0	0.25	0.5	0.75	1.0	1.5
0.025	11.6	10.2	10.0	10.1	9.7	9.4
0.050	13.6	12.9	12.9	12.0	11.1	10.6
0.065	13.7	13.0	12.7	11.6	10.9	10.8
0.075	14.1	13.1	12.8	11.7	11.7	11.4
0.090	15.4	—	12.6	12.6	12.3	12.1
0.010	16.2	13.9	13.5	12.7	12.8	11.9
0.012	18.9	14.0	13.8	13.3	13.6	12.8
0.014	20.2	15.5	14.4	14.1	13.8	13.3

Table 2.5. Effect of tin and silver on corrosion resistance of lead–calcium–tin alloys. (Corrosion weight loss in mg cm^{-2}.)

	0.6 wt.% Sn	1.2 wt.% Sn	1.5 wt.% Sn	3.0 wt.% Sn
0.1 wt.% Ca	126	80	76	54
0.08 wt.% Ca	75	37	33	32
0.08 wt.% Ca + 0.05 wt.% Ag	39	22	—	—

believed [84] to contribute to the corrosion. The weight loss passes through a minimum at about 1.3 wt.% Sn [82]. At higher tin contents, however, the grains become coarser and this results in deeper intergranular corrosion in accord with other studies [21,85,86]. Similar corrosion behaviour has been found [87] on cast and expanded grids, as seen in Fig. 2.6. As the tin content is increased further, corrosion becomes more regular and occurs primarily at interdendritic boundaries. This results in a higher corrosion rate but lower rates of penetration into the grain structure.

Very regular corrosion, without grain boundary attack, was found [88] on alloys that had low calcium content (0.06 wt.%), a relatively high tin content (0.7 wt.%), and contained aluminium. Evidently, when present at sufficiently high concentrations, tin prevents localized penetrating corrosion and macro-pitting, and also reduces the volume of the corrosion product. The reduced attack was attributed to the lower number of grain boundaries per unit volume in low-calcium–high-tin alloys. The structure was thought to induce low grid growth and to be desirable for the long life of VRLA batteries. Unfortunately, the results contradicted those of other workers [83] who obtained evidence of extensive attack at grain boundaries in similar lead–calcium–tin alloys. The difference in findings may be due to the fact that aluminium was present in the alloys used in the more recent work [88], but absent from the alloys examined by the earlier researchers [83].

Even higher tin contents (up to 2 wt.%) have been reported [89] to provide reduction in the rate of corrosion and growth of positive lead–calcium grids in VRLA batteries employed in standby service at elevated temperatures. The beneficial effects of high tin on positive-grid corrosion in VRLA batteries have recently been confirmed [90]. It is proposed that the improved corrosion resistance is due to the large number of fine precipitate particles and better accommodation of the stresses of corrosion by the high mechanical properties of the alloys.

2.5.4 Tin effects on conductivity of battery grids

Following the studies on pure lead [57,64], a great deal of work has been undertaken to determine the effects of tin on the corrosion layer of lead–calcium–tin alloys, which are the major alloys for VRLA batteries. One study [82] showed that the corrosion rate of lead–calcium alloys was significantly reduced by the addition of tin and the thickness of the α-PbO layer was substantially reduced. It was further found that tin enrichment at grain boundaries in cast alloys induced a high level of tin in the corrosion layer that was able to suppress passivation. Finally, it was suggested

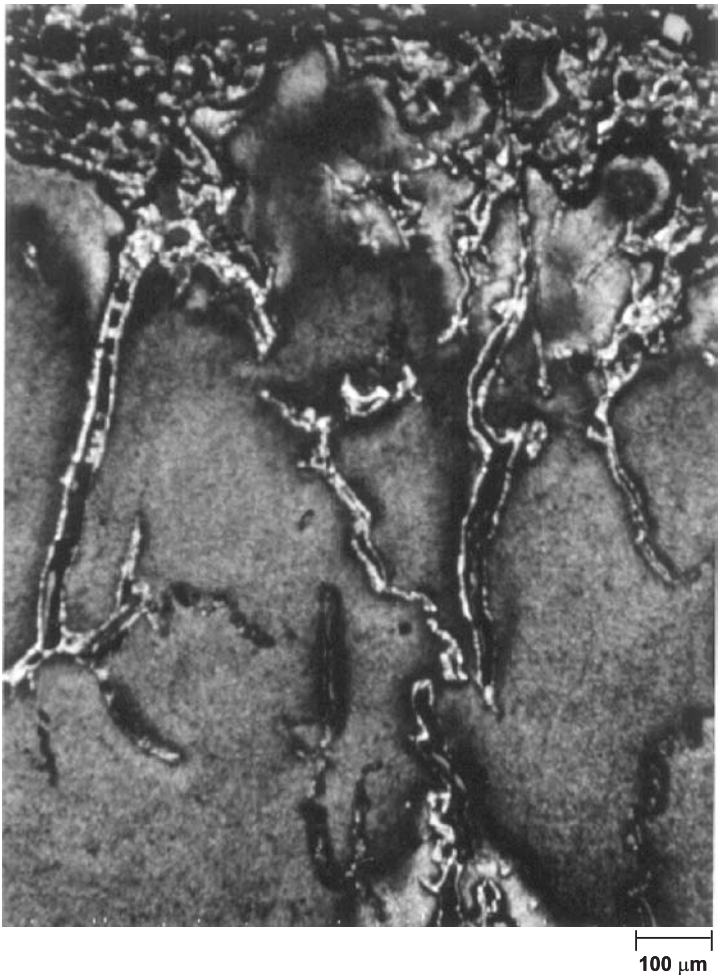

Fig. 2.6. Penetrating corrosion into grain boundary of Pb–Ca–Sn alloys, Pb–0.06 wt.% Ca–0.7 wt.% Sn alloy.

that the decrease in the passive layer thickness might be due to the acidity of Sn^{4+} which is incompatible with the stability of α-PbO.

Tin has been shown to increase greatly the conductivity of the passive corrosion layer in lead–calcium alloys. The presence of tin can exercise an important influence on the corrosion resistance of lead–calcium–tin alloys, as well as on the thickness and conductivity of the passive layer formed on the alloys [91]. Tin additions of about 1.2 wt.% or more have been shown [90,92] to increase markedly the conductivity of the corrosion layer, particularly of the α-PbO, which can develop under deep-discharge conditions. Lead–calcium alloys show significant differences from pure-lead counterparts [65]. A lead–calcium alloy with 0.6 wt.% Sn shows no enrichment of tin in the oxide layer [91], while an alloy with 1.2 wt.% Sn exhibits only moderate enrichment. It is not until the tin concentration reaches 1.5 wt.% that significant

enrichment occurs. The resistance of the interface as a function of tin content for Pb–0.08 wt.% Ca alloys is presented in Fig. 2.7. These differences may be due to the discontinuous precipitation processes which occur at low 'r' values. There is significant segregation of tin to the interdendritic boundaries as well as to the grain boundaries in both lead–calcium–tin and lead–tin alloys [93,94]. The segregation is shown in Fig. 2.8 [41].

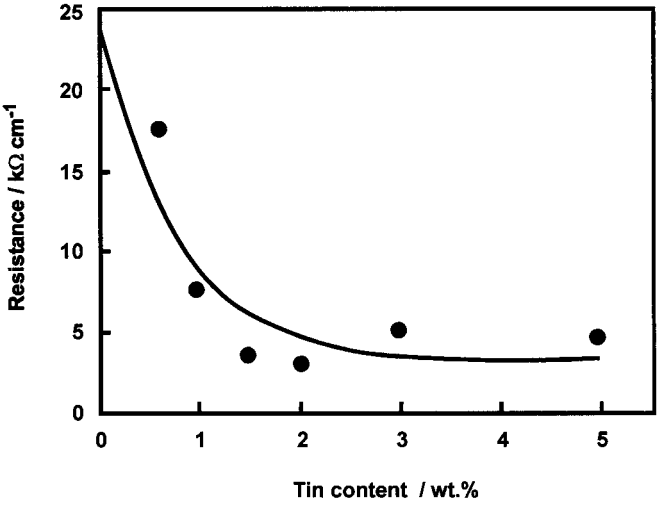

Fig. 2.7. Effect of tin on polarization resistance of Pb–0.008 wt.% Ca–*x* wt.%Sn alloys in 0.5 M H_2SO_4 after passivation at 700 mV for 24 h.

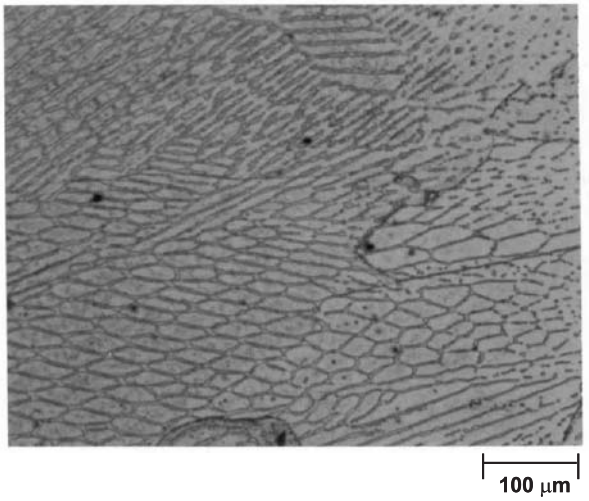

Fig. 2.8. Segregation of tin in lead–calcium–tin alloys to grain and sub-grain boundaries.

When the '*r*' value is less than 9:1, and more likely when the calcium is at high levels, significant precipitation of calcium Pb_3Ca occurs by grain-boundary movement. This movement in discontinuous precipitation destroys the tin segregation found in the lead–calcium–tin alloys with low '*r*' values and homogenizes the alloy. Significant segregation of up to 2 wt.% Sn has been observed [94] in an alloy which contained 0.6 wt.% Sn and a low calcium content, and for which the precipitation of $(PbSn)_3Ca$ or Sn_3Ca continuous particles resulted in no change in the microstructure. Much lower segregation was also found in a cast alloy with 1.2 wt.% Sn but a much higher calcium content, viz., 0.09 wt.%. Such compositions may not produce the stable Sn_3Ca precipitate within the cast structure, but may undergo discontinuous precipitation of Pb_3Ca, despite a favourable '*r*' value, due to segregation of calcium as well as tin [95]. The modified grain structure, which disperses the tin segregation, may make the tin less accessible to the corrosion product because it is not concentrated in the grain boundaries.

At tin contents of 2 wt.% and higher, three phases are present in the alloy, namely, a solid solution of 1.9 wt.% Sn, fine precipitates of $(PbSn)_3Ca \rightarrow Sn_3Ca$, and coarse crystals of pure tin primarily at grain boundaries and interdendritic boundaries [91]. The tin crystals appear to inhibit the formation of $PbSO_4$ on the surface. During oxidation, the corrosion layer is doped with sufficient tin, in the form of SnO_2, to increase the conductivity of the passive layer. Improvements in conductivity at tin contents below 1.5 wt.% could be due to the presence of SnO_2 precipitated at the grain boundaries of the PbO [96]. Alloying with tin also increases the overpotential of both the oxygen and hydrogen evolution reactions. The high segregation of tin to the grain and sub-grain boundaries can increase locally the concentration of SnO_2 in the PbO lattice. The doping can alter the electrical properties of the corrosion layer [55]. Lead–tin alloys are able to maintain the tin segregation to the grain boundaries [65,21]. The internal resistance and life of VRLA batteries under float service is a function of tin content [89], as shown in Fig. 2.9.

The phase diagram [97] presented in Fig. 2.10 shows the tin level above the '*r*' value of 9:1 that is sufficient to force the calcium within the cast matrix to react and produce continuous $(PbSn)_3Ca$ precipitates and dope the grain and interdendritic boundaries. The high tin content of the segregated boundaries enhances the localized doping of the corrosion product at the grid surface (Fig. 2.11).

Doping the active material of the battery and corrosion layer of the grid surface with a solution of tin sulfate to produce localized high conductivity greatly improves cycling ability and increases capacity [98]. The extremely high resistance to oxidation of the lead surface in the presence of high amounts of tin might be a problem when curing these grids, particularly for spiral-wound configurations [95]. The tin may reduce the PbO formed on the surface to lead, while the tin maybe oxidized to SnO_2. This would lower the pH at the grid|active-material interface and thus prevent further alkaline attack and attachment of basic lead sulfates.

Silver additions to lead–calcium–tin alloys. Silver has been added to lead–calcium–tin alloys to increase the resistance to creep and corrosion, and to prevent growth of the positive grids at elevated temperatures. Valve-regulated lead–acid batteries often operate at elevated temperatures and/or produce high internal

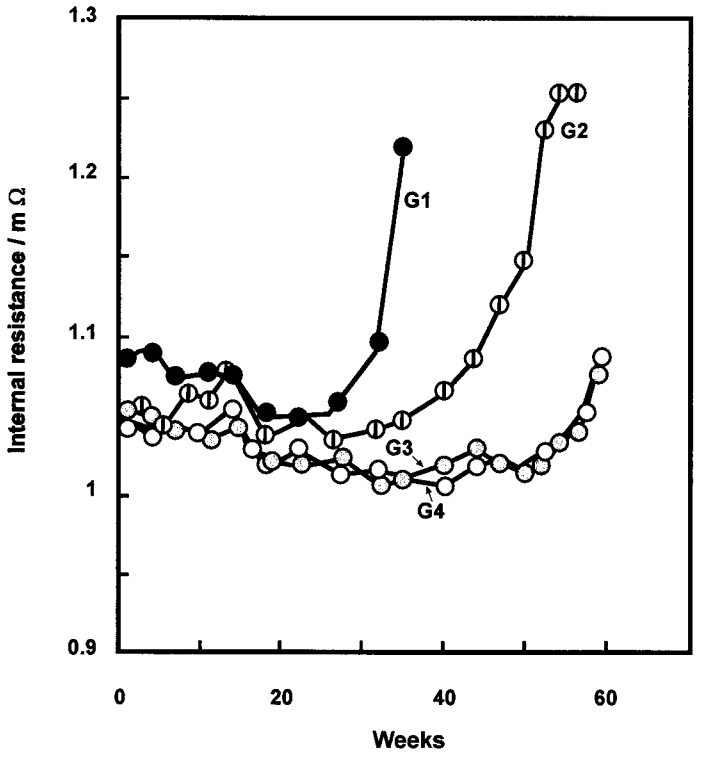

Fig. 2.9. Evolution of internal resistance of 6-V, 100-Ah, VRLA batteries under float at 2.28 V and 60°C as function of grid alloy: G1: 0.7 wt.% Ca–0.7 wt.% Sn; G2: 0.7 wt.% Ca–1.0 wt.% Sn; G3: 0.7 wt.% Ca–2.0 wt.% Sn–0.05 wt.% Ag; G4: 0.7 wt.% Ca–2.0 wt.% Sn.

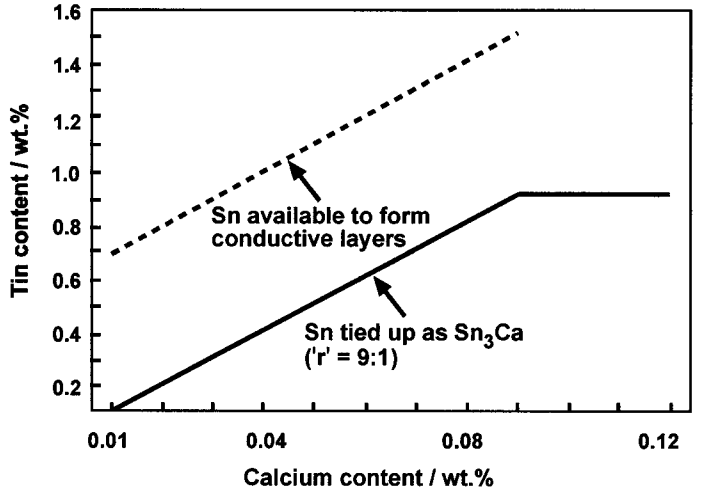

Fig. 2.10. Amount of tin required to form stable SnCa precipitates (solid line) and dope the corrosion layer (dashed line) as function of calcium content.

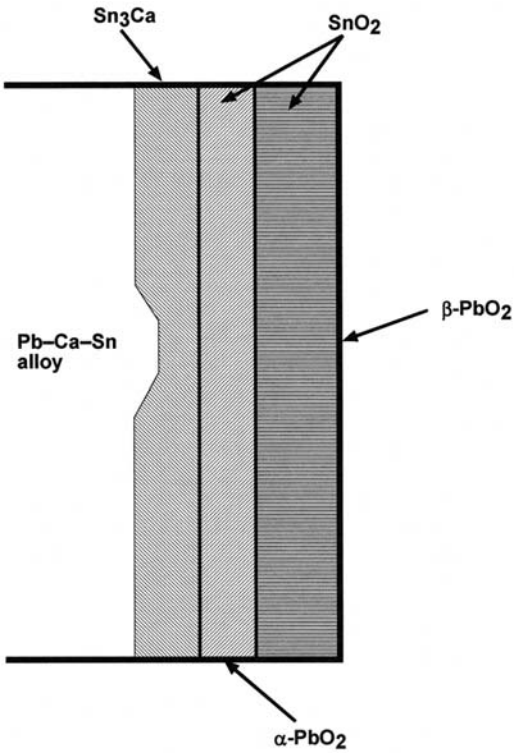

Fig. 2.11. Schematic of corrosion product on lead–calcium–tin alloy.

temperatures during recombination of oxygen at the negative plate. High temperature leads to enhanced grid corrosion and subsequent growth. Lead–calcium–tin alloys with silver contents up to 0.1 wt.% have been evaluated recently [81]. Tin-rich alloys contained large grains oriented in the direction of heat flows. Silver additions caused large segregation at grain boundaries and sub-grain boundaries. The segregated particles contained aluminium, silver, and Ag_xSn_y intermetallic particles. Tin-rich alloys with 0.05 wt.% Ag significantly increased the mechanical properties of the lead–calcium–tin alloys.

Silver has a significant effect in delaying the discontinuous precipitation reaction as well as the overageing of calcium precipitates [90]. Silver also increases the corrosion resistance of lead–calcium–tin alloys — particularly under conditions that simulate end-of-discharge (high pH) conditions — and improves the cycle-life and capacity of VRLA batteries. Silver decreases the thickness of the PbO layer but produces a harder, more compact, corrosion layer than tin. Silver does not, however, increase the conductivity of the corrosion layer.

Silver imparts little improvement to the mechanical properties of lead–calcium–tin-(silver) alloys which are fully aged (Table 2.6), but gives lower elongation in both cast and rolled alloys. There is no effect on the microstructure at 0.03 wt.% Ag [51]. Significant improvement in creep resistance has been observed in alloys which contain silver [99]. Significant increases in cycle-life and capacity have been described

Table 2.6. Comparison of mechanical properties of lead–calcium–tin–silver alloys.

Calcium (wt.%)	Tin (wt.%)	Silver (wt.%)	YS (MPa)	UTS (MPa)	YS:UTS	Elongation (%)
Continuously cast (12 mm thickness) before rolling						
0.044	0.50	—	38.2	47.7	80	31
0.042	0.73	—	41.1	50.0	82	28
0.043	1.17	—	45.6	55.0	83	31
Conventionally cast						
0.048	0.48	—	38.8	48.6	80	30
0.046	0.70	—	44.0	53.6	82	30
0.043	1.18	—	47.1	57.5	82	29
0.045	0.55	0.036	41.6	50.7	82	28
0.042	0.77	0.030	44.2	53.2	83	28
0.046	1.05	0.032	46.0	55.5	83	27
Continuously cast						
0.040	0.95	—	42.6	47.5	89	30
0.037	0.48	0.034	36.3	40.3	90	24
Concast rolled to 1.2 mm						
0.044	0.50	—	46.8	57.1	82	17
0.042	0.73	—	54.6	63.5	86	16
0.042	1.17	—	57.8	64.3	90	15
0.040	0.62	0.034	64.6	65.4	98	9

for VRLA batteries that employ lead–calcium–tin alloys which contain various amounts of silver [100,101].

Silver is reported to segregate to the grain and sub-grain boundaries of lead–calcium–tin alloys [94]. Microprobe analysis of the cross-section of grid wires produced from cast and rolled lead–calcium–tin alloys with a bulk silver content of 0.03 wt.% indicates segregation of 1.6–6 wt.% Ag to the grain and sub-grain boundaries. The variation in the silver content to the boundaries is due to different solidification conditions. This segregation to the grain boundaries, and reaction with tin, can result in the formation of low-melting, tin–silver intermetallic compounds. Special techniques [102] may be required for handling thick grids containing high silver and high tin in order to prevent cracking in grid production. The incorporation of silver up to 0.05 wt.% has been found to impose no detrimental effects on cast lead–calcium–tin alloys for stationary VRLA batteries [89].

After years of research, alloys for the positive grids of VRLA batteries for cycling or stationary service have evolved to be primarily lead–calcium alloys which utilize low calcium content (0.04–0.07 wt.%), a relatively high tin content (1.2 wt.% or higher), and a low silver content of 0.01–0.04 wt.%. These alloys show exceptional resistance to corrosion in float or cycling service, achieve high mechanical properties and resistance to creep or grid growth, produce excellent conductivity through the corrosion layer, yield good rechargeability from deep discharge, and offer low self-discharge rates.

2.6. Lead–Antimony–Cadmium Alloys

One battery company (GNB-Exide) has developed an antimony alloy suitable for use in cycling, as well as stationary, VRLA batteries [103]. Antimony and cadmium react in this alloy to form the intermetallic compound SbCd [104]. There is a pseudo binary equilibrium with a eutectic of about 10 wt.% PbSn and a maximum solubility in lead of 6 wt.% SbCd. Grid alloys containing SbCd have satisfactory properties for casting grids in the factory, but grid cracking can be a problem. The creep and corrosion properties, although less favourable than those of lead–calcium–tin alloys, are satisfactory for use in VRLA batteries. The alloys must have a higher cadmium content than is required to react with the antimony to form CdSb [104,105].

The basis for the performance of the alloy in VRLA batteries is corrosion of the lead–cadmium–antimony alloy to produce antimony in the corrosion layer of the positive grid, which thus eliminates the antimony-free effect of pure lead or lead–calcium alloys. During corrosion, small amounts of antimony and cadmium present in the lead matrix are introduced into the corrosion product and thereby dope it with antimony and cadmium oxides. The antimony and cadmium give excellent conductivity through the corrosion product. The major component of the alloy, the CdSb intermetallic alloy, is not significantly oxidized upon float service, but may become oxidized in cycling service.

Small amounts of cadmium and antimony are leached from the grid corrosion layer during cycling. These deposit on the negative during recharge. The cadmium is believed to plate over the antimony on the negative plate and raise the potential of the negative plate. Even in the presence of antimony, this process reduces gassing to levels where the alloy can be used for VRLA batteries.

References

1. D.H. McClelland, J.L. Devitt, U. S. Patent 3,862,861 (1975).
2. E.F. Wolf, C.F. Bonilla, *Trans. Electrochem. Soc.*, **79** (1941) 307.
3. J.J. Lander, *J. Electrochem. Soc.*, **98** (1951) 220.
4. J.J. Lander, *J. Electrochem. Soc.*, **103** (1956) 1–8.
5. J. Burbank, *J. Electrochem. Soc.*, **106** (1959) 369–376.
6. S. Tudor, A. Weisstuch, S.H. Davang, *Electrochem. Technol.*, **5** (1967) 21.
7. P. Ruetschi, B.D. Cahan, *J. Electrochem. Soc.*, **106** (1959) 1079–1081.
8. D. Pavlov, *Ber. Bunsenges.*, **71** (1967) 398.
9. D. Pavlov, *Electrochim. Acta*, **13** (1968) 2051–2061.
10. D. Pavlov, R. Popova, *Electrochim. Acta*, **15** (1970) 1483–1491.
11. D. Pavlov, N. Iordanov, *J. Electrochem. Soc.*, **117** (1970) 1103–1109.
12. P. Ruetschi, *J. Electrochem. Soc.*, **120** (1973) 331–336.
13. K. Fuchida, K. Okada, S. Hattori, M. Kono, M. Yamane, T. Takayama, J. Yamashita, Y. Nakayama, Yuasa Battery Co., *ILZRO Project LE–276 Antimony-free grids for deep discharge, Final Report 1 January 1978 to 31 December 1981*, International Lead Zinc Research Organization, Inc., Research Triangle Park, NC, USA, 1982.
14. I.K. Gibson, K. Peters, F. Wilson, in: J. Thompson (Ed.), *Power Sources 8. Research and Development in Non-mechanical Electrical Power Sources*, Academic Press, London, UK, 1981, pp. 565–580.
15. K.R. Bullock, M.A. Butler, *J. Electrochem. Soc.*, **133** (1986) 1085–1090.
16. K.R. Bullock, E.C. Laird, *J. Electrochem. Soc.*, **129** (1982) 1393–1398.

17. B. Culpin, A.F. Hollenkamp, D.A.J. Rand, *J. Power Sources*, **38** (1992) 63–74.
18. J. Garche, *J. Power Sources*, **30** (1990) 47–54.
19. D. Pavlov, S. Ruevski, *J. Electrochem. Soc.*, **126** (1979) 1100–1104.
20. K. Weisner, J. Garche, N. Anastasijevic, in: J. Thompson (Ed.), *Power Sources 9. Research and Development in Non-mechanical Electrical Power Sources*, Academic Press, London, UK, 1983, p. 17–37.
21. R.F. Nelson, D.M. Wisdom, *J. Power Sources*, **33** (1991) 165–185.
22. E.E. Schumacher, G.M. Bouton, *Metals & Alloys*, **14** (1941) 865.
23. H.F. Haring, U.B. Thomas, *Trans. Electrochem. Soc.*, **68** (1935) 293.
24. U.B. Thomas, A. Forster, H.E. Haring, *Trans. Electrochem. Soc.*, Preprint 92-12 (1947). The Electrochemical Society.
25. G.W. Mao, J.G. Larson, P. Rao, *Metall.*, **1** (1969) 399.
26. E. Hoehne, *Z. Metallkde.*, **30** (1938) 52.
27. J. Burbank, A.C. Simon, E. Willihnganz, in: P. Delahay (Ed.), *Advances in Electrochemistry and Electrochemical Engineering 8*, Wiley Interscience, London and New York, 1971, p. 157.
28. J. Bohmann, U. Hullmeine, E. Voss, A. Winsel, Varta Batterie AG, *ILZRO Project LE–277 Active material structure related to cycle life and capacity, Final Report 1 July 1982 to December 1982*, International Lead Zinc Research Organization, Inc., Research Triangle Park, NC, USA, 1983.
29. E.E. Schumacher, G.S. Phipps, *Trans. Electrochem. Soc.*, **68** (1935) 309.
30. A.F. Hollenkamp, *J. Power Sources*, **36** (1991) 567–585.
31. T.G. Chang, in: K.R. Bullock, D. Pavlov (Eds.), *Proc. Symp. Advances in Lead–Acid Batteries*, *Proc. Vol. 84–14*, The Electrochemical Society, Pennington, NJ, USA, 1984, pp. 86–97.
32. Z. Takehara, K. Kanamura, M. Kawanami, *J. Electrochem. Soc.*, **137** (1990) 800–804.
33. A. Kita, Y. Matsumaru, M. Shinpo, H. Nakashima, in: L.J. Pearce (Ed.), *Power Sources 11. Research and Development in Non-mechanical Electrical Power Sources*. International Power Sources Symposium Committee, Leatherhead, UK, 1986, pp. 31–44.
34. R.D. Prengaman, *Proc. 4th International Lead-Acid Battery Seminar*, 25–27 April, 1990, San Francisco, CA, USA, International Lead Zinc Research Organization, Inc., Research Triangle Park, NC, USA, 1990, pp. 19–30.
35. A. Winsel, E. Voss, U. Hullmeine, *J. Power Sources*, **30** (1990) 209–226.
36. *Summary Report and Minutes of Lead–Calcium Alloy Workshop*, *Wantage*, *UK*, *Appendix D*, ILZRO Lead–Acid Battery Task Force, International Lead Zinc Research Organization, Inc., Research Triangle Park, NC, USA, 1989.
37. *Proc. First Meeting of the PCL Study Group*, West Sussex, UK, Advanced Lead-Acid Battery Consortium, Research Triangle Park, NC, USA, 1993.
38. D.A.J. Rand, R.F. Nelson, Proc. 2nd Meeting of the PCL Study Group, Montreux, Switzerland, Advanced Lead-Acid Battery Consortium, Research Triangle Park, NC, USA, 1995.
39. M. Hansen, K. Anderko, *Constitution of Binary Alloys*, McGraw-Hill, New York, USA, 1958.
40. T.W. Caldwell, U.S. Sokolov, *J. Electrochem. Soc.*, **123** (1976) 972–977.
41. R.D. Prengaman, *Proc. 7th International Lead Conference*, *Pb–80,* Madrid, Lead Development Association, London, UK, 1980, p. 34.
42. A.M. Howard, E. Willihnganz, *J. Electrochem. Technol.*, **6** (1968) 370.
43. G.W. Mao, J.G. Larson, P. Rao, *J. Electrochem. Soc.*, **120** (1973) 11–17.
44. M. Myers, H.R. Van Handle, C.R. Di Martini, *J. Electrochem. Soc.*, **121** (1974) 1526–1530.
45. R.D. Prengaman, *Proc. Fall Meeting Electrochem. Soc.*, Las Vegas, NV, USA, 1976, Paper 9.
46. J. Perkins, G.R. Edwards, *J. Mat. Sci.*, **10** (1975) 136.
47. W. Sharfenburger, S. Henkel, *Z. Metallkde.*, **64** (1973) 478.
48. L. Bouirden, J.P. Hilger, J. Hertz, *J. Power Sources*, **33** (1991) 27–50.
49. J.L. Caillerie, J. Hertz, A. Boulahrouf, M. Dirand, J.P. Hilger, *Proc. International Lead Conference Pb–86*, Goslar, Federal Republic of Germany, Lead Development Association, London, UK, 1986, pp. 57–67.
50. H. Borchers, W. Scharfenberger, S. Henkel, *Z. Metallkde.*, **66** (1975) H2, 111.
51. R.D. Prengaman, *J. Power Sources*, **53** (1995) 207–214.
52. D. Kelly, P. Niessen, E.M.L. Valeriote, *J. Electrochem. Soc.*, **132** (1985) 2533–2538.

53. H.K. Giess, in: K.R. Bullock, D. Pavlov (Eds.), *Proc. Symp. Advances in Lead–Acid Batteries*, *Proc. Vol. 84–14*, The Electrochemical Society, Pennington, NJ, USA, 1984, pp. 241–251.
54. J.J. Lander, *J. Electrochem. Soc.*, **99** (1952) 467–473.
55. D. Pavlov, *J. Electroanal. Chem.*, **118** (1981) 167–185.
56. H. Döring, J. Garche, H. Dietz, K. Wiesener, *J. Power Sources*, **30** (1990) 41–45.
57. D. Pavlov, B. Monahov, M. Maja, N. Penazzi, *J. Electrochem. Soc.*, **136** (1989) 27–33.
58. H. Yasuda, S. Furuya, N. Hoshihara, T. Yamaguchi, K. Takahashi, T. Ishii, U.S. Patent 4,805,277 (1989).
59. S. Saito, M. Terada, T. Hayakawa, A. Miura, A. Komaki, G.B. Patent 2,209,241-A (1989).
60. K. Takahashi, H. Yasuda, N. Takami, S. Horie, Y. Suzui, *J. Power Sources*, **36** (1991) 451–460.
61. C. Morris, *Proc. 10th International Lead Conference*, Nice, France, Lead Development Association, London, UK, 1990, p. 226.
62. K.H. Christian, H. Döring, J. Garche, K. Wiesener, G.E. Schadlich, Ger. Patent DD 257,144-A1 (1988).
63. H. Döring, J. Garche, W. Fischer, K. Wiesener, *J. Power Sources*, **28** (1989) 367–380.
64. P. Simon, N. Bui, F. Dabosi, *J. Power Sources*, **50** (1994) 141–152.
65. P. Simon, N. Bui, N. Pebere, F. Dabosi, *J. Power Sources*, **53** (1995) 163–173.
66. M. Calabek, P. Baca, V. Smarda, K. Micka, *ALABC Project AMC-003A*, *Characterization of changes in resistance related to premature capacity loss in lead–acid battery plates, Final Report 1 July to 30 June 1995,* Advanced Lead-Acid Battery Consortium, Research Triangle Park, NC, USA, 1995.
67. M. Terada, S. Saito, T. Hayakawa, A. Komaki, *Prog. Batt. Solar Cells*, **8** (1989) 214–216.
68. H. Borchers, H. Assmann, *Metall.*, **69** (1978) 43.
69. Z.W. Chen, J.B. See, W.F. Gillian, D.M. Rice, *J. Power Sources*, **42** (1993) 35–45.
70. J.P. Hilger, L. Bouirden, *J. Alloys Comp.*, **236** (1996) 224–228.
71. T.W. Caldwell, U.S. Sokolov, L.M. Bocciarelli, *J. Electrochem. Soc.*, **123** (1976) 1265–1271.
72. J.P. Hilger, *Structural Transformation in Lead Alloys, Short Intensive Training Course,* COMETT, Nancy, France, 25–26 March, 1993.
73. J. Hertz, C. Fornasieri, J.P. Hilger, M. Notin, *J. Power Sources*, **46** (1993) 299–310.
74. M.V. Rose, J.A. Young, *Proc. 5th International Lead Conference*, Paris, France, Lead Development Association, London, UK, 1974, p. 37.
75. A.B. Townsend, *US-AEC Research and Development Report, Metallurgy and Ceramics, Y-1307* (1960).
76. R.J. Sims, U. S. Patent 3,920,473 (1975).
77. N.E. Bagshaw, H. McWhinnie, U.S. Patent 4,125,690 (1978).
78. R.D. Prengaman, in: K.R. Bullock, D. Pavlov (Eds.), *Proc. Symp. Advances Lead–Acid Batteries*, *Proc. Vol. 84–14*, The Electrochemical Society, Pennington, NJ, USA, 1984, pp. 201–213.
79. R.D. Prengaman, *J. Power Sources*, **67** (1997) 267–287.
80. K. Takahashi, N. Hoshihara, H. Yasuda, *J. Power Sources*, **30** (1990) 23–31.
81. Université de Nancy, CEAC-France, École Nationale Supérieure de Chimie de Toulouse, Metaleurop Recherche, *Bright|Euram Project BE-7297, Task 8 Effect of alloying elements on the mechanical properties, corrosion resistance and passivation of the positive grid, Final Report, 1 January 1994 to 31 December 1997*, Advanced Lead-Acid Battery Consortium, Research Triangle Park, NC, USA, 1998.
82. R. Miraglio, L. Albert, A. El Ghachcham, J. Steinmetz, J.P. Hilger, *J. Power Sources*, **53** (1995) 53–61.
83. E.M.L. Valeriote, J. Sklarchuk, M.S. Ho, in: K.R. Bullock, D. Pavlov (Eds.), *Proc. Symp. Advances in Lead–Acid Batteries*, *Proc. Vol. 84–14*, The Electrochemical Society, Pennington, NJ, USA, 1984, pp. 224–240.
84. D.B. Williams, E.P. Butler, *Intern. Met. Rev.*, **3** (1981) 153.
85. N.E. Bagshaw, *Proc. 3rd International Lead Conference*, Venice, Italy, Lead Development Association, London, UK, 1968.
86. E.M.L. Valeriote, A. Heim, M.S. Ho, *J. Power Sources*, **33** (1991) 187–212.
87. E.M.L. Valeriote, *J. Electrochem. Soc.*, **128** (1981) 1423–1433.
88. H.K. Giess, *J. Power Sources*, **53** (1995) 31–43.

89. H.K. Giess, C. Ohlin, *Proceedings of the 18th International Telecommunications Energy Conference*, Boston, MA, IEEE, 1996, pp. 334–343.
90. L. Albert, A. Chabrol, L. Torcheux, Ph. Steyer, J.P. Hilger, *J. Power Sources*, **67** (1997) 257–265.
91. N. Bui, P. Mattesco, P. Simon, J. Steinmetz, E. Rocca, *J. Power Sources*, **67** (1997) 61–67.
92. P. Mattesco, N. Bui, P. Simon, L. Albert, *J. Power Sources*, **64** (1997) 21–27.
93. R.D. Prengaman, *J. Power Sources*, **33** (1991) 13–20.
94. S. Fouache, A. Chabrol, G. Fossati, M. Bassini, M.J. Sainz, L. Atkins, *J. Power Sources*, **78** (1999) 12–22.
95. R.D. Prengaman, *J. Power Sources*, **95** (2001) 224–233.
96. A. El Ghachcham, Ph. Steyer, J. Steinmetz, P. Delcroix, G. Le Caër, *J. Power Sources*, **64** (1997) 35–37.
97. R.D. Prengaman, *Proc. 14th Annual Battery Conference*, Long Beach, CA, USA, IEEE, 99 TH 8371, 1999, pp. 171–176.
98. M. Shiomi, Y. Okada, T. Shiroya, European Patent Application EP 0849816 A1 (1998).
99. N.E. Bagshaw, *J. Power Sources*, **53** (1995) 25–30.
100. P. Rao, U.S. Patent 5,298,350 (1994).
101. P. Rao, T.F. Uhlemann, U.S. Patent 5,691,087 (1997).
102. S.R. Larsen, U.S. Patent 5,948,566 (1999).
103. G.W. Mao, P. Rao, J.F. Trenter, U.S. Patent 4,166,155 (1979).
104. W.C.M. Couch, U.K. Patent 613,308 (1948).
105. N.E. Bagshaw, in: T. Keily, B.W. Baxter (Eds.), *Power Sources 12, Research and Development in Non-mechanical Electrical Power Sources*, International Power Sources Symposium Committee, Leatherhead, UK, 1988, pp. 113–129.

This page intentionally left blank

Valve-Regulated Lead–Acid Batteries
D.A.J. Rand et al., editors

—CHAPTER 3—

FORMATION OF LEAD–ACID BATTERIES AND STRUCTURE OF POSITIVE AND NEGATIVE ACTIVE MASSES

D. Pavlov

3.1. Introduction

3.1.1. Manufacture of lead–acid battery plates

The classical scheme for the manufacture of flat pasted plates for automotive, traction and stationary lead–acid batteries is shown in Fig. 3.1. There is no difference between the technology of plate manufacture for conventional (flooded) and valve-regulated (VRLA) lead–acid batteries. The two versions do differ, however, in the method of separation of the plates, the quantity and type (liquid or gel) of electrolyte, and in the design of the battery itself.

The basic steps in the process of plate manufacture are as follows.

Grid manufacture. The grids for positive and negative plates are produced either through casting, or through rolling and expansion techniques. Lead–antimony or lead–tin–calcium alloys are used. Grids for VRLA batteries are produced from the latter type of alloy. Grid alloys and grid manufacture are discussed in detail in Chapter 2 [1].

Production of leady oxide. Pure lead ingots are subjected simultaneously to abrasion and surface oxidation in a ball mill, or are melted in a Barton pot and oxidized in an air atmosphere [2]. A 70–85% oxidized lead powder (called 'leady oxide') is obtained with a characteristic grain size-distribution. The same leady oxide is used for the production of both positive and negative plates.

Paste preparation. The leady oxide is placed in a reactor (mixer). Fine polymer fibres, cut into small pieces (3 mm), are added to the paste to reduce the processing waste during paste preparation. Measured amounts of water and H_2SO_4 solution are also added under continuous stirring. Basic lead sulfates are formed during this step. After mixing for 10–20 min, during which the crystals of the basic lead sulfates grow, the paste is ready for the preparation of positive plates. The negative paste is prepared in a similar way, except that lignosulfonate (expander), $BaSO_4$, carbon, and inhibitors are added. The paste must have a precise density and consistency.

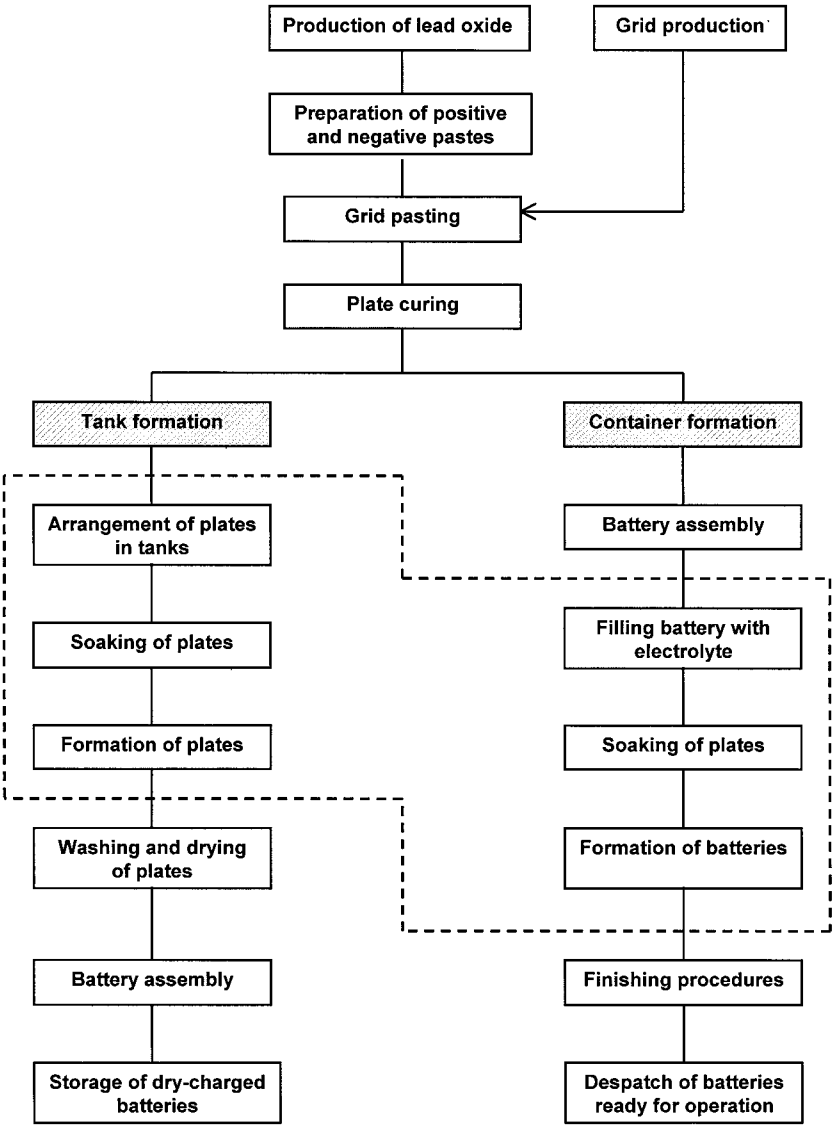

Fig. 3.1. General scheme of technological procedures involved in manufacture of lead–acid battery plates.

Depending on the temperature of paste preparation, two types of basic lead sulfates are formed, namely: $3PbO{\cdot}PbSO_4{\cdot}H_2O$ (termed: 3BS) or $4PbO{\cdot}PbSO_4$ (termed: 4BS). If the temperature of paste preparation is kept below 65°C, 3BS is formed. The particles are between 1 and 4 μm in length, and 0.5 and 0.8 μm in diameter. If the temperature of paste preparation exceeds 75°C and there are no surface-active substances (e.g., expanders), 4BS crystals are formed. These particles are larger than those of 3BS, viz., 15–50 μm in length and 3–15 μm in width, as determined by the

conditions of paste preparation. The size of the above crystals and the amount of liquid in the paste determine the porosity of the paste, which, in turn, is responsible for the porosity of the active masses obtained.

Grid pasting. Paste of the required density and consistency is spread on to the grids by means of a specially designed machine. When expanded grids are used, the paste is applied to the expanded strip and then both sides of the pasted strip are covered with paper, after which the individual plates are separated. The pasted plates are partially dried in a tunnel oven and are then stacked on pallets.

Plate curing. During this procedure, the individual 3BS (or 4BS) and PbO particles interconnect to form a continuous skeleton, which is attached to the grid (current-collector). The lead in the paste is oxidized to PbO, the grid undergoes partial corrosion, and the 3BS (or 4BS) and PbO particles partially recrystallize. The paste is then dried. During this step, the hydroxides contained in the solution that fills the pores crystallize mostly at the sites of contact between the crystals, which thus interconnect to form a continuous 'skeleton' structure. In order to obtain a connection of good mechanical strength between the grid and the positive active-mass (PAM), a corrosion layer with a thickness above a certain critical value should be formed during plate curing. The process is conducted in special chambers with controlled temperature, humidity, and duration of both the curing and drying stages. For both types of pastes (3BS and 4BS), high-temperature curing (at 60°C for 3BS pastes; at >80°C for 4BS pastes) facilitates the formation of a corrosion layer of the appropriate thickness. Crystals of 4BS can also be obtained during the curing process by treating 3BS plates with steam at a temperature above 90°C for 2–4 h. If the duration of vapour treatment exceeds this period, it may lead to the formation of large 4BS crystals, which are difficult to convert ('form') into the desired active materials.

Positive and negative active-mass formation. The cured pastes of both positive and negative plates comprise identical mixtures of bivalent lead compounds (3BS, 4BS, PbO), which cannot create electromotive forces when the pasted plates are assembled into cells. The purpose of the formation step is to convert the cured pastes into electrochemically active porous materials — PbO_2 in the positive plates and Pb in the negative plates — which are connected mechanically and electrically to the grids. The process of formation can be conducted via two basic schemes, as shown in Fig. 3.1.

(i) *Tank formation*. Cured positive and negative plates (usually 50–200 pieces) are arranged, individually or in couples, in large electrolytic tanks containing H_2SO_4 of 1.08–1.10 rel. dens. Plates of similar polarity are connected to each other. The plates are left in the tanks for a definite period of time ('soaking step'). Then, the multi-plate cell is switched to an electrical source which supplies the formation current according to a precise algorithm. The amount of electrolyte is calculated on the basis of 2–3 $l\,kg^{-1}$ of dry paste. The formation temperature is controlled within the range of 25–55°C. For conventional

technology, the formation current varies between 0.7 and 2.5 mA cm^{-2} during the stages of the formation process. Formation usually lasts from 18 to 40 h for automotive battery plates, and from 48 to 73 h for traction battery plates. The quantity of electricity that is passed through the plates is about 1.7 to 2.5 times their theoretical capacity. When accelerated formation methods are applied for automotive battery plates, the formation time can be reduced to 8–12 h. After formation, the plates are removed from the tanks, washed with water to remove H_2SO_4 solution from their pores, and dried under appropriate conditions. Negative plates are dried either in an oxygen-free atmosphere or under vacuum. Positive and negative plates are assembled, with separators between them, into dry-charged batteries.

(ii) *Container formation*. Cured positive and negative plates, together with the separators, are assembled into 'plate groups', which are then placed in battery containers. For VRLA batteries with absorptive glass mat (AGM) separators, the plate group should be compressed to a definite pressure and then fastened with polymer tapes before insertion into the battery container (for both traction and stationary cells). If the cells are small and the container is designed to maintain the required compression, the plate groups are placed in the container without fastening. The next step is to fill the container with electrolyte. This is a rather delicate procedure with VRLA batteries that use AGM or gelled electrolyte. After a definite period of soaking, the battery is connected to the current source and formation commences. Depending on the concentration of the acid used, two formation methods are applied: (i) 'double-shot formation', in which the battery is filled with H_2SO_4 of 1.08–1.15 rel. dens.; after formation the electrolyte is replaced with H_2SO_4 of 1.30–1.32 rel. dens., which decreases to 1.28 rel. dens. as a result of dilution by the residual acid in the plates; (ii) 'single-shot formation', in which the battery is filled with H_2SO_4 of 1.24 to 1.25 rel. dens.; during formation the H_2SO_4 concentration increases to 1.28 rel. dens., and after some finishing procedures the batteries are ready for use.

In this Chapter, the discussion is confined to the processes that occur during soaking and formation of the positive and negative plates, as well as to the structures of the two types of active mass obtained as a result of the formation procedure. These steps are identified in the dashed-line frame in Fig. 3.1.

3.1.2. Survey of soaking and formation phenomena

Chemically prepared positive (PbO_2) and negative (Pb) active-masses show somewhat poorer capacity than electrochemically prepared materials in the early discharges of cycling batteries. In the case of positive plates, the electrochemical formation process is associated with the formation of PbO_2 of high surface-area and of a special structure. The positive and negative active materials must have an appropriate structure in order to provide good capacity. This structure is obtained by a complex combination of chemical and electrochemical reactions and crystallization processes that proceed during plate formation.

Generally, formation is carried out under constant-current conditions. The changes in temperature, electrolyte concentration, and cell voltage during plate soaking and formation are presented in Fig. 3.2 [2]. Chemical reactions commence between PbO, basic lead sulfates, and H_2SO_4 when the plates come into contact with the solution.

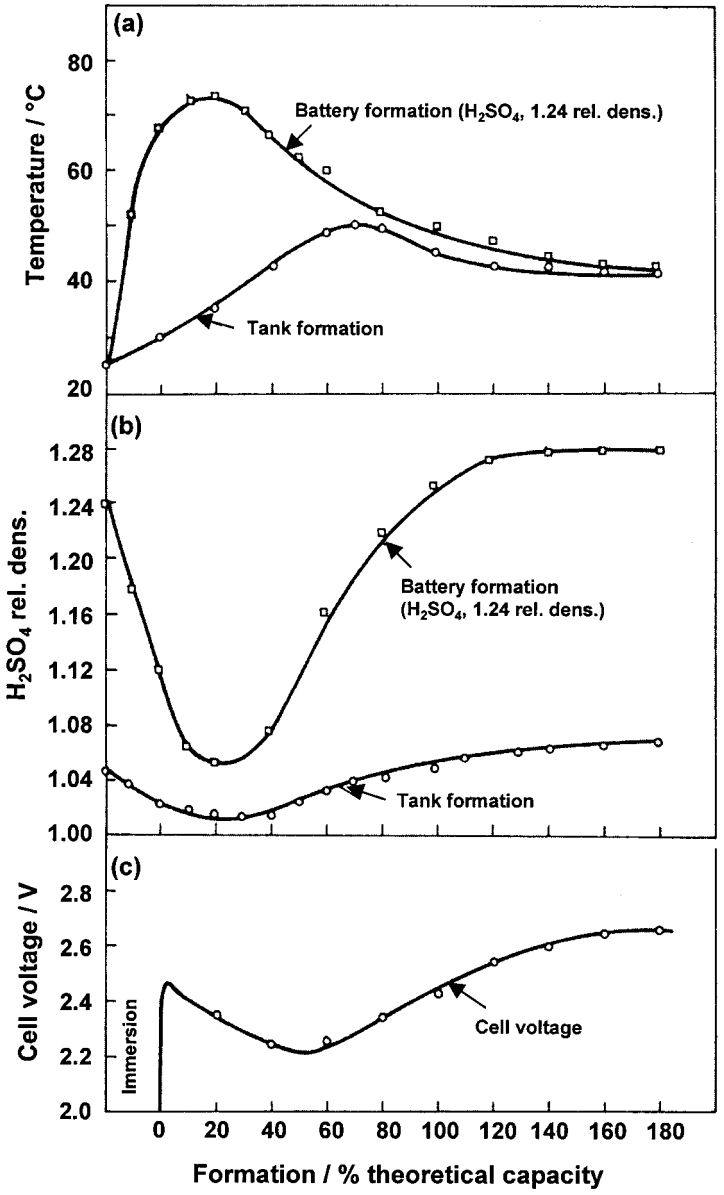

Fig. 3.2. Changes in temperature, electrolyte concentration, and cell voltage during soaking and formation of battery plates [2].

Since the reactions during the soaking procedure are exothermic, the temperature in the tank or battery starts to rise. The electrochemical reactions involved in the formation process also contribute to the overall thermal balance (in the battery or in the tank). These reactions are endothermic and can be represented by the following equations:

$$2PbO = Pb + PbO_2 \qquad \Delta H_f = +160\,kJ \qquad (3.1)$$

$$2PbSO_4 + 2H_2O = Pb + PbO_2 + 2H_2SO_4 \qquad \Delta H_f = +363\,kJ \qquad (3.2)$$

$$H_2O = H_2 + \tfrac{1}{2}O_2 \qquad \Delta H_f = +286\,kJ \qquad (3.3)$$

In addition, when electric current flows through the electrolyte, Joule heat is released. Heat exchange occurs between the formation tank (or battery) and the surrounding atmosphere. The reactions during the different formation stages all provide individual contributions to the overall thermal balance of the system. Consequently, the temperature curves feature a maximum, and with attenuation of the exothermic chemical reactions of sulfation, the temperature of the tank (battery) decreases slowly. Battery manufacturing practice has shown that the optimum temperature range for the formation process is between 25 and 55°C.

The data in Fig. 3.2 show that, initially, the H_2SO_4 concentration decreases, not only during the soaking period but also during the early stages of formation. A decrease in the formation tank (battery) voltage is also observed during the initial period of formation, Fig. 3.2(c).

Later in the formation process, the electrochemical reactions cause H_2SO_4 to be extracted from the plates and, consequently, the acid concentration increases. At the end of the formation process, the acid concentration is higher than that at the beginning of formation. This increase is due to the extraction from the plates of the acid used in the production of basic lead sulfates during paste preparation and in sulfation of the paste during plate soaking.

3.2. Soaking of Plates

3.2.1. Filling VRLA cells with H_2SO_4 solution

When VRLA batteries are container-formed, filling of the cells with H_2SO_4 solution is a delicate process, especially when using gelled electrolyte. Since the plate group is under compression, the efficacy of the filling process depends on the following parameters.

(i) *Pore system in AGM and plates*. Both the plates and the AGM separators have a porous structure. The transport of the H_2SO_4 solution through the pores is strongly impeded, however, and depends on the total pore volume and the pore-size distribution as well as on the hydrophilicity of the pore walls, in both the AGM and the plates.

(ii) *Plate-group design and dimensions*. Sulfation proceeds by reactions between the H_2SO_4 and the PbO and the basic lead sulfates in the plates, as a result of which water is formed and H_2SO_4 concentration gradients are created in the different parts of the plate group and hence the degree of sulfation of the various parts of the plates will also be different. The H_2SO_4 in the electrolyte may become so diluted when penetrating into the interior of the plate group that only a weak H_2SO_4 solution or even pure water remains. In the latter case, the paste particles are hydrated. This process depends on the plate-group design and on the method of filling the cells with H_2SO_4 solution. A very important design parameter is the ratio between the plate height (h_p) and the separator thickness (d_{AGM}) [3]. For $h_p{:}d_{AGM} < 50$, filling the plate group with electrolyte is easy. If this ratio is between 50 and 100, there are some difficulties with filling, and the process is strongly impeded at ratios between 100 and 200. At ratios greater than 200, the access of H_2SO_4 solution to some parts of the plate group may be blocked and hence 'dry zones' may be formed.

(iii) *Phase composition of cured paste*. The processes of sulfation of basic lead sulfates and of the PbO in the paste are exothermic. The heat released from these reactions causes the temperature of the plate group as a whole to rise. As the acid concentration is not the same in all parts of the plate group, the temperature in the different zones will also be different. In some zones, it may rise so much that water vapour may form. In this case, oxides from the cured pastes may be blown out into the separators. Through heat exchange between the different zones in the plate group, and between the plate group and the surrounding medium, the temperature will be equalized after a certain period of time (0.5–1.0 h). In order to reduce the rates of the above reactions of sulfation, the H_2SO_4 solution is most often cooled to temperatures below 0°C before being poured into the cells.

The most widely used filling techniques include the following.

- Gravity filling of the cells with H_2SO_4 electrolyte. This is the slowest method and results in the most uneven H_2SO_4 distribution throughout the plate group. This method is applied in filling cells with $h_p{:}d_{AGM} < 50$.
- 60% of the H_2SO_4 solution is gravity filled into the cells and then they are vacuum treated. The remaining electrolyte is then added.
- The cells are vacuum treated. 35% of the electrolyte volume is filled and the cells are vacuum treated again. Another 35% of the electrolyte is added. The cells are vacuum treated and the remaining 30% of the electrolyte volume is filled. Most often, however, this procedure is reduced to two vacuum treatments only. The method is applied mainly to gel designs of VRLA battery. There are two types of vacuum treatment: (i) 'soft vacuum', in which a pressure slightly lower than atmospheric pressure is maintained in the cells; (ii) 'hard vacuum', in which the cell pressure is < 15 mm Hg column. The hard vacuum treatment ensures faster filling of the plate group with electrolyte.

The basic criteria for selecting an appropriate method of electrolyte filling are: (i) small H_2SO_4 concentration gradients between the different parts of the

plate group; (ii) an almost equal temperature throughout the whole volume of the plate group.

After the reactions of paste sulfation start, plates that have been partially carbonated during the paste preparation, and especially during the plate-curing process, release CO_2.

The VRLA cells are filled with H_2SO_4 electrolyte until a layer of electrolyte is formed over the plate groups. On completion of the formation process, the excess H_2SO_4 solution is removed from the cells. A mirror-like electrolyte surface, interrupted only by the tops of the separators, forms in the plate group. This corresponds to 100% saturation of the AGM separator with electrolyte. At the beginning of cycling, the oxygen cycle operates with low efficiency. This leads to water loss and when the electrolyte saturation drops below 96%, the efficiency of the oxygen cycle increases and the water loss decreases. When a considerable part of the water in the electrolyte decomposes, water should be added to restore that which is lost.

3.2.2. Chemical zonal processes during soaking

Zonal processes are due to the reactions that proceed between the ions of the solution and the solid porous mass as a result of which a new solid porous phase is formed [4]. The latter occupies a certain zone in the volume of the solid porous mass, see Fig. 3.3.

The reaction between the ions of the solution and the initial solid porous phases proceeds in a reaction layer, which is located between the zone of the initial phases and the zone occupied by the reaction products. The reaction layer shifts in space and penetrates the volume of the initial phase zone. Thus, the volume of the zone occupied by the reaction products grows at the expense of the initial phase zone. The direction in which the reaction product zone grows depends on the transport hindrances experienced by the ions on their way from the solution volume to the reaction layer and/or on the transport difficulties met by the ions formed in the reaction layer on their way to the solution volume. On soaking and formation of the positive and negative plates, some zonal processes occur. During soaking, only chemical reactions proceed in the reaction layer (i.e., chemical zonal processes).

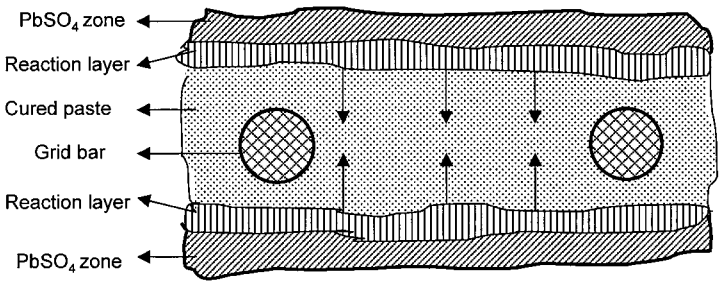

Fig. 3.3. Schematic of zones through cross-section of cured plate after soaking.

During plate formation, electrochemical reactions proceed in the reaction layer (i.e., electrochemical zonal processes).

The following chemical processes take place during soaking of the plates. These result in sulfation of the basic lead sulfates and of PbO, as follows.

$$4PbO + SO_4^{2-} + 2H^+ = 3PbO \cdot PbSO_4 \cdot H_2O \qquad pH = 14.6 + 0.5 \ln a_{SO_4^{2-}} \tag{3.4}$$

$$3PbO \cdot PbSO_4 \cdot H_2O + SO_4^{2-} + 2H^+ = 2(PbO \cdot PbSO_4) + 2H_2O \qquad pH = 9.6 + 0.5 \ln a_{SO_4^{2-}} \tag{3.5}$$

$$PbO \cdot PbSO_4 + SO_4^{2-} + 2H^+ = 2PbSO_4 + H_2O \qquad pH = 8.4 + 0.5 \ln a_{SO_4^{2-}} \tag{3.6}$$

$$4PbO \cdot PbSO_4 + 4SO_4^{2-} + 8H^+ = 5PbSO_4 + 4H_2O \qquad pH = 13.2^* + 0.5 \ln a_{SO_4^{2-}} \tag{3.7}$$

(*No experimentally determined value for the equilibrium coefficient for reaction (3.7) has been found in the literature. The value 13.2 has been obtained by approximate calculations based on similar reactions.)

The above reactions start at the two surfaces of the plates and form two zones rich in $PbSO_4$, which grow towards the core of the plate (Fig. 3.3). Cured pastes are yellow in colour (basic lead sulfates and PbO are hydrated), while sulfated zones are grey. This difference in colouring allows easy determination of the growth rate of the sulfate zones towards the interior of the plate. The rate of movement of the reaction layer (V_{sul}) into the bulk of the cured paste depends on the following parameters:

$$V_{sul} = f(C_{H_2SO_4}, T, C_{paste}, d, l, H_2SO_4\text{: PbO}) \tag{3.8}$$

where T is the temperature; C_{paste} is the phase composition of the paste; d is the density of the cured paste; l is the thickness of the plate; H_2SO_4:PbO is the acid-to-oxide ratio; PbO is the amount of free and bonded PbO.

When soaking is conducted in H_2SO_4 of 1.06 rel. dens., there still remains unreacted paste even after 20 h of soaking. When the plate group of an automotive cell is soaked in H_2SO_4 of 1.20 rel. dens., 30–40 min is sufficient for the whole cured paste of a plate of 2.8 mm in thickness to turn grey in colour, but it is not completely sulfated [5].

In H_2SO_4 solution of low rel. dens., the zonal processes should be carefully controlled as they create an inhomogeneity in the phase composition of the paste throughout the plate cross-section, which leads to inhomogeneity of the PAM structure.

On the microstructural level, sulfation of the cured paste depends on crystal size. Thus, both 3BS crystals (which are generally small) and the small PbO particles

undergo sulfation relatively quickly, whereas the cores of 4BS crystals, of the large PbO particles and of the unoxidized Pb particles remain non-sulfated even after 24 h of soaking. The processes that take place on soaking of 3BS and 4BS cured pastes will be discussed separately.

3.2.3. Soaking of 3BS-cured pastes

A study has been made of the chemical processes that take place on soaking 3BS-cured pastes in three H_2SO_4 solutions of different relative densities [6]. In these investigations, 1.425 g of cured paste (both positive and negative) reacts with 1 cm^3 of electrolyte. The changes in chemical and phase composition of 3BS pastes when soaked in H_2SO_4 solutions of 1.05, 1.15, and 1.25 rel. dens. have been studied. The resulting changes in electrolyte relative density are shown in Fig. 3.4. The highest rate of sulfation is observed during the first hour of soaking.

The changes in PbO and $PbSO_4$ content in the paste (determined by wet analysis) during soaking of the positive plates are presented in Fig. 3.5. Similar changes in chemical composition have also been observed with the negative plates. After 8 h, the amount of $PbSO_4$ in the positive paste increases by 22, 47, and 60% for acid solutions of 1.05, 1.15, and 1.25 rel. dens., respectively.

The data in Figs. 3.4 and 3.5 indicate that despite the presence of PbO and H_2SO_4 the reaction between them proceeds at a very low rate. Our recent investigations have provided an explanation for this phenomenon. It has been found that in the plate

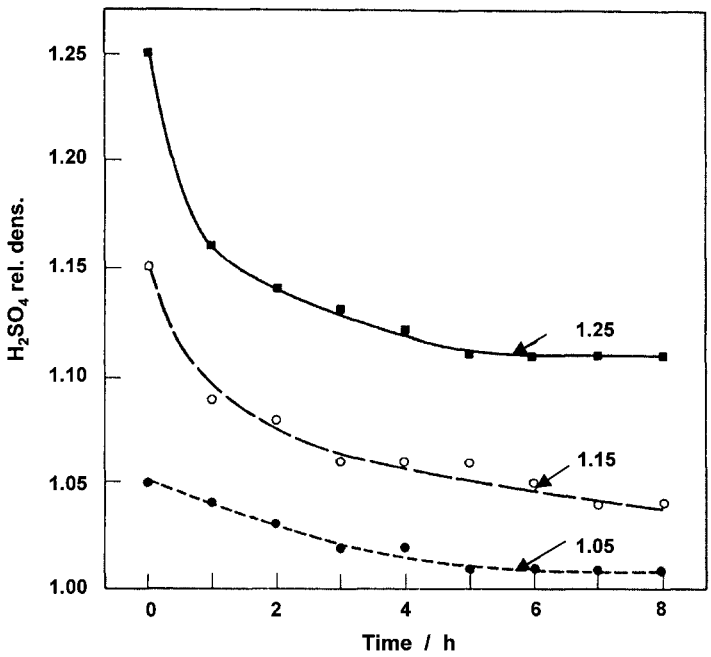

Fig. 3.4. Changes in electrolyte concentration of cells during soaking in 1.05, 1.15, or 1.25 rel. dens. H_2SO_4 [6].

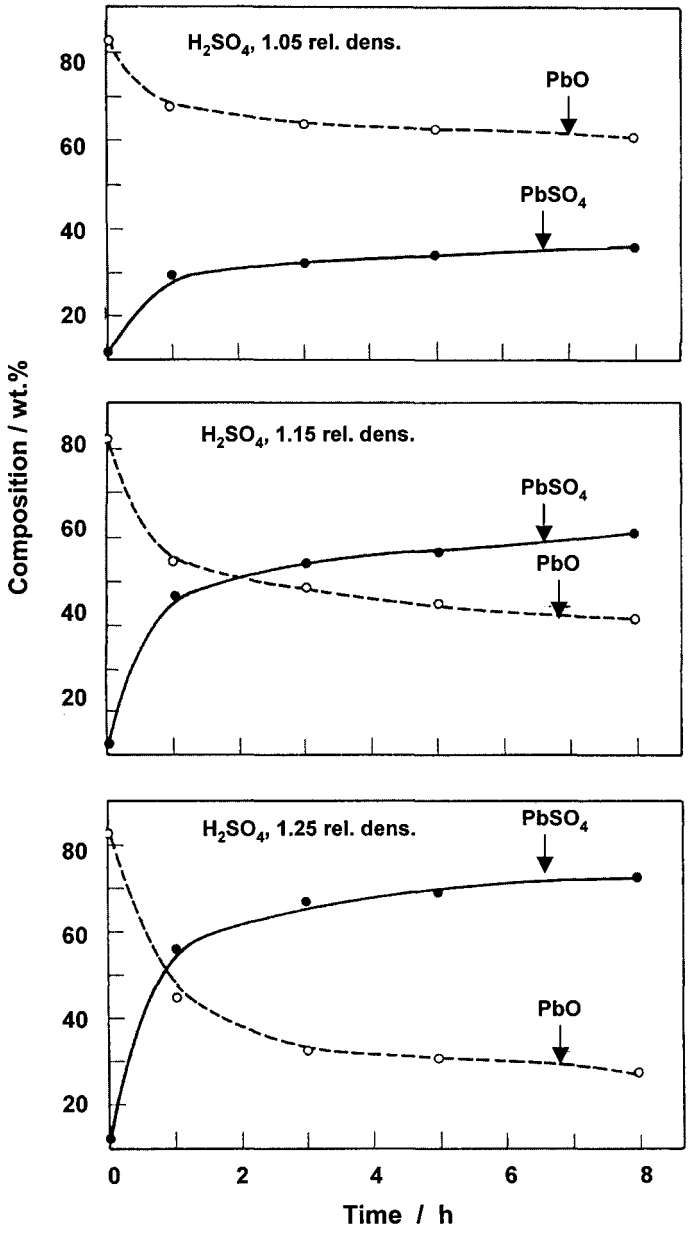

Fig. 3.5. Changes in chemical composition of cured positive plates during soaking in 1.05, 1.15, or 1.25 rel. dens. H_2SO_4 [6].

interior, between the two $PbSO_4$ zones (Fig. 3.3), the H_2SO_4 concentration is very low and water reacts with 3BS (or 4BS) and PbO as a result of which hydroxides and hydroxy-sulfates are formed. These products are greater in volume than the initial compounds and, hence, the small pores are filled and the radii of the larger pores are

reduced. When H_2SO_4 flows through the pores of the $PbSO_4$ layers, it penetrates only the remaining free large pores in the hydrated inner zone and reacts with the pore surface to form a $PbSO_4$ layer that has membrane properties. This layer blocks the access of H_2SO_4 to the hydroxides in the inner plate zone and, consequently, the reaction of sulfation is slowed down substantially. Thus, during soaking of the plate, two $PbSO_4$ layers are formed on the two plate surfaces, whereas in the hydrated plate interior, $PbSO_4$ is formed only on the surface of the large pores. The relative amounts of $PbSO_4$ in the former two layers and in the hydrated inner zone are determined by the concentration of H_2SO_4 during soaking of the plate.

The cured paste contains α-PbO (tetragonal), β-PbO (orthorhombic), and 3BS. During soaking, $PbO{\cdot}PbSO_4$ (1BS) and $PbSO_4$ are formed. The changes in intensity of the characteristic X-ray diffraction (XRD) lines for these phases on soaking are shown in Fig. 3.6. During the first 15 min, the contents of α-PbO and 3BS decrease rapidly, while β-PbO undergoes sulfation more slowly.

On soaking in H_2SO_4 of 1.05 rel. dens., the principal crystal products of sulfation are 1BS and 3BS, with small amounts of $PbSO_4$ formed after 4 h of soaking. The 1BS phase is formed at the beginning of soaking, and the 3BS 1–2 h later. The higher the H_2SO_4 concentration, the greater the amount of $PbSO_4$ formed in the paste.

Changes in both the structure and the crystal morphology of the cured pastes during the 8-h period of soaking have been monitored by means of scanning electron microscopy. Electron micrographs of paste crystals, and of the structure of the paste after 3 h of soaking in H_2SO_4 of 1.15 rel. dens., are presented in Fig. 3.7. The paste structure at the surface of the plate is shown in Fig. 3.7(a,b). During soaking in H_2SO_4, the surface layers of the plate feature $PbSO_4$ crystals. These crystals are much smaller in the interior of the plate.

The hydrated basic lead sulfates and lead oxide crystals, formed in the plate interior on soaking, are presented in Fig. 3.7(c,d), and the structure of the $PbSO_4$ layers in the large pores of the hydrated zone are shown in Fig. 3.7(e,f). At the end of soaking, well-shaped prismatic $PbSO_4$ crystals are also observed in the plate surface layers. These $PbSO_4$ crystals have resulted from recrystallization processes following the Gibbs–Thompson equation [7].

The above electron micrographs of soaked pastes indicate that $PbSO_4$ crystals retain no memory of the initial 3BS crystals, which has also been reported by other researchers [8,9]. On the other hand, the micrographs in Fig. 3.6 show that considerable quantities of 3BS crystals remain unsulfated even after 5 h of soaking in H_2SO_4 of 1.25 rel. dens., i.e., there is a trace of memory of the initial paste composition. The remaining 3BS crystals are involved in the processes of formation and exert an influence on the organization of the PAM structure, and hence on the performance of the battery.

The influence of soaking on the performance of automotive batteries has also been investigated [6]. The capacities of batteries manufactured with plates that have been soaked in H_2SO_4 solutions of three concentrations (1.05, 1.15, and 1.25 rel. dens.) for 0, 2, 5, and 8 h are given in Fig. 3.8. The utilization of the PAM is 50%. The capacity measurements are performed at the 20-h rate of discharge (C_{20}) and 25°C. The time of discharge at −18°C with a discharge current of 5 C_{20} amperes (cold-cranking test, CCA) is shown in Fig. 3.8(b).

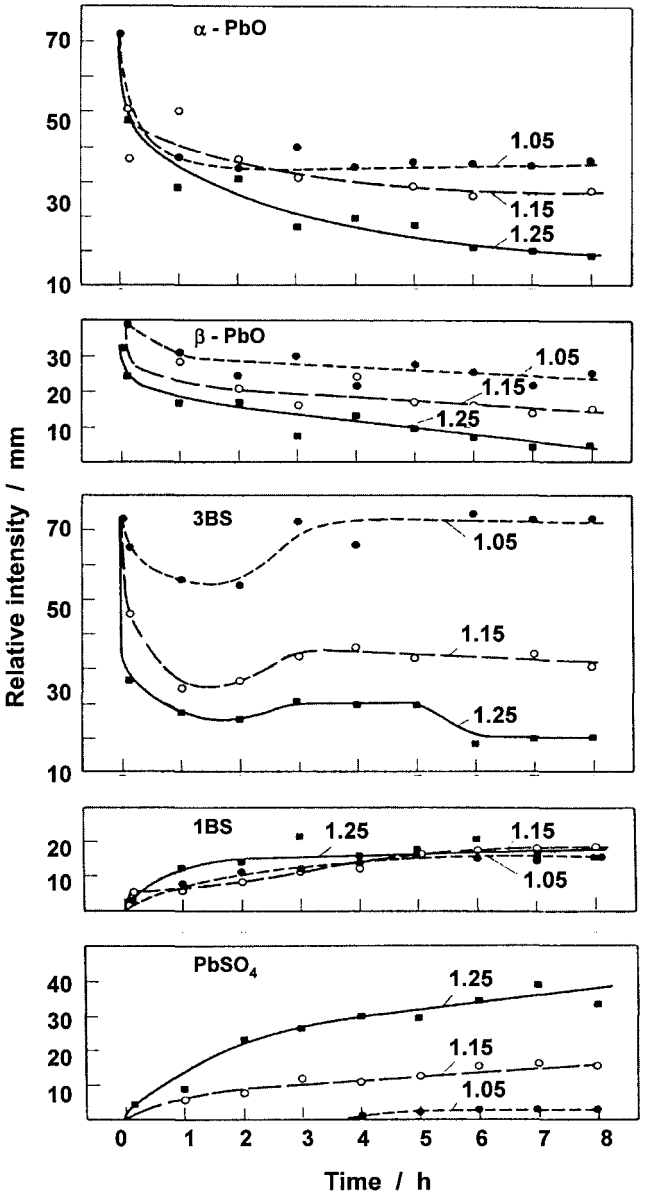

Fig. 3.6. Changes in relative intensity of characteristic XRD lines (peak heights measured in mm from diffraction record) for different phases in pastes during soaking in 1.05, 1.15, or 1.25 rel. dens. H_2SO_4. $PbSO_4$, 1BS, and some 3BS are formed during soaking [6].

The cycle-lives of the above batteries under the DIN 43539/2-test protocol for automotive batteries are presented in Fig. 3.9. The end-of-discharge voltage at the tenth charge–discharge cycle (i.e., after one week of cycling) is given in Fig. 3.9(a), and the voltage after 30 s of the CCA test in Fig. 3.9(b). The batteries were soaked

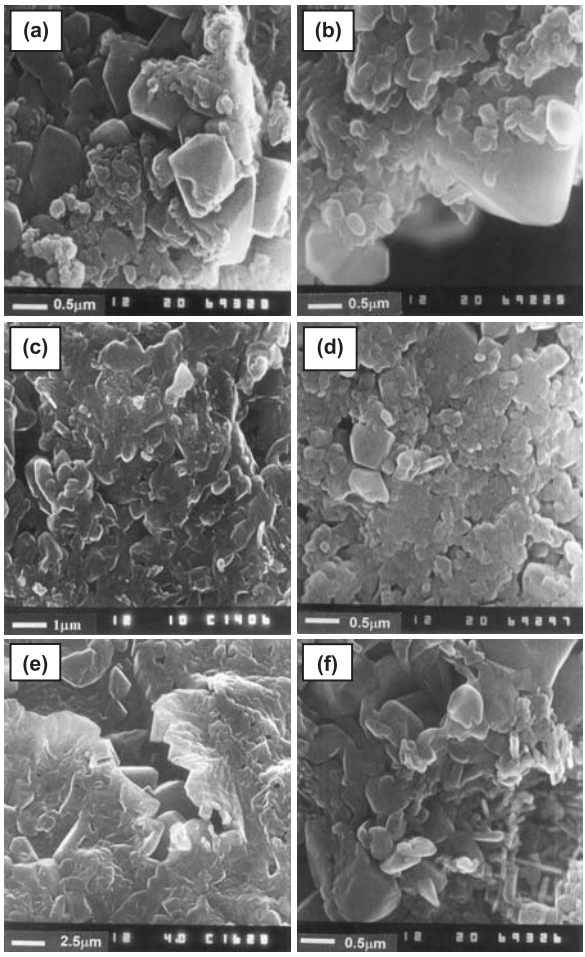

Fig. 3.7. Structure of soaked paste and crystal morphology in: (a), (b) sulfated surface layers of paste; (c), (d) hydrated inner plate zone; (e), (f) sulfated surfaces of pores in hydrated inner zone.

for 2 h and then formed in H_2SO_4 of 1.05, 1.15, or 1.25 rel. dens. The results indicate that the optimum conditions of soaking are: H_2SO_4 of rel. dens. 1.15 and a soaking time of 2 h. Under these conditions, the initial capacity of the battery is high, the CCA performance is acceptable, and the battery cycle-life is sufficiently long.

It has been established that the processes of soaking are affected by the density of the 3BS paste. Thus, at a paste density of $3.89\,g\,cm^{-3}$, the amount of H_2SO_4 that reacts during the soaking step is greater than that for pastes with density $4.39\,g\,cm^{-3}$ [5].

It can be concluded that the soaking procedure changes significantly both the phase composition and the structure of the cured 3BS paste. These changes depend strongly on the concentration of the H_2SO_4 solution and on the duration and temperature of soaking. Accordingly, the structure of the active mass during

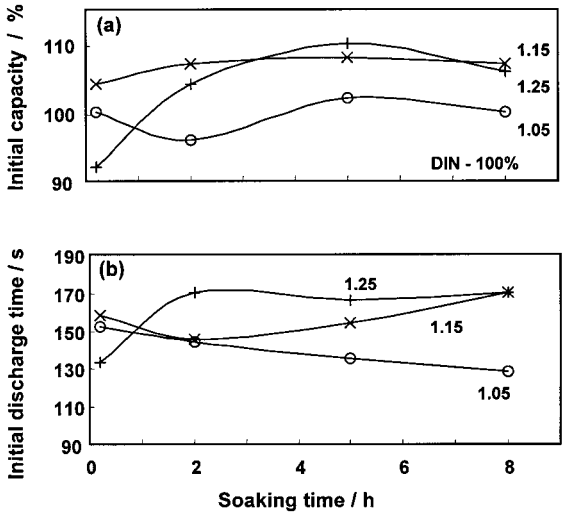

Fig. 3.8. Dependence of (a) initial capacity and (b) initial discharge time during CCA test of batteries soaked and formed in 1.05, 1.15, and 1.25 rel. dens. H_2SO_4 on time of soaking. Tests carried out according to DIN 43539/2 standard [6].

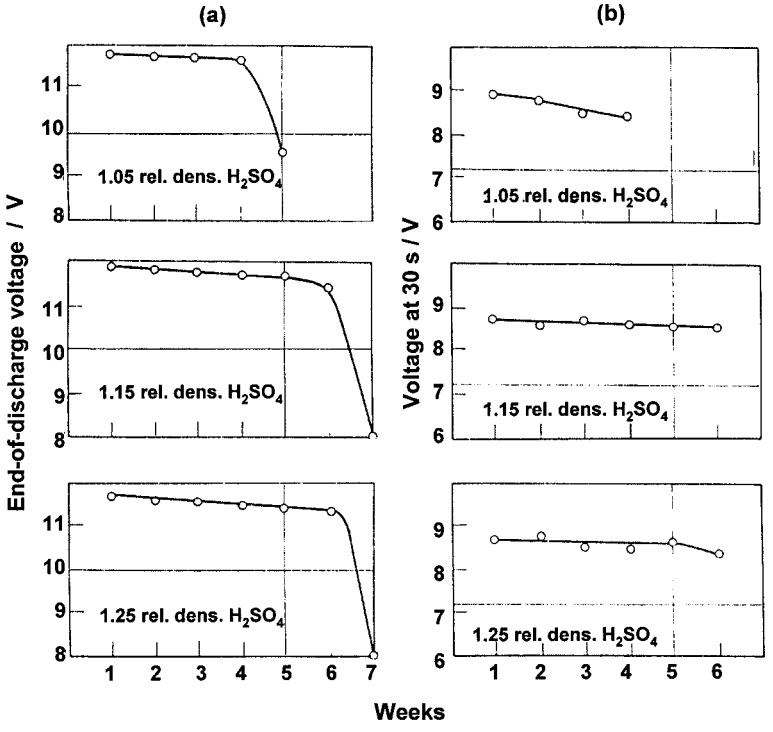

Fig. 3.9. (a) End-of-discharge voltage at 10th charge–discharge cycle (10 cycles carried out within one week). (b) Voltage after 30 s of discharge during CCA test (DIN 43539/2). Batteries soaked for 2 h and formed in 1.05, 1.15, or 1.25 rel. dens. H_2SO_4 [6].

formation will be influenced by the structure of the soaked paste rather than by that of the cured paste. Hence, soaking exerts an effect on both the capacity and the cycle-life of the battery. That is why the soaking procedure should be considered as an autonomous technological step with a definite role in determining battery performance and, therefore, should be controlled very carefully.

3.2.4. Soaking of 4BS-cured pastes

With the introduction of Pb–Ca–Sn alloys for the production of positive grids, the phenomenon known as premature capacity loss (PCL) was observed. Positive plates lost capacity during the initial cycles because of impaired electronic and mechanical contact between the PAM and the grid (termed the 'PCL-1 effect'). One of the possible methods to suppress this effect was to use 4BS pastes [10]. The 4BS crystals are large and build up a strong PAM skeleton. Due to their large size, however, 4BS crystals are difficult to form and plates produced with 4BS pastes require more time for formation. This presents some technological problems. A possible solution is to prolong the time of soaking to allow deep sulfation of the 4BS crystals [5,11–14].

The dependence of the amount of H_2SO_4 that has reacted with 10 g of 3BS or 4BS paste as a function of soaking time is shown in Fig. 3.10. 4BS pastes react with H_2SO_4 much more slowly than do 3BS pastes. The smaller surface area and the greater thickness of the crystals in 4BS pastes cause the rate of the reaction of sulfation to slow down within the first 30 min of soaking [11–16]. The structure of the lead sulfate layer that covers the 4BS crystals has been examined [11–14]. First, polyhedral particles with an average size of up to 2 μm are formed on the surface of

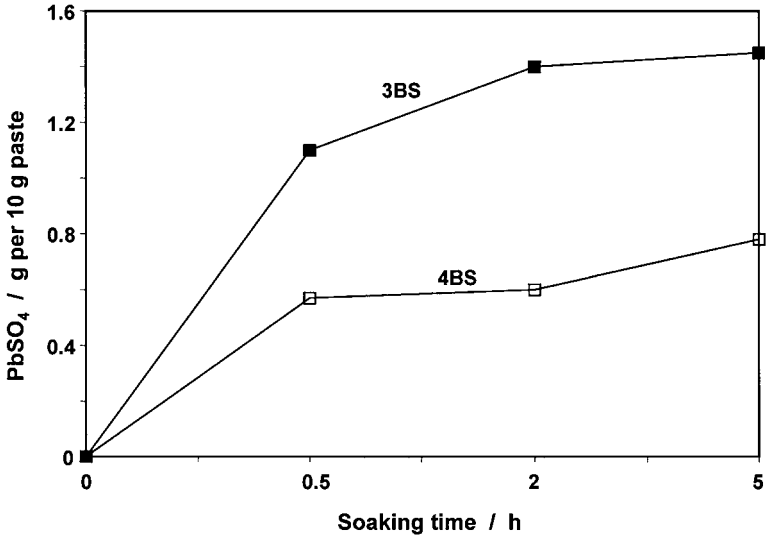

Fig. 3.10. Changes in $PbSO_4$ content formed on soaking 3BS and 4BS pastes as a function of time of soaking [13].

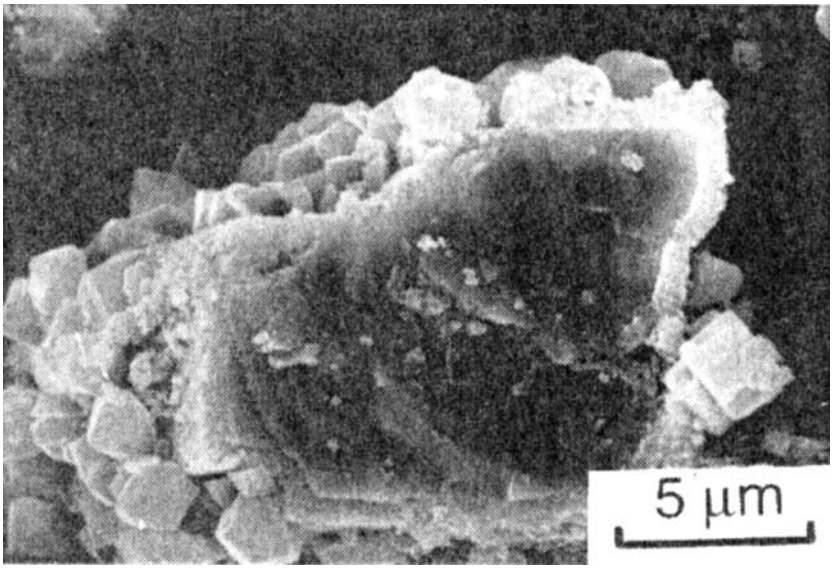

Fig. 3.11. Photograph of cross-section of broken 4BS crystal with $PbSO_4$ layer on surface [13].

the 4BS crystals. Then, the sulfation proceeds into the volume of the 4BS crystals to form a layer of small agglomerates which are composed of $PbSO_4$ nodules of a size that does not exceed 0.2 μm [11–14]. The cross-section of a partially sulfated 4BS crystal is shown in Fig. 3.11 [13]. A superficial $PbSO_4$ layer composed of large and small crystals, and the unreacted core of the 4BS crystal can be clearly distinguished.

The processes of 4BS sulfation proceed within the matrix of the 4BS crystal through a metasomatic chemical reaction [15]. This allows the 4BS macrostructure of the paste to be preserved and transferred, through the formation process, into the macrostructure of the PbO_2 active mass. The progress of the sulfation reaction deep into the core of the 4BS crystals is slowed down and (in practice) a definite thickness of the $PbSO_4$ layer is reached, which depends on the temperature of soaking. These dependences are given in Fig. 3.12 for different temperatures [13]. The higher the temperature of soaking, the thicker is the $PbSO_4$ layer formed on each 4BS crystal. Elevated temperatures increase the depth of sulfation by increasing the porosity of the structure of the granular $PbSO_4$ layer. This facilitates the transport of H^+ and SO_4^{2-} ions and water through the layer towards the core of the crystal.

Heat generation during the soaking step is proportional to the specific surface of the cured paste [14]. Thus, the temperature rise on soaking of 4BS pastes is half that for 3BS pastes. It is therefore not necessary to cool down the H_2SO_4 solution before filling into batteries with 4BS cured plates.

It has been established that the rate of sulfation on soaking of 4BS pastes depends on the method of 4BS crystal formation. The various methods of 4BS production yield not only crystals of different size, but also different nature [17].

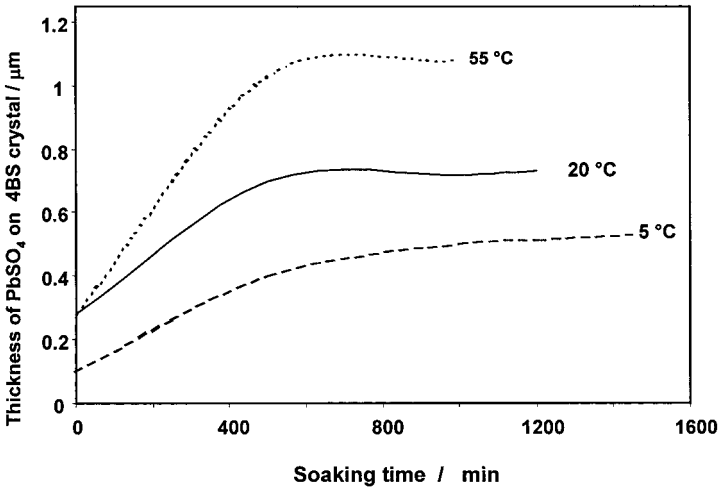

Fig. 3.12. Changes in thickness of superficial $PbSO_4$ layer on 4BS crystals during soaking at three different temperatures [13].

3.3. Formation of Positive Plates

3.3.1. Thermodynamics of formation processes

The electrochemical reactions that proceed during the formation of positive plates can be represented by the following equations. E_h represents the equilibrium potential for the reaction at 298.15 K.

$$\begin{aligned} &PbO_2 + SO_4^{2-} + 4H^+ + 2e^- = PbSO_4 + 2H_2O \\ &\quad E_h = 1.685 - 0.118pH + 0.029 \ln a_{SO_4^{2-}} \end{aligned} \tag{3.9}$$

$$\begin{aligned} &PbO_2 + HSO_4^- + 3H^+ + 2e^- = PbSO_4 + 2H_2O \\ &\quad E_h = 1.628 - 0.088pH + 0.029 \ln a_{HSO_4^-} \end{aligned} \tag{3.10}$$

$$\begin{aligned} &2PbO_2 + SO_4^{2-} + 4e^- + 6H^+ = PbO \cdot PbSO_4 + 3H_2O \\ &\quad E_h = 1.468 - 0.088 + pH + 0.015 \ln a_{SO_4^{2-}} \end{aligned} \tag{3.11}$$

$$\begin{aligned} &4PbO_2 + SO_4^{2-} + 8e^- + 10H^+ = 3PbO \cdot PbSO_4 \cdot H_2O + 4H_2O \\ &\quad E_h = 1.325 - 0.074pH + 0.007 \ln a_{SO_4^{2-}} \end{aligned} \tag{3.12}$$

$$\begin{aligned} &PbO_2 + 2e^- + 2H^+ = PbO + H_2O \\ &\quad E_h = 1.107 - 0.059pH \end{aligned} \tag{3.13}$$

$$3PbO_2 + 4e^- + 4H^+ = Pb_3O_4 + 2H_2O$$
$$E_h = 1.122 - 0.059pH \tag{3.14}$$

$$O_2 + 4H^+ + 4e^- = 2H_2O$$
$$E_h = 1.228 - 0.059pH + 0.015 \ln Pb_{O_2} \tag{3.15}$$

All equilibrium potentials are referred to a standard hydrogen electrode. The $Hg|Hg_2SO_4$ electrode is widely used in lead–acid battery investigations. This electrode has a potential which is 0.620 V more positive than that of the standard hydrogen electrode at pH = 0 [18].

The above reactions involve bivalent lead compounds with different PbO and $PbSO_4$ contents. The higher the content of PbO in a given compound, the more negative is the potential of its oxidation to PbO_2. Thus, on oxidation of a mixture of $PbSO_4$, 1BS, 3BS, and Pb_3O_4 in the cured paste after soaking, first PbO and then the basic lead sulfates will be oxidized. When the amount of the starting compounds diminishes, the potential of the positive plates will increase and when it exceeds the equilibrium $PbO_2|PbSO_4$ potential, oxidation of $PbSO_4$ will start. The higher the H_2SO_4 concentration, the more positive is the equilibrium potential of the $PbO_2|PbSO_4$ electrode. Consequently, different potential plateaux will be observed during formation of the soaked paste, as determined by the phase composition of the paste. The development of potential plateaux for the different paste phases in the potential–time curve depends on the kinetics of the redox reactions. For purely kinetic reasons, some of the phases in the paste may not manifest themselves by a specific plateau in the potential curves.

3.3.2. Reactions during formation of PAM from 3BS-cured pastes

The reactions that proceed during positive-plate formation have been identified by the accompanying changes in the phase and chemical compositions of the plates, as well as by the changes in both the open-circuit and charge potentials of the plates, see Fig. 3.13 [19,20]. The phase composition has been determined by XRD analysis. The pastes are prepared at 30°C using an acid-to-oxide ratio of 4.5% and water is added to give a paste density of 4.0 g cm^{-3}. The formation electrolyte is H_2SO_4 of 1.05 rel. dens. and the time of soaking is 10 min. Small regions of the pasted plates are sulfated during the soaking step. The chemical composition is determined through conventional analytical methods; the potentials are measured vs. a $Hg|Hg_2SO_4$ reference electrode.

Depending on the phase and chemical compositions of the paste and of the active mass, the formation process may be divided into two stages, as follows.

(i) *First stage*. The lead oxide and basic lead sulfates are oxidized to α-PbO_2 and small amounts of β-PbO_2, and the paste also reacts with H_2SO_4 to form $PbSO_4$ (reaching approximately 25% at the end of the first stage); the potentials under load and at open-circuit are low.

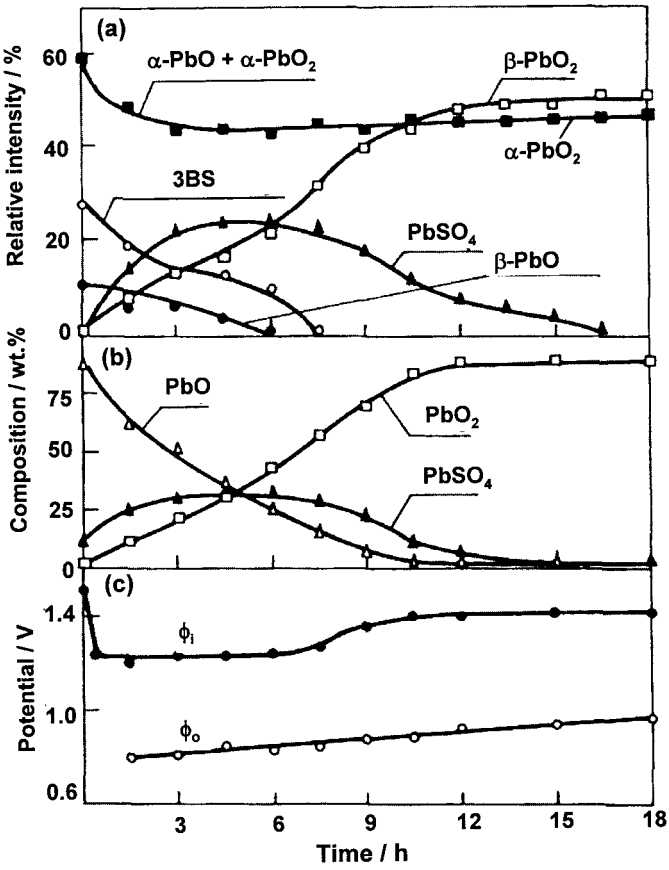

Fig. 3.13. Dependence on formation time of: (a) phase composition and (b) chemical composition of paste and active mass, and (c) plate potential under formation current (φ_i) and on open-circuit (φ_0). Formation electrolyte is 1.05 rel. dens. H_2SO_4 [19].

(ii) *Second stage* (*after about 6 h*). The $PbSO_4$ formed on soaking and during the first stage of formation is oxidized to β-PbO_2; the potential under load increases. The low degree of sulfation of the paste, the short time of soaking and the low H_2SO_4 concentration on formation yield approximately equal amounts of α-PbO_2 and β-PbO_2.

Based on the analytical data for the changes in the phase and chemical compositions of the plates during formation, schemes for the chemical and electrochemical reactions that proceed during the two formation stages have been proposed. The reactions of formation of PbO_2 from 3BS during the first stage are shown in Fig. 3.14. The parameter n represents the amount of Pb^{2+} ions that participate in the electrochemical process (B_1) leading to the formation of PbO_2 according to reaction (C_1); ($4-n$) is the remainder of the lead ions which react to form $PbSO_4$ (reaction E_1).

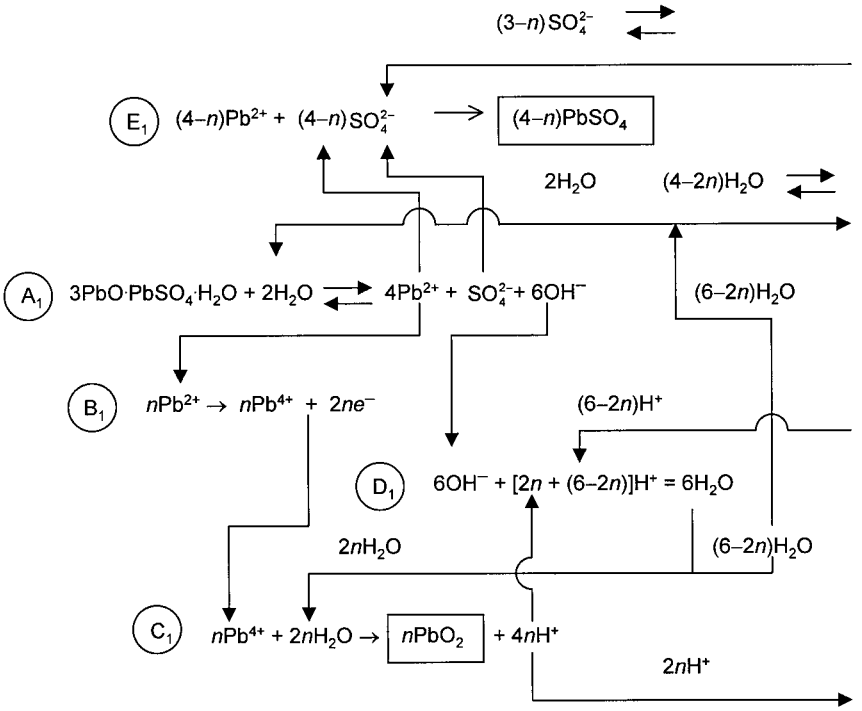

Fig. 3.14. Reactions of $3PbO{\cdot}PbSO_4{\cdot}H_2O$ oxidation to PbO_2 and sulfation to $PbSO_4$ during first stage of formation [19].

For the above reactions to proceed, it is necessary that flows of H^+, SO_4^{2-}, and H_2O enter or exit the plate. These flows, together with the electronic charge shown in reaction B_1, maintain the electroneutrality of the solution in the reaction layer. The direction of each flow depends on the formation current as well as on the degree of sulfation of the cured paste and on the concentration of H_2SO_4 in the formation electrolyte [19,21].

During both the soaking step and the first formation stage, H_2SO_4 penetrates into the plate and the paste is sulfated. Sulfation starts first in the surface layer of the plate during soaking and then proceeds inside the plate during formation. The 3BS, 4BS, and PbO in the plate interior are hydrated and the pH of the solution in the pores increases. In these inner zones, the electrochemical reaction B_1 proceeds and α-PbO_2 is formed (reaction C_1). It can be seen from eqns. (3.11) to (3.13) that 1BS, 3BS, and PbO are oxidized to PbO_2 at potentials more negative than those at which $PbSO_4$ is oxidized (eqns. (3.9) and (3.10)). The potential of the plates during the first stage of formation is more negative by 150–200 mV than that during the second stage of formation (see Fig. 3.13).

The X-ray data for the phase composition of the $PbO_2 + PbSO_4$ zone indicate that both the electrochemical reaction B_1 and the reaction of sulfation E_1 proceed in the same reaction layer. During the first stage of formation, there are two reaction layers in the plate. In the first layer, the electrochemical reaction B_1 and the chemical

reactions C_1 and E_1 proceed. This layer is located in the interior of the plate. The second reaction layer is near the plate surface and this is the layer where the reactions of sulfation of PbO and of basic lead sulfates to $PbSO_4$ and 1BS proceed. The distribution of the two reaction layers (*v.s.*) is responsible for the formation of different structures in different parts of the PAM.

When PbO and 3BS have been depleted, the pH of the solution will decrease. In order to maintain a constant formation current, the potential of the plate will increase and reach the value required for the oxidation of $PbSO_4$ to PbO_2 to proceed. At this point, the second stage of formation will commence according to the scheme of chemical and electrochemical reactions shown in Fig. 3.15. $PbSO_4$ is oxidized to β-PbO_2. This process is associated with generation of H_2SO_4 (reaction D_2). The solution in the pores becomes strongly acidic and a flow of H_2SO_4 leaves the plate. Consequently, the concentration of H_2SO_4 in the electrolyte increases (Fig. 3.2(b)). The PbO_2 formed during this stage is of the β modification.

When sulfation of the paste is high (acid-to-oxide ratio = 5–6%), longer soaking time and higher H_2SO_4 concentrations during formation (1.20–1.25 rel. dens.) shorten the first stage of formation (< 2 h) [19], and the amount of β-PbO_2 in the PAM exceeds several times that of the α-PbO_2 modification. Under the above

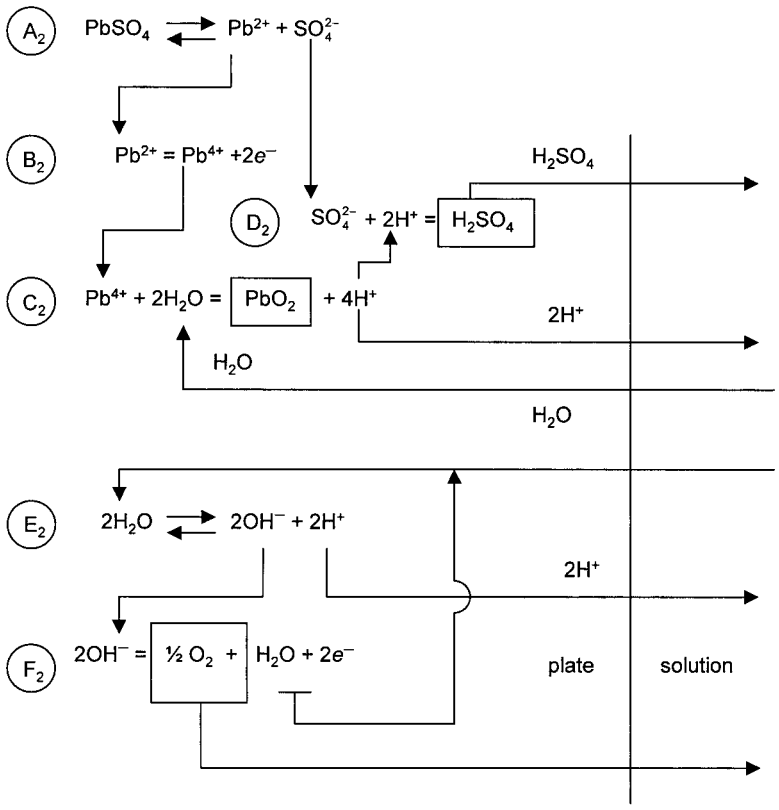

Fig. 3.15. Electrochemical and chemical reactions during second stage of formation [19].

conditions, the formation of $PbSO_4$ on the plate surface is not always complete and there are white regions in the plates, which are not fully formed. The reason for this lies in the development of a thick layer of large $PbSO_4$ crystals, which are oxidized to PbO_2 only during the first charge–discharge cycles.

The distribution of the α-PbO_2 and β-PbO_2 phases through the cross-section of the plate depends on the local pH of the solution that fills the pores of the reaction layer. It has been established that β-PbO_2 predominates in the outer layers of the plate, whereas α-PbO_2 is found mostly in the plate core [19–27]. It has also been found that high pH values are created as a result of transport difficulties that affect the flow of H_2SO_4 into the interior of the plate. The transport of H_2SO_4 may be impeded as a result of the formation of a dense layer of $PbSO_4$ crystals that covers the plate surface or a high PbO content and a high density of the cured paste, low formation H_2SO_4 concentration, considerable plate thickness, etc. [19,26,27]. In general, the distribution of α-PbO_2 and β-PbO_2 depends on the conditions of paste preparation, of soaking and of formation of the plates.

3.3.3. Zonal processes during formation of PAM from 3BS-cured pastes

Lead oxides and basic lead sulfates are white or yellow in colour, whereas PbO_2 is dark brown or black. This difference in colour allows the formed and unformed zones in the plate to be clearly distinguished. Photographs of the cross-section of the plate during different stages of formation in H_2SO_4 of 1.15 rel. dens. are shown in Fig. 3.16. Since the lead grid is the only electronic conductor in the plate, the growth of PbO_2 starts at the grid bars and can be clearly seen as a dark-brown zone. Phase analysis shows that this zone consists of PbO_2 and $PbSO_4$ crystals. During formation, the $PbO_2 + PbSO_4$ zone grows first in the interior of the plate. White zones of $PbSO_4$ crystals, which are formed on both surfaces of the plate during the soaking step and during the first formation stage, grow into the plate core. The $PbO_2 + PbSO_4$ zones of two adjacent grid bars advance towards each other until they coalesce, and then the zone grows towards the surface of the plate, whereby $PbSO_4$ is oxidized to β-PbO_2. As at this stage of formation, the electrode potential is highly positive (Fig. 3.13), the $PbSO_4$ formed in the interior of the plate during the first stage is also oxidized to β-PbO_2. The direction of the growth of the $PbO_2 + PbSO_4$ zone is determined by the transport hindrances that affect H^+ and SO_4^{2-} ion flows and of water transfer between the reaction layer and the bulk of the electrolyte, as well as by the paste composition and the formation current density [21].

The influence of paste composition on the direction of growth of the $PbO_2 + PbSO_4$ zones is shown in Fig. 3.17 [4]. The data are for cross-sections of partially formed plates prepared with pastes containing 0, 2, 4, 6, 8, 10, and 12% H_2SO_4. Examinations have been carried out after 8 h of formation of 12-Ah battery plates. In all cases, formation starts at the grid bars and the growth of the zones depends on the amount of H_2SO_4 in the paste. If the paste is prepared with water alone (i.e., 0% H_2SO_4), the zones advance initially along the surface of the plate and then into its interior. With pastes containing more than 8% H_2SO_4, the growth of the zones proceeds in the reverse direction. On formation of pastes prepared with 2–6%

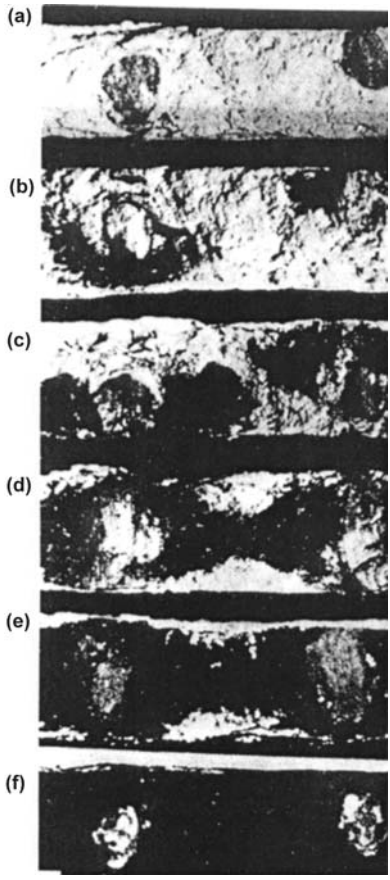

Fig. 3.16. Cross-sections through plate at various stages of formation in 1.15 rel. dens. H_2SO_4. Dark regions are $PbO_2 + PbSO_4$ zones [19,20]. Plate thickness is 1.8 mm. This is a vertical cross-section of the plate.

H_2SO_4, the growth may follow different patterns as dictated by the acid-to-oxide ratio in the paste and the density of the formation current [21]. Hence, the phase composition of the active mass (α-PbO_2 or β-PbO_2) will differ for the different regions within the cross-section of the plate and will depend on the direction of $PbO_2 + PbSO_4$ zone growth during formation [20].

Zonal processes are slow processes. They are responsible for the long duration of plate formation. Hence, it is important to find methods to by-pass the zonal processes. In order to accelerate the formation of positive plates, some conductive additives have been added to the positive pastes [28]. These additives increase the conductivity of the cured paste and formation proceeds almost uniformly throughout the whole plate volume as the electric current flows along the conductive additive network. The additives should be chemically stable in H_2SO_4 solution. Data have been reported about successful attempts to reduce the duration of the formation procedure to 8 h.

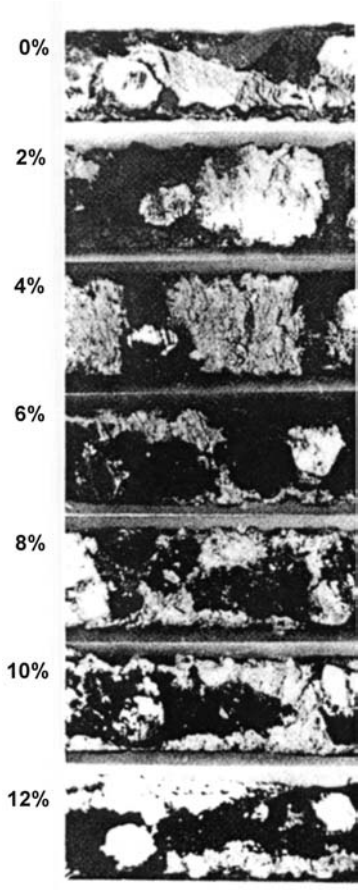

Fig. 3.17. $PbO_2 + PbSO_4$ zones in partially formed plates prepared with pastes of different acid-to-oxide ratios (%) [4]. Plate thickness is 1.8 mm. This is a vertical cross-section of the plate.

Conductive additives that are commonly used are as follows:

(i) Carbon, anisotropic graphite, graphite.
(ii) Conductive polymers, i.e., polyaniline, polypyrrole, polyparaphenylene, and polyacetylene, in the form of powders or fibres. These polymers are added to the positive paste. The maximum amounts of these additives should not exceed a few percent. To date, there are no data that indicates wide application of these polymers by the battery industry.
(iii) Glass fibres coated with SnO_2 have been developed and used in lead–acid battery positive plates with the aim to improve the process of plate formation and the performance of the plate.
(iv) Barium plumbate is a relatively stable conductive ceramic having the perovskite structure. Addition of this material to PAM [29–31] improves significantly the formation efficiency.

(v) Lead dioxide or red lead (25–50%) are widely used by many major battery manufacturers. When H_2SO_4 is added to red lead the following reaction proceeds:

$$Pb_3O_4 + 2H_2SO_4 \rightarrow 2PbSO_4 + \beta\text{-}PbO_2 + 2H_2O \tag{3.16}$$

β-PbO_2, when present in sufficient amounts, may suppress the zonal processes and thus improve substantially the efficiency of the formation process. This can be achieved, however, only if the leady oxide does not contain too much lead. In this case, the following reaction proceeds:

$$Pb + PbO_2 + 2H_2SO_4 \rightarrow 2PbSO_4 + 2H_2O \tag{3.17}$$

and the role of Pb_3O_4 as an additive that suppresses the zonal processes is eliminated.

The various types of positive-plate additives and their effect are discussed in detail in Chapter 4.

3.3.4. β-PbO_2:α-PbO_2 ratio and its effect on capacity of positive plates

Based on the processes that occur during the two formation stages and taking into account that α-PbO_2 is formed in weak acidic to alkaline media, whereas β-PbO_2 is formed in acidic media, the following overall equation for the β-PbO_2:α-PbO_2 ratio in the active mass at the end of the formation process has been proposed [19]:

$$\beta\text{-}PbO_2{:}\alpha\text{-}PbO_2 = (q^0_{PbSO_4} + q^1_{PbSO_4} + q^1_{PbO}) : (q^0_{PbO} - q^1_{PbSO_4} - q^1_{PbO}) \tag{3.18}$$

where $q^0_{PbSO_4}$ is the initial quantity of $PbSO_4$ in the basic lead sulfates; $q^1_{PbSO_4}$ is the amount of $PbSO_4$ produced during soaking and the first formation stage; q^1_{PbO} is the amount of PbO transformed into β-PbO_2, a process which may proceed at the end of the first formation stage; q^0_{PbO} is the total initial amount of PbO (free and bonded in basic lead sulfates).

Many scientists have investigated the influence of the β-PbO_2:α-PbO_2 ratio on the capacity of plates [22,25,26,32,33]. It has been established that this ratio does indeed affect capacity, but there is no direct correlation, as demonstrated by the following experiments [34]. Two series of plates were produced using pastes with the same acid-to-oxide ratio in the range 0–12%, but mixed at two different temperatures, namely, 30°C to yield 3BS crystals and 80°C to facilitate the formation of 4BS crystals. Note, 3BS and 4BS pastes form different PAM structures. If the capacity were determined directly by the β-PbO_2:α-PbO_2 ratio, then both series of plates should have the same capacity determined only by this ratio. The ratio as a function of the acid-to-oxide ratio in the paste is presented in Fig. 3.18. It can be seen that the β-PbO_2:α-PbO_2 ratio is the same for the two series of plates when the acid-to-oxide ratio in the paste is up to 8%. The dependence of the capacity of the plates during the second cycle on discharge at 0.7 A or 42 A as a function of the acid-to-oxide ratio is given in Fig. 3.19. The capacity of the plates increases at both discharge currents.

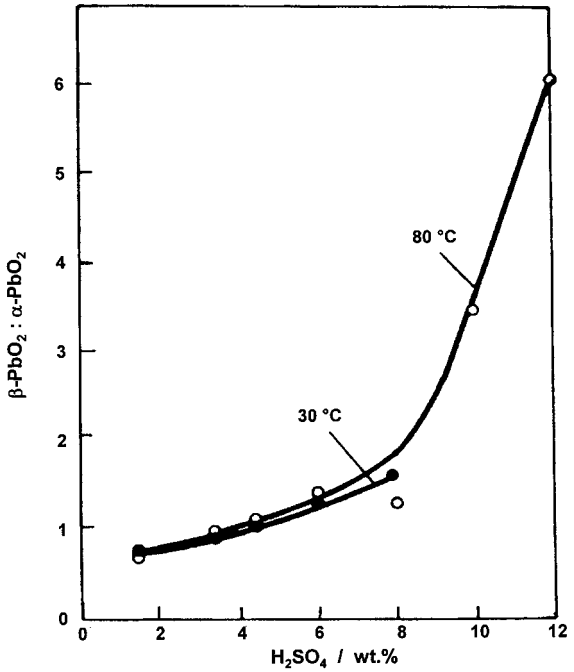

Fig. 3.18. Experimentally determined β-PbO_2:α-PbO_2 ratio as a function of acid-to-oxide ratio in paste [34].

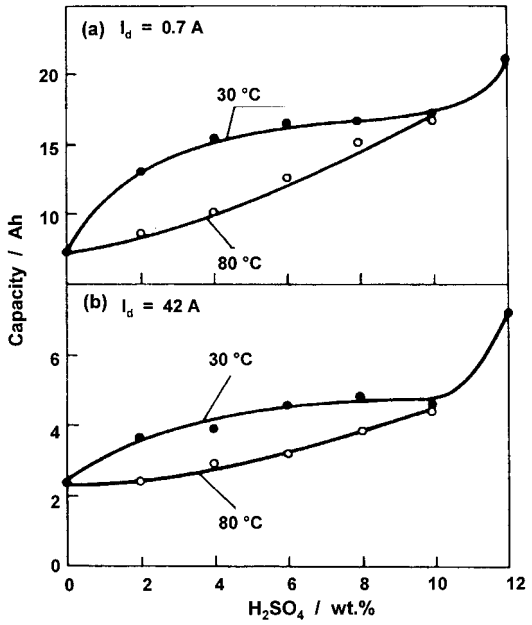

Fig. 3.19. Capacity of positive plates at second charge–discharge cycle as a function of acid-to-oxide ratio in paste [34].

Moreover, the higher the discharge current, the weaker is the dependence of the plate capacity on the β-PbO_2:α-PbO_2 ratio.

A comparison of the data in Figs. 3.18 and 3.19 shows that although the β-PbO_2:α-PbO_2 ratio for a given acid-to-oxide ratio is the same, the active mass prepared from pastes containing 3BS yields a higher capacity than plates produced with 4BS pastes. Thus, the capacity of the active mass depends not only on the ratio between the two PbO_2 modifications in PAM, but also, and much more so, on the type and structure of the PAM that are determined by the type of basic lead sulfates in the paste subjected to formation. Hence, the capacity of the positive plate is determined by the structure of the active mass and the relative proportions of β-PbO_2 and α-PbO_2.

3.3.5. Structure of PAM

The structure of the PAM obtained during formation of the plates has been studied through scanning electron microscopy and a model for this structure has been proposed, see Fig. 3.20 [35–37]. The following two structural levels can be distinguished.

(i) *Microstructural level*. The smallest building element of the PAM structure is the PbO_2 particle. A certain number of PbO_2 particles interconnect into agglomerates. In some cases (usually after cycling of the battery), these agglomerates contain micro-pores between the particles. In other cases, the particles have coalesced and only the boundaries between them are distinguished at high magnifications (> 30 000 X). At this microstructural level, the electrochemical reaction of discharge proceeds. This level determines the active surface-area of the PAM.

(ii) *Macrostructural level*. A huge number of agglomerates, and in some cases individual particles, interconnect to form aggregates or a porous mass. Micro-pores are formed between the agglomerates that constitute the aggregate. Thus, the aggregate has the nature of a microporous structure. Aggregates interconnect to form a 'skeleton', which is connected to the grid through an interface. Macro-pores are formed between the aggregates and allow H^+ and

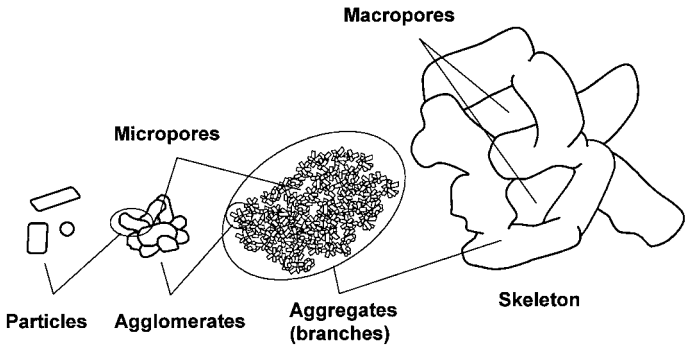

Fig. 3.20. Schematic of basic structural elements of PAM [38].

SO_4^{2-} ions and water to move between the plate interior and the bulk of the electrolyte. Thus, the macrostructural level provides the main transport system in the PAM.

The type of macrostructure that will be formed in the PAM depends on the size of the crystals in the cured paste. Crystals and particles of 3BS, 4BS, PbO, and $PbSO_4$ are converted into aggregates and agglomerates, which build up the macrostructure of the PAM. It should be noted that 3BS and 4BS crystals, as well as PbO particles, vary in size. Three different types of macrostructures are formed, as follows.

(i) *Skeleton*. When the cured paste contains large particles ($>10\,\mu m$), the macrostructure has a pronounced skeleton appearance. This is best manifested in PAM obtained from the formation of 4BS pastes. An electron micrograph of a cured paste with 4BS crystals and the active mass obtained from these paste is shown in Fig. 3.21(a) and (b), respectively. During formation, the shape of the 4BS crystals is transferred to the aggregates, which interconnect into a skeleton. On cycling of the plates, the skeleton undergoes evolution and the well-shaped aggregates visible in Fig. 3.21(b) gradually change in appearance. The shape of the skeleton is now determined by the charge and discharge current algorithms, but the micro- and macrostructural levels and their functions are preserved.

(ii) *Porous mass*. When the cured paste contains small particles ($<1.5\,\mu m$) that are chaotically interconnected, a porous mass is formed (Fig. 3.22). This type of macrostructure lacks the pronounced skeleton structure that features aggregates with macro-pores in-between. The basic building elements of this type of macrostructure are the agglomerates of interconnected particles. The 3BS particles are small in size (1–2 μm long, 0.3–0.8 μm wide). They are

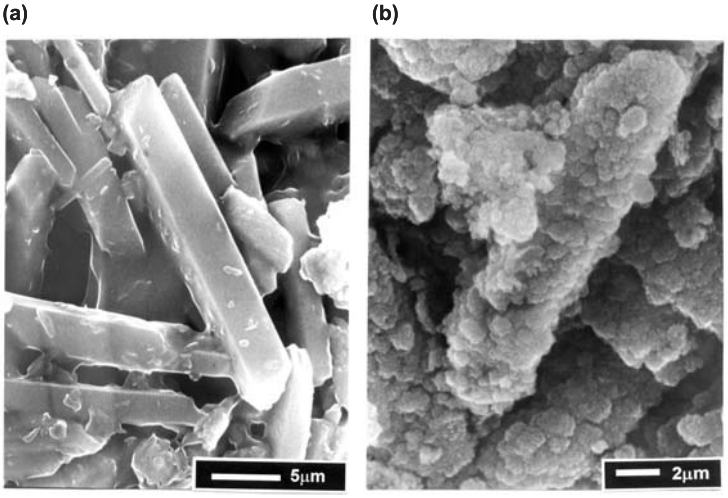

Fig. 3.21. Scanning electron micrographs of structure of (a) cured paste and (b) PAM obtained from 4BS pastes. PAM skeleton built up of interconnected aggregates obtained from oxidation of 4BS crystals [17].

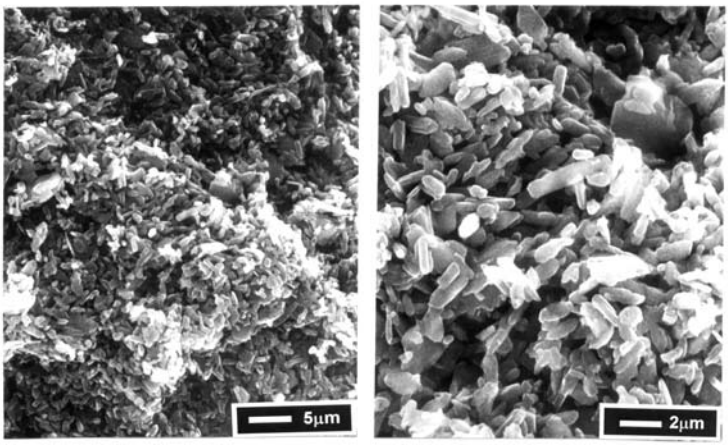

Fig. 3.22. Scanning electron micrographs of cured paste produced from 3BS particles. Chaotically interconnected 3BS crystals form a porous mass.

grouped fairly chaotically during paste preparation and curing and are converted into a porous mass during formation. An electron micrograph of the positive PbO_2 mass obtained by formation of a 3BS paste is presented in Fig. 3.23(a) [38]. The agglomerates, which are tightly interconnected with macro-pores in-between, are shown in Fig. 3.23(b) and the agglomerate and the constituent particles and nuclei in Fig. 3.23(c). It can be clearly seen that this type of structure creates a large contact surface between the agglomerates and the solution in the pores of the PAM. On cycling of the plates, the macro-structure of the PAM formed from 3BS pastes also undergoes evolution [38].

(iii) *Mixed macrostructure*. This comprises zones with skeleton structure and porous mass zones. Such a macrostructure is observed in the PAM obtained from cured pastes that have experienced prolonged soaking or on formation of pastes containing both 4BS and 3BS crystals.

3.3.6. Gel–crystal forms of PbO_2 particles

From electron micrographs of PbO_2 particles which are interconnected in agglomerates (Fig. 3.23 and 3.24), the following types of particles can be distinguished:

- Spherical or egg-shaped particles as if obtained from a liquid phase (Fig. 3.23(c) and Fig. 3.24(a,b)), in which PbO_2 particles have coalesced into small agglomerates (Fig. 3.24(a)) or into individual particles with good contact between them (Fig. 3.24(b)).
- PbO_2 crystal particles, which are relatively small in size but are in contact with each other (Fig. 3.24(c)), or large crystallites with well-shaped faces, apexes, and edges. Some of the crystallites have partially built faces of prismatic form. These forms are a result of metasomatic oxidation of undissolved parts of the $PbSO_4$

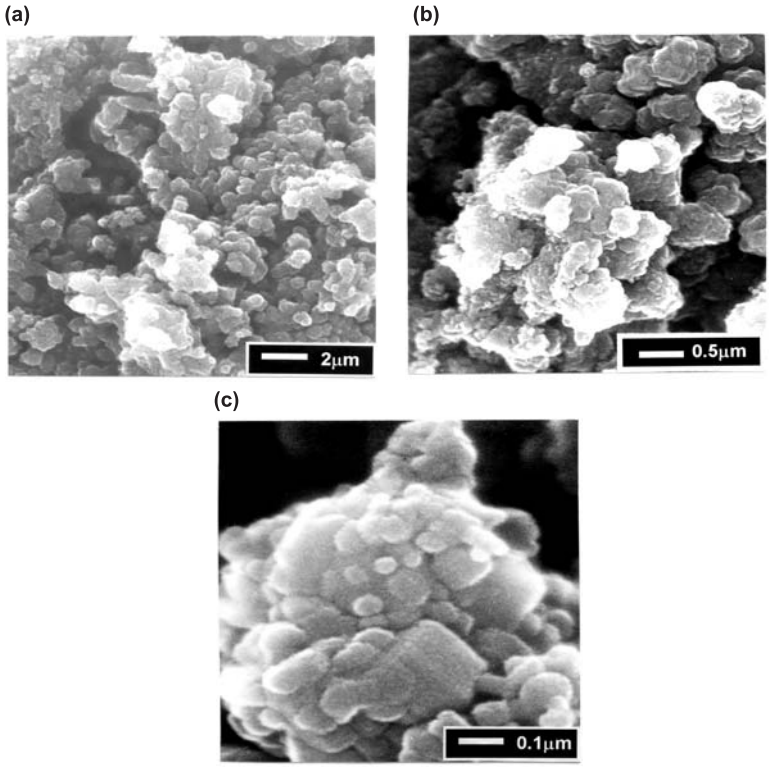

Fig. 3.23. Scanning electron micrographs of PAM obtained from 3BS pastes: (a) porous PAM; (b) agglomerate structure of macroporous mass; (c) agglomerate comprising particles of various shapes [38].

crystals, which have converted into PbO_2 during charge. Several small particles exhibit heterogeneous structures (Fig. 3.24(d)). The contact surface-area between these particles is not so large.

- Needle-like particles, possibly with a common base (Fig. 3.24(e)), or individual needle-like particles possibly with contacts between them (Fig. 3.24(f)).

The following question arises: Are the particles homogeneous in material and phase composition? The answer is provided by the images obtained by means of transmission electron microscopy, see Fig. 3.25 [39]. The patchy appearance of the image contrast suggests some degree of heterogeneous structure. Hence, the PbO_2 particles consist of zones of different composition.

A transmission electron micrograph and a diagrammatic representation of the phase composition (determined by electron diffraction analysis) of a particle of formed PAM are presented in Fig. 3.26. The electron diffraction analysis demonstrates the predominance of zones with β-PbO_2 structure in the middle part of the particle. By contrast, the uppermost and bottom parts, which are far more electron-transparent, have an amorphous structure. A $PbSO_4$ nucleus is also detected in the bottom part near the amorphous zone.

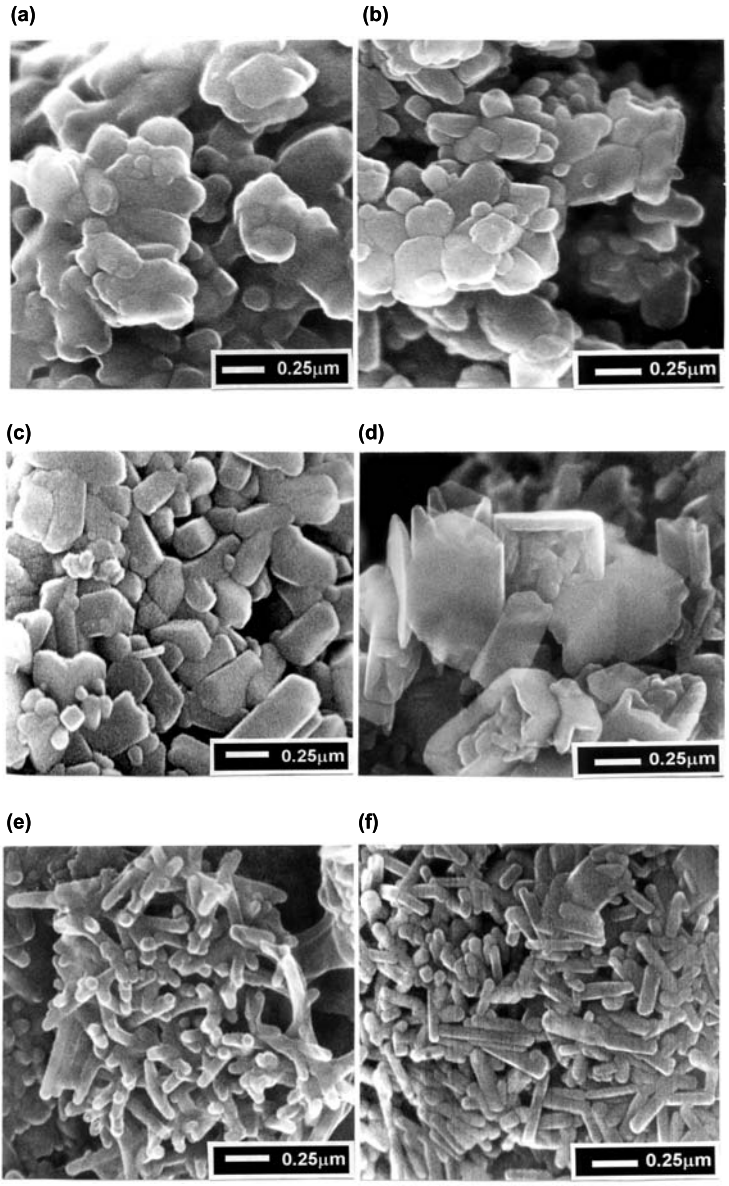

Fig. 3.24. Scanning electron micrographs of PbO_2 particles of various shapes formed during plate formation and cycling [38].

It has been established, through XRD analysis, that the average dimensions of PbO_2 crystals in PAM are between 45 and 60 nm [39–41]. The micrographs in Figs. 3.25 and 3.26 show that the size of some PbO_2 particles exceeds 100 nm.

It is to be expected that the amorphous zones are strongly hydrated. To verify this conjecture, PbO_2 particles have been subjected to heating inside a scanning

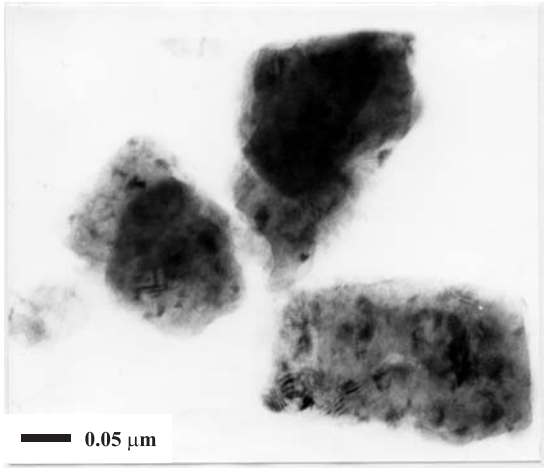

Fig. 3.25. Transmission electron micrograph of PbO_2 particles. The particles have a non-homogeneous composition [39].

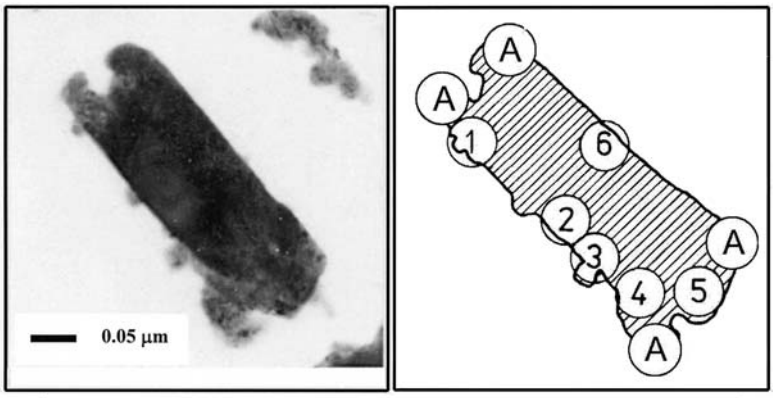

Zone #	Interplanar distance (d), Å	Phase
1	3.51 3.33	β-PbO_2 $PbSO_4$
2	2.81	β-PbO_2
3	3.33; 3.00; 1.64	$PbSO_4$
4	3.50; 1.75; 1.86; 2.23	β-PbO_2
5	2.80; 1.09	β-PbO_2
6	3.50; 2.22	β-PbO_2
A	Amorphous structure	

Fig. 3.26. Transmission electron micrograph of a PbO_2 particle and distribution of structural zones as determined through electron diffraction analysis [39].

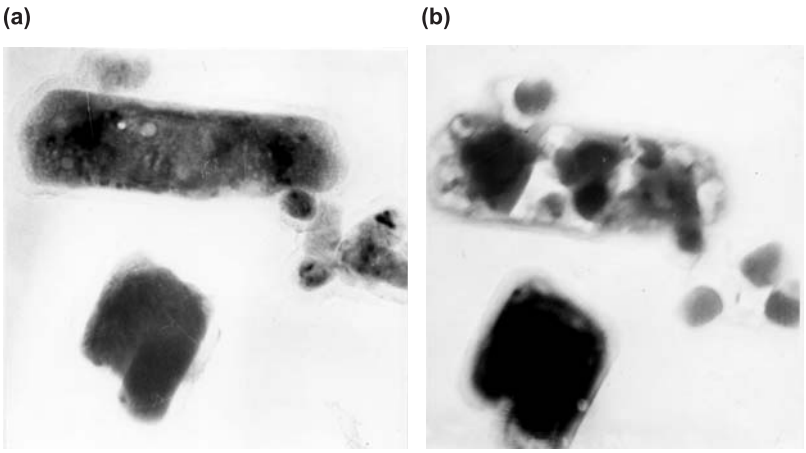

Fig. 3.27. Transmission electron micrographs of PbO_2 particles: (a) before and (b) after heating inside microscope [42].

electron microscope. Micrographs of particles prior to and after heating are presented in Fig. 3.27 [42]. The small particle contains only a small amorphous zone; the longer one contains several amorphous zones (Fig. 3.27 (a)). When heated at 100°C for 20 min, the long particle boils for a short time and water evaporates from inside the particle. The material is concentrated in several zones which are mainly around the crystal part of the particle (Fig. 3.27(b)). Empty zones (voids) also appear. It follows then that the lighter zones in the particle are hydrated and are of an amorphous nature. These regions are referred to as 'gel zones'.

3.3.7. *Mechanism of formation of PbO_2 particles*

Studies with X-ray photoelectron spectroscopy have found that the formed PAM contains 34% OH groups when obtained from 3BS pastes and 31% OH groups when the PAM is formed from 4BS pastes [39]. Hydrothermogravimetric analysis has shown that in the temperature range from 260 to 450°C, water evaporates from the PAM at $0.00323\,cm^3\,g^{-1}$ PAM [43].

The finding that there are hydrated zones in the PbO_2 particles has allowed the following mechanism for the formation of PbO_2 particles to be proposed [37,39]:

$$Pb^{4+} + 4H_2O \rightarrow Pb(OH)_4 + 4H^+ \tag{3.19}$$

$Pb(OH)_4$ has a sol character, i.e., it dehydrates partially as a result of which gel particles are formed:

$$nPb(OH)_4 \rightarrow [PbO(OH)_2]_n + nH_2O \tag{3.20}$$

$[PbO(OH)_2]_n$ represents a gel particle. Further dehydration takes place and PbO_2 crystallites and crystal zones are formed in the particles or in particles that have coalesced into agglomerates.

$$[PbO(OH)_2]_n \leftrightarrows \underset{\text{crystal zone}}{[k(PbO_2)} + \underset{\text{gel zone}}{(n-k)PbO(OH)_2]} + kH_2O \tag{3.21}$$

Hydrated zones exchange ions with the solution. Hence, the lead dioxide particle is an open system [39,42]. $PbO(OH)_2$ may also be represented by the formula H_2PbO_3. Thus, both OH^- and H^+ ions in the gel zones are in equilibrium with the anions and cations of the solution, which facilitates the discharge reaction [44]. It has been established that the crystallites which build up the crystal zones of the formed PAM particles are sized between 25 and 40 nm, whereas the size of the particles themselves varies from 50 nm to about 150 nm, and a single particle may contain several crystallites [38]. These particle sizes give a specific surface-area of 5–7 $m^2 g^{-1}$ PAM.

When the size of the crystal zones substantially exceeds that of gel zones, the particles have a recognizable crystal habit (Fig. 3.24(c,d)). If the gel zones occupy a relatively thick layer on the surface of the particles, the latter have rounded shape (Fig. 3.23(c), Fig. 3.24(a,b)). When, however, the particles are completely hydrated (which is usually the case with small particles Fig. 3.23(c)), the shape is drop-like or egg-like. It has been found that there is equilibrium between gel zones and crystal zones, and this equilibrium depends on the temperature, the types of ion in the solution [42], and the alloying additives used. Antimony increases the share of gel zones to about 30% [45]. As PbO_2 particles are an open system, an ion-exchange may proceed between the solution outside the particles and their hydrated zones. This suggests that PbO_2 particles resemble biological cells in their behaviour. The crystal zones of α-PbO_2 and β-PbO_2 particles have the nature of degenerate semiconductors and are characterized by high electroconductivity ($\sim 10^2\,\Omega^{-1}\,cm^{-1}$) [46]. Hydrated zones have proton (H^+) conductivity.

The reaction of discharge involves both electrons and protons (eqns. (3.9) and (3.10)). When these two types of charged particles reach a given point in the gel zone of the lead dioxide particle simultaneously, the discharge reaction proceeds. This may happen most readily at the boundary between crystal and hydrated zones. When the PAM is composed only of PbO_2 crystals, it will have high electron conductivity but low proton conductivity. The capacity of the plate will be low [47]. By contrast, if the PAM is composed of gel alone, it will exhibit high proton conductivity, but low electron conductivity. Again, the plate capacity will be low. If the PAM is a gel–crystal system, electron and proton conductivities will both be high, as will the plate capacity [47,48].

3.3.8. Formation of pore system in PAM and its functions

One of the requirements for metasomatic transformations is that the volume changes between the host and metasomate are minimal. The changes during formation of PbO_2 from several lead compounds contained in the cured paste are listed in

Table 3.1. Volume changes during formation of PbO_2 [15].

Compound	Moles of PbO_2 per mole of compound	$\triangle V^*$ (cm^3)	% $\triangle V^*$ per Pb atom
$PbSO_4$	1	−23.12	−48.12
β-PbO	1	1.69	7.18
α-PbO	1	0.96	4.02
Pb_3O_4	3	−0.72	−2.81
$PbO{\cdot}PbSO_4$	2	−12.66	−33.77
$3PbO{\cdot}PbSO_4{\cdot}H_2O$	4	−13.00	−34.00
$4PbO{\cdot}PbSO_4$	5	−4.51	−15.38

$\triangle V^*$ is volume change upon conversion to β-PbO_2 per gram atom of Pb in compound.

Table 3.1 [15]. The volume of the particles increases during the oxidation of PbO to β-PbO_2, and decreases during the oxidation of $PbSO_4$ and basic lead sulfates to PbO_2. Thus, the overall volume change of the crystals will depend on the phase composition of the paste.

The changes in porosity of pastes, prepared with 6% H_2SO_4 at 30°C and containing 3BS during formation at a current density of $2\,mA\,cm^{-2}$ are presented in Fig. 3.28 [4]. The porograms for the surface layers and for the interior of the plate are plotted and compared with those for an unformed plate. The paste in the interior of the plate is hydrated, which accounts for the pore volume being smaller than that of the unformed plate. During the first formation stage (12 Ah, 18 Ah), the average pore radius remains virtually unchanged; the number of fine pores increases whilst that of large pores decreases. The total volume of the pores decreases, which shows that sulfation and hydration processes have a predominant effect on pore volume. The $PbSO_4$ is formed in two reaction layers. During the second stage (28 Ah, 60 Ah), $PbSO_4$ is oxidized to PbO_2 and the average radius of the pores increases from 0.15 to 0.80–1.00 μm, whereas the total pore volume of the active mass increases from 0.065 to $0.085\,cm^3\,g^{-1}$ PAM.

The data in Table 3.1 show that oxidation of PbO to PbO_2 leads to an increase of 4–7% in the volume of the solid phase. By contrast, oxidation of basic lead sulfates to PbO_2 causes shrinkage of the solid phase volume by 15–34%. Thus, plates containing only basic lead sulfates may have cracks after formation. To reduce such cracking, the paste should contain PbO and basic lead sulfates in an appropriate ratio.

The pore volume and pore surface-area as a function of pore radius for an active mass formed from 3BS paste on lead–antimony grids are presented in Fig. 3.29(a) and (b), respectively. The pore volume begins to rise at a pore radius of 1 μm and the surface area at a pore radius of 0.1 μm. Pores with 0.1 μm radius have a specific pore volume of $0.065\,cm^3\,g^{-1}$, which is about 62% of the total pore volume. The surface area of the pores of this same size is only 6% of the total surface-area of the PAM. These results demonstrate that the macrostructure of the PAM is basically built up of pores with radii larger than ~0.1 μm (macro-pores), and these pores serve as the main transport system for the flows of ions and H_2O between the bulk of the solution

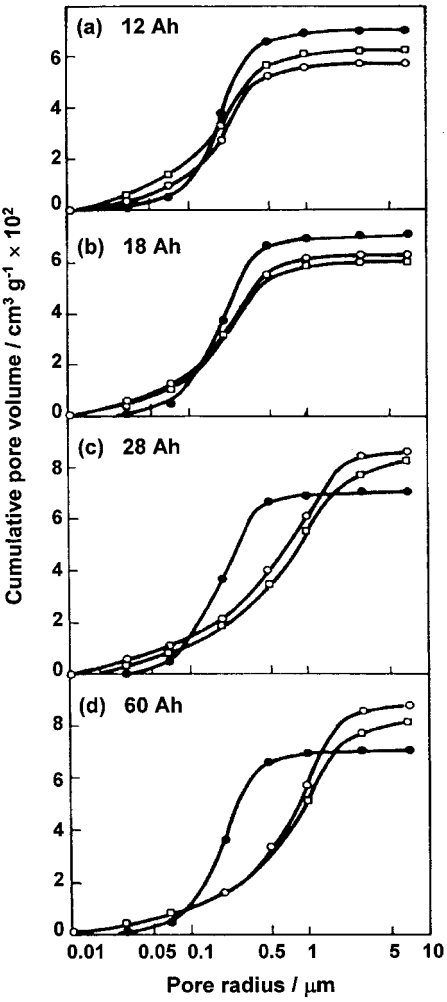

Fig. 3.28. Changes in total pore volume and pore-size distribution by radius for 3BS paste and active mass during formation with current density of 2 mA cm^{-2}: (●) unformed plate; (○) plate surface; (□) plate interior [4].

and the aggregates inside the plate. Pores with radii smaller than ~0.1 μm (micropores) are located in the interior of the aggregates between the agglomerates. The electrochemical processes of discharge take place on the surfaces of these small 'reaction pores' [36].

The pore volume and surface-area distribution vs. pore radius for PAM formed from pastes with various phase compositions and densities are given in Fig. 3.30 [36]. The curves for chemically prepared PbO_2 are also provided for comparison. When the PAM is obtained by formation of basic lead sulfate pastes, the pore volume grows gradually within a wide range of radii (0.05–1.2 μm). For chemically prepared PbO_2, the total pore volume attains its limiting value within a very narrow range of

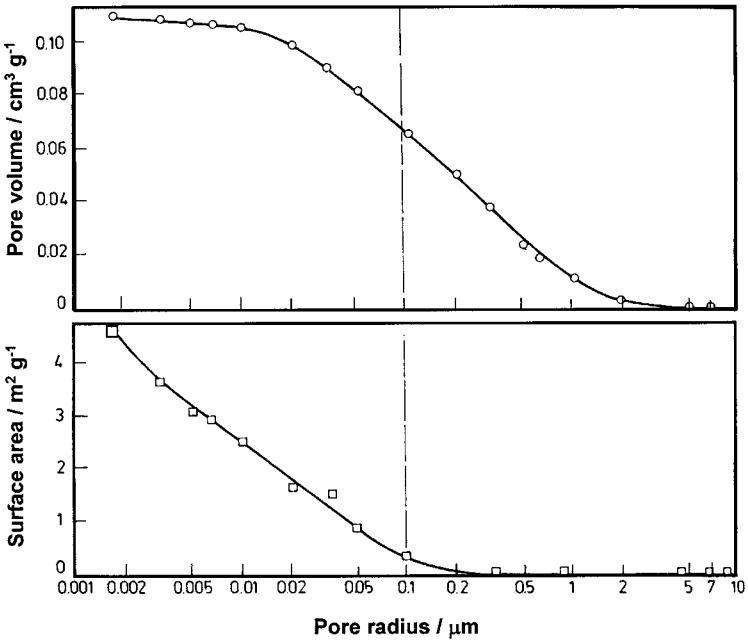

Fig. 3.29. Pore volume and pore surface-area distribution for PAM formed from 3BS paste. Pore radius of ~0.1 μm is assumed to be the limit between micro- and macro- (transport) pores [36].

radii. A steep rise in the surface-area curve for PAM prepared from basic lead sulfate pastes is observed for pore radii smaller than 0.5–0.1 μm. In the case of chemical PbO_2, this rise starts at radii ten times smaller (0.01 μm). Both the pore volume and the surface area are strongly dependent on the phase composition and density of the paste. These experiments suggest that the porosity of the PAM can be controlled through the phase composition and the density of the initial paste.

The boundary between micro- and macro-pores in Fig. 3.30 is marked by an arrow on the porograms. The surface area of the PAM is determined mainly by the surface of the micro-pores; the contribution from the macro-pores is negligible. Hence, the boundary between the macro-pores and the micro-pores is determined by the pore radius from which the PAM surface-area starts to increase rapidly (Fig. 30(b)). As the agglomerates and particles that surround the micro-pores differ in size for PAMs obtained from different pastes, the macro-pore|micro-pore boundary varies between 0.05 and 0.2 μm (Fig. 30(b)). In the literature, it is often assumed that the boundary micro-pore radius has an average value of ~0.1 μm. The correlation between the total pore volume (V_p) and the micro-pore volume ($V_{\mu p}$) and the capacity of the plate at the fifth cycle is given in Fig. 3.31 [36]. The capacity increases with increase in the total pore volume and does not depend on the volume of micro-pores. The difference $V_p - V_{\mu p}$ gives the volume of the transport pores. Hence, the volume of the transport pores is the capacity-limiting parameter for positive plates with lead–antimony grids.

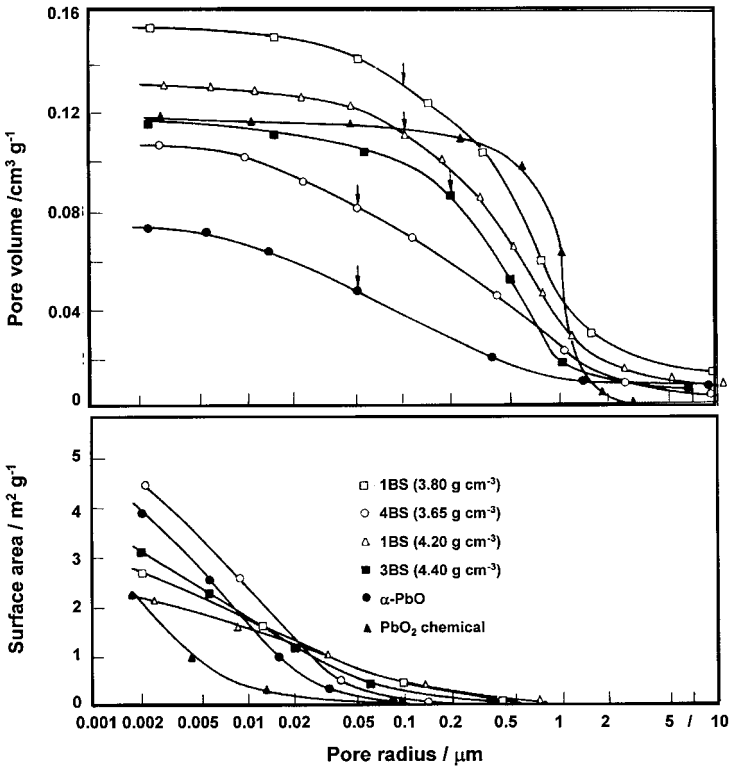

Fig. 3.30. Pore volume and pore surface-area distribution for PAM formed from pastes with various phase compositions. Arrows mark the assumed boundary between micro- and macro-pores [36].

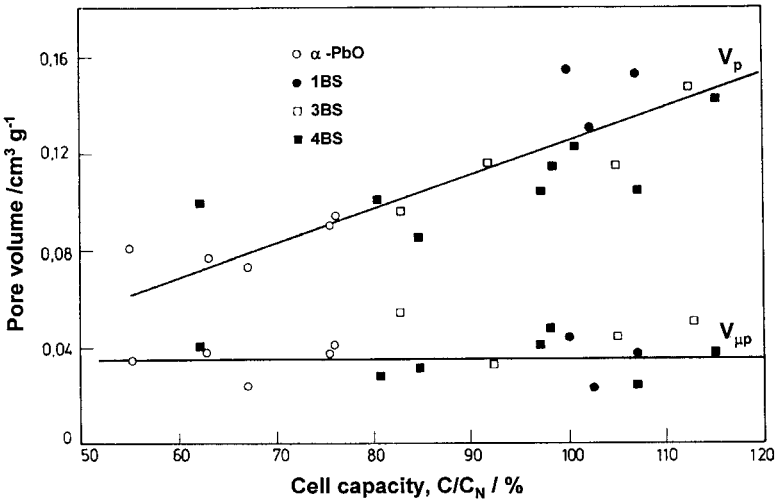

Fig. 3.31. Dependence of cell capacity on total pore volume (V_p) and on volume of micro-pores ($V_{\mu p}$) for PAM prepared from pastes with various phase compositions [36].

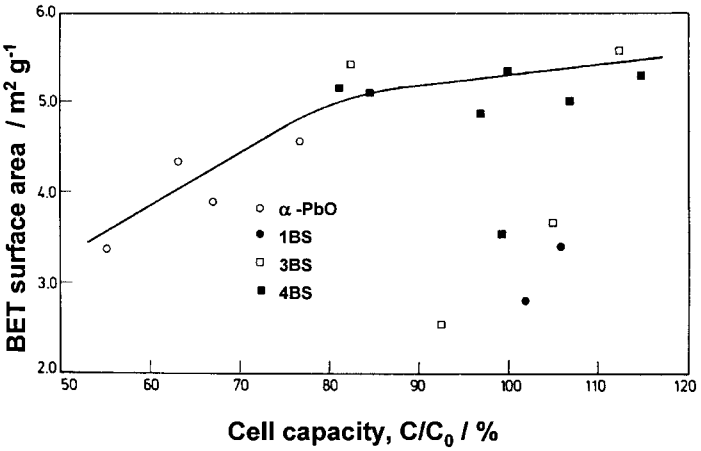

Fig. 3.32. Plate capacity as a function of BET surface-area for PAM prepared from pastes with various phase compositions [36].

The capacity of plates with lead–antimony grids and different phase composition and density of the pastes as a function of the BET surface-area of the PAM (at the fifth cycle) is shown in Fig. 3.32 [36]. In general, the plate capacity increases with increase in BET surface-area. Several plates have comparatively low BET surface-area but high capacity. Hence, the BET surface-area of the PAM is not the sole parameter that determines plate capacity.

The above porosity, BET surface-area, and capacity measurements have been carried out at the fifth cycle, i.e., when the structure of the PAM is determined by the formation process. On further cycling, the PAM structure undergoes changes, as a result of which one or more of the above parameters may become capacity-limiting.

3.3.9. Influence of basic lead sulfates on cycle-life of positive plates

The dependencies of the phase composition of the paste and the cycle-life of the positive plates on the acid-to-oxide ratio used for paste preparation are presented in Fig. 3.33 [34]. The relative intensities of the characteristic diffraction lines for the different phases in pastes prepared using different acid-to-oxide ratios are shown in Fig. 3.33 (a) and (b). The sulfation of the pastes increases with increase in acid content.

(i) *Pastes prepared at 30°C* (*Fig. 3.33(a)*). 3BS is the main basic lead sulfate formed in the paste when acid-to-oxide ratios of up to 10% are used. At ratios above 8%, 1BS appears in the paste and its amount increases with increase in the ratio. When the acid-to-oxide ratio is above 10%, the amount of 3BS in the paste decreases at the expense of an increase in 1BS. Pastes prepared with acid-to-oxide ratios between 1 and 8% contain β-PbO as well.

(ii) *Pastes prepared at 80°C* (*Fig. 3.33(b)*). Hydrated 4BS ($4PbO{\cdot}PbSO_4{\cdot}xH_2O = 4BS{\cdot}xH_2O$) is formed in pastes at acid-to-oxide ratios between 1 and

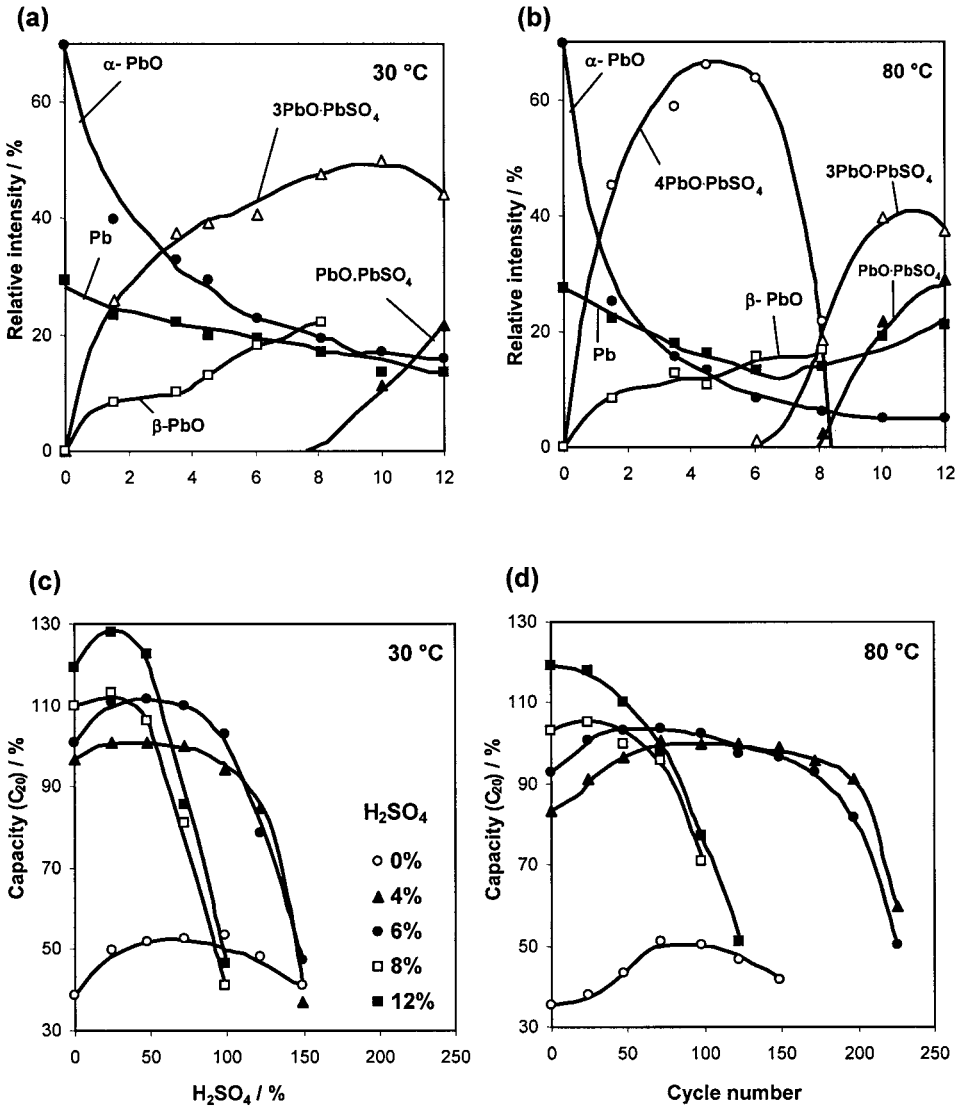

Fig. 3.33. (a), (b) Phase composition of pastes prepared with different amounts of acid at 30 and 80°C; (c), (d) Changes in C_{20} capacity of 12-V/42-Ah automotive batteries with positive plates produced from 3BS, 4BS, and 1BS pastes (depending on acid strength and preparation temperature) on cycling at 50% DoD. The battery capacity is limited by the positive plates [34].

8%; the maximum amount of $4BS{\cdot}xH_2O$ is detected at ratios between 4 and 6%. At higher acid contents in the paste, the amount of $4BS{\cdot}xH_2O$ decreases abruptly at the expense of the formation of 3BS. The quantity of the latter phase increases with acid-to-oxide ratios up to 10%, and decreases thereafter. The pastes prepared with acid-to-oxide ratios above 8% also contain 1BS,

which gradually increases with ratios up to 12%. β-PbO is also formed in the pastes at ratios between 1 and 8% (Fig. 3.33(b)).

A study has been made of the effect of the above basic lead sulfates formed in the PAM on the cycle-life of 12-V/42-Ah batteries. In order to allow the PAM structure to manifest fully its influence, the batteries were cycled with no compression applied, i.e., the PAM was allowed to expand freely on cycling. The results, presented in Fig. 3.33(c) and (d), demonstrate clearly the marked effect of paste composition on the cycle-life performance of the positive plates.

During cycling, the positive plates retain 'a memory' of the pastes used for their production. The positive plates produced with pastes without H_2SO_4 yield less than 60% of the rated capacity but have a long cycle-life. By contrast, plates with an acid-to-oxide ratio of 8–12% have high initial capacity but poor cycle-life due to shedding of the positive active-material. The 1BS crystals are thin and elongated in shape and they produce a weak skeleton, which disintegrates rapidly on cycling (Fig. 3.33). These crystals are formed on soaking 3BS pastes, though in small amounts (Fig. 3.6), and they adversely affect battery cycle-life.

Batteries produced with pastes containing 4BS (4–6% H_2SO_4 at 80°C) exhibit the longest cycle-life. The initial capacity of these batteries is, however, lower than that of their 3BS counterparts. These results reflect the effect of the PAM structure on the performance of the battery. It is true that the PAM structure changes substantially on cycling, but the initial structure formed during formation is of utmost importance. This structure affects the conversion of one type of porous mass or skeleton to another on cycling.

In positive-plate manufacture, 3BS and 4BS phases are never used alone. They are always in combination with PbO, which improves the connection between the basic lead sulfate crystals and hence facilitates the formation of a mechanically strong porous mass or skeleton. The ratio between the basic lead sulfates and the PbO in the pastes exerts an influence on the initial capacity and the cycle-life performance of the battery, namely the higher the PbO content in the paste, the lower is the initial capacity of the positive plates (Fig. 3.33).

When the leady oxide used for 3BS paste preparation has a degree of oxidation of 80–84%, the acid-to-oxide ratio is low (4%), the soaking step is short and the formation of the plates is conducted in H_2SO_4 solutions with relative density below 1.10, the degree of sulfation of the paste is low and the first formation stage is long. The PAM obtained is intact (no cracks are observed) and the degree of formation is 70–75% PbO_2. A great amount of PbO remains unoxidized because of the formation of a porous mass rather than a skeleton and part of this mass is encapsulated by the PbO_2 layer formed on its surface. The initial capacity of the formed plates is 75–80% of the rated value and about 4–10 cycles are required to reach 100%. Usually, such plates have relatively long cycle-life.

When 3BS pastes are prepared using a leady oxide with 80% oxidation, an acid-to-oxide ratio of 6%, a relatively long soaking step and formation in H_2SO_4 of 1.15 rel. dens. or higher, the first formation stage is relatively short and the degree of formation is 90–92% PbO_2. The initial capacity of the plates is about 100% of the rated value. The PAM macrostructure formed during the first

formation stage is not particularly strong, which leads to a gradual decline in capacity on cycling.

3.3.10. *Formation of plates prepared with 4BS-cured pastes*

The size of 4BS crystals varies from 10 to 100 μm in length and from 2 to 15 μm in diameter. The changes in the phase and the chemical compositions of the plate on the formation of 4BS pastes are illustrated in Fig. 3.34 [49]. Within 20 h of formation, 70% of the paste has been converted into PbO_2 (Fig. 3.34(b)). The remaining unformed 4BS crystals can be easily identified by immersing a piece of PAM in a mixture of $H_2O_2 + HNO_3$. PbO_2 dissolves in this solution and the remaining core consists of 4BS and $PbSO_4$ phases, as confirmed by the XRD data. A scanning electron micrograph of the plate core is presented in Fig. 3.35 [49]; the circles mark the remnants of unformed 4BS in the interior of particles.

As mentioned above in Section 3.2.4, only a superficial layer of 4BS crystals (1–2 μm thick) is sulfated during the soaking procedure. Further sulfation stops thereafter. If the diameter of 4BS crystals is kept constant (at about 10 μm), the length does not influence the efficiency of the formation process [9]. In fact, the formation efficiency depends very strongly on the diameter of the 4BS crystals [9,12,49].

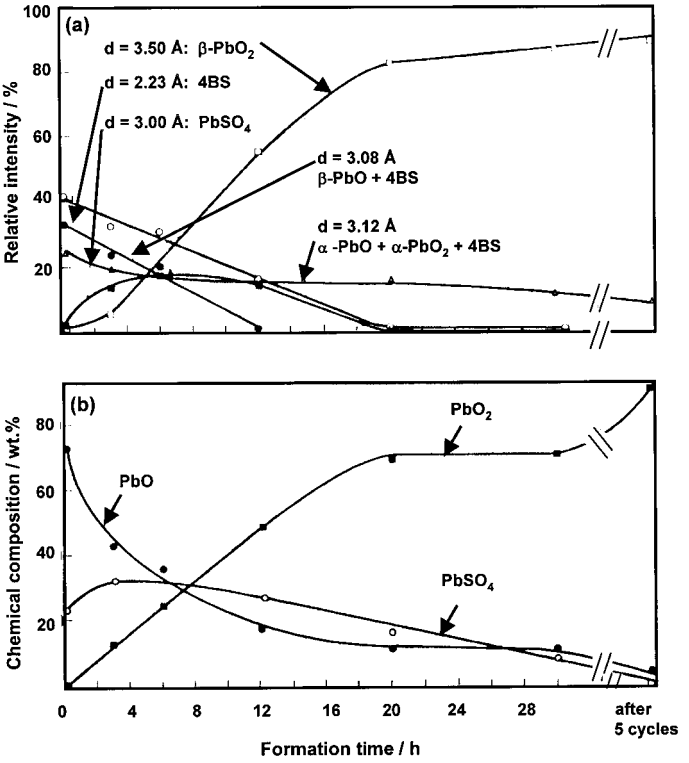

Fig. 3.34. Changes in (a) phase and (b) chemical composition of 4BS pastes during active-mass formation. Maximum degree of formation is 70% at 30 h [49].

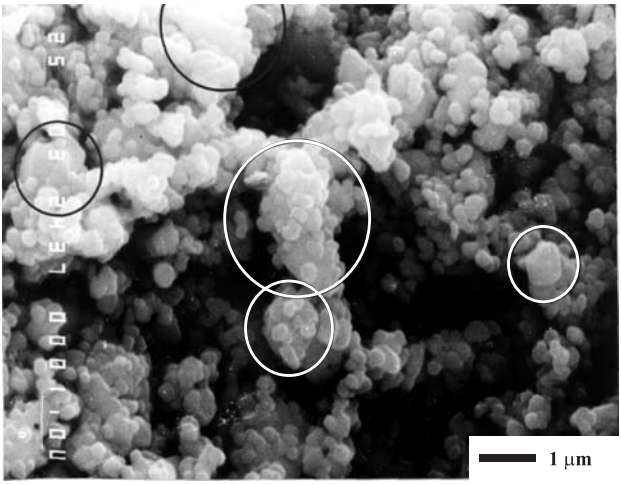

Fig. 3.35. Scanning electron micrograph of non-formed parts of 4BS crystals in interior of PbO_2 agglomerates after 30 h of formation. PbO_2 is dissolved in $H_2O_2 + HNO_3$. X-ray diffraction analysis shows presence of $PbSO_4$ crystals. Magnification bar = 1 μm [49].

The formation of 4BS crystals is influenced by the conditions of soaking, which determine the thickness of the $PbSO_4$ layer that forms on the 4BS crystals. The stages of formation of a partially sulfated 4BS crystal (short soaking period) are shown schematically in Fig. 3.36 [12]. First, the superficial $PbSO_4$ layer is oxidized to PbO_2 (Fig. 3.36(b)). As a result of the electrochemical and chemical reactions involved in formation of the latter compound, H_2SO_4 is formed, which reacts partially with the 4BS crystals to produce more $PbSO_4$ and part of it leaves the crystals. Consequently, a layer of ($4BS + PbSO_4$) is formed in the crystal interior (Fig. 3.36(c)). The unoxidized interior of the large 4BS crystals is easily dissolved by treating the formed PAM with ammonium acetate solution at 80°C. The bivalent compounds dissolve and only PbO_2 remains in the PAM. An electron micrograph of a treated sample of PAM after 6 h of formation is shown in Fig. 3.37. The PbO_2 surface layer consists of small agglomerates with micro-pores in-between. During formation, H_2O and H^+ ions have to penetrate through these pores into the interior of the aggregate and SO_4^{2-} ions have to escape. These flows have to overcome some transport hindrances on their way. The data in Fig. 3.34 show that formation of the remaining part of the 4BS crystals cannot be completed even after 30 h of formation. Ion transport difficulties are the reason for the low efficiency of formation of the 4BS crystals. The interior of the aggregates is formed only after 5–10 deep discharge–charge cycles.

The time for formation of the 4BS crystals depends on their thickness. The latter, in turn, is determined by the method of production of these crystals. The following technologies for the production of 4BS-cured pastes have been put into practice.

(i) 4BS crystals are produced during plate curing [50]. This is the most common method for 4BS paste production. The plates are subjected to steam treatment for 2–4 h. During this period, the temperature of the plates rises to over

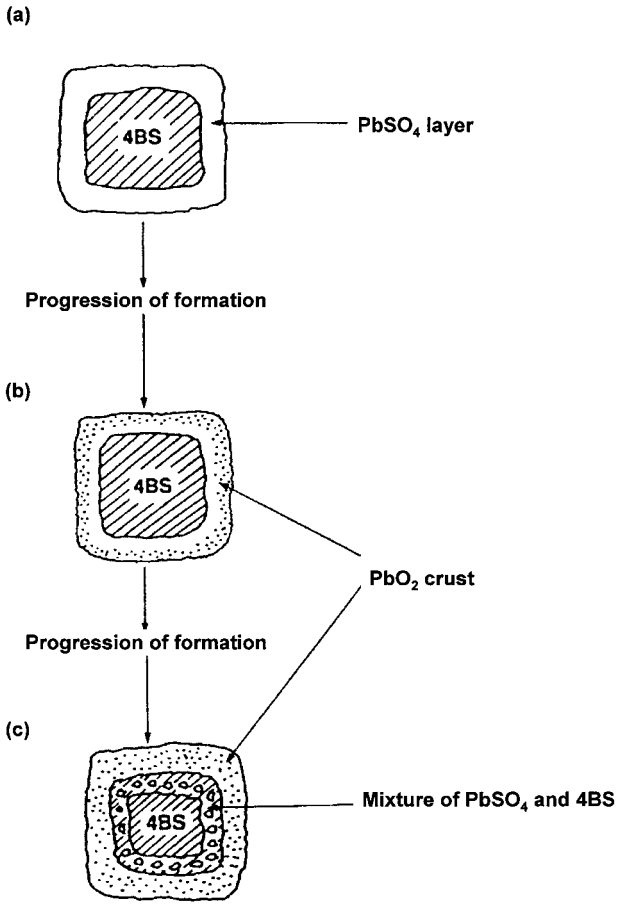

Fig. 3.36. Schematic of formation of 4BS crystals to PbO_2 after short soaking period [12].

80°C and 3BS crystals are converted into 4BS crystals of irregular shape (Fig. 3.38), with good connection between themselves and with the current-collector. Formation of such pastes takes more than 48 h. This technology is used for the production of all types of positive plates. If the time of steam treatment is extended to 8–10 h and the temperature of the plate is higher than 90°C, the resulting 4BS crystals are very thick and the formation of such pastes requires several days. When this method is applied to the manufacture of positive plates for stationary batteries, service lives of over 15 years are achieved.

(ii) 4BS crystals are obtained during paste preparation at temperatures higher than 80°C [51]. This technology yields long, well-shaped, 4BS crystals with a thickness that varies depending on the time of paste mixing and the temperature of paste preparation. When the paste is mixed for 10–20 min, the crystals are 2–4 μm thick and require 20–30 h for formation. The PAM

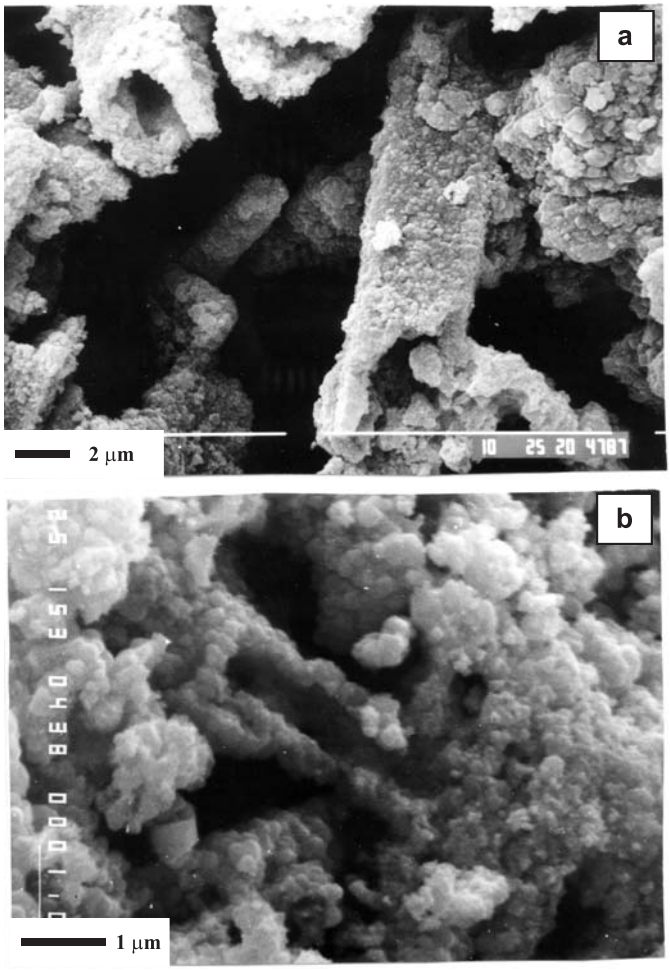

Fig. 3.37. Electron micrographs of PbO_2 aggregates treated with ammonium acetate after 6 h of formation. Inner parts of aggregates have dissolved to form channels. Magnification bar: (a) 10 μm; (b) 1 μm [49].

skeleton obtained is stable and well connected to the current-collector, especially if combined with high-temperature curing ($>80°C$) for 2 h.

(iii) Semi-suspension method [17]. This method is analogous to the one described in (ii) above, except for the fact that the 4BS crystals are obtained from a semi-suspension (density = 3.2–3.4 $cm^3\,g^{-1}$) instead of a paste at temperatures higher than 80°C. After stirring of the semi-suspension for 10–20 min, the excess water is evaporated under vacuum [52] until the desired paste density is achieved. The 4BS crystals (15–25 μm in length, 2–6 μm in diameter) obtained by this method are hydrated and their formation is relatively easy (20–35 h). The resulting PAM skeleton is very stable and hence the cycle-life of the

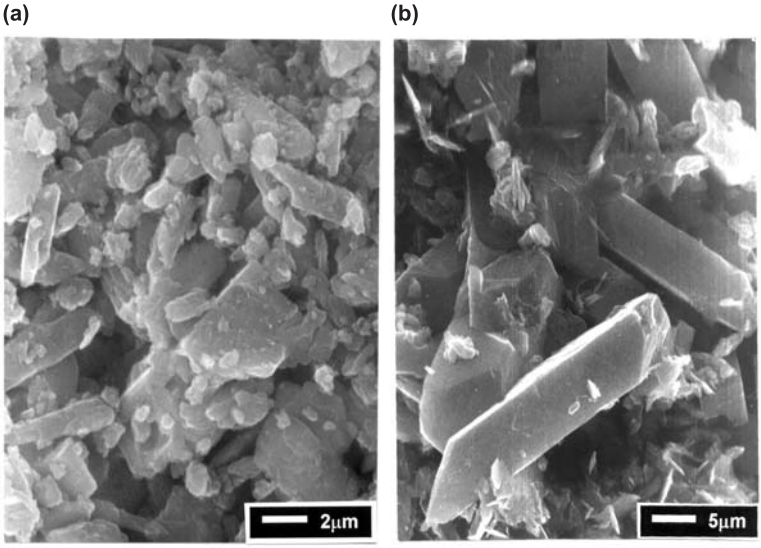

Fig. 3.38. Scanning electron micrographs of 4BS crystals formed during high-temperature curing.

plates is long. Longer stirring of the semi-suspension yields larger 4BS crystals (30–50 μm in length). These pastes are suitable for the production of long-life batteries.

(iv) 4BS crystals are obtained from a slurry of lead oxide in water to which H_2SO_4 solution is added slowly in stoichiometric quantities with respect to the oxide. The temperature of stirring is 80°C [15,53]. After filtration, the powder obtained is heated to 55°C. The 4BS crystals thus produced are sized between 30 and 40 μm and formation requires 6–7 days with several charge–discharge cycles. This method has been used for the production of cylindrical stationary batteries for the AT&T company, with a service life of over 20 years.

Selection of a particular method for the production of 4BS pastes depends on the type of battery application, the time of plate formation and the planned service life of the battery. 4BS pastes are gaining an ever-increasing share in the production of positive plates for lead–acid batteries.

3.3.11. Influence of current-collector surface on formation of $PbSO_4$ crystals at grid–PAM interface

It has been established that on cycling of tubular positive plates with die-cut strap grids (SGTP) or of positive plates with expanded grids with flat ribs, a rapid capacity loss is observed (the PCL-1 effect, see Section 2.3, Chapter 2 and Chapter 9) [54]. The reason for this capacity loss is the formation of groups of $PbSO_4$ crystals in the layer of the PAM that contacts the current-collector (Fig. 3.39). These $PbSO_4$

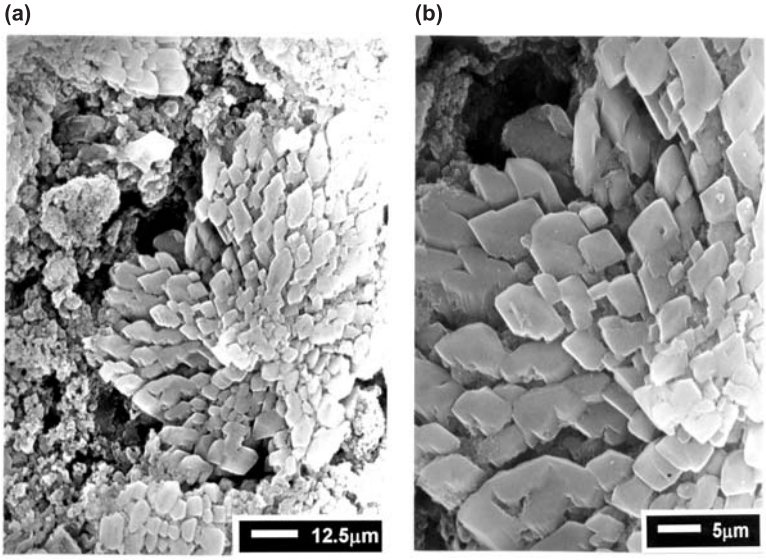

Fig. 3.39. Scanning electron micrographs of groups of $PbSO_4$ crystals formed in layer close to current-collector with smooth surface [54].

crystals are not oxidized to PbO_2 during charge. Hence, even though the PAM is in good health, the plates have low capacity and power.

What is the cause of this phenomenon? The smooth metal surface encourages the processes of discharge to proceed at a uniform rate in a layer close to the grid|PAM interface, as a result of which large plate-like $PbSO_4$ crystals are formed in this layer (Fig. 3.39). These crystals 'eat up' and interrupt the branches of the PAM skeleton and consequently their number at the interface decreases, which impairs the contact of the PAM with the current-collector. On battery charge, the $PbSO_4$ crystals are not oxidized to PbO_2 because of the interrupted branches and the impeded transport of H_2SO_4 in the PAM [54].

A model for the grid|PAM interface of a plate with a smooth metal surface is presented in Fig. 3.40(a). Through roughening of the metal surface of rolled Pb–Sn–Ca or Pb–Ca grids (or straps), the formation of groups of plate-like $PbSO_4$ crystals can be prevented (Fig. 3.40(b)). Such roughening can be achieved by various techniques, as follows:

(i) Through mechanical treatment of the grid or strap current-collector.
(ii) Through subjecting the battery to negative polarization for 30–45 min before formation [54]. As a result of this procedure, lead is deposited irregularly on the smooth metal surface and hence causes roughening (Fig. 3.40(b)). After such pre-treatment, the connections of the battery poles to the power source terminals are reversed and formation proper starts. Test results for batteries that have been formed with an algorithm which includes prior negative polarization are given in Fig. 3.41. The capacity curve is similar to that for batteries that use cast grids with rough surfaces.

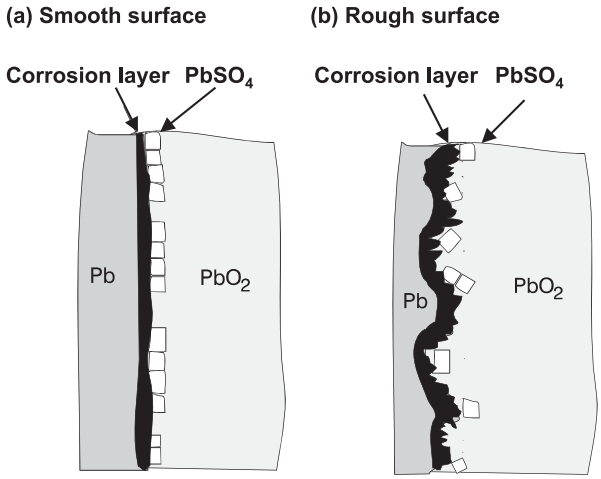

Fig. 3.40. Models for current-collector surface profiles and $PbSO_4$ crystals formed on: (a) smooth surface; (b) rough surface.

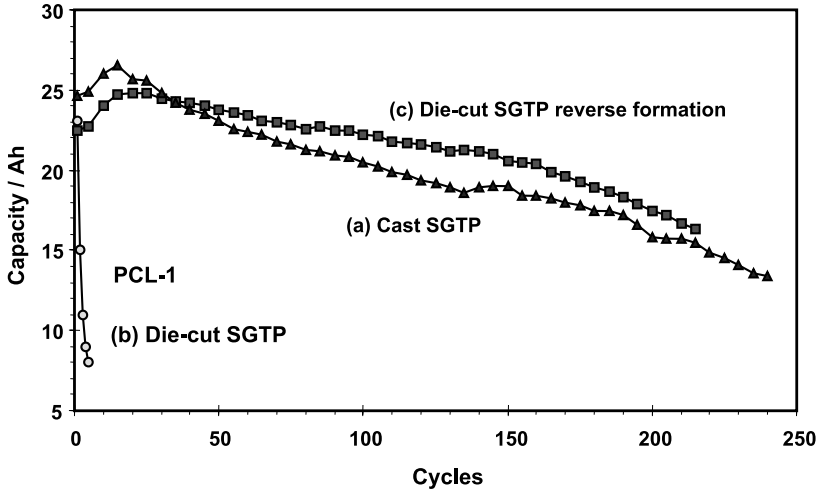

Fig. 3.41. Capacity curves for strap grid tubular positive plates (SGTP): (a) cast strap grids with smooth surface; (b) die-cut strap grids with smooth surface (PCL-1 effect); (c) die-cut strap grids with rough surface obtained after reverse-current treatment prior to formation proper [54].

3.4. Formation of Negative Plates

3.4.1. Thermodynamics of formation processes

The electrochemical reactions that proceed during formation of negative plates can be represented by the following equations. E_h represents the equilibrium potential

for the reaction at 298.15 K. All equilibrium potentials are referred to a standard hydrogen electrode.

$$PbO + 2e^- + 2H^+ = Pb + H_2O \qquad (3.22)$$
$$E_h = 0.248 - 0.059pH$$

$$3PbO \cdot PbSO_4 \cdot H_2O + 8e^- + 8H^+ = 4Pb + H_2SO_4 + 4H_2O \qquad (3.23)$$
$$E_h = 0.030 - 0.044pH - 0.007 \ln a_{SO_4^{2-}}$$

$$PbO \cdot PbSO_4 + 4e^- + 4H^+ = 2Pb + H_2O + H_2SO_4 \qquad (3.24)$$
$$E_h = -0.113 - 0.029pH - 0.015 \ln a_{SO_4^{2-}}$$

$$PbSO_4 + 2e^- + 2H^+ = Pb + H_2SO_4 \qquad (3.25)$$
$$E_h = -0.356 - 0.029 \ln a_{SO_4^{2-}}$$

$$PbSO_4 + 2e^- + 2H^+ = Pb + HSO_4^- + H^+ \qquad (3.26)$$
$$E_h = -0.302 - 0.029pH - 0.029 \ln a_{HSO_4^-}$$

$$2H^+ + 2e^- = H_2 \qquad (3.27)$$
$$E_h = -0.059pH - 0.029 \ln Pb_{H_2}$$

It is generally assumed in electrochemistry that the standard potential of the hydrogen electrode is equal to 0 V at all temperatures. Hence, there is no numerical term in eq. (3.27). On comparing the values of the numerical terms in eqns. (3.22)–(3.27), it can be seen that after the reduction of PbO and 3BS, water decomposition will start with the evolution of hydrogen. Due to kinetic limitations, however, this does not actually occur. The hydrogen overpotential on lead electrodes is one of the highest observed for different metals. Hence, 1BS and $PbSO_4$ are reduced to lead first and then, on increase of the potential, the hydrogen reaction commences.

3.4.2. Reactions during formation of negative plate

The changes in phase composition of negative plates (12 Ah) when formed in H_2SO_4 of 1.05 rel. dens. at a current density of 5 mA cm^{-2}, after a 10-min soaking period, are presented in Fig. 3.42 [55]. The XRD data show that the formation process can be divided into two stages. During the first stage, the amounts of PbO and 3BS decrease, whilst those of Pb and $PbSO_4$ increase. This suggests that PbO and 3BS are partially reduced to Pb, and partially react with H_2SO_4 to form $PbSO_4$. During the second stage, the XRD lines for $PbSO_4$ indicate a decrease in the amount of $PbSO_4$ and an increase in Pb content.

Based on the above XRD data, a general scheme has been proposed for the electrochemical and chemical reactions that proceed during the first formation stage

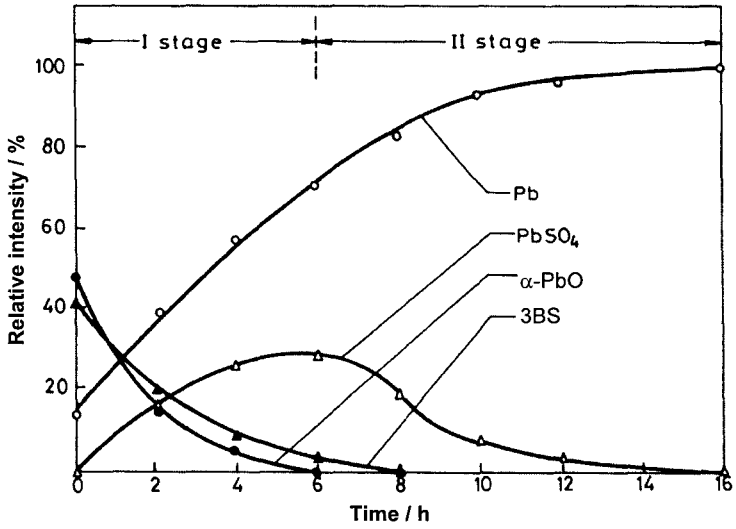

Fig. 3.42. Changes in phase compositions of paste and active mass of negative plates during formation [55].

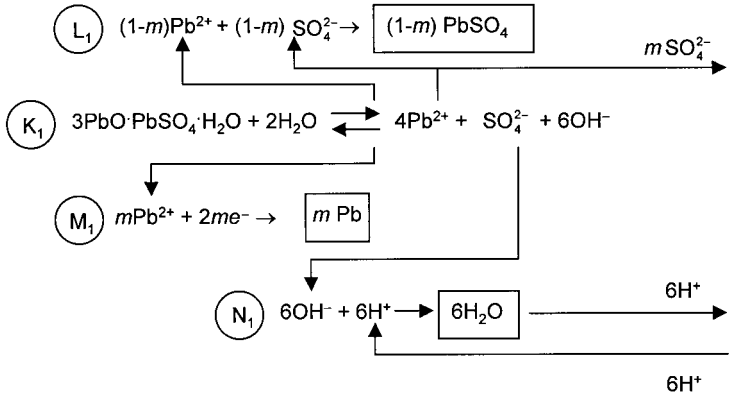

Fig. 3.43. Electrochemical and chemical reactions during first stage of formation of NAM obtained from 3BS pastes [56].

[55,56]. These processes occur in a reaction layer. This reaction scheme for the formation of Pb active mass from 3BS pastes is shown in Fig. 3.43. A similar scheme for the reactions that proceed during the second formation stage is given in Fig. 3.44.

It can be seen from the above reaction schemes that during the first formation stage Pb, $PbSO_4$, and H_2O are formed in the reaction layer, i.e., the latter has an almost neutral pH. During the second stage, H_2SO_4 is produced in the pores of the plate and hence a Pb phase grows in this strongly acidic solution. It is well known that Pb^{2+} ions form different complexes, depending on the pH of the solution. In neutral solutions, $Pb(OH)^+$ and $Pb(OH)_2$ types of complexes are produced, whilst in strongly acidic solutions, Pb^{2+} and $PbSO_{4\,sol}$ are present. The different lead

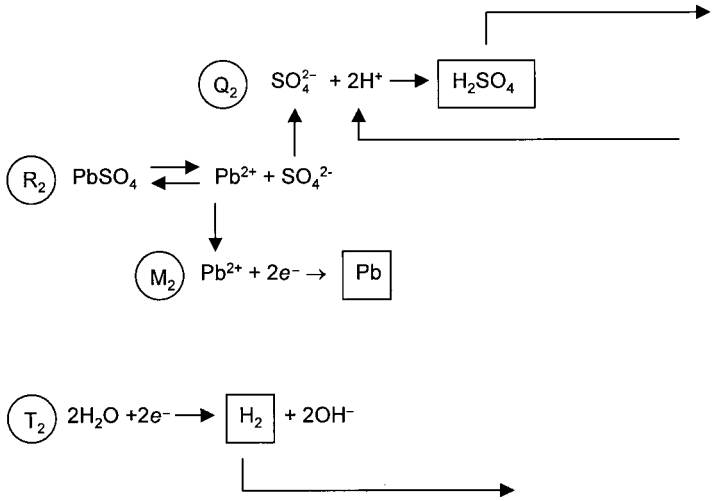

Fig. 3.44. Reactions during second stage of formation of NAM [56].

complexes may affect the electro-crystallization process of lead. This fact has encouraged the notion that a 'primary' lead structure is created during the first formation stage and a 'secondary' structure during the second stage.

3.4.3. Zonal processes

How do the formation processes proceed through the cross-section of the plate? Photographs of the plate cross-section prior to formation as well as during different stages of formation are presented in Fig. 3.45 [56]. Formation starts on the grid surface. A grey zone is formed, which grows along the two surfaces of the plate. According to the X-ray data, this zone is composed of Pb and $PbSO_4$. After covering the whole surface of the plate, the $Pb + PbSO_4$ zones grow towards the interior of the plate until the entire cross-section is formed.

According to the reaction scheme in Fig. 3.43 , an exchange of H^+, SO_4^{2-} ions, and H_2O occurs between the bulk of electrolyte and the reaction layer located between the $Pb + PbSO_4$ zone and the non-formed paste. The electrochemical reaction $Pb^{2+} + 2e^- \rightarrow Pb$ decreases the concentration of the positive charges in the reaction layer. The charges of OH^- and SO_4^{2-} ions in this layer remain uncompensated. In order to preserve the electrical neutrality of the solution in the reaction layer, H^+ ions must migrate from the bulk of the electrolyte into the reaction layer and SO_4^{2-} ions must move in the reverse direction. The rates of these flows control the rate of the electrochemical reactions in the reaction layer. Since H^+ ions are much more mobile than SO_4^{2-} ions, they will maintain the electric neutrality of the reaction layer. The H^+ (and OH^- and $SO_4{}^{2-}$) ions experience the least transport difficulties and hence pass along the shortest paths between the surface layers of the plate and the bulk of electrolyte. Therefore, the $Pb + PbSO_4$ zones will first grow in the plate surface layers and, after the plates are fully covered by the

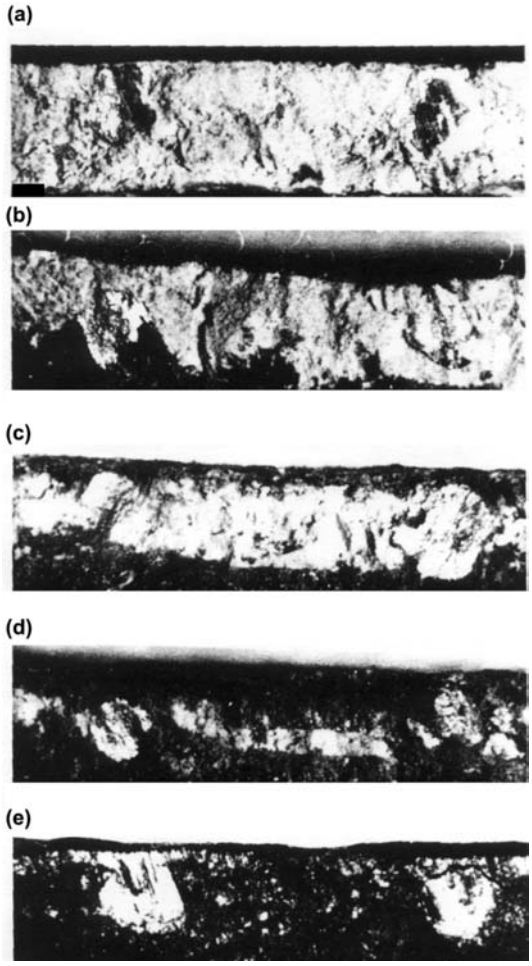

Fig. 3.45. Photographs of cross-section of negative plate during formation: (a) prior to formation; (b)–(d) during different formation stages, dark regions are $Pb + PbSO_4$ zones; (e) completely formed plate [56]. Plate thickness is 1.8 mm. This is a vertical cross-section of the plate.

$Pb + PbSO_4$ zones, the latter will progress towards the interior of the paste. These zonal processes are illustrated in Fig. 3.45.

The question arises as to when does the second stage of formation start? Does this occur when PbO and 3BS in the plate are completely depleted, or does it begin earlier? In an attempt to find the answer to this question, the changes in $PbSO_4$ distribution throughout the cross-section of the plate during formation have been followed by means of electron microprobe analysis [56]. These changes in $PbSO_4$ content after each 2 h of formation are shown in Fig. 3.46. During the first 4 h of formation, $PbSO_4$ is formed only in the surface layers of the plate and the resulting $Pb + PbSO_4$ zones grow towards the interior of the plate. After 6 h, the $PbSO_4$

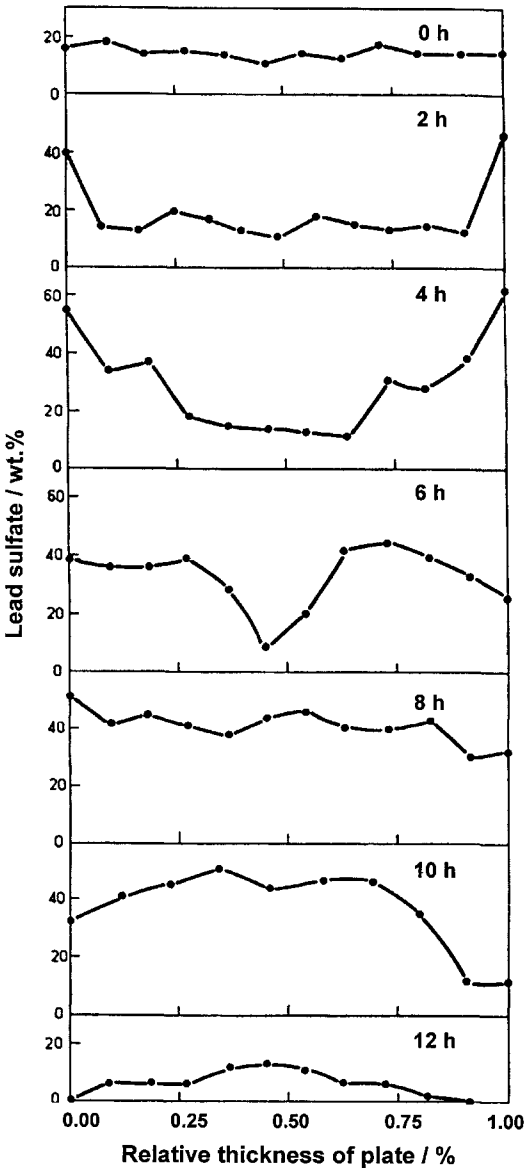

Fig. 3.46. Changes in $PbSO_4$ distribution through cross-section of plate during formation [56].

content in the surface layers begins to decrease, *i.e.*, the reaction $PbSO_4 \rightarrow Pb$ proceeds, though the PbO and 3BS phases in the inner plate layers have not yet fully reacted. This indicates that two reaction layers have formed — one in the interior of the plate where Pb is produced as a result of the electrochemical reactions of PbO and the reduction of 3BS (first stage), and a second reaction layer near the plate surface where $PbSO_4$ is reduced to Pb. With time of formation, the first reaction

layer disappears as the amounts of PbO and 3BS are exhausted, and the second reaction layer grows towards the interior of the plate. Through model investigations, it has been established that these phenomena are due to impeded transport (diffusion and migration) of the H^+ and SO_4^{2-} ions into the plate interior [57].

3.4.4. Structure of negative active mass

The morphology of the crystals in the $Pb + PbSO_4$ zone during the first stage of negative-plate formation has been investigated by means of scanning electron microscopy. An electron micrograph of the crystal structure of the $Pb + PbSO_4$ zone is shown in Fig. 3.47 [55]. The $PbSO_4$ crystals exhibit miscellaneous morphology. Part of the negative plate has been immersed in a boiling saturated solution of ammonium acetate for 30 min to allow all divalent compounds to dissolve and leave only the lead phase. The structure of this lead phase (Fig. 3.48) consists of a network (skeleton) of bonded crystals of irregular shape. The length and width of the separate branches is 3–10 and 2–5 μm, respectively. If Figs. 3.47 and 3.48 are compared, it becomes evident that the $Pb + PbSO_4$ zone is composed of a network of Pb crystals that is covered with $PbSO_4$ crystals.

The lead structure of a completely formed plate is presented in Fig. 3.49. Small, dendrite-shaped lead crystals are formed from $PbSO_4$ during the second formation stage. These crystals grow on the lead skeleton surface. Therefore, it can be assumed that the negative active-mass (NAM) consists of a skeleton of primary lead crystals that are bonded to each other and to the plate grid, and are covered with small secondary lead crystals. The lead crystals in a completely charged plate, after 10 charge–discharge cycles at a current density of $5\,mA\,cm^{-2}$, are shown in Fig. 3.50. A comparison between Figs. 3.49 and 3.50 shows that the overall appearance of the lead crystals after cycling is different from that after formation. This difference is due to the different H_2SO_4 concentrations in which the lead crystals have been formed during plate formation and cycling.

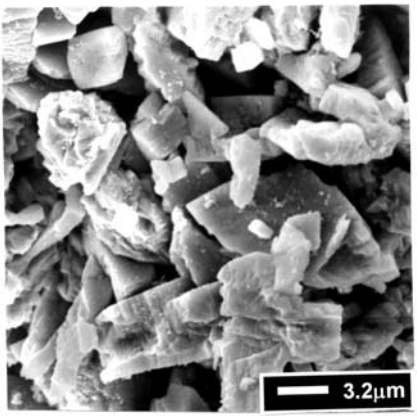

Fig. 3.47. Scanning electron micrograph of crystals within $Pb + PbSO_4$ zone during first stage of formation of negative plate [55].

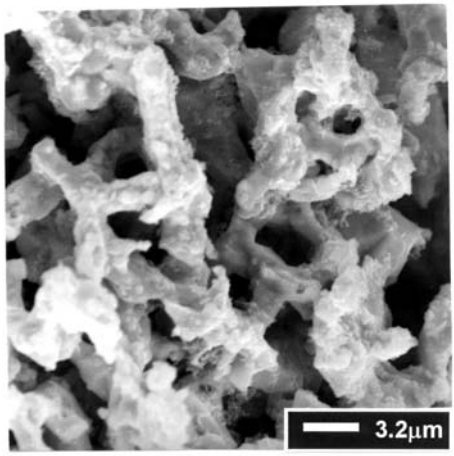

Fig. 3.48. Scanning electron micrograph of lead skeleton obtained during first formation stage [55].

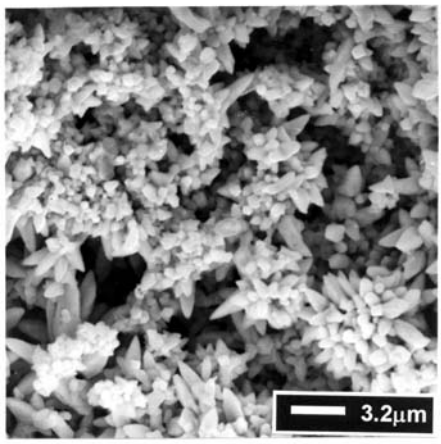

Fig. 3.49. Scanning electron micrograph of lead crystals in completely formed negative plate [55].

The morphology of the crystals in the discharged active mass is shown in Fig. 3.51. Densely packed $PbSO_4$ crystals (1–4 μm) are observed in the micrograph. The morphology of the lead crystals located beneath has been determined after dissolving the $PbSO_4$ in ammonium acetate solution. An electron micrograph of this lead substructure is given in Fig. 3.52. A comparison of Figs. 3.48 and 3.52 reveals that the lead structure obtained during the first formation stage has been but slightly affected during charge–discharge cycling. The lead skeleton has a double function: it serves as a current-collector for all parts of the active mass and provides mechanical support to the lead crystals which participate in the current-generation process. It has been established that the capacity of the plate is equivalent to the amount of electricity

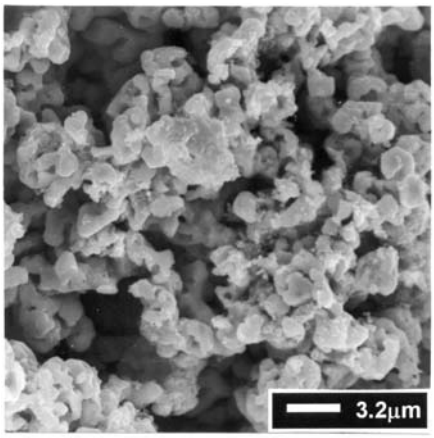

Fig. 3.50. Scanning electron micrograph of lead crystals in charged negative plate after 10 charge–discharge cycles [55].

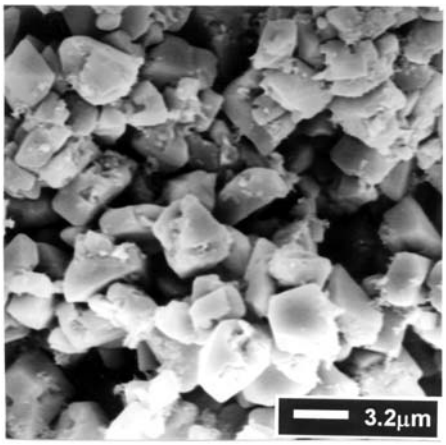

Fig. 3.51. Morphology of crystals in fully discharged negative plate [55].

obtained during the oxidation of the secondary lead structure. Only 10–15% of the lead skeleton structure participates in the current-generation process. Thus, the secondary lead structure has been identified as the 'energy providing' structure.

During pasting of the grids, the paste is homogeneous in all parts of the plate. During formation, however, the electrochemical processes occur in two stages. Due to the different equilibrium potentials of the divalent lead compounds contained in the paste, different products are formed during these processes. Micro-heterogeneity is thus created by the occurrence of a primary and a secondary structure [55]. During battery operation (charge–discharge cycling), these two structures play different roles. It may be expected that the capacity, power, and cycle-life of the plate will depend on the relative proportions of these structures. By keeping an optimum ratio

between these two structures, it is possible to maintain stable operating parameters of the negative plates.

The secondary structure of the negative plate builds up and disintegrates during each charge–discharge cycle. On the other hand, the skeleton structure changes slowly throughout the cycle-life of the battery. Hence, the primary structure created during the first stage of formation constitutes the 'memory' for the technology of negative-plate manufacture [55].

3.4.5. Evolution of pore structure of plate during formation

The changes in molar volume on conversion of one lead compound into another or on reduction to Pb are given in Table 3.2 [15]. The molar volume increases during the reactions of sulfation and decreases during the electrochemical reaction of reduction of lead compounds to lead.

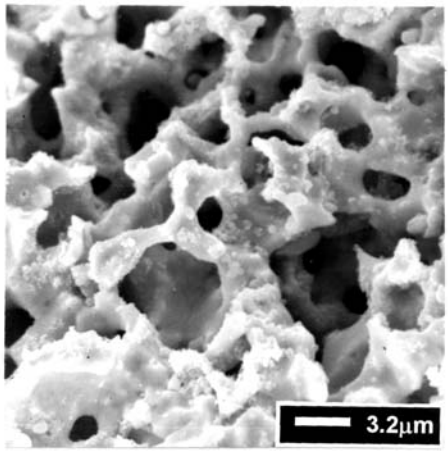

Fig. 3.52. Scanning electron micrograph of skeleton of discharged negative plate after dissolving $PbSO_4$ crystals [55].

Table 3.2. Volume changes during formation of lead [15].

Reaction		Relative volume change with respect to initial product (%)
Starting product	End product	
PbO	Pb	−23
	$3PbO{\cdot}PbSO_4{\cdot}H_2O$	+60
	$PbSO_4$	+100
$3PbO{\cdot}PbSO_4{\cdot}H_2O$	Pb	−52
	$PbSO_4$	+23
$PbSO_4$	Pb	−60

Changes in pore-volume distribution by radius during formation of a negative plate have been determined for both the surface layers and the interior of the plate. The results are presented in Fig. 3.53 [56]. Prior to formation, the pore radii vary between 0.1 and 0.3 μm; after formation, they are in the range 0.6–4 μm. The two stages of formation can be clearly distinguished by the behaviour of the porograms. During the first formation stage (first 6 h), the total pore volume in the surface layers of the plate decreases slightly. This indicates that the rate of the chemical reaction of $PbSO_4$ formation is higher than that of the formation of Pb. After 8 h, the reaction of Pb formation becomes dominating both in the surface layers and in the interior of

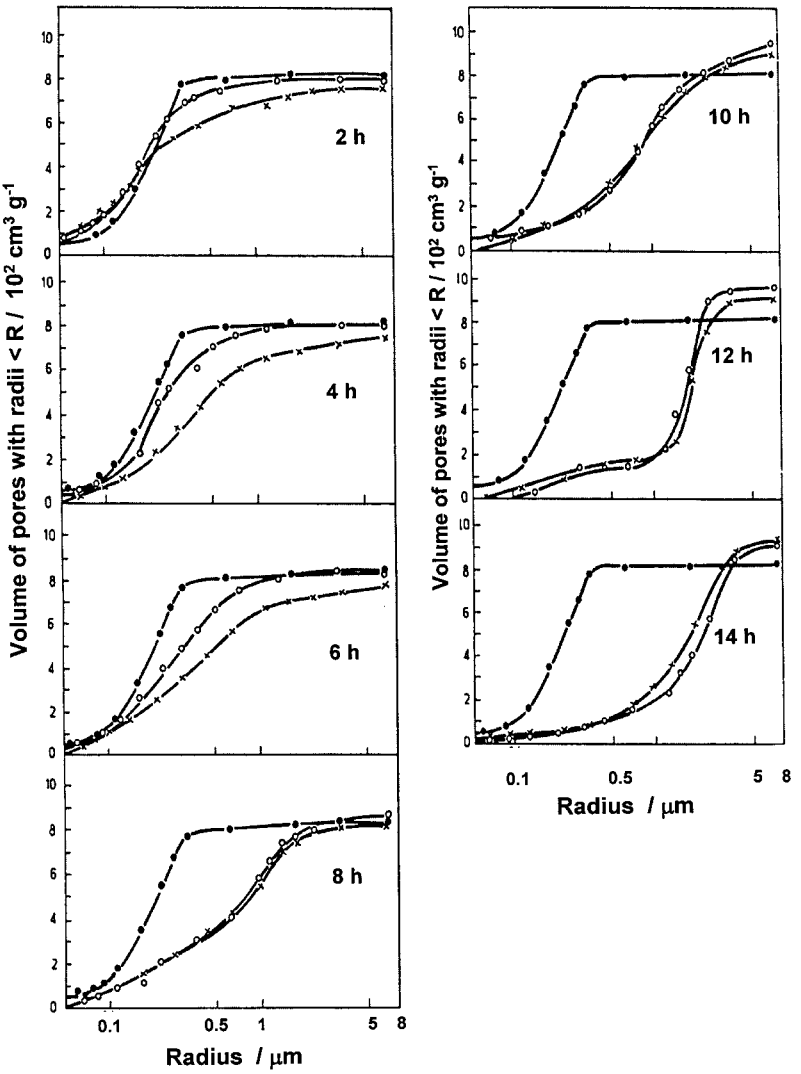

Fig. 3.53. Changes in pore volume and pore-size distribution on formation of NAM: (●) unformed plate; (○) plate surface layers; (×) plate interior [56].

the plate, whilst the rate of the reaction of paste sulfation decreases sharply or ceases altogether as the 3BS and PbO phases become exhausted. The total pore volume increases and so does the average pore radius after 10, 12, and 14 h of formation (Fig. 3.53).

3.4.6. Effect of expanders on NAM

The NAM contains some additives, i.e., 0.2–2.0 wt.% $BaSO_4$ (most often 0.8 wt.%), 0.2–0.3 wt.% carbon, and 0.2–0.5 wt.% chemically treated lignins or their derivatives. The lignin additive has the highest activity and hence it is often called the 'expander'. The expander improves the capacity performance of the plates at low temperatures and high charge currents (cold-cranking ability), and also prolongs the life of the battery on cycling. Expanders exert a strong influence on the crystallization processes of Pb on charge and of $PbSO_4$ on discharge [58–67]. They also suppress the formation of β-PbO and 4BS crystals [20,68].

How does the organic expander affect the skeleton and the secondary structure? Negative plates with or without expander (lignosulfonate) have been investigated. The changes in potential (*vs.* $Hg|Hg_2SO_4$ electrode) and the content of $PbSO_4$ during formation are presented in Fig. 3.54 for negative plates with and without expander [66]. Formation of the plates containing expander is completed within 10 h, while those without expander require 12 h of formation. Hydrogen evolution starts on plates with expander at an overpotential which is 160 mV more negative than that on plates with no expander.

The dependence of plate potential on current density during the first and the second formation stages is presented in Fig. 3.55 [66]. The processes of PbO and 3BS reduction during the first stage of formation proceed at a lower potential in the plates without expander. The same tendency is observed with the reduction of $PbSO_4$ to Pb. This indicates that the expander impedes all the electrochemical reactions involved in the formation process.

The morphology of the Pb crystals that build up the NAM skeleton for plates with or without expander is presented in Fig. 3.56. A more pronounced roughness of the skeleton surface is observed in expander-containing plates. Different expanders yield different NAM skeletons, which may serve as a 'memory' of the technology of plate production [66].

The secondary lead structure of the completely formed plates with or without expander is shown in Fig. 3.57. In NAM without expander, the secondary lead structure covers the skeleton in the form of a smooth layer, whereas the secondary lead structure in the NAM of expander-containing plates comprises individual Pb crystals which are located over the skeleton structure. Hence, organic expanders regulate the processes involved in the formation of both types of structure in the lead active-mass during the formation of negative plates.

In VRLA batteries, oxygen reaches the negative plates and is reduced to form water. It also oxidizes the expander and thereby produces carbon dioxide. Consequently, the morphology of the secondary Pb crystals is changed and they become dendrite-like, similar to those shown in Fig. 3.57(a). This results in capacity

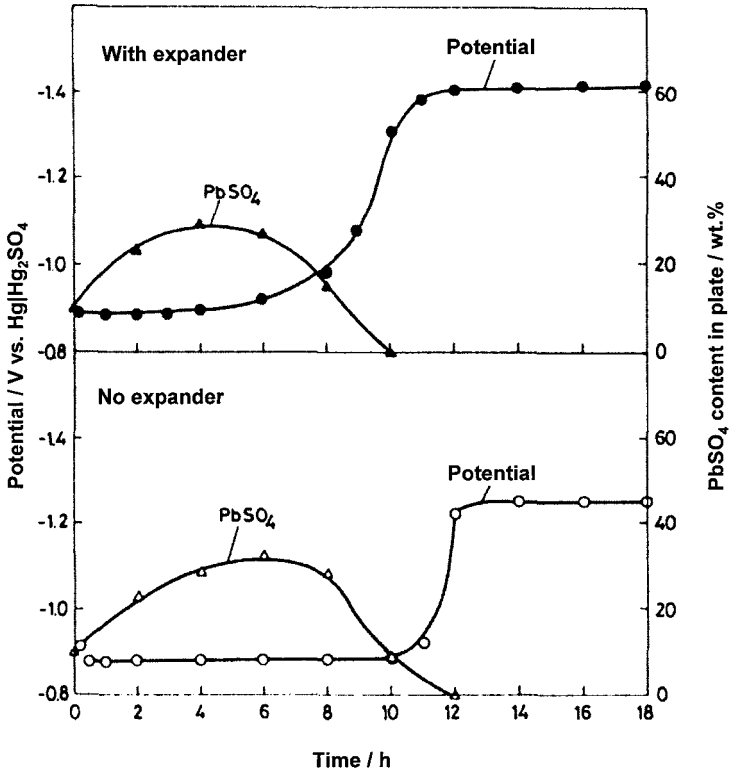

Fig. 3.54. Changes in plate potential and $PbSO_4$ content on formation of NAM with or without expander [66].

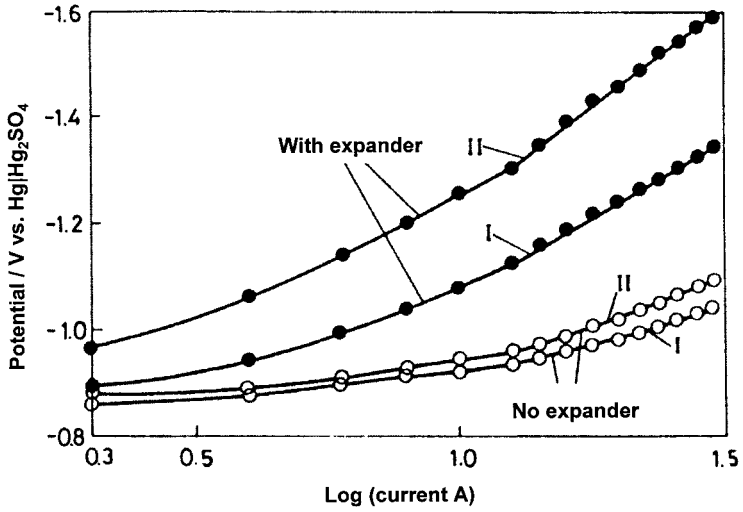

Fig. 3.55. Polarization curves during second hour (first stage — I) and seventh hour (second stage — II) of formation of negative plates with or without expander [66].

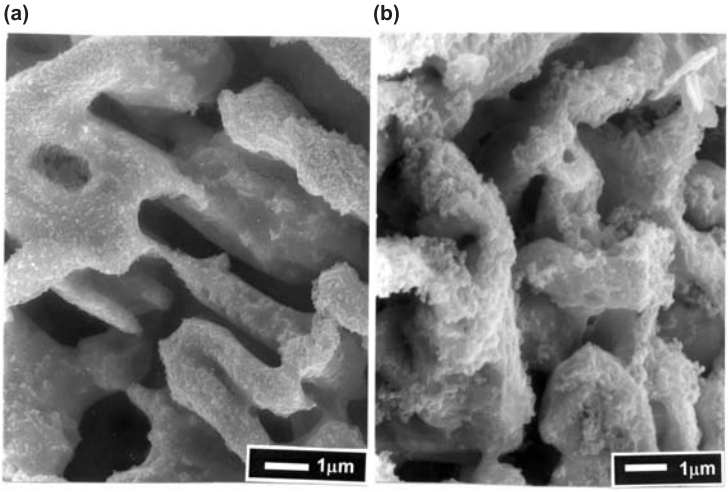

Fig. 3.56. Scanning electron micrographs of skeleton structure of NAM formed during first formation stage: (a) no expander; (b) with expander [66].

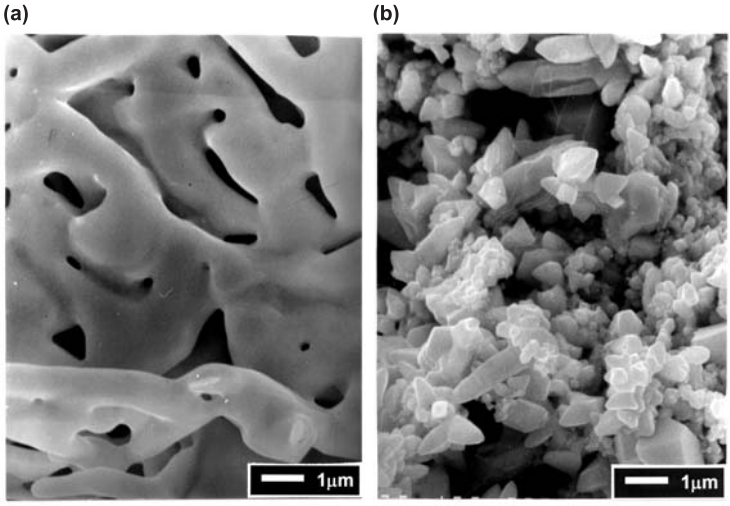

Fig. 3.57. Morphology of crystals of secondary lead structure formed in plates during second formation stage: (a) no expander; (b) with expander [66].

loss and often the cycle-life of VRLA batteries is limited by the type and chemical stability of the expander.

The most widely used expander for automotive batteries is Vanisperse A (VS-A) produced by Borregaard LignoTech (Norway). By contrast, a great variety of expanders is used by manufacturers of industrial and standby batteries. In the case of batteries for cycling applications, the use of an expander blend of Indulin and VS-A guarantees a much longer cycle-life than when the two organic substances are used

alone [69]. The choice of an appropriate expander for a given type of battery is very important for the overall performance of the battery.

3.4.7. Effect of expander structure on battery performance

Organic expanders are complex polymer substances which contain different functional groups such as methoxy, phenolic, carboxy, ketonic, and carbinol groups. The correlation between the structural groups that build the different expanders and the performance of the negative plates (e.g., capacity, CCA, cycle-life, self-discharge, charge-acceptance) is very complex [62–65,67,70–75, see also Chapter 5]. Lignosulfonates contain a great number of functional groups that occupy different positions in the structure of the expander and these active groups affect battery performance in different ways, depending on their position in the polymer structure, and the physicochemical, electrochemical, and crystallization processes involved in the formation and disintegration of the NAM structure.

Through studying the influence of eight members of a family of expanders on the performance of automotive batteries (according to the DIN43539-2 test protocol), a correlation has been found between the content of the different structural groups in the expander and the performance of the battery [73,74]. Expanders with low average molecular weight (LMW) have the greatest beneficial effect on battery performance. Smaller molecules adsorb to the surface of Pb or $PbSO_4$ faster than polymer molecules with higher molecular weight (HMW). Smaller molecules are more mobile and have a better chance of adsorption on the lead nuclei and the growing crystals. Hence, in batteries, which are subjected to continuous cycling (i.e., they are in a dynamic state), expanders with LMW have a stronger effect on the NAM performance than do HMW expanders.

On the other hand, the HMW polymer fractions are adsorbed preferentially on the lead surface under equilibrium conditions [73]. A large molecule has many points of contact with the surface and adheres more tightly to it. A large polymer molecule has less freedom in solution. Hence, smaller polymer molecules will first be adsorbed on the lead surface and then these molecules will gradually be substituted by larger ones. Due to the above processes, the beneficial effect of the expanders on the performance of standby batteries will differ from their influence on automotive batteries.

It has been established that an increase in the carboxylic acid group (–COOH) content in the expander leads to an increase in capacity and a decrease in the self-discharge of plates. Methoxy groups ($-O\cdot CH_3$) render the expander more hydrophobic and consequently, the voltage during the 30 s of the CCA test decreases. The higher the organic sulfur content in the expander, the higher is the rate of the self-discharge processes. Phenolic groups (Ar–OH) improve the cycle-life performance of automotive batteries, but reduce charge-acceptance and accelerate self-discharge. It has also been established that the higher the purity of the lignins, the higher are the CCA performance parameters and the longer the cycle-life of the negative plates [73]. From these observations, it follows that an appropriate expander with optimum functional group content and average polymer molecular weight should be selected for each type of battery so as to achieve optimum battery performance.

3.5. Technology of Formation

3.5.1. Technological parameters of formation process

The following parameters play an essential role in the technology of formation.

(i) *Formation current*. This determines the rates of the electrochemical reactions as well as those of the chemical reactions caused by the electrochemical ones, that proceed in both types of plate. The formation current algorithm takes account of the different stages during which the various structural elements (i.e., corrosion layer, adjacent PAM layer, two types of active material) are formed. An appropriate current profile should yield optimum performance parameters for the plates, but should also shorten the duration of the formation procedure and minimize the amount of water that decomposes during this step. The maximum admissible current density is limited by the temperature and the battery voltage.

(ii) *Battery voltage*. Battery voltage should be lower than that which causes intense evolution of hydrogen and oxygen as such gassing would increase energy losses and harmful emissions to the environment. The voltage limit for formation depends on the temperature, the type of grid alloy, the H_2SO_4 concentration and the phase composition of the pastes.

(iii) *Temperature*. The temperature of formation should not exceed 55–60°C. Otherwise, the performance of the battery will be impaired. This temperature limit should be taken into account when selecting the formation current. Elevated temperatures reduce the voltage of water decomposition and temperatures higher than 65–70°C reduce the cold-cranking ability of the battery.

(iv) *H_2SO_4 concentration*. The H_2SO_4 concentration exerts an influence on the processes of sulfation of the plates during soaking and formation, and hence on the structure and phase composition of the active masses.

(v) *Quantity of electricity flowing through plates*. This quantity should amount to between 1.7 and 2.5 times the theoretical capacity of the plates and depends on the thickness of the plates, the phase composition of the cured paste, the size of the particles which constitute the individual phases, and the current and voltage algorithms of formation.

Each of the above parameters exerts an influence on the formation of the structure of the active masses and on the nature of their interfaces with the grids. Thus, the parameters affect the performance of the battery. The algorithm of the formation should take into account the zonal processes that occur on both types of plate so as to ensure the formation of appropriate active-mass structures, which would guarantee high battery performance characteristics.

3.5.2. Stages of formation of positive and negative plates

Positive-plate formation. As discussed earlier (Figs. 3.16 and 3.17), zonal processes occur during formation of the positive plates. In the case of the positive-plate

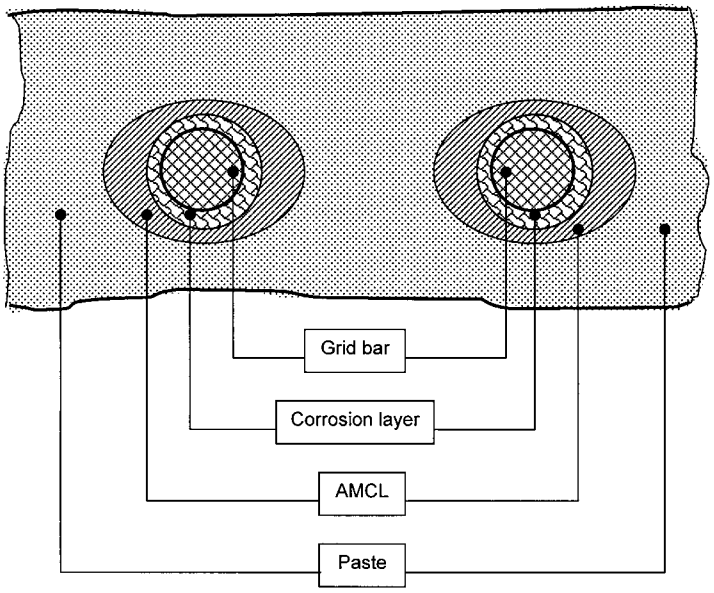

Fig. 3.58. Schematic of cross-section through structure of positive plate during formation.

structure presented in Fig. 3.58, these processes can be summarized as follows.

(i) First, a corrosion layer is formed around the grid bars.
(ii) Next, the active-mass layer which contacts the corrosion layer is formed. This layer is called the 'active-mass collecting layer — AMCL' [76] and its role will be discussed later.
(iii) The final stage is formation of the volume of the cured paste. The reactions which proceed during this stage are presented schematically in Figs. 3.14 and 3.15, and by eqns. (19)–(21).
(iv) When a small part of the cured paste remains unformed, the potential of the positive plate starts to increase and reaches the values at which decomposition of water and evolution of oxygen proceed.

The processes that occur during each of these stages should be taken into account when establishing the current (voltage) algorithm for formation of positive plates. The specific current and voltage values for the different formation stages are discussed below in Section 3.5.3.

Negative-plate formation. The stages in the formation of negative plates have been determined in terms of the zonal processes as presented in Fig. 3.45. The reactions involved in each of the formation stages are presented schematically in Figs. 3.43 and 3.44, and are summarized in Fig. 3.59. The formation can be divided into the following stages.

(i) First, a contact lead layer is formed on the grid surface.
(ii) Then, a lead skeleton and a $Pb + PbSO_4$ zone begins to grow from this layer and covers both plate surfaces.

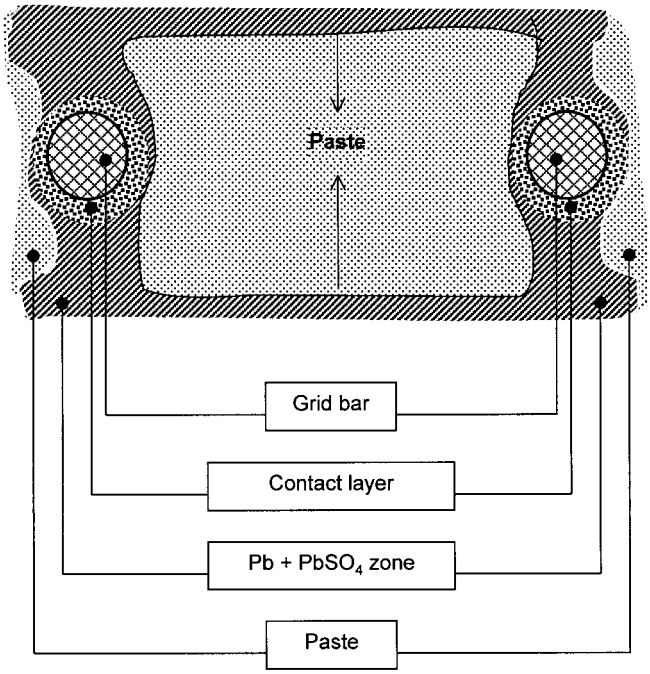

Fig. 3.59. Schematic of cross-section through structure of negative plate during the formation stage when $Pb + PbSO_4$ zones have covered the whole plate surface.

(iii) When the plate surface is covered by the $Pb + PbSO_4$ zone, the direction of growth of the Pb skeleton changes towards the interior of the cured paste. With progress of the growth front deep into the plate core, the resistance of the electrolyte filling the pores of the $Pb + PbSO_4$ zone increases. In order to keep the current constant, the potential of the negative plates increases and when it exceeds the equilibrium potential of the $Pb|PbSO_4$ electrode, a second reaction layer is formed and reduction of $PbSO_4$ to Pb commences. This process starts at the plate surface and advances towards the interior of the $Pb + PbSO_4$ zones [57].

(iv) When PbO and 3BS are reduced to a Pb skeleton and $PbSO_4$ crystals are formed, which in turn are reduced to Pb, the plate potential increases to values higher than the potential for H_2 evolution and water decomposition commences.

The current and voltage algorithm should account for the above stages of the formation process. Formation of the NAM results directly in the formation of Pb (cf., reaction schemes in Figs. 3.43 and 3.44) and the processes involved are not complicated. This is not the case, however, with the formation of the positive plates. As is evident from the reaction schemes presented in Figs. 3.14 and 3.15, the formation process of the positive plates involves a number of chemical reactions (reactions (19)–(21)), which result in the formation of PbO_2 with a gel–crystal form.

These processes depend strongly on the local conditions at a given site within the plate and lead to the formation of different macrostructures. That is why a more complex algorithm is needed for the current and voltage of formation of the positive plates. Hence, the overall battery (formation tank) algorithm should be based mainly on that required for positive-plate formation. The individual stages in this algorithm will be outlined below.

3.5.3. General current (voltage) algorithm for formation of positive plates

The algorithm is based on the structure of the positive plate as presented in Fig. 3.58. Changes in the potential of positive plates (125 g paste per plate) have been monitored during plate formation. The plates were produced with 3BS and 4BS pastes of two densities, viz., 4.0 and 4.3 g cm^{-3}. The electrolyte used was H_2SO_4 of rel. dens. 1.06. The duration of the soaking step was 2 h. Formation was conducted with a constant current of 12 mA g^{-1} of cured positive paste [5]. The initial positive-plate potentials during constant-current formation and the capacities of the plates on the first, second, and eighth cycles are given in Fig. 3.60.

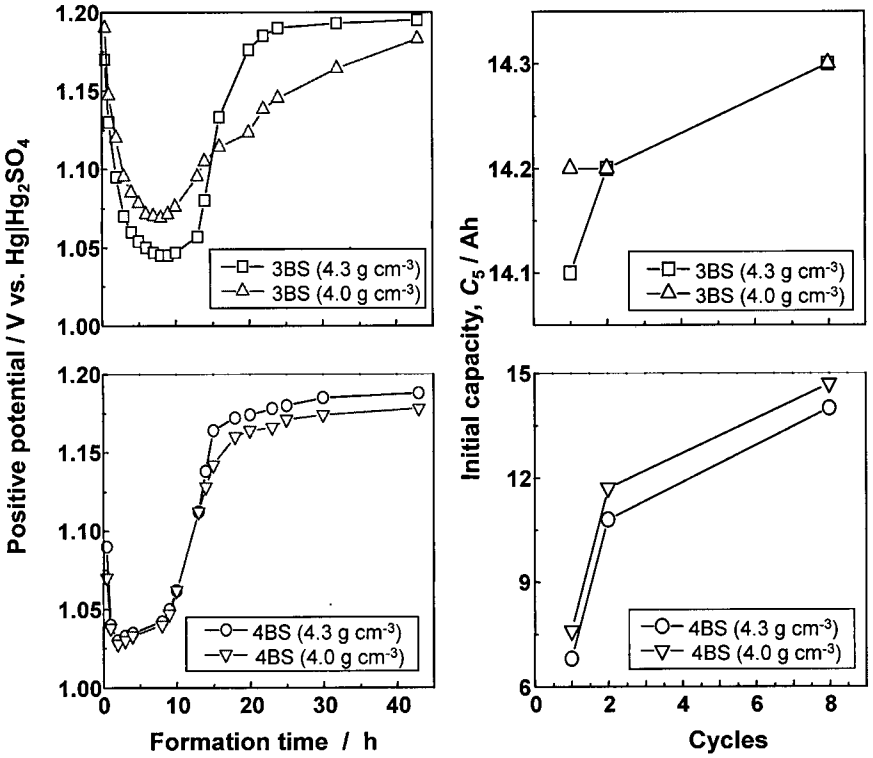

Fig. 3.60. Positive-plate potential during constant-current formation and initial capacity of four different types of cured pastes [5]. The former data show the decline in potential after the maximum value.

In view of the potential–time curve profile, as well as the reaction schemes and zonal processes presented in Figs. 3.13 to 3.17, and the structure of the plate as shown in Fig. 3.58, formation can be divided into four stages.

(i) *Formation of corrosion layer* (*initial*). The potential passes through a maximum and declines thereafter. According to Fig. 3.16, this stage is related to the formation of a corrosion layer on the grid surface. As the only electron conductor in the cured paste is the grid (current-collector), and its surface is small, the current density at the beginning of formation will be high. Consequently, the polarization of the positive plate will be high. The corrosion layer forms mainly during the curing process. It is composed of PbO and $Pb(OH)_2$, in amounts that depend on the conditions of curing. These compounds are electron insulators. For their oxidation to PbO_2, the potential increases abruptly and when the corrosion layer is oxidized to PbO_2 and the latter comes into contact with the solution, the active surface increases and the polarization of the plate decreases. The potential curve passes through a maximum and declines thereafter. The basic problem during this formation stage is the creation of a homogeneous corrosion layer all over the grid surface, with a thickness above a certain critical value. In order to prevent high polarization of the plate, which may lead to intense oxygen evolution, and detachment of the cured paste from the grid, the current density during this initial period should be low (0.02–0.05 C, where C is the rated capacity). The current value and the duration of this initial period depend on the type of grid alloy used. Pb–Sb grids are oxidized at a higher rate, and a thick corrosion layer is formed on their surface relatively quickly during plate curing. When the thickness of the layer is above a certain critical value, it is resistant to the mechanical influences during the first charge–discharge cycles.

Corrosion of Pb–Sn–Ca grids proceeds at a low rate, and the thickness of the corrosion layer obtained during the curing step is below the critical value, hence it cracks easily, its contact with the PAM is impaired, and the PCL-1 effect occurs on cycling of such plates. To avoid this phenomenon, a thick corrosion layer should be formed on the surface of Pb–Sn–Ca grids during plate curing. This can be achieved by introducing into the curing procedure a step of treating the plates (either 3BS or 4BS) at high temperature in the presence of oxygen and water steam. The duration of this step depends on the corrosion rate of the particular grid alloy and the method of grid production, and it is aimed at formation of a corrosion layer which is well bound to the 3BS or 4BS paste. During this high-temperature step, CO_2 is supplied along with the air blown into the curing chamber and part of the paste undergoes carbonization. The CO_2 gas is then released on soaking and during the initial stages of formation.

Through formation of the PbO_2 corrosion layer, the electron-conductive surface of the plate increases and thus the current density is reduced and the cell voltage decreases. This allows an increase in the formation current to a higher value (to a rate of 0.2 C) for a certain period of time. The

formation current may be increased step-wise using one, two, or more current steps. The overall duration of this initial period of current increase is about 1–2 h, during which time a quantity of electricity amounting to approximately 1 Ah per plate flows through the battery. This period is needed because of the non-uniform oxidation of the corrosion layer over the grid surface. The outermost parts of the grid oxidize faster than those in the interior of the plate. The oxidation of the corrosion layer to PbO_2 marks the beginning of the oxidation of the cured paste.

(ii) *Formation of the active-mass collecting layer* (*AMCL*). This is an active-mass layer of a certain thickness which is in contact with the corrosion layer. During charge, the AMCL has the function of collecting the electrons generated in the active mass and conducting them through the corrosion layer to the current-collector. During discharge, the AMCL conducts the electrons that come from the grid and pass through the corrosion layer, and then distributes them throughout the PAM [76]. To be able to perform these functions, the AMCL should be composed of a great number of highly conductive, thick skeleton branches, or of a porous shapeless mass. Such a layer can be formed in the presence of high oversaturations of Pb^{4+} ions in the pores of the AMCL, which can be achieved at high formation current densities. The current is kept high (e.g., 0.2–0.3 C) for about 2–3 h or a cell voltage of about 2.35–2.40 V is maintained for 2 h, whereby the current passes through a maximum and is reduced thereafter. During this period, the grid|PAM interface is oversaturated with Pb^{4+} ions, which leads to intense nucleation and growth of small PbO_2 particles. These particles form an AMCL of adequate mechanical strength and elasticity, and of high electrical conductivity.

(iii) *Formation of PAM and NAM*. This period involves the processes that proceed during the two stages of active-mass formation described earlier for both the positive and the negative plates (Figs. 3.13–3.15 and 3.42–3.44). The battery (tank) temperature should be kept below 55°C and the voltage should not exceed 2.60 V per cell. This voltage limit is only provisional and depends on the type of grid alloy. If antimony-free alloys are used, the voltage limit is higher, namely, 2.70 V per cell. The upper voltage limit also depends on the thickness of the plate.

If the temperature rises above 55°C, the formation current should be reduced. When the voltage reaches the upper voltage limit, further formation is conducted at this value and the current declines. During this formation stage, the PAM and NAM skeletons are built and most of the $PbSO_4$ is converted into β-PbO_2 and Pb, respectively. During this period, the amount of electricity that flows through the battery (or formation tank) is equal to about 1.4–1.5 of the theoretical capacity and the formation current is 0.15–0.2 C for most of the time. The current is reduced when intense gas evolution (i.e., that exceeding an acceptable rate) commences. Most formation current algorithms include a pause (rest period) of about 1–2 h at the end of this stage, followed by another 2–4 h of formation with a current of 0.1–0.15 C with certain voltage limitations. Recrystallization processes occur in the PAM and the NAM during the rest

period, as well as desorption of oxygen and hydrogen from the active mass. It is not recommended that a rest period be included in the first stage of formation.

The formation current algorithm should also include one charge–discharge cycle when processing: (i) 4BS-cured pastes with large crystals; (ii) 3BS-cured pastes with considerable PbO content, which forms a porous mass with a small surface-area; (iii) thick plates. In these three cases, when 1.8–2.0 of the theoretical electricity passes through the plates, a formation efficiency of 72–78% PbO_2 is usually reached and intense water decomposition proceeds. In order to 'open' new surfaces of the non-formed cured paste to the solution, the battery (formation tank) is discharged to 40–60% DoD and is then recharged to 120–140%. As a result of these steps, the quantity of electricity that passes through the battery plates during the formation process increases to 2.3–3.0 of the theoretical value. Such batteries reach their rated capacity within the first three cycles.

(iv) *Water decomposition*. During this fourth stage of formation, the reactions of water decomposition predominate. The overvoltage of hydrogen and oxygen evolution depends on the formation current, the temperature, and the additives to the grid alloy and to the paste. Organic additives increase the overpotential of hydrogen and oxygen evolution (see Chapters 4 and 5). These reactions reduce the efficiency of the formation process. Therefore, the rates of these reactions should be kept very low through control of the voltage applied to the battery (or formation tank). Moreover, the evolved hydrogen and oxygen flows may sweep amounts of H_2SO_4 into the atmosphere and thus create serious environmental problems.

3.6. Conclusions

The above formation current (voltage) algorithm has been developed taking into account the processes that are involved in formation as well as the reaction zones in the plate cross-section where these processes take place. This is only a general algorithm. It should be modified to account for the specific type of plate (automotive, traction, or stationary), size and thickness of plate, type of battery (flooded, VRLA), phase composition, and structure of the cured pastes.

The efficiency of a given formation algorithm should be judged not only by the initial capacity and CCA performance of the battery, but also by the profile of the capacity vs. cycle number curve and the cycle-life of the battery. As discussed earlier, the structure of the PAM and NAM and of the grid|active-material interface, which are formed during battery manufacture, though changing substantially on subsequent cycling, still exert a strong influence on the life of the battery. Therefore, elaboration of an appropriate current, voltage, and temperature algorithm for battery formation involves conducting the symphony of processes that take place during formation, so as to ensure the manufacture of positive and negative plates that will endow batteries with high-performance characteristics and long cycle-life.

References

1. R.D. Prengaman, Chapter 2 of this book.
2. H. Bode, in: R.J. Brodd, K. Kordesch (Eds.), *Lead–Acid Batteries*, John Wiley, New York, 1977, p. 251.
3. R. Nelson, *Lecture Course on VRLA*, LABAT'99 Conference, Sofia, Bulgaria, June 1999.
4. D. Pavlov, G. Papazov, *J. Electrochem. Soc.*, **127** (1980) 2104.
5. I. Drier, F. Saez, P. Scharf, R. Wagner, *J. Power Sources*, **85** (2000) 117.
6. D. Pavlov, S. Ruevski, T. Rogachev, *J. Power Sources*, **46** (1993) 337.
7. D. Pavlov, I. Pashmakova, *J. Appl. Electrochem.*, **17** (1987) 1075.
8. W.O. Butler, C.J. Venuto, D.V. Visler, *J. Electrochem. Soc.*, **117** (1970) 1339.
9. S. Grugeon-Dewaele, S. Laruelle, L. Torcheux, J.-M. Tarascon, A. Delahaye-Vidal, *J. Electrochem. Soc.*, **145** (1998) 3358.
10. D. Pavlov, *J. Power Sources*, **46** (1993) 171.
11. L.T. Lam, A.M. Vecchio-Sadus, H. Ozgun, D.A.J. Rand, *J. Power Sources*, **38** (1992) 87.
12. L.T. Lam, H. Ozgun, L.M.D. Craswick, D.A.J. Rand, *J. Power Sources*, **42** (1993) 55.
13. S. Grugeon-Dewaele, J.B. Leriche, J.M. Tarascon, H. Delahaye-Vidal, L. Torcheux, J.P. Vaurijoux, F. Henn, A. de Guibert, *J. Power Sources*, **64** (1997) 71.
14. L. Torcheux, J.P. Vaurijoux, A. de Guibert, *J. Power Sources*, **64** (1997) 81.
15. J. Burbank, *J. Electrochem. Soc.*, **113** (1966) 10.
16. D. Pavlov, N. Kapkov, *J. Electrochem. Soc.*, **137** (1990) 21.
17. D. Pavlov, S. Ruevski, *J. Power Sources*, **95** (2001) 191.
18. P. Ruetschi, R.T. Angstadt, *J. Electrochem. Soc.*, **111** (1964) 1323.
19. D. Pavlov, G. Papazov, V. Iliev, *J. Electrochem. Soc.*, **119** (1972) 8.
20. D. Pavlov, in: B.D. McNicol, D.A.J. Rand (Eds.), *Power Sources for Electric Vehicles*, Elsevier, Amsterdam, 1984, p. 328.
21. G. Papazov, *J. Power Sources*, **18** (1986) 337.
22. V.H. Dodson, *J. Electrochem. Soc.*, **108** (1961) 401, 406.
23. A.C. Simon, E.L. Jones, *J. Electrochem. Soc.*, **109** (1962) 760.
24. J.R. Pierson, *Electrochem. Technol.*, **5** (1967) 323.
25. J. Armstrong, I. Dugdale, W.J. McCusker, in: D.H. Collins (Ed.), *Power Sources 1966*, *Research and Development in Non-mechanical Electric Power Sources*, Pergamon Press, Oxford, 1967, p. 163.
26. S. Ikari, S. Yoshizawa, S. Okada, *Denki Kagaku*, **27** (1959) 487.
27. B. Culpin, *J. Power Sources*, **25** (1989) 305.
28. P.T. Moseley, *J. Power Sources*, **64** (1997) 47.
29. K.R. Bullock, W.H. Kao, US Patent 5,045,170, September 3 1991.
30. W.H. Kao, K.R. Bullock, *J. Electrochem. Soc.*, **139** (1992) 4L, 41.
31. K.R. Bullock, T.C. Dayton, Chapter 4 this book.
32. S. Satori, J. Tensuo, *J. Electrochem. Soc.*, **31** (1963) 15.
33. K. Wiesener, W. Hoffmann, O. Rodemacher, *Electrochim. Acta*, **18** (1973) 913.
34. D. Pavlov, G. Papazov, in: *Electrochemical Power Sources*, *Proceedings of First Symposium EPS*, Dum Techniky, Praha, 1975, p. 49.
35. D. Pavlov, E. Bashtavelova, *J. Electrochem. Soc.*, **131** (1984) 1468.
36. D. Pavlov, E. Bashtavelova, *J. Electrochem. Soc.*, **133** (1986) 241.
37. D. Pavlov, E. Bashtavelova, D. Simonson, P. Ekdunge, *J. Power Sources*, **30** (1990) 77.
38. M. Dimitrov, D. Pavlov, *J. Power Sources*, **93** (2001) 234.
39. D. Pavlov, I. Balkanov, T. Halachev, P. Rachev, *J. Electrochem. Soc.*, **136** (1989) 3189.
40. A. Santoro, P. D'Antonio, S.M. Caulder, *J. Electrochem. Soc.*, **130** (1983) 1451.
41. K. Kordesch, *Chem. Ing. Tech.*, **38** (1966) 638.
42. D. Pavlov, I. Balkanov, *J. Electrochem. Soc.*, **139** (1992) 1830.
43. D. Pavlov, E. Bashtavelova, V. Manev, A. Nasalevska, *J. Power Sources*, **19** (1987) 15.
44. D. Pavlov, I. Balkanov, P. Rachev, *J. Electrochem. Soc.*, **134** (1987) 2990.
45. B. Monahov, D. Pavlov, *J. Electrochem. Soc.*, **141** (1994) 2316.

46. W. Mindt, *J. Electrochem. Soc.*, **116** (1969) 1076.
47. P. Faber, *Electrochim. Acta*, **26** (1981) 1435.
48. D. Pavlov, *J. Electrochem. Soc.*, **139** (1992) 3075.
49. D. Pavlov, E. Bashtavelova, *J. Power Sources*, **31** (1990) 243.
50. J.R. Pierson, in: D.H. Collins (Ed.), *Power Sources 2, Research and Development in Non-mechanical Electrical Power Sources*, Pergamon Press, Oxford, 1969, p. 103.
51. D. Pavlov, G. Papazov, *J. Appl. Electrochem.*, **6** (1976) 339.
52. H.J. Vogel, *J. Power Sources*, **48** (1966) 71.
53. R.V. Biagetti, M.C. Weeks, *Bell Syst. Tech. J.*, **49** (1970) 1305.
54. G. Papazov, D. Pavlov, B. Monahov, *Proc. Vol. II, 4th ALABC Members & Contractors Conference*, Scottsdale, AZ, USA, April 1999, p. 425.
55. D. Pavlov, V. Iliev, *J. Power Sources*, **7** (1981/82) 153.
56. D. Pavlov, V. Iliev, G. Papazov, E. Bashtavelova, *J. Electrochem. Soc.*, **121** (1974) 854.
57. D. Pavlov, *J. Electroanal. Chem.*, **72** (1976) 319.
58. A.C. Simon, S.M. Caulder, P.J. Gurlusky, J.R. Pierson, *Electrochim. Acta*, **19** (1974) 739.
59. J. Burbank, A.C. Simon, E. Willihnganz, in: P. Delahay, C.W. Tobias (Eds.), *Advances Electrochem. Engineering*, *Vol. 8*, Wiley Interscience, New York, 1971, p. 229.
60. A.C. Zachlin, *J. Electrochem. Soc.*, **98** (1951) 321.
61. E. Willihnganz, *Trans. Electrochem. Soc.*, **92** (1947) 148.
62. E.G. Yampol'skaya, M.I. Ershova, I.I. Astakhov, B.N. Kabanov, *Elektrokhim.*, **2** (1966) 1211; **8** (1972) 1209.
63. B.K. Mahato, *J. Electrochem. Soc.*, **127** (1980) 1679.
64. T.F. Sharpe, *Electrochim. Acta*, **1** (1969) 635.
65. G.I. Aidman, *J. Power Sources*, **59** (1996) 25.
66. V. Iliev, D. Pavlov, *J. Appl. Electrochem.*, **15** (1985) 39.
67. D. Pavlov, S. Gancheva, P. Andreev, *J. Power Sources*, **46** (1993) 349.
68. D. Pavlov, I. Iliev, *Elektrokhim.*, **11** (1975) 1627.
69. Central Laboratory for Electrochemical Power Sources, Bulgaria, S.E.A. Tudor, Politecnico di Torino, *Brite/Euram Project BE97–4085*, *Task 3 Improvements in negative plate performance*, *Annual Report 1 January 1999 to 31 December 1999*, Advanced Lead-Acid Battery Consortium, Research Triangle Park, NC, USA, 2000.
70. E.J. Ritchie, *J. Electrochem. Soc.*, **127** (1980) 1679.
71. A. Hayeshi, Y. Namura, *Tappi*, **21** (1967) 393.
72. D. von Borstel, G. Hoogenstraat, W. Ziechmann, *J. Power Sources*, **50** (1994) 131.
73. D. Pavlov, B.O. Myrvold, T. Rogachev, M. Matrakova, *J. Power Sources*, **85** (2000) 79.
74. B.O. Myrvold, D. Pavlov, *J. Power Sources*, **85** (2000) 92.
75. C. Francia, M. Maja, P. Spinelli, *J. Power Sources*, **85** (2000) 110.
76. D. Pavlov, *J. Power Sources*, **53** (1995) 9.

Valve-Regulated Lead–Acid Batteries
D.A.J. Rand et al., editors

—CHAPTER 4—

POSITIVE-PLATE ADDITIVES TO ENHANCE FORMATION AND BATTERY PERFORMANCE

K.R. Bullock and T.C. Dayton

4.1. Introduction

This chapter reviews the effects of additives in the positive active-material of the lead–acid battery. Common materials found in the oxide and the positive-plate paste, such as lead oxides, basic lead sulfates, and lead carbonate, are not included. Additives and impurities that derive from grid corrosion or from the reaction of the plate with the electrolyte are also beyond the scope of this chapter.

The lead–acid battery has inherent characteristics that make it attractive for many applications. These include high specific power and power density, high volumetric energy density, and low initial cost. One shortcoming of the lead–acid battery, whether in its flooded or valve-regulated (VRLA) form, is its low specific energy (i.e., energy per unit weight). This limits its usefulness in more demanding applications such as in electric-vehicle duty. The theoretical specific energy of the lead–acid battery is $218\,\mathrm{Wh\,kg^{-1}}$ for 100 wt.% sulfuric acid. This value is based on a cell voltage of 2.606 V for 100% sulfuric acid going to 100% water on battery discharge. If it is assumed that 40% sulfuric acid is used and the weight of water is included, then the theoretical specific energy drops to $123\,\mathrm{Wh\,kg^{-1}}$. The specific energy actually achieved depends on the discharge rate but is around 20% of the theoretical capacity. The major reason for the low specific energy is that much of the active material in both the positive and negative plates is not discharged. Thus, non-reacting additives in the active material provide structure and conductivity to the plates, but do not contribute to the cell reaction [1].

4.2. Modelling the Effects of Additives

In an attempt to reach a better understanding of lead–acid batteries and the physical processes that limit capacity, computer programs were developed that simulate the conductivity of the positive active-material and the diffusion of sulfate ions [2].

The ‘conductivity model’ estimates the critical volume fraction of paste that contains non-conducting or conducting additives which are not chemically active. In order to model the conductivity of the active material, the material is assumed to be made of spherical particles and modelled as nodes on a two-dimensional grid. Each node is connected to the surrounding eight nodes by a conductive pathway. The grid

contains over one million nodes, i.e., 1024×1024 nodes. The model randomly chooses a node and attempts to find a conductive pathway to the edge of the grid. If a pathway can be found, the starting node is considered discharged and marked as non-conductive. If a pathway is not found, the starting node is marked as isolated. After all nodes have been selected and pathways have been tried, the model reports the number of nodes that have been either discharged or isolated. The critical volume fraction is calculated as the ratio of discharged nodes to the initial number of available nodes.

The model can take into account any non-conductive additives by initially marking those nodes as discharged. For conductive additives, the model marks those nodes as always conductive. The amounts of additives are given as volume percentages and the size of the individual additive is given relative to the base node size. For example, a non-conductive glass microsphere, approximately 20–50 μm in diameter, is represented as a particle of 10×10 nodes.

Using this model, Fig. 4.1 was created to show the effect on the critical volume fraction of adding conductive and non-conductive additives. This figure shows how different loadings and types of additives can modify the percentage of the active material that can react during discharge. With regards to non-conductive additives, the larger-sized additives are most effective in displacing active material without seriously decreasing the critical volume fraction. If 40% by volume of larger additives were added to the active material, the critical volume fraction would only drop to around 50%. Conversely, for conductive additives, the model predicts the

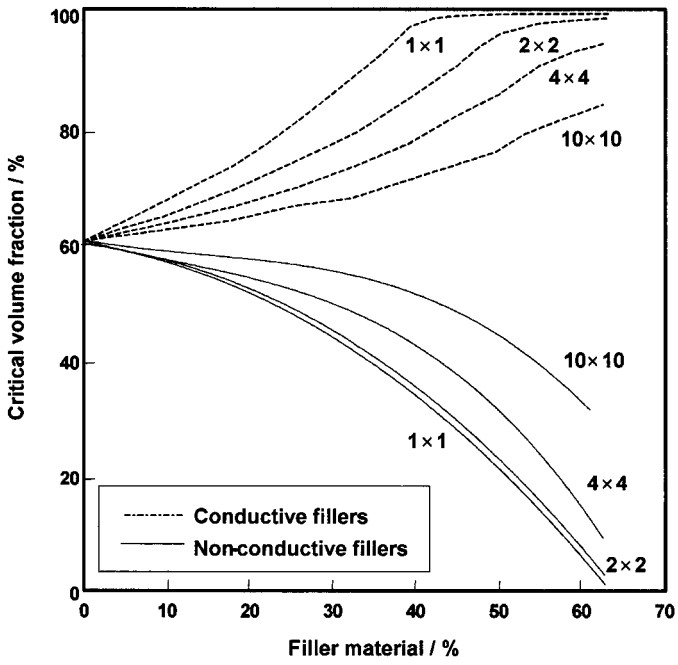

Fig. 4.1. Critical volume fraction with material additives [2].

most performance increase from small particles. The particle size represented by the 1×1 additive would be similar in size to the lead oxide particle. If 40% by volume of these small additives were added to the active material, then nearly 100% of the remaining active material would react.

The conductivity model is limited to a two-dimensional representation and the conductive pathways have no resistance. Additionally the model assumes a homogeneous material without any pores. Even with these limitations, the model has been used to predict the effects of non-conductive additives with good correlation to experimental data [3].

The 'diffusion model' employs finite difference equations and Fick's law to estimate the acid concentration in both the negative and positive active-material, as well as between them as a function of time. The Nernst equation is then used to determine the battery voltage. The model combines diffusion and conductivity parameters, which include the critical volume fraction from the conductivity model, to estimate battery performance over a wide range of discharge rates. The model produces voltage vs. time curves, percentage material reaction curves, and acid concentration plots. The model is helpful in understanding the behaviour of lead–acid batteries and can be used to develop new cell designs. Once the plate and cell parameters are established, the model can predict the performance of the cell and allows for iterations to determine optimum parameter values.

With these two models a battery can be designed, modelled, and optimized for the use of inert additives. Since each type of additive has different effects on battery performance, it is necessary to design the battery to utilize the selected additive to its fullest. The models are also very useful in designing experiments to test the effects that the additives will have on battery performance.

4.3. Non-conductive Additives

Using non-conductive additives, the specific energy can be increased either by minimizing the weight of the battery or by improving the porosity of the plates. Additives replace the lead active-material, which is typically heavier than the additive. If, however, the plate has an excessive amount of the additive, the energy that the plate will deliver is reduced because less active material is available. Non-conductive additives also lower the electrical conductivity of the plate. When the weight is reduced more than the energy, the specific energy of the battery increases. If the porosity of the positive active-material is increased by the additive, the diffusion of electrolyte into the plate is enhanced and thus more of the active material will react, which again increases the specific energy. The magnitude of both these effects depends on both the discharge rate and the battery design.

4.3.1. Hollow glass microspheres

A simple way of reducing the weight of the battery is to use lightweight fillers in the plates. If the filler replaces active material that does not contribute to the energy of the battery, the specific energy can increase dramatically. One type of filler material

Table 4.1. Effect of glass microspheres on performance of positive plates [1].

Plate type	Stoichiometric capacity (Ah)	Measured utilization, $C_{ave.}$ (%)
Production plate	18.96	11.64
Hand pasted, 0 wt.% additive	17.41	5.02
Hand pasted, 1.1 wt.% additive	12.89	24.57
Hand pasted, 2.2 wt.% additive	12.83	30.32
Hand pasted, 4.4 wt.% additive	8.44	33.12
Hand pasted, 6.6 wt.% additive	9.08	19.94

that has been studied is hollow glass microspheres. These spheres have a solid surface, which prevents any liquid from penetrating to their hollow centres. The glass spheres are chemically inert and non-conductive.

In one study [1], positive plates were pasted with varying amounts of glass microspheres added to the active material as a weight percentage of lead oxide. The plates were produced by the hand-pasting of production grids. The cast grids were 4.25 in. high, 4.5 in. wide, and 0.077 in. thick. Each plate was pasted to a thickness of 0.085 in. After curing, one positive plate was combined with two production negative plates to form a cell. Two cells were constructed for each type of plate. The cells contained excess electrolyte and excess negative material to ensure that the positive plate was the limiting component. After the cells were formed, the relative density of the acid was adjusted to 1.3 and the cells were cycled. Each cell was then tested at several rates to evaluate the performances of the plates. The results of the discharge tests are presented in Table 4.1 as percent utilizations. Utilization is determined by dividing the discharged ampere-hours by the stoichiometric capacity of the paste. The data show that the utilization increases when glass microspheres are added to the paste. The increase is greatest at the higher discharge rates and is negligible at the lower discharge rates. The maximum increase in utilization is reached with 4.4 wt.% loading of glass microspheres. The glass microspheres lower the density of the positive paste so that the amount of active material in the plate is reduced while the surface area and pore volume remain essentially unchanged. Therefore, a larger volume of electrolyte for reaction surrounds each gram of active material [1].

One disadvantage to using filler-type additives, such as glass microspheres, is that there will most likely be an increase in the battery volume. The increased volume will degrade the energy density of the battery. Depending on the application, this trade-off may be acceptable.

4.3.2. Carboxymethyl cellulose

Attempts to assist the supply of acid to the positive active-material have focused on increasing the porosity of the paste to enhance diffusion or by providing fine local reservoirs of acid within porous particles throughout the plate [4]. One such

additive is carboxymethyl cellulose (CMC). The effects of adding CMC to positive active-material have been investigated by using flooded cells that each comprised one positive plate and two negative plates. The positive plates were loaded with CMC at 0.2 and 2 wt.% with respect to leady oxide. The addition of CMC was found to increase the water absorption of the paste without decreasing the workability of the paste. This is probably due to the known swelling and dispersion-stabilizing properties of CMC [5]. Capacity tests showed little improvement at 2 wt.% CMC. By contrast, a loading of 0.2 wt.% gave a 10% increase in initial capacity at a high discharge rate ($C/3$) and a 5% increase at a low discharge rate ($C/20$). Poor cycle-life was reported due to the swelling effect of CMC, which weakened the mechanical strength of the active material [6].

4.3.3. Silica gel

Silica gel has also been studied as a porosity-increasing additive [5]. The addition of 0.2 wt.% resulted in improved capacity at both low and high rates. Although the addition of silica gel was not observed to cause significant physiochemical changes to the positive active-material, it is possible that silica gel promotes nucleation which consequently leads to a finer pore structure in the active material. Since this form of silica is porous, the additive may act as an acid reservoir. Further study of silica gel as an additive, especially at high discharge rates, has been recommended [6].

4.3.4. Designer additives

A recently completed research programme examined the use of porosity-enhancing additives. Two types of such additives were tested and reported [7–9]. One additive was an inorganic particle that contains a major amount of silica (ES-60); the other additive was a porous polyolefin (ES-100). Both additives had a maximum particle size of 150 μm and were elongated [7]. The additives were incorporated into hand-pasted, positive plates at 1.5 wt.%. After the plates were cured, 5-plate, flooded cells were assembled and formed in the container. The cells were tested at discharge rates which ranged from 2.5–75 A. The results are shown in Table 4.2 in terms of capacity per unit weight ($Ah\,kg^{-1}$). The data confirm that the additives significantly increase the utilization of positive active-material and thus enhance the capacity. This is most noticeable at the higher discharge rates. Life-cycle testing at constant current

Table 4.2. Effect of additives on performance of positive plates in terms of Ah per kg active material [7].

Current (A)	75	50	18.7	6.3	2.5
No additive	10.3	14.8	54.8	98.2	107.7
ES-60	28.9	34.5	65.7	107.6	118.8
ES-100	19.5	26.5	69.5	113.4	124.3

was then applied to the additive-doped cells. The cell with the ES-100 additive continued to show a 20% improvement over the cell without additive to 140 cycles. The performance of the cell with the ES-60 additive declined rapidly around 50 cycles and failure occurred at 80 cycles.

As these additives showed merit in flooded cells [8], the test was extended to include VRLA batteries of the absorptive glass mat (AGM) design. The additives, ES-60 and ES-100, were incorporated separately in the positive-plate paste at loadings of 2 and 3% by weight of dry lead oxide. Grids of golf battery size (6.625×7.250 in.) were hand-pasted, cured, and tank-formed. Sealed test cells were constructed, each with two positive plates and three negative plates. Compression was maintained on the plates at 40% of the original thickness of the separator. These test cells were cycled 15 times and then discharged at rates similar to those listed in Table 4.2. The resulting capacities showed 17–47% increases over the control cells for the various discharge rates and additive types. After 100 cycles, the capacity tests were repeated. At the higher discharge rates, the capacity was about 20% greater than that of the control cell. When the test cells were loaded with 3 wt.% additive, the resulting capacity was little different from that obtained at the 2 wt.% loading [8].

Tests were also performed using VRLA batteries with gelled electrolyte [9]. The additives gave benefits similar to those obtained with AGM batteries. It was concluded that the porosity additives could have a positive effect on battery capacity. Future work with these additives will continue and involve full-scale batteries.

4.4. Conductive Additives

One of the main reasons for the high power capability of the lead–acid battery is the high conductivity of the active materials. Lead dioxide is a semiconductor with a conductivity of up to 10^3 $(\Omega\ \text{cm})^{-1}$ at room temperature, while 35% sulfuric acid has a conductivity of 0.8 $(\Omega\ \text{cm})^{-1}$. Lead, which is a metallic conductor, is used for both the current-collector and the negative active-material. Because of the high conductivities of these materials, a fully charged lead–acid battery has a resistance of only a few mΩ.

Unfortunately, the lead (II) compounds are not very conductive. Lead sulfate is an insulator and the lead oxides and basic lead sulfates are semiconductors. Before they are given the first charge, called 'formation', battery plates are composed of mixtures of these materials. Plate formation cannot proceed until a conductive pathway is formed. Pavlov and co-workers [10] have shown that in acid solutions, the materials next to the current-collector are first converted to conductive lead and lead dioxide. Formation then proceeds inward towards the centre of the pellet (see Chapter 3). Lead sulfate is the last material to be converted in the formation process. The rate of formation is thus limited by the non-conductive nature of lead oxide, especially in the positive plate.

During discharge, the conductive positive plate is covered with an insulating layer of lead sulfate crystals that precipitate on to the surfaces of the porous lead dioxide. The discharge capacity is limited by the rate of diffusion of acid to the underlying

lead dioxide. Total material utilization of the lead dioxide is also limited by the need to maintain a stable, conductive structure in the plate to conduct current from the reaction site to the current-collector. If the plate becomes too heavily sulfated, it will be difficult or impossible to recharge. Storage of the battery in a discharged condition can exacerbate this problem by allowing the lead sulfate crystals to grow into a 'hard sulfate' with a low surface area.

To overcome these limitations, lead–acid battery researchers have been searching for conductive additives that are stable in the battery environment. The ideal additive would have a conductivity that is at least as high as carbon, a long-range order to minimize the amount of material needed, and stability within the positive plate during formation. It must also not contaminate or degrade the battery during subsequent use. This is a difficult task, since many conductive materials oxidize in the positive plate because of its high potentials and the strongly oxidizing properties of PbO_2 and H_2SO_4.

4.4.1. Barium plumbate

One conductive additive which is relatively stable is barium plumbate ($BaPbO_3$) [11]. This is a ceramic [12] with the perovskite structure and is easily made by standard ceramic-powder technology. Addition of this material to positive plates in a lead–acid battery significantly improves the formation efficiency. The formation mechanism is changed when the conductive particles are dispersed in the plate. Formation not only proceeds from the grid towards the centre of the pellet, but also takes place slowly around the conductive particles in the plate. The conductive paths of PbO_2 grow and make connection with each other during formation to establish a network, which further facilitates the formation.

The beneficial effect of $BaPbO_3$ has been illustrated by the results of a study of the formation of positive plates made from orthorhombic lead oxide (β-PbO), 1 wt.% glassy fibre, and 5.8 M H_2SO_4. The weight ratio of lead oxide to acid was about 9. Because β-PbO is harder to oxidize than typical leady oxides, formation enhancement by conductive additives would be more pronounced. The chemical compositions of plates with and without the conductive additive after formation with 200% theoretical input capacity are listed in Table 4.3. The formation efficiency is significantly enhanced by the additive, as indicated by the higher content of PbO_2. The formed plates were discharged at a current density of about 13.3 mA cm^{-2}, which is equivalent to a 2-h rate to a cut-off voltage of 1.75 V. The results, summarized as the material utilization in the first reserve capacity, are also listed in Table 4.3. The material utilization of the plate with $BaPbO_3$ is the same as that of a completely formed, conventional, positive plate. Without $BaPbO_3$, the material utilization is only 6%.

The formation mechanisms for plates with and without $BaPbO_3$ appear to be different. As shown in Fig. 4.2, the formation of a plate without the conductive additive proceeds from the grid towards the centre of the pellet (Fig. 4.2(a) to (d)); this is consistent with the results of other studies [10]. When the conductive particles are dispersed in the plate (Fig. 4.2(e)), long-range conductive paths are apparently

Table 4.3. Effect of barium plumbate on positive-plate formation [11] (reproduced by permission of *J. Electrochem. Soc., Inc.*).

	Characterization of formed β-PbO plates	
	Without $BaPbO_3$	With 10 wt.% $BaPbO_3$
Chemical content (wt.%)		
PbO_2	43.9	76.0
PbO	16.7	16.5
$PbSO_4$	38.4	4.4
First reserve capacity material utilization (%)	6.0	43.3

Experimental error ± 2% absolute.

established. This will allow formation to proceed not only from the grid but also slowly around the conductive particles inside the plate (Fig. 4.2(f)). As the conductive paths of PbO_2 grow and make connection with each other (Fig. 4.2(g)), a conducting network is formed which further facilitates the formation (Fig. 4.2(h)). The plate with the $BaPbO_3$ additive appears to be completely formed after the passage of about 180% of the theoretical plate capacity.

The effect of loading of $BaPbO_3$ in a positive plate on the formation efficiency is summarized in Table 4.4. The data show that significant improvement in formation starts at a loading level as low as 0.5 wt.%. This formation enhancement increases with $BaPbO_3$ loading and approaches a plateau. Beyond about 7 wt.%, additional $BaPbO_3$ has no influence on the formation efficiency.

Once the battery is formed, a stable conductive additive can enhance the current-acceptance of deeply discharged batteries. This has been demonstrated [12] by the addition of 10 wt.% $BaPbO_3$ to a conventional positive plate made by adding 1.325 rel. dens. H_2SO_4 to a water-based, ball-mill, leady oxide and 0.1 wt.% polyester fibres. The plates were prepared via a standard process for commercial automotive batteries and used to construct flooded test cells with one positive and two negative plates. The cells were first given two cold-cranking tests alternately with three reserve-capacity tests. Then, the cells were discharged over 20 h to 1.5 V, discharged on a 2-Ω resistive load for five days, and finally left on open-circuit at 1.975 V. When subjected to a current-acceptance test to 2.67 V, the cell with $BaPbO_3$ in the positive plate and a control cell without the additive required 2 and 4 min, respectively, to accept 10 A.

The stability of $BaPbO_3$ and its effect on the performance of a battery over its useful life have also been investigated for automotive applications [12–14]. A conventional automotive cell with 1 wt.% $BaPbO_3$ in the positive paste and a control cell were formed by means of a standard high-rate formation procedure. Cell performance was then evaluated by means of a standard Battery Council International (BCI) sequence of reserve capacity and cold-cranking tests. The cell containing $BaPbO_3$ formed three times faster with 12% less input capacity. The BCI test results of the two cells were comparable.

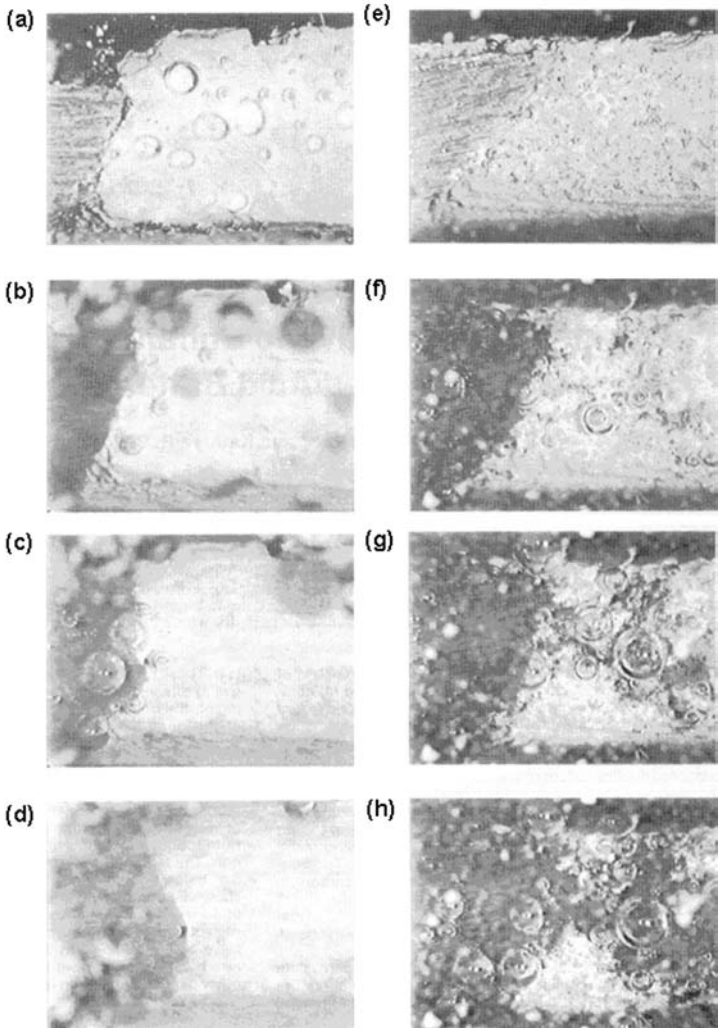

Fig. 4.2. Effect of conductive additive on formation efficiency. Cross-section of positive β-PbO plates without (a) to (d) and with (e) to (h) 10 wt.% $BaPbO_3$ after (a),(e) 0%, (b) 70%, (f) 125%, (c),(g) 144%, (h) 169% and (d) 200% of theoretical capacity is passed. The grid is on the left-hand side. (Reprinted from *J. Electrochem. Soc.*, Vol. 139, No. 4, April (1992) by permission of J. Electrochemical Society, Inc. Photographs courtesy of Johnson Controls, Inc.)

Barium plumbate is electrochemically stable in the positive plate. Chemically, however, it can be slowly attacked by dilute sulfuric acid. The first-order rate constant for decomposition of barium plumbate in dilute sulfuric acid was determined to be $k = 2.6 \times 10^{14} \{H^+\} \exp(-E_a/RT)$, where E_a is 31.6 kcal, R is the gas constant, and T is the absolute temperature. The half-life of this material in

Table 4.4. Effect of barium plumbate loading on positive-plate formation [11] (reproduced by permission of *J. Electrochem. Soc., Inc.*).

$BaPbO_3$ loading (wt.%)	Material utilization (%)
0.0	6.0
0.1	8.7
0.5	22.6
1.0	32.7
2.5	37.4
5.0	41.1
10.0	43.3

Experimental error ± 2% absolute

sulfuric acid of 1.265 rel. dens. at 20°C is estimated from the rate constant to be 3.4 years, but is much less at higher temperature.

The products from decomposition of $BaPbO_3$ in sulfuric acid include $BaSO_4$ and PbO_2. Barium sulfate in a positive plate is known to facilitate the nucleation of lead sulfate and to alter the morphology of the plate (see Section 4.5.1). Cycle-life during 100% DoD testing of a positive plate is shortened if the content of $BaSO_4$ becomes greater than 0.3 wt% [12–14]. Based on the half-life and fraction of barium in the additive, $BaSO_4$ would not reach this detrimental level during the service life of an automotive battery if the loading of $BaPbO_3$ is limited to about 1 wt.%. This was confirmed in 100% DoD cycling of cells formed with positive pastes which contained 0, 1, 2.5, or 5 wt.% $BaPbO_3$. The cell with 1 wt.% $BaPbO_3$ had a cycle-life comparable with the control that had no $BaPbO_3$, while the cells with 2.5 and 5 wt.% exhibited significantly shortened cycle-life.

4.4.2. Titanium oxide

Magneli phase TiO_x ($x = 1.67$ to 1.9) is conductive. A proprietary material of this composition in the form of solid sheets or a honeycomb has been patented for use as current-collectors in either monopolar or bipolar lead–acid batteries [15]. The honeycombed structure holds the paste and thereby improves paste adhesion and the mechanical stability of the plate, as well as the electrical conductivity. The material is stable at the potentials of the positive plate [16,17].

Conductive TiO_x has been evaluated as a positive-plate additive in spirally wound, VRLA batteries of the AGM design [18]. Both fibres and powders at a 2 wt.% concentration were examined in a sequence that consisted of five conditioning cycles, variable rate discharges, polarization, and cycle-life tests. For each additive, 3–6 single cells with nominal capacity of 15 Ah were conditioned by discharging at 7.5 A to a 1.75 V cut-off, followed by a 1.5 A charge to 12 h. In the remaining testing, charging was conducted at constant current (15 A)–constant voltage (2.45 V to 1 A)–constant current (1 A for 1 h). Variable-rate discharges at 1.5, 5, 15, and 25 A were performed to a 1.75 V cut-off. Polarization testing consisted of current pulses

for 10 s (charging and discharging) that were separated by rests for 10 min at 100, 80, 50, and 20% SoC. Cycle-life testing used 15 A discharges to a 1.75 V cut-off. Results showed that discharge capacities were not significantly enhanced by the conductive TiO_x and cycle-life was reduced.

A further disadvantage of TiO_x is the narrow range of non-stoichiometric oxidation states that are both stable and conductive. Uniform oxidation of TiO_x materials is difficult to maintain in a large-scale, commercial, manufacturing process.

The reduction of TiO_2 to the conductive Magneli phases is accommodated by a crystallographic shear process in which two layers of the MO_6 octahedra that compose the oxide move closer together and eliminate a layer of oxygen ions [4]. This systematically generates a number of Ti^{3+} ions that contribute to the conductivity via the mechanism: $Ti^{3+} \rightarrow Ti^{4+} + e^-$. Moseley [4] has suggested two alternative materials for further study: (i) niobium could be substituted on to the cationic sub-lattice of rutile, and donors would be generated by $Nb^{4+} \rightarrow Nb^{5+} - e^-$; (ii) fluorine could be substituted on to the sub-lattice of tin dioxide, and donors would be generated by $Sn^{2+} \rightarrow Sn^{4+} + 2e^-$.

4.4.3. Conductive polymers

Polymeric tubes for clad lead–acid battery plates have been made from intrinsically conductive polymers [19] by weaving fibres of polypyrrole, poly(phenylene vinylene), or polythiophene of several hundred microns in thickness. Polyaniline [20] as well as polypyrrole, polyparaphenylene, and polyacetylene doped with anions (ClO_{4-}, $FeCl_3^-$, AsF_5^-, SO_4^{2-}, and HSO_4^-) have also been added as 1.15 μm powders or fibres to positive pastes to improve capacity [21].

The polymers contained 0.02–0.35 mole fraction of dopant, which gave a typical conductivity of 80 $(\Omega\ cm)^{-1}$. Discharge tests on positive pastes made from PbO and aqueous H_2SO_4 (1.40 rel. dens.) showed higher material utilization when 50 vol.% of conductive polypyrrole was added to the paste. Positive active-material with the additive had 85% material utilization of the PbO_2 and 0.28 Ah, compared with 60% material utilization and 0.40 Ah without the additive [20]. It is evident that the lower capacity without the additive is due to the large volume of inactive polymeric material in the plate. An earlier patent [21] showed that, except for polyaniline, the additives degraded during recharge and could not withstand overcharge. The first and second discharge capacities of plates containing 10 vol.% of either conductive polyaniline or polyparaphenylene are compared in Table 4.5 with those of a control without the additive.

Table 4.5. Effect of conductive polymers on performance of positive plates [21].

Plate composition	First capacity after formation ($Ah\ kg^{-1}$)	Second capacity after 2.5 V charge ($Ah\ kg^{-1}$)
PbO_2	108	114
PbO_2 + polyaniline	117	130
PbO_2 + polyparaphenylene	115	95

The conductive polymers were also tested at levels of 1–3 wt.% in a positive plate which contained $PbSO_4$, α-PbO_2, and β-PbO_2 [22]. The optimum concentration was found to be 1 wt.%. At 2–3 wt.% additive, the discharge capacity was increased by about 30% and the specific surface-area from 3–4 to 5–6 $m^2 g^{-1}$. Cycle-life declined at additive concentrations above 5 wt.% due to mechanical instability of the electrode. Polypyrrole and polythiophene oxidized during overcharge, but polyaniline remained stable.

4.4.4. SnO_2

In the VRLA battery studies described above [18], the plates with the tin dioxide additive showed a slightly higher capacity at the highest discharge rate ($0.6\,C$) applied. The SnO_2 migrated out of the plate during cycling, however, and gave rise to cell failure by shorting.

Tin dioxide doped with about 10 at.% of fluorine is conductive and stable in the positive electrode, but is unstable during cell reversal and in the negative electrode during normal operation. Glass fibres coated with this material have been developed and used in lead–acid battery pastes to improve formation and plate performance [23–25]. The fibres are coated by a spray-pyrolysis process, in which an aqueous solution of $SnCl_4$ is sprayed on to the fibres at 500°C in air [26]. Unwanted impurities, such as iron and chloride ions, are eliminated by rinsing the fibres in sulfuric acid of 1.300 rel. dens. at 70°C and distilled water. The SnO_2 coating is 0.5 to 1 μm in thickness and has a tetragonal (cassiterite) structure. Positive active-material which contains these fibres delivers utilization efficiencies in excess of 50% at the 1-h rate [27]. A 20% increase in utilization at the 5-min rate can be achieved when fibres are added to the positive active-material of bipolar VRLA batteries [28].

4.4.5. Iron boride

Positive plates with a density of 1.15 g cm^{-3} have been made from 8.2 wt.% ball-milled lead oxide, 10 wt.% iron boride, and 8 wt.% polyethylene [29]. The mixture was pressed, sintered, and put in a honeycomb conductive matrix. The battery delivered 60 Wh kg^{-1} with this lightweight electrode. The patent claims that shedding and morphology changes during cycling were reduced and nucleation of the lead oxide crystals was improved. The utilization of positive active-material was increased by 50% at the $C/3$ rate compared with typical positive active-material. Other conductive additives claimed in the patent are TaB_2, TaN, $ZrSi_2$, $NbSi_2$, TiP, and CrP.

4.4.6. Lead-coated glass wire

Materials made by a co-extrusion process for coating glass, copper, or titanium wire with lead [30] have been proposed as a substitute for the lead grid. The diameter of

the wire thicknesses can vary from 0.038 to 0.635 cm. The wires are too thick to be used as an additive in battery pastes but have been woven together to form lead grids and have also been incorporated in tubular plates to add strength and save weight. Lead-coated glass fibres of 0.025 cm diameter have also been suggested as additives to the positive plate [31].

4.4.7. Carbon

Carbon is insoluble in acid and is stable in the negative plate, but it tends to decompose in the positive-plate environment at a rate that depends on the form of the material.

Although carbon has been investigated as an additive to the positive plate for many years, its use has not yet achieved much commercial success. A grid made from lead wire with carbon fibres protruding from the grid wires into the paste was developed to improve cycle-life and high-rate performance [32]. The addition of an isotropic graphite to the positive plate was also found to improve capacity and cycle-life [33,34]. It was claimed that the improvement was due to expansion of the material which increased plate porosity, rather than to an increase in conductivity. The addition of graphite, carbon, and/or titanate whiskers to both the positive and negative pastes has also been patented [35]. When long carbon whiskers were added to the positive plate at concentrations up to 1.5 wt.%, the ohmic resistance of the cured plate decreased and the formation efficiency increased [36]. Half of the carbon decomposed during formation. This resulted in increased pore size and greater utilization of positive active-material on discharge. The average pore size increased from 0.13 μm without carbon to 2.7 μm with 1 wt.% carbon, and the pore volume from 0.10 to 0.15 $cm^3 g^{-1}$. Cycle-life on a JISC8702 test with 50% DoD at 25°C was not affected by the carbon additive.

The addition of 0.1–0.5 wt.% graphite fibres made from either acrylonitrile or a pitch precursor has been patented [37]. On average, the chopped fibres were about 3.0 mm in length and 0.05 mm in diameter. Positive plates were made from a paste composed of 81.3 wt.% PbO, 9.5 wt.% H_2SO_4 (1.35 rel. dens.), 8.7 wt.% deionized water, 0.1 wt.% Dynel^{TM} fibre, and 0.4 wt.% polyacrylonitrile graphite fibre. Formation of a battery made with this paste was compared with a control that had no graphite additive. Only 39% of the energy required to form the control was required to form the battery that contained graphite in the positive plate.

The effects of adding 0.3 wt.% of either carbon or glass fibre to the positive paste have been compared [38]. Plate thickness, discharge rates, and temperatures were varied, and the capacities of cells that contained one positive and two negative plates were measured. Under a discharge of 12.25 mA cm^{-2} at 25°C, positive plates of thickness 2.77 mm had less capacity with carbon than with glass, but more capacity than the control with 4.25-mm thick plates. Neither the volume % nor the density of the fibres was given, and the loss of carbon during formation was not determined. In this study, therefore, it is difficult to distinguish the effect on discharge capacity of conductivity enhancement from that of acid transport.

Adding carbon black to the positive paste not only enhances formation slightly (a maximum of 2%) by increasing the conductivity of the paste, but also promotes the formation of α-PbO_2 [5]. The porosity and coarseness of the active mass also increases. A paste was made by mixing ball-milled leady oxide with 0.2 or 10 g carbon black and adding aqueous sulfuric acid and water. Positive plates prepared from this paste were formed and cycled at the 10-h rate; each cycle involved discharge for 1 h and charge for 5 h. After 216 cycles, the α-PbO_2:β-PbO_2 ratio in the cell with 0.2 wt.% carbon black was still 41% higher than that in the control cell with no carbon added. It was also found that the carbon was not stable in the positive plate. For a cell with 1.0 wt.% carbon black, 0.4 wt.% remained after formation and only 0.05 wt.% after cycling. It was further observed that oxidation of carbon black occurred even when the positive electrode was at open-circuit. Cycle-life, however, was not affected. The findings thus agree substantially with those of Hojo *et al.* [35,36]. Both sets of studies show that additions of carbon to the positive electrode have the greatest benefit during formation. Although the carbon influences the plate morphology, it does not appear to have much effect on cell performance or cycle-life. This is probably because carbon is oxidized in the positive-plate environment to form gaseous carbon dioxide.

In a flooded lead–acid battery, carbon dioxide will evolve without imparting any significant effect on battery performance. In VRLA batteries, however, the gas will increase the internal cell pressure. This could accelerate a common failure mode, namely, cell dry-out, by causing the valve to open more frequently. The pressure increase and bubble formation may affect the rate of oxygen evolution of the positive plate, and/or the rate of oxygen transport, and/or oxygen recombination at the negative plate. Another failure mechanism of VRLA batteries is progressive sulfation of the negative plate by oxygen recombination. If carbon dioxide interferes with either oxygen formation or recombination, it may reduce the rate of negative plate sulfation and increase float life.

Measurements of the effect of graphite concentration in the positive plate on gas evolution have been made on flooded stationary cells with a nominal capacity of 4.5 Ah at the 10-h rate [39]. Standard plates with grids made from pure-lead, lead–calcium, or lead–antimony alloys were tested and gave similar results. In cells with lead–calcium grids, gas evolution increased significantly as the graphite content was increased from 0.5 to 5 wt.%. For all alloys, when cells with 0.5 wt.% graphite were floated at 2.23 V per cell, the initial rate of gas evolution was less than that for cells without graphite. At the end of an 8-week float test, however, the cells with and without 0.5 wt.% graphite had similar gassing rates. Cell capacities were initially higher with graphite, but cycle-life remained unchanged. These results suggest that the effects of graphite additions on the oxygen cycle in VRLA batteries should be evaluated.

Another study [40] examined the effect of adding 10 g of natural graphite with a grain size of 520 μm to positive plates in 4.5-Ah VRLA cells. The active material was prepared by mixing 2 kg of leady oxide and 0.8 g of polyester fibre with 150 ml of water and then 271 ml of 1.200 rel. dens. sulfuric acid. The pastes were applied to lead–calcium–tin grids, cured at 80°C for 72 h, and dried in air. The test cells, composed of one positive and two negative plates, were formed and then floated at a

constant voltage of 2.25 V. Each month, the cells were discharged at a constant current of 0.45 A to a 1.80 V cut-off. The cell with graphite retained its capacity better than the cell without graphite. The capacity of both cells increased somewhat when they were 'reactivated' by discharging at a low current of 0.1 A and charging at 0.45 A. When the cells were dismantled, the active material that contained graphite was found to be very brittle. It was suggested that this was due to intercalation of sulfate ions into the graphite grains. The total amount of graphite remaining in the plate was not reported. Other studies on flooded batteries show that the carbon gradually oxidizes to carbon dioxide, as reported above.

The initial utilization of active material was found to increase when 0.5 wt.% of expanded graphite, carbon fibre, needle coke, or polyacene was added to positive pastes [41]. Expanded graphite was the most beneficial in this respect. The addition of this graphite did, however, reduce the number of cycles due to softening and shedding of the active materials when the cell was subjected to constant-current discharges at a 3 to 4-h rate to a 1.65 V cut-off. Addition of a nitrogenous heterocyclic compound along with the graphite overcame this problem. Cycle-life was equivalent to that of a control cell with no additives, but the material utilization increased from 38 to 53% by the 30th cycle. Further tests on commercial batteries showed that 1 wt.% of the composite additive gave good results. Comparable battery performance could be achieved with 14% less active material at the expense of only a small reduction in cycle-life.

Fibres made from carbon-filled polyolefin or polyester have been added to battery paste to increase life [42]. In another approach [43], a battery plate was made by filling a non-conductive polyvinylchloride grid with paste and covering the plate with a sheet of partly carbonized, organic, non-conductive fibres. The carbonized layer on the fibres provided the electrical conductivity.

The capacity of densely packed tubular electrodes made of chemically prepared PbO_2 was improved by the addition of 1–12 wt.% graphite of 8-μm diameter [44]. The increase in capacity was ascribed to an improved acid supply which resulted from two effects of the graphite, viz., pore formation and electro-osmotic pumping.

4.4.8. Lead dioxide

Although much work has been undertaken to find a stable, conductive additive for the positive plate, lead dioxide is still the additive which is most commonly employed to improve the efficiency of the formation process. A traditional way to enhance the conductivity of the positive plate during formation is to use 25–100 wt.% of red lead ($Pb_3O_4 = 2PbO{\cdot}PbO_2$). When sulfuric acid is added to this oxide to make a paste, the red lead reacts to form lead dioxide and lead sulfate. This well-demonstrated approach is adopted for hard-to-form batteries, particularly those with tubular positive plates. Plates made of red lead have poor cycle-life unless the positive active-material is highly compressed. This requirement has limited the use of red lead in flat-plate designs, such as those used for automotive batteries. Three paste-mixing processes in which red lead is added to the paste have recently been patented [45–47]. These pastes can be cured at higher temperatures to

form tetrabasic lead sulfate that provides longer cycle-life and only slightly less initial capacity than pastes that contain tribasic lead sulfate. The direct addition of lead dioxide to paste mixtures containing tetrabasic lead sulfate enhances formation [48].

Particles of lead dioxide in lead monoxide, such as those formed in a ball-mill, can be formed by treating the oxide with ozone before paste mixing [49]. The use of persulfate [50–53] and peroxides [54] to effect the partial conversion of lead oxide in the paste to lead dioxide has also been proposed. A proprietary process for treating the surfaces of unformed plates with ozone gas produced a thin coating of lead dioxide, which enhanced formation [55,56]. Much lower quantities of lead dioxide are needed with this approach than when red lead is added to the plate, and the normal battery paste mix can be used. Dipping or spraying the plate with a persulfate solution has also been adopted to oxidize the surface PbO to conductive PbO_2 [57].

4.5. Chemically Active Additives

4.5.1. Sulfate salts

Sulfate salts are sometimes added to batteries to depress the formation of large lead sulfate crystals that are difficult to recharge. Failure by 'sulfation' is common when the battery is deeply discharged or left on open-circuit in the discharged state. Because crystals of barium sulfate and strontium sulfate are isomorphous with lead sulfate and are relatively insoluble, they can nucleate the lead sulfate crystals and thus reduce their size.

The addition of sulfates to the positive plate was evaluated by Lorenz (as described in Ref. 58). Results showed that 0.5 wt.% barium sulfate or strontium sulfate added to the positive active-material reduced the cycle-life from 100 cycles without the additive to 30–50 cycles with the additive under the same conditions. The end-of-life was taken as a 40% decline in the initial capacity. Lorenz further reported that calcium sulfate is not isomorphous with lead sulfate and therefore has no effect on battery life. (Note, calcium sulfate also does not act as an inorganic expander for negative plates.)

The cycle-life of cells discharged at the $C/5$ rate to 0.7 V was found to decrease when 0.3 or 3 wt.% $BaSO_4$ was added to the positive plate [59]. Compared with an undoped plate, the addition of 3 wt.% $BaSO_4$ decreased the cycle-life by a factor of 10. The expansion of a free-standing positive plate increased by a factor of 4, and the loss of active material increased by a factor of 8. Addition of 0.3 wt.% $BaSO_4$ had an effect that was half-way between 0 and 3 wt.% $BaSO_4$. Although compression of the cell stack increases cycle-life, the relative effect of adding $BaSO_4$ is similar. The cycle-life was estimated to be 320, 80, and 35 cycles for cells with 0, 0.3, and 3 wt.% $BaSO_4$, respectively. (See Section 4.4.1 above for further discussion.)

Sodium sulfate is not isomorphous with lead sulfate and is more soluble. The solubility of lead sulfate in sulfuric acid containing sodium sulfate is given in Table 4.6 for acid concentrations from 0 to 10 wt.% [60,61]. When dissolved in the

Table 4.6. Solubility of lead sulfate in sulfuric acid + sodium sulfate solutions[a].

H_2SO_4 (wt.%)	Na_2SO_4 (wt.%)	pH		Solubility of $PbSO_4$ (mg Pb per l)	
		25°C	66°C	25°C	66°C
0	0.05	6.1	8.1	4.3	9.9
	0.2	6.4	7.2	3.2	7.2
	0.5	5.0	5.0	5.0	5.6
	2.0	5.6	5.6	4.0	7.5
	10.0	5.7	5.7	10.8	18.4
0.5	0.05	1.34	1.23	3.7	7.6
	0.2		1.26		6.1
	0.5	1.42	1.42	3.4	6.8
	2.0	1.63	1.63	3.9	6.8
	5.0	1.83	1.70	5.4	9.5
	10.0	1.93	1.93	9.5	17.1
2.0	0.5	0.87	0.87	4.2	8.8
	2.0	0.96	0.96	4.4	6.6
	10.0	1.22	1.22	8.3	13.2
10.0	0.5	0.08	0.08	5.3	6.3
	2.0	0.12	0.12	5.6	6.5
	10.0	0.18	0.18	12.3	10.4

[a]Private communication from Marsh of data shown in graphical form in Refs. [60,61]. Marsh measured the data cited in Refs. [60,61].

electrolyte, up to about 2 wt.% sodium sulfate decreases the solubility of lead sulfate at all acid concentrations, due to the common-ion effect. At concentrations of sodium sulfate between 2 and 10 wt.%, the solubility of lead sulfate is higher at all acid concentrations. The growth of large crystals, called 'hard sulfate', occurs by a dissolution–precipitation process when the battery is on open-circuit. At the low acid concentrations in a discharged battery, the solubility of lead sulfate is higher than in a fully charged battery with high acid concentrations. Addition of sulfate salts to the battery electrolyte to reduce the solubility of lead sulfate reduces the number of failures from shorting when the battery is deeply discharged or stored with minimal electrolyte [60,61]. Addition of sulfate salts is common in VRLA batteries, where the limited electrolyte volume can, at the end of the discharge or on open-circuit, result in a more dilute acid than in the case of flooded batteries. Unfortunately, sodium sulfate accelerates the corrosion of the negative plate lugs and connecting strap when lead–tin alloys are used for these parts [62]. This effect occurs in VRLA batteries because the negative lugs and strap are exposed to air and wetted with only a thin film of electrolyte. Addition of selenium to the alloy suppresses this effect.

In the early 1950s, the United States National Bureau of Standards evaluated a battery electrolyte additive which contained sodium sulfate and magnesium sulfate. The manufacturer's claim was that the additive could restore the performance of

Table 4.7. Effect of sodium sulfate on performance of positive plates [44].

Na_2SO_4 (wt.%)	Total packing efficiency as % of theoretical ($PbO_2 + Na_2SO_4$)	% Theoretical capacity obtained at cycles			
		1	2	3	4
3.8	39	15.1	5.6	10.6	12
2.2	36	2.4	2.8	2.8	2

heavily sulfated batteries, but the Bureau of Standards concluded that the material was without merit. When a strong controversy erupted, the National Academy of Sciences appointed a Committee to appraise the work of the National Bureau of Standards [63]. The Report of the Committee on Battery Additives [64] supported the Bureau of Standards conclusion.

Tubular plates have been made with chemically prepared lead dioxide and 2.2 or 3.8 wt.% sodium sulfate in the positive active-material [44]. Test results on cells cycled at constant-current are shown in Table 4.7. It was concluded that sodium sulfate increases the utilization of material by dissolving to create a more porous structure in the positive plate. It was also noted that graphite has an even greater effect in the same concentration range (see Section 4.4.7).

Sulfate salts have been introduced into the positive paste of VRLA cells during the paste-mixing process. In a recent study [65], sodium sulfate was added to positive pastes at 0, 0.01, 0.05, 1, and 2 M levels (note, the authors did not explain how the molarity levels were calculated). The plates were cured at 85°C to form tetrabasic lead sulfate and α-PbO. The tetrabasic lead sulfate crystals had sizes of 1–20 μm in the paste without sodium sulfate. The crystal size decreased and the specific surface-area increased most with the lowest amounts of sodium sulfate, viz., 0.01 and 0.05 M. Five, 4.0-Ah, VRLA cells, one for each additive concentration, were subjected to 100% DoD cycling. The cells with 0.01–0.05 wt.% sodium sulfate in the positive plate had about 4% higher initial capacity and 4% more average capacity per cycle than the cell with no sodium sulfate. Under duty that simulated the driving of an electric scooter, the cells that had 0.01–0.05 wt.% sodium sulfate in the positive plate showed about 8% increase in both initial and average capacity per cycle.

In another study [66], three-plate, 1.2-Ah cells with a Pb–5.5 wt.%Sb grid, 1.250 rel. dens. acid and PVC separators were discharged at 200 mA for 5 h and recharged at 70 mA for 17 h. Capacities were measured after every five cycles to an end-of-life at 80% of initial capacity. The performance of positive plates containing 0.5 or 1.5 wt.% of sodium or magnesium sulfate were compared with undoped plates. The cycle-life of the positive plate was improved by the addition of magnesium sulfate, but the negative plates shed material after 60 cycles (note, no explanation for this plate deterioration was given). The authors also studied the behaviour of cells that contained 0.5 and 1.5 wt.% sodium sulfate in the electrolyte. It was concluded that addition of sodium sulfate is more effective in the electrolyte than in the paste.

The effect of the addition of calcium sulfate to positive pastes has also been investigated [67]. Pasted electrodes were cycled three times as well as to the end of the battery cycle-life. The positive active-material was washed with water, dried, pulverized, and used to pack tubular electrodes. Additions of 0, 0.1, 0.2, 0.8, and 1.2 wt.% calcium sulfate were included in the study. When the tubular electrodes were cycled, the capacity of the ground positive active-material was gradually restored. Cycle-life increased as a function of the content of calcium sulfate; the most stable capacity was with 0.8 wt.% calcium sulfate. It was concluded that the addition of calcium sulfate increases the rate of lead sulfate nucleation during discharge and modifies the β-PbO_2 and lead sulfate structure. The positive active-material contains regions of crystalline lead dioxide, as well as regions of amorphous, hydrated, lead oxide — called 'gel'. The calcium ions increase the gel:crystal ratio in the positive active-material and act as binders for the skeletal structure of the material. This conclusion appears to be in conflict with Lorenz's conclusion that $CaSO_4$ does not nucleate $PbSO_4$ (see above).

Another investigation [68] found that calcium sulfate in paste improves the cold-cranking ability of automotive batteries. Two types of batteries were tested, namely, a standard 12-V, 60-Ah unit and a tubular, 8-V, 450-Ah diesel electric locomotive battery. Either 0.25 or 2 wt.% calcium sulfate was dry blended with the oxide before acid and water additions. The automotive batteries were tested at the $C/20$ rate and also discharged at high rates at 0 and -15°C. The tubular batteries were discharged at 2300 A for 15 s, followed by a rest period for 15 s. Calcium sulfate increased the voltage at all concentrations and discharge rates, and the effect was more pronounced at higher currents and lower temperatures. Lead–acid batteries typically show a sharp voltage drop at the beginning of discharge, and this is followed by a voltage increase. The phenomenon is called the 'coup de fouet'. In the above study, the voltage drop was not reduced by calcium sulfate and the voltage increase was only seen after the first 5 s of discharge, except under a high rate of discharge at -15°C. An alternative approach involved dipping dry pasted plates in calcium nitrate solution, draining off the excess nitrate solution, immersing the plates in dilute sulfuric acid to form calcium sulfate in the pores, and then washing to remove acid and nitrate. Although this treatment decreased the porosity by as much as 25%, the battery performance was still improved.

4.5.2. Phosphates

Voss [69] has published a comprehensive review of the effects of phosphoric acid on the performance of lead–acid batteries. This review included previously unpublished tests by Kugel, Rabl, and Woost conducted between 1926 and 1935, in which phosphoric acid was added to the positive paste at the 0.9, 2.0, 2.9, or 4.0 wt.% level, and at 0.9 wt.% in the electrolyte. The results showed that, during cycling, the phosphoric acid concentration increases in the electrolyte but decreases in the phosphated positive active-material. It is also higher in the electrolyte when the cell is discharged. Tables 4.8–4.10 show the results of these studies.

Table 4.8. Content of phosphoric acid in electrolyte and charged positive active-material of Fauré plates during the first six cycles [69].

Charge no.	1		2		3		4		5			6
Discharge no.		1		2		3		4		5		
H_3PO_4 in electrolyte												
charged state (g l^{-1})	3.6		3.9		4.3		4.7		5.1			5.3
discharged state (g l^{-1})		4.7		5.3		6.0		6.5		6.8		
H_3PO_4 in positive material												
charged state (%)	2.5		2.4		2.1		1.9		1.7			1.6

Table 4.9. Cycle-life data of 4 Ky 225 Fauré plates with/without phosphoric acid [69].

Cycle	Discharge rate (h)	Nominal $C/5$ capacity (%)		Voltage at start of discharge (V per cell)	
		with H_3PO_4	without H_3PO_4	with H_3PO_4	without H_3PO_4
300	5	60	68	2.04	2.02
325	5	58	66	2.03	2.02
326	10	58	67	2.04	2.03
327	1	50	59	2.03	2.02

Table 4.10. Effect of phosphoric acid dosage on cycle-life of Ky Fauré type cells [69] (end-of-life taken as 60% $C/5$).

H_3PO_4 dosage (g per kg lead oxide)	Cycle-life
9	220
20	330
29	490
40	720

Cells with four positive and five negative electrodes were constructed with 0 and 2–3 wt.% phosphoric acid in the paste. The cells with phosphoric acid had 13–18 wt.% lower capacity than cells without phosphoric acid. The cell voltage at the beginning of discharge was 10–20 mV higher in the phosphated cells. The positive active-material with phosphate adhered more firmly to the grid than in cells without phosphate, and this reduced the shedding of the material by about 50%. Thus, phosphoric acid in the paste significantly improved cycle-life. At 6 wt.% phosphoric

acid, however, mossing due to formation and reduction of soluble lead (IV) material on charge resulted in early cell failure due to short-circuits.

Many other workers have studied the effects of adding phosphoric acid to the electrolyte. The results vary dramatically with the acid concentration, paste composition, acid:paste ratio, and application. Voss recommends that cells should be operated above 15°C to decrease mossing, and summarizes the effects of phosphoric acid in lead–acid cells as follows:

- retards sulfation on stand after deep discharge;
- promotes the formation of lead (IV) species on charge, which may increase mossing and may oxidize organic materials;
- reduces lead corrosion;
- reduces self-discharge;
- affects the cell voltage, more specifically the potential of the positive plate;
- reduces the shedding rate of the positive active-material;
- increases the cycle-life of positive plates;
- reduces the capacity of positive pasted plates by about 15%;
- may increase the capacity of Planté plates due to lower shedding rates;
- behaves opposite to the sulfate ion with regard to its concentration in the electrolyte.

Phosphoric acid and phosphate salts have been added to improve the performance of many different battery designs in many applications. Frequently, use of the additive has been discontinued when unexpected test or field results contradicted earlier laboratory results. The many conflicting effects listed by Voss explain why phosphates have been so controversial. A series of studies of the effects of phosphates in sulfuric acid on the positive electrode [70–72] may help to explain this quandary. The activity of the phosphate ion in sulfuric acid solution is determined by the acid concentration. The degrees of dissociation of H_3PO_4 into $H_2PO_4^-$, HPO_4^{2-}, and PO_4^{3-} are dependent on the activity of the hydrogen ion. When the sulfuric acid concentration is high, the phosphate activity will be low, and vice versa. Thus, during formation or at the end of discharge, phosphate additions will have a higher effective concentration than in a fully charged battery. In the alkaline environments that can exist in the corrosion film or during plate formation, lead phosphates are more stable than basic lead sulfates [72]. Lead phosphates in the positive paste can significantly alter the structure and reactivity of the paste during formation or the corrosion film during battery use.

One of the most successful applications of phosphoric acid has been in gelled electrolytes that are made by adding fumed silica to sulfuric acid [73,74]. Larger phosphate concentrations appear to be tolerated in the gelled acid without adversely affecting cell performance. One reason may be that the plates in these batteries are formed by the dry-charge process and the phosphate is added to the battery with the electrolyte. Addition of silica may also affect the equilibria of phosphate dissociation and/or lead phosphate formation. Further study of these effects may lead to a better understanding of how to control phosphate activities to enhance battery performance.

One study [75] explored additions of 0.06 wt.% silicide, 0.26 wt.% phosphate, 0.12 wt.% cobalt salts or 0.15 wt.% fibre to positive plates of 4-Ah capacity. The plates were formed in acid with 50–100% overcharge and discharged at a 5-h rate to 1.75 V. It was found that cobalt (II) salts increased the α-PbO_2 in the plate, and that phosphate promoted the development of smaller PbO_2 crystals. Addition of silicide or phosphate increased the initial capacity. Cycle-life increased from 19 to 26 cycles with phosphate and to 28 cycles with cobalt. Silicide and fibre mechanically strengthened the active material but only slightly increased the cycle-life. Silicide with fibre and cobalt salt with phosphate were claimed to be the best formulations for increasing the capacity of the active material (by 10–15%).

4.5.3. Bismuth

Because bismuth is a common impurity in lead, its effects in lead–acid batteries have been extensively studied. A review of the literature [76] has concluded that the investigations have produced many conflicting results. Nevertheless, it is generally agreed that bismuth accelerates oxygen evolution from the positive plate. Formation of a mixed oxide, $PbO_2 \cdot BiO_x$, has been suggested as the reason for the lower oxygen overpotential. Bismuth may also possibly suppress hydrogen evolution on lead and enhance oxygen reduction. This suggests the need for further study of the action of the oxygen cycle in VRLA batteries with bismuth additions.

In a recent study [77], positive plates were made from either bismuth-free oxide, or from high-purity oxide that contained 0.05 wt.% bismuth. The resulting active material was removed from the grid, washed and dried, pulverized, and compressed into disc-shaped electrodes at 2.9 kPa. The electrodes were immersed in acid of 1.275 rel. dens. and subjected to a 'full charge' at 0.05 A for 16 h. Capacity tests were then performed (20 cycles; discharge: 0.125 A to 1.75 V; charge: 0.05 A, no voltage limit, 120% charge return) with the electrode compressed under a given pressure in the range 1.4–60 kPa. Below 40 kPa, bismuth was found to increase the initial capacity. Moreover, at all pressures studied, bismuth enhanced the rate at which the capacity developed on cycling. Both these observations are consistent with the findings of other studies [78,79], which have shown that bismuth in the grid alloy or in the electrolyte restores the capacity of tubular electrodes made from pulverized positive-plate material. It was concluded [77] that bismuth encourages the growth of fine, acicular crystals of lead dioxide that interconnect and, thereby, consolidate and strengthen the porous mass of the positive electrode.

In a parallel investigation [80], VRLA batteries (6 V, nominal $C_{20} = 4$ Ah) were manufactured either from lead oxide containing 0.05 wt.% bismuth or from standard factory lead oxide. Cycle tests were performed under the Japanese Industrial Standard (JIS) and the International Electrotechnical Commission (IEC) tests protocols. In the JIS test, the battery is discharged at $0.25C_{20}$ A for 2 h and then recharged at a constant voltage equivalent to 2.45 V per cell with a maximum current of $0.1C_{20}$ A for 6 h. Twenty-four of these discharge–charge sequences are applied. On the next cycle, the battery is discharged at the same current until the voltage reaches 1.7 V per cell. The 25-cycle test is repeated until either the

discharge capacity on the 25th sub-cycle is lower than 50% of the nominal capacity or the battery reaches the 1.7 V per cell cut-off during the 2-h discharge test. Under the JIS protocol, the cycle-life was increased from 675 to 800 with the bismuth-bearing oxide. The failure mode of the batteries without bismuth was positive-plate expansion.

The IEC protocol, run at 22°C, consists of discharging at $0.17C_{20}$ A and recharging at a constant voltage equivalent to 2.35 V per cell with a current maximum of $0.3C_{20}$ A for 9 h. Fifty discharge–charge cycles are applied and then the battery is discharged at the $C_{20}/20$ rate to 1.75 V per cell. This is repeated until the capacity either declines to 60% or less of the nominal C_{20} value or the voltage during the 3-h discharge reaches 1.75 V per cell. The batteries with bismuth gave 675 cycles compared with 510 cycles for the controls. The failure mode of batteries subjected to the IEC protocol was undercharge or sulfation of the negative, which suggests that bismuth may improve negative-plate rechargeability. This possibility was later verified [81] in experiments that showed that bismuth contents up to 0.06 wt.% can improve the charging ability of negative plates, especially when cycling within a low and narrow partial state-of-charge window (40–70% SoC) of the type that will be experienced in 42-V powernet automotive and hybrid electric vehicle duties.

It has recently been demonstrated that other benefits to be gained by incorporating bismuth in active material include: lower rates of hydrogen and oxygen gassing [82] (note, this effect on oxygen evolution is opposite to the traditional view [76]); less risk of selective discharge of negative or positive plates and lower float current [83]; lower self-discharge rates [84].

4.5.4. Polyvinylsulfonic acid and its salts

The tests of additives in spirally wound VRLA batteries [18] also included a proprietary 'AD7' additive, which was chemically described as polyvinylsulfonic acid or its salts, called polyvinylsulfonates [85,86], together with crystal carbon fibres, polyester fibres and SnO_2 powder. None of the additives were found to increase the initial discharge capacities compared with the control. The 'AD7' additive did, however, show significantly better maintenance of capacity during cycling than the control. It was further claimed [81,82] that typical additive concentrations of about 0.001–0.5 wt.%, in either the positive paste or the negative paste or both, function as a binder and a plasticizer to improve life, capacity, and low-temperature performance.

4.6. Conclusions

This review of work on additives to the positive plate shows that a variety of effects can be achieved. The choice of additives is very dependent on the intended application and corresponding battery requirements. Additives that enhance material utilization and/or reduce plate weight may be desirable for batteries in electric vehicles, where high specific energy is required. In automotive batteries,

specific power may be enhanced by additives that increase plate porosity and facilitate acid transport. Batteries that require long cycle-life under deep-discharge conditions may benefit from binders to reduce active-material shedding.

Most studies of additives to the positive plate have focused on flooded lead–acid batteries. The results are probably applicable to VRLA batteries in most cases. One exception may be when additive effects are dependent on acid concentration. For example, the addition of soluble sulfate salts may be more effective in VRLA batteries with AGM separators than in gelled or flooded designs. This is because the acid in VRLA batteries may reach lower concentrations under deep discharge or prolonged open-circuit conditions. Soluble sulfate salts will reduce shorting and may prevent freezing under such conditions. It should be noted, however, that soluble sulfate salts may also accelerate corrosion of the negative plate lugs and connecting strap when these parts are exposed to oxygen and wetted with a thin film of electrolyte. Another additive worthy of consideration is phosphoric acid. Control of the effects of phosphoric acid additions appears to be better in gelled batteries formed by dry-charging than in AGM or flooded batteries made with an in-case formation process. This may be due to better control of the degree of dissociation of the phosphoric acid in such gelled batteries.

A second restriction to the use of additives in VRLA batteries may be when they affect the oxygen cycle. For example, carbon may increase the internal cell pressure by oxidizing to produce carbon dioxide. Bismuth may accelerate oxygen evolution. And sulfate salts may have some effect on the recombination of oxygen at the negative plate by nucleating lead sulfate crystals. At the positive, additives that increase the plate surface-area or porosity may accelerate oxygen evolution on overcharge. Further study of such effects is needed to determine what additives are most beneficial in VRLA batteries.

References

1. D.B. Edwards, V.S. Srikanth, *J. Power Sources*, **34** (1991) 217.
2. T.C. Dayton, D.B. Edwards, *J. Power Sources*, **85** (2000) 137.
3. D.B. Edwards, P.W. Appel, *J. Power Sources*, **46** (1993) 39.
4. P.T. Moseley, *J. Power Sources*, **64** (1997) 47.
5. H. Dietz, J. Garche, K. Wiesener, *J. Power Sources*, **14** (1985) 305.
6. K. McGregor, *J. Power Sources*, **59** (1996) 31.
7. J.A. Wertz, T.J. Clough, *Proc. 13th Annual Battery Conference on Applications and Advances*, Long Beach, CA, USA, 1998, p. 311. (IEEE Paper 98H8299.)
8. J.A. Wertz, T.J. Clough, *Proc. 14th Annual Battery Conference on Applications and Advances*, Long Beach, CA, USA, 1999, p. 189. (IEEE Paper 99TH8371.)
9. J.A. Wertz, T.J. Clough, *Proc. 15th Annual Battery Conference on Applications and Advances*, Long Beach, CA, USA, 2000, p. 77. (IEEE Paper 00TH8490.)
10. D. Pavlov, G. Papazov, V. Iliev, *J. Electrochem. Soc.*, **119** (1972) 8.
11. W.H. Kao, K.R. Bullock, *J. Electrochem. Soc.*, **139** (1992) L41.
12. N.K. Bullock, W.H. Kao, US Patent 5,045,170 (Sept. 3, 1991).
13. W.H. Kao, N.K. Bullock, R.A. Peterson, US Patent 5,302,476 (April 12, 1994).
14. W.H. Kao, S.L. Haberichter, P. Patel, *J. Electrochem. Soc.*, **141** (1994) 3301.
15. P.C.S. Hayfield, US Patent 4,422,917 (1983).
16. R.L. Clarke, J.F. Cheng, Eur. Pat. Appl. 0.360,942 (April 4, 1990).

17. N.E. Bagshaw, R.L. Clarke, K. Kendall, in: *Ext. Abstr. Electrochem. Soc. Fall Meeting*, The Electrochemical Society Inc., Pennington, NJ, USA, 1990, p. 2.
18. J.B. Olson, E.D. Sexton, K.E. Murray, IEEE Paper 0-7803-4098 (1998), p. 169.
19. M. Matsumoto, S. Ito, Jpn. Kokai Tokkyo Koho JP 61/455565A2 [86/45565] (1986).
20. P. Mirebeau, G. Chedeville, E. Genies, French Patent 2,553,581 (1985).
21. P. Mirebeau, French Patent 2,519,191 (1983).
22. B.Z. Lubentsov, Ya.H. Samovarov, G.I. Zvereva, M.L. Khidekel, *Mater. Sci. Forum*, **62** (1990) 485; B.Z. Lubentzov, G.I. Zvereva, V.E. Dmitrienko, M.L. Khidekel, *Mater. Sci. Forum*, **62** (1990) 487.
23. J.J. Rowlette, US Patent 4,507,372 (March 26, 1985).
24. J.J. Rowlette, T.J. Clough, J.Y. Josefowicz, J.W. Silbert, US Patent 4,547,443 (1985).
25. J.J. Rowlette, S.A. Alkaitis, N. Pinsky, J.Y. Josefowicz, *The American Chemical Society*, Paper No. 8412-0986-3/86/0869-231 (1986).
26. J.J. Rowlette, A.I. Attia, *Proc. 2nd Annual Battery Conf. on Applications and Advances*, Long Beach, CA, USA, 1987, p. 209.
27. A.I. Attia, D.E. Perone, paper presented at ILZRO Lead–Acid Battery Seminar, May 5, 1989.
28. A.I. Attia, J.J. Rowlette, *Proc. 33rd Intl. Power Sources Symp.*, Cherry Hill, NJ, USA, The Electrochemical Soc., Pennington, NJ, USA, 1988, p. 624.
29. T.S. Lee, A.F. Sammells, R.J. Remich, US Patent 4,289,835 (Sept. 15, 1981).
30. R. Walk, G. Mayer, P. Howard, R. Blanyer, C. Mathews, B.E. Jay, *Proc. 32nd Intl. Power Sources Symposium*, Cherry Hill, NJ, USA, The Electrochemical Society Inc., Pennington, NJ, USA, 1986, p. 368.
31. D.B. Edwards, W.E. Rippel, *NASA Tech Briefs*, (1991) p. 20.
32. L. Weininger, C.R. Morelock, *J. Electrochem. Soc.*, **122** (1975) 1161.
33. A. Tokunaga, M. Tsubota, K. Yonezu, K. Ando, in: K.R. Bullock, D. Pavlov (Eds.) *Advances in Lead-Acid Batteries*, *Proc. Vol. 84–14*, The Electrochemical Society Proceedings Series, Pennington, NJ, USA, 1984, p. 314; *J. Electrochem. Soc.*, **134** (1987) 525.
34. A. Tokunaga, M. Tsubota, K. Yonezu, *Proc. Vol. 87-2*, The Electrochem. Soc. Fall Meeting, Honolulu, HI, USA, October 18–23, 1987, Abs. 129, p. 187.
35. E. Hojo, K. Kishimoto, Y. Kasai, N. Nakashima, O. Matsushita, Eur. Pat. Appl. EP 352,115 (July 21, 1988).
36. E. Hojo, J. Yamashita, K. Kishimoto, N. Nakashima, Y. Kasai, *Yuasa Jiho*, **72** (1992) 23.
37. R.V. Pitts, J.B. Williamson, M.J. Gough, T.E. Bolner, US Patent 5,223,352 (June 29, 1993).
38. C.C. Wan, C.M. Yeh, American Institute of Aeronautic and Astronautics, Inc., Paper 869400 (1987) p. 1119.
39. J. Kwásnik, J.D. Milewski, T. Pukacka, B. Szcześniak, *Prog. Batteries and Battery Materials*, **13** (1994) 219.
40. B. Szcześniak, J. Kwásnik, J.D. Milewski, T. Pukacka, *J. Power Sources*, **53** (1995) 119.
41. S. Wang, B. Xia, G. Yin, P. Shi, *J. Power Sources*, **55** (1995), 47.
42. S. Kunitomo, S. Tanaka, *Jpn. Kokai Tokkyo Koho JP*, 61/455565 A 2 [86145565], 1986.
43. P. Reasbeck, Brit. Pat. GB 1,553,504 (1979).
44. S.V. Baker, P.T. Moseley, A.D. Turner, *J. Power Sources*, **27** (1989) 127.
45. D. Pavlov, N. Kapkov, Bulgarian Pat. 43,335 and 43,336 (May 1988).
46. D. Pavlov, N. Kapkov, *J. Electrochem. Soc.*, 137 (1990) 16.
47. D. Pavlov, N. Kapkov, *J. Electrochem. Soc.*, 137 (1990) 21.
48. G.N. Reich, US Patent, 4,415,410 (1983).
49. G.A. Parker, US Patent, 4,415,410 (1983).
50. A.R. Reid, US Patent, 2,159,226 (1939).
51. C.H. Ling, Belgian Patent 723,018 (1968).
52. Y. Matsumura, S. Saito, A. Muira, Y. Ishikawa, A. Komaki, T. Hayakawa, Japanese Pat. Pub. No. 61/145664 (1985).
53. J.A. Lopez-Doriga, Spanish Patent 8,801,559 (1988).
54. J.A. Orsino, US Patent 2,658,077 (1953).
55. B. Mahato, W. Delany, US Patent 4,656,706 (April 14, 1987).
56. K.R. Bullock, B.K. Mahato, W.J. Wruck, *J. Electrochem. Soc.*, **138** (1991) 3545.
57. N.K. Bullock, R.A. Petersen, US Patent 5,149,606 (September 22, 1992).

58. H. Bode, *Lead–Acid Batteries*, Wiley, New York, USA (1977), p. 336.
59. S. Atlung, B. Zachau-Christiansen, *J. Power Sources*, **30** (1990) 131.
60. G.W. Mao, A. Sabatino, U.S. Patent 3,948,680 (April 6, 1976).
61. G.W. Mao, A. Sabatino, U.S. Patent 3,988,165 (Oct. 26, 1976).
62. D. Pavlov, M. Dimitrov, G. Petkova, H. Geiss, C. Gnehm, *J. Electrochem. Soc.*, **142** (1995) 2919.
63. G.W. Vinal, *Storage Batteries*, 4th Edition, John Wiley, USA (1955), p. 158.
64. National Research Council, *Report of the Committee on Battery Additives of the National Academy of Science*, Washington, D.C. (Oct. 30, 1953).
65. J.-S. Chen, *J. Power Sources*, **90** (2000) 125.
66. R. Janakiraman, P.G. Balakrishnan, M. Devasahayam, *Trans. SAEST*, 27 (1992) 177.
67. T. Rogachev, D. Pavlov, *J. Power Sources*, **64** (1997) 51.
68. C.S. Ramanathan, *J. Power Sources*, **35** (1991) 83.
69. E. Voss, *J. Power Sources*, **24** (1988) 171.
70. K.R. Bullock, D.H. McClelland, *J. Electrochem. Soc.*, **124** (1977) 1478.
71. K.R. Bullock, *J. Electrochem. Soc.*, **126** (1979) 360.
72. K.R. Bullock, *J. Electrochem. Soc.*, **126** (1979) 1848.
73. O. Jache, German Patent 1,671,693 (Dec. 12, 1967).
74. K. Eberts, in: D.H. Collins (Ed.), *Power Sources 2*, *Research and Development in Non-mechanical Power Sources*, Pergamon, Oxford (1970), p. 69.
75. C. Yupu, J. Zhiyun, *Chinese J. Appl. Chem.*, **4** (1987) 12.
76. M.J. Koop, D.A.J. Rand, B. Culpin, *J. Power Sources*, **45** (1993) 365.
77. L.T. Lam, N.P. Haigh, D.A.J. Rand, *J. Power Sources*, **88** (2000) 11.
78. D. Pavlov, A. Dakhouche, T. Rogachev, *J. Power Sources*, **30** (1990) 117.
79. D. Pavlov, *J. Power Sources*, **33** (1991) 221.
80. L.T. Lam, N.P. Haigh, D.A.J. Rand, J.E. Manders, *J. Power Sources*, **88** (2000) 2.
81. L.T. Lam, H. Ceylan, N.P. Haigh, J.E. Manders, *J. Power Sources*, **107** (2002) 155.
82. L.T. Lam, O.V. Lim, N.P. Haigh, D.A.J. Rand, J.E. Manders, D.M. Rice, *J. Power Sources*, **73** (1998) 36.
83. L.T. Lam, N.P. Haigh, C.G. Phyland, N.C. Wilson, D.G. Vella, L.H. Vu, D.A.J. Rand, J.E. Manders, C.S. Lakshmi, *Proceedings of the 20th International Telecommunications Energy Conference*, San Francisco, CA, USA, IEEE (1998), p. 452–460.
84. L.T. Lam, N.P. Haigh, O.V. Lim, D.A.J. Rand, J.E. Manders, *J. Power Sources*, **78** (1999) 139.
85. J.B. Olson, US Patent 5,871,862 (Feb. 16, 1999).
86. J.B. Olson, US Patent 5,998,062 (Dec. 7, 1999).

Valve-Regulated Lead–Acid Batteries
D.A.J. Rand et al., editors

—CHAPTER 5—

NEGATIVE PLATES IN VALVE-REGULATED LEAD–ACID BATTERIES

K. Peters

5.1. Introduction

The period between 1950 and 1980 saw several changes in the design and manufacture of negative plates for lead–acid batteries. In particular, new types of additives were introduced following the change from wood to synthetic separators. There followed many investigations into the mechanisms and influence of the chosen additives [1–4]. Until that period, negative plates were perceived as the life-limiting component due to a progressive loss in their surface area during battery service. As a result of this work and the subsequent changes in technology, both the service-life and the coulombic output of lead–acid batteries were greatly improved.

In recent years, with the progressive introduction of valve-regulated lead–acid (VRLA) batteries, the behaviour of negative plates under typical operating conditions of limited overcharge and an internal oxygen cycle has assumed new importance. There is concern that without a better understanding and subsequent improvement of charge maintenance, the negative plate will again be the life-limiting component, in both cycling and standby applications.

The rapid reaction of oxygen with lead is the keystone to the functioning of the internal oxygen cycle in VRLA batteries, and ways to ensure that gas recombination proceeds efficiently without progressive loss of negative-plate capacity constitute the subject of many present studies. The self-discharge of the negative-plate by the oxidation reaction must be balanced by equivalent secondary reactions at the positive plate or, at least, decreased by appropriate charging conditions. Where high specific energy is desirable in, for example, new designs of electric-vehicle (EV) batteries, there is also the problem that negative failure may be exacerbated by a decrease in the mass of the active material to a value which is just sufficient to meet the required capacity, without due allowance for progressive loss of capacity as the battery ages.

Resolution of the above problems is made more difficult by the sensitivity of negative plates to various secondary reactions, such as those caused by impurities and additives. These may affect the self-discharge rate, as well as the charge-acceptance and the efficiency at which the charge input is subsequently used. The transient nature of these effects increases the difficulty of understanding their influence. Several studies are now underway to increase this understanding and

thereby improve the performance of negative plates in VRLA batteries, particularly under the high-rate, partial state-of-charge (HRPSoC) conditions that are experienced in all types of hybrid electric vehicle (HEV) applications. Much of this effort is supported and coordinated by the Advanced Lead–Acid Battery Consortium (ALABC) under the auspices of the International Lead and Zinc Research Organization. Whilst more work is required to ensure that negative plates in VRLA designs meet duty requirements and provide long and trouble-free service, this chapter reviews the present state-of-knowledge and includes a discussion of the effects of impurities and additives and their influence on charging methods.

5.2. Basic Electrochemical Characteristics

The first step in the conventional process for the manufacture of porous lead electrodes is to mix a powder of lead and lead oxide (so-called 'leady oxide') with sulfuric acid, water, and certain additives. The resulting paste is then applied to the grids and 'cured' under controlled conditions of temperature, relative humidity, and time to produce basic lead sulfates which assist consolidation of the material as well as its adherence to the grid. Finally, the basic lead sulfates are reduced to a porous lead plate by a prolonged electrochemical charge operation, so-called 'formation' (see Chapter 3). The chemical and physical structure of the active material produced by this process must be capable of meeting the design capacity and be sufficiently durable for the required battery service-life. With conventional manufacturing methods, the paste must also have the correct consistency to enable application to grids without loss, slumping, or excessive shrinkage.

Within these constraints, the apparent density of negative active-material is usually in the range 3.8–4.2 $g\,cm^{-3}$ with a surface area of 0.3–0.8 $m^2\,g^{-1}$ and a porosity of 48–55%. These properties change during service according to the types of additives used and the treatment history of the plates, i.e., depth-of-discharge (DoD) and charging practice.

The structure of negative active-material has been described as consisting of a skeleton which is produced during the initial stage of the formation process, with small lead crystals — a so-called 'energetic structure' — being developed on the surface in the latter stages [5]. It has been further suggested that the decline or increase in capacity during cycling is due to the fact that the microstructure developed during plate processing undergoes morphological changes with consequent changes in surface area.

During discharge, lead is oxidized to Pb^{2+} ions with the production of lead sulfate and the release of two electrons, i.e.,

$$Pb + HSO_4^- \rightarrow PbSO_4 + H^+ + 2e^- \tag{5.1}$$

The theoretical consumption of lead during discharge is 3.86 g per Ah (259 mAh g^{-1}), but the capacity is invariably limited by the surface coverage of sulfate and the restricted accessibility of acid within the pores so that the actual value is much less than theoretical. The capacity depends on several factors, which

include: discharge rate; temperature; plate thickness and internal structure, i.e., density, pore size, and surface area.

Functional characteristics, such as the specific energy and specific power at various rates of discharge and temperature, generally refer to cells or batteries as a whole. The properties of individual electrodes can be assessed, however, by monitoring the performance of single plates under experimental conditions where they limit the discharge, for example by discharging single negative plates against two opposing positive electrodes in excess electrolyte with a suitable reference electrode.

A good approximation of the relationship between current, I, and discharge duration, t, is given by the empirical Peukert equation, i.e.,

$$I^n t = K \tag{5.2}$$

where n and K are constants over a specific range of discharge conditions and can be determined experimentally. The value of n approaches unity at very small current densities at which the discharge capacity approaches the limit imposed by exhaustion of reactants. For intermediate current densities at 25°C, values of $K = 0.42$ and $n = 1.39$ have been reported for negative plates [6]. At high current densities, n approaches 2 as the capacity is limited by diffusion.

Diffusion limitations and their influence on capacity and the utilization of the active mass are progressively reduced with thinner plates, and the Peukert equation can be modified [7] to include both temperature and thickness parameters, namely:

$$I^n[t/d^{(2-n)}] = K_o(1 + aT) \tag{5.3}$$

where d is the plate thickness in mm; T is the temperature in °C; a is a constant over the range -20 to $+20$°C. The capacity and material utilization of negative plates that vary in thickness from 1 to 5.9 mm for discharge rates of 5 min, 1 h, and 5 h are shown in Fig. 5.1. The data illustrate the high efficiency of the negative active-mass

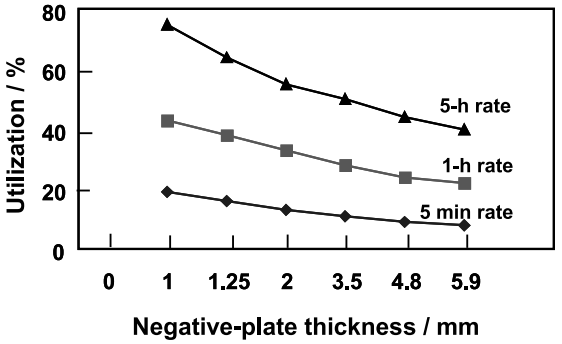

Fig. 5.1. Utilization of negative active-material at various plate thicknesses.

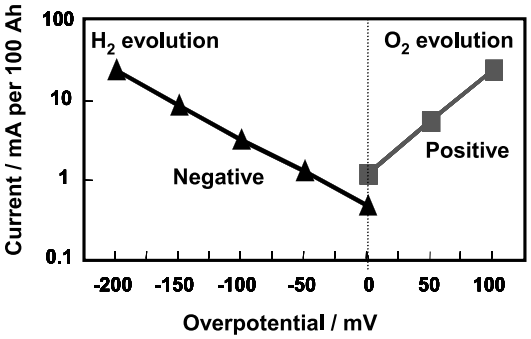

Fig. 5.2. Tafel plots for hydrogen and oxygen evolution at 20°C.

under conditions of excess electrolyte and low discharge rate; the coulombic utilization of thin plates approaches 80% of the Faradaic value.

Within the normal range of electrolyte concentrations (4.5–5.6 M H_2SO_4), the equilibrium potential, E_o, of the negative electrode is -0.330 to -0.345 V with respect to a standard hydrogen electrode (SHE). Deviations from this value during charge and discharge (i.e., the overpotential, η) as a result of kinetic hindrances and resistive losses can be conveniently related to the current density, i, by the Tafel equation

$$\eta = E - E_o = a + b \log i \tag{5.4}$$

where E is the electrode potential under load; a is a constant; b is the slope of the Tafel line. Tafel plots for negative and positive electrodes in a standby battery that had been float-charged for an extended period at 20°C are shown in Fig. 5.2.

The evolution of hydrogen on lead in sulfuric acid, though thermodynamically favoured, is strongly inhibited due to its high overpotential. The lead → lead sulfate and hydrogen evolution reactions occur simultaneously and can be represented by a mixed-potential [8]. In Fig. 5.3, the lead → lead sulfate reaction is shown to occur rapidly due to its low overpotential, whilst the overpotential associated with hydrogen evolution results in a slow and gradual rise in current. Under open-circuit conditions, i.e., no external current, self-discharge occurs with the gradual conversion of lead to lead sulfate at a mixed potential, E_M. The position of the mixed potential is determined mainly by the faster of the two reactions, whilst the (equal) rate of each reaction, i, is dominated by the slower reaction. For example, as shown in Fig. 5.3, an increase in the rate of hydrogen evolution (the slower reaction) results in a marked increase in the rate of self-discharge (the faster reaction), viz., $i_1 \rightarrow i_2$, but in only a slight shift in the mixed potential, viz., $E_{M_1} \rightarrow E_{M_2}$.

Electrode behaviour is strongly influenced by several factors, particularly by impurities, certain additives, and dry-charging treatments (especially those which are oil-based). Contamination by metals which have a lower hydrogen overpotential than lead, progressively increases gassing at lower applied potentials and accelerates

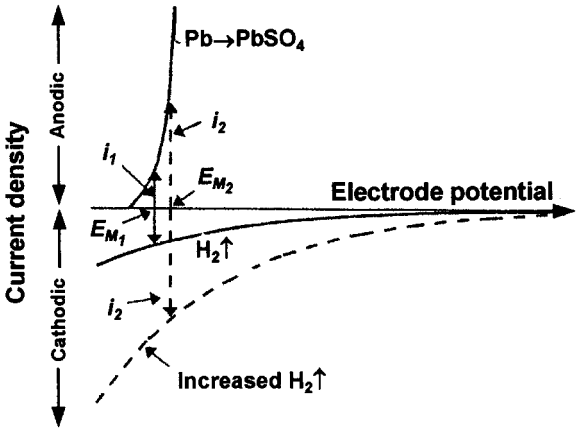

Fig. 5.3. Schematic of the mixed potential, E_M, established at the negative plate of a lead–acid battery due to the competing lead discharge and hydrogen evolution reactions (diagram based on that presented by Berndt [8]).

self-discharge. Trace amounts of these metals can increase the current when charging at the same potential and result in substantially higher gassing rates. Certain types of organic additives, such as lignosulfonates, can have the reverse effect and increase the overpotential [9], although usually not to the same extent as some metallic impurities. The complexity of the situation is further exacerbated by the transient nature of these influences. For example, the deposition of impurities may increase with service but, at the same time, coverage by lead sulfate may suppress their effect. Additionally, some metallic impurities may be gassed off as hydrides, particularly if certain organic additives or separators derived from natural products are used [10].

These factors have a major effect on the charging response. For example, where charging is limited to a pre-set voltage level, the amount of charge to this point, i.e., the charge-acceptance, will vary according to the influence of the contaminant or the additive. Constant-current charging provides some control of charge-acceptance, but the amount of charge which is efficiently used to convert discharged product to charged product will depend on the extent to which these factors effect the overpotential.

Manufacturing materials are the main source of impurities. The quality of lead used during manufacture varies widely and high purity is essential if the response to specific charging procedures is to be uniform. The difference in the current–voltage relationship during the charging of negative plates made with lead from two sources is shown in Fig. 5.4. One source is high-purity primary lead and the other is secondary (recovered) lead with higher impurity levels [11]. Batteries containing negative plates made from the secondary lead have higher charge currents at the same potential with much higher gassing rates, particularly as plates approach full charge.

Several attempts have been made to specify acceptable purity levels more accurately [12,13], but the strong influence of quite small amounts of certain metals

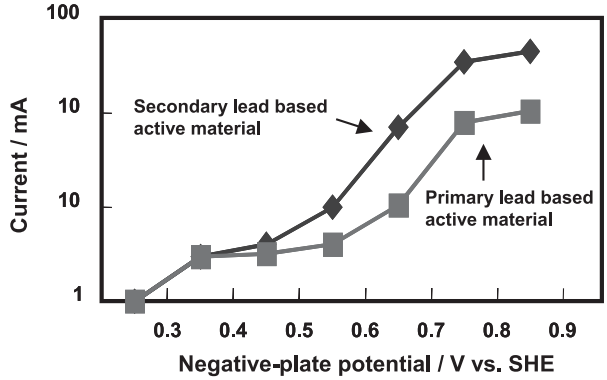

Fig. 5.4. Charging patterns of negative plates made from two sources of lead.

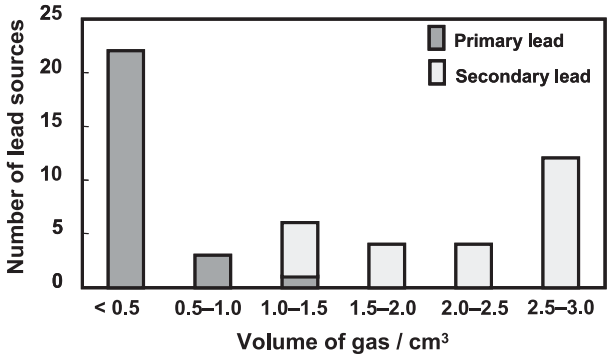

Fig. 5.5. Gassing on negative active-material made from primary and secondary lead.

makes this difficult. Additionally, there is a widely held view that combinations of trace amounts of certain metals have a greater effect than the individual metals themselves.

A simple and convenient method for assessing the scale of impurity effects is to measure the gassing rates of negatives made with lead from various sources when immersed in sulfuric acid [11]. The amount of gas evolved from negative active-material made from 50 different sources of lead, split approximately equally between primary and secondary lead, is shown in Fig. 5.5. The active material was fully formed, evacuated to remove absorbed gas, and immersed in acid for 70 days at 25°C. The primary lead samples gave much lower gassing rates. More recently [14], this technique has been used to demonstrate the variable effects of raw materials on both the gassing rate and the float currents of standby batteries, particularly in relation to the use of internal catalytic gas-recombination devices, as discussed later in Section 5.5. Quantification of the influence of specific impurities is presently being undertaken in a research project that is being conducted by CSIRO as part of the ALABC research programme [15].

Table 5.1. Impurity standards of primary and secondary lead (wt.%).

Element	Primary	Purified secondary	Element	Primary	Purified secondary
Al	< 0.0001	< 0.0001	Mn	< 0.00005	< 0.00005
Sb	0.0005	0.0003	Ni	< 0.0001	0.0001
As	< 0.0001	0.0001	Se	< 0.00005	< 0.00005
Bi	0.006	0.018	Ag	0.0005	0.0017
Co	< 0.00005	< 0.00005	Sn	0.0001	0.0001
Cr	< 0.00005	< 0.00005	Te	< 0.00005	< 0.00005
Cu	0.0004	0.0003	S	< 0.0001	< 0.0001
Fe	< 0.0001	< 0.0001	Zn	0.0006	0.0001

Several sources of refined secondary lead with higher purity standards, produced specifically for the manufacture of VRLA designs, are now available. Typical purity standards are shown in Table 5.1.

Whilst the influence of impurities and additives on charge or float conditions is common to all types of lead–acid batteries, with VRLA batteries there is the additional concern of self-discharge of the negative by reduction of the oxygen generated at the positive electrode, i.e.,

$$Pb + \tfrac{1}{2}O_2 + H_2SO_4 \rightarrow PbSO_4 + H_2O \tag{5.5}$$

The reduction of oxygen has been studied on porous lead plates of industrial design by using two-electrode models of the lead–acid battery, with close packing of the plates and with the space between the plates sealed along the edges [16]. The rate of absorption of oxygen in the system, j_a, was derived from the current flow when using a fully charged lead electrode held at an overpotential of 50 mV, i.e., −0.390 V vs. SHE. Oxygen entered the system at a rate, j_e, which was equivalent to that evolved from a PbO_2 electrode charged at current densities of up to 50 mA cm^{-2}. The ratio $j_a : j_e$ for different charging rates was determined for a flooded system without separators, as well as for cells which contained lower amounts of electrolyte with various separator materials (Fig. 5.6). The recombination of oxygen on the fully immersed (flooded) electrode is equivalent to a gassing rate of 0.1–0.2 mA cm^{-2}. This is in agreement with the convectional flow of oxygen in sulfuric acid; oxygen has a diffusion coefficient of 0.8×10^{-5} cm^2 s^{-1} and a solubility of 0.65×10^{-6} g mol cm^{-3}. In sealed systems that have glass-fibre separators with pore diameters between 10 and 20 μm and with an oxygen pressure sufficient to displace some electrolyte, recombination efficiencies greater than 50% are obtained at a current density of 50 mA cm^{-2}. This is a very high rate of charge for most applications.

Unlimited diffusion and the rapid reduction of oxygen will have an effect on the potential of the negative plate. It will remain close to the open-circuit value, with the potential of the positive plate becoming more positive under the usual

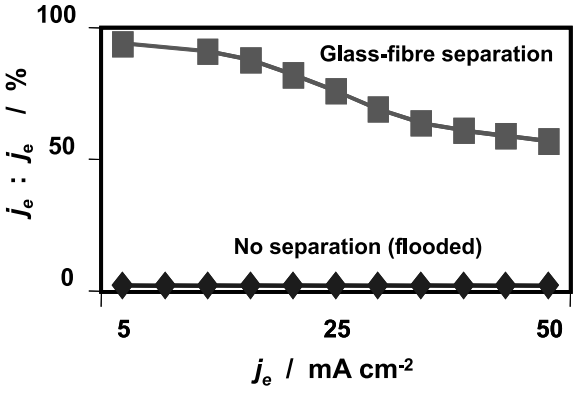

Fig. 5.6. Relative reduction rates of oxygen on porous lead electrodes.

voltage-limiting conditions of charge and with oxygen evolution increasing further according to the Tafel relationship. Under these conditions, a steady decline in the state-of-charge (SoC) of the negative plate is likely. Attempts to prevent this decrease in SoC by increasing overcharge will accelerate the problem unless secondary reactions, such as grid corrosion at the positive plate or oxidation of organic materials, reduce the evolution of oxygen to a value which allows the potential of the negative plate to become more negative.

Several possible ways to ensure that the negative plate is adequately charged are under investigation. It is important to balance the secondary reactions of grid corrosion at the positive, and hydrogen evolution at the negative, in such a way that the charge current more than compensates for the self-discharge at the negative. Alternatively, oxygen recombination can be limited by diffusion constraints, for example with highly saturated separators or by the use of separators which have a higher percentage of much smaller pores than the materials normally used in VRLA designs (see Chapters 6 and 7). Lowering of the recombination efficiency by these means implies some water loss from the system with the possibility of premature drying out. A further option is the use of internal catalysts to recombine the hydrogen evolved as the negative approaches full charge with a proportion of the oxygen evolved at the positive, to produce water. This approach is now used commercially [17,18] and the results are discussed, together with the influence of charging conditions on the SoC of the negative plate in Sections 5.4 and 5.5, below.

5.3. Negative-plate Additives

Traditionally, negative plates in lead–acid batteries contain a combination of carbon black, barium sulfate, and an organic additive which is usually a wood extract. These additives are collectively called an 'expander', although this term is often used purely for the organic component of the mix. The presence of the expander helps to

maintain a porous lead structure with a high surface-area during cycling. The three components are usually premixed by the supplier and the composition varies according to requirements. Typical proportions used in automotive batteries are: 0.15–0.25 wt.% carbon, 0.3–0.5 wt.% barium sulfate, 0.2–0.4 wt.% organic additive. Higher levels are used in industrial batteries. The total amount of expander used in industrial VRLA designs varies between 1.0 and 2.5% of the weight of oxide in the paste mix [9] and the ratio of organic, carbon, and barium additions vary according to the manufacturer's specifications. The organic component is not added to the negative plates of some products in order to avoid possible changes in the on-charge potential during service. In these cases, as much as 2.0 wt.% barium sulfate may be added to compensate for the absence of the organic additive.

The effects of expanders have been investigated extensively, particularly in the period between 1940 and 1955 [1,19,20]. The work was aimed at extending the service life of negative plates, which was the usual failure mode of lead–acid batteries at that time, and at increasing engine starting power, particularly under cold conditions. The additives influence the development of lead crystals during charge and control the formation of lead sulfate during discharge [21]. The three materials function in different ways to provide independent beneficial features, but also give further improvements when combined [22–24].

As mentioned above in Section 5.1, attention has focused again on the need to maintain the negative plate in a good SoC in VRLA batteries, and the more recent studies have concentrated on the choice of expanders. This is mainly because of the concern that the strong oxidizing atmosphere and higher temperature at the surface of the negative plate under the internal oxygen cycle will degrade the organic component and thus cause premature battery failure. Whilst there is little quantitative evidence of such degradation, some manufacturers increase the amount of barium sulfate, which modifies the crystal size of lead sulfate, to about 1.0 wt.%. The higher amount is presumed to maintain a small crystal size for the discharge product in the event of loss of effectiveness of the organic component.

A second concern is the fact that naturally occurring materials contain metallic impurities, which may reduce the hydrogen overpotential. In cycling applications, it is usual with VRLA designs to limit charge to a pre-set voltage. Additives which increase the plate overpotentials will reduce gassing, i.e., the coulombic input during charge to these pre-set levels will be used more efficiently, although the total charge accepted may be lower. Conversely, under the same conditions, additives which decrease the overpotentials will cause the ampere-hour input during charge to be higher but because the plates will gas earlier, the charge efficiency will be lower. These influences may be compensated by suitable charge algorithms (see Chapter 9), but it is their transient nature during service that is difficult to manage. The other two additives, namely, carbon black and barium sulfate, when supplied at the required purity and quality standards, have little or no effect on the overpotentials.

The final reason for the renewed interest in expanders — and indeed in all types of additive — is the desire to improve the coulombic output of negative plates, primarily in order to improve the specific power and specific energy of lead–acid batteries. This objective has assumed more importance recently given the need to develop batteries for EV and HEV applications.

5.3.1. Carbon

Early studies on the effects of carbon addition to negative pastes [21,25] showed that carbon functions primarily as a conductor, and thereby enhances formation efficiency and reduces the level of residual sulfate. It may also improve recharge, particularly under deep-discharge conditions. It was further concluded that, when combined with barium sulfate and an organic component, a typical carbon addition of ~ 0.2 wt.% has little influence on the discharge performance and cycle-life of batteries.

More recently, Shiomi *et al.* [26] reported that much higher amounts of carbon not only improve the formation process with less charge required to reduce the lead sulfate, but also extend cycle-life in tests designed to simulate HEV service. The schedules provide only limited overcharge and VRLA batteries with negative plates made with ten times the normal levels of carbon exhibit much improved cycling performance and generally have higher finishing voltages throughout cycling, see Fig. 5.7.

Similar improvements in cycling performance have been reported by Saez *et al.* [27] with high levels of carbon in negative plates in 15-Ah VRLA motorcycle batteries that were operated under typical EV schedules. The batteries contained negative plates made with 0.2 wt.% Vanisperse A, 1.0 wt.% barium sulfate, and three levels of carbon, viz., 0.28, 0.56, and 2.8 wt.%. The initial capacities at the 1*C*, 2*C*, and 5*C* discharge rates increased by about 10% when the carbon content was raised to 0.56 wt.%, but were lower at the higher carbon level of 2.8 wt.%. This effect on capacity was confirmed when trials were repeated prior to conducting the EUCAR ECE15L cycle test. This schedule consists of a repetitive series of constant-power

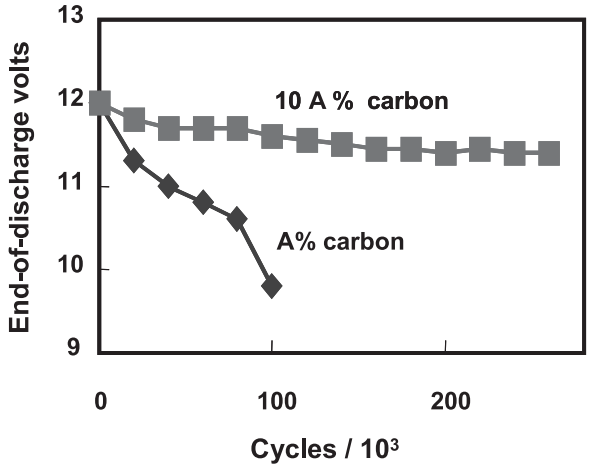

Fig. 5.7. Life-cycle tests on 65-Ah VRLA batteries made with two levels of carbon in the negative plates [26].

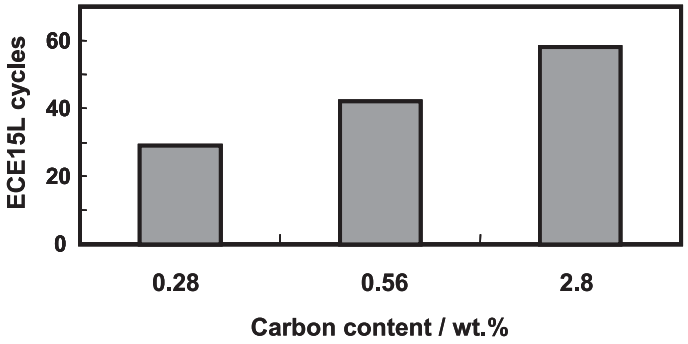

Fig. 5.8. Life-cycle tests on batteries with different amounts of carbon in the negative plates.

Table 5.2. Properties of negative plates made with different amounts of carbon.

Carbon content (wt.%)	Free-lead content (wt.%)	Porosity (%)	Mean pore size (μm)	Specific surface-area ($m^2 g^{-1}$)
0.28	2.5	49	0.38	1.53
0.56	1.1	45	0.28	1.65
2.8	1.4	41	0.25	1.62

discharges, charges, and rest periods. Battery failure usually occurs during the high-power discharge stage with the battery voltage decreasing below the required level. The performance of batteries with three levels of carbon when tested to 80% DoD is shown in Fig. 5.8. The cycle-life improves when the carbon addition is doubled to 0.56 wt.%, and there is a further marked increase when the content is raised to 2.8 wt.%. The properties of these negative plates were measured and are listed in Table 5.2. The data show a trend of decreasing porosity, smaller pore size, and greater specific surface-area as the carbon content is increased.

Both Shiomi *et al.* [26] and Saez *et al.* [27] have suggested that high levels of carbon improve the rechargeability of negative plates by providing conductive networks around the peripheries of lead sulfate crystals and, thereby, extend battery cycle-life.

In a third study, Newnham *et al.* [28] constructed cells with negatives that contained up to ten times the normal level of standard grade carbon, high surface-area carbon, and graphite powder. Each cell was fitted with an electrolyte pump to minimize the influence of acid stratification, and then subjected to a simple HEV driving schedule (1-min discharge, 1-min charge between 50 and 53% SoC). Negative-plate potentials were measured at the end of each charge and each discharge period. The effect of high levels of carbon was noticeable during the first charge — the potential of cells made with negatives that contained normal levels of carbon (0.2 wt.%) displayed a progressive rise at an early stage of charging, but the potential of cells with 2.0 wt.% carbon or graphite remained low until substantial

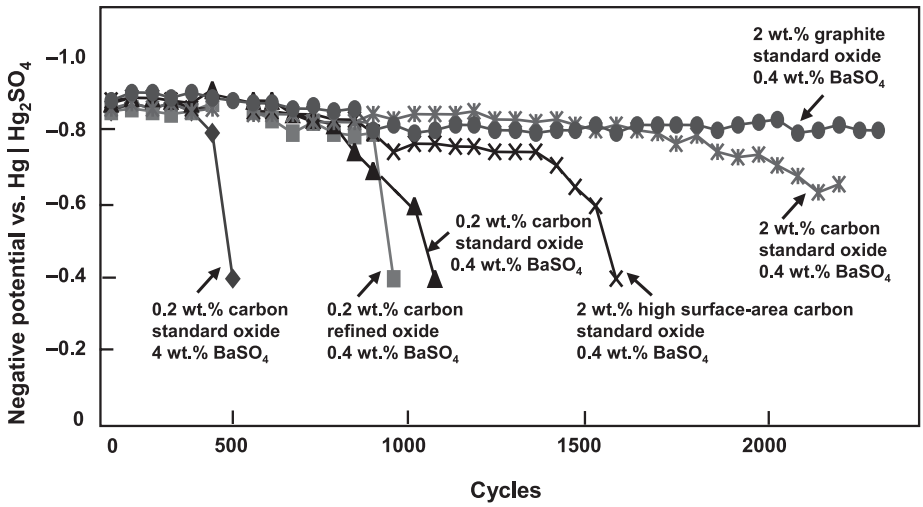

Fig. 5.9. End-of-discharge potential of negative plates in prototype cells during simple HEV duty [28].

charging had taken place. Under the HEV schedule, cells with the higher levels of carbon showed a substantial improvement in cycle-life, particularly when using negatives made with 2.0 wt.% graphite, as shown in Fig. 5.9. During charging in the early stages of cycling, it was found that the potential of the negatives increased in a negative direction into regions where significant evolution of hydrogen, and hence a lower charge efficiency, can be expected. In most cases, a high content of carbon delayed this effect, and the use of graphite was even more effective, see Fig. 5.9.

5.3.2. Barium sulfate

The influence of barium sulfate additions on the performance of negative plates has been studied extensively [21,25]. Barium sulfate is isomorphous with lead sulfate and therefore functions as a nucleation centre ('seed') for the precipitation of the discharge product and favourably restricts its crystal size (see Section 4.5.1, Chapter 4). Strontium sulfate behaves similarly. It has been suggested that the effectiveness of barium sulfate is directly attributable to the number of nucleii present rather than to the amount added. The optimum amount of barium sulfate when combined with other additives for use in automotive batteries has been found to be between 0.3 and 0.5 wt.%.

These early developments were carried out on flooded batteries but similar conclusions have been shown to apply to VRLA designs. There is no indication that barium sulfate additions affect negative-plate overpotentials. Thus, there is a trend towards using greater amounts in VRLA batteries on the basis that the level of organic additive can be reduced so as to avoid overpotential influences on the performance of positive and/or negative plates during charge and to maintain good

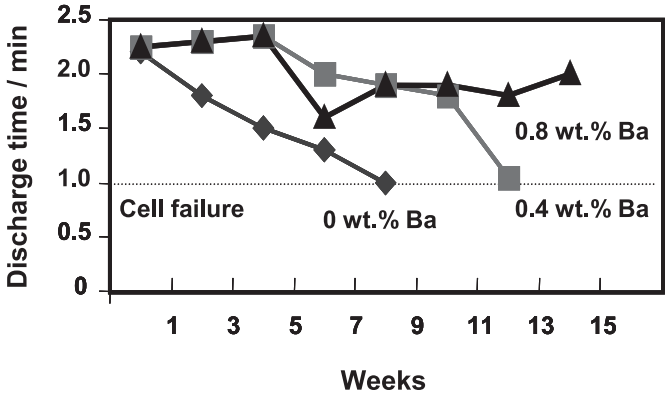

Fig. 5.10. Effect of barium sulfate additions on battery cycle-life.

negative-plate activity in the event of degradation of the organic additive during service. Several manufacturers have doubled, or even trebled, the barium content in negative plates used in VRLA batteries. This is particularly the case in some standby batteries where only barium sulfate and carbon are used as a precaution against varying float currents during service.

From tests conducted on negative-limited, nine-plate cells with three levels of barium sulfate, it was found that cycle-life improved as the amount of barium sulfate was increased [29]. The negatives contained 0.15 wt.% Vanisperse A and 0.2 wt.% carbon, and the cells subjected to an automotive battery test schedule of 2-h discharge/4-h charge at $0.25C_{20}$ A over 5 days followed by open-circuit stand for 65 h and a check discharge at $5C_{20}$ A at -18°C. With a failure point of 1-min discharge duration, cells without barium additions survived for only seven weeks on this schedule. The cycle-life increased to 13 weeks with 0.4 wt.% barium sulfate, and to more than 15 weeks with 0.8 wt.% barium sulfate, as shown in Fig. 5.10. Studies on negative plates in VRLA batteries revealed a similar trend [27]. Cells with 1.0 wt.% barium sulfate gave initial capacities which were similar to those for cells with lower additions, but had better cycle-lives on the ECE15L life test. The improvement when higher levels of barium were used in negative plates with two different organic additives is demonstrated in Fig. 5.11.

5.3.3. Organic additives

Traditionally, the organic components of expander formulations are derived from natural products such as wood pulp. The composition of such materials is poorly defined. Lignin extracts, frequently obtained from waste sulfite liquors in the papermaking industry, are purified by removing sugars and various metals, and then depolymerized to different degrees. Lignin molecules are formed from three primary precursors, *p*-coumaryl alcohol, coniferyl alcohol, and sinapyl alcohol; the

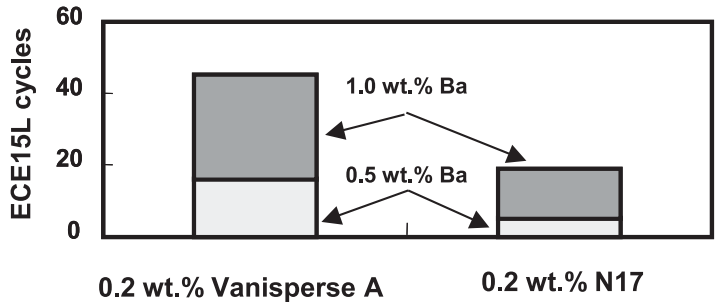

Fig. 5.11. Performance of batteries with two levels of barium sulfate and two organic additives under ECE 15L life test.

proportion of each varies with the origin of the lignin [30]. They can be sulfonated to different levels with sulfurous acid and then prepared as salts with various cations.

The preferred structure appears to be a low average molecular weight with a high proportion of carboxyl and phenolic groups, and a low content of methoxy and thionyl radicals. It has been suggested [31] that structural groups of the pyrocatechol type are particularly beneficial. Lignosulfonates produced by sulfonation can be partially oxidized, a process which reduces the number of sulfonic and methoxy groups and increases the number of functional phenolic and carboxyl groups. Such materials are commonly known as 'oxylignins'.

Lignin-derived compounds are dispersing agents which reduce the particle size of the active material and greatly increase the surface area. During discharge, the surface coverage of active lead sites is modified and passivation is delayed, with consequent improvement and maintenance of capacity, particularly when discharges are carried out at high rates and under cold conditions. In common with most organics, these materials may affect the overvoltage during charge with consequent effects on charging patterns. The extent of this varies with the type and amount of expander and as explained earlier, charge responses may change during service due to degradation of the organic. A further feature of these materials is the cleansing or immunizing effect of purging metallic impurities from the lead surface. This is similar to the mechanism by which certain separators, namely those made from natural products such as rubber or wood, reduce the effect of trace contaminants, such as antimony, by promoting the evolution of their hydrides, e.g., stibine in the case of antimony [10].

The concern over the performance of negative plates in VRLA batteries has resulted in renewed interest in the influence and mechanisms of organic additives and extensive research programmes have been carried out under the auspices of the ALABC. This work has included an assessment of 34 materials, five of which were synthetic organic compounds that were identified to have the potential to act as effective expander components in lead–acid batteries [32]. Preliminary screening tests for stability in acid, impurities and thermal stability, followed by studies of potentiostatic transients, impedance plots, and cyclic voltammograms [33], have

reduced the number to five naturally occurring and three synthetically produced materials for cell testing. A parallel research programme [27] started with 19 possible materials from natural and synthetic sources. These were reduced to seven for performance and life-cycle testing in cells and batteries. All the tested organic substances changed the structure of the lead sulfate layer and this change had an influence on its subsequent reduction to lead. Further work on the effects of blends of organic materials on capacity and service has been carried out in a project under the Brite Euram Programme of the European Union [34]; the project was also partly funded by the ALABC.

In the above studies, batteries with negative plates that contain both lignins and oxylignins exhibit improved cycling performance. With the likelihood that VRLA batteries will have higher operational temperatures due to the exothermic reduction of oxygen and that thermal degradation will therefore be accelerated, it has been suggested that a combination of a low level of a highly electrochemically active material with a higher amount of a less electrochemically active material may be desirable for optimum cycle-life. Combinations of Indulin AT (lignin), Vanisperse A (oxylignin), and proprietary materials identified as UP313 (a purified softwood Kraft lignin) and UP414 (a desulfonated, high molecular weight, sodium lignosulfonate made from softwood) have been used in capacity and cycle-life tests at 25, 40, and 60°C. The life of all test cells was much reduced at the higher temperature, but unlike tests with other additives, there was no fall in capacity at the beginning of cycling. It was found that the charge mode strongly influences both the capacity and the cycle-life. If the charge is conducted to a small overcharge, the capacity of the negative plates first declines rapidly, increases to about 80% of the useful capacity within 10–15 cycles, and then remains almost constant at this level. If the charge is conducted to high overcharge levels, no initial decline in capacity is observed and negative plates that contain a combination of the three additives give the longest cycle-life.

In the study conducted by Boden [32], the effectiveness of the eight organic materials which passed the screening test was determined by measuring the capacities of negative plates made with three levels of each additive at three constant-current discharge rates. The experiments were conducted with negative-limiting cells which each consisted of three plates with a central negative fitted with a reference electrode. Capacity measurements were made after several conditioning cycles and with five replicates. In addition, initial capacities were measured at room temperature and at −18°C under the Dynamic Stress Test for EVs in accordance with the United States Advanced Battery Consortium Procedure 5B. This has a variable discharge profile based on specific power requirements, with a maximum of $150\,W\,kg^{-1}$ when related to a full-sized EV battery. For the experimental cells, the peak power was equivalent to a current density of $16.3\,mA\,cm^{-2}$.

All the organic additives increased the BET specific surface-area of the negative plate. In the absence of an additive, the surface area was $0.2\,m^2\,g^{-1}$. Vanisperse A — probably the organic material which is most commonly used by the battery industry — increased the surface area to $0.67\,m^2\,g^{-1}$ at the lowest addition level (0.25 wt.%), and to $0.82\,m^2\,g^{-1}$ at 0.75 wt.%. Other materials increased the surface area similarly, but not to the same extent. For all the materials, the surface area increased with the

dosage. For example, plates made with the synthetic material BNF had a surface area of $0.4\,m^2\,g^{-1}$ at the lowest level (0.25 wt.%) and $0.8\,m^2\,g^{-1}$ at the highest addition level.

The utilization of negative active-material at three discharge rates was determined, and Table 5.3 shows the range of mean values for plates made with 0.22 wt.% carbon black, 0.8 wt.% barium sulfate, and three levels of the experimental materials. The data have been normalized to eliminate small variations in paste weight. At 0.25 wt.%, the least-effective additive increased the material efficiency at a current density of $5.7\,mA\,cm^{-2}$ (5-h rate) from approximately $90\,mAh\,g^{-1}$ (no organic) to $101\,mAh\,g^{-1}$, after conditioning cycles, whilst the most-effective material gave $147\,mAh\,g^{-1}$. This is 57% of the theoretical value of $259\,mAh\,g^{-1}$. Additives which showed the greatest improvement at $5.7\,mA\,cm^{-2}$ are listed in Table 5.4 and include two synthetically produced materials, Lomar B and GKD. The difference between the effects of various additives is more noticeable at high discharge rates. Higher capacities were obtained with greater amounts of some materials, especially Indulin AT (a natural wood lignin), Kraftplex (a sulfonated modified Kraft lignin), and

Table 5.3. Range of mean active-material utilization ($mAh\,g^{-1}$) of negative plates with varying amounts of additive.*

Additive concentration (wt.%)	Discharge rate		
	$5.7\,mA\,cm^{-2}$ ($C/5$)	$8.5\,mA\,cm^{-2}$ ($C/3$)	$21.7\,mA\,cm^{-2}$ ($C/1$)
0	90	84	64
0.25	101 to 147	95 to 143	79 to 122
0.50	119 to 144	106 to 132	92 to 121
0.75	101 to 147	93 to 142	74 to 123

*Values are the mean of five cells for each experimental variant and the range shown covers the values for all of the eight different organic additives [30].

Table 5.4. Additives with highest utilization of negative active-material at $5.7\,mA\,cm^{-2}$.

Material	Type	Concentration (wt.%)	Improvement* (%)
Lomar B	Naphthalene sulfonate	0.25	170
Lomar B	Naphthalene sulfonate	0.75	169
Kraftplex	Sulfonated Kraft lignin	0.75	161
Maracell XC-2	Partially desulfonated sodium lignosulfonate	0.25	157
GKD	Composition unknown	0.50	155
Vanisperse A	Partially desulfonated sodium lignosulfonate	0.25	152

*Negatives with no organic additive = 100%.

Table 5.5. Utilization of negative active-material under Dynamic Stress Test.

Material	Concentration (wt.%)	Utilization ($mAh\,g^{-1}$)	
		Room temperature	−18°C
Lomar B	0.5	116	55
Lomar B	0.25	115	49
Lomar B	0.75	112	50
Kraftplex	0.75	108	49
GKD	0.5	106	33
GKD	0.75	101	49
Maracell XC	0.75	100	50
Vanisperse A	0.25	100	45
Vanisperse A	0.75	100	45

Lignotech D-1380 (a partially desulfonated sodium lignosulfonate). With other materials, for example BNF (a beta-naphthol formaldehyde condensate) and Vanisperse A (a partially desulfonated sodium lignosulfonate), the capacities were lower at higher concentrations.

The capacities and utilizations obtained under the variable power Dynamic Stress Test at 25°C and −18°C followed a similar trend. The results for materials which gave good utilizations are summarized in Table 5.5.

Saez *et al.* [27] used seven additives from the original nineteen for cell testing at a level of 0.2 wt.%, together with the addition of 1.0 wt.% barium sulfate and 0.28 wt.% carbon. Three additives were also tested at the 0.4 wt.% level, namely, DD5 (a blend of Kraft lignin and condensed naphthalene sulfonate), N17 (a sodium lignosulfonate), and Vanisperse A. At the 5-h rate, the best results, which cannot be directly compared with those of Boden [32] because of the difference in cell design, gave material utilizations of 120–128 $mAh\,g^{-1}$ and 114–124 $mAh\,g^{-1}$ for 0.2 and 0.4 wt.% additions, respectively, i.e., utilization was generally slightly lower at the higher level. A small decrease in efficiency with the higher amount of additive was also observed on the variable power ECE15L schedule; cells with 0.2 wt.% additive had utilizations between 96 and 108 $mAh\,g^{-1}$, whilst those with 0.4 wt.% gave 92–96 $mAh\,g^{-1}$. At both additive levels, there was an appreciable decrease in both capacity and material utilization on subsequent ECE15L cycles.

Whilst there are clear differences between the effects of the various organic materials, the influence of increasing levels of addition is variable. In both the recent research programmes [27,32], some additives give better results at the lower concentrations, whilst higher amounts of others improve performance. It is suggested that there exists a point at which the maximum surface adsorption of a given organic material takes place, above which little, if any, benefit is obtained at higher concentrations. Greater utilizations may be possible with higher additions, but because of the apparent high specificity of the organic–active-material surface chemistry, comparing the performance at a constant loading of active material may not be the most effective method of evaluation.

Table 5.6. Cycle-life of three-plate cells at two temperatures.

Additive	Concentration (wt.%)	Cycle-life	
		25°C	40°C
Vanisperse A	0.75	1000	500
Vanisperse A	0.25	680	110
Lomar B	0.75	510	390
BNF	0.75	370	320
GKD	0.50	100	480
Lignotech D-1380	0.75	150	460
Maracell XC	0.75	180	420

Although the influence of the above materials over extended battery service has yet to be quantified, experimental trials at 25 and 40°C with three-plate cells which had an excess of positive active-material have provided an indication of their effectiveness during cycling [9]. The cells were discharged at 1.50 A (16.3 mA cm^{-2}) to 1.70 V, and recharged at 2.45 V with a current limit of 5 A. The failure point was when the utilization of the negative active-material fell by 20 mAh g^{-1} from its initial value. Cells with no organic additives had mean cycle-lives of 70 and 115, and material utilizations of 58 and 70 mAh g^{-1} at 25 and 40°C, respectively. All additives improved the cycle-life but to different extents, see Table 5.6. With certain materials, the cycle-life was increased on raising the temperature to 40°C, whilst others gave a lower cycle-life at that temperature. There was also a considerable difference in the effect of different concentrations of the same material, as can be seen for the two levels of Vanisperse A. To some extent, this may be explained by the pre-defined failure point used in the tests.

A better representation of the effectiveness of the additives is given in Fig. 5.12 which shows the actual material efficiency of each additive after the first 100 cycles. Additives which had a better initial performance at the lower concentration of 0.25 wt.%, such as Lomar B, Vanisperse A, and Maracell XC-2, maintained efficiencies that were greater than 100 mAh g^{-1} after 100 cycles. At the higher concentrations (0.75 wt.%), the utilization of negatives with synthetic materials Lomar and GKD was about 20% higher than most of the natural products. In most cases, but particularly with the natural products, the material utilization was higher when cells were cycled at 40°C. With the synthetic material Lomar B, there was little difference in utilization at the two temperatures.

During cycling, the surface area of negatives made with natural products decreased and the lead sulfate content increased. For example, the surface area of negative plates that contained Vanisperse A decreased from ~ 0.8 to 0.3 $m^2 g^{-1}$ at about 400 cycles. BET surface-area analysis of negatives appears to be a good indicator of the effectiveness of the organic material — there is a correlation between surface area and capacity. It is noteworthy that the plates made with Lomar B maintained a surface area of 0.4 $m^2 g^{-1}$ through more than 500 cycles, at both 25 and 40°C.

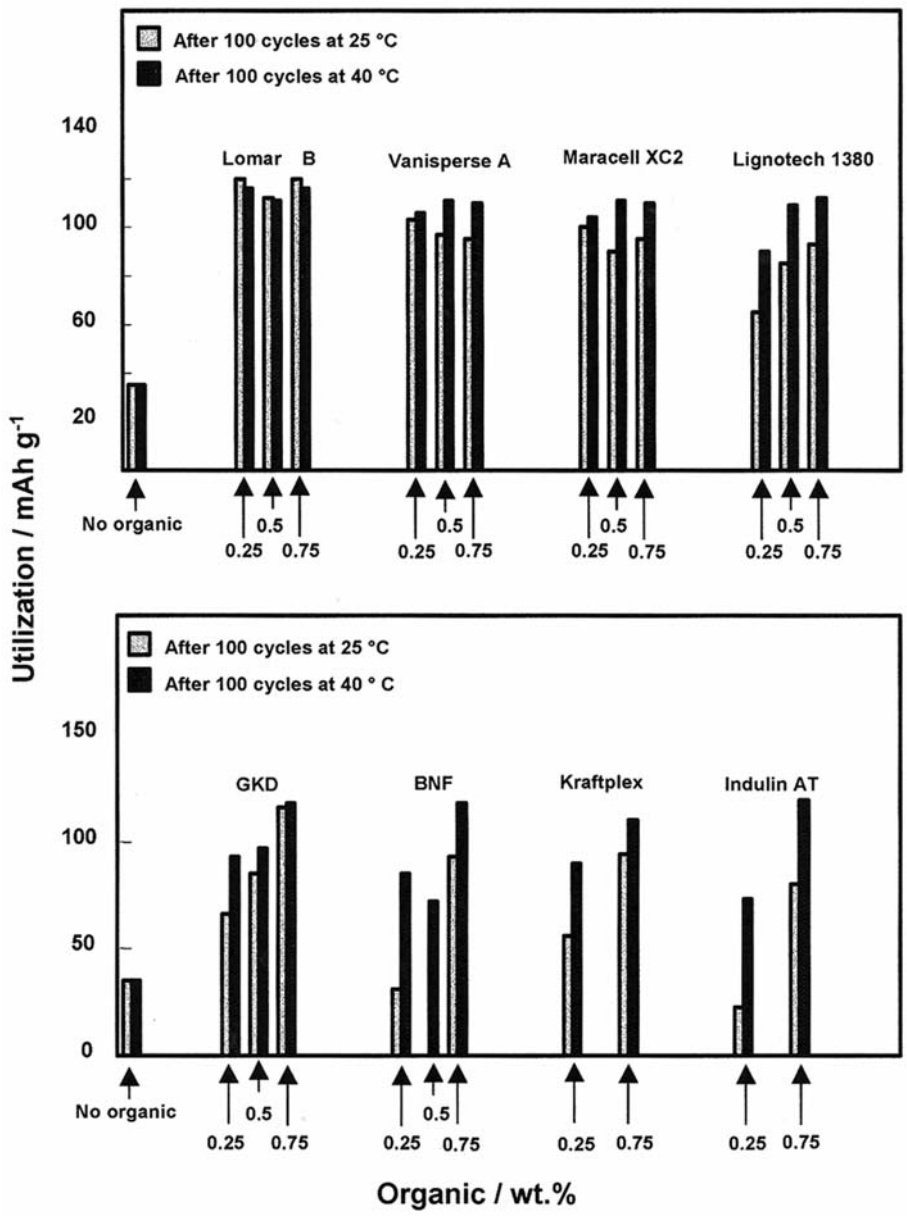

Fig. 5.12. Effect of type and amount of organic additive on utilization of negative-plate material after 100 cycles at 25 and 40°C.

The best cycle-lives at room temperature were obtained with the organic materials that gave the highest initial utilization. This is not always the case at higher temperatures, where, though material utilization is improved, the cycle-life with the more efficient additives decreases and those negatives containing the less efficient

additives cycle longer before significant deterioration in battery performance. This suggests that the more electrochemically efficient materials are also the most degradable. In support of this view, additives (e.g., Vanisperse A) which showed a decrease in cycle-life with temperature were the most severely decomposed when soaked for five days in 40% sulfuric acid at 65°C.

In summary, it is clear that the experimental organic materials exhibit different behaviour. Additions of synthetic Lomar B yield the highest initial capacity both on constant-current discharges and on the Dynamic Stress Test, as well as a good mean cycle-life. The widely used Vanisperse A provides a somewhat longer cycle-life, particularly at high addition levels, but produces a lower capacity and, more seriously, is found to exhibit substantial batch-to-batch variability in electrode properties [33]. This latter problem may ultimately encourage the use of synthetic materials. All the experimental work conducted to date suggests that highly compressed designs of VRLA cell enable increased amounts of additives to be used without overexpansion being a major concern. Additions of up to 0.75 wt.% have been used so far, and it is possible that even higher amounts can be used in VRLA cells to provide further improvement in performance.

5.4. Charging Influences

As described above in Section 5.2, the high hydrogen overpotential on lead allows the negative plate to charge efficiently with minimal gassing until the charge reaction is almost complete. This situation applies over a wide range of charging rates and temperatures. By comparison, recharge of the positive plate is less efficient, with the evolution of oxygen occurring early during charge and increasing progressively as the charge proceeds [35].

Several factors influence the hydrogen overpotential, especially metallic impurities which can reduce its value and therefore increase gassing and self-discharge and thereby decrease the charge efficiency. In extreme cases of contamination only hydrogen is produced, i.e., it is impossible to recharge the negative plate. Organic additives increase the hydrogen overpotential to various degrees according to the type and amount of the organic material. This implies more efficient conversion of the discharged product to active material. Under limiting charging conditions (voltage or time), however, an increase in the absolute value of the potential at the negative may reduce the charge-acceptance and consequently the positive plate, which is the less-efficient charge acceptor, may not be adequately charged.

The influence of organic materials on charge inhibition has been demonstrated by means of cyclic voltammetry [36]. All the materials increase the anodic peak area, which is an indication of the developed capacity. In addition, the expanders modify, to varying degrees, the shape and peak values of the cathodic sweep, which are indicators of the charge-acceptance. Consequently, the voltammograms enable two main performance features of organic materials to be examined, namely: (i) the ability to increase the capacity of the lead electrode; (ii) the higher or lower hindrance that the additive imparts to the charging process. Saez *et al.* [27] identified seven preferred additives. The differences between the cathodic peak potentials of

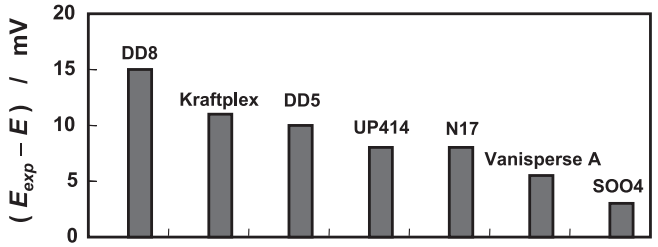

Fig. 5.13. Change in cathodic peak potential ($E_{exp} - E$) of negative plates with (E_{exp}) and without organic additive (E).

Table 5.7. Gas evolution currents from negative plates with different organic materials before and after cycling (charge at 1.35 V vs. $Hg|Hg_2SO_4$).

Organic material	Gas evolution (mA)	
	Initial	After 40 cycles
DD5	6.3	241.4
DD8	9.7	133.2
Kraftplex	9.3	392.6
N17	12.2	46.3
S004	11.4	58
UP414	3.3	144
Vanisperse A	6.5	81.6

negatives with each of these materials (E_{exp}) and those of undoped negative plates (E) are shown in Fig. 5.13. The practical significance of these effects was shown by measuring gassing rates during the charging of cells made with negatives containing the additives, both before and after cycling. The data given in Table 5.7 show a marked and variable increase in hydrogen evolution after 40 cycles. It may be possible to counter these effects by the use of charge algorithms that accommodate such changes, or by making appropriate corrections to the selected charging procedure during service.

In VRLA designs, there is the added complication that self-discharge as a result of the oxygen-recombination process renders the potential of the negative plate less negative. Consequently, under similar limiting conditions of voltage or time, it is possible to recharge the positive plate effectively with only a low overcharge factor, whilst the recharge of the negative plate may be insufficient because of the self-discharge reaction. Further overcharge only serves to increase both the temperature of the battery and the rate of self-discharge. Moreover, the situation at the negative is exacerbated if impurities that promote self-discharge are also present.

Negative plates made with different organic materials, as described previously [31] had end-of-charge potentials between -1.00 and -1.30 V (with respect to $Hg|Hg_2SO_4$) when charged during cycling with a voltage limit of 2.45 V per cell for 5 h. The potentials of the positive plate varied by a similar amount in the positive direction, i.e., over a range of $+1.45$ to $+1.15$ V. At room temperature, the shift in the potential of the negative plate to less negative values during cycling was most noticeable with those plates that had the highest initial value. Usually, though not always, cycle-life was improved at 40°C. It has been suggested [32] that this behaviour reflects the effect of the organic component of the expander on the charge-acceptance under voltage-limiting conditions and would account for the improved cycle-life at higher temperatures.

The majority of VRLA batteries produced today are used in standby applications to provide a reliable source of power in the event of failure of the mains supply. Discharges are infrequent and the batteries are maintained by float charging at a pre-set voltage. For example, European practice is to use parallel strings (usually 48 V) across a 54.5 V supply (2.27 V per cell). Adequately designed new cells, after conditioning and free of impurities, have a float current of < 1 mA per Ah at 20°C.

Under normal operating conditions, the battery is fully charged and the float current, I_{float}, should maintain this condition by compensating for self-discharge and secondary reactions. In a VRLA cell, the current distribution at each electrode is:
At negative electrode

$$I_{\text{float}} = I_{H_2} + I_R \tag{5.6}$$

At positive electrode

$$I_{\text{float}} = I_{O_2} + I_{\text{corr}} \tag{5.7}$$

where the current consumed by hydrogen evolution, oxygen reduction, oxygen evolution, and grid corrosion is denoted by I_{H_2}, I_R, I_{O_2}, and $I_{\text{corr.}}$, respectively.

The hydrogen evolution current, I_{H_2} follows the Tafel relationship, and is the main reaction at the negative plate in vented cells. At high oxygen-recombination efficiencies ($\sim 100\%$), all the oxygen produced at the positive plate is reduced at the negative. In this situation, if the hydrogen evolution rate, I_{H_2}, exceeds the corrosion rate, $I_{\text{corr.}}$, the negative plate will not be fully charged. Most likely, it will be progressively self-discharged and lose capacity. If, however, $I_{\text{corr.}}$ is greater than I_{H_2}, the float current will be sufficient to sustain the charge on the negative. With less oxygen recombination, for example in the case of cells that have highly saturated separators, or if gas transport is impeded by using separators with small diameter pores [37], the float current may sustain the charge on the negative unless impurities increase the hydrogen evolution current excessively. In this situation, oxygen that is not recombined will exhaust through the vent and the system may dry out prematurely.

To ensure reliability over long periods of service, good purity standards are essential. With proper control of temperature and float voltage, service-lives in excess of 10 years are normal and positive grid corrosion is the usual failure mode. At high

temperatures, however, corrosion may be excessive and intermittent float charging has been proposed to minimize corrosion rates [38].

In cycling applications where charging is invariably time-limited, the effectiveness of recharge is influenced by the relative efficiencies of the oxidation and the reduction of $PbSO_4$ in the respective plate polarities. Marginal differences in the SoC of the positive and negative plates will accumulate over several cycles. Several charging algorithms have been proposed in an attempt to overcome this problem (see Chapter 9). The simplest approach, now widely used, is to continue the recharge at a low constant current for a set time after the normal voltage-limited termination. Stepped constant-current and 'current-interrupt' algorithms operate on a similar principle and help to complete the recharge of the negative without undue build-up of heat. Improved cycle-lives of VRLA batteries have been reported [39] by limiting the charge to 105% of the discharge output, followed by an extended charge of 115% after every six cycles. With a similar procedure, up to 1000 cycles have been reported with spiral-wound cells on a rapid charging schedule [40]. The cells were undercharged during rapid charging with an overcharge every five cycles. Subsequent examination showed that the rate of growth of the negative active-material particles was slower during rapid charging compared with that observed during conventional charging.

A similar approach, used experimentally with some success, is to conduct cycling with only partial recharge. Under these conditions, the charge efficiency at both electrodes is high and the secondary reactions of gas production are reduced. Extended cycle-lives were obtained with batteries cycled between 20 and 80% of full charge [41] and, more recently, 12-V VRLA batteries recharged to 80% capacity with a 14.35 V limit and a full recharge with a constant current every 10 cycles gave 800 cycles to a failure limit of 80% of the initial capacity [42]. Beyond 800 cycles, there was a more rapid decline in capacity and the negative plates could not be fully charged without causing unacceptable thermal problems. Many applications do not require a full discharge on each cycle (e.g., HEV and remote-area power supply duties, see Chapters 11 and 14, respectively) and operating procedures of this type could extend service-life appreciably [43].

5.5. Use of Internal Catalysts

Several early patents exist on the use of gas-recombining catalysts inside vented cells to combine gases produced on overcharge and thereby reduce watering periods and the hazard of gassing in closed environments [43–46]. More recently, such catalysts have been fitted in VRLA batteries to recombine some of the oxygen produced at the positive plate during charge with the small amount of hydrogen produced at the negative [47,48]. As explained earlier, unless the secondary reactions at each electrode are properly balanced, the negative plate will progressively lose capacity. Assuming 100% recombination of oxygen, this requires the corrosion rate at the positive plate to be equal to or greater than the hydrogen evolution rate at the negative plate. The results from both trials and the commercial operation of VRLA batteries

have shown that this balance can be shifted if a proportion of the oxygen evolved at the positive plate reacts with hydrogen on the catalyst to produce water [17,18].

Catalytic recombination of only a small proportion of the oxygen is sufficient to reduce the internal oxygen cycle to such an extent that the negative plate can be fully charged. During five years operation of standby batteries fitted with catalysts, the float currents were found to be much more stable and the negatives remained in a fully charged condition. In the same application, negative plates in batteries without catalysts became extensively sulfated. The use of these catalysts substantially reduces the deleterious effects of impurities and VRLA cells that are out of balance initially can be corrected.

More recently, a range of 6-V and 12-V, 125-Ah monobloc batteries with/without catalysts have been tested under standby float conditions for extended periods at room temperature and the gassing rates recorded. The results for the 6-V batteries are presented in Table 5.8. Batteries 1 and 2 were not fitted with catalysts and had individually sealed cell compartments. Batteries 3 and 4 had a single catalyst located in a common headspace. The data obtained from tests on 12-V, 25-Ah batteries with two catalysts in the common headspace are shown in Fig. 5.14. Those without

Table 5.8. Gassing rates for batteries under standby service at room temperature.

Battery*	Catalyst	Gassing rate (cm^3 per cell per h)	
		2.26 V per cell	2.35 V per cell
1	no	0.93	16.8
2	no	1.4	7.8
3	yes	nil	0.62
4	yes	nil	nil

*Batteries 1 and 2: 6 V, 125 Ah with cells separately sealed.
Batteries 3 and 4: 6 V, 125 Ah with common headspace.

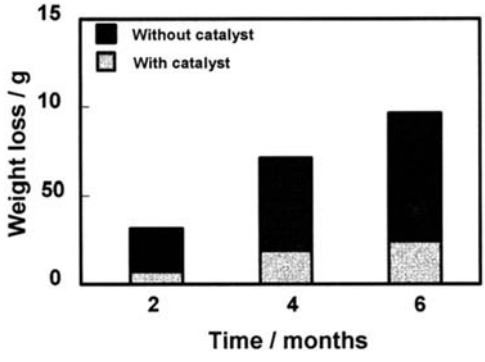

Fig. 5.14. Weight loss of 12-V/25-Ah batteries on float at 40°C.

catalysts had individually sealed cells and showed four times more weight loss than cells with catalysts when charged continuously at 2.26 V per cell at 40°C.

5.6. Summary

Recent studies have provided a better understanding of the behaviour of negative plates in VRLA lead–acid batteries. The major conclusions of this work can be summarized as follows.

(i) Under conditions where oxygen recombination operates efficiently, battery cycle-life may be reduced if the balance of the charge input and the self-discharge at the negative plate does not allow the potential of the negative plate to reach a sufficiently negative value during charge. The self-discharge rate can be reduced by improving purity standards. Further improvement in cycle-life is possible with the correct choice of charge algorithm.

(ii) The influence of additives on the performance and life of batteries has been investigated extensively with confirmation of the previously reported benefits of high levels of carbon and/or barium sulfate. Higher addition levels have little effect on capacities and the improved cycle-life appears to be due to the greater effectiveness of charge, particularly when the coulombic input is restricted in order to minimize gassing.

(iii) Several natural and synthetic organic materials, identified as having the potential to act as effective expander components, have been tested. All materials increase the surface area of the negative plate, particularly when using higher amounts of materials derived from natural products. The surface area of negative plates containing synthetic materials shows little change during cycling. All materials improve the initial capacity, but to varying extents. The best materials give 50–60% improvement in coulombic efficiency at the 5-h rate of discharge. With some materials, higher amounts increase charge outputs. With others, however, increasing the addition level has the reverse effect. Differences between additives are more noticeable at higher rates of discharge.

(iv) The effect of the organic additives on the cycle-life of experimental cells varies considerably. The best results have been obtained with negative plates that contain 0.75 wt.% Vanisperse A and that are cycled at room temperature. With some additives, there is an improvement at 40°C, but with others the cycle-life is decreased. Similarly, higher amounts of some additives result in improved cycle-lives but, again, the reverse is true for others. It is noteworthy that the synthetic Lomar B gives the highest initial capacity on both constant-current discharges and the Dynamic Stress Test, as well as a good mean cycle-life. The widely used Vanisperse A provides a somewhat lower capacity and has been reported to suffer from batch-to-batch variability but a better cycle-life, particularly at high addition levels.

(v) The above differences, namely, the influence of higher or lower additions of organic materials on initial performance and cycling and the diverse behaviour at two temperatures are not fully understood and further work is proceeding.

It has been suggested that comparing the performance at a constant loading in the active material may not be the most effective method of evaluation. Whilst the best cycle-lives at room temperature are found with organic materials which give the highest initial utilization, these same materials tend to cause a lower cycle-life at higher temperatures. This suggests that the more electrochemically efficient materials are also the most degradable. Evidence in support of this possibility has been provided by degradation tests in strong sulfuric acid.

(vi) All organic additives affect the hydrogen overpotential, but the extent depends on the type and the amount of additive that is used. Under voltage-limited charging where the charge is restricted, these influences affect the coulombic input and this can account for the different cycle-lives of negatives with the various additives. Changes in the cycling performance at 25 and 40°C can also be explained by the differing action of additives at these two temperatures.

(vii) Several methods of charging VRLA batteries to improve the durability and life of negative plates have been investigated. Under limiting conditions of charge, the charge effectiveness is dependent on several factors, namely, the purity of the raw materials; the influence of the organic additions; cell design; the specific algorithm that is being used. Charging problems are increased in cycling applications due to the varying charge efficiencies of the positive and negative plates, as well as the difficulties of ensuring a correct balance between charge input and self-discharge.

(viii) Internal catalysts have been used in VRLA batteries to promote the recombination of a proportion of the oxygen produced at the positive plate in order to reduce the self-discharge from the internal oxygen cycle to such an extent that the negative can be fully charged. Experience with standby batteries indicates that the deleterious effects of impurities that cause VRLA cells to become out of balance can be corrected through the use of gas-recombining catalysts.

References

1. E.J. Ritchie, *Trans. Electrochem. Soc.*, **100** (1953) 53–59.
2. J. Burbank, A.C. Simon, E. Willihnganz, in: P. Delahay, C.W. Tobias (Eds.), *Advances in Electrochemistry and Electrochemical Engineering*, *Vol. 8*, Wiley, New York, USA, 1971, pp. 157–251.
3. P. Ruetschi, *J. Power Sources*, **2** (1978) 3–24.
4. N.A. Hampson, J. Lakeman, *J. Power Sources*, **6** (1981) 101–109.
5. D. Pavlov, S. Ignatova, *J. Appl. Electrochem.*, **17** (1987) 715–723.
6. M.I. Gillibrand, G.R. Lomax, *Electrochim. Acta*, **8** (1963) 693–702.
7. K. Peters, unpublished work (1972).
8. D. Berndt, in: N.E. Bagshaw (Ed.), *Maintenance-Free Batteries*, Wiley, New York, USA, 1997, p. 31.
9. D. Boden, J. Arias, F.A. Fleming, *J. Power Sources*, **95** (2001) 277–292.
10. W. Böhnstedt, C. Radel, F. Scholten, *J. Power Sources*, **19** (1987) 427–441.
11. B. Culpin, G. Pilling, F. Fleming, *J. Power Sources*, **24** (1988) 127–136.
12. J.R. Pierson, C.E. Weinlein, C.E. Wright, in: D.H. Collins (Ed.), *Power Sources 5*, *Research and Development in Non-mechanical Electrical Power Sources*, Academic Press, London, UK, 1975, pp. 97–108.

13. D.M. Rice, J.E. Manders, *J. Power Sources*, **67** (1997) 251–255.
14. W.E.M. Jones, *Proceedings of the 22nd International Telecommunications Energy Conference*, Phoenix, AZ, USA, IEEE, 2000, pp. 447–452.
15. L.T. Lam, H. Ceylan, N.P. Haigh, T. Lwin, C.G. Phyland, D.A.J. Rand, D.G. Vella, *ALABC Project N3.1*, *Influence of residual elements in lead and expander materials on the oxygen- and/or hydrogen-gassing rates of lead–acid batteries*, *Semi-annual Report 1 July to 31 December 2001*, Advanced Lead-Acid Battery Consortium, Research Triangle Park, NC, USA, 2001.
16. E.A. Khomskaya, N.F. Gorbacheva, T.V. Arkhipova, N.F. Burdanova, *Sov. Electrochem.*, **21** (1985) 331–334.
17. D. Berndt, W.E.M. Jones, *Proceedings of the 19th International Telecommunications Energy Conference*, San Francisco, CA, USA, 1997.
18. D. Berndt, W.E.M. Jones, *Proceedings of the 20th International Telecommunications Energy Conference*, San Francisco, CA, USA, 1998, pp. 443–451.
19. E. Willihnganz, *Trans. Electrochem. Soc.*, **92** (1947) 281–284.
20. G.W. Vinal, *Storage Batteries*, John Wiley & Sons, New York, USA, 1951.
21. A.C. Zachlin, *J. Electrochem. Soc.*, **98** (1951) 325–333.
22. B.K. Mahato, *J. Electrochem. Soc.*, **127** (1978) 1679–1687.
23. E.G. Yampo'skaya, M.I. Ershova, I.I. Astakhov, B.N. Kabanov, *Sov. Electrochem.*, **2** (1966) 1211–1214.
24. E.G. Yampo'skaya, M.I. Ershova, V.V. Surikov, I.I. Astakhov, B.N. Kabanov, *Sov. Electrochem.*, **8** (1972) 1209–1210.
25. E. Willihnganz, Presentation to Association of American Battery Manufacturers, October 22–23, 1942; *Natnl. Lead Publn.*, 63 (1942).
26. M. Shiomi, T. Funato, K. Nakamura, K. Takahashi, M. Tsubota, *J. Power Sources*, **64** (1997) 147–152.
27. F. Saez, F. Trinidad, B. Martinez, D. Martin, P. Spinelli, *J. Power Sources*, **95** (2001) 174–190.
28. R.H. Newnham, W.G.A. Balding, A.F. Hollenkamp, O.V. Lim, C.G. Phyland, D.A.J. Rand, J.M. Rosalie, D.G. Vella, *ALABC Project C/N 1.1*, *Advancement of valve-regulated lead–acid battery technology for hybrid-electric and electric vehicles*, *Semi-annual Report 1 July to 31 December 2001*, Advanced Lead-Acid Battery Consortium, Research Triangle Park, NC, USA, 2001.
29. S. Ruevski, D. Pavlov, *Proc. Ext. Abstr. Labat '96 International Conference*, Varna, Bulgaria, June 1996, p. 46.
30. K.V. Sarkanan, C.H. Ludwig in: *Lignins: Occurrence, Formation, Structure and Reactions*, Wiley Interscience, New York, 1971.
31. D. Pavlov, B.O. Myrvold, T. Rogachev, M. Matrakova, *J. Power Sources*, **85** (2000) 79–91.
32. Hammond Expanders Division of Hammond Group, Inc., Hawker Energy Products, Inc., Bipolar Power Corporation, *ALABC Project B–0008.5, Development of new expander for the VRLA battery in electric vehicle applications, Final Report 1 July 1997 to 30 June 1999*, Advanced Lead-Acid Battery Consortium, Research Triangle Park, NC, USA, 1999.
33. C. Francia, M. Maja, P. Spinelli, *J. Power Sources*, **85** (2000) 110–116.
34. Central Laboratory for Electrochemical Power Sources Bulgaria, S.E.A. Tudor, Politecnico di Torino, *Brite/Euram*, *Project BE 97–4085*, *Task 3. Improvements in negative plate performance*, *Annual Report 1 January 2000 to 31 December 2000*, Advanced Lead-Acid Battery Consortium, Research Triangle Park, NC, USA, 2001.
35. K. Peters, A.I. Harrison, W.H. Durant, in: D.H. Collins (Ed.), *Power Sources 2*, Pergamon Press, Oxford, UK, 1970, pp. 1–16.
36. Central Laboratory for Electrochemical Power Sources Bulgaria, S.E.A. Tudor, Politecnico di Torino, *Brite/Euram Project BE97–4085, Task 3. Improvements in negative plate performance, Final Report 1 January 1998 to 31 August 2001*, Advanced Lead-Acid Battery Consortium, Research Triangle Park, NC, USA, 2001.
37. B. Culpin, J.A. Hayman, in: L.J. Pearce (Ed.), *Power Sources 11*, *Research and Development in Non-mechanical Power Sources*, International Power Sources Symposium Committee, Leatherhead, England, 1986, pp. 45–66.
38. X. Munaret, M. Coux, P. Lenain, *Proceedings of the 22nd International Telecommunications Energy Conference*, Phoenix, AZ, USA, 2000, paper 16–3.

39. T. Ikeya, N. Sawada, S. Takagi, J.-I. Murakami, K. Kobayshaya, T. Sakabe, E. Kousaka, H. Yoshioka, S. Kato, M. Yamashita, H. Narisoko, Y. Mita, K. Nishiyama, K. Adachi, K. Ishihara, *J. Power Sources*, **91** (2000) 130–136.
40. T.G. Chang, D.M. Jochim, *J. Power Sources*, **91** (2000) 177–192.
41. K. Tomantschger, E.M. Valeriote, J. Sklarchuk, T.G. Chang, M. Dewer, D. Jochim, *Proceedings of the 3rd ALABC Members and Contractors Conference*, London, UK, March 1998, Advanced Lead-Acid Battery Consortium, Research Triangle Park, NC, USA, 1998.
42. R.F. Nelson, J.B. Olson, E.D. Sexton, A.A. Pesaran, M.A. Keyser, *ALABC Project No. B–007.2*, *Development of improved cycle life by design of charge algorithms specifically aimed at VRLA batteries*, *Progress Report 21 July to 20 September 1999*, Advanced Lead-Acid Battery Consortium, Research Triangle Park, NC, USA, 1999.
43. R.H. Newnham, W.G.A. Balding, *J. Power Sources*, **11** (1997) 26–39.
44. T.A. Edison, U.S. Pat. 1,016,874 (1912).
45. Accumulatorenwerk Hoppecke Carl Zoellner & Sohn, Patent DE 20 08 218 (1976).
46. Accumulatorenwerk Hoppecke Carl Zoellner & Sohn, Patent DE 26 38 899 (1976).
47. D. Feder, W.E.M. Jones, *Proceedings of the 17th International Telecommunications Energy Conference*, The Hague, Holland, 1995.
48. S.S. Misra, T.M. Noveske, A.J. Williamson, *Proceedings of the 22nd International Telecommunications Energy Conference*, Phoenix, AZ, USA, 2000, paper 3–2.

Valve-Regulated Lead–Acid Batteries
D.A.J. Rand et al., editors

—CHAPTER 6—

THE FUNCTION OF THE SEPARATOR IN THE VALVE-REGULATED LEAD–ACID BATTERY

M.J. Weighall

6.1. Introduction

The separator, or more precisely the system employed to immobilize the electrolyte, is the key component in a valve-regulated lead–acid (VRLA) cell since it provides the means for valve-regulated operation. Provision must be made for the electrolyte to have ready access to the active material on the positive and negative plates, and for free passage of oxygen from the positive plate to the negative plate during charging. This latter requirement effectively demands gas channels between the plates because the coefficient of diffusion of oxygen through the aqueous electrolyte phase is some four orders of magnitude smaller than that through air [1]. Simultaneously, the separator system must offer all the properties necessary for the flooded version of the lead–acid cell, from which the VRLA design has been developed. These properties include: chemical stability in the acid environment, electronic insulation, sufficient open porosity to allow low ionic resistance through the electrolyte phase, good dimensional stability, and adequate strength to prevent puncture by lead 'dendrites'.

As mentioned briefly in Section 1.3, Chapter 1, two principal methods have been developed for providing the special combination of electrolyte accommodation and directed porosity that are required in a VRLA cell. The first system to be introduced [2] had the electrolyte immobilized as a gel by the addition of 5–8 wt.% of fumed silica. Partial dry-out of the gel opens out the gas spaces necessary for oxygen transport, while acid within the gel remains available for participation in the cell reaction. A sheet of microporous material is usually added to protect against metallic short-circuits and to fix the inter-plate separation. The second system [3] makes use of a glass-micro-fibre separator, which has a very high porosity and can thus absorb a large volume of electrolyte. Batteries using absorptive glass mat (AGM) are more widely used than gel alternatives by virtue of their lower cost and higher power ratings. On the other hand, gel technology is less prone to acid stratification and drainage (*v.i.*), and is preferred where long life, especially under deep-cycling applications, is the prime requirement. It should be noted that since separator materials now used in the former battery technology may not be comprised solely of glass mat, some authors have preferred to use the generic term 'recombinant-battery

separator mat — RBSM' in place of 'AGM'. It has been decided to adopt the more common 'AGM' terminology in this and other chapters.

Separator properties must be taken into account when considering the performance required in specific applications. For example, the compression properties of the separator exercise a direct influence on plate-group pressure and the prevention of active-material expansion. Separator properties also affect aspects of battery manufacture, especially the process of battery formation. For reasons of cost and convenience, many VRLA manufacturers prefer to assemble the batteries with unformed plates and use container formation, rather than to construct batteries from dry-charged plates. Problems may arise with container formation if the cell groups are built with a very high plate-group pressure [4] to maintain positive-plate integrity during cycling and prevent premature capacity loss. When an AGM separator is compressed, it reduces the pore size significantly and thus decreases the space available for electrolyte between the plates. This adversely affects the wicking properties of the electrolyte (*v.i.*). During discharge, the reaction of the electrolyte with the plate active-materials is exothermic, so that as the liquid penetrates into the plate stack it becomes hotter as well as more dilute. In the extreme case, lead sulfate from the plates dissolves into the dilute electrolyte, releases soluble Pb^{2+} ions into the separator, and gives rise to hydration shorts during subsequent charge when the Pb^{2+} ions are converted back into lead in the pores of the separator. The reduced electrolyte availability aggravates this problem if the separator is under high compression or if there is a small inter-plate spacing.

Another potential problem with the filling process is that individual cells may retain dry areas in which little or no liquid is present. This may arise if the filling process is non-uniform and leaves pockets of trapped gas. These dry areas will slowly become wetted both during and after formation, but there is a risk of severe grid corrosion due to the high temperatures and alkaline conditions prior to, and during, formation [4].

In summary, the separator materials required to accommodate the electrolyte in a VRLA cell perform a function that is not only vital for the operation of the cell, but is also extremely demanding in terms of the complex combination of properties that are necessary.

6.2. Characteristics of Absorptive Glass Mat (AGM)

6.2.1. Wetting behaviour of AGM materials

The micro-fine glass material chosen for the separator in the cells originally produced by the Gates Rubber Company [3] is still used in the majority of present-day VRLA batteries. The material is made from borosilicate glass via a flame-attenuation process which produces fibres with diameters in the range 0.1–10 μm, and with a typical length of around 1 mm (Fig. 6.1). As prepared, the material has the consistency of cotton wool and is processed into sheet form by a wet-laying procedure on a conventional paper-making machine [6]. This gives the sheet a three-dimensional anisotropy, and most of the fibres lie in the plane of the sheet with a

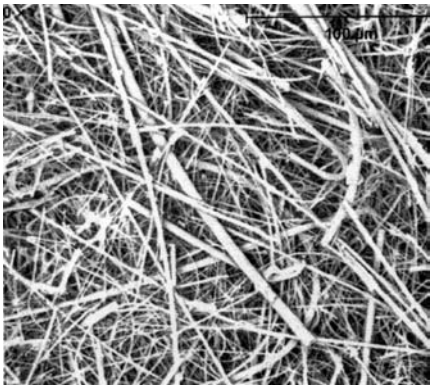

Fig. 6.1. Scanning electron micrograph of glass micro-fibre mat [5].

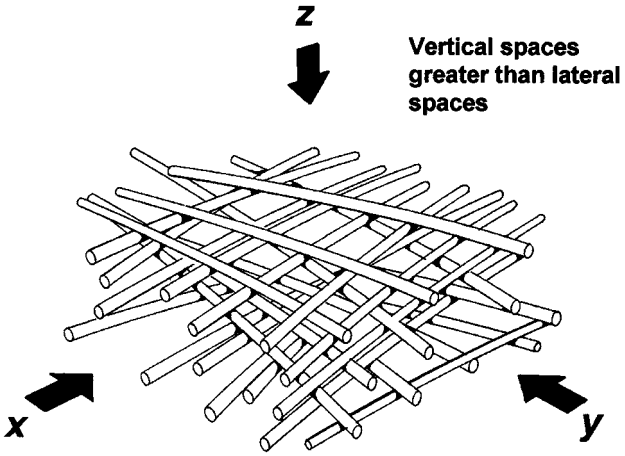

Fig. 6.2. Schematic drawing of AGM microstructure [1].

slight preference for the machining direction. The structural anisotropy is illustrated schematically in Fig. 6.2 in terms of a scheme of orthogonal co-ordinates in which the x and y axes lie in the plane of the sheet and the z axis is perpendicular to that plane. The pores in the z direction are much larger (10–30 μm) than those in the x–y plane of the separator (2–4 μm). These structural properties exercise an important influence on the manner in which the material performs as a separator.

Wetting characteristics can be improved by maximizing the surface area through the use of densely packed fibres of small diameter — but at a higher cost and with the likelihood of a decrease in the efficiency of oxygen recombination. The fibre blend and subsequent treatment influence the resulting pore size and associated properties such as tensile strength and compressibility. In addition, some manufacturers use

Table 6.1. Influence of fibre diameter on separator characteristics [7].

Fibre diameter (μm)	0.1	0.5	1.0	2.0	5.0	10.0
Fibre length						
($m\,kg^{-1}$)	4.7×10^{10}	1.9×10^{9}	4.7×10^{8}	1.2×10^{8}	1.9×10^{7}	4.7×10^{6}
($m\,m^{-3}$)	1.1×10^{13}	4.5×10^{11}	1.1×10^{11}	2.8×10^{10}	4.5×10^{9}	1.1×10^{9}
Surface area						
($m^2\,kg^{-1}$)	14 800	2960	1480	741	296	148
($m^2\,m^{-3}$)	3.5×10^{6}	7.1×10^{5}	3.5×10^{5}	1.8×10^{5}	7.1×10^{4}	3.6×10^{4}
Pore size	→ increasing →					
Tensile strength	→ decreasing →					
Cost	→ decreasing →					

chopped fibres to provide the separator with more uniform compression characteristics. This influence of small-diameter fibres is summarized in Table 6.1 [7]. Separators that contain a high proportion of very fine fibres are more costly, but some batterymakers accept this penalty in order to improve battery quality or to enhance certain operational characteristics such as tensile strength and separator behaviour under compression. The separator material is purchased in terms of a 'basis weight' which usually varies from 100 to $300\,m^2\,g^{-1}$, in either cut or roll form, and can be used in single- or multi-layers. Because various manufacturing processes result in slight differences in the uncompressed thickness, this parameter is quoted at a standard pressure which is normally specified as 10 kPa.

The following definitive analysis of the function of the AGM has been given by Culpin and Hayman [1]. Capillary systems in porous media involve a solid phase and at least two fluid phases (here, air/oxygen and sulfuric acid, respectively). The interface between a solid and a liquid phase is subject to surface tension forces. Clean glass surfaces are perfectly wetted by sulfuric acid solution (i.e., the contact angle is zero) so that the micro-fibres in the separator become coated with a layer of acid. The liquid phase arranges itself spatially in order to minimize its surface energy, i.e., the liquid tries simultaneously to maximize its area of contact with the glass and to minimize its surface area of contact with the gas phase (sulfuric acid has a high air|liquid interfacial tension of $0.75\,mN\,cm^{-1}$).

In order to minimize the area of contact with the gas phase, the liquid will tend to bridge across smaller pores initially, since to bridge across large pores will expose a larger surface area to the gas phase. Thus, as saturation of the fibre mat by the liquid phase increases, liquid will first fill the small pores, which are oriented within the x–y plane of the separator. At this stage, the larger pores, which are oriented in the z direction (i.e., perpendicular to the plane of the separator), are essentially open and free to the passage of gas. Therefore, up to a certain level of saturation, the volume of liquid in the separator presents no obstruction to the passage of oxygen by gas-phase diffusion. As saturation increases, the size of pores which are blocked by liquid films increases progressively until, at around 90% saturation, the largest pores are

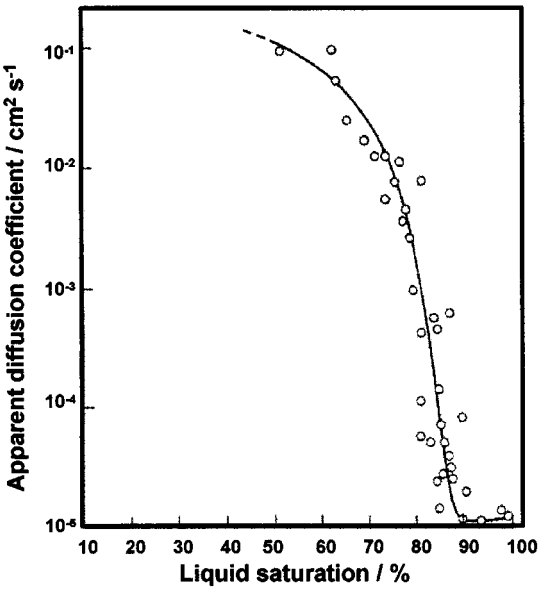

Fig. 6.3. Apparent diffusion coefficient of oxygen as a function of separator saturation [1].

covered and the residual 10% of porosity represents isolated pockets of gas which do not play any effective part in oxygen transport. The apparent diffusion coefficient for oxygen transport across a glass micro-fibre separator falls as saturation reaches 90%, as shown in Fig. 6.3 [1]. (Note, the apparent diffusion coefficient is the measured value. This will be the all-gas value when there is no liquid and the all-liquid value when there is no gas, but a weighted-mean when there are two phases, i.e., as in a real separator.)

The progressive blocking of larger and larger pores in the separator as saturation proceeds is effectively a capillary-wicking process. The rate of wicking, dh/dt, of a wetting liquid in a porous structure is given by the Washburn equation [8]. This relationship comprises two terms: the first defines the influence of surface tension, while the second defines the effect of gravity, as follows:

$$dh/dt = 2r\gamma \cos\theta/8\eta h - r^2\rho g/8\eta \tag{6.1}$$

where h is the height of the wicking front; t is time; r is the pore radius; γ is interfacial tension; θ is the contact angle; η is the viscosity of the liquid; ρ is the density of the liquid; g is the gravitational constant.

Integration of eqn. (6.1) and invoking the limit that $h = 0$ at time zero gives:

$$r^2\rho g t/8\eta = h_m \ln[(h_m)/(h_m - h)] - h \tag{6.2}$$

where h_m is the maximum height reached by the fluid at infinite time and is given by:

$$h_m = 2\gamma \cos\theta/\rho g r \tag{6.3}$$

If the gravity term in eqn. (6.1) is ignored, integration yields the expression:

$$h^2 = \gamma r t \cos\theta / K^2 2\eta \tag{6.4}$$

where K represents a tortuosity factor.

The driving force for liquid penetration is governed by the pressure gradient, P, across the curved liquid|gas interface. The pressure drop across the interface in a uniform capillary of radius r is given by:

$$P = 2\gamma \cos\theta / r \tag{6.5}$$

Equation (6.1) indicates that a plot of dh/dt versus $1/h$ should give a straight line, and indeed data for specimens of glass micro-fibre do show such a relationship, see Fig. 6.4 [1]. It follows that the velocity of the wicking front is directly proportional to the pore size, i.e., capillary rise is most rapid in the largest pores. By contrast, eqn. (6.3) suggests that the maximum height to which the liquid will rise (after infinite time) is inversely proportional to the size of the pore, i.e., the smaller the pores, the higher will the liquid wick.

The above two predictions have been verified by the results of experiments with materials that offer different pore sizes by virtue of different mass fractions of fine fibres — the more fine fibres, the smaller the pore size, see Fig. 6.5 [6]. The effect of fibre mix on wicking characteristics for wicking heights up to 12 cm is shown in Fig. 6.6 [6]. A good linear relationship between the square of the wicking height and time is obtained, as predicted by eqn. (6.1). Furthermore, it is clear that the greater the percentage of fine fibres, i.e., the smaller the mean pore size, the slower is the

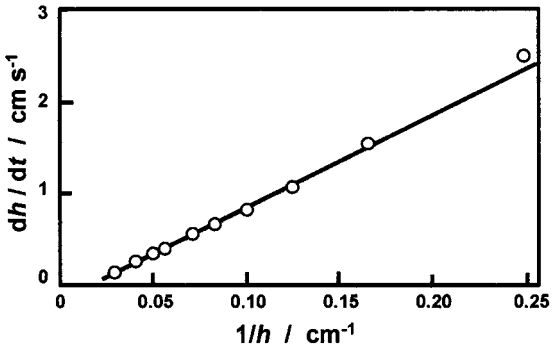

Fig. 6.4. Wicking data fitted to Washburn equation [1].

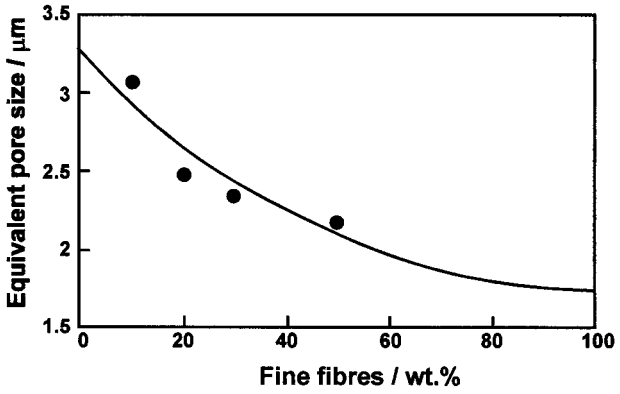

Fig. 6.5. Effect of fibre mix on pore size [6].

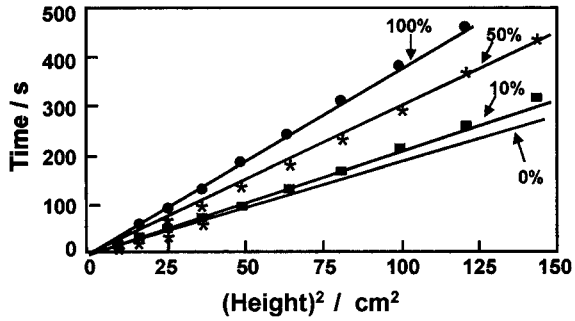

Fig. 6.6. Effect of fibre mix on wicking characteristics; percentage of fine fibres as shown [6].

wicking process. In agreement with the prediction given by eqn. (6.3), the liquid phase ultimately wicks to a greater height in a glass mat with a fine pore size than in one with a coarse pore size, as shown in Fig. 6.7 [9] and Table 6.2 [7].

The contrasting structure of the plates and the separators is also relevant to the functioning of the battery. For example, the capillary pressures dictate that electrolyte fills the plates preferentially. This preferential filling appears to be the ideal situation since it can best support the electrochemical reaction, i.e., it leaves the separator partially saturated so that movement of electrolyte can provide pathways for gas transport. If, however, the overall saturation is too low or there is excessive loss of water, the separator will dry out and give rise to an increase in the internal resistance of the battery and the possibility of thermal runaway. An increase in internal resistance, and consequent low service-life, can also result if the compression between separators and battery plates relaxes over a period of time. Over-compression may cause fibres to fracture with a loss of resilience, i.e., the separators lose the ability to return to original thickness after a high pressure is applied and

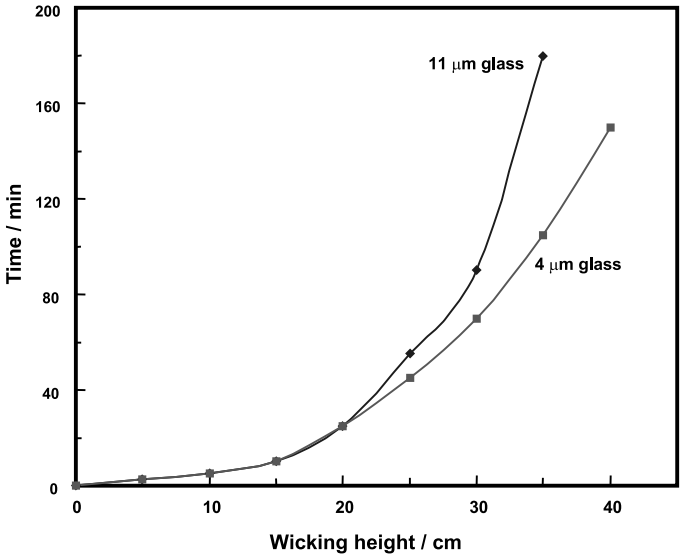

Fig. 6.7. Respective wicking rates for AGM separators with large (11 μm) and small (4 μm) pore sizes [9].

Table 6.2. Properties of all-glass AGM separators [7].

Property		Sample			
		1	2	3	4
Specific surface area ($m^2 g^{-1}$)		0.5	0.9	1.2	2.6
Maximum pore size (μm)		45	31	24	14
Thickness (mm)					
mm at 10 kPa	dry	2.58	1.78	1.65	1.39
	wet	2.51	1.71	1.60	1.35
mm at 20 kPa	dry	2.03	1.49	1.47	1.27
	wet	1.99	1.47	1.44	1.26
mm at 30 kPa	dry	1.86	1.40	1.40	1.23
	wet	1.87	1.39	1.41	1.21
Grammage ($g m^{-2}$)		280	240	240	180
Wicking height (mm)					
1.300 rel. dens. acid					
−1 min		42	39	37	33
−5 min		94	88	83	75
−1 h		195	205	210	220
−2 h		240	280	300	370
−10 h		360	410	455	550
Tensile strength after 25 min (g)[a]		1900	1870	1950	1600

[a]In this test, a strip of separator (25 × 150 mm) is clamped in a tensile testing machine. The rate of jaw separation is set at 25 ± 5 mm per min and the breaking force is recorded.

then released. Also, fine fibres may dissolve during prolonged service, particularly at higher temperatures. Both these effects will reduce compression.

6.2.2. *Physical properties of AGM materials*

The AGM materials used in VRLA batteries must sustain the required plate-group pressure, must hold the electrolyte in place, and must allow sufficient (but not excessive) transport of oxygen from the positive plate to the negative. Some of the properties of typical all-glass AGM separators are shown above in Table 6.2 [7]. The following important features are noted:

- The maximum wicking height after an extended period is inversely proportional to the pore size, as seen previously in Fig. 6.7.
- The separator is compressible and the separator thickness decreases with increasing applied pressure, see Fig. 6.8 [7]. For example, for a separator with a grammage of $280\,g\,m^{-2}$, the dry thickness at 30 kPa is 28% less than that at 10 kPa. Compression also reduces the pore size in the vertical plane of the separator. For instance, measurements of capillary rise on sample 3 (Table 6.2) at 15 and 25% compression gave pore sizes of 1.3 and 1.1 μm in the vertical plane, compared with 2.1 μm when uncompressed.
- A separator with a high surface area exhibits a smaller reduction in thickness for a given applied pressure than a separator with a low surface area. Therefore, a higher applied pressure is needed to achieve the same percentage compression with the former type of separator.

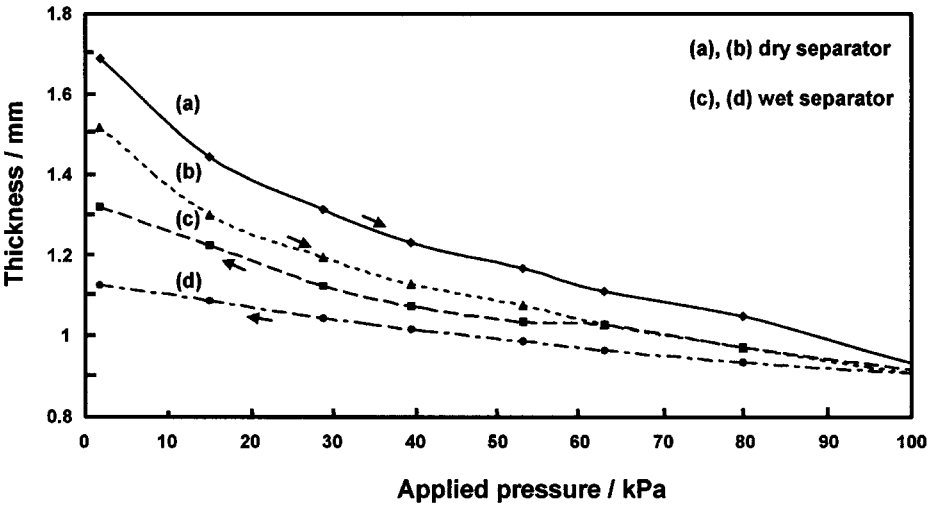

Fig. 6.8. Thickness–compression curves for AGM separator; arrow denotes direction of increasing/decreasing pressure [7].

The characteristics of the key physical parameters of AGM separators are discussed below. Reference should also be made to the BCI test methods for these materials [10].

Thickness. Because of the delicate and very compressible nature of AGM, it is necessary to measure the thickness at a controlled, standard pressure. The pressure chosen is 10 kPa (1.5 psi). Thus, calculation of the percentage compression is based on the initial thickness of the separator as measured at 10 kPa and, ideally, the BCI test method is employed [10]. It should be noted that the relative humidity of the test conditions and prior handling of the material may affect the result.

Basis weight (or 'grammage'). This is the weight per unit area and is usually expressed in terms of g m^{-2}. Since AGM is normally sold by weight but used by area, this is a critical specification. The weight is measured on a moisture-free sample, and then corrected for the moisture content of the test specimen (AGM may pick up moisture between manufacture and testing/use).

Volume porosity. This is the ratio of the total void volume to the total apparent volume, expressed as a percentage. The apparent volume is obtained by multiplying the sample area by the thickness measured at a specified pressure. The void volume is that portion of the apparent volume which is not occupied by the solids used to make the separator, and is usually determined by subtracting the volume of the solids from the apparent volume. The volume porosity of the AGM in the compressed state limits the maximum amount of acid between the plates. Determination of the volume porosity requires knowledge of the thickness, basis weight, and average density of the solids in the sample.

Pore size. The bubble point method (BCI Test Method 3–015) [10] is used to measure the maximum pore diameter. The maximum pore size and the pore-size distribution can be determined by means of the liquid porosimetry method which uses, for example, a Coulter porosimeter (BCI Test Method 3–017) [10].

A more detailed characterization of the pore-size characteristics of AGM can be obtained with the mercury intrusion technique. This is based on the principle that the external pressure required to force a non-wetting liquid into a pore against the opposing force of surface tension depends on the pore size. The technique is widely employed to characterize porous materials, and provides data on pore diameter, pore-size distribution, and pore volume. Some caution must be applied in interpreting the results, however, because of the assumptions that are made concerning cylindrical pores, contact angle, and the surface tension of mercury.

Surface area. This can be determined using BET adsorption [11]. The significance of this parameter is that the performance of a VRLA battery is partly dependent on the surface area of the mat between the plates. For example, surface area has an influence on acid stratification.

Compressibility. The AGM is typically used while under compression, and therefore it is necessary to know the pressure required to give the desired level of compression within the battery. The separator thickness is measured under various forces and the resulting relationship is used to determine the pressure required to compress the AGM into the available space between the plates in the battery. A typical 'compression curve' has been shown above in Fig. 6.8.

Electrical resistance. Measurement of electrical resistance (i.e., the resistance to an ionic current through the electrolyte) is a standard procedure for characterizing separators used in flooded lead–acid batteries; the electrical resistance is usually included in the separator specification. By contrast, AGM separators are used in a partially saturated state and account must therefore be taken of gas-filled pores which contribute an extremely high electrical resistance. Partial de-saturation of a porous medium which is initially saturated with a conducting wetting fluid causes an increase in the electrical resistance, provided that the conducting liquid is replaced by a non-conducting fluid. Archie's Law [12] is an empirical relationship which relates the resistivity of a partially saturated medium, R, to the degree of saturation of the wetting phase, S_w, and the resistivity of the liquid at 100% saturation, R_o, as follows:

$$R = R_o S_w^{-n} \tag{6.6}$$

where n is known as the 'saturation exponent'. Measurements of the resistance ratio, R/R_o, of glass micro-fibres in the z direction (i.e., perpendicular to the plane of the sheet) indicate [1] that such material obeys Archie's Law with a rather high saturation exponent, viz., $n = 4$. The behaviour is evidently attributable to the anisotropic structure of the material.

6.3. Gel Batteries

As mentioned earlier, the electrolyte in gel batteries is immobilized by gelatinization with silicon dioxide. The preferred agent is a 'fumed silica' with a very small mean particle size ($\sim 10\,\text{nm}$) and, hence, a very high surface area ($200–300\,\text{m}^2\,\text{g}^{-1}$). When fumed silica (typically around 5 wt.%) is mixed with sulfuric acid electrolyte, a viscous solution is formed and develops into a gel on standing. The thickening process can be reversed by subjecting the material to a significant impact, although the gel will re-form if the solution is left in an undisturbed state. It is claimed that weak hydrogen-bonding is responsible for this thixotropic behaviour. Oxygen transport occurs via fissures in the gel that are formed during the early stages of battery life through partial drying out (water loss) and concomitant shrinkage of the gel. A supplementary sheet of a micro-porous (pores $< 1\,\mu\text{m}$) material is required in batteries with the gelled electrolyte in order to prevent electrical short-circuits and fix the inter-plate separation. Typical materials used for this supplementary separator sheet are discussed in Section 7.2.2, Chapter 7.

The manufacturing costs of gel batteries are higher than those of batteries with AGM separators and the specific power is generally lower because of the higher level

of internal resistance. On the other hand, gel technology is a more effective means of immobilizing the electrolyte and the batteries are less prone to electrolyte drainage and acid stratification than are AGM batteries.

6.4. Separator Properties and Function

6.4.1. Compression characteristics

The micro-fine glass separator mat used in VRLA batteries is extremely compressible, and this property serves to mould the separator to the structure of the plate surface. Unfortunately, changes in plate volume can take place during charge–discharge cycling, with the result that the glass mat may lose compressibility. There may also be some dissolution of the fine fibres which, again, will have an adverse effect on the compression characteristics.

The positive plate, in particular, undergoes structural changes during deep-discharge cycling. If unrestrained, the active material softens, and particle-to-particle contact becomes weaker and is eventually lost. This process gives rise to shedding of the active material and loss of capacity. If the active material can be constrained by the separator, expansion and shedding are delayed and battery cycle-life extended [13]. For many years, conventional heavy-duty batteries, e.g., for motive-power applications, have been constructed with thick glass mats adjacent to the positive plates. Nevertheless, the applied compression in these batteries has not necessarily been controlled accurately. A clear relationship has been demonstrated [14,15] between positive-plate compression and cycle-life. For example, Takahashi *et al.* [14] have demonstrated that a critical plate-group pressure of $>40\,\text{kPa}$ is necessary to control plate growth.

During a study of the factors that affect the failure modes of VRLA batteries [13], it was pointed out that compression of the positive active-material via the separator is a critical factor in eliminating premature capacity loss. As a result of this work, it was concluded that the progressive expansion of the positive active-material leads ultimately to a breakdown of conductivity through the porous structure. As this breakdown intensifies, less and less of the material is accessible to discharge and, therefore, capacity falls. Compression and constraint of the active material mitigate against this breakdown by opposing the expansion of the material. If the separator is compressed against the positive plate at a sufficiently high pressure, the expansion and shedding of the active material are controlled and battery life is extended. In effect, the fibres in the AGM separator act as 'springs' in constraining the expansion of the positive active-material during cycling. As the force of the spring is directed against not only the plates but also the cell container, it is important that the latter is rigid and does not distort. This requirement may necessitate the development of special container designs [16].

The beneficial effect of compression in extending the cycle-life of VRLA batteries was confirmed in a project carried out by the Advanced Lead-Acid Battery Consortium (ALABC) [17]. The work also showed that the composition of the micro-fine glass separator has an important influence on cycle-life, namely, a higher

content of fine fibres results in longer cycle-life. Accordingly, attention was focused on the need to improve the properties of the glass separator, and to search for alternative separator materials of superior performance.

The behaviour of AGM separators under compression depends on a range of parameters which include the glass source, ratio of fine to coarse fibres, grammage, and surface area. The compression curve for a particular separator needs to be taken into account in battery design given the performance and life requirements of the particular application. An example of the compression characteristics of a typical material used in this application together with the consequences of the material becoming wetted with sulfuric acid is shown in Fig. 6.9. The following general conclusions can be drawn from these curves.

- For an applied force up to — and possibly beyond — 50 kPa, the separator thickness is reduced with increasing applied force.
- When the applied force is released, the separator recovery is incomplete such that the separator does not return to its original thickness.
- The separator tends to contract on wetting, and for a given applied force has a lower thickness than in the dry state.

To achieve a compression of 30% (i.e., a reduction in thickness of 30% compared with the original value at 10 kPa) an applied force in excess of 50 kPa may be required. (Note, the percentage compression must be referenced to the dry state, because the original thickness is measured with the separator in this state.)

If high plate-group pressure is required, special attention needs to be paid to the cell-assembly equipment to enable sufficient pressure to be applied to the plate group for it to be inserted into the cell container. Over-compression at this stage may actually damage the fibres. On the other hand, if a high compression cannot be

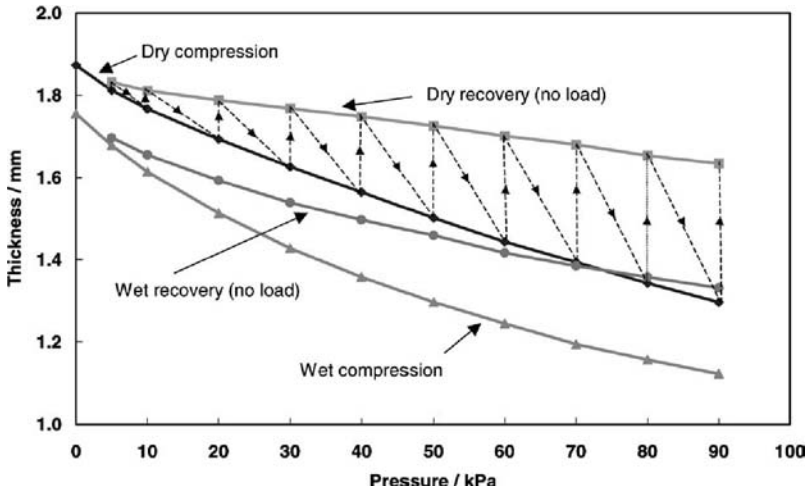

Fig. 6.9. Compression vs. applied pressure for typical all-glass separator. Dashed line indicates alternation between compression and recovery measurements [18].

maintained within the cell, there may be a rapid fall in capacity caused by expansion and loss of active material from the positive plates. In this connection, a study carried out by Hollingsworth & Vose [19] has provided some reassurance. For applied forces as high as 500 kPa, the results demonstrated that AGM separators can in fact maintain resilience. A reduction in tensile strength and an increase in elongation were observed during compression testing and this suggests that the matrix of AGM separators changes as the force increases. Evidence from scanning electron microscopic studies indicated that fibre displacement rather than fibre breakage was occurring, with fibres rotating, spreading out and even grouping together. For standard separators, it was found that over 92% of the original thickness was recovered after the pressure was released. It may be possible to improve tensile strength with modified materials (e.g., by including organic fibres).

Only the properties of separators in the dry state were reported by Hollingsworth & Vose [17]. Separators with a range of surface areas and grammages were tested, but the ratio of fine to coarse fibres in each separator was not given. The compression tests were conducted over short periods (30 min) and therefore concern remains over the effect of long-term, high compressive forces on glass-fibres in the wet state. Nevertheless, the results do indicate that the limitation on the maintenance of a high plate-group pressure within a VRLA battery is more likely to be due to the battery design and methods of assembly, rather than to the properties of the separator itself. It is worth noting that the design of the first commercially available battery using micro-fine glass separators — the Gates cell — had a spirally wound configuration which caused the plates and separators to be restrained under a firm assembly pressure. Thus, serendipitously, this first design provided the high compression of the separator against the positive electrode that is necessary to achieve a long cycle-life.

In practice, it may be difficult to maintain the required plate-group pressure throughout the life of a battery. An initial pressure of 40 kPa soon drops to 30 kPa or less. This is the result of several factors: wetting of the separator; formation of the battery; loss of fibre resilience during cycling. To maintain the integrity of the positive plates, the compression needs to be kept as high as possible during the early stages of cycling. Plate-group pressure does increase again later in cycling, but this is due to expansion of the positive active-material. A separator with a high surface area (i.e., a high fine-fibre content) may be better able to resist 'crush' under high levels of compression, and may also minimize acid stratification. Another possibility is to use a separator that resists compression. To be effective, this also requires a device that acts as an external spring to exert force on the plate group.

6.4.2. Oxygen cycle and recombination efficiency

The essential function of the VRLA battery relies on the transport of oxygen from the positive plate through the separator to the negative plate during charging. This transport can only take place effectively if the separator is not fully saturated. A saturation level of 95% or less is preferred.

Table 6.3. Comparison of transport rates through an orifice (length = 5 mm, radius as shown) at 20°C by pressure-assisted flow ($\triangle p = 10$ kPa) and by diffusion [20].

Orifice radius (μm)	Pressure-assisted out-flow of oxygen ($cm^3\,s^{-1}$)	Flux of oxygen due to diffusion ($cm^3\,h^{-1}$)
10	0.341	0.0009
50	213	0.022

The transport of oxygen can take place by pressure-aided gas flow and/or by diffusion [20]. Gas flow through an orifice is described by the Poiseuille equation, i.e.,

$$\Delta V/\Delta t = \pi r^4/(8\eta l) \cdot \Delta p \tag{6.7}$$

where ΔV is the volume of gas in cm^3; Δt is time in s; r is the radius of the orifice in cm; η is the viscosity in $N s\,cm^{-2}$; l is the length of the flow route in cm; $\triangle p$ is the pressure difference in $N\,cm^{-2}$. The rate of diffusion is governed by Fick's first law:

$$dn/dt = -(DA)\,dc/dx \tag{6.8}$$

where n is the number of moles transported; t is time in s; D is the diffusion coefficient in $cm^2\,s^{-1}$; A is the cross-sectional area in cm^2; dc/dx is the concentration gradient in mole cm^{-3} per cm. The relative importance of the transport mechanisms is shown in Table 6.3 in terms of the volume of oxygen transported by pressure-assisted flow and by diffusion through orifices of radius 10 and 50 μm, respectively. Both mechanisms are likely to contribute in the changing circumstances of an ageing VRLA system. Initially, most pores will be partly closed and oxygen will only penetrate when assisted by the build-up of pressure at the positive electrode. Under these circumstances, the radius of the opening through which the gas ultimately passes is extremely significant given the dependence of the rate of transport on the fourth power of the radius, see eqn. (6.7). Later in life, when separator/gel dry-out due to water loss causes channels to be permanently open between the electrodes, the internal pressure in the battery will be less and diffusion may become more important. In such a situation, the radius of the orifice will become less dominant.

At first sight, during recharge of the VRLA battery, it would seem that the oxygen cycle should be 100% efficient. This would ensure that no gas is released and vented to the outside atmosphere so that water loss is minimized. In recent years, however, it has become apparent that 100% oxygen recombination may not be desirable, as this may lead to negative-plate degradation. The secondary reactions of hydrogen evolution and grid corrosion are very important in the lead–acid battery, and may have a significant impact on VRLA cell behaviour. The rates of the two reactions need to be balanced, otherwise one of the electrodes — usually the negative — may not become fully charged. The negative electrode may actually self-discharge at the reversible potential and therefore its potential will have to rise above this value

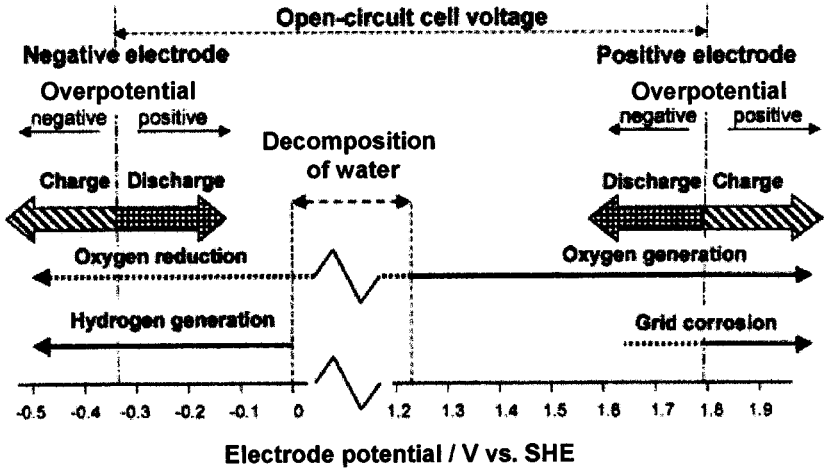

Fig. 6.10. Possible reactions in VRLA batteries as function of electrode potential. Origin of arrows represents equilibrium potential of given reaction [22].

(i.e., become more negative) to compensate for self-discharge and to prevent capacity decline. While the negative plate is occupied in recombining oxygen, its potential cannot become more negative in the required manner. There is then a risk that it will slowly lose capacity because of self-discharge due to local action from impurities in the active materials. This situation will arise if the rate of oxygen recombination is high and the rate of local action at the negative plate exceeds the rate of grid corrosion at the positive plate [21]. The possible reactions in VRLA batteries are shown in Fig. 6.10 as a function of electrode potential [22].

The actual structure of the separator exercises an important influence on the efficiency of oxygen recombination. A separator with a high surface area and a small average pore size may wick acid to a greater height and provide a higher resistance to the diffusion of oxygen. This may imply the use of a separator with a high percentage of fine fibres, or a hybrid separator containing, for example, organic fibres.

6.4.3. Stratification and drainage

A uniform distribution of sulfuric acid electrolyte between the plates of the battery is essential if the battery is to provide an optimum service. Two types of departure from this ideal are encountered in practice: (i) a heterogeneous distribution of the liquid phase when saturation is incomplete; (ii) and the development of concentration gradients within the liquid phase.

The heterogeneous distribution of electrolyte between the plates not only influences the oxygen cycle but also prevents complete utilization of the active material since regions of the plate which dry out are unable to take part in the discharge reaction. This phenomenon becomes a progressively more serious problem as water is lost and the total volume of electrolyte decreases.

A related issue, when the plates are oriented in a vertical plane, is drainage. There is a limiting height to which the forces of surface tension are able to carry liquid in defiance of the forces of gravity (see eqn. (6.3)). Plates that are taller than this limit will become incompletely saturated at the top with the same consequences that result from falling levels of saturation. Conversely, electrolyte drainage from the separator in a fully assembled cell would be expected to reduce performance, particularly at low discharge rates, where acid starvation would limit capacity. Drainage imposes a maximum height for the element if optimum capacity is to be retained. For commonly used grades of AGM, the height limit is 30–40 cm. If capacity requirements demand larger plates than this to be used, then either the plates must be mounted horizontally or a material with a finer pore structure must be used as the separator.

Concentration gradients ('acid stratification') occur readily in the electrolyte of flooded cells. As the cells are charged, sulfuric acid is produced at a high concentration adjacent to the plate surface and sinks to the base of the cell because it has a higher relative density than the rest of the electrolyte. If left uncorrected, this situation will lead to a non-uniform utilization of active material (with a reduced capacity), aggravated local corrosion and, consequently, shortened cell-life. Flooded cells are periodically set to produce gas during charging, which stirs the electrolyte and overcomes these problems. The immobilization of the electrolyte in a VRLA cell with an AGM separator reduces the tendency for acid stratification but also removes the possible remedy for the problem since gassing is not an option. A gelled electrolyte practically eliminates stratification effects because the molecules of acid immobilized in the gel are not free to move under the influence of gravity.

6.5. Future Developments

The above discussion has shown how the separator–electrolyte-immobilization system in a VRLA battery performs a complex combination of functions. Recently, McGregor *et al.* [18] have listed the following separator properties that are considered to be generally desirable for most battery applications:

- acceptable tensile strength (0.875–1.75 $kN\,m^{-1}$) and elongation (0.5–10%) for processing;
- high porosity ($\sim$ 95% uncompressed) to allow for effective acid filling and oxygen transport;
- serve as an electronic insulator, but when partially saturated display low ionic resistivity (50–70 $m\Omega\,cm^2$);
- readily wettable by sulfuric acid over the life of the battery;
- minimal shrinkage on wetting, sustain a high level of applied pressure at the positive-plate, and conform to the surface of the plates at the required level of force;
- resistance to attack by battery-strength acid at high temperatures (80–120°C) and by oxidation at high potentials;
- high chemical purity, i.e., must not release metal or organic impurities, such as transition metals or chloride species;

- have a pore-size distribution (1–20 μm) which provides a sufficient supply of acid to the plates at the desired rate, but presents no risk of dendritic growth;
- have the ability to wick acid electrolyte to heights of up to 30 cm and minimize stratification and drainage.

None of the present-day AGM separator materials meets the requirements perfectly. The separators appear to allow expansion (and softening) of the positive active-material unless they are employed with compressive forces that are so high as to be impracticable in conventional designs of battery container. The separators also enable high rates, and hence high-power performance, to be obtained from VRLA batteries, but they can also cause the internal oxygen cycle to be overworked as cell life advances and this could give rise to charging and heating problems. This characteristic is, at least partly, a consequence of the pore structure of the AGM materials.

It is obvious that the search for modified or new separator materials for VRLA batteries should be a research topic of high priority. Compared with traditional materials, a separator with a high surface area and a small average pore size may reduce acid stratification, wick acid to a greater height, and provide a higher resistance to the diffusion of oxygen. Such novel materials could moderate the adverse effects of the oxygen cycle (i.e., generation of heat and suppression of negative-plate potential) and hence extend battery life by facilitating complete recharge. Research and development into improved separators is reviewed in Chapter 7.

References

1. B. Culpin, J.A. Hayman, in: L.J. Pearce (Ed.), *Power Sources 11, Research and Development in Non-mechanical Electrical Power Sources*, International Power Sources Symposium Committee, Leatherhead, England, 1987, pp. 45–66.
2. O. Jache, US Patent 3,257,237 (1966).
3. D.H. McClelland, J.L. Devitt, US Patent 3,862,861 (1975).
4. R.F. Nelson, *Batteries International*, **36** (1998) 95–103.
5. A. Ferreira, *J. Power Sources*, **95** (2001) 255–263.
6. B. Culpin, *J. Power Sources*, **53** (1995) 127–135.
7. K. Peters, *J. Power Sources*, **42** (1993) 155–164.
8. E.W. Washburn, *Phys. Rev.*, **17** (1921) 273.
9. E. Nann, V. Toniazzo, U. Lambert, R.F. Nelson, *ALABC Project S1.2, Engineered separators for optimization and performance in VRLA batteries, six-month Project Report 1 June to 30 November 2000*, Advanced Lead-Acid Battery Consortium, Research Triangle Park, NC, USA, 2000.
10. Battery Council International, Battery Technical Manual Test Methods for Recombinant Battery Separator Mat (RBSM) 5/93 (1993).
11. S. Brunauer, P.H. Emmett, E. Teller, *J. Am. Chem. Soc.*, **60** (1938) 309.
12. G.E. Archie, *Trans. AIME*, **146** (1942) 54.
13. A.F. Hollenkamp, *J. Power Sources*, **59** (1996) 87–98.
14. K. Takahashi, M. Tsubota, K. Yonezu, K. Ando, *J. Electrochem. Soc.*, **130** (1983) 2144.
15. J. Alzieu, J. Robert, *J. Power Sources*, **13** (1984) 93–100.
16. W.A. Lincoln, *The Battery Man*, 42 (March 2000) 24, 26–29, 32.
17. Hawker Batteries, ENTEK International, *Brite/Euram Project BE 7297 Task 6, Separator optimization for VRLA batteries, Final Report 1 January 1994 to 31 December 1997*, Advanced Lead-Acid Battery Consortium, Research Triangle Park, NC, USA, 1998.

18. K. McGregor, H. Ozgun, A.J. Urban, G.C. Zguris, *J. Power Sources*, **111** (2002) 288–303.
19. C. Pendry, *J. Power Sources*, **78** (1999) 54–64.
20. D. Berndt, *Maintenance-Free Batteries*, Research Studies Press, Taunton, UK, 1997.
21. W. Brecht, *Batteries International*, **39** (1999) 35–44.
22. D. Berndt, *J. Power Sources*, **95** (2001) 2–12.

This page intentionally left blank

Valve-Regulated Lead–Acid Batteries
D.A.J. Rand et al., editors

—CHAPTER 7—

SEPARATOR MATERIALS FOR VALVE-REGULATED LEAD–ACID BATTERIES

K. Ihmels and W. Böhnstedt

7.1. Introduction

The function of the separator in the VRLA battery has been reviewed in Chapter 6, where the need for the separator to satisfy a complex set of requirements simultaneously has been described. The development of an effective separator clearly represents a challenge for the materials scientist. This chapter outlines the materials that have been used to date and introduces others which are emerging as candidates during the search for improved performance.

Two VRLA battery technologies are currently predominant, i.e., absorptive glass mat (AGM) and gel designs. In the former, the AGM immobilizes the electrolyte and simultaneously functions as a separator. In gel batteries, the acid is immobilized by means of fumed silica, and an additional separator is required to fix the plate distance and to prevent electronic shorts.

State-of-the-art separators for these batteries are described here only to the extent required to illustrate trends and to highlight the need for further development. The greater part of the discussion is descriptive of the new materials which are currently being investigated in pursuit of improved separator performance in VRLA batteries.

7.2. State-of-the-art Separators

7.2.1. Absorptive glass mat (AGM) separators

The most commonly used AGM separators are microfibre-glass fleeces without organic components such as binders or polymeric fibres. The fleeces are composed of blends of acid-resistant glass fibres from two size ranges: (i) 'microfibres', with an average fibre diameter below 1 μm; (ii) 'coarse' fibres, with an average diameter of $\sim 3\,\mu m$. The microfibres (approximately 20–30% of the total) increase the internal surface, improve the tensile strength, and decrease the pore diameter; but they significantly increase the product cost. The driving force for the incorporation of larger fibres is mainly cost reduction, but they also facilitate the filling of

Table 7.1. Typical properties of AGM separators [1].

Basis weight ($g\,m^{-2}$)[a]	200
Porosity (%)	93–95
Average pore size (μm)	5–10
Thickness (acid filled) (mm)	
at 10 kPa	1.3
at 35 kPa	1.0
Puncture strength (N)	7.5

[a]Defined in Chapter 6.

batteries by creating larger pores with faster acid pick-up, often referred to as the 'wicking rate'.

Typical data for conventional AGM separators are shown in Table 7.1 [1]. The separators have a very high porosity, i.e., in excess of 90%. This high porosity, together with a good wettability, results in a very high acid absorption and a low electrical resistance. In addition, the chemical and oxidative stability of the material is very good and the purity, in terms of trace elements and organic contamination, is high.

In the battery, the acid saturation of AGM separators is usually in the range of 95 to 85% [2]. This increases the effective electrical resistance over that of fully saturated separators by 20% for 95% saturation and by 90% for 85% saturation [3], but it also creates open channels of relatively large pores that enable very efficient oxygen transport from the positive to the negative plate. Too high an oxygen transport rate may, however, result in thermal runaway due to the exothermic consumption of oxygen on the negative plate [4], and in premature capacity loss (PCL) by undercharging of the negative plate, a mechanism now referred to as PCL-3 [5,6].

Given the relatively large pores and the good wettability, the wicking rate (speed of acid pick-up) of AGM is fairly high. On the other hand, the comparatively large pores present the risk of internal shorts through the separator, especially when using a narrow plate-spacing and in cycling applications. Additionally, the larger pores reduce resistance to vertical flow of the acid in the separator. Therefore, AGM separators are prone to acid drainage and acid stratification. The term 'acid drainage' describes a gravity-driven migration of the acid to the bottom of the separator, while 'acid stratification' relates to the diffusion of concentrated acid generated during charge towards the bottom of the battery. Acid drainage occurs when the cell is too tall for the capillary forces to overcome the forces of gravity. The liquid phase then 'sags' within the pore structure until the two forces are balanced. When the plates are taller than this critical value, and 'sagging' takes place, an upper part of the separator is left with gas in its pores rather than liquid and this obviously alters dramatically the rate of oxygen transfer. Drainage is thus a process which involves two non-solid phases — liquid and gas. By contrast, stratification only takes place within the liquid phase. Clearly, the two phenomena limit the height of AGM batteries. Furthermore, since acid stratification is accelerated by deep-discharge cycles, AGM batteries are predominantly used in applications that do not involve frequent service under such cycles.

Another feature of AGM separators is their compressibility. With compression of the plate and separator stack, this AGM property guarantees good plate–separator contact, even if the plates are not perfectly smooth. Also, battery assembly is facilitated since the stack can be easily inserted into the cell after compression to a thickness lower than the cell dimension. An undesirable result of the compressibility is that the AGM separator does not exert sufficient resistance against expansion of the positive plate during battery cycle-life. This expansion is particularly prevalent in deep-cycle applications and can cause the battery to suffer premature capacity loss (PCL) via reduced inter-particle conductivity — a phenomenon known as 'PCL-2' [7]. In the literature, two additional characteristics, which are related to the PCL-2 failure mode, are discussed, namely, AGM separators shrink when first wetted with electrolyte and their fibres can be crushed at high pressure levels [8–10]. These features result in a loss of separator resilience, i.e., a lessening of the ability to display a reversible spring effect.

7.2.2. Separators for gel batteries

In gel batteries, the addition of 5–8 wt.% of fumed silica (pyrogenic silica) with a specific (BET) surface-area of 200–300 $m^2 g^{-1}$ serves to immobilize the electrolyte. Cracks in the gel provide voids for oxygen transport to the negative electrode. Compared with AGM batteries, the manufacturing cost of gel batteries is considered higher, and their specific power is lower due to a higher internal resistance. Because of the very effective immobilization of acid in the fumed-silica gel, the batteries are less prone to electrolyte drainage and acid stratification than AGM batteries. Accordingly, gel technology offers some advantage in cycle applications, e.g., in motive power for in-plant vehicles and wheelchairs [11].

Gel batteries require an additional separator to fix the plate distance and to prevent electronic shorts. The most effective protection against shorts is achieved by means of separators with low pore size; ideally, microporous materials should be used (pore size less than 1 μm). Additionally, the separator should have a low acid-displacement since the fumed silica and the cracks in the gel already reduce the volume available for electrolyte. To minimize the internal resistance of the battery, the electrical resistance of the separator should be as low as possible. These two requirements, viz., low acid-displacement and low electrical resistance, translate into a need for separators with good wettability, high porosity, and low geometrical volume, i.e., rib configuration and backweb thickness should both be optimized.

In contrast to most conventional separators for flooded batteries, separators for gel batteries have ribs positioned not only towards the positive plate, but also towards the negative plate in order to facilitate the gel-filling process. For batteries with pasted positive plates, the separator is usually laminated with a glass fleece, which protects the positive plate against shedding, especially in cycle applications. Although this surface fleece stabilizes the active material, the present design of gel batteries cannot prevent completely the expansion of the positive material and the occurrence of PCL-2. The most important characteristics of separators used in gel batteries are listed in Table 7.2 (adapted from Ref. 12).

Table 7.2. Properties of separators used in gel batteries.

Property	Phenol–formaldehyde/ resorcinol separators	Microporous PVC separators	Coated glass-mat separators
Backweb thickness (mm)	0.4	0.55	0.4
Porosity (%)	70	71	70
Pore size (average) (μm)	0.5	0.2	0.1
Acid displacement ($ml\,m^{-2}$)	165	260	n.a.
Electrical resistance ($m\Omega\ cm^2$)[a]	100	160	140

[a]This is the resistance offered by one square centimetre of the separator material in question.

Table 7.3. Characteristics of state-of-the-art separator technologies for VRLA batteries.

System	Advantages	Disadvantages
Absorptive glass mat (AGM)	• Very high porosity of separator	• Relatively large separator pores – acid stratification – electrolyte drainage – risk of internal shorts – risk of thermal runaway – risk of PCL-3
	• High purity and stability of separator	• Low tensile strength of separator
	• Low internal electrical resistance	• High compressibility of separator – risk of PCL-2
	• Easy acid filling	• Low crush resistance of separator – risk of PCL-2
	• Relatively low cost	• Contraction on wetting of separator – risk of PCL-2
Gel	• Little acid stratification	• Difficult gel-filling processes
	• Little electrolyte drainage	• Relatively high internal resistance
	• Small separator pores – low risk of internal shorts	• Low compressive forces – risk of PCL-2
		• Relatively high cost

7.3. Development Trends for VRLA Battery Separators

The advantages and disadvantages of state-of-the-art AGM and gel separator technologies for VRLA batteries are given in Table 7.3.

Much recent effort on separator development has been devoted to the optimization of existing products. Since the separator dictates the performance of

an AGM battery much more than does the separator in a gel battery, work has focused primarily on the improvement of microfibre separators, namely:

- minimization of acid stratification, electrolyte drainage, and the risk of electric shorts
  – separator with small pore size
- prevention of PCL-2 (expansion of positive active mass)
  – separator with low compressibility, high crush resistance, and low contraction on wetting
- prevention of PCL-3 (undercharging of negative plate) and thermal runaway
  – separator that allows controlled transport of oxygen.

Attempts to satisfy these requirements have involved several different development strategies:

- optimization of the share of fine and coarse fibres in AGM
- addition of polymeric fibres or silica
- lamination with membranes
- novel separator concepts.

All of these development concepts are described in the next section.

7.4. Separator Developments

7.4.1. Modified AGM

7.4.1.1. AGM — high surface-area. When first introduced into the market, AGM separators had a relatively high content of fine fibres. These separators had specific surface-areas in the range of 1.6–2.0 $m^2 g^{-1}$ (note, a surface area of 2.0 $m^2 g^{-1}$ represents a separator with close to 100% fine fibres). Today, separators with a lower share of fine fibres (20–30%) are common and, consequently, surface areas are typically between 1.1 and 1.3 $m^2 g^{-1}$ [13]. The driving force for this lower fine-fibre content has been mainly the higher cost of such fibres, a welcome side effect is a faster wicking rate due to larger pores [13,14]. Most of these AGM separators went into stationary batteries, which experience less acid stratification and expansion of the positive plates than batteries in cycling applications.

With VRLA batteries recently becoming the focus of attention for cycling applications, requirements for the AGM separator have changed. In particular, the AGM separator must better withstand the forces caused by the expansion of the active material, and acid stratification must be reduced. Both these requirements call for a higher share of fine fibres, which is known to improve the mechanical properties and to decrease the pore size. The latter property, in turn, should reduce acid stratification. The expected improvement in mechanical properties can be illustrated by calculating the number of fibres for a given sample weight. For example, a two-gram sample contains about 5.6 billion fine fibres (diameter 0.8 μm) vs. 28 million coarse fibres (diameter 3.5 μm). If the fibres are viewed as springs, fine fibres should offer substantially more resilience to provide for sustained pressure

against the plates [14]. The data compiled in Table 7.4 illustrate the trend to lower pore size and lower compressibility with the higher surface area which results from a higher share of fine fibres [15]. It has also been reported [10] that AGM separators with high surface area exhibit greater crush-resistance.

As a result of such considerations, the surface area, particularly fine-fibre content of AGM separators has been the subject of two ALABC projects on EV batteries. In the first project [16], acid stratification was found to decrease as the surface area of the separator was increased, see Table 7.5. Nevertheless, any advantage in terms of battery cycle-life was less clear-cut, see Table 7.6.

Post-service examination revealed that all positive plates had undergone softening and considerable expansion. In addition, lead dioxide particles had penetrated the separator. The general condition of the positive plates was better with separators of higher fine-fibre content, which was related to the lower degree of acid stratification.

Table 7.4. Pore size and compressibility of AGM separators with different surface areas [15].

Specific surface-area ($m^2\,g^{-1}$)	0.5	0.9	1.2	2.6
Maximum pore size (μm)	45	31	24	14
Thickness (dry) (mm)				
at 10 kPa	2.58 (100%)	1.78 (100%)	1.65 (100%)	1.39 (100%)
at 20 kPa	2.03 (79%)	1.49 (83%)	1.47 (89%)	1.27 (91%)
at 30 kPa	1.86 (72%)	1.40 (78%)	1.40 (85%)	1.23 (88%)
Thickness (acid filled) (mm)				
at 10 kPa	2.51 (100%)	1.71 (100%)	1.60 (100%)	1.35 (100%)
at 20 kPa	1.99 (79%)	1.47 (86%)	1.44 (90%)	1.26 (93%)
at 30 kPa	1.87 (75%)	1.39 (81%)	1.41 (88%)	1.21 (90%)

Note, figures in brackets represent percentage of initial thickness at 10 kPa.

Table 7.5. Acid densities after tests of cells using AGM separators with different contents of fine fibre [16].

Cycles at end-of-service	Specific surface-area ($m^2\,g^{-1}$)	Fine-fibre content (%)	Acid densities in different separator regions ($g\,cm^{-3}$)		
			Upper region	Middle region	Lower region
142	0.7	10	1.250	1.323	1.346
230	0.7	10	1.231	1.308	1.326
202	1.45	55	1.255	1.289	1.307
205	1.45	55	1.293	1.301	1.305
180	2.2	100	1.293	1.296	1.299
188	2.2	100	1.283	1.283	1.308
260	2.2	100	1.305	1.305	1.308

Table 7.6. Cycle-life of cells using AGM separators with different contents of fine fibre [16].

Specific surface-area ($m^2\,g^{-1}$)	Fine-fibre content (%)	Cell pressure (kPa)	Cycles when capacity loss first reaches 20%	Cell pressure at initial cycles (kPa)
0.7	10	~40[a]	54	29
0.7	10	40[b]	63[c]	—
1.45	55	~40[a]	70	12
1.45	55	~40[a]	40	14
2.2	100	< 10[a]	55	4
2.2	100	~55[a]	59	30
2.2	100	40[b]	130[d]	—

[a]Initial pressure at cell build, operated at fixed plate-group thickness.
[b]Operated at constant pressure by means of piston cell.
[c]Permanent fall to below 80% of initial capacity after ~90 cycles.
[d]Permanent fall to below 80% of initial capacity after ~180 cycles.

Table 7.7. Cycle-life of cells using AGM separators with different contents of fine fibre at different compression levels [17].

Fine-fibre content (%)	Cycle-life[a] at compression level (%)		
	20%	25%	30%
50	325	350	680
66	820	460	840
75	890	870	620

[a]End of cycle-life estimated for capacity falling below 80% of initial value.

The best cycle-life was obtained for a separator with 100% fine fibres when the cell was operated under constant pressure by means of a piston cell. For cells operated at fixed plate-group thickness, there were strong indications of crushing of the separators very early in service, and this allowed expansion of the positive plates that resulted in a substantial loss of capacity. The separator crushing is reflected in the low cell pressures listed in the last column of Table 7.6. In general, the cycle-life of all the cells was low compared with those employed in other ALABC projects with AGM separators. This is at least partly explained by the 100% DoD operation of the former cells (end-of-discharge-voltage, 1.75 V) at a 3-h discharge rate, which was much more demanding than most of the regimes adopted in the other ALABC projects.

In a second ALABC project [17], separators with 50, 66, and 75% fine-fibre content were assembled into cells at compression levels of 20, 25, and 30%, respectively. These cells were operated to 75% DoD (3 h at $C_5/4$) at a constant plate-group thickness; the cycle-lives are listed in Table 7.7. Although there were some

anomalies (e.g., 75% fine-fibres and 30% compression), it can be concluded from the results that cycle-life increases with higher fine-fibre content and higher compression. It should be noted, however, that this tendency with higher compression is less clear-cut, which may be due to uncontrolled loss of compression during cycling, as was observed in the earlier ALABC project [16] (*v.s.*) for cells operated at constant plate-group thickness (see Table 7.6).

7.4.1.2. AGM — high|low surface-area composite. In a different approach aimed at taking advantage of the separate merits of high and low surface-area glass fibres, multi-layered AGM separators were investigated [18]. It was found that two interspersed layers — one with fine fibres and one with coarse fibres — showed better properties than when those fibres were dispersed ('mixed') in a single, uniform sheet. This was especially true for pore size and tensile strength, as shown in Table 7.8. These results can be explained by assuming that the fine fibres are not 'diluted' in a two-layer separator, but they are in a uniformly mixed fibre material. In addition to these results, a 100% fine-fibre layer facing the electrodes can also be expected to prevent shorts and acid stratification more effectively than a mixed fibre separator.

With the preceding as background, a two-layered AGM separator was evaluated in a further ALABC project [19,20]. This separator consisted of a layer of 100% fine fibres (high surface area) and a second layer made of a mixture of 40% fine fibres with the addition of coarse fibres and chopped structural fibres (low surface area) [21]. Both the positive and negative plates were wrapped by this separator, with the 100% fine-fibre layer facing the electrodes; the cell configuration is shown

Table 7.8. Comparison of properties of AGM separators, one consisting of a layer of fine fibres in contact with a layer of coarse fibres, and the other consisting of a single-layer of mixed fibres [18].

Fibre ratio fine (%)/coarse (%)	Separator type	Average pore size (μm)	Tensile strength ($kN\,m^{-1}$)
0/100	coarse fibres	10.4	0.20
17/83	mixed fibres	6.9	0.37
	two layers	3.6	0.41
25/75	mixed fibres	5.8	0.37
	two layers	3.2	0.47
33/67	mixed fibres	4.8	0.44
	two layers	3.0	0.57
42/58	mixed fibres	4.2	0.43
	two layers	2.8	0.62
50/50	mixed fibres	4.0	0.68
	two layers	2.5	0.72
100/0	fine fibres	2.6	0.69

in Fig. 7.1. The compressive force in these cells, applied on the dry separator, was 35 kPa, and cycling was performed to 75% DoD (3 h at 0.25 C_5). The best two of six cells went below 80% of their initial capacities at approximately 340 cycles. This was of a low cycle-life compared with other separators tested in the project, which may be partly explained by the relatively low compression level that was employed.

7.4.1.3. AGM — membrane sandwich. The combination of a membrane with an AGM separator has been investigated with a view towards controlling the oxygen transport as well as improving the compressive properties of the separator. With reference to the latter aspect, a AGM–membrane sandwich has been evaluated [19]. The AGM consisted of 100% fine fibres, and the incompressible polymer membrane was a mixture of polyvinyl chloride and 5–10 wt.% silica, which was partly extracted to increase the pore size and porosity. The properties of the two separator components are summarized in Table 7.9 [22].

The cell configuration, illustrated in Fig. 7.2, placed a layer of the AGM in contact with each electrode and the membrane was located between the two layers of AGM. The compressive force in the cells, applied on the dry separator, was > 50 kPa, and cycling was performed to 75% DoD (3 h at $0.25C_5$). Under these conditions, the cells

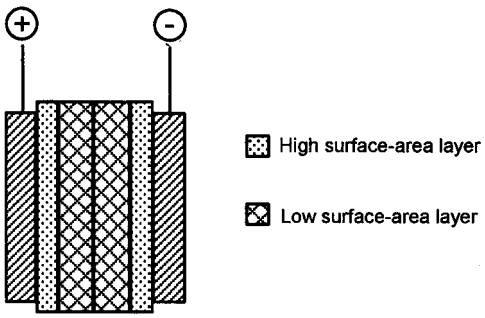

Fig. 7.1. Cell construction with two-layered AGM.

Table 7.9. Properties of AGM–membrane sandwich components [22].

Property	Micro-glass fibre	Organic membrane
Total thickness (dry) (mm)	0.52	0.57
Backweb thickness (mm)	0.52	0.47
Porosity (%)	93	81
Specific surface-area ($m^2\,g^{-1}$)	2.0	—
Pore size (mean) (μm)	2.5	5.0
Electrical resistance ($m\Omega\,cm^2$)[a]	—	45

[a]This is the resistance offered by one square centimetre of the separator material in question.

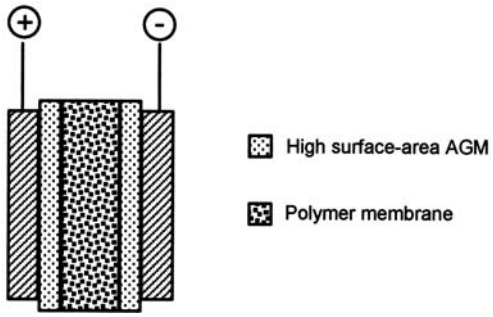

Fig. 7.2. Cell construction with AGM–membrane sandwich [22].

ran approximately 600 cycles before dropping to below 80% of their initial capacity [23]. Tear-down analysis of one intact cell after 500 cycles showed both the plates and the separators to be in good condition. Compared with hybrid separators and the two-layered AGM separator described earlier, the sandwich separator gave the best cycle performance. This finding may stimulate further work on such separator systems.

7.4.1.4. AGM — with organic fibres. AGM separators made from a blend of glass fibres and about 10 wt.% of polymeric fibres have been used by the battery industry for many years [24–26]. Compared with traditional AGM separators, these so-called 'hybrid separators' show an improved tensile strength and a 2–5 times higher puncture strength [26]. Depending on the weight fraction of the polymer fibres, hybrid separators can be sealed into pockets. In addition, the polymer fibres (e.g., made from polyethylene, polypropylene, polyester, or bi-component polymers) create hydrophobic sites. These sites allow the use of a 'fill and spill' process in which batteries are flooded with acid and, after formation, the excess acid is decanted. The hydrophobic sites then allow the passage of oxygen to the negative plate [13].

Although hybrid separators appear to offer advantages in battery manufacture and, additionally, might show an improved resilience after compression [25], there have been few published reports on their performance. Recently, a hybrid separator with 15 wt.% organic fibres was the subject of an ALABC investigation. The properties of this separator are compared with those of conventional AGM separators in Table 7.10 [27]. The hybrid separator shows a slightly lower compressibility in the dry state and a significantly lower shrinkage on wetting. Several cells were cycled at the 2-h rate to 80% DoD. The conditions and results are summarized in Table 7.11. For all the cells that showed a positive-plate limitation, softening and expansion of the positive active-material was observed. For the cells subjected to a pressure of 80 kPa, this was accompanied by a compaction of the separator and of the negative active-material, with the latter causing a reduction in the capacity of the negative plate.

The above results indicate that hybrid separators are more of an advantage for the battery production process than for improving battery performance.

Table 7.10. Compressive properties of hybrid and AGM separators [27].

Property	Hybrid[a]	AGM
Thickness (dry) (mm)		
at 10 kPa	1.55 (100%)	1.64 (100%)
at 20 kPa	1.51 (97%)	1.58 (96%)
at 50 kPa	1.39 (90%)	1.37 (84%)
Thickness (acid filled) (mm)		
at 10 kPa	1.38 (100%)	1.27 (100%)
at 50 kPa	1.30 (94%)	1.20 (94%)
Contraction on wetting (%)[b]		
at 10 kPa	11	23
at 50 kPa	6	12
Specific surface-area ($m^2\ g^{-1}$)	0.83	—

Note, figures in brackets represent percentage of initial thickness at 10 kPa.
[a]Designation II-P15.
[b]Contraction = (dry thickness – acid-saturated thickness)/dry thickness × 100%.

Table 7.11. Summary of cycle-life tests with hybrid separators [27].

Pressure (kPa)	Cell type	Separator	End-of-life[a] (cycles)	Limiting plate-group
40	standard	II-P15	90	positive
40	standard	II-P15 + pasting paper[b]	335	positive
40	standard	II-P15 + PE separator[b]	194	positive
40	piston cell	II-P15	155	positive
80	piston cell	II-P15	156	positive
80	standard	II-P15	120	negative (slightly)
80	piston cell	II-P15	63	neither plate

[a]To 80% of initial capacity.
[b]To restrict movement of positive active-material into separator.

7.4.1.5. Silica-loaded glass mat (SLGM). As mentioned earlier, the cost of AGM increases substantially with the share of fine fibres. Therefore, the incorporation of cheap fillers with high surface area has been pursued as a low-cost alternative to increase the surface area of AGM [13]. Various patents have been granted on AGM separators filled with silica. The claimed advantages include: reduced acid stratification when AGM is immersed in a colloidal solution of silica and the water is dried off [28]; high tensile strength, resiliency and crush resistance when silica particles are incorporated together with a binder [29]; and smaller pore size, higher surface area and, therefore, improved battery performance when AGM is filled with silica particles [30].

Table 7.12. Compressive properties of silica-loaded glass mat and AGM separators [27].

Property	SLGM	AGM
Thickness (dry) (mm)		
at 10 kPa	1.90 (100%)	1.64 (100%)
at 20 kPa	1.88 (99%)	1.58 (96%)
at 50 kPa	1.82 (96%)	1.37 (84%)
Thickness (acid filled) (mm)		
at 10 kPa	1.84 (100%)	1.27 (100%)
at 50 kPa	1.79 (97%)	1.20 (94%)
Contraction on wetting (%)[a]		
at 10 kPa	3	23
at 50 kPa	2	12
Specific surface-area ($m^2\ g^{-1}$)	3.86	—
Pore size (average) (μm)	16	—

Note, figures in brackets represent percentage of initial thickness at 10 kPa.
[a]Contraction = (dry thickness − acid-saturated thickness)/dry thickness × 100%.

Considering these potential advantages, a glass-fibre separator filled with silica (SLGM) was included in an ALABC project that evaluated various separator systems [27]. No details of the composition and manufacturing of this particular SLGM separator were disclosed, but a comparative evaluation against other separators was performed. The data are summarized in Table 7.12. Because of their favourable compressibility and shrink-on-wetting characteristics, these separators were also examined in a battery test programme. Two cells subjected to an initial pressure of 80 kPa and cycled to 80% DoD failed very early (less than 50 cycles). Surprisingly, these failures were found to be due to significant contraction of the separators accompanied by a partial loss of contact between the plates and the separators. In a subsequent cycling test in which the plate-group pressure was adjusted during cycling, a notably better cycle-life (~470 cycles) could be achieved with frequent adjustments of the plate-group pressure to compensate for the contraction of the separator. It remains to be investigated whether this unexpected contraction is related to the particular separator version that was employed in the study or if it is a general feature of SLGM.

In another ALABC project [31], a so-called 'Silica Powder AGM' composed of 70 wt.% silica, 10 wt.% polyester fibres (with low melting point and acting as a binder) and 20 wt.% glass fibres was subjected to cycling tests to 72% DoD. The initial pressure was 42 kPa and the cell achieved about 250 cycles before its capacity fell below 80% of the initial value.

Within the framework of a project for the optimization of batteries for storing photovoltaic and wind energy, an AGM separator with an inorganic filler of high surface-area was developed. The surface area was found to increase and the pore size to decrease significantly with incorporation of the filler, but the tensile strength suffered, see Table 7.13 [32]. With this separator (regardless of how much filler was

Table 7.13. Properties of unfilled (standard) AGM and filled separators [32].

Property	Filler content		
	Standard	Low	High
Specific surface-area ($m^2\ g^{-1}$)	1.17	7.28	14.83
Pore size (average) (μm)	4.78	3.29	2.84
Tensile strength ($kN\,m^{-1}$)	0.96	0.67	0.47

used) and additional modifications of the battery design (high ratio of positive to negative active-material, relatively high compression of the separator, relatively low saturation degree), the cycle-life of batteries operated at 60% DoD could be improved by up to 50%.

7.4.1.6. Other AGM modifications. Some recently published patents have described AGM separators produced from dry-laid instead of wet-laid fibres [33,34]. In the wet-laid paper process, the glass fibres break during their dispersion in water. Since the dry-laying process avoids such 'fibre degradation', it is claimed to produce sheets with longer fibres and better mechanical properties, e.g., higher tensile strength, resiliency, and crush resistance. Other patents deal with pre-compressed AGM separators, which expand on filling with acid [35], or AGM treated with polymer dispersions for improved mechanical properties [36]. A special variety of VRLA battery separators composed of a very small amount of fibrillated PTFE (Teflon) and silica has also been disclosed [37,38]. It remains to be seen which of these technologies can be converted into commercial products.

7.4.2. Alternative separators

7.4.2.1. Synthetic wood-pulp separators (SWP). So-called 'synthetic wood-pulp' (SWP) separators are used widely in Japan for automotive batteries. These are fleeces made from fibrillated polyethylene or polypropylene and small amounts of additional fibres (e.g., polyester fibres); sometimes, the fleeces are also filled with silica. The organic sheets are laminated with a glass mat, which serves to stabilize the positive active-material [39].

Within the ALABC programme, various new SWP separators have been evaluated with respect to their suitability for VRLA batteries [31,40]. These separators vary in their fibre composition, and some also contain silica powder and microglass fibres. The porosity is in the range of 85–88%, which is somewhat less than that of AGM separators. Due to the hydrophobic nature of the organic fibres, the electrical resistance is about 3–5 times higher than that of conventional AGM separators. On the other hand, the SWP separators exhibit lower compressibility, lower contraction on wetting, and better recovery compared with AGM separators. In a separate ALABC task [27], one of these SWP separators (referenced as SWP-7) was compared with a standard AGM; the results are compiled in Table 7.14.

Table 7.14. Compressive properties of SWP-7 and AGM separators [27].

Property	SWP-7	AGM
Thickness (dry) (mm)		
at 10 kPa	1.50 (100%)	1.64 (100%)
at 20 kPa	1.48 (99%)	1.58 (96%)
at 50 kPa	1.46 (97%)	1.37 (84%)
Thickness (acid filled) (mm)		
at 10 kPa	1.39 (100%)	1.27 (100%)
at 50 kPa	1.34 (96%)	1.20 (94%)
Contraction on wetting (%)[a]		
at 10 kPa	7	23
at 50 kPa	8	12
Pore size (average) (μm)	13	—

Note, figures in brackets represent percentage of initial thickness at 10 kPa.
[a]Contraction = (dry thickness − acid-saturated thickness)/dry thickness × 100%.

In battery cycle tests to a regular 72% DoD, the initial discharge capacities of the SWP-7 cells were 10% lower than for the AGM cell. This difference was attributed to the lower porosity of the SWP-7 separator and the attendant lower acid volume. Cells with SWP-7 separators achieved 300 cycles, but the AGM cell failed after 150 cycles (failure point: 80% of initial capacity). It should be mentioned that whereas the SWP-7 cells were built with an assembly pressure of 48–58 kPa, the AGM cell used only 22 kPa and this may have contributed to its shorter cycle-life.

In a different battery test with a simulated EV load pattern, a SWP-7 cell with an assembly pressure of 60 kPa achieved 450 cycles versus 270 cycles for an AGM cell with 73 kPa. The failure mode was found not to be the expansion of positive plate but, rather, sulfation of the negative plate. This led to the conclusion that the favourable mechanical properties of SWP-type separators suppress degradation of the positive active-material.

7.4.2.2. Polymeric microfibre mat. Until recently, the production of absorptive separators from 100% polymeric fibres was limited by the fact that fibre diameters of less than 1 μm could not be produced at reasonable cost. Further developments in polymers, as well as refinements in fibre production, have resulted in the manufacture of mats with a high percentage of fine fibres with a diameter below 1 μm [41]. As these organic fibres (usually polypropylene) are hydrophobic by nature, wettability has to be imparted by additional treatments such as grafting with hydrophilic agents or by co-extrusion with hydrophilic polymers [1].

A comparison between typical data for a microfibre-glass mat and that for a polypropylene microfibre mat is given in Table 7.15 [1]. Glass mats attain a higher porosity and smaller pore size, probably due to the higher stiffness of the individual fibres and a higher portion of microfibres. Polypropylene microfibre mats distinguish themselves by higher tensile and puncture strengths. In addition, they can

Table 7.15. Properties of microfibre-glass mat and polypropylene microfibre mat separators [1].

Properties	Microfibre-glass mat	Polypropylene
Porosity (%)	93–95	90–92
Pore size (mean) (μm)	5–10	5–15
Fibre diameter (μm)	0.5–5	0.5–30
Puncture strength (N)	7.5	15
Tensile strength ($kN\,m^{-1}$)		
–MD	0.32	0.75
–CMD	0.25	0.92

Table 7.16. Compressive properties of polypropylene microfibre mat and AGM separators [27].

Property	Polypropylene	AGM
Thickness (dry) (mm)		
at 10 kPa	0.97 (100%)	1.64 (100%)
at 20 kPa	0.95 (97%)	1.58 (96%)
at 50 kPa	0.88 (91%)	1.37 (84%)
Thickness (acid filled) (mm)		
at 10 kPa	0.95 (100%)	1.27 (100%)
at 50 kPa	0.87 (92%)	1.20 (94%)
Contraction on wetting (%)[a]		
at 10 kPa	2	23
at 50 kPa	1	12
Pore size (average) (μm)	32.5	—

Note, figures in brackets represent percentage of initial thickness at 10 kPa.
[a]Contraction = (dry thickness − acid-saturated thickness)/dry thickness × 100%.

be welded into pockets and, thus, can be integrated into highly automated assembly processes.

The compressive properties of a polypropylene microfibre mat and a standard AGM were compared in one of the ALABC projects discussed above [27]. The findings are shown in Table 7.16. Although the compressibility of the dry separator and especially the shrink-on-wetting look favourable, the capacities of cells assembled at 40 kPa and 80 kPa were significantly lower than for cells with hybrid separators (mix of glass and polymer fibres). Tear-down analysis revealed that this was due to release of acid from the separators. In the light of this phenomenon, no further work on this separator type was conducted within the project.

7.4.2.3. Staflex. A separator named 'Staflex' has been evaluated in the ALABC programme [27]. The properties of this separator are compared with those of a

Table 7.17. Compressive properties of Staflex and AGM separators [27].

Property	Staflex	AGM
Thickness (dry) (mm)		
at 10 kPa	1.12 (100%)	1.64 (100%)
at 20 kPa	1.12 (100%)	1.58 (96%)
at 50 kPa	1.09 (97%)	1.37 (84%)
Thickness (acid filled) (mm)		
at 10 kPa	1.05 (100%)	1.27 (100%)
at 50 kPa	1.05 (100%)	1.20 (94%)
Contraction on wetting (%)[a]		
at 10 kPa	6	23
at 50 kPa	4	12
Specific surface-area ($m^2\ g^{-1}$)	6.94	—
Pore size (average) (μm)	0.63	—

Note, figures in brackets represent percentage of initial thickness at 10 kPa.
[a]Contraction = (dry thickness − acid-saturated thickness)/dry thickness × 100%.

standard microfibre-glass separator in Table 7.17. Although no details of its composition have been published, Staflex is claimed to be an organic material. The separator does not yield as much as AGM when subjected to pressure, and it also shrinks less upon wetting with acid. Based on its relatively low compressibility, it was anticipated that it would allow high levels of plate-group pressure and thereby could control positive-plate expansion and, thus, sustain capacity. At a pressure of 80 kPa, however, cells cycled to 80% and 100% DoD failed after only 50 and 25 cycles, respectively. The capacity was negative-limited, and post-service analysis revealed that this was due to significant compaction and porosity loss of the negative active-material. There may also have been a contribution from a strong interaction of this active material with the separator, which would limit diffusion of acid into the plate and cause an insufficient recombination efficiency.

7.4.2.4. Acid jellying separator. Recently, a microporous separator known as the 'Acid Jellying Separator' (AJS) has been developed [42]. This is a highly filled polymer separator with fumed silica as the major filler component. Important properties of the AJS are given in Table 7.18 for a sample with a thickness of 1 mm [1]. In contrast to microfibre-glass mats, the AJS swells slightly when filled with acid. The very low compressibility is also remarkable, as shown in Fig. 7.3 where its properties are compared with those of a microfibre-glass mat separator [1]. For a design pressure of 100 kPa, the AJS thickness decreases by only about 1% in contrast to more than 40% for microfibre-glass mats. This low pressure sensitivity of the AJS, in conjunction with a suitable battery design, should allow the expansion of the positive active-material to be strictly limited. In addition, its microporosity should largely prevent the growth of active material into the separator.

Table 7.18. Properties of AJS [1].

Porosity (%)	81
Pore size (mean) (μm)	0.2
Dimension change on wetting (%)	+1
Thickness (acid filled) (mm)	
at 10 kPa	1.000
at 35 kPa	0.995
at 100 kPa	0.990
Electrical resistance ($m\Omega\ cm^2$)[a]	90

[a]This is the resistance offered by one square centimetre of the separator material in question.

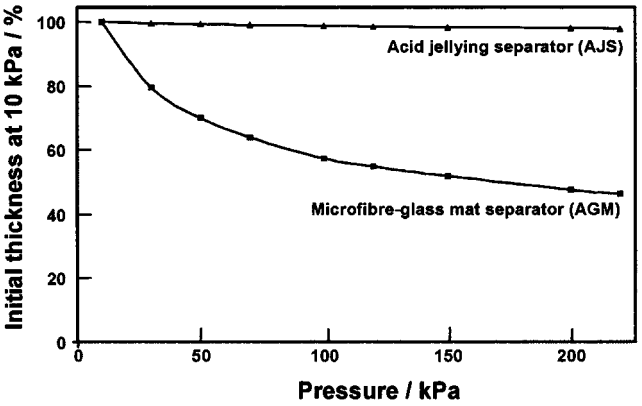

Fig. 7.3. Compressibility of AJS and AGM separator (acid filled) [1].

Acid stratification is also not expected to have a significant effect on cycle-life, since the electrolyte is contained in a gel inside these separators. This is due to the fumed silica used as the major filler and the resulting large internal surface area of some $150\,m^2\,g^{-1}$. The following laboratory investigation was undertaken. Separator strips (8×2.5 cm) were soaked with sulfuric acid — one half of each strip with acid of $1.6\,g\,cm^{-3}$ rel. dens. and the other half with acid of $1.2\,g\,cm^{-3}$ rel. dens. The strips were then suspended with the higher density acid in the top half. Due to gravity effects, with time, the densities equalize from top to bottom. The acid densities for the AJS and a microfibre-glass mat separator are shown in Fig. 7.4 as a function of time [1]. The intersection of the straight lines yields the extrapolated time for acid density equalization within the separator. Due to the substantially larger internal surface area and the lower average pore size, the acid density change proceeds some six times slower in the AJS than in the microfibre-glass mat. This should effectively delay acid stratification in cycling service, or even completely eliminate it, because the time for forming denser acid within the few hours of one charge–discharge cycle is short in comparison with the time of acid diffusion exchange inside the separator (some 50 h).

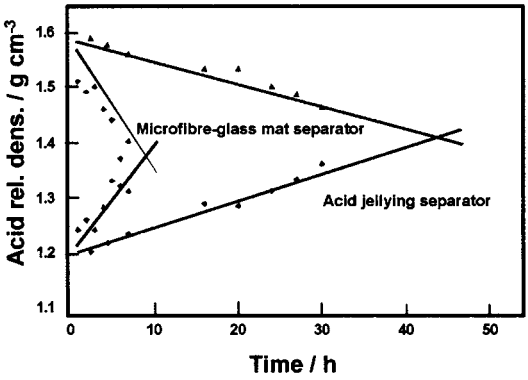

Fig. 7.4. Acid stratification experiment for AJS and AGM separator [1].

Acid Jellying Separators have been compared with AGM and gel in cells tested for EV duty [43]. Cells with a nominal capacity of 48 Ah (C_5/5 rate) were assembled with various separation systems, and pressure was applied to the cell walls. The cells were subjected to 25 cycles (C_2/2 rate) followed by two capacity checks (C_5/5 rate), by means of the following regime:

discharge: 100%DoD: 20 A to 1.6 V(C_2/2); 9.6 A to 1.75 V(C_5/5).
charge: IU: 14.4 A, 10 h, 2.4 V for AGM; 2.45 V for AJS and gel.

The C_5 capacities of three cells are shown in Fig. 7.5. Two cells were separated with AJS and subjected to 30 and 80 kPa initial external pressure, respectively, and one cell was separated with AGM and 30 kPa initial pressure [44]. With the end-of-life defined as the moment when the capacity fell below 80% of its initial value, the AJS (30 kPa), AJS (80 kPa), and AGM (30 kPa) cells completed 510, 1005, and 250 cycles, respectively. Thus, compared with this particular sample of AGM, twice the cycle-life is achieved with AJS cells at the same initial mechanical pressure. By increasing the mechanical pressure from 30 to 80 kPa, the cycle-life of the AJS cell is doubled (i.e., four times that of an AGM cell), which demonstrates the beneficial effect of applying pressure to the electrodes in combination with a non-compressible separator. This is supported by thickness measurements on positive plates removed from service after 450 cycles, see Table 7.19 [43]. The expansion of the positive plate is significantly constrained by the use of AJS and simultaneous application of higher mechanical pressure in comparison with a cycled gel cell under lower mechanical pressure. After cycling, the positive active-material of the AJS cells is still in good condition without any visual evidence of substantial softening. In agreement with the above-mentioned laboratory experiments, only very slight acid stratification and electrolyte drainage is found in these cells. Failure of the AJS (80 kPa) cell after 1005 cycles is attributed to grid corrosion.

7.4.2.5. Ceramic separator. A rigid ceramic separator has been developed by Corning, Inc. [45], with the purpose of improving the cycle-life of VRLA batteries by

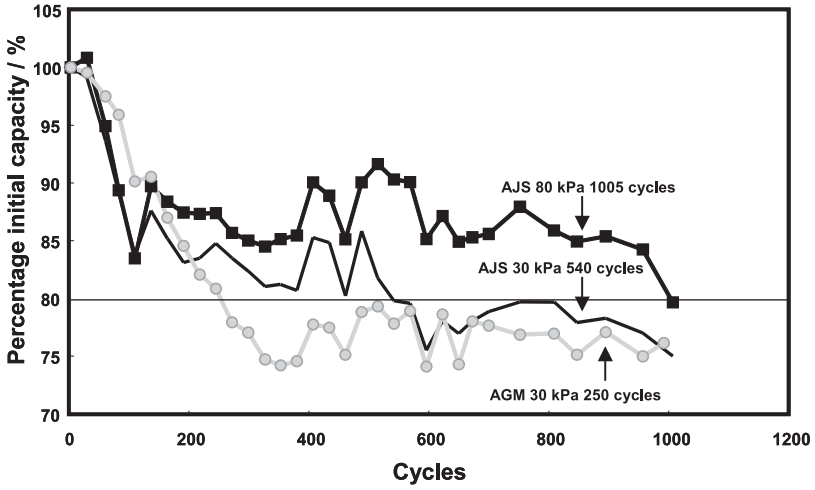

Fig. 7.5. C_5 capacity evolution of cells with different separation systems and different initial external mechanical pressure [44].

Table 7.19. Positive-plate thickness for new cell and two cells after 450 cycles (100% DoD) [43].

Property	Cell type		
	New	Cycled AJS	Cycled gel
Mechanical pressure (kPa)	—	60	30
Positive-plate thickness (mm)			
– top	2.85	3.3	4.0
– middle	2.85	3.4	4.2
– bottom	2.85	3.5	4.1

means of a compressed battery design. Follow-up patents were filed [46–48], and encouraging test results were obtained with batteries [49].

In an ALABC project, rigid ceramic separators were tested with the purpose of preventing the expansion of the positive plate and thereby extending the battery life [50]. Two types of completely rigid separators were evaluated, one characterized by a porosity of 70% and an average pore diameter of 20 μm, and the other by a porosity of 82% and an average pore diameter of 26 μm. Due to mechanical limitations of the separator, the plate-group pressure was limited to 20 kPa. In the first battery tests, the initial cell capacity was rather low. This was due to an insufficient contact between the rigid separators and the plates, which by their nature are not perfectly smooth. This problem was circumvented by inserting a thin paper sheet between the plate and separator. Subsequent cycle tests with

this revised configuration were performed on the second type of ceramic separator that had a larger pore size and a porosity of 82%. The thickness of the separators was around 1.5 mm. The battery capacity declined significantly after only 40 cycles and, after 60 cycles, one cell failed completely. Battery tear-down revealed a short through the separator for the failed cell as well as substantial softening of the positive mass and deep penetration of the active material into the separator pores in all cells.

Additional cycle tests, with both separator versions under slightly modified conditions, confirmed these results, although with slightly better results for the separator with the lower pore size, see Fig. 7.6. The cycle tests were stopped after 80 cycles with 42% of the initial capacity, and after 110 cycles with 47% of the initial capacity, for the two types of ceramic separators, respectively. Although no shorts were found in these batteries, a considerable amount of softening of the positive active-material was evident. These results underline the need for a separator with small pore size (preferably microporous) in order to prevent shorts and the expansion of the active material into the separator.

A similar ceramic separator was used in a different ALABC project [27]. This separator had a thickness of 3.39 mm, an average pore size of 100 μm, and a surface area of $0.36\,m^2\,g^{-1}$. Compared with the test described above, a higher stack pressure, between 58 and 130 kPa, was applied. The cell with this separator failed after only 33 cycles, i.e., gave less than 80% of its initial capacity. The failure was due to severe negative-plate compaction and subsequent capacity limitation of this plate.

7.4.2.6. Granular silica. In the early 1990s, Japan Storage Battery developed a VRLA battery in which the acid was immobilized by closely packed granular silica that was filled between and around the plates [51–53]. The silica consists of fine primary particles and of coarser secondary particles formed by agglomerates of the primary particles. While the fine primary particles immobilize the acid, the interstices

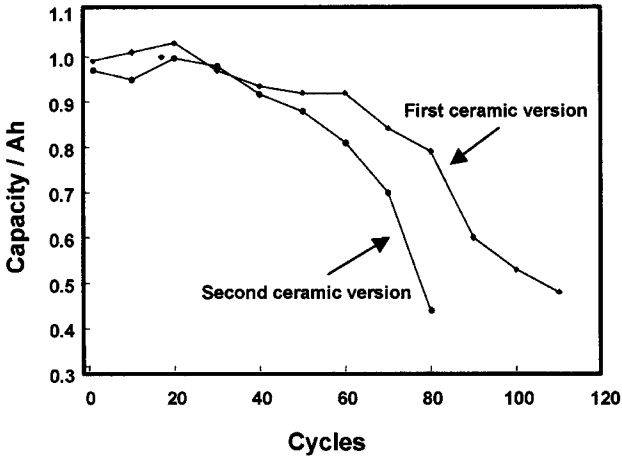

Fig. 7.6. Cycle test (discharge rate 1.25 A, 100% DoD) of 8 V batteries with two versions of ceramic separator [50].

Table 7.20. Properties of granular silica and AGM separator [53].

Property	Granular silica	AGM
Porosity (%)	88–90	92–95
Electrical resistance ($m\Omega\ cm^2/mm$)[a]	80–100	60–80
Specific surface-area ($m^2\ g^{-1}$)	100–300	1–3

[a]This is the resistance offered by one square centimetre of the separator material per millimetre of thickness.

between the agglomerates create the channels for oxygen transport. A separator was also used which had a thickness of 0.02–0.3 mm and a porosity of 70–80%. The properties of the granular silica are compared with those of an AGM separator in Table 7.20 [53].

Since it was assumed that plate growth can be reduced by the densely packed silica, batteries with this concept have been the subject of an ALABC project for EV batteries [31]. It was found that, in contrast to AGM separators, granular silica does not contract either upon wetting with sulfuric acid or when water is lost from the battery. This should be beneficial for maintaining a stabilizing effect on the plates. Batteries of various plate thickness (2.2, 3.2, and 4.5 mm) with AGM and with granular silica were cycled at 60°C to 52% DoD. While the best AGM battery failed after approximately 500 cycles (failure point: 80% of initial capacity), the granular silica batteries achieved around 700 cycles. In addition, all three batteries with granular silica had a similar cycle-life independent of the plate thickness, while the AGM battery with the thinnest plates had a significantly shorter cycle-life. Post-test evaluations showed substantial grid growth for the AGM cells, but only small grid growth for all the granular silica batteries. The failure mode for the granular silica batteries appeared to be the grid corrosion.

7.5. Conclusions

The essential attributes of the ideal material for use as a separator in VRLA cells are now well understood. A wide range of materials and material combinations has been evaluated for this purpose, and it has emerged that materials with small pore size (high surface area) and very little compressibility show good prospects for extending the cycle-life of VRLA batteries.

It remains to be seen which of the many separator materials will be successful in commercial applications. Obviously, this will depend on costs and market requirements, as well as on performance. Although most of the developments reviewed here have been directed towards EV batteries, many of the findings are equally applicable to valve-regulated lead–acid batteries intended for use in other applications.

References

1. W. Böhnstedt, *J. Power Sources*, **78** (1999) 35–40.
2. R.F. Nelson, *Batteries International*, **43** (2000) 51–60.

3. B. Culpin, J.A. Hayman, in: L.J. Pearce (Ed.), *Power Sources 11. Research and Development in Non-mechanical Electrical Power Sources*, International Power Sources Symposium Committee, Leatherhead, England, 1986, pp. 45–66.
4. K. Jana, *The Battery Man*, **41(4)** (1999) 28–36.
5. W.B. Brecht, *The Battery Man*, **40(5)** (1998) 24–45.
6. R.D. Prengaman, *The Battery Man*, **42(9)** (2000) 16–25.
7. A.F. Hollenkamp, *J. Power Sources*, **59** (1996) 87–98.
8. K. McGregor, A.F. Hollenkamp, M. Barber, T.D. Huynh, H. Ozgun, C.G. Phyland, A.J. Urban, D.G. Vella, L.H. Vu, *J. Power Sources*, **73** (1998) 65–73.
9. K. Peters, *J. Power Sources*, **59** (1996) 9–13.
10. G.C. Zguris, *J. Power Sources*, **59** (1996) 131–135.
11. D. Berndt, *Maintenance-Free Batteries*, Research Studies Press Ltd., Taunton, England, 1997, p. 152.
12. W. Böhnstedt, in: J.O. Besenhard (Ed.), *Handbook of Battery Materials*, Wiley VCH Weinheim, Germany, 1999, p. 281.
13. G.C. Zguris, *The Battery Man*, **34(9)** (1992) 42–48.
14. G.C. Zguris, *The Battery Man*, **39(3)** (1997) 14–24.
15. K. Peters, *J. Power Sources*, **42** (1993) 155–164.
16. A.F. Hollenkamp, K. McGregor, M. Barber, J.A. Hamilton, T.D. Huynh, H. Ozgun, C.G. Phyland, A.J. Urban, D.G. Vella and L.H. Vu, *ALABC Project AMC-009*, *Final Report: December 1999 – November 1997*, Advanced Lead-Acid Battery Consortium, Research Triangle Park, NC, USA, 1998.
17. Hawker Batteries, Entek International, *BE 7297 Task 6*, *Final Report*, *Volume 3*, *January 1998*, Advanced Lead-Acid Battery Consortium, Research Triangle Park, NC, USA, 1998.
18. A.L. Ferreira, *J. Power Sources*, **78** (1999) 41–45.
19. Oldham France, Amer-Sil, Hollingsworth & Vose, University of Kassel, *BE97-4085 Task 1*(*a*), *3 Months Periodic Progress Report*, *10 August 1988*, Advanced Lead-Acid Battery Consortium, Research Triangle Park, NC, USA, 1998.
20. Oldham France, Amer-Sil, Hollingsworth & Vose, University of Kassel, *BE97-4085 Task 1*(*a*), *Second Annual Progress Report*, *29 February 2000*, Advanced Lead-Acid Battery Consortium, Research Triangle Park, NC, USA, 2000.
21. M. Weighhall, *ALABC Project No. R/S-001*, *October 2000*, Advanced Lead-Acid Battery Consortium, Research Triangle Park, NC, USA, 2000.
22. U. Lambert, Proc. 5th ALABC Members & Contractors Conference, Nice, France, 28–31 March, 2000, Advanced Lead-Acid Battery Consortium, Research Triangle Park, NC, USA, 2000.
23. Oldham France, Amer-Sil, Hollingsworth & Vose, University of Kassel, *BE97-4085 Task 1*(*a*), *Periodic Progress Report Six Months*, *22 August 2000*, Advanced Lead-Acid Battery Consortium, Research Triangle Park, NC, USA, 2000.
24. K. Peters, B. Culpin, U. S. Patent 4,373,015 (1980).
25. J.P. Badger, U. S. Patent 4,908,282 (1987).
26. G.C. Zguris, *The Battery Man*, **42(8)** (2000) 14–25.
27. A.F. Hollenkamp, K. McGregor, R.H. Newnham, W.G.A. Baldsing, P. Howlett, T.D. Huynh, C.G. Phyland, A.J. Urban, D.G. Vella, L.H. Vu, *ALABC Project No. B-001.2*, *Final Report*, *February 2000*, Advanced Lead-Acid Battery Consortium, Research Triangle Park, NC, USA, 2000.
28. E. Voss, R. Bräutigam, European Patent Application 0 253 987 A1 (1986).
29. M.J. Isaacson, European Patent Application 0 466 302 A1 (1990).
30. G.M. Fernandez, F.L. Trinidad, European Patent Specification EP 0 680 105 B1 (1994).
31. M. Tsubota, M. Shiomi, K. Nakamura, Y. Okada, K. Sawai, *ALABC Project No. B-003.4*, *Final Report*, *10 September 1999*, Advanced Lead-Acid Battery Consortium, Research Triangle Park, NC, USA, 1999.
32. M. Fernández, A.J. Ruddell, N. Vast, J. Esteban, *J. Power Sources*, **95** (2001) 135–140.
33. G.C. Zguris, U. S. Patent 6,071,641 (1997).
34. D.A. Forte, J. Rumiesz, M.J. Cusick, P.C. Martin, U. S. Patent 6,071, 651 (1998).
35. G.C. Zguris, F.C. Harmon, European Patent 0 672 304 B1 (1992).
36. D. Pavlov, S.I. Ruevski, V.B. Naidenov, V.V. Mircheva, G.A. Petkova, M.K. Dimitrov, T.V. Rogachev, M.H. Cherneva-Vasileva, International Patent Application (PCT) WO 99/01902 (1997).
37. M. Khavari, U. S. Patent 5,928,811 (1997).

38. H.B. Johnson, S.B. Laferty, M.P. Wagner, S.M. Mohnot, U. S. Patent 5,009,971 (1989).
39. W. Böhnstedt, in: J.O. Besenhard (Ed.), *Handbook of Battery Materials*, Wiley VCH Weinheim, Germany, 1999, p. 267.
40. K. Sawai, M. Shiomi, Y. Okada, K. Nakamura, M. Tsubota, *J. Power Sources*, **78** (1999) 46–53.
41. J. Zucker, International Patent Application (PCT) WO 98/31060 (1997).
42. W. Böhnstedt, J. Deiters, K. Ihmels, J. Ruhoff, U. S. Patent 6,124,059 (1998).
43. ZSW, Accumulatorenfabrik Sonnenschein, Daramic, *BE97-4085 Task 1(b)*, *Periodic Progress Report Six Months*, *22 August 2000*, Advanced Lead-Acid Battery Consortium, Research Triangle Park, NC, USA, 2000.
44. M. Perrin, H. Döring, K. Ihmels, A. Weiss, E. Vogel, R. Wagner, *J. Power Sources*, **95** (2001) 85–96.
45. J.L. Stempin, R.L. Stewart, D.R. Wexell, U. S. Patent 5,514,494 (1995).
46. V.A. Edwards, J.L. Stempin, International Patent Application (PCT) WO 98/33222 (1997).
47. J.L. Stempin, R.L. Stewart, D.R. Wexell, U. S. Patent 5,728,331 (1996).
48. T.N. Gardner, A.J. Salkind, J.L. Stempin, D.R. Wexell, U. S. Patent 5,738,955 (1996).
49. A.G. Cannone, A.J. Salkind, J.L. Stempin, D.R. Wexell, *Proc. Eleventh Annual Battery Conference on Applications and Advances*, Long Beach, NY, USA, 1996, 279–282.
50. Accumulatorenfabrik Sonnenschein, *BE97-4085 Task 1(c)*, *Annual Report*, *February 1999*, Advanced Lead-Acid Battery Consortium, Research Triangle Park, NC, USA, 1999.
51. A. Tokunaga, T. Hayashi, T. Hatanaka, M. Kasai, T. Omae, European Patent Specification 0 443 451 B1 (1990).
52. M. Shiomi, K. Takahashi, M. Tsubota, *J. Power Sources*, **42** (1993) 173–184.
53. K. Takahashi, A. Tokunaga, M. Tsubota, *The Battery Man*, **37(11)** (1995) 24–32.

This page intentionally left blank

Valve-Regulated Lead–Acid Batteries
D.A.J. Rand et al., editors

—CHAPTER 8—

BATTERY MANAGEMENT

A. Jossen

8.1. Introduction

As is well known, the operational functions of valve-regulated lead–acid (VRLA) batteries are more complex than those of vented type ('flooded') lead–acid batteries. The main reasons for this are the use of an immobilized electrolyte and the participation of the internal oxygen cycle (see Section 1.3, Chapter 1). The VRLA design allows the development of very compact storage units, for example, those employed in uninterruptible power supplies (UPSs). One effect of such compact storage is an inhomogeneous battery temperature. A further factor influencing performance is that modern energy-storage applications require higher reliability than has been demanded in the past. These characteristics and requirements have resulted in marked improvements in VRLA batteries during the past decade. In addition, systems have been developed for monitoring and managing the batteries so as to achieve optimum duty in service.

Monitoring systems measure and display key battery parameters. The main objective is to detect cell or battery module failures at an early stage. The replacement of a cell or module can then be accomplished with a short system down-time as and when necessary. Monitoring systems normally measure cell/module voltages, current and temperature, and estimate cell/module state-of-charge (SoC) and/or state-of-health (SoH). Such systems have been used in UPS applications for many years.

Battery management systems (BMSs) are based on such monitoring systems. The information gained from the monitoring system is fed back to the battery system for the purpose of electrical management. Thus, for example, the electrical management takes account of the SoH of the battery. The target is not only to predict cell failures, but also to increase battery life. The principle of a typical BMS is shown in Fig. 8.1. For simplicity, only the charge control part is shown.

It is very important that the BMS be optimized for the particular type of battery that is being used. That is, the BMS should be matched to the battery. The combined battery plus BMS unit is then called a 'battery system'. Additionally, the BMS should also be matched to the application. For example, a BMS that is optimized for photovoltaic applications may not be suitable for UPS applications.

Optimized operation of a BMS is not only important for lead–acid batteries. It is even more important for advanced battery systems such as lithium batteries and high-temperature batteries. Indeed, successful operation of high-temperature

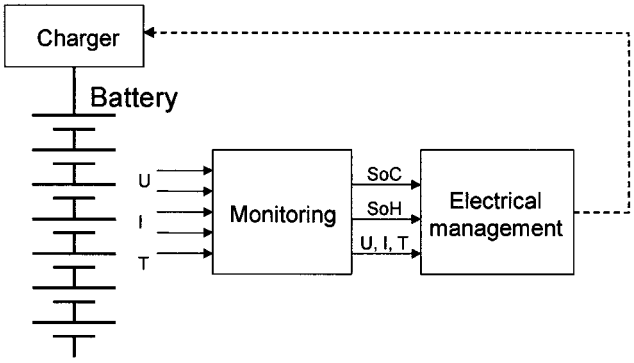

Fig. 8.1. Principle of BMS (only for charge process).

batteries is not possible without a BMS. Therefore, the development of BMSs for such batteries has a high priority and is normally carried out by the battery manufacturer. In the case of VRLA batteries, a BMS is still useful, but is not essential. Accordingly, most VRLA battery manufacturers have tended to devote only a low priority to BMS development. Nowadays, however, the rapid development of automobile electrical systems, for example the 42-V powernet, steering by wire and other advances, has increased the need for battery monitoring and management systems for lead–acid batteries to be developed both by battery manufacturers and by car manufacturers and their component suppliers.

Battery management systems are based on micro-controller systems. Therefore, it is possible to integrate additional, helpful features. For example, storage of historical data (data logging) and communication via the internet are possible.

8.2. Tasks of Battery Management Systems

Independent of the battery type and the application, the structure of the BMS is always broadly the same. The functions of a BMS can be split into the following tasks:

- data acquisition
- battery state determination
- electrical management
- thermal management (not always necessary)
- storage of historical data
- safety management
- communication.

The calculated control parameters are transmitted via an interface to the control units, such as the charger and the load. The task with the highest priority is safety management. Any critical failure must be detected by this task and substitute

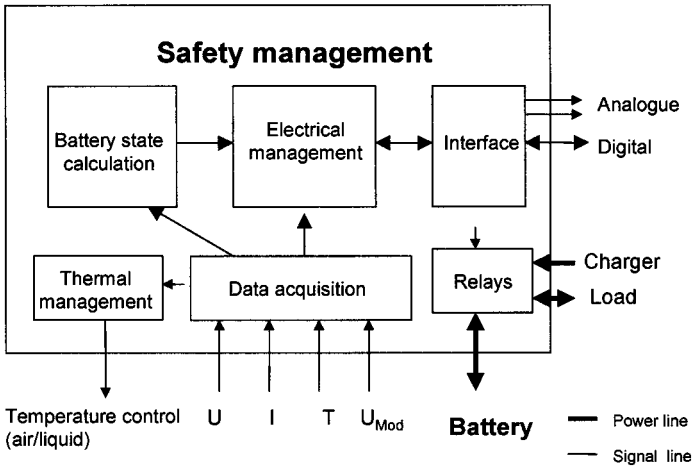

Fig. 8.2. Schematic of BMS.

functions used or, in a worst-case situation (e.g., short-circuit), the system shut down. A simplified block diagram of a BMS is shown in Fig. 8.2.

Depending on the application and the battery chemistry, the functions within the tasks are different. For small batteries, some of the listed functions are available as single- or multiple-chip solutions. For example, lithium-ion battery packs for cellular phones and laptop computers contain, as a minimum, a safety-management function. In the case of larger battery systems, the BMS is more complex and must be individually developed for the battery technology and the application.

8.3. Designs of Battery Management System

In general, there are two different architectures for BMSs namely, decentralized systems and centralized systems. These two architectures are illustrated for an electric vehicle (EV) application in Fig. 8.3 (decentralized) and Fig. 8.4 (centralized). In the decentralized system (Fig. 8.3), the individual BMS tasks are located in different devices. The charge control is part of the charger, the discharge control is part of the EV drive system, the battery state determination is carried out within a range meter, and so on. Some BMS tasks must be implemented in more than one device, especially in the case of safety management. Normally, there is little or no communication between the devices, so an optimized operation is not possible. Another disadvantage is that the battery-relevant control functions are located in different devices. Thus, each device must be adapted to the particular battery used.

A centralized BMS for the same EV application is presented in Fig. 8.4. All BMS tasks are located in the battery management unit, which is positioned close to the battery. The main advantages of this architecture are:

- unlimited communication between BMS tasks is possible
- safety management is facilitated

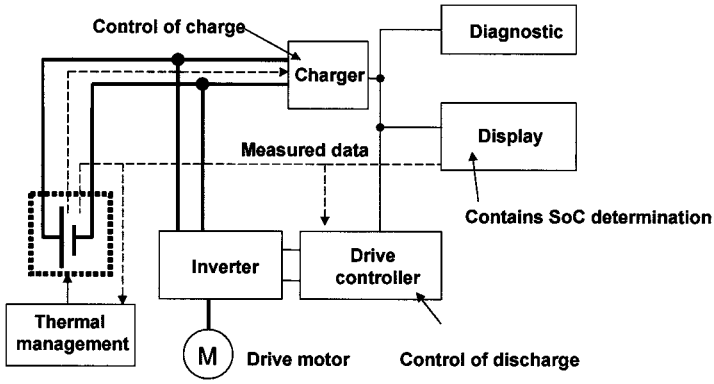

Fig. 8.3. Example of decentralized BMS (electric vehicle).

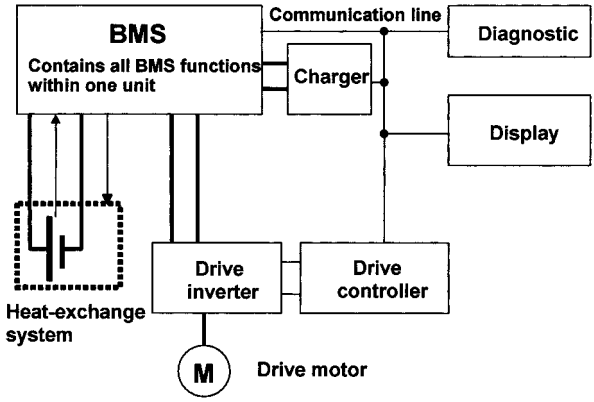

Fig. 8.4. Example of centralized BMS (electric vehicle).

- battery relevant functions are located in one unit; therefore, parameter adjustment and adaptation to different batteries is simplified
- a dumb charger is used; it is totally controlled by the BMS (which contains the charge algorithm).

For these reasons, more and more BMSs are of the centralized structure type.

8.4. Battery Data Acquisition

All the algorithms of the BMS use measured and calculated data as input information. Therefore, the accuracy, sampling rate, and the characterization of front-end filtering are very important and, again, these depend on the type of application. For example, the sampling rates for EV applications are much faster than one sample per second, whereas in the case of photovoltaic or UPS applications, sampling rates are less than 1 sample per second. Battery current(s),

voltages, and temperatures are used as input values. The use of special sensors to measure other physical values (e.g., acid rel. dens., pressure) is very expensive. A critical factor within most applications is the incidence of single cell/module failures, which leads to reduced performance or, in the worst case, to sudden drops in voltage. Therefore, measurements cell/module voltage are very important, but this does increase costs. Finally, there remains the question of how many cells can be grouped to one measurement channel. The literature suggests the optimum number is in the range of 1 to 10 cells.

The purpose of single-cell or single-module voltage measurements is a cell/module-based electrical management scheme (see Section 8.6) to avoid single-cell/module failure. The measurements can also be used to detect, or better to predict, cell/module failures (see Section 8.5).

Two different architectures for cell/module measurements are used, namely, centralized and decentralized architectures. In the centralized system (Fig. 8.5), the data acquisition unit is located within the BMS. The advantage of this technology is lower material cost. The main disadvantage is the necessity of replicated wiring between the BMS central unit and each battery cell (module). In the decentralized measurement system (Fig. 8.6), data acquisition is decentralized, i.e., one unit for each cell/module. These units communicate with the central BMS via a digital communication bus. The advantages of this configuration include reduced wiring, the possibility of expanding the system, and the ease of adding measurements of cell/module temperature. This additional information gives the possibility for a better, but also more complex, battery-state calculation. Decentralized systems become more economical in the case of larger batteries. Bus structures or ring structures are used for communication. The ring structures have the advantage that identification of the module position can be done automatically and the modules require no address. An example of a decentralized measurement system based on a ring structure is described in Ref. [1], and an example with a bus structure is described in Ref. [2]. At present, there is a move to integrate the decentralized measurement units into the battery and to decentralize management tasks, such as SoC and SoH determination.

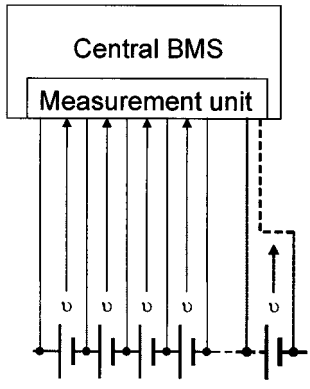

Fig. 8.5. Centralized data acquisition.

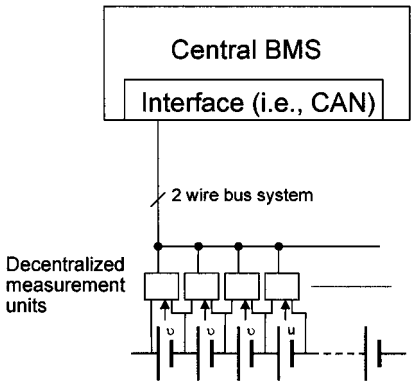

Fig. 8.6. Decentralized data acquisition.

Within the BMS, the measured values are used for state determination and for system control. Therefore, it is important that the measured values are correct, failures are detected, and substitute functions are available in case of measurement failures. Thus, the following processing should be carried out: (i) analogue filtering; (ii) digital filtering; (iii) broken wire checking; (iv) range check; (v) check of deviation (only for temperature measurement); (vi) comparison with other measured signals (e.g., average cell voltage with battery voltage); (vii) in case of a measurement failure: generation of a substitute value (e.g., room-temperature instead of battery temperature) and signaling the measurement failure. Functions (iii) to (vii) are often called plausibility checks. Such checks are most critical in the case of battery current and voltage. Even if there are no redundant measurements available, it is still possible to check the correlation between voltage and current for the detection of broken wires. Voltage measurements can be used to identify battery connector bolts that need to be tightened [3]. Indications of measurement failures are used within the electrical management system (to prompt use of substitute values) and are stored in an error register.

8.5. Determination of Battery State

Battery state is used as an input parameter for the electrical management system and, additionally, is an important parameter for the user. The battery state, which is described in terms of SoC and SoH, can be used to estimate both the bridging time (the period of time for which the battery will be able to provide power during an interruption of the normal power supply) and the expected life of the battery. In general, the SoC describes the actual available charge whereas the SoH describes the available charge of the fully charged battery. Both parameters are relative values, normalized to the full battery capacity, i.e.,

$$\mathrm{SoC} = \frac{\text{remaining capacity}}{\text{capacity of fully charged battery}} \tag{8.1}$$

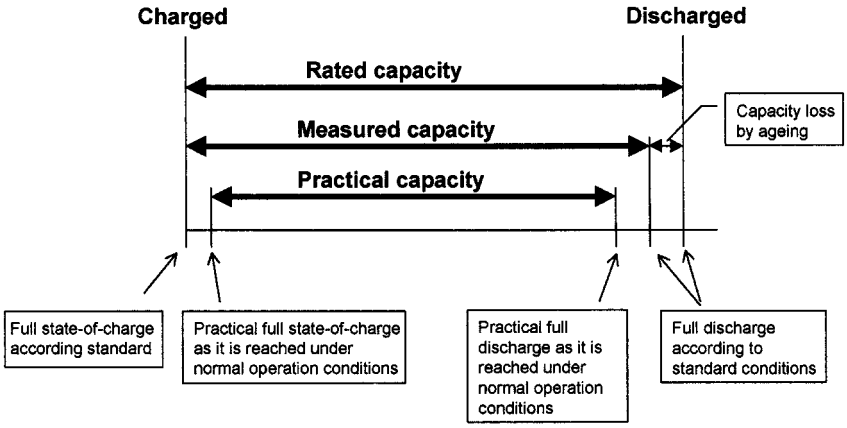

Fig. 8.7. Comparison of different definitions of battery capacity.

$$\mathrm{SoH} = \frac{\text{measured capacity}}{\text{rated capacity}} \tag{8.2}$$

One issue is how to define the capacity of a fully charged battery. It can be the rated capacity (given by the manufacturer), the measured capacity (which changes with age), or the practical capacity (battery capacity that is available during operation conditions). The differences between these capacities is illustrated in Fig. 8.7. Definitions of SoC, SoH, measured capacity, practical capacity etc. are given in Table 8.1. A detailed discussion of these terms has been presented by Sauer *et al.* [4].

8.5.1. Battery state-of-charge

The determination of SoC can be based on the measurement of internal parameters (electrolyte or active mass parameters) or external parameters (temperature, voltage, current). The possible measurement methods are shown in Fig. 8.8.

Internal battery parameters can only be measured by the use of special sensors [5], which leads to high costs. Most of the known methods are based on electrolyte measurements. According to the cell reaction of the lead–acid battery, the electrolyte is not only necessary for the ionic transport but is also necessary for the charge and discharge reactions. The SO_4^{2-} ions of the electrolyte take part in the reactions. This results in a linear relation between the SoC and the ionic concentration of the electrolyte. Other electrolyte parameters vary approximately linearly with concentration. The relationship between acid rel. dens. and these other parameters is given in Table 8.2.

For SoC measurements, it is possible to measure a representative electrolyte parameter e.g., measurement of buoyant force, refractive index, concentration, acid rel. dens. measurement by hydrostatic pressure, conductance, dielectric

Table 8.1. Definitions for capacity, SoC, full state-of-charge, and SoH [4].

Parameter	Symbol	Definition	Unit	Range
Rated capacity or nominal capacity	C_N	The rated or nominal capacity is the value for the capacity given by the manufacturer at nominal operating conditions (defined by temperature, current, and end-of-discharge voltage). As a standard, the 10 h capacity ($N = 10$) should be used. A transformation between any temperature between 10 and 30°C and the nominal temperature is possible with the given equation. If the manufacturer only specifies values for the 100-h, 20-h, or 5-h capacity, then a rough approximation of the C_N capacity can be gained from the rules-of-thumb: $C_N = C_{100h}/1.2$; $C_N = C_{20h}/1.1$; $C_N = C_{5h}/0.9$ $C_N = \frac{C_T}{1 + z \cdot (T - 20°C)}$ with $z = 0.006\,K^{-1}$	Ah	> 0
Initial capacity	C_0	The initial capacity is the capacity available at a capacity test with I_{10} down to 1.8 V/cell (according to DIN 43539) starting at state-of- charge FULL (DIN 43539) after taking the battery into operation according to the manufacturers recommendations.	Ah	>0
Measured capacity	C_m	The measured capacity is the capacity available at a capacity test with I_{10} down to 1.8 V/cell (according to DIN 43539) starting at state-of- charge FULL at any time after taking the battery into operation.	Ah	>0
Practical capacity	C_p	The practical capacity is the capacity between the practical state-of-charge $FULL_p$ and the end-of- discharge threshold defined in the system.	Ah	>0
Remaining capacity	Q_r	The remaining capacity is the amount of charge available at a certain time without any previous charging with an I_{10} discharge down to 1.8 V/cell.	Ah	>0
Charge balance	Q_b	Net discharged charge from a battery since the last state-of-charge FULL $Q_b = \int_t I_{MR} \cdot dt$, $I_{MR} \equiv$ main reaction current	Ah	> 0

continued

Table 8.1. Continued.

Parameter	Symbol	Definition	Unit	Range
Depth-of-discharge	DoD	The depth of discharge is the ratio of the charge balance and the rated capacity. The depth of discharge is 0 when reaching the full state-of- charge and 1 after a net discharge of the rated capacity. $\mathrm{DoD} = \frac{Q_\mathrm{b}}{C_N}$	–	0 to >1 or 0 to >100%
State-of-charge	SoC	The state-of-charge is the ratio between the difference of the rated capacity and the charge balance on the one hand and the rated capacity on the other hand. State-of-charge is 1 when state-of-charge FULL is reached and 0 after a net discharge of the rated capacity. $\mathrm{SoC} = 1 - \mathrm{DoD} = \frac{C_N - Q_\mathrm{b}}{C_N}$	–	1 to <0 or 100 to < 0%
Relative state-of-charge	$\mathrm{SoC_r}$	The relative state-of-charge is the ratio between the difference of the measured capacity and the charge balance on the one hand and the measured capacity on the other hand. The relative state-of-charge is 1 when state-of-charge FULL is reached and 0 after a net discharge of the measured capacity $\mathrm{SoC_r} = \frac{C_\mathrm{m} - Q_\mathrm{b}}{C_\mathrm{m}}$	–	1 to 0 or 100 to 0%
Practical state-of-charge	$\mathrm{SoC_p}$	The practical state-of-charge is the ratio between the difference of the practical capacity and the charge balance on the one hand and the practical capacity on the other hand. The practical state-of-charge is 1 when the practical state-of-charge FULL is reached and 0 after a net discharge of the practical capacity $\mathrm{SoC_o} = \frac{C_\mathrm{p} - Q_\mathrm{b}}{C_\mathrm{p}}$	–	1 to 0 or 100 to 0%

continued

Table 8.1. Continued.

Parameter	Symbol	Definition	Unit	Range
Dynamic relative state-of-charge	SoC_{rd}	only of relevance at currents > I_{10}, dynamic correction of the measured capacity with the available battery current and the battery temperature $SoC_{rd} = \frac{C_m \cdot F - Q_b}{C_m \cdot F}$; $F = f(T, I_{battery})$	–	1 to <0 or 100 to < 0 % F ∈ [0, 1]
Dynamic practical state-of-charge	SoC_{pd}	only of relevance at currents > I_{10}, dynamic correction of the practical capacity with the available battery current and the battery temperature $SoC_{pd} = \frac{C_p \cdot F - Q_b}{C_p \cdot F}$; $F = f(T, I_{battery})$	–	1 to <0 or 100 to <0% F ∈ [0, 1]
Full state-of-charge	FULL	Full state-of-charge is reached (according to DIN 43539), if the battery current is not changing within 2-h at a constant charge voltage and constant temperature.		
Practical full state-of-charge	$FULL_p$	The practical full state-of-charge is the state-of-charge, which can be reached in a system under normal operating conditions (depending on the charge voltage, the maximum charge current and the short-time history of the battery).		
Open-circuit voltage	OCV	The open-circuit voltage is the voltage measured at a battery at open-circuit ($I_{batt} = 0$) while the voltage changes less than 0.5 mV/cell within 2 h.	V	2.2–1.9
Approximate open-circuit voltage	OCV_x	The approximate open-circuit voltage is the voltage of a battery at open-circuit ($I_{batt} = 0$) while the voltage changes less than x mV/cell/h. The approximate open-circuit voltage with x = 0.25 mV/cell/h is equivalent to the open-circuit voltage ($OCV_{0.25}$ = OCV).	V	2.2–1.9
State-of-health	SoH	The state-of-health is the ratio between the measured capacity and the rated capacity. State of health is 1, when the measured capacity equals the rated capacity. A state-of-health greater than 1 means more measured capacity than promised by the rated capacity. As per definition, a battery is at its end of lifetime at a state-of-health of 0.8. $SoH = \frac{C_m}{C_N}$		>1 to 0

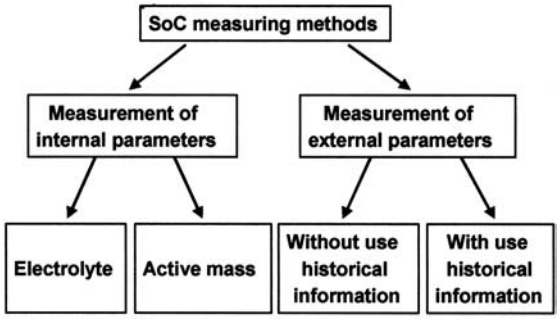

Fig. 8.8. Methods of SoC measurement.

Table 8.2. Electrolyte parameters for dilute sulfuric acid (room temperature).

Wt.%	Relative density	Concentration (g l^{-1})	Concentration (mol l^{-1})	Refractive index	Relative viscosity
8.0	1.0541	84.2	0.858	1.3427	1.180
10.0	1.0068	106.6	1.087	1.3451	1.228
12.0	1.0821	129.6	1.322	1.3475	1.279
14.0	1.0966	153.3	1.563	1.3500	1.334
16.0	1.1114	177.5	1.810	1.3525	1.396
18.0	1.1265	202.4	2.064	1.3551	1.467
20.0	1.1418	228.0	2.324	1.3576	1.543
22.0	1.1575	254.2	2.592	1.3602	1.621
24.0	1.1735	281.1	2.866	1.3628	1.703
26.0	1.1893	308.7	3.147	1.3653	1.793
28.0	1.2052	336.9	3.435	1.3677	1.890
30.0	1.2213	365.7	3.729	1.3701	1.997
32.0	1.2353	395.3	4.030	1.3725	2.118
34.0	1.2518	425.6	4.339	1.3749	2.250
36.0	1.2685	456.7	4.656	1.3773	2.387
38.0	1.2855	488.5	4.981	1.3797	2.528
40.0	1.3028	521.1	5.313	1.3821	2.685

characteristic, ultrasonic properties, and measurement by additional electrodes. Additional information about these several methods is given in Table 8.3.

SoC determinations by measurement of external parameters can be grouped into short-term and long-term measurements. The latter take historical factors into account.

Short-term measurements are based on the relation between current and voltage. It is possible to observe the system and wait for a defined event (e.g., open-circuit operation, starting of an engine, etc.), or it is possible to inject a defined current and measure the voltage response. Most methods are based on an electric circuit that consists of a voltage source, an over-voltage network, and a side-reaction current (Fig. 8.9).

Table 8.3. Electrolyte measurements for SoC determination.

Method	Accuracy	Type of measurement	Measurement influenced by	Usable for VRLA	Cost
Buoyant force (depth of dip)	C	Local, at the top electrolyte	• gassing • acceleration forces • inclination • acid level • acid stratification	No	High
Buoyant force (compensation of forces)	B	Local, at the top electrolyte	• gassing • acceleration forces • inclination • friction of mechanism • acid stratification	No	High
Refractive index (prism)	A	Local, at the top electrolyte	• gassing • dirt • acid stratification	Possible	Medium
Refractive index (fibre optic)	B	Local, at the top electrolyte	• Gassing • dirt • acid stratification	Possible	Medium
Hydrostatic pressure	A	Average	• acceleration forces • inclination	No	Medium
Concentration measurement (Ion exchange membrane)	B	Average value over sensor length	• friction of mechanism • ageing of membrane	Possible	High
Additional electrodes: Open-circuit measurement	C	Local	• ageing of electrode • gassing • acid stratification	Possible	Medium
Additional electrodes: principle of intercalation	C	Local	• ageing of electrodes • acid stratification	Possible	Medium
Dielectric measurement	D	Local	• gassing • acid stratification	Possible	Medium
Conductance of electrolyte	D	Local	• gassing • acid stratification • temperature	Possible	Medium
Viscosity	D	Local	• gassing • acceleration forces • friction of mechanism • temperature	No	High

A very accurate.
B accurate.
C approximate.
D inaccurate.

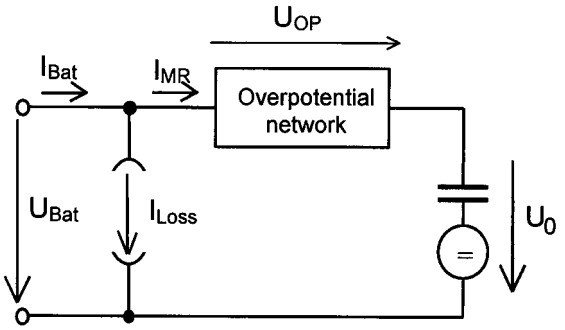

Fig. 8.9. Electric circuit for open-circuit voltage measurement.

The open-circuit voltage (OCV, approximately U_0) is in good correlation with the acid rel. dens. and can be used directly for SoC determination:

$$\mathrm{SoC} = 1 - \frac{a - U_0}{a - b} \tag{8.3}$$

where a is open-circuit voltage at full SoC and b is open-circuit voltage at fully discharged state. Using Table 8.1, it is possible to calibrate this equation for several SoC definitions. The main disadvantage of direct OCV measurement is the dynamic behaviour, which is caused by overvoltages. Rest periods of five or more hours are necessary to get the true OCV value [6]. Improved methods predict the OCV by extrapolation of the voltage curve [7,8], which yields good results after 5–10 min.

The overpotential network of Fig. 8.9 can be simplified by exploiting the internal d.c. resistance of the battery, and the side-reaction current, I_{Loss}, can be neglected when discharging at a SoC below 90%. The differential internal resistance, $R_{i_{\mathrm{diff}}}$, can then be computed by inserting a current step ($I_1 \rightarrow I_2$) and measuring the voltage response ($U_1 \rightarrow U_2$):

$$R_{i_{\mathrm{diff}}} = \frac{U_2 - U_1}{I_2 - I_1} = \frac{\Delta U}{\Delta I} \tag{8.4}$$

It must be taken into account that differential internal resistance varies with temperature and current [9]. Therefore, the measurement must be carried out under defined conditions. The differential resistance of a VRLA, gel-type traction battery vs. SoC is given in Fig. 8.10. The data show that the differential resistance increases with decreasing SoC, and increases more strongly when the SoC is below 20%. At a high SoC, the statistical uncertainty is greater than the change in the differential resistance with SoC. Thus, the measurement is of limited value under these conditions.

Measurement of the d.c. resistance can, however, be used to detect a low SoC. Finally, it should be noted that the d.c. resistance increases with battery age.

Although this feature complicates SoC measurements, it does lead to the possibility of using d.c. resistance values in SoH determination.

It is also possible to measure the complex impedance or complex admittance of an overpotential network. Instead of measuring the whole complex impedance (or admittance) curve, it is usually sufficient to measure only one or two values at given frequencies. The frequencies used are in the range 50–10,000 Hz, most often 1000 Hz. The admittance of a gel VRLA battery during discharge at the 10-h rate is shown in Fig. 8.11 [8]; note that, frequency and SoC are parameters. Instead of

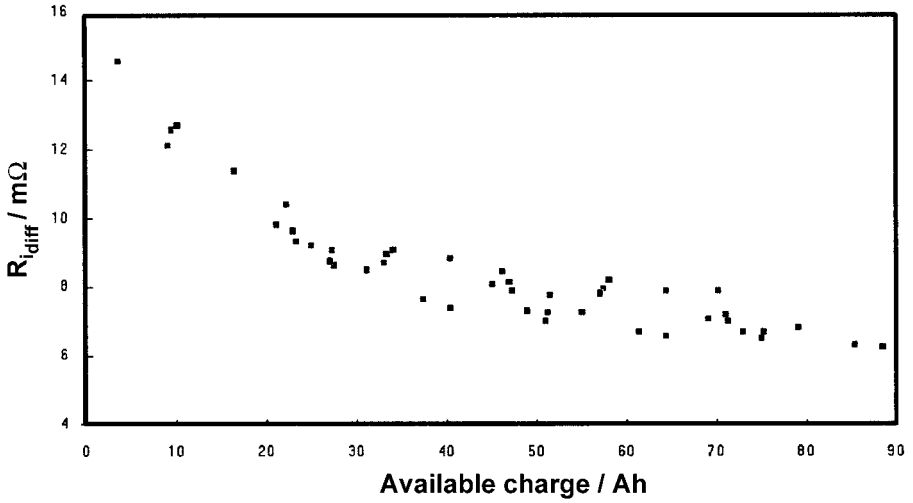

Fig. 8.10. Differential d.c. resistance as function of SoC.

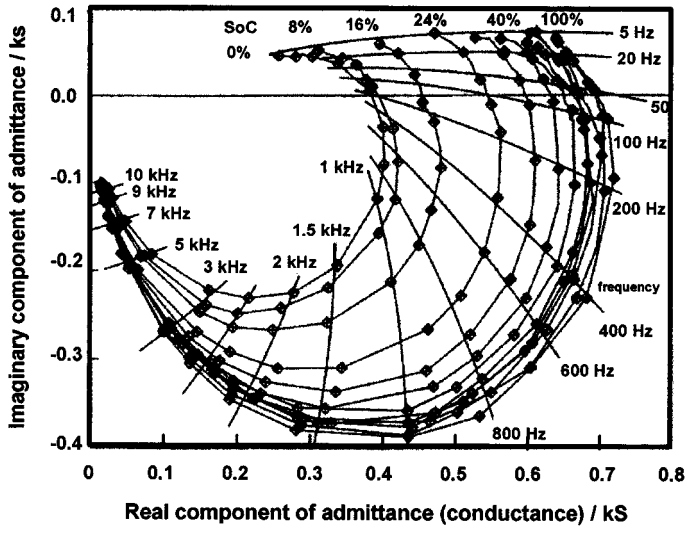

Fig. 8.11. Admittance of VRLA battery as a function of SoC and frequency.

admittance, its real part, conductance, is often determined. It can be seen that, over a wide range of frequency, the value of the complex impedance is sensitive to SoC from 0% to around 50% SoC. At high SoCs, the complex impedance is much less sensitive to SoC.

On the other hand, the impedance changes with the battery age and this can be used as an SoH indicator. According to Feder *et al.* [10], conductance is in good correlation with available capacity. Therefore, if the SoC is known by another method, the conductance can be used for SoH determination.

There exist different methods for impedance measurement. Normally, a sine-wave current is injected and the voltage response is measured. In some special applications, it is possible to use an existing current ripple instead of the sine-wave current source. For example, the a.c. ripple from an alternator that is a part of the system can, perhaps, be used [11].

The actual battery state is mainly influenced by the historical operation of the battery. Therefore, methods for SoC determination should ideally take into account the history of the battery. Such (long-term) methods include simple charge balance and more complex adaptive methods.

Charge balance, or Ah counting, is a simple and often used method for SoC determination. With reference to Fig. 8.9, the charge balance (Q_b) is approximately the integral of the main reaction current (I_{MR}):

$$Q_b = \int_t I_{MR} \cdot dt, \quad I_{MR} \equiv \text{main reaction current} \tag{8.5}$$

$$Q_b = Q_{b,0} + \int_0^t I_{MR} \cdot d\tau \tag{8.6}$$

where ($Q_{b,0}$) is the initial value of the charge balance.

The main reaction current is the battery current minus the loss current (I_{Loss}). The loss current must be calculated. A simple empirical method is the use of a charge factor:

$$I_{Loss} = I_{Bat} * (CF - 1) \quad \text{for charge} \tag{8.7}$$

$$I_{Loss} = 0 \qquad \text{for discharge} \tag{8.8}$$

where CF is the charge factor (1.0–1.2).

An improvement is possible if a constant self-discharge rate is taken into account. In the case of varying operation conditions (temperature, SoC, current), this simple approach will not fit the real loss current. Jossen *et al.* [12] describe a method based on Tafel and Arrhenius characteristics. This takes into account changes in the efficiency of the oxygen cycle. The model is calibrated at the full SoC. A more complex model for loss calculation is described in Ref. [13].

The main problems with Ah counting are:

- drift of the SoC, by reason of integration of errors:
  – measurement offset
  – error in estimation of the self-discharge rate
- high accuracy measurement of current is necessary
- for installation, the actual SoC must be known to calibrate the algorithm; it is therefore necessary to charge the battery to a full SoC
- several different mechanisms of loss must be taken into account, especially for VRLA designs
- battery ageing must be accommodated because of changes in the overcharge characteristic and in battery capacity.

The following improvements have been made:

- recalibration of charge balance by
  – full SoC detection [12]
  – open-circuit voltage [14]
  – battery models [15]
  – other recalibration methods
- change in the self-discharge rate must be determined by adaptive methods.

A simple Ah counter with recalibration is shown in Fig. 8.12. The Ah counter is reset to the battery capacity when the full SoC is detected, and it is set to zero when a fully discharged state is detected. Additionally, the Ah counter can be used to measure battery capacity.

A disadvantage of the charge-balance method described is that the equation for loss calculation varies with battery type and age. Therefore, it is difficult to determine the exact parameters. As a result, normally standard parameters are often used, which can lead to an increased calculation error and a drift of the SoC meter.

The manual setting of parameters and the ageing of model parameters are the main disadvantages of the methods described above. One solution is the self-learning

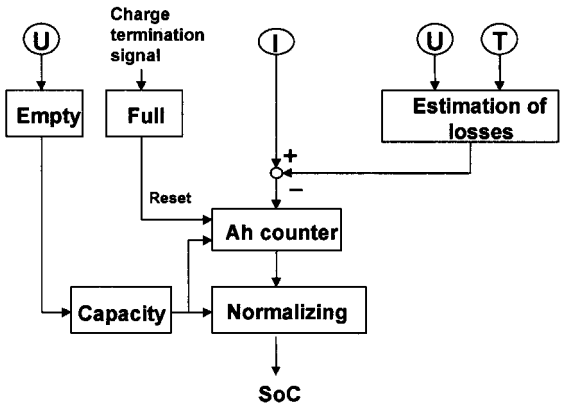

Fig. 8.12. Principle of a SoC meter based on Ah counting.

adaptive system. As an example, the estimation of losses of the Ah-counter of Fig. 8.12 can be improved if the difference between the Ah-counter and the reset capacity is used to adapt the parameters of the equation.

Other adaptive systems are based on a comparison of the battery voltage with the calculated voltage of a battery model. The differences are used to adapt the parameters of the battery model. The parameters and state values of the model are used for SoC and SoH calculations. The principle of such a system is illustrated in Fig. 8.13.

Other methods for parameter adaptation are known. The use of a Kalman filter is the most popular one. The basis of such a filter is the battery model shown in Fig. 8.14. The Kalman filter takes the statistical knowledge of the parameter and the measurement into account. Applications are described in Refs. [16] and [17].

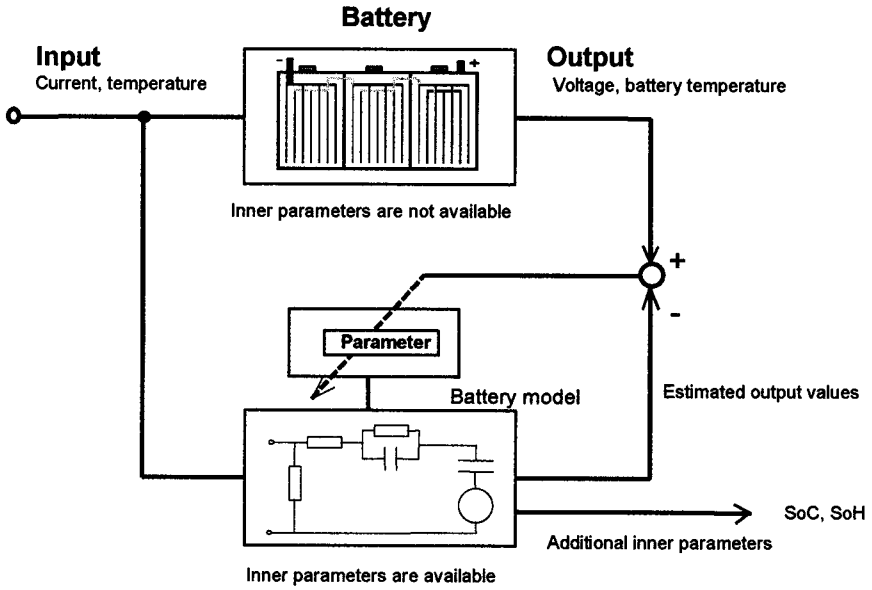

Fig. 8.13. Adaptive method for battery state determination.

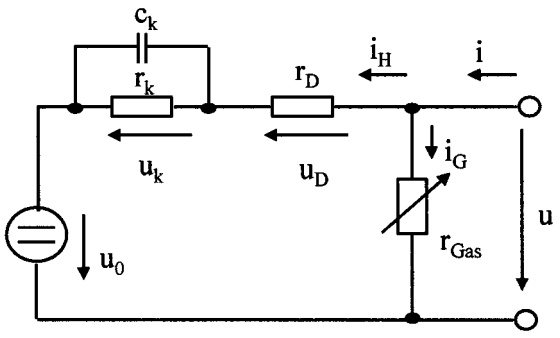

Fig. 8.14. Battery model used within a Kalman filter.

The main advantage of this method, as compared with Ah-counting, is its drift-free operation. Measurement errors lead to a calculation error. After some operation time, however, the calculated SoC goes back to the actual value (see Fig. 8.15).

There are many other known methods for SoC determination. Piller [16] describes an artificial neural network (ANN) and a simple linear equation method. The structure of the ANN is given in Fig. 8.16. For training the ANN, measured values of temperature, voltage, current and a SoC value (calculated with a reference method) are necessary.

Instead of the ANN, it is possible to use a simple linear equation:

$$\Delta Q(i) = \alpha_0 + \alpha_1 \cdot U(i) + \alpha_2 \cdot U(i-1) + \alpha_3 \cdot I(i) + \alpha_4 \cdot I(i-1) + \alpha_5 \cdot Q(i-1) \tag{8.9}$$

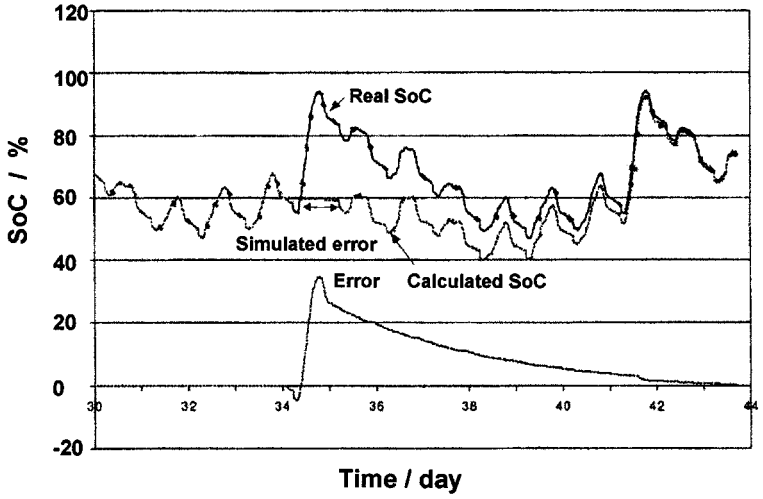

Fig. 8.15. Error of SoC calculation with Kalman filter after a forced measurement error. (Measured current was set to zero for 20 h.)

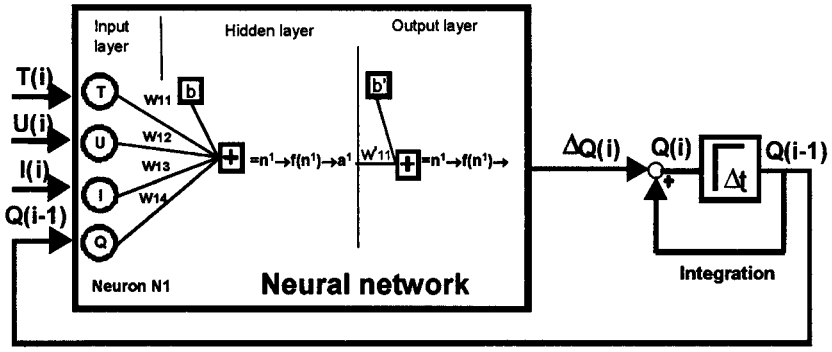

Fig. 8.16. Structure of a feed-back artificial neural network: I(i) = current; Q(i) = SoC; U(i) = voltage; ΔQ(i) = change of SoC; α = parameter.

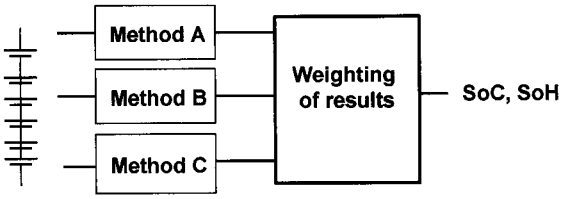

Fig. 8.17. SoC determination by different methods.

Parameter determination is accomplished by laboratory measurements or by a least-mean-squares method if reference data are available. With such methods, it is possible to use a current measurement with a low accuracy. This can reduce costs for a SoC measurement capability. Singh *et al.* [18] and Heinemann [19] describe SoC determination methods based on fuzzy logic. This approach relies on the use of expert knowledge in lieu of complex mathematical models. It is also possible to combine a fuzzy SoC algorithm with other methods to increase the accuracy.

Kozlowski *et al.* [20] have described a method where three different SoC calculation methods are used, and these results are compared and weighted to combine the advantages of the three methods. The principle is illustrated in Fig. 8.17.

Statistical analysis is often used to determine differences between battery cells. If no charge-equalizing equipment is installed, the current through each cell is equal. Therefore, the cell/block voltages can be compared to estimate differences between cells. It is known that the voltage is not a direct indication of the battery state. Voltage can be used for relative analyses, however, and can show the changes of one cell in comparison with others.

8.5.2. Battery state-of-health

The SoH is defined as the quotient of the measured capacity and the rated capacity. The measured capacity is the capacity of a fully charged battery at standard discharge conditions. In some applications (e.g., automotive), the high-power capability is of interest. Therefore, other definitions for SoH are also possible.

SoC and SoH are not independent. Both reflect the battery performance in a similar way. For example, both parameters provide an indication of high-power capability. The relation between the two parameters, however, is not linear and depends on the ageing mechanism. A simplified relationship between SoH and SoC is illustrated in Fig. 8.18.

In general, SoC describes the short-term changes of battery parameters whereas SoH describes the long-term changes. SoH determination does not need to be carried out continuously. Periodic measurements (e.g., once a week) are adequate for most applications. The period of measurement depends on the application. Extrapolation of SoH measurements allows a prediction of battery life. Sudden battery failures, however, also occur, e.g., cracking of a faulty weld. Failures such as these are very difficult to predict. To determine the SoH, it is necessary to know the actual SoC or to measure the SoH, always at the same SoC (i.e., full SoC).

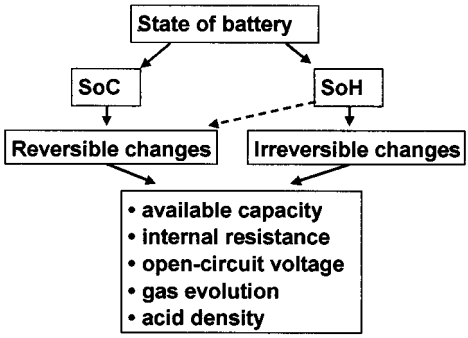

Fig. 8.18. Relationship between SoC and SoH.

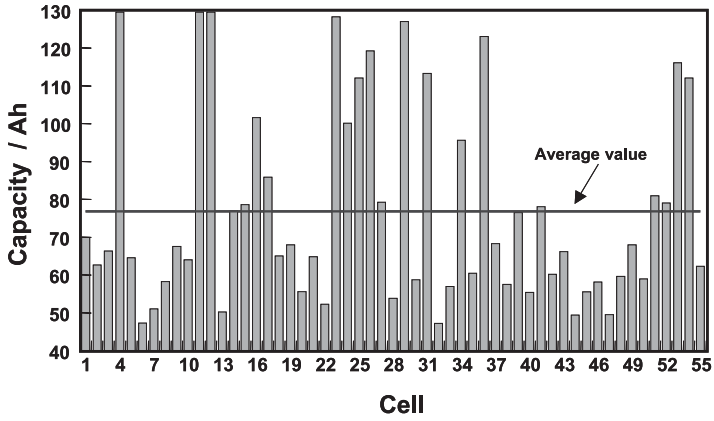

Fig. 8.19. Capacity test of 100-Ah VRLA battery (gel type) after five years of photovoltaic operation.

It is well known that the cells of a battery age individually. This characteristic stems from manufacturing tolerances and different operating conditions (e.g., different cell temperatures). The single-cell characteristic within a large battery cannot be detected by monitoring the battery voltage, but cell/block voltage measurement is necessary in order to get information about individual cells/blocks and to predict failures at an early stage.

The results of a capacity test on a 55-cell, VRLA gel-type battery after five years of operation are given in Fig. 8.19. It can be seen that the cell capacities are very different and that no systematic pattern develops during ageing.

The determination of SoH can be achieved by discharging a fully charged battery until the end-of-discharge voltage is reached. This method is consistent with the definition of SoH and, therefore, the exact value of SoH can be computed. In most applications, however, it is not possible to carry out discharge tests, due to limitations of the power equipment or the lack of access to the battery. In the case of

a multi-string battery architecture within UPS systems, each string is discharged separately while the other strings are still in UPS operation. Lohner [21] describes another method for UPS batteries, in which ageing is determined by a partial discharge test between 100% and 90% DoD, and Pascoe and Anbuky [22] describes a method that exploits an analysis of the Coup de Fouet region for estimating the battery capacity.

The simplest method for SoH estimation is to count the throughput of charge and to compare it with a defined value. Improvements are possible if this method is corrected for depth-of-discharge (DoD) per cycle, temperature, ageing by time, and ageing by abuse conditions (over-discharge, over-charge). Ter Horst *et al.* [23] describe three methods:

$$N \cdot q_{\text{cyc}} = \text{constant} \tag{8.10}$$

$$N \cdot \ln\left(1 - \frac{q_{\text{cyc}}}{q_{\max}}\right) = \text{constant} \tag{8.11}$$

$$\frac{N}{1 - q_{\text{cyc}}/q_{\max}} = \text{constant} \tag{8.12}$$

where N is the number of cycles; q_{cyc} is the DoD; $q_{\max}$ is the parameter.

Other equations take the discharge current and the temperature into account [24]. The main disadvantage of these models is that there is no feed-back between the battery and the calculated state. Therefore, such models can be used for life estimation within the planning phase, but not for online state estimation.

A method based on the detection of end-of-discharge involves the measurement of the practical capacity of a battery by observing the Ah difference between a full SoC and a fully discharged state of the battery during normal operation. This method is simple to implement if an Ah counter is available. The time between the full SoC and the discharged state should not be too high (i.e., less than 1 week). This method is only practical if the two reference points are reached within the application.

The internal resistance of a battery increases with battery age due to corrosion, sulfation, water loss, and loss of conductivity between grid and active mass. Therefore, the d.c. resistance or the complex admittance are good indicators of battery age. As described previously, battery resistance is also influenced by the SoC and the temperature.

Lohner [21] describes a cell/block-based method for estimating SoH in UPS applications. This method includes the resistance of the wiring. The system measures the resistances of the new battery blocks and compares these reference values with measured resistance during life. The measurements are carried out at a 95% SoC. The SoH determination is based on the change in the resistance. Feder [25] has discussed the measurement of conductance. This value is in good correlation with the measured capacity. If the SoC is known, it is possible to calculate the SoH.

Impedance-based measurements are often used for UPS batteries. Measurements are carried out at full SoC and the results of all cells/blocks are compared.

Spaeth *et al.* [26] have developed a method for SoH determination that is based on fuzzy clustering [27]. This method separates the life of a battery into three phases, namely, new, working, and capacity-drop phases. The sum of the populations of all the phases is constant. An algorithm is used to quantify the phases by analysing existing reference data. A periodically measurable event is used for the reference data, e.g., the current drop during a constant-voltage charge. The reference data must be available for the entire battery lifetime. Results obtained using this method for three identical batteries operated under different conditions for three years are presented in Fig. 8.20.

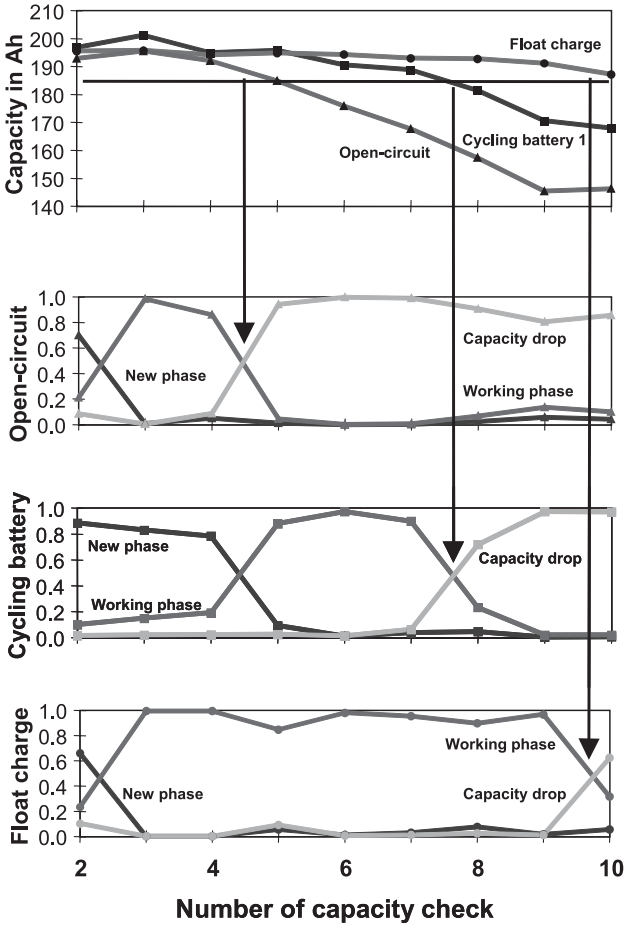

Fig. 8.20. Capacity and fuzzy classification of cycling, floating and self-discharge performance of lead–acid batteries operated for three years.

8.6. Electrical Management of Batteries

With electrical management of the battery, the input parameters of current, voltage, temperature, SoC, and SoH are used to control the charge and discharge processes. The following tasks must be fulfilled:

- control of the charge process:
  - standard charging
  - equalization charging (e.g., via a charge-equalization circuit)
  - float charge
  - auxiliary charge (e.g., charging by diesel within a photovoltaic hybrid system)
  - recuperation charge (e.g., electric vehicle)

  control of discharge:

  - deep-discharge protection
  - current/power limitation
  - avoid other critical operation parameters

The charge control process and the discharge limitation depend strongly on the particular battery technology and type. For UPS systems, the recharging of the battery must be adapted to the depth of the previous discharge, the temperature, and (optionally) the battery age. Quick recharge and lowest possible ageing rate are the main targets. The control of float charge is very important.

8.6.1. Control of charge

The targets of charging are: (i) charge as fast as is practical; (ii) avoid ageing; (iii) periodic equalization of cells. Charge methods are described in Chapter 9 and are not discussed here.

8.6.2. Control of discharge

The BMS features necessary for discharge operation depend strongly on the application. The main task is to avoid overload and deep discharge. Either of these factors will reduce the life of the battery. In some applications (e.g., automotive), it is important to guarantee a special performance (e.g., starting). Therefore, discharging below a critical state must be avoided.

Deep-discharge protection is provided in order to avoid life-reduction by over-discharge of the cells. Over-discharge, especially to the point of causing some reverse charge, must be avoided [28].

In most state-of-the-art systems, deep-discharge protection is controlled by voltage. The relation between end-of-discharge voltage, discharge current, and depth of discharge is shown in Fig. 8.21. It can be seen that the voltage is not a good parameter for protecting the battery against deep discharge, especially if the currents are small ($< I_{10}$) or the current is not constant. An improvement can be

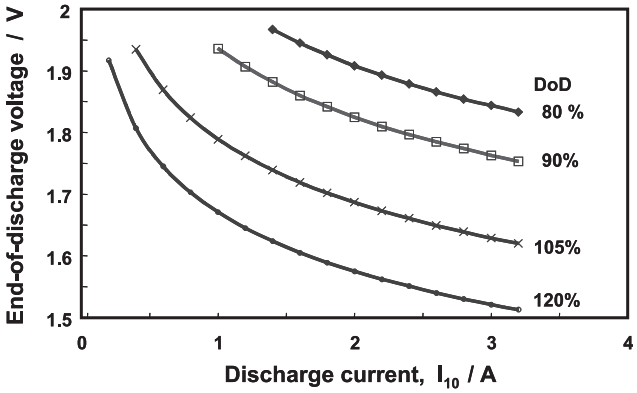

Fig. 8.21. Battery voltage as function of discharge current for various depths-of-discharge.

achieved if the voltage threshold value is corrected or compensated for different current values:

$$U_{\mathrm{D,off}} = U_{\mathrm{D,off,o}} - I * R \tag{8.13}$$

where I is the discharge current; $U_{\mathrm{D,off,0}}$ is the turn-off voltage for $I = 0$. This equation can be used for discharge currents above I_{10} and a current dynamic ($I_{\max}/I_{\min}$) of up to 3. For smaller currents or for high dynamic operation, a quadratic equation or two or more linear equations are necessary. It is not possible, however, to limit the DoD to values below 90% at currents below I_{10} by use of the voltage and current, because the cut-off voltage is very close to the open-circuit value.

If there is no charge-equalizing circuit that operates during discharge [29], the cell/block voltages must be monitored and the discharge must be terminated if the worst-case cell voltage reaches the cut-off value.

In high-power applications, e.g., hybrid electric vehicles (HEVs), UPS, over-load by current and by temperature must be avoided. A significant difference between applications is whether it is practical to limit the discharge current (e.g., HEV applications) or not practical to limit the discharge current (e.g., UPS applications). If it is not practical to limit the discharge current, it may be reasonable to implement a priority-controlled load system (see below).

An approach to limiting the discharge current to a HEV as a function of SoC, temperature, and voltage is presented in Fig. 8.22. Such methods use knowledge about the internal resistance as a function of the SoC and the temperature. The target is to avoid low battery voltages during operation. Improved methods allow the prediction of the maximum current (or power) for a given load period. This is vital information that enables constant power to be guaranteed during acceleration of an EV.

If loads within a utility system have different power requirements, it may be reasonable to protect critical loads by implementing a load prioritization scheme.

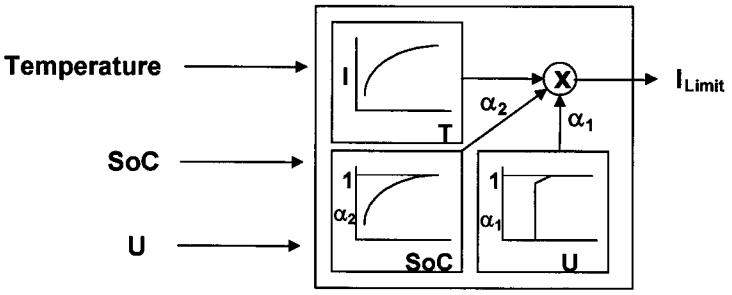

Fig. 8.22. Function for current limitation in electric vehicles.

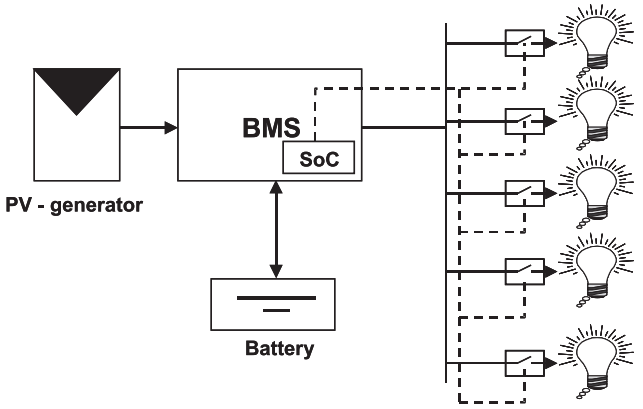

Fig. 8.23. Example of priority-controlled, deep-discharge, protection system.

For example, within a PV system, a medical refrigerator is likely more important than a television set. Consequently, during periods of low solar insolation, turning off the television could protect the refrigerator.

Individual loads can be prioritized and controlled remotely or, alternatively, a distribution grid with lines of different priority can be used. A simple method would be to base the turn-off and turn-on of the load on battery SoC values. Such a system is shown in Fig. 8.23. An advantage of the grid-control option is that the control switches are then centralized.

8.6.3. Multiple battery systems

Systems with two or more independent batteries may be used for any or all of the following reasons: (i) they combine the advantages of different battery systems; (ii) they provide increased redundancy; (iii) they provide the possibility of improved control and measurement methods; examples of such methods would be: discharge tests with UPS systems or the ability to charge batteries in photovoltaic systems fully.

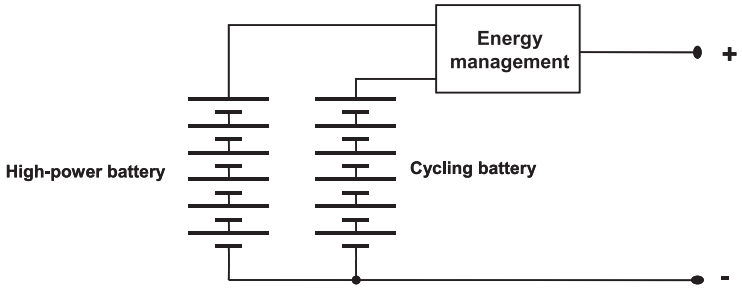

Fig. 8.24. Two-battery system for automotive applications from Gemini TwinPower.

The use of two or more different battery technologies can exploit the advantages of each. It is also possible to combine batteries of the same chemistry but with different designs. For example, one battery is optimized for high power and a second battery (energy) is optimized for cycle-life. Such a system for automotive applications is shown in Fig. 8.24. The battery-management system would preferentially discharge the cycling battery and preferentially charge the power battery. Discharging of the power battery is only done for starting the engine, and the operational strategy ensures that this battery is always at a very high SoC.

It is also possible to combine storage systems of different technologies. The targets are the same as those mentioned above. One idea is to combine a lead–acid battery with a double-layer capacitor (DLC). Within HEVs, DLCs can be used for storing the recuperation energy whereas a lead–acid battery is used for energy storage and low power loads.

Applications with special safety requirements demand highly reliable energy storage. Such applications are UPS and x-by-wire systems. If one battery bank fails, system operation can continue for a limited time with the remaining batteries.

If there are two or more independent batteries within a system, it is possible to control charge and discharge currents separately. If one battery is not available because it is under a diagnostic or maintenance procedure, limited system operation is still possible. Such diagnostic and maintenance procedures can be:

– discharge test (e.g., UPS)
– open-circuit voltage measurement
– full charge and equalization charge in photovoltaic systems
– other procedures, e.g., resistance measurements.

A special type of two-battery system is the 42-V/14-V automotive network. This system has two separate networks; one with 42-V and one with 14-V charge requirements, and each network is buffered with a battery. The 42-V battery is necessary to meet the requirements of the high power loads, and the 14-V battery is used for operating the other loads. The electrical management of a multiple battery system is more complex and the investment costs of the whole system are higher than for a single battery system.

8.7. Thermal Management of Batteries

From the literature, it is known that temperature affects the performance of a battery in multiple ways. With decreasing temperature, battery capacity is reduced and cycle-life is increased. Charge-acceptance is reduced at decreasing temperature, especially if the temperature is below 0°C [30]. Temperature gradients between cells in a battery reduce capacity and lifetime [31]. Peak power increases with increasing temperature [32]. Therefore, control of battery temperature (thermal management) is an important task for a battery management system.

A thermal-management system is helpful for:

- high power applications (e.g., HEVs), where the battery is heated by internal processes;
- applications where cell temperatures differ due to local heat sources or sinks (e.g., UPS systems where batteries and rectifiers/inverters are located in a single cabinet) or in high-power applications where heat dissipation from the battery cells (blocks) is inhomogeneous;
- solar applications where the batteries are located in cabinets exposed to solar radiation;
- high-power, low-temperature applications (e.g., military) where heating is necessary to guarantee a high power capability;
- applications where fast recharging at low temperatures is necessary; here, heating may be necessary to increase charge-acceptance.

The tasks of thermal-management systems may include temperature equalization among cells, cooling of the battery and, in other applications, heating of the battery. Liquid coolants, forced air, and direct electric systems are among the methods used. Additionally, insulation can moderate the effects of high and low temperatures and maintain the battery near the average temperature. A major problem is achieving adequate heat transfer from inside the battery cells to the outside, which must overcome the thermal resistance of the electrolyte, the plastic container, and the balance of the transfer path (see Section 1.4, Chapter 1). Immobilized electrolytes, especially, limit the heat-transfer. The reasons are: (i) no convection inside the battery; (ii) inadequate heat conductivity between electrolyte and container. Thermal management and the particular system used exert a significant influence on the temperature differences between cells, as illustrated in Fig. 8.25.

Most manufacturers recommend that the maximum temperature difference between cells does not exceed 5°C. Depending on the application, the power consumption of the thermal-management system may be very important. Pumps, fans, and heating devices are energy-consuming. Therefore, the control of these components should be optimized. Different types of thermal-management system have been discussed by Pesaran [33].

8.7.1. Air systems

The use of forced-air convection is the simplest method for cooling, heating, and temperature equalization. Electric vehicles, like General Motors' EV_1 and Chrysler's

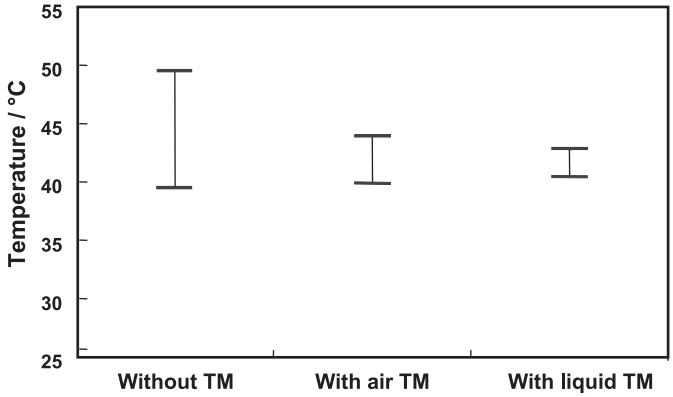

Fig. 8.25. Influence of different thermal-management systems on temperature difference between single monoblocs.

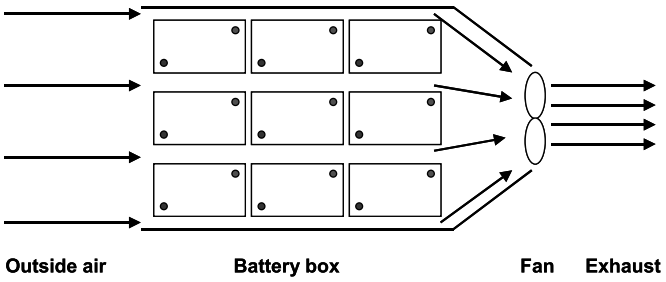

Fig. 8.26. Principle of thermal management using air.

EPIC, used air as the medium for battery cooling and heating. The principle of a thermal-management system using air is shown in Fig. 8.26.

The temperature of the battery depends on the outside air temperature and the operation parameters. Therefore, in lieu of thermal management, the battery temperature cannot be below the ambient temperature. If battery temperatures below the ambient temperature are necessary, the incoming air must be cooled. This can be done with an evaporator, for example. In the case of very low ambient temperatures, it is also possible to heat the incoming air.

8.7.2. Liquid systems

Cooling systems based on a liquid heat transfer medium have a higher efficiency than air systems, but are more complex. Heat transfer from the battery to the liquid can be accomplished by means of plates glued on to the container wall or integrated in the container wall, for example. Also, integrated heat-exchangers can exploit the high thermal conductivity of the battery terminals, by either cooling or heating the

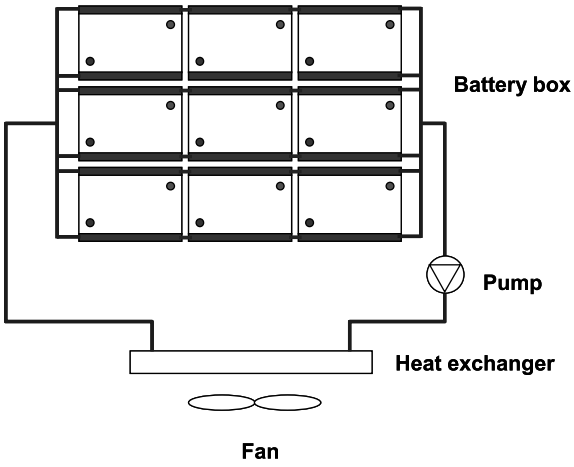

Fig. 8.27. Principle of thermal management using liquid.

terminals, as appropriate to maintain the required temperature [34]. Regardless of the heat-exchange method, the batteries are connected within the cooling loop in series and/or parallel. A layout for a liquid-cooled battery with nine battery blocks is given in Fig. 8.27. The cooling system should be designed in such a way that the temperature difference between the first and last cells is within the allowed specifications (typically $< 5°C$). The system shown in Fig. 8.27 holds the battery temperature close to the ambient temperature and equalizes block temperatures. For active cooling and heating, an additional heat exchanger is necessary. Independent of the heat-transfer medium used, the layout (parallel–series connection) of the blocks is an important design parameter.

8.7.3. Electrical systems

In the case of applications where only heating is necessary, electrical heat systems are the least-expensive solution. Heat plates are simply mounted on the outside of the battery container. It is then very simple to control the heating power. In the case of stand-alone systems, however, heating uses energy from the battery. This reduces efficiencies and also battery SoC. Therefore, battery performance is reduced, and an accurate balance between improvement of battery performance via increased temperature and performance reduction via lower SoC is necessitated. The effect of heating by discharging can be expressed in terms of the ratio of the specific energy and specific heat capacity of the system. Several advantages and disadvantages of electric heating are listed in Table 8.4.

The use of Peltier elements for cooling of batteries is also possible. Koppenhoefer [35] describes field tests with and without active cooling with Peltier elements. Such a system for the case of a fibre-cable distribution shelter is shown in Fig. 8.28.

Table 8.4. Advantages and disadvantages of electrical-heating systems.

Advantages	Disadvantages
Inexpensive	Only for small batteries
Simple control	No temperature equalization between cells
No noise	Stand-alone systems use energy from the battery

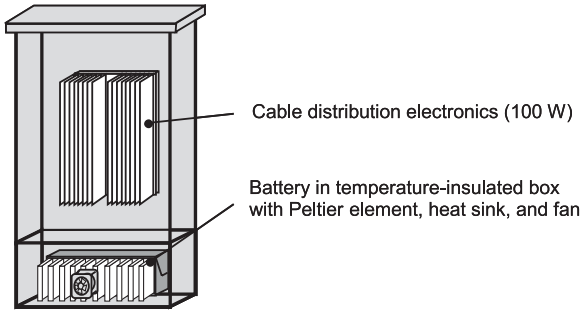

Fig. 8.28. Cable distributor cabinet with air-conditioned battery.

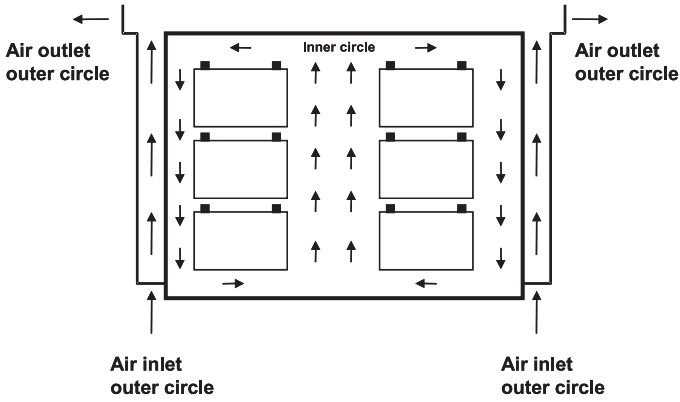

Fig. 8.29. Double-shell housing as passive cooling device.

8.7.4. Passive cooling systems and isolation

In some applications, where it is necessary to protect the batteries from heat via solar radiation (e.g., PV systems), passive-cooling systems can be used (Fig. 8.29). An example of a passive-cooling system in telecommunications applications is described in Ref. [36]. This design reduces the effects of heating by direct solar radiation and by heat generated inside the housing. Additionally, the batteries are protected against other effects of the environment.

8.7.5. *Phase-change materials*

The latent heat of a phase change can be used to hold a battery at a constant temperature. The phase-change temperature should be adapted to the average operation temperature. The use of a phase-change material (PCM) increases the total heat capacity of the system and this leads to equalization of temperature over time. The heat dissipation of the whole system (battery + PCM) is not increased. The latent heat of a PCM (e.g., 190 kJ kg^{-1} for the material ISO-T27) is about 200 times higher than the thermal energy that a typical VRLA battery (specific heat capacity: about 0.8 kJ kg^{-1} K^{-1}) gains or loses for a change in temperature of 1 K. Therefore, the necessary mass of the PCM can be in the range of 10% of the battery weight. Barnes *et al.* [37] showed that a temperature reduction of 10 K is possible through the use of a PCM.

8.7.6. *Other systems*

There are other possibilities for the thermal control of batteries, namely:

- use of variable heat conductance insulation [38];
- placement in the ground in a special box, i.e., insulate;
- inductive heating [39].

8.8. Storage of Historical Battery Data

Measured data can be stored in several different ways, e.g., data logging, storing of integrated values (cycles, Ah, etc.), storing of statistically analyzed data, error storage. Data logging is used to store interesting and important values, often as a function of time. These data can be used to analyze the operation conditions in detail. This does require, however, a large memory. Integrated values summarize interesting parameters of a battery. These are: (i) charged and discharged Ah; (ii) charged and discharged Wh. Statistically analyzed data summarize the operation of the battery. For example, the number of cycles vs. DoD, as illustrated in Table 8.5, is a useful and interesting data field. In this example, it is possible to get an overview of the cycling operation with only 5 stored parameters.

Other statistical analyses could encompass the following parameters:

- current
- temperature
- voltage
- SoC
- over-load/abuse conditions
- number of full charges/equalization charges.

With such data, it is possible to see how the battery has been operated and how it has performed. This information is interesting and could be of value for warranty purposes.

Table 8.5. Example for statistical data storage (c1–c5 are the labels for the cycles).

DoD	< 20%	20–40%	40–60%	60–80%	> 80%
cycles	c1	c2	c3	c4	c5

Error storage technology is well known for automotive systems. For example, sensor failures, battery failures, and failures of the charger are detected and stored. Normally, these errors are displayed (e.g., via a red warning light) and, in some instances, may signal a requirement for maintenance.

8.9. Safety Management of Batteries

Safety management has to protect the battery against critical operation conditions and against failure of the BMS or its associated sensors and wiring. In the case of failure, substitute functions may be necessary in order to continue battery operation, perhaps at a lower performance.

In the case of a BMS for an electric vehicle, the tasks of the safety-management system are:

- protection against deep discharge
- protection of single cells against over-discharge
- protection against over-temperature (thermal runaway)
- detection of short-circuits
- detection of isolation failures
- battery turn off in case of a crash.

Over-current and over-voltage conditions should also be detected by the safety-management system.

8.10. System Communications

Communication between the BMS and other systems is another important feature. The different communication lines are illustrated in Fig. 8.30. The specific type of physical interface and the protocol used depend mainly on the application. In general the following systems are used:

- analogue signals
- pulse-width modulated signals
- digital bus systems, e.g., CAN
- use of the powerline.

It is also possible to have communication between external systems and the BMS. As an example, it is possible to transmit data from a vehicle to a central database. Such a feature is interesting for fleet operators in order to optimize the range or operation time of the vehicles. Data transmission can be carried out during charging at a charge station (wired communication) or with a wireless communication line while the vehicle is in use.

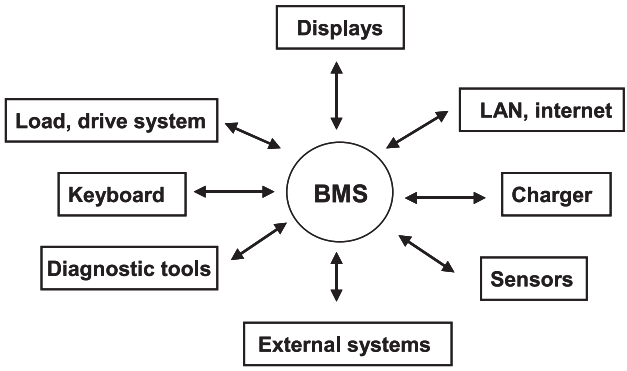

Fig. 8.30. Communications between BMS and other systems.

8.11. Conclusions

Battery management systems are used to improve the performance and lifetime of batteries. In order to perform this function effectively, a BMS should contain all the battery-relevant parameters and algorithms for charging, control of discharge, and control of battery temperature. The systems are also used to obtain knowledge about the actual battery state (SoC and SoH). The improved performance of microcontrollers in combination with on-line battery models will lead to a more accurate calculation of the SoC and SoH in the future. One of the driving forces for the development of improved methods for SoH calculation is the new 42-V powernet for vehicles. In the case of steering-by-wire and braking-by-wire, the battery is a safety-relevant component and monitoring of the state parameters is essential in order to guarantee the performance of the powernet.

References

1. A. Lohner, *Proceedings of 15th Electric Vehicle Symposium EVS-15*, Brussels, Belgium, 1998.
2. B. Hauck, J. Altmeier, 1998, *Proceedings of 15th Electric Vehicle Symposium EVS-15*, Brussels, Belgium, 1998
3. E. Gotaas, *Batteries International*, **48** (2001) 87–92.
4. D.U. Sauer, G. Bopp, A. Jossen, J. Garche, M. Rothert, M. Wollny, *Proceedings of the 21st International Telecommunications Energy Conference*, Copenhagen, Denmark, 1999, paper 31–32.
5. J. Burbank, E. Goldstein, *J. Electrochem. Soc.*, **113** (1966) 1329–1331.
6. T. Higginson, K. Peters, in: L.J. Pearce (Ed.), *Power Sources 11. Research and Development in Non-mechanical Electrochemical Power Sources*, International Power Sources Symposium Committee, Leatherhead, England, 1986, pp. 21–30.
7. J.H. Aylor, A. Thieme, B. Johnson, *IEEE Transactions on Industrial Electronics*, **39** (1992) 398–409.
8. H.P. Hoenes, Doctoral thesis, University of Stuttgart, Germany, 1994.
9. J.B. Copetti, F. Chenlo, *Proceedings of 11th E.C. Photovoltaic Solar Energy Conference*, Montreux, Switzerland, 1992, pp. 1116–1119.
10. D.O. Feder, M.J. Hlavac, W. Koster, *J. Power Sources*, **46** (1993) 391–415.
11. J. Walter, *Workshop on Impedance-Based Techniques in Monitoring and Diagnostics of Lead–acid Batteries*, Aachen, Germany, 27–28 March 2001, Paper No. 15.

12. A. Jossen, A. Bosch, H.P. Hoenes, H. Karl, G. Lehner, G. Saupe, A. Zahir, *Proceedings of 10th E.C. Photovoltaic Solar Energy Conference*, Lisbon, Portugal, 1991, pp. 1012–1015.
13. U. Teutsch, *Proceedings of TELESCON*, Berlin, 1994.
14. M. Rothert, B. Willer, C. Schmitz, G. Bopp, D.U. Sauer, A. Jossen, *Proceedings of workshop 'Electrochemical Storage Systems for Solar Energy Systems'*, 4–5 May 1999, Ulm, Germany, 1999, pp. 211–232 (German).
15. R. Weiss, J. Appelbaum, *J. Electrochem. Soc.*, **129** (1982) 1928–1933.
16. S. Piller, C. Ehret, W. Schroer, A. Jossen, *Proceedings of 45th International Scientific Colloquium*, Ilmenau Technical University, 2000, pp. 245–250.
17. M. Ceraolo, *Proceedings of 13th Electric Vehicle Symposium EVS-13*, Osaka, Japan, 1996, pp. 659–665.
18. P. Singh, C. Fenni, D.E. Reisner, A.J. Salkind, *Proceedings of 15th Electric Vehicle Symposium, EVS-15*, Brussels, Belgium, 1998.
19. D. Heinemann, *Proceedings of 14th Electric Vehicle Symposium EVS-14*, Orlando, FL, USA, 1997.
20. J.D. Kozlowski, C.S. Dyington, A.K. Garga, M.J. Watson, T.A. Hay, *The Battery Man*, **43(4)** (2001) 14–29.
21. A. Lohner, Doctoral thesis, University of Aachen, Germany, 1998.
22. Ph E. Pascoe, A.H. Anbuky, *Proceedings of the 21st International Telecommunications Energy Conference*, Copenhagen, Denmark, 1999, paper 6–1.
23. E.W. ter Horst, K. Blok, W.C. Turkenburg, *Proceedings of 8th E. C. Photovoltaic Solar Energy Conference*, Florence, Italy, 1988, pp. 1564–1568.
24. ZVEI, Product Division Batteries, *Information Sheet: Considerations on the Life of Traction Batteries*, ZVEI, Hannover, Germany, 2001.
25. D.O. Feder, *Proceedings of the 17th International Telecommunications Energy Conference*, Den Haag, Netherlands, 1995, pp. 22–27.
26. V. Spaeth, A. Jossen, H. Doering, J. Garche, *Proceedings of the 19th International Telecommunications Energy Conference*, Melbourne, Australia, October 1997, pp. 681–686.
27. H.J. Zimmermann, *Fuzzy Set Theory and its Application*, Academic Publishers, London, UK, 1992.
28. J. Garche, A. Jossen, H. Doering, *J. Power Sources*, **67** (1997) 201–212.
29. H. Schmidt, C. Siedle, L. Anton, *Proceedings of 13th E. C. Photovoltaic Solar Energy Conference*, Nice, France, 1995, pp. 1846–1849.
30. T.F. Sharpe, R.S. Conell, *J. Appl. Electrochem.*, **17** (1987) 789–799.
31. B. Dickinson, D. Swan, *Proceedings of Future Transportation and Technology Conference*, 1995, pp. 145–154. (SAE paper 951949).
32. F. Wicks, E. Doane, *Proceedings of 28th Intersociety Energy Conversion Engineering Conference*, 1993.
33. A.A. Pesaran, *The Battery Man*, **43(5)** (2001) 34–39.
34. R.J. Sanders, US Patent 4,600,665 (1986).
35. R. Koppenhoefer, *Proceedings of Telescon* 2000, Dresden, Germany, 2000, pp. 137–142.
36. R. Korte, *Proceedings of Telescon 2000*, Dresden, Germany, 2000, pp. 147–152.
37. S.G. Barnes, F.A. Fleming, W.J. Longardner, A.P. Ravalovich, *Proceedings of 12th Electric Vehicle Symposium EVS-12*, Anaheim, CA, USA, December 1994, pp. 27–37.
38. S.D. Burch, T.F. Potter, M.A. Keyser, M.J. Brady, K.F. Michaels, SAE Tech. Paper 950409, 1995.
39. G. Looke, G. Voelkel, *E.T.Z.*, **106(11)** (1995) 552–558.

Valve-Regulated Lead–Acid Batteries
D.A.J. Rand et al., editors

—CHAPTER 9—

CHARGING TECHNIQUES FOR VRLA BATTERIES

R.F. Nelson

9.1. Introduction

The life of a lead–acid battery is often considered to be a function of materials and design parameters such as grid alloy and thickness, paste composition, plate thickness, positive active-material:negative active-material (p:n) ratio, and electrolyte strength, as well as discharge conditions such as rate and depth. While it is readily acknowledged that charging can also have a significant impact on life, it is remarkable how little standard charging methods have varied over the past several decades. Moreover, the quantum shift in technologies in moving from flooded to valve-regulated lead–acid (VRLA) has seen only minimal adjustments to the charging algorithms developed in the first 70 years of the past century — this in spite of the profound effect that the so-called 'oxygen cycle' operative in VRLA batteries has on the chemistry of the charging process.

In hindsight, it may be regrettable that, by and large, the same companies that developed flooded lead–acid products were the ones that now manufacture the vast majority of VRLA batteries. Moreover, the few 'outsider' companies such as Gates Energy Products (now Hawker/Invensys), Electrosource and Portable Energy Products appear to have paid scant attention to modifications in charging algorithms tailored to the performance and life of their VRLA products. While it seems to be obvious now, it was not clear in the early development of VRLA that it bore more similarities to sealed nickel–cadmium products than to its flooded cousin in terms of charging technologies.

In the early days of VRLA development, the influence of the oxygen cycle was exalted and designs were created to optimize its effect, particularly during the charging process. It is only now becoming apparent (after all this technology has been in existence for only about 35 years) that the oxygen cycle must be managed and moderated in VRLA products in order to realize the lifetimes in both float and cyclic duty that are inherent in this fascinating and important technology. While materials and design changes may result in moderate percentage increases in lifetimes, truly effective charging algorithms can lengthen both float and cyclic lifetimes by multiples rather than by percentages. This chapter first presents a review of the state-of-the-art in charging to see how the industry arrived at the present practice (largely based upon flooded technology), and then examines how approaches that are 'outside of the box' can be taken to achieve the true lifetimes of which these remarkable VRLA products are capable.

9.1.1. *Basic charging — chemistry/secondary reactions*

The chemistry of charging is identical to the fundamental lead–acid equations presented elsewhere in this book. On both plates, lead sulfate is converted to active materials through the passage of electrical current, initially at virtually 100% efficiency (except for energy dissipation due to ohmic effects). When the conversion of lead sulfate to sponge lead on the negative and lead dioxide on the positive cannot support the applied charging current, the efficiencies drop below 100%. Because the charge-acceptance efficiencies of the two electrodes are different, this does not occur for both at the same state-of-charge (SoC). Typically, the charge-acceptance of the positive electrode is poorer than for the negative and, thus, the positive goes into overcharge at ~70–80% SoC, depending upon pore structure, surface area, and the magnitude of the charging current. The charge-acceptance of the negative plate is significantly higher and so it goes into overcharge at ~90% SoC [1].

Where the overcharge processes begin is a function of a number of design factors and the charging conditions. In general, it can be said that the positive electrode goes into overcharge first, followed by the negative some time later. The overcharge, or secondary, reactions on the positive electrode are water breakdown and grid corrosion, as follows:

$$\text{Water decomposition: } 2H_2O \rightarrow O_2 + 4H^+ + 4e^- \tag{9.1}$$

$$\text{Grid corrosion: } Pb + 2H_2O \rightarrow PbO_2 + 4H^+ + 4e^- \tag{9.2}$$

Both reactions are very sensitive to the applied voltage, and both occur at slightly higher potentials than the primary $PbSO_4/PbO_2$ charging reaction. Thus, when much of the lead sulfate on the positive electrode has been converted back to lead dioxide and the diffusion rate of water into the interior plate pores cannot keep up with the applied current, these secondary reactions take place. For some period of time, the charging current is distributed between the primary process and the secondary overcharge reactions. If charging continues for a sufficient period of time, at some point virtually all of the lead sulfate will have been converted to lead dioxide and all of the charging current then goes into these secondary reactions. Obviously, a proper charge algorithm will minimize the amount of energy consumed in these parasitic secondary reactions.

On the negative electrode, the primary lead sulfate → sponge lead process takes place with high efficiency until ~90% SoC. Its charge-acceptance is greater than that of the positive largely due to its coarser, more open, pore structure that facilitates acid diffusion into the plate interior. At some point, however, secondary reactions will also begin at the negative electrode, primarily the reduction of hydrogen ion to hydrogen gas by simple electron transfer (occurring at ~350 mV above the $Pb/PbSO_4$ reversible potential):

$$2H^+ + 2e^- \rightarrow H_2 \tag{9.3}$$

Thermodynamically, this occurs at a lower potential than the primary charging reaction but, as with oxygen generation at the positive, the overpotential for hydrogen generation on the lead electrode is relatively great and so recharge can be largely completed before hydrogen evolution begins in earnest. The kinetics of hydrogen evolution on metal surfaces, however, are highly variable, and so the presence of even small amounts of active impurities (platinum, palladium, tellurium, etc.) will lower the hydrogen-evolution potential significantly, sometimes to the point where full recharge of the negative electrode is difficult or impossible.

In a flooded lead–acid system, the two plates charge independently of one another due to the saturated electrolyte condition and to the low diffusion rates of oxygen and hydrogen gases in sulfuric acid. Thus, these gases escape from the cell before they can interact with the opposite electrode. Both are still affected by impurity effects on overpotentials and thus perfectly efficient recharge of both plates is not guaranteed.

In a VRLA cell, interaction between the plates and electro-generated gases is not only possible but is enabled via the partially saturated condition, so the picture is more complex. At the positive electrode, the chemistry is identical to that for a flooded lead–acid cell. Grid corrosion can and does occur, as does water decomposition. Early in life, much of the oxygen generated escapes from the VRLA cell as molecular oxygen gas, as in a flooded lead–acid product, due to designing for a high level of electrolyte saturation (90–95%). With time in float or cycling use, however, gas paths can be created between the plates during charging and the process at the negative electrode becomes more complicated. As shown in Fig. 9.1, the diffusion rate of oxygen in air is considerably greater than

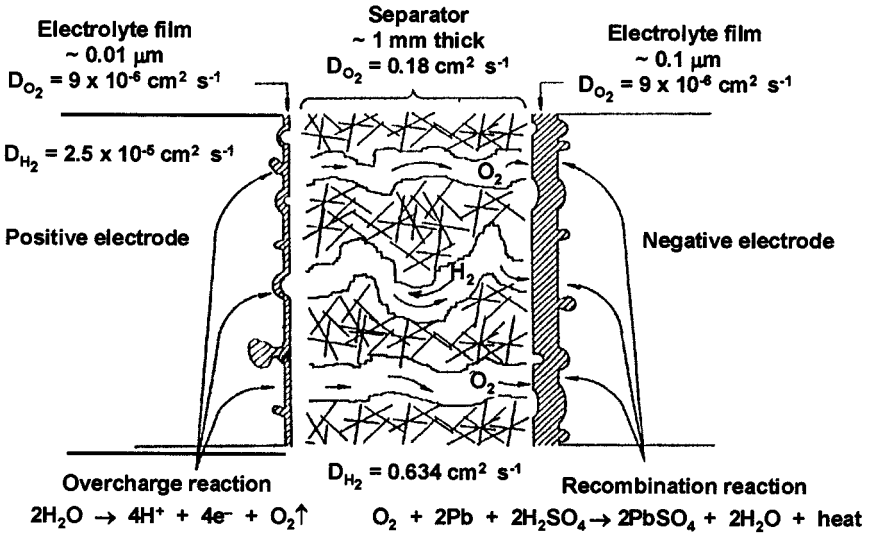

Fig. 9.1. Conceptual view of gas-transport process and diffusion characteristics through glass-mat separator in typical VRLA cell.

in the sulfuric acid electrolyte. Taking into account gas solubility, the diffusion rate of oxygen in the gas phase is effectively $\sim 10^7$ times that in acid. Thus, with a plate spacing of, say, 2 mm, unhindered oxygen transport in the gas phase takes place within a few seconds. In practice, separator saturation levels, compressed pore structures and tortuosity effects, combined with a thin-film electrolyte condition in the negative plate pores, result in transport times of minutes or hours. When oxygen does reach the surface of the negative electrode, however, it is spontaneously reduced back to water at the negative-plate charging potentials:

$$\text{Oxygen reduction at the negative: } O_2 + 4H^+ + 4e^- \rightarrow 2H_2O \text{ (+heat)} \qquad (9.4)$$

As can be seen, this is the reverse of reaction (1), decomposition of water at the positive electrode. The net effect of this oxygen cycle is to convert electrical energy to heat. Thus, any oxygen gas that reaches the negative plate surface will be converted back to water and, thus, will not be lost from the cell. In addition, because the standard potential for oxygen reduction is less negative than the open-circuit value for the negative electrode, significant levels of oxygen reduction will 'drag down' the plate potential so that hydrogen evolution is diminished or completely eliminated. Combined, these two factors result in much-reduced gas (and water) losses from VRLA cells compared with flooded lead–acid analogs, approximately by an order of magnitude.

In practice, the negative electrode assumes a 'mixed-potential' condition, with some portions of the surface supporting oxygen reduction and others continuing to generate hydrogen gas, as shown in Fig. 9.2. This is a balanced, delicate condition, and small changes in saturation levels or choices of separator characteristics can

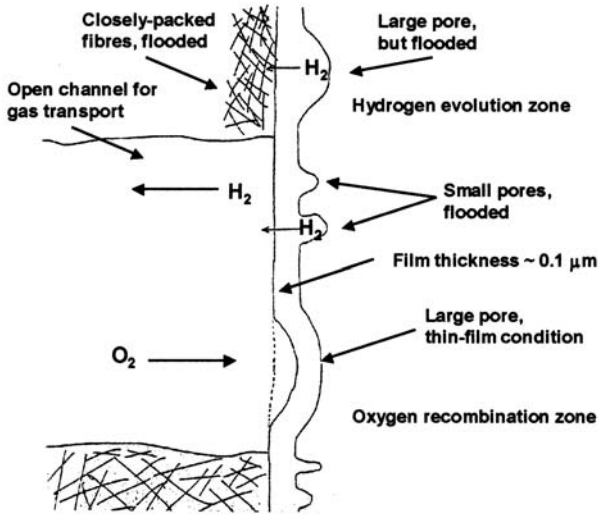

Fig. 9.2. Model depicting 'mixed-potential' condition at negative-plate surface due to simultaneous functioning of hydrogen-evolution zones and oxygen-recombination gas paths.

have a large effect on driving cell performance to one of the two extremes of virtually no oxygen reduction (also called 'oxygen recombination' in some texts) or complete conversion back to water. This 'closed oxygen cycle' with its associated heat effects [2] and the mixed-potential condition at the negative plate, is key to understanding the design and recharge behaviour of VRLA cells and batteries, as is discussed in the following sections.

9.1.2. *Traditional charging methods*

As noted earlier, charging methods used for VRLA batteries have largely been similar or identical to those developed for flooded counterparts. This is natural, as both are lead–acid chemistries and most battery companies' experience began with flooded versions. In fact, these traditional approaches work very well for VRLA products early in life, when their highly saturated conditions closely approximate flooded lead–acid environments.

9.1.2.1. Constant-voltage charging. Constant-voltage (CV) charging is a technique where a discharged battery is recharged with a voltage setting in the overcharge region and a current limit that will not damage the battery. Thus, a more descriptive term is current-limited CV charging; in European convention it is referred to as IU charging. Early in recharge, the voltage will be relatively low and the current limit will be reached almost immediately. The charging process will stay in current limit until the battery charge voltage reaches the pre-set charging voltage, as shown in Fig. 9.3 [3]. When the battery voltage equals the charger voltage setting, the charging current will begin to fall, as lower amounts

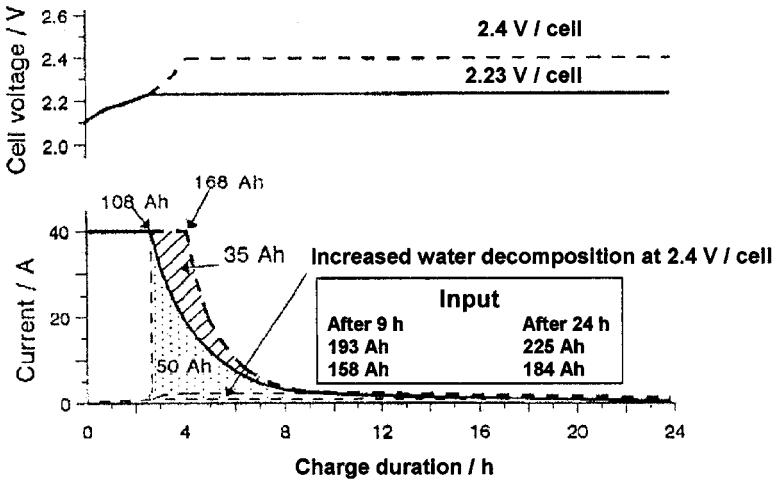

Fig. 9.3. Example of current-limited constant-voltage (CV or IU) charging for a 200-Ah VRLA battery at 2.23 VPC (solid line) and 2.40 VPC (dotted line). Larger Ah charge returns are for 2.40 VPC charge. (From Ref. [3], p. 84.)

of charge will now be required to hold the pre-set voltage value. The current will decrease exponentially and at some point will achieve a steady-state value — a so-called 'float' voltage value (see Section 9.3.1). As seen in the example shown in Fig. 9.3, roughly 60% of the total recharge is accomplished within the first 2.7 h when the current limit is sustained. As the current falls, the time per ampere-hour delivered increases so that, in the last 15 h, only ~14% of the total charge is delivered. This long 'tail' on the charging curve is probably the greatest drawback to CV charging. When recharge time is not important, however, it is an effective (and the most common) method for float or cyclic charging of VRLA products.

Selection of the charge voltage will largely determine the charging time. If higher charge voltages per cell (VPC) are used, as shown in Fig. 9.3, the battery stays in current limit for a longer time in order to reach the higher voltage. This results in a significantly higher charge input during the early hours of recharge (here, 35 Ah more at 2.40 V compared with 2.23 V within the first 9 h) and delivers a full recharge in a shorter time. A faster recharge can also be realized using a higher current limit, but care must be taken not to generate harmful amounts of heat due to ohmic (I^2R) effects. As can be seen in Fig. 9.3, charging at higher voltages results in more water decomposition (and hydrogen evolution) and, thus, higher weight losses and accelerated grid corrosion. These two problems are more severe in flooded lead–acid products. Thus, the amplitude of the charging voltage must be balanced against the time available for charging and the threat of undercharging, which is more likely at lower charge voltages, particularly with grid constructions that are susceptible to interface-related premature capacity loss (PCL-1) effects. The relationship between recharge time and charge voltage in CV charging is shown in Fig. 9.4 [4] for a typical VRLA product.

In summary, the advantages of CV charging are as follows:

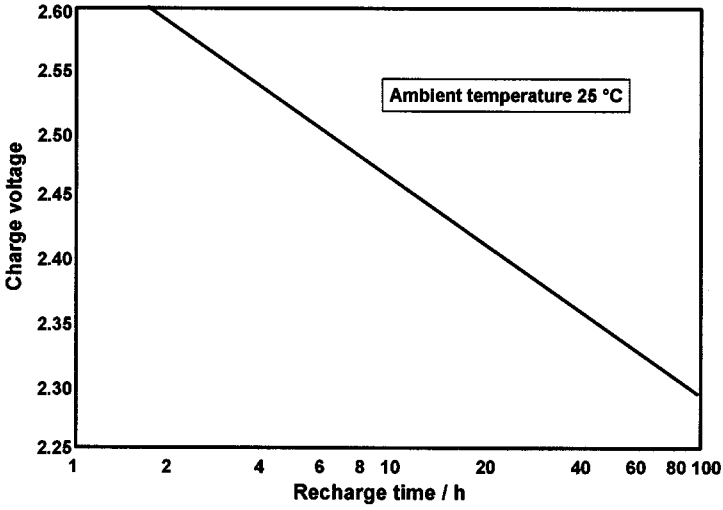

Fig. 9.4. Relationship between charge voltage and recharge time on CV charge.

- precise voltage regulation is possible (but is relatively expensive and may not be necessary);
- overcharge is minimized, with most of the current going into lead sulfate charging;
- charge voltage and limiting current can be varied to have a fast or slow charge;
- it is usable for float charge, as there are low float currents but relatively fast recharge.

On the other hand, several significant drawbacks also exist:

- there is a long-duration charge 'tail', which creates long charge times in most cases;
- Ah input is indeterminate and must be measured by current integration;
- undercharging and capacity 'walkdown' can easily occur;
- cell-to-cell charge equalization is not likely due to low, uncontrolled string voltages;
- with relatively high current limits for fast recharge, thermal runaway is possible on float or cycling due to high finishing-current draws as VRLA batteries age;
- without environmental controls, temperature compensation may be necessary.

9.1.2.2. Constant-current charging. Constant-current (CC) charging is also a viable approach for VRLA products, particularly in multi-cell strings — and the longer the string, the more it is appropriate. In this approach, a constant charging current is applied to the battery, usually in a multiple of at least two steps and often several more. Because voltages are not usually controlled, there is the danger of cells spending an appreciable amount of time at high voltages where gassing and grid corrosion can occur. On the other hand, this type of charging ensures that all cells will be able to achieve full recharge on each cycle or during float charging. In fact, it is the case that overcharge is the great concern for CC charging, whereas undercharging is the primary danger with CV algorithms. True CC charging is performed with a voltage of ~ 3.0 VPC, i.e., a level that is sufficient to allow cells to attain very high gassing potentials. To counter this, finishing currents are either very low ('trickle' levels) or high currents are used for only short periods of time.

A common CC algorithm, first proposed for small VRLA batteries by Gates Energy Products [4], involves a two-step process where the battery is brought up to $\sim 90\%$ SoC using a relatively high CC, typically at the C_{10}–C_5 rate. A step-down to a 'trickle' current of C_{500}–C_{1000} follows using a 2.50 VPC trigger point. If, for some reason, the battery voltage drops below 2.35 VPC, the charger goes back to the high-current mode. In this way, the battery is kept at, or near, full charge with minimal overcharge.

The problem with using a single-step CC charge is illustrated in Fig. 9.5. In order to complete the recharge in a reasonable amount of time, a relatively high CC level needs to be employed, as noted above. As can be seen in the lower curve, however, this will entail the application of very high overcharge amounts of 20–30% compared with an 'ideal' charging curve, one that approximates a truncated CV

charge. This high amount of overcharge will ensure full recharge, but cycle-life will be sharply curtailed. Moreover, long-term float charging is not possible with this approach whereas it can be done, for example, with the two-step 'trickle'-charge approach.

The upper curve in Fig. 9.5 shows, perhaps, the other extreme, a multi-step CC algorithm that very closely matches the 'ideal' charging curve. While this may seem excessive, it will minimize overcharge and such programs can be easily done with inexpensive 'smart' chargers now on the market. In fact, recent work by a consortium of Japanese workers looking at charging methods for VRLA batteries in load-levelling and EV applications has shown that multi-step CC charging may be a superior approach in many cases [5–7].

In summary, CC charging has a number of advantages and drawbacks; the primary advantages are as follows:

- CC chargers are relatively inexpensive (although today all commercial chargers are easily affordable);
- rapid, controlled charging is possible with a fixed, easily measured Ah input (adding up currents and times);
- cell-to-cell charge equalization takes place on every charge event;

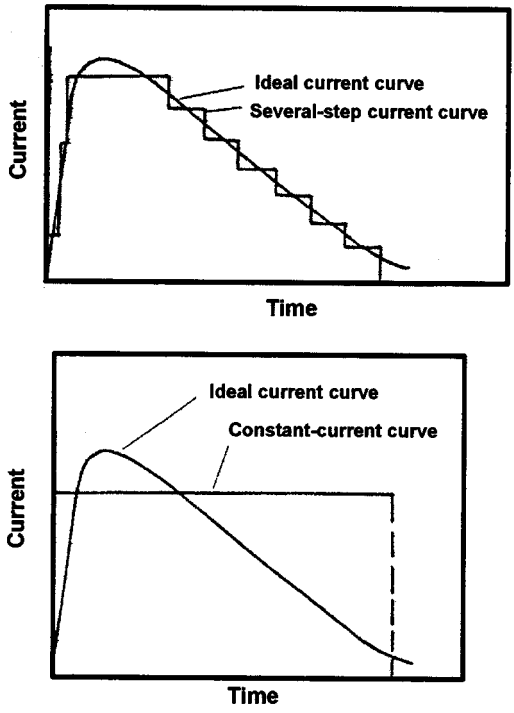

Fig. 9.5. Constant-current charge curves compared with 'ideal current curve' representative of truncated CV charge curve. Lower curves are for single-step CC charge, upper curves are for programmable multi-step CC charge.

- temperature compensation is not necessary;
- thermal runaway is not likely to occur due to the low, controlled float or finishing current at the end of charge;
- undercharging is not as likely as with CV charging due to the well-defined Ah input and charge factor.

The drawbacks of CC charging are as follows:

- single-rate CC charging may produce heavy overcharge (see Fig. 9.5) and result in gassing/dry-out, grid corrosion and, thus, shortened life;
- voltage is uncontrolled; high voltages may produce more grid corrosion, gassing;
- finishing currents must be adjusted as VRLA batteries age to ensure that they are greater than the current draw for the oxygen cycle.

9.1.2.3. Constant voltage–constant current combinations. It is also possible to combine the CV and CC approaches; in fact, one of the most effective methods for charging VRLA batteries is the so-called IUI algorithm. This is simply a current-limited, CV charge with a CC finishing step at some low current level; an example is shown in Fig. 9.6. In this example, a CV charge at 2.45 VPC is first applied with a $0.7C_5$ current limit. As with a simple IU charge, the battery stays in current limit until the battery charge voltage equals the pre-set charger voltage (U_1), at which point the current begins to decrease exponentially. At some point, defined by time or

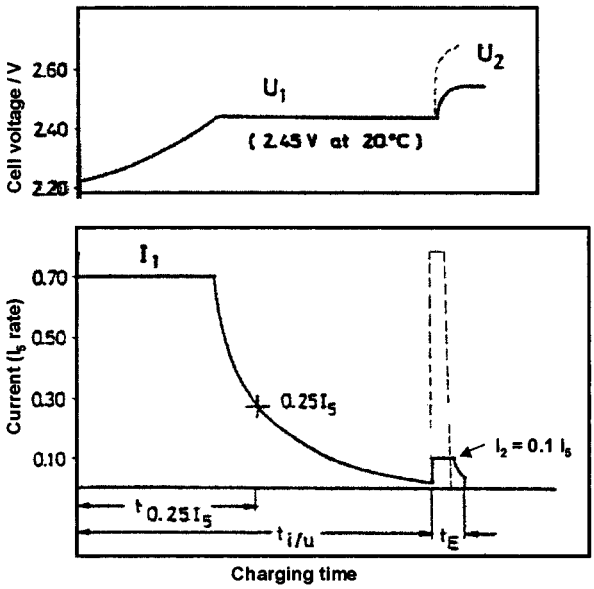

Fig. 9.6. Example of CV charge followed by CC finish (IUI). The finish can be either a voltage-limited, low-current step (solid line) or a high-current step with no voltage limit (dotted line).

current, a CC finishing step is initiated, usually at some low current level such as C_{50} for, usually, 1–2 h. The voltage may, or may not, be controlled (in Fig. 9.6, it is controlled, as can be seen by the current decay at the end of charge), but in any event the finishing voltage is high (U_2) relative to a normal CV charge. Thus, this approach is a 'hybrid' of the two previous algorithms, with some good aspects of both.

The major problem with an IUI charge algorithm for VRLA batteries, one that will eventually cause premature failure, is related to the magnitude of the finishing step. Early in life, when the saturation level is high, the CC finishing step is adequate to charge the negative plate fully, and it provides some degree of cell-to-cell charge equalization. As the battery ages and the saturation level drops, more current is drawn by the oxygen cycle. When this parasitic current draw exceeds the magnitude of the finishing current level, the battery will not be fully charged; indeed, at some point before this, full recharge is not likely to be achieved. Conceptually, it is evident that when all of the finishing current is being consumed by oxygen reduction, it cannot go into completing recharge of the active material. A recommendation for more effective IUI charging of VRLA batteries, particularly after the first few hundred cycles, is to use a higher, shorter-duration finishing step (as shown by the dotted line in Fig. 9.6) in order to keep the finishing-step Ah input at a reasonable level. The maximum allowable current and duration will be dictated by the heat-generation and dissipation properties of the VRLA product, as thermal build-up will limit the application of this approach. The rationale and conditions for this will be discussed more fully in Section 9.3.

A second CV–CC approach is a 'pseudo-CC' algorithm, which is really a multi-step, current-limited CV charge. In this algorithm, a first current-limited CV step with a relatively high current is applied, but with a low voltage limit (unlike true CC charging, which does not employ voltage limits), as shown in Fig. 9.7 with 2.45 VPC. When the battery voltage reaches this level the current limit is stepped down and

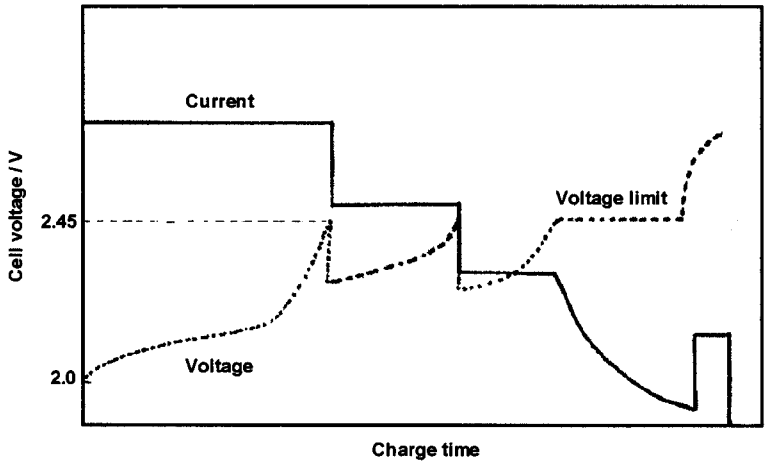

Fig. 9.7. Example of multi-step voltage-limited CC charge ('pseudo-CC') with a 2.45 VPC step trigger and pure CC finishing step (no voltage limit).

results in a voltage drop followed by a gradual climb back to 2.45 VPC. This can be repeated for several steps, perhaps with a CC finishing step as in IUI charging. This is a more cautious approach than true CC charging, and it will result in lower levels of grid corrosion and gassing. Like true CV charging, however, there is a significant risk of undercharging, particularly as the battery ages.

9.1.2.4. Taper-current charging. An approach that is well suited to VRLA products, but one that is seldom used, is taper-current (TC) charging. Perhaps one fundamental reason that it is not commonly used is that, in this technique, neither current nor voltage is controlled; rather, current drawn and voltage attained (up to a pre-set voltage limit) are determined largely by the battery charging requirements.

In TC charging, a power supply is wired in series with a load resistor and the cell or battery to be recharged. Current flows according to the load resistance and the voltage difference between the power supply (typically set at ~2.5–3.0 VPC) and the cell/battery being charged. A simplified TC circuit is given in Fig. 9.8. Initially, the voltage difference is great, of the order of 1 VPC following a full discharge; thus, the inrush current is high. As the cell/battery voltage climbs during recharge, the charging current falls because of the decreasing voltage difference. When the cell/battery voltage climbs into the gassing region the charge current falls to a minimum value, but one significantly higher than for conventional CV charging because of the moderating effect of the load resistor. Early in life, when the saturation level is high, the current will stay low because the end-of-charge voltage will be high, as for a flooded lead–acid battery, and the current–time curve will be similar to that for a traditional CV algorithm. As the battery ages and the oxygen cycle becomes more prominent, a voltage 'rollover' is observed (a peak, or plateau, followed by a drop-off) where the voltage might rise to ~2.7 VPC and then drop to 2.4–2.5 VPC. When this happens, there will be an automatic increase in

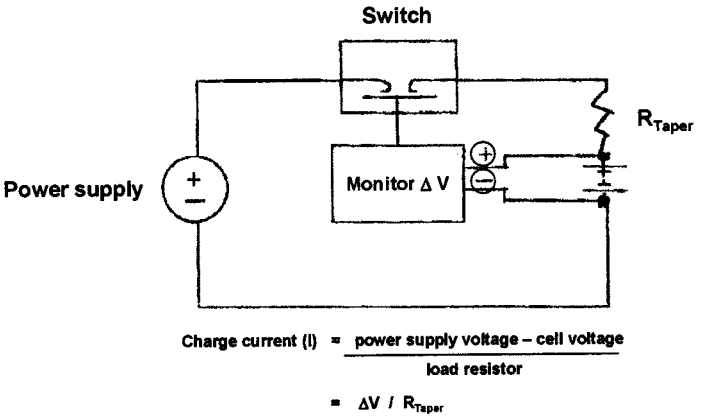

Fig. 9.8. Simplified schematic diagram for TC charging circuit. Centre box is a feedback element to use electrical signals from battery for termination.

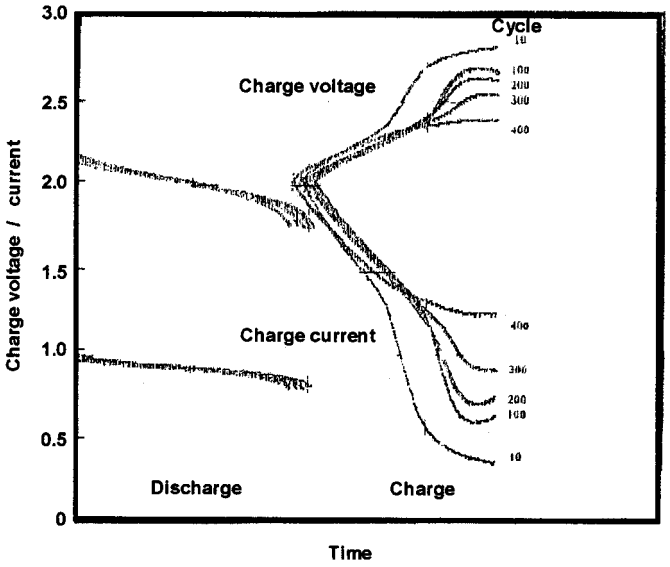

Fig. 9.9. Discharge and charge current (lower traces) and voltage (upper traces) curves for a 2-V/1.2-Ah VRLA cell for cycles 10–400. Note transition from 'flooded' behaviour (cycle 10) to heavy charge current draw due to low saturation level (cycle 400).

the finishing current to compensate for the increasing voltage difference between the cell/battery and the power supply (whose voltage is fixed). Thus, as a cell/battery ages, or if it was manufactured with a relatively low saturation level, the higher draw for oxygen recombination will automatically be accommodated by higher finishing currents, as shown in Fig. 9.9.

Power supply voltages and resistor values are chosen based upon the desired inrush/end-of-charge currents and charging time. Typically, for a 2-V/1.0-Ah cell one might use a power-supply setting of 3.0 V and a 0.3 Ω load resistor rated for 5 W. This will provide an inrush current of ~3.3 A for the 1.0-Ah cell. Clearly, for large batteries much lower inrush currents would be used. For larger voltages and Ah ratings, power supply and resistor values are specified by linear multiplication of the per-cell values. Also, lower limiting voltages can be ensured by reducing the power-supply setting. This will significantly lengthen the charge time, however, as currents throughout the recharge will be greatly reduced and only limited cell-to-cell equalization will be realized. On the plus side, the lower voltage limit will minimize the amounts of gassing and grid corrosion.

The advantages and disadvantages of TC charging are similar to those for CV and CC algorithms; the advantages are as follows:

- TC chargers are very inexpensive
- with the proper power supply and load resistor settings, it is unlikely that batteries will be undercharged
- fast charging is possible with moderate levels of overcharge

- charge input adjusts as the cell/battery characteristics change as a result of aging and/or variable saturation levels, separator characteristics, temperature, and other factors that directly define the strength of the oxygen cycle.

There are, however, a number of negative aspects to TC charging, largely due to the unregulated nature of the chargers:

- significant levels of a.c. line 'noise' (a.c. ripple, harmonics, etc.) can be applied to the battery unless filters are used; in extreme cases line fluctuations may even be amplified
- Ah input is indeterminate and must be measured using current integration
- relatively high amounts of overcharge are applied
- this technique is not suitable for float charging for a variety of reasons (no voltage/current regulation, possibly high finishing currents)
- VRLA products can experience thermal runaway due to the high finishing currents available, as with CV charging.

9.1.2.5. Pulsed-current charging. Pulsed-current charging is an old technique that is enjoying a renaissance of sorts in applications involving VRLA batteries; excellent summaries and overviews are available in the recent literature [8,9]. Another technique called 'resistance-free pulse charging', discussed in detail in Section 9.3.3, has been pioneered by Norvik and Cominco to carry out very fast charging of nickel–cadmium (Ni–Cd) and lead–acid batteries [10]. A summary of the various pulsing techniques is given in Fig. 9.10. As can be seen, there are two general approaches, one utilizing a constant period with decreasing amplitude and the other a constant amplitude with decreasing period. In both cases, each pulse delivers a

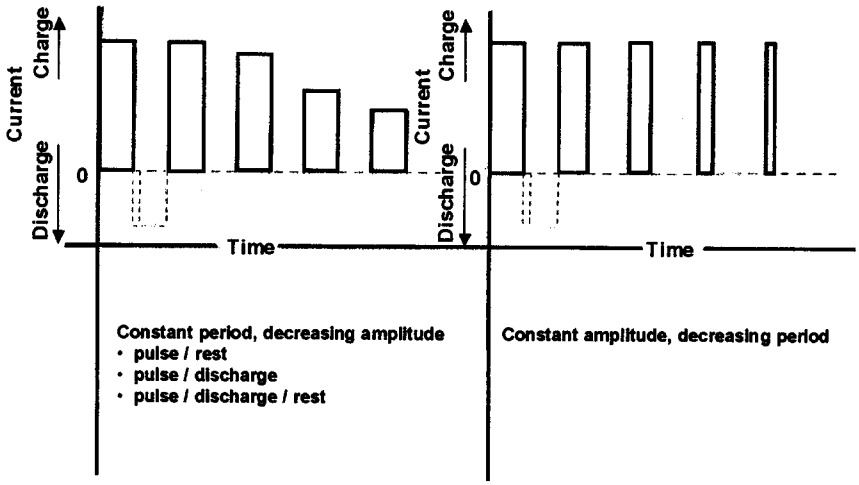

Fig. 9.10. Examples of pulsed-current charge techniques. Dotted lines are for rests (zero current), low-current discharges or discharge–rest combinations.

decreasing coulombic input to the cell/battery as the end of charge is approached, which thus minimizes the amount of overcharge and resultant gassing.

A further variant is seen in the 'off' periods, which can be either a complete rest, a discharge, or a combination of the two (in Fig. 9.10, dotted lines). In all cases, these 'off' periods allow time for heat dissipation and liquid diffusion to take place, increasing the efficiency of the charging process and allowing the use of high finishing currents. Discharges are used in the belief that they remove surface charges from the plates and make the following charge periods more efficient. Further flexibility can be achieved by varying the 'on:off' ratio through a single recharge event and throughout cycle-life. Pulse techniques have also been used in float applications for telecom and UPS batteries [11].

The foregoing is a brief summary of charging algorithms that may be applicable to VRLA products. As shall be seen in Section 9.2, each of these has strengths and weaknesses when it comes to VRLA charging algorithms. None is completely satisfactory, largely because all were developed to charge flooded lead–acid products and the two technologies are fundamentally different, primarily due to the oxygen cycle being operative in one and almost completely inoperative in the other. Given this, charging technology specifically targetted at VRLA batteries is now considered.

9.2. Charging of VRLA Products

As noted previously, the functioning of the oxygen cycle in VRLA products makes them fundamentally different from the more traditional flooded lead–acid batteries. The charging algorithms described previously, largely developed for flooded products, work well for VRLA batteries but will not deliver optimal cycle and float lifetimes due to various limitations. In all cases, these limitations are related to the oxygen cycle, which is variable throughout life. In flooded lead–acid batteries, the initial conditions apply throughout life as long as the batteries are properly maintained (mostly periodic watering). In VRLA products the physical (and, thus chemical) conditions vary significantly going from freshly formed to well-aged. This variability is connected to the saturation levels existing in the plate pores and the glass-mat separator; the 'saturation level' is the ratio of liquid volume to the total void volume in the unfilled cell element (non-solids volume), expressed as a percentage. Most VRLA designs use an initial saturation level of $\sim$95%. This level is really the crux of the proper charging of VRLA products. If saturation effects are handled properly, VRLA batteries can have the same lifetimes as the best, purpose-built, flooded technology; if they are not, lifetimes can be extremely short. The key is in understanding saturation effects and how they impact float and cyclic charging of VRLA batteries.

9.2.1. The oxygen cycle and saturation effects

The important design difference between VRLA and flooded lead–acid batteries is the partially saturated condition of the plates and separator in VRLA products. As noted earlier, the diffusion rates for oxygen and hydrogen are $\sim 10^7$ times greater

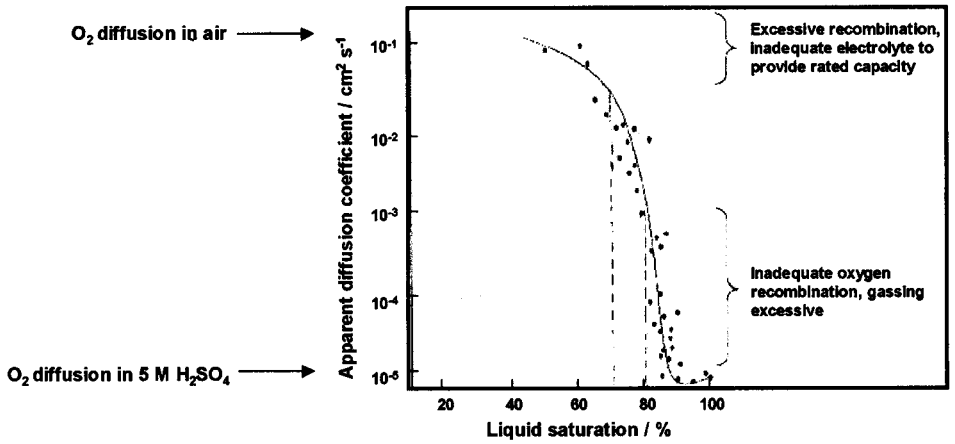

Fig. 9.11. Apparent diffusion coefficient of oxygen as a function of AGM separator acid-saturation percentage. Dotted vertical lines represent the operational range for VRLA cell, ~10%. In practice, this operational range is shifted to ~85–95% [14].

in the gas phase than in the liquid electrolyte. Thus, reasonable levels of oxygen recombination depend upon some degree of lack of saturation existing in the plates and separator. It has been shown that the saturation level in the separator has a tremendous impact upon VRLA cell/battery performance [12,13]. Moreover, this occurs over a relatively small range of saturation, as shown in Fig. 9.11 [14]. This has implications for both manufacturing and performance. In building VRLA batteries, a saturation level of 90–95% after formation is targetted. In order to achieve this accurately cell-to-cell, very tight tolerances on grid, paste, separator, and electrolyte weights are required. In practice, this is difficult to achieve so many manufacturers finish formation in a fully saturated state, sometimes with a follow-on adjustment to ~95% saturation level. This serves as a uniform starting point for all cells, but the variable solids volumes from cell-to-cell will result in equally variable void volumes after a relatively short period of use.

The biggest problem with VRLA cells is that oxygen-transport properties can change dramatically with relatively small changes in saturation levels, as shown in Fig. 9.11. The ease of oxygen transport can directly influence performance through its effect on recharge times and voltages. The lower the saturation level, either initially or as batteries age, the greater the recharge time due to a portion of the recharge current going into the oxygen cycle (which does nothing for recharge of either plate). This is graphically illustrated in Fig. 9.12 [15], which shows three S-shaped charge curves at different initial saturation levels. In a saturated state, overcharge is reached in the minimum time (left-hand curve). At 92 and 84% saturation levels, overcharge is progressively delayed due to an increasing contribution to the total Ah input (and, hence, the SoC or total charge time), which is a result of a stronger oxygen cycle. Note also that the end-of-charge voltages are lower for the partially saturated samples, and if these charging processes had been continued, it is likely that the curve for the 84% saturation battery

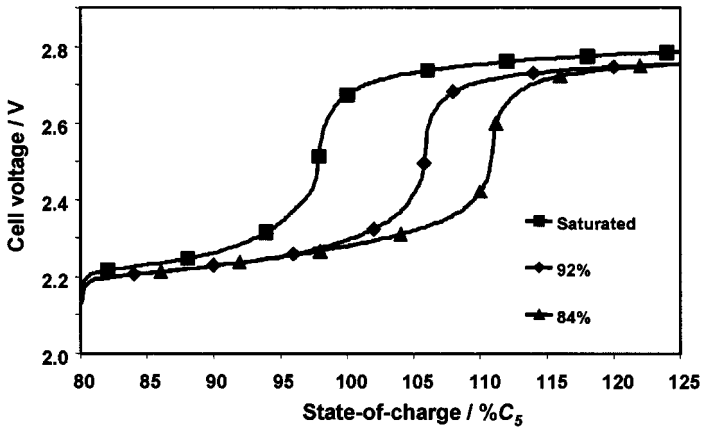

Fig. 9.12. Voltage vs. SoC curves for CC charging of thin tubular-plate VRLA cells with three different saturation levels. Charging S-shaped curves (left to right) are for 100, 92, and 84% saturation [15].

would have shown a voltage 'rollover' to a lower level earlier than for the 92% saturation condition. At lower saturation levels, gas paths are created more easily and, thus, earlier in recharge, and more charge current then goes into the parasitic oxygen cycle (see below). This results in a lowering of the top-of-charge voltage and an earlier voltage 'rollover' if the end-of-charge current level is sufficiently great to establish discrete gas paths and a resultant steady-state oxygen cycle, see Ref. [15] for details. This same phenomenon had been reported previously for commercial EV battery packs [12,13] and appears to be generic for VRLA batteries.

In the more common case when a VRLA cell starts out at $\sim$95% saturation, it behaves electrochemically very much like a flooded lead–acid cell. As the cell ages, however, the saturation level of the separator drops significantly due to the following processes:

- gassing water loss
- water-vapour transport out through the plastic walls of the battery container
- water consumption due to grid corrosion
- electrolyte re-distribution from the separator into the plate pores due to increases in porosity (and a later re-distribution back to the separator as porosity decreases).

As shown in Fig. 9.11, it only takes an approximate 10% increase in void space in the separator to change gas transport from essentially a liquid-diffusion process to one almost completely in the gas phase [14]. This has enormous electrochemical consequences. It means that the oxygen cycle will become a dominant overcharge process and this must somehow be addressed in both float and cyclic charging. In both duty cycles, the result is suppression of the potential of the negative plate. Since the reversible potential for oxygen reduction is below the open-circuit value for the negative plate, this can result, in the extreme, in partial negative-plate discharge.

Clearly, this is unacceptable. This is what must be dealt with, however, in properly charging VRLA products. If this thermodynamic fact is not addressed, VRLA products will fail prematurely, not due to dry-out or grid corrosion, but due to insufficient recharge of the negative plate.

9.2.2. Gas transport and oxygen cycle

In order to adapt the charging process to the changes that take place in VRLA batteries with different initial saturation levels and/or as they age, it is necessary to understand how gas transport takes place plate-to-plate. It has been seen above that when a VRLA battery is recharged, the positive electrode, due to its poorer charge efficiency, goes into gassing overcharge first and generates oxygen micro-bubbles within its pores. These micro-bubbles then coalesce and are expelled from the positive active-material (PAM) pores along with some electrolyte. Thus, although the separator may have been only partially saturated before overcharge, it may become saturated, or close to it, as electrogenerated gas continues to expel electrolyte from the plate pores. When these gas bubbles reach the glass-mat separator, they will 'pump' electrolyte out of the largest pores first as pressure builds. At the same time, the negative plate will continue charging with high efficiency. At some later point it, too, will go into overcharge and generate hydrogen gas; the hydrogen will enter the separator from the negative-plate side and electrolyte will be 'pumped' from the pores into the separator via the same mechanism as that for the positive plate.

The structure of the AGM separator is such that the 'pore structure' (as it is a tangled mat of fibres, there are no real pores but it is useful to represent it in this way) is much coarser in the z direction (plate-to-plate) than in the x–y plane (up, down, and sideways) [16,17]. This means that as pressure builds due to gas accumulation, the direction of void paths will be in the desired direction, i.e., plate-to-plate. Moreover, it is likely not a smooth, uniform process but, rather, one where a large pocket is filled with gas (and cleared of electrolyte at the same time). Subsequently, when the pressure reaches a critical level, the gas path will be propagated in the direction of least resistance (in any of the possible directions). The ease of this process is determined largely by the tortuosity, average fibre diameter (specific surface-area) and compressed density of the glass mat. In float charging, this means that higher steady-state current levels may occur with separators that possesses more 'open' pore structures. In cyclic charging at a given saturation level, larger pore structures will likely result in longer recharge times with a greater percentage of the total Ah input taken up by the oxygen cycle (see Chapter 6 for more details). In this piecemeal fashion, complete gas paths will form; but early in battery life, at least in cyclic charging, it may be that recharge will be completed before this occurs. As the battery ages and more void space is progressively created, this process of gas-path formation becomes more and more efficient and occurs earlier in overcharge. As was seen in Fig. 9.12, this will also be the case with relatively low initial saturation levels.

At some point, significant oxygen reduction begins to take place before the plates are fully recharged. It should be noted that hydrogen oxidation at the positive

electrode, while thermodynamically favoured, is kinetically hindered to the point where it is not considered a significant contributor to the overcharge process. At the negative, however, the impact of oxygen reduction is to decrease the charge efficiency of the lead sulfate material that still remains. If the charge algorithm is not adjusted to account for this new situation, a slight undercharge of the negative plate will occur. While it may only be a fraction of a percent, it is cumulative and becomes more pronounced cycle-to-cycle as the strength of the oxygen cycle grows. The result is a 'walk-down' in discharge capacity that results in early failure. Autopsies show, however, that the failure mode is not grid corrosion or dry-out but, more often, softening of the PAM and heavy sulfation of the negative active material (NAM). Usually, these two effects are more pronounced at the plate bottoms.

Once charging is terminated, residual oxygen gas is scavenged by the negative plate and any hydrogen generated will slowly diffuse out through the plastic walls of the container. The gas paths created by gas generation will, thus, collapse and be re-filled with electrolyte. In addition, electrolyte is likely to re-fill the plate pores to some extent. Thus, when the next recharge process begins, the same gas-path formation must take place from an almost-flooded starting point that will probably be similar to that for the previous cycle.

In float charging, gas paths will form more slowly; but with a small, constant, oxygen generation rate at the positive plate, these channels are likely to be maintained as long as charging continues. Because of the current draw for oxygen recombination, float currents are roughly three times higher for VRLA batteries than for flooded products, as has been pointed out by Berndt [18]. Most of this excess current goes into the oxygen cycle and is converted to heat. This does not lead to increased grid corrosion or higher gassing levels for VRLA batteries; in fact, gassing levels are lower for VRLA batteries by a significant amount, as shown in Fig. 9.13 [18]. As can be seen, at a typical float-charge voltage of 2.25 VPC, a flooded lead–acid battery has an equilibrium float current of 14 mA per 100 Ah, which corresponds to an energy input of 31.5 mW (2.25 V × 14 mA). The area in diagonal lines represents the free energy of reaction, nFE^{o}, while the hatched area corresponds to the reversible heat effect. Because gas venting is stoichiometric (two moles of hydrogen and one of oxygen per two moles of water) and essentially complete, roughly two-thirds of the heat generated in this cell is removed via gassing.

In the equivalent VRLA battery, the float current is at 45 mA per 100 Ah due to the effect of the oxygen cycle, with an equivalent energy input of 101.3 mW. Because the potential of the negative electrode is just above the open-circuit value, the positive is 'pushed' more positive by the CV charge. This results in more water decomposition and oxygen evolution relative to the flooded cell. Because most of this oxygen is reduced at the negative electrode (thus lowering its potential, reducing the hydrogen evolution rate) and gassing is minimal in this VRLA cell, the net result is conversion of almost 95% of the float charging current to heat. Because of the huge difference in gassing rates, it can be seen that the heat remaining in a VRLA cell is almost nine times that for a comparable flooded cell (i.e., 95.4 vs. 10.8 mW).

Under normal float-charging conditions this heat, though excessive, can be easily dissipated. If conditions hinder heat dissipation and/or higher float currents are drawn, however, this process can become a vicious cycle that can result in thermal

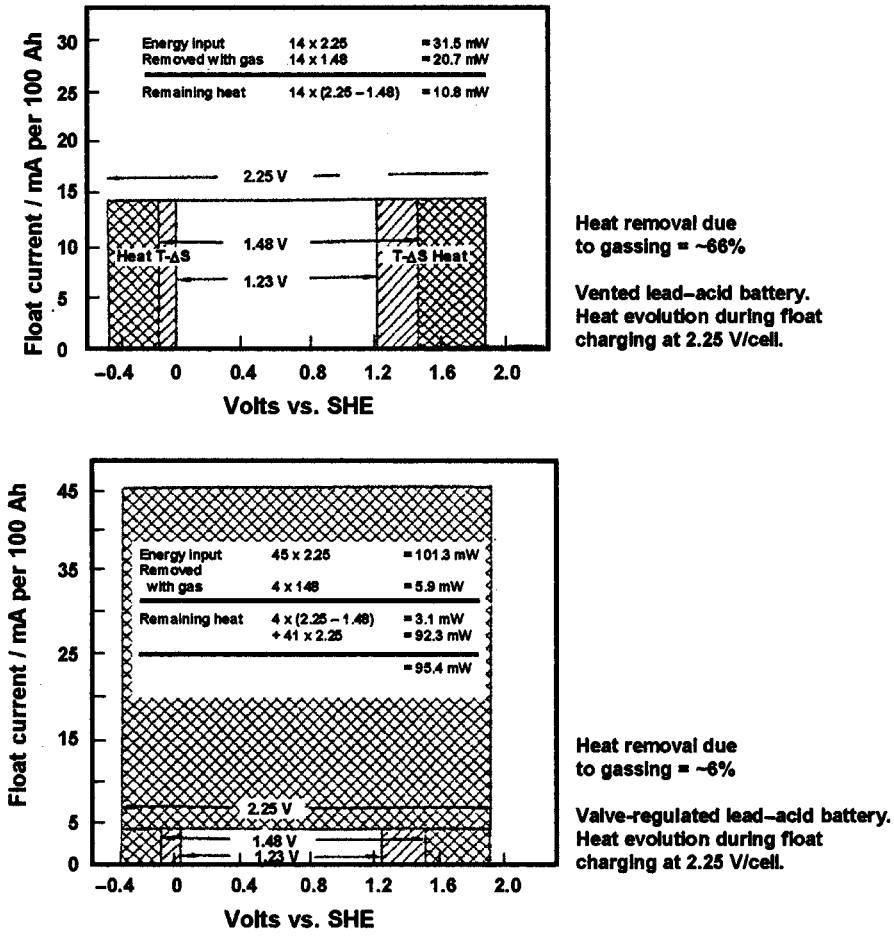

Fig. 9.13. Comparison of float currents, heat evolution, and heat removal for a vented (flooded, upper graph) and VRLA (lower graph) battery [18].

runaway, which destroys the cell [19]. As the cell heats up, higher float currents are drawn. This causes the generation of more oxygen at the positive, which diffuses to the negative and is reduced, thus lowering the negative-plate potential further. On CV charge, this pushes the positive-plate potential to higher values, which causes more water decomposition and oxygen generation. This is the cyclic process that leads to thermal runaway.

9.2.3. Overcharge processes

The overcharge process is fundamentally different in VRLA batteries as compared with flooded products, and this is reflected in lifetimes and failure

modes. In flooded batteries, as noted, the plates charge independently and the secondary reactions of hydrogen evolution at the negative and oxygen evolution and grid corrosion at the positive also take place in isolation. Because of this, water loss and grid corrosion are roughly linear processes as the battery ages as long as it is well maintained by water additions and the charge/float current is constant. There is little or no oxygen recombination due to the flooded condition in the plate stack.

In VRLA batteries, the saturation level starts out at 95–100% and so, initially, much or all of the overcharge/float current goes into hydrogen evolution, oxygen evolution, and grid corrosion. Cumulative weight loss and corrosion rate are linear, as shown in Fig. 9.14. This continues until a saturation level of ~92 to 90% is achieved, at which point the oxygen cycle takes effect. The scenario is somewhat different for float charging, as will be discussed in Section 9.3.1. As overcharge continues, the distribution of overcharge current shifts towards the oxygen cycle and the cumulative weight loss and grid corrosion begin to taper off. For purposes of discussion, it is assumed that the charge factor (ratio of Ah of charge to Ah of discharge) is constant at ~1.1.

At a critical saturation level of ~88 to 84% (the point will vary with design), the strength of the oxygen cycle increases dramatically. Correspondingly, the amount of

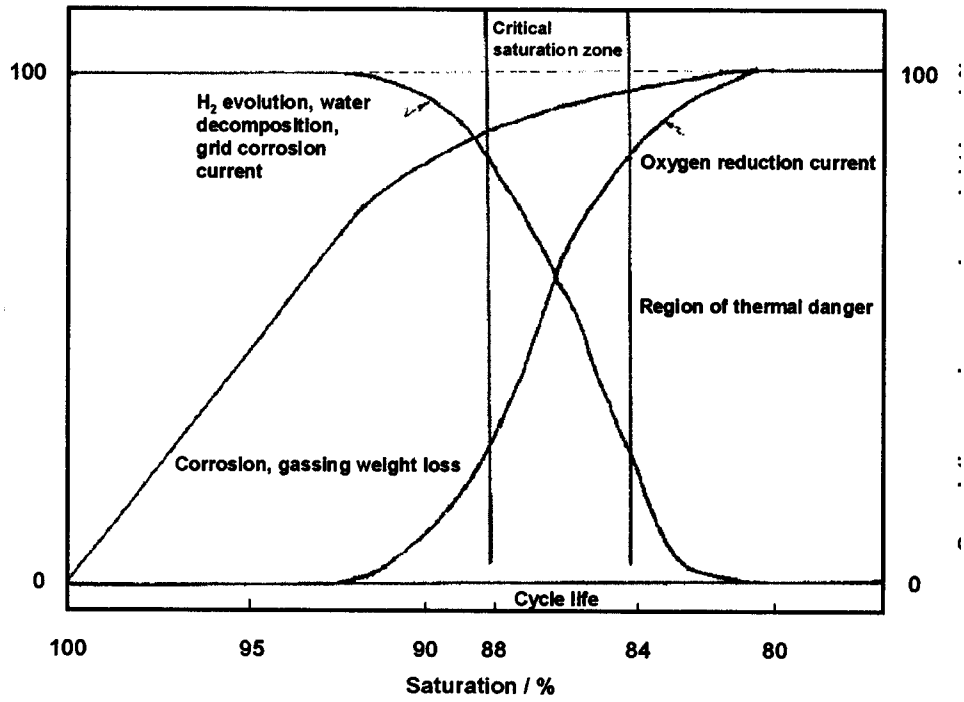

Fig. 9.14. Relative distribution of overcharge current as a function of VRLA saturation level between H_2 evolution/H_2O decomposition/grid corrosion and the oxygen cycle throughout cycle-life.

overcharge current going into the other parasitic processes drops and the water loss and corrosion rates drop sharply (note the similarity to the curve shape and position relative to percentage of saturation in Fig. 9.11). Shortly after this, the 'region of thermal danger' is entered; here, virtually all of the overcharge current is going into heat production and the gassing rate has dropped off dramatically. This is also the region where full recharge becomes difficult or impossible due to the excessive current draw for the oxygen cycle. If the finishing current is not sufficiently high, recharge cannot be completed; but the more the overcharge current that is applied, the greater is the heat generation and build-up. As shall be seen in Section 9.4.2, this condition can only be overcome by novel approaches to charging and, even with these, a 'thermal wall' is hit that cannot be counter-acted without changes in design and materials. Thus, it is not cell failure or undercharging in the traditional sense that limits VRLA battery life but a condition where higher finishing currents cannot be applied because of dangerous heat build-up.

Beyond the considerations above in the 'region of thermal danger', there are several other important points that can be gleaned from Fig. 9.14, as follows.

- As noted earlier, new VRLA batteries behave very much like flooded products in overcharge for a period of time; the saturation level is so high (95% +) that gas paths between the plates are not created during overcharge, and thus the plates finish charge independently;
- At about 92 to 90% saturation, gas paths begin to form before recharge is completed and some oxygen reduction occurs. If the charge factor is fixed, this necessarily demands that the amount of charge going into the other processes drops, as does the rate of weight loss (cf., Fig. 9.12);
- The position of the critical saturation zone can be controlled somewhat through changes in materials and design that all relate to changes in fluid dynamics in the separator; anything that makes the creation of significant numbers of gas paths more difficult 'buys time' to complete recharge;
- The ease of creation of gas channels is not linear with percent saturation but is, rather, exponential. This makes it imperative that the amount of overcharge per cycle (or float charge per unit time) be minimized, as this reduces the rate of decrease of saturation levels;
- After the critical saturation zone has been passed, water loss and grid corrosion become minor processes, and the primary concern in VRLA recharging becomes how to handle the oxygen cycle and the resultant thermal build-up;
- If at all possible, this should be done with minimal increases in the charge factor, as more overcharge only accelerates the above processes.

Clearly, this is a different situation than that experienced with flooded lead–acid products. The dominance of the oxygen cycle changes the distribution of the overcharge current and, thus, it must change how VRLA batteries can be charged effectively. In cyclic charging, it will be seen that the rate of the finishing charge is much more important than the amount of overcharge. In float charging, it is critical either to minimize the amount of charge or keep the saturation level as constant as possible; in practice, both of these can be done.

9.3. Existing Charging Methods Applied to VRLA Products

As noted earlier, most VRLA products are charged in both float and cyclic applications much as flooded batteries have been charged for nearly 100 years. For float, this means conventional CV charging, possibly with temperature compensation. For cyclic charging, either IU or IUI methods are used, but in both cases the finishing steps are relatively long and are at low currents. As has been seen, this may not be the best approach for obtaining maximum lifetimes out of VRLA products, but all have been successful in obtaining reasonably good lifetimes in a variety of applications. Because of this, most of the battery world continues to use these conventional approaches, so it is useful to review them in more detail, as follows.

9.3.1. Float charging

Back-up, or standby, power applications involve the charging of a cell or battery string in such a way that it is always at full capacity should the mains power fail and it becomes the sole mode of maintaining the device that it supports. The most common applications are back-up for distributed-power telecom systems and uninterruptible power supply (UPS) systems for computers, burglar alarms, emergency lighting, etc. In such service, the battery string must not be heavily overcharged as this will drastically shorten the desired lifetime of some 6–10 years. This creates a delicate balancing act in that all of the cells in what may be a very large series string or a series–parallel array must be maintained in a narrow range of SoC at all times. This is almost always done by applying a CV charge that is a multiple of the charge voltage of 2.25–2.40 VPC, as determined by the relative density of the electrolyte. Because self-discharge rates are significant for many VRLA products, charging is usually continuous between interruptions in a.c. power.

The above charging approach has been used successfully for many years for flooded lead–acid batteries. Although such batteries are susceptible to serious performance problems, mostly related to impurities and resultant variations in charging voltages and grid-corrosion levels, the cell-to-cell variability is usually quite low for a given battery installation. Thus, the use of per-cell multiple charging voltages (i.e., nominal VPC times the number of cells) can be used with the assurance that each cell will adopt roughly the same charging voltage. It is still possible to undercharge or overcharge a flooded lead–acid standby battery on CV float, but if this happens all of the cells will be affected in a roughly uniform fashion. In addition, these batteries are generally quite large with correspondingly great electrolyte reservoirs. The gas stoichiometric ratios of oxygen and hydrogen on float and the amounts of these gases are roughly equivalent to the magnitudes of the charging currents which, as have been seen, are relatively low. Thus, the batteries have excellent thermal stability and, in fact, cannot fail due to thermal runaway (for a detailed explanation of the various factors involved in thermal runaway, see Ref. [3]).

Voltage uniformity does not exist in VRLA batteries unless all cells are fully saturated — and even then, this will change as water is lost and electrolyte is re-distributed from the separator into the plates. As noted previously, the ease of

oxygen transport is directly related to the saturation level, so when cells vary in their void volumes there will be a comparable variation in oxygen-recombination current. This, in turn, creates variations in voltages on float. While the individual voltages will add up to the applied string voltage, they are likely not all the same. An example of this is given in Table 9.1. This is a listing of half of the cell voltages in a series–parallel array of 2 × 24-Ah VRLA cells. Initially, there is a relatively small variation in cell voltage (90 mV), but this varies with time through 106 days, at which point the spread is 250 mV. Individual cell voltages 'bounce' around with time, which is typical of VRLA cells on float. Even though the applied string voltage is set at 2.28 VPC, the voltage of cell 32 on day 106 is well below the open-circuit value (2.15 V) and cell 30 is clearly in the gassing region (2.40 V). This is reinforced by the data shown in Table 9.2 for a different type of VRLA product in a single 12-cell string. Here, not only voltages but also gas volumes are recorded and, again, it is seen that even though the nominal float voltage is just below the gassing potential (2.35 VPC), several cells are gassing fairly heavily [20].

Table 9.1. Individual cell voltage data for 300-Ah prismatic cells in a 48-V/600-Ah array floated at 2.28 VPC.

Cell number	Original voltage (V)	Voltage at 30 days (V)	Voltage at 78 days (V)	Voltage at 106 days (V)
2	2.25	2.25	2.22	2.24
4	2.25	2.31	2.42	2.37
6	2.27	2.25	2.24	2.24
8	2.26	2.25	2.24	2.24
10	2.31	2.27	2.27	2.26
12	2.26	2.29	2.38	2.31
14	2.26	2.24	2.23	2.23
16	2.27	2.21	2.18	2.20
18	2.26	2.24	2.22	2.22
20	2.32	2.29	2.30	2.31
22	2.26	2.32	2.18	2.20
24	2.29	2.24	2.23	2.23
26	2.25	2.31	2.32	2.25
28	2.25	2.37	2.39	2.34
30	2.27	2.28	2.32	2.40
32	2.32	2.22	2.14	2.15
34	2.27	2.25	2.15	2.22
36	2.27	2.22	2.28	2.24
38	2.29	2.28	2.28	2.28
40	2.26	2.26	2.22	2.24
42	2.27	2.24	2.22	2.23
44	2.27	2.22	2.17	2.22
46	2.30	2.27	2.30	2.34
48	2.23	2.22	2.20	2.22
Range (mV)	80	160	280	250

Table 9.2. Float voltage and gassing characteristics in a 24-V/5.0-Ah cell string floated at 2.35 V/cell.

Cell number	Pre-float OCV (V)	Float voltage[a] (V)			
		Float time (h)			
		0	16	24	42
1	2.126	2.30	2.37	2.42	2.41
2	2.126	2.22	2.25	2.27	2.28
3	2.129	2.22	2.22	2.22	2.22
4	2.132	2.24	2.24	2.29	2.31
5	2.132	2.57 (0.0)	2.48 (12)	2.45 (21)	2.43 (35)
6	2.135	2.21	2.23	2.22	2.23
7	2.135	2.24	2.26	2.37	2.39
8	2.139	2.38	2.46	2.35	2.38
9	2.140	2.55 (0.0)	2.24 (50)	2.26 (55)	2.26 (57)
10	2.140	2.38	2.51 (8)	2.48 (26)	2.45 (46)
11	2.140	2.36	2.48 (10)	2.45 (24)	2.42 (36)
12	2.142	2.38	2.48	2.43	2.41
Float voltage variation (mV)		36	29	26	23

[a]Numbers in parentheses are ml of gas evolved. Gas composition is exclusively hydrogen and carbon dioxide.

This illustrates a critical point in CV float charging of VRLA arrays, namely, individual cell voltages on float can and do vary significantly in both directions from the nominal voltage that is applied per cell. This is the major problem with conventional approaches to float charging of VRLA batteries. The variation in cell voltage may even out somewhat over time (as opposed to the data in Table 9.1), but the duration may be substantial for some battery designs because, as seen, some cells will float at low voltages and some will be high. Those that are high (relatively high saturation levels) will gas and lose water, which will lower their saturation levels and thus lower their voltages on float. This will bring up the low-voltage cells because the sum of the individual cell voltages must add up to the applied string voltage. The net result is a tightening of the voltage spread, but because the average saturation level has been reduced the float current will increase somewhat. As the battery as a whole ages, the voltage range of the population will narrow and approach the applied VPC value as it loses weight and the saturation level decreases further. The float current will increase because it will require a higher charge input to maintain the nominal VPC as the oxygen cycle strengthens. This strengthening of the oxygen cycle makes it more likely that one or two cell voltages may drop sufficiently to be below their respective open-circuit values, even though all the cells are on charge (this may have been even more likely when the string was new due to the presence of a number of high-voltage cells).

The operation of the oxygen cycle in VRLA batteries is a 'knife edge' of sorts. A properly working cell will have enough void space for limited oxygen transport, but at the same time it must have sufficient electrolyte to provide the needed nominal discharge capacity; thus, the initial ~95–98% saturation level. In this state of 'almost flooded/almost starved' electrolyte saturation, effective float charging of all cells becomes an exercise in 'dancing on the head of a pin' [21,22]. The phenomenon is illustrated in Fig. 9.15. On the negative plate, the primary $Pb/PbSO_4$ reaction occurs in a narrow potential range. The secondary reaction of hydrogen evolution, while kinetically hindered, does take place at a low level in the same voltage window, but it becomes significant in terms of current draw at higher potentials, typically ~350 mV higher (to the left). The negative plate 'ideal' float zone is a potential sufficient to drive the $PbSO_4/Pb$ reaction to completion, but not so high as to promote hydrogen evolution. If the potential drops too much (moves to the right), the risk is run of partially discharging the lead electrode. In practice, this can occur if and when significant levels of oxygen reduction take place, as its reversible potential for conversion back to water (the vertical arrow just to the left of the *y*-axis in Fig. 9.15) is well below the open-circuit value for the negative electrode.

The picture is somewhat more complicated at the positive electrode. Again, the float voltage must be sufficiently positive to drive the $PbSO_4/PbO_2$ reaction to completion and maintain it, but this must be balanced against the secondary

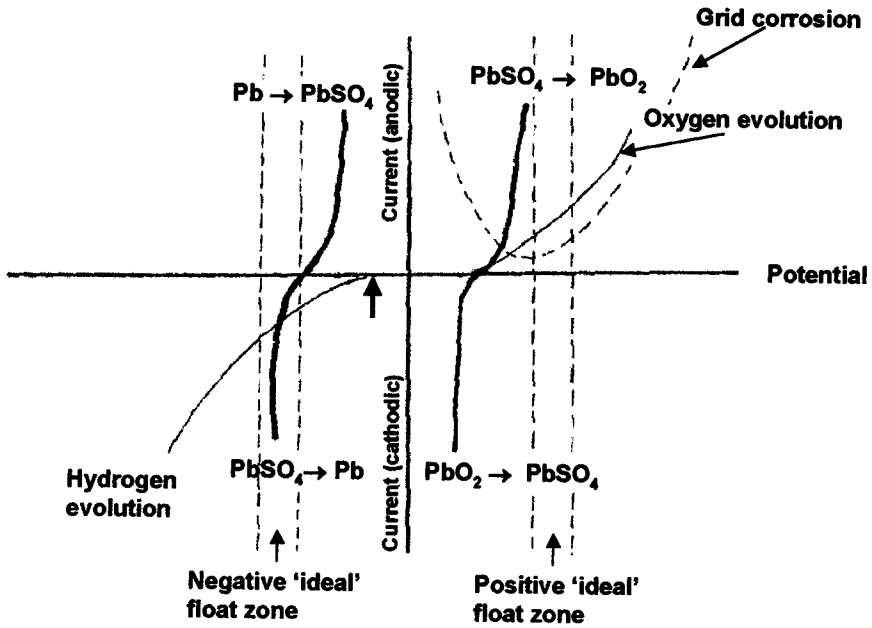

Fig. 9.15. Representation of primary charge–discharge processes and overcharge reactions in VRLA cell. Vertical arrow just to the left of *y*-axis denotes potential for oxygen reduction to water.

reactions of water decomposition and grid corrosion. Water decomposition, like hydrogen evolution at the negative, is kinetically hindered and becomes significant about 500 mV above (to the right of) the reversible $PbSO_4/PbO_2$ potential. Grid corrosion is a more complex parabolic relationship with a minimum roughly 100 mV above the reversible potential [23]. Again, a positive-plate 'ideal float zone' exists, and it is a compromise between the three processes. If this zone shifts to the right (higher positive-plate polarization), grid corrosion and water decomposition rates become large. If it shifts to the left (depolarization of the positive plate), partial discharge will take place and the grid corrosion rate also increases.

The voltage difference between these two zones is the nominal applied float voltage. If charging is done on an individual-cell basis (such an approach was pioneered by Ericsson in Sweden in the early 1980s), then these zones can be fairly well maintained. Almost all VRLA float applications, however, involve applying a string voltage instead. For example, a 48 V-telecom battery will be charged at, say, 54.5 V, which is 2.27 VPC. As seen in Tables 9.1 and 9.2, this does not ensure that all cells will be at 2.27 V; in fact, it is well known that indeed this is not the case. Because of the oxygen cycle, there is a tendency in some cells with the lowest saturation levels to experience a drop in the negative-plate voltage to the point where partial discharge occurs, as noted earlier. This also further raises the potential of the positive plate, producing more oxygen and grid corrosion. The oxygen produced by more water decomposition will then complete the cycle and further 'drag down' the negative plate, thus intensifying the process.

The variation in string voltages is fundamentally tied to variations in saturation levels [12,24], but it is so pronounced because the float process is, by design, such a 'balancing act' of minimal charge voltages and currents. The aim is to ensure that the battery (and all of its individual cells) is fully charged, but the charging should not be so strong that battery life is shortened. All of the above examples use CV charging, but the use of low-level CC charging, while feasible, results in the same scenario. Low charging currents and voltages allow individual VRLA cell voltages to 'wander' due to the variable influence of the oxygen cycle. In cells, float voltages can and do vary significantly over time (see Tables 9.1 and 9.2), probably due to small perturbations of the gas-transport process through the glass-mat separator, with fluid movements shutting off some gas channels and creating others in a somewhat random fashion. Because of the low float current and resultant miniscule oxygen-generation rate, there is not a sufficient stream of electro-generated gas to maintain a consistent fluid distribution in the glass-mat separator.

Added to this are the vagaries of VRLA standby applications, which are often poorly controlled in terms of charging equipment (e.g., significant voltage drift and minimal power-line filtering, exposing the battery to significant levels of a.c. ripple currents) and temperature (e.g., little or no environmental control, modules packed together, sometimes in proximity to rectifiers). Since predicted lifetimes are often estimated from accelerated testing done under tightly controlled laboratory conditions [25], it is little wonder that VRLA batteries have not performed as expected in standby applications. In summary, it is clear that conventional CV or CC float string charging is not reliable for VRLA products. Some new approaches that

are being applied and which promise to extend field lifetimes significantly in these demanding applications are discussed later in this chapter.

The above data on float charging of VRLA batteries raise several significant points:

- because of differences in saturation levels, VRLA cells in series strings will float at different voltages unless they are individually charged
- conventional CV or CC float charging is such a delicate 'balancing act' that the energy applied to the string is not sufficient to affect this voltage spread greatly
- there is some leveling of voltages over time as high-voltage cells are drawn down due to gassing/corrosion water loss, and low-voltage cells are pulled up due to the necessity for all cell voltages to add up to the string voltage; this can result in an increase in float current
- if there is enough variability and/or some cells are sufficiently under-saturated, the discharge capacity of the string can be reduced by partial discharge of negative plates in some of the cells
- this partial discharge (see above) is apparently due to extreme depolarization of some cells due to excessive oxygen transfer to the negative plate; this condition can worsen as cells age and saturation levels decrease due to fluid removal from the separator via several well-characterized mechanisms.

9.3.2. Cyclic charging

In cyclic charging, the condition of 'dancing on the head of a pin' that exists under float conditions must be avoided because of the higher voltages and currents that are employed. Even here, however, the oxygen cycle introduces unique challenges not seen in comparable flooded lead–acid products. With high-voltage/high-current recharges over several hundred cycles, VRLA technologists have, perhaps, become pre-occupied with dry-out and grid corrosion as life-limiting factors. The result has been that many VRLA batteries fail due to undercharging rather than to excessive overcharge, shown pictorially in Fig. 9.16. Clearly, overcharge will shorten life relative to an 'ideal' cycle-life, particularly if it is severe (dotted line), but undercharging will shorten lifetime even more, with a gradual walk-down in capacity beginning as early as within the first 10–20 cycles. This has become even more the case as corrosion-resistant alloys have been developed for VRLA products, producing a resurrection of PCL-1 failures due to interface passivation reducing the effectiveness of CV charging. These alloys also offer the possibility of greater resistance to overcharge, opening up new possibilities for VRLA products.

Still, most cyclic charging is done with simple IU or IUI algorithms. In both cases, a current-limited CV charge is applied (the IU step), followed by a second current-limited CV charge at a higher voltage or with no voltage limit for the IUI finishing step (Fig. 9.6). For flooded lead–acid batteries this is not a problem, as the two plates charge independently and the oxygen cycle has little or no effect. Here, low finishing currents present no difficulty and the biggest issue is the time required to finish the recharge. Higher currents and voltages will accelerate the recharge, but this may result in more overcharge for products with poor charge-acceptance.

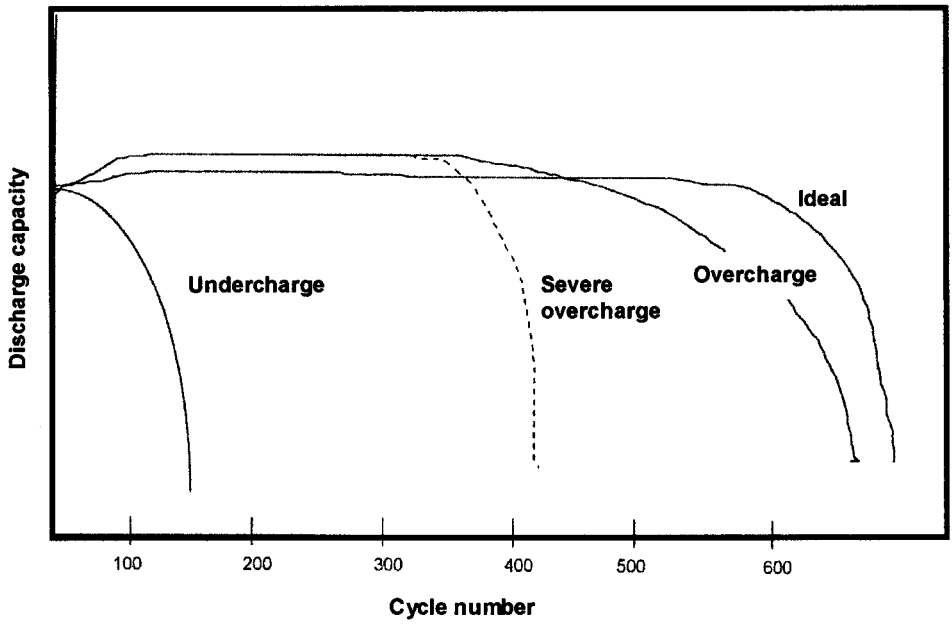

Fig. 9.16. Representational cycle–capacity curves for various overcharge conditions for VRLA battery. The *y*-axis is in arbitrary units with all curves starting at 100%.

For VRLA batteries, CV charging is an effective approach, but it will only result in cycle-lives of 200–300 in many cases and, further, there is the danger of the battery going into thermal runaway. This will not happen early in cycle-life, and the battery may, in fact, have failed to deliver 80% of rated capacity before end-of-charge currents rise to dangerous levels. If cycling is continued and more void space is created by grid corrosion and water loss, the finishing current can, in the extreme, rise to the original current limit, which is typically in the range of C_5–C_3. Such behaviour will occur because the end-of-charge voltage is severely reduced due to high levels of oxygen reduction, and at the end of charge the battery will go back to current limit in an attempt to achieve the nominal charge voltage. Thermal runaway will eventuate because virtually all of this high finishing current is being converted to heat by the oxygen cycle, whereas, at the beginning of charge (the current-limited portion of the CV charge), virtually all of the current is going into active-material conversion.

What is insidious about this chain of events is that they happen within relatively few cycles (not in a linear fashion), as shown in Fig. 9.17 for an IUI charge process. To some extent, the cycle interval for this transformation is a function of plate thickness and spacing; the greater these values the slower is the change. The end-of-charge voltages and currents for deep cycling of a 12-V/50-Ah, spiral-wound VRLA battery are shown in Fig. 9.17; plate thicknesses and spacings are of the order of 1.0–1.2 mm. There is a gradual drop in capacity, which reaches the 80% cut-off point in only 133 cycles, and at cycle 312 the capacity drops to 50% of rated. The switch to a 2-A/1-h finishing step (no voltage limit) is when a 1-A current taper point is

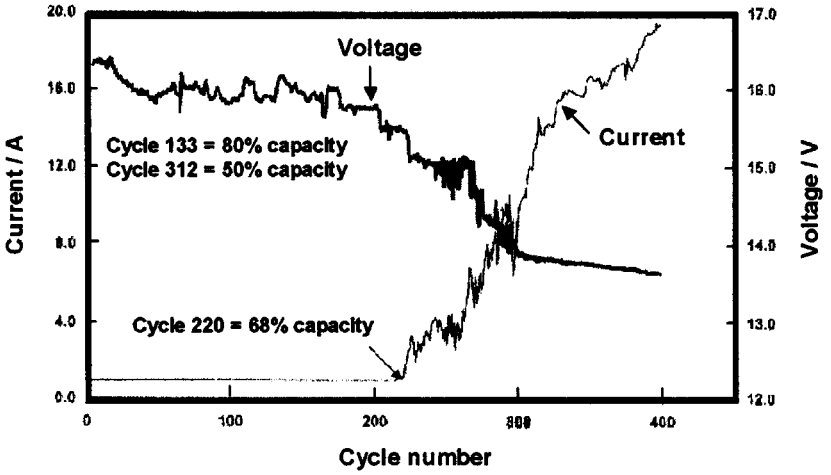

Fig. 9.17. End-of-charge voltage (CC finishing step) and end-of-charge current (CV step) as function of cycle-life for 12-V/50-Ah VRLA battery using the standard Optima IUI recharge algorithm.

reached on the CV charge or at a charge factor of 1.2, whichever occurs first. As can be seen, the 1-A current taper level is reached before the 1.2 charge factor out to cycle 220, at which point the CV end-of-charge current begins to rise steeply when the charge factor is reached. At cycle 400, cycling is terminated due to the battery temperature approaching 70°C at the end of the CV charge. At the same time that the CV end-of-charge current is rising, the voltage at the end of the finishing CC charge is dropping and eventually flattens out at ~ 13.7 V. This is typical behaviour created by an increasingly strong oxygen cycle as the battery ages. Initially, the IUI charge algorithm works acceptably because of the relatively high saturation levels in the cells, which allows for a full recharge before the oxygen cycle begins. At some point, however, the saturation levels reach a 'trigger' point where the amount of overcharge current from oxygen reduction grows exponentially (refer to Fig. 9.11 for a corresponding decrease in saturation), and the switchover to the finishing CC step has to be done sooner and sooner on the taper portion of the current-time curve. Even at that, the 2-A current magnitude of the finishing step (here, a C_{25} level) is not sufficient to recharge the battery fully because the current draw for oxygen reduction exceeds this value and grows cycle-to-cycle. When the finishing current amplitude is less than the steady-state current draw for the oxygen cycle the battery must, necessarily, be undercharged. In fact, because the discharge capacity reaches the 80% failure level at only 133 cycles, it is clear that, for this product, this type of IUI algorithm is not adequate.

Better results using IUI charging have been reported recently in other programs. In the ALABC European Brite-EuRam IMPLAB program, cycling results on thick-plate (2–3 mm) single cells with experimental separator configurations exhibited deep-cycle lifetimes of some 327–750 cycles [26]. In evaluating these results, it should be kept in mind that the cycle-lives of these types of cells in 12-V batteries would be likely to experience decreases of some 30–50%. Even earlier work

showed that thick-plate AGM single cells and batteries could be cycled to 300–600 cycles using a simple IU charge algorithm with a 2.40 V limit [27,28]. Work reported by FIAMM focused on IUI charging and ways to minimize gas emissions and weight loss [29]. This was achieved by using fast-charge techniques with minimal overcharge, but the approach employed a low-voltage CV step (2.37 VPC) and this increased the recharge time. A low finishing current (0.005 C_5) was also employed, which would do little to overcome the oxygen cycle and complete recharge as the battery ages.

A more recent study looked at the effects of inrush current, charge voltage, and the nature of the finishing step using various IUI algorithms [30]. Work was carried out with 12-V/60-Ah and 6-V/180-Ah, VRLA commercial products with relatively thick plates (2–3 mm or more). Deep-cycle lifetimes of 500–700 cycles were obtained, and it was found that high-inrush currents and high charge voltages, i.e., fast charging with a low charge factor, gave superior lifetimes. Still, it was found that the charge factor slowly increased through cycling, starting at $\sim$1.08 and finishing at $\sim$1.15. Concerned with this, the authors used a finishing charge level of C_{50} and proposed using even lower levels to minimize grid corrosion.

Another study, employing 3-step CC charging on a 144-V string composed of 12-V/60-Ah modules, found that fast charging with minimal overcharge gave superior results [7]. It was determined that using the same charge algorithm (30, 12, 2A) with variable times for finishing produced markedly different results. With a continuous charge factor of 1.15 (charge time of $\sim$5 h), a cycle-life of 310 cycles was obtained with an energy efficiency of $\sim$74%. Failure was reportedly due to sulfate build-up at the bottoms of the negative plates. With a charge factor of 1.05 (charge time of $\sim$4 h) and a 1.15 charge factor conditioning charge every sixth cycle, a lifetime of 431 cycles was realized with an energy efficiency of 82.5%. Interestingly, autopsy of these cells showed sulfate build-up at the tops of the negative plates. Recent work by Panasonic on a 12-V/60-Ah, EC-EV1260 battery, using a 5-step CC charging algorithm, has also produced superior results [31]. With a standard DST120 discharge step, this battery yielded $\sim$1200 cycles to 80% of rated capacity.

Given these studies, it is apparent that application of traditional current-limited CV charging (IU algorithm), with (IUI) or without (IU) a CC finishing step, can yield good results with VRLA products; but it is also apparent that more can be drawn from these batteries due to the almost-universal failure mode of PAM softening and/or negative-plate sulfation. As with float charging, there are some significant points that emerge from the studies cited above:

- deep-cycle lifetimes of 300–600 or more can be realized using simple IU or IUI algorithms or multi-step CC charging on thick-plate VRLA cells and batteries;
- rapid charging (of the order of a few hours) with minimal overcharge appears to significantly extend cycle-life for a variety of products;
- all these studies use low finishing currents to minimize gassing and grid corrosion;
- charge factors tend to increase throughout cycle-life, typically beginning at 1.05–1.10 and gradually rising to 1.15–1.20.

All these observations are consistent with the mechanism that has been developed for VRLA products where the strength of the oxygen cycle increases as the cell/battery ages and the saturation level correspondingly decreases. Fast charging with minimal overcharge is necessary to minimize the amount of charge going into the parasitic oxygen cycle. With the low finishing currents employed, however, it appears that eventually even this approach fails. None of these studies included temperature data, which would have been helpful in possibly attributing the results directly to the oxygen cycle.

9.3.3. Fast charging

Up until about 10 years ago, it was believed that lead–acid batteries of any type could not be fast charged because there would be irreparable damage to the positive active-material. In addition, in VRLA batteries, it was felt that this approach would result in excessive levels of grid corrosion and gassing, leading to early, rapid failure. Rapid charging of sealed Ni–Cd cells and batteries was first proposed by Kordesch [32] and was subsequently developed by Norvik Technologies in commercial products. Using their Minitcharger^{TM}, it was found that it was possible to recharge deep-discharged Ni–Cd products fully in 5–10 min because of the endothermic nature of the charging process (except for overcharge) [33].

In the early 1990s, Valeriote at Cominco advanced this technology for, first, flooded lead–acid batteries [10] and, later, for thin-plate VRLA products ([34] and references therein). This approach is a variant of standard current-limited CV charging, but using a so-called constant 'resistance-free voltage' (RFV). The RFV value for any product is offset somewhat from the normal CV value by an amount proportional to the *IR* magnitude for the battery being charged; the technique is illustrated in Fig. 9.18 [34]. Following a deep discharge, a RFV charge begins with a low current and voltage 'spike' due to the high resistance of the discharged battery; voltage then drops sharply and the current rises to the current limit, I_{LIMIT}. The applied voltage, V_{APP}, rises as the battery charges, reaching a maximum value of $V_{APP} = V_{RF} + IR$. The voltage and current then decrease until $V_{APP} = V_{RF}$. This is done using ohmic-compensation feedback circuitry that reduces the applied voltage as the ohmic component decreases. Using this approach, it was found that ~ 50 Ah flooded lead–acid, gel, and AGM batteries could be fast charged to 80% SoC within 15 min or less, with a temperature rise of less than 25°C. In order to realize these rapid charge times, a high-inrush current limit of $\sim 5\,C$ (here, 250 A) must be used. It was found at these rates that ohmic factors dominate heat generation up to 40–50% SoC, at which point polarization and enthalpic heating become dominant, particularly in VRLA batteries. Given this, it was found that flooded batteries experienced lower temperature rises due to their high gassing levels (an effective source of heat dissipation) and greater volumes of electrolyte (a heat sink effect), in spite of their higher battery resistances. In VRLA batteries, minimal resistance (thin plates, glass-mat separator) and a design optimized for effective heat dissipation were found to facilitate fast charging, but overheating was still more of a problem than for flooded products.

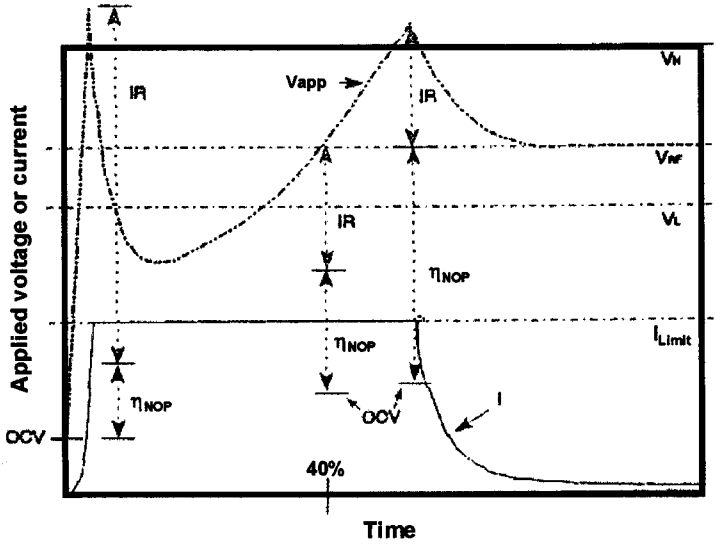

Fig. 9.18. Schematic illustration of constant resistance-free-voltage charging [33].

This work was later extended to a wide range of lead–acid products in ALABC programs RMC-002, RMC-009, and A001.3. Follow-on ALABC work has extended the Cominco pioneering studies to commercial applications (Project A001.1). Later work on Hawker Genesis, thin-plate, prismatic VRLA products [35] demonstrated that simple CV charging with current limits of up to 9 *C* could be carried out on individual batteries in laboratory tests. With a 6 *C* current limit, 80% charge return from 0% SoC was done within 10 min. Field testing on a full pack in an hybrid electric vehicle (HEV) duty cycle using a 5 *C* current limit also showed good results.

Given all of this, it is now abundantly clear that thin-plate, VRLA batteries can be fast charged with excellent results. Contrary to previous beliefs, for a given VRLA product, the imposition of aggressive charging algorithms that minimize the effects of the oxygen cycle and finish the charge relatively quickly, can result in superior cycle-lives.

9.3.4. Charge-termination strategies

In cyclic charging, the method of termination can be as important as the charging algorithm itself, in some cases more so. Again, this is because the growing presence of the oxygen cycle changes the dynamics of charging, particularly during the finishing phase, to a significant degree. With flooded lead–acid batteries, the point of termination and the charge factor can remain fairly constant because the shape of the voltage–time charge curve does not change greatly throughout cycle-life. Charges are always terminated based upon time or Ah input (charge factor), and the amount of overcharge is fairly constant.

With VRLA products, the amount of overcharge needed increases with cycling as the amount of charge drawn by the oxygen cycle gradually grows. This is in contrast to Ni–Cd charging, where the shape of the voltage–time curve remains almost constant because the saturation level varies little throughout the cycle-life. Thus, termination points such as 'zero $\triangle V$' or '$-\triangle V$' can be used for Ni–Cd batteries, as shown in Fig. 9.19 [36]. For VRLA batteries, a fixed amount of overcharge (fixed charge factor, 1.05–1.20) or a timed charge can be used for the first 100–200 cycles when the saturation level is high and recharge performance is much as it would be for a flooded lead–acid product, as seen in Fig. 9.19, solid line. As VRLA batteries are cycled, however, the charge factor must be increased to account for the oxygen cycle, so use of a fixed charge factor will eventually result in undercharge (see also Fig. 9.12). Use of a timed charge with CC charging will also lead to undercharging and, with CV charging, it will result in significant overcharge and, in the extreme, thermal runaway due to increasing current draw at the end of the charge 'tail'.

Further complicating the picture is the fact that, as VRLA batteries age, the shape of the voltage–time charge curve collapses and lowers as shown in Fig. 9.19, dotted lines. For these situations, the use of a zero $\triangle V$ or $-\triangle V$ termination strategy with CC charging may result in continuous charge, as the $\triangle V$ events are no longer as well defined as they were initially and the resultant gradual voltage slope change may not be sensed; a circumstance that may lead to significant overcharge. As most VRLA charges are still done with IU or IUI charging, termination is based upon time with a switch to the finishing CC step, or they use some form of

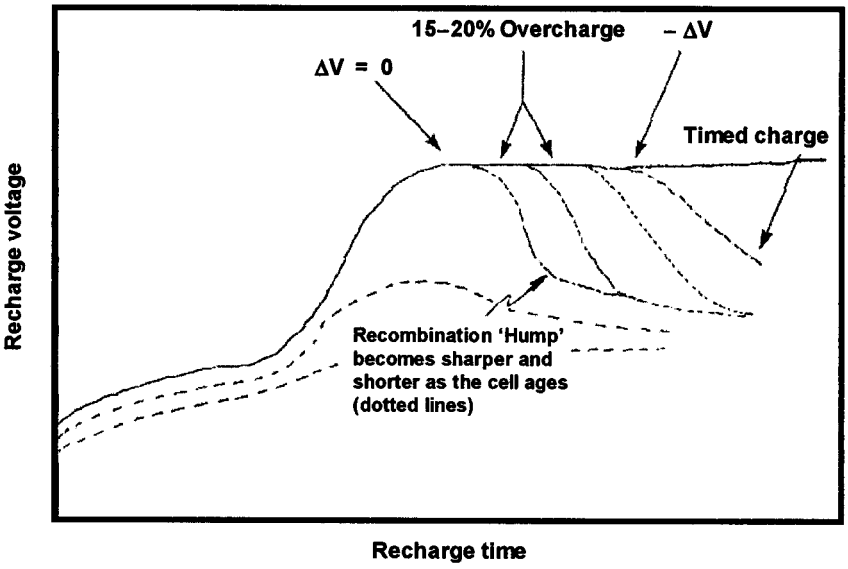

Fig. 9.19. Various termination methods as they relate to recharge time. As VRLA cells age, recombination 'hump' shortens and maximum voltage drops; eventually, charge voltage stays just above open circuit throughout the charge.

logic similar to that described in Section 9.3.2. These types of considerations are more relevant for thin-plate products because they develop active oxygen cycles earlier in life. Thick-plate products can go for several hundred cycles before their saturation levels drop to a point where the oxygen cycle becomes a dominant factor in overcharge.

In practice, some form of iterative process is best used to obtain maximum cycle-life with VRLA products; a fixed algorithm will eventually fail, even for thick-plate products. The simplest approach is to apply a step-wise increase in charge factor once the performance of the battery has been characterized, e.g., 1.05–200 cycles, 1.10 for 200–300, 1.15 for 300–400 and so on. For each product the timing of the increases will vary, depending upon the initial saturation level and the plate thicknesses. For CC charging, time could also be lengthened throughout cycle-life but this is a cruder approach that will probably not be optimal.

9.3.5. Failure modes attributable to charging

VRLA batteries often fail for different reasons than seen for flooded lead–acid products. The latter usually fail due to grid corrosion or growth or to PAM softening or both. These are easily understood failure modes that can be addressed to some extent through materials/design changes or by changes to the charging/termination algorithm.

VRLA batteries are subject to a number of potential failure modes that can be linked to charging. In fact, it is rare that they will fail in cyclic duty due to fatal grid corrosion. In the early days of the ALABC research program, the first major task was to extend the cycle-life of the positive plate in EV-type applications. In the early 1990s, most VRLA batteries failed in cycling either within the first few cycles or within 100–200 cycles, as shown schematically in Fig. 9.20 [37]. So-called 'PCL-1' was found to be a grid|PAM interface effect where a passivation layer formed with grid surfaces that were resistant to grain-boundary corrosion; the development of Pb–Ca–Sn alloys has, in most cases, overcome this. PCL-2 is a condition within the PAM where connective PbO_2 preferentially sulfates and is resistant to recharge;

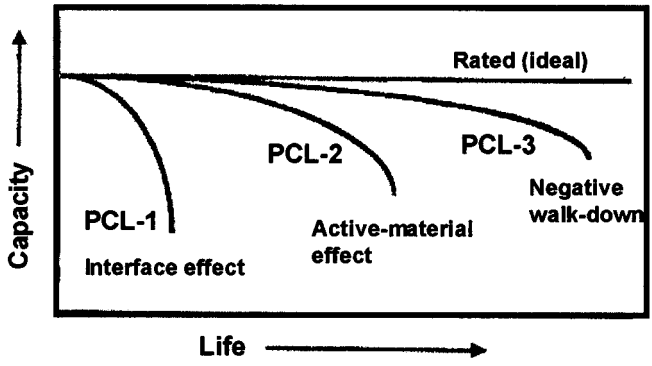

Fig. 9.20. Three categories of premature capacity loss (PCL) in deep-cycling applications.

this causes progressive isolation of portions of the PAM. Chemical additives such as H_3PO_4 and tin salts have a beneficial effect, but the greatest improvement has come from higher plate-stack compression levels and the use of separators that have greater 'spring-back' properties.

PCL-3, called here 'negative walk-down', is really the subject of this chapter. It has also been referred to as 'insufficient negative-plate recharge' and has been identified only recently as a major failure mode for VRLA batteries [38–40]. As noted, it occurs when the oxygen cycle becomes so strong during recharge that most or all of the overcharge current is drained off and largely converted to heat (with a minor amount sometimes going into oxygen venting). It is often accompanied by progressive sulfation of the bottom areas of the negative plates, apparently due to extreme depolarization and sulfation which then sets up a voltage gradient that makes recharge more difficult.

Several other failure modes can and do occur with VRLA batteries in both float and cyclic applications, as follows.

- Reversible capacity decay or reversible insufficient mass utilization (RIMU), perhaps another term for PCL-2 [41]. This is a phenomenon explored by Winsel, Meissner and co-workers at Varta where capacity loss can be reversed by changes in charging algorithms or by chemical modifications as noted for PCL-2.
- Negative top-lead corrosion, a phenomenon related to overcharge and oxygen recombination occurring on the top lead, creating water that leads to an alkaline condition with calcium alloys that then results in runaway corrosion of the negative top-lead material [42]. The condition is easily avoided by coating the top lead with acidified gel or wrapping it with glass-mat separator soaked with acid and contacting the functional separator in the plate stack.
- Acid stratification is a situation that is common in flooded lead–acid batteries if equalizing charges are not applied periodically, charges that create vigorous gassing that physically mixes the electrolyte. With cycling, small changes in acid relative density top-to-bottom are amplified due to gravity effects, with a gradual increase in density at the bottom of the cell. This also occurs in VRLA products that employ very high saturation levels and/or low surface-area or so-called 'hybrid' (glass/organic fibre) separators. It is further aggravated by low compression levels; this, by itself or together with the above factors, results in insufficient retention of electrolyte during cycling. The more a VRLA cell resembles a flooded lead–acid product, the more likely acid stratification is to occur. It is also more likely to take place in tall cells and batteries (which are, as a result, often used in a horizontal position). If present in a given design, it can be avoided by changing the orientation of the battery on cyclic charge periodically, as this is largely a gravity effect [43].
- Acid drainage is an extreme case of gravity effects in VRLA cells. In very tall cells or in cells built with low surface-area or glass/organic hybrid separators combined with low compression levels electrolyte can actually 'pool' in the bottom of the cell, even at moderate or high saturation levels. This creates a condition where the bottom of the cell charges as if it were a flooded lead–acid cell (which it is) and the upper portions of the cell try to function as a normal,

or even low-saturation, VRLA product. This condition has not been studied extensively, but it is certain that it will not result in long cycle or float lifetimes. It is not easily corrected.

- Negative-plate densification can occur as an alternative to PAM failure in highly compressed products such as the spiral-wound Optima 12-V/50-Ah battery studied by Cominco [44]. It was found that when positive-plate growth and expansion occurs in a tightly compressed cylindrical design the soft negative-plate sponge lead densifies, which can contribute to failure due to a loss of porosity. Interestingly, this failure mode has not been reported in a variety of other ALABC projects that employ comparable or higher compression levels than those in the Optima spiral-wound product. In the Cominco work, it was found that this process was operative in both conventional and fast-charge processes.

Other common VRLA failure modes such as dry-out, water consumption, and grid growth/corrosion have been well documented in the literature [45,46].

9.4. Evolving and Optimized Charging Methods

Given all of the foregoing, what are the best ways to float and cyclic charge VRLA products? To some extent, it depends upon the application and the expectations of the user. If optimal lifetimes are the goal, then much can be said about how these products could be charged. In a word, most of the existing commercial methods are not likely to be successful in pursuing this goal. As has been noted, these methods are based largely upon flooded lead–acid technology, which is not affected by the oxygen cycle. The oxygen cycle really changes everything and brings VRLA closer to nickel–cadmium chemistry, particularly in terms of charging. For both float and cyclic charging, it is the growing presence of the oxygen cycle as the battery ages that dictates the need for different charging approaches. This need is further amplified by the fact that individual VRLA cells, with varying saturation levels, react differently to the oxygen cycle and experience variable amounts of saturation at any time and throughout life. This extreme variability requires unusual charging approaches that are more aggressive than normal algorithms and may even be changeable throughout battery life. Another charging condition that has recently become important for VRLA batteries in HEV and photovoltaic applications is the so-called 'partial state-of-charge', or PSoC, cycling. This puts extreme constraints on the VRLA battery and will be discussed in some detail. With these comments as a backdrop, let's look at some possible approaches to optimal float, cyclic and PSoC charging of VRLA batteries.

9.4.1. Optimized approaches to float charging

The fundamental problems to be overcome in float charging of VRLA cell strings are the cell-to-cell variability in saturation levels and the gradual decrease in saturation during life due to water loss and consumption in grid corrosion. Both these conditions, combined with the mild charging that attempts to keep all cells just fully

charged without excessive overcharge, lead to some cells losing capacity on charge due to extreme depolarization of some of the negative plates. It would seem, then, that optimized approaches to charging would involve either more aggressive charging algorithms or better control of the oxygen cycle, or both. Some of the methods available that may lead to more effective float charging of VRLA products are as follows.

Gelled-electrolyte batteries. One of the benefits of gel batteries, particularly early in life, is that their oxygen-transport properties are poor due to the impervious nature of the gel. With time, cracks and channels form in the gel, and these match up with the pores in the polymeric support separator to eventually create gas paths from the positive to the negative plates [47]. It is likely to take months or years (depending upon the battery design and the application conditions) before the gas-transport characteristics of a gel battery are similar to those of a standard AGM product. Until this time, conventional charging may be successful in maintaining sufficient polarization of all negative plates to maintain full discharge capacity. It must be kept in mind, however, that gel products are not suitable for high-rate applications due to their relatively large plate thicknesses and spacings and the lower diffusion rates of the sulfuric acid electrolyte in the gel (about one-third of that in the liquid phase). Still, in traditional standby applications requiring low or moderate discharge rates, the moderation of the oxygen cycle by the gel separator system can be a distinct advantage. The larger electrolyte quantities in gel batteries relative to comparable AGM products compensates for the higher gassing levels and resultant weight losses; this can be an added advantage for gel products in high-temperature standby applications.

Recombination catalysts. The use of noble-metal, recombination catalysts is a technology that has been in use for decades in both flooded and VRLA products. Recently, they have been touted for use in, particularly, VRLA telecom batteries, and they are currently being marketed commercially by C&D [48]. Catalysts, which are positioned in the head space of a cell, operate on the principle of recombining hydrogen and oxygen gases generated by float or overcharge on active platinum or palladium surfaces and returning the resultant water to the cell. In this way, oxygen partial pressures are kept low and the amount of oxygen recombining at the negative plate is reduced, thus allowing proper polarization and maintenance of a fully charged state in all cells. Catalysts add cost, they may require additional head space and they can malfunction in a number of ways, but they do improve the functioning of VRLA cells in long telecom strings by facilitating proper charging.

Intermittent charging. This is a charging approach first proposed by Northern Telecom in 1984 [49]. It has been developed in a number of forms, but all these involve aggressive charging on a periodic basis with rest, or off-line, times in between charge events. It has been proposed with pulsed-current algorithms [11,50] and high-voltage CV charging [51], and it is available in commercial packages that combine intermittent charging (IC) with battery monitoring systems [52]. When the technique

was first proposed in 1984, high-speed switching circuitry was not available, so it was applied by charging and resting alternating parallel strings so that part of the battery was always on-line. Now, such circuitry is available such that, if an outage occurs during a rest period, the battery can be brought on-line rapidly to function normally. Intermittent charging has a number of advantages and drawbacks [51], but, for the purposes of this discussion, there are two major pluses. First, each charge event provides cell-to-cell equalization since they are usually at relatively high voltages that will heavily polarize all cells (but for a short period of time, typically $\sim$30 min every 10 days or with on:off ratios of $\sim$1:17). Second, the amounts of charge and overcharge relative to continuous low-voltage CV float charging are extremely low. For example, the amount of charge for a 48-V/100-Ah telecom battery with normal continuous CV charging at an average current of 100 mA is about 876 Ah over one years' time; it can be estimated that $\sim$80% of this will be overcharge (thus promoting gassing and grid corrosion). With IC charging at 60 V (full rectifier output, 2.50 VPC) for 30 min every 10 days with rest, or off-line, periods in between, the total Ah input over the same one-year period will be 216 Ah, with $\sim$36 Ah of that being overcharge [51]. The methods used in IC ensure that the battery is between 95 and 100% SoC at all times, and it is clear that longer life due to equalized cells and low water loss/grid corrosion will be ensured. In addition, temperature compensation is not required regardless of the environmental conditions, and thermal runaway cannot occur due to the short charging periods. Taking into account cost, changes in battery design, and disruption of existing standby sites, it is clear that this is an effective, if not optimal, approach to long-term float charging of VRLA batteries.

Wrapped negative plates. This is a design approach reportedly developed by Matsushita for their long-life EV battery line [31]. Here, the negative plates are wrapped with a microporous polymer membrane that inhibits, but does not eliminate, oxygen transport during overcharge, thus improving the polarization and rechargeability of the negative plate in cyclic applications. In float use, this may not be so effective, as steady-state diffusion levels of oxygen through the membrane may be significant enough to depolarize negative plates in cells with relatively low amounts of saturation. Still, it merits further investigation.

Sub-micron pore size separators. As noted in Atlung's landmark paper on oxygen transport in VRLA systems [38], effective recharge can only be accomplished by impeding oxygen transport to some extent; in float applications, it may be possible to minimize negative-plate depolarization by doing this. One approach that is being investigated is to engineer the structure of the separator system to create fine pores and/or a high level of tortuosity to impede gas transport. This can be done by using fine-fibre, all-glass separators or glass/polymer 'sandwich' systems [53,54], or by using high-density glass separators with high compression levels of 60–80 kPa in the finished batteries [55] (see also Chapters 6 and 7). As with the wrapped-negative approach, it is not possible to say at this time whether such separator systems will control oxygen transport continuously (necessary for traditional CV float charging)

and thus keep oxygen reduction at a reduced level. It should be pointed out that this type of approach, if successful, will result in higher gassing water loss amounts due to reduced oxygen-cycle efficiencies. This is a compromise that will necessarily accrue when the effectiveness of the oxygen cycle is retarded. In designs such as this, optimal performance and life may be realized by incorporating catalysts to deal with the higher oxygen levels created by hindrance of the oxygen cycle.

9.4.2. Optimized approaches to cyclic charging

In cyclic charging, the effect of the oxygen cycle is temporary, occurring only during the overcharge process. However, as VRLA batteries age, this effect becomes stronger and stronger and at some point becomes completely dominant. Up to this point, charge algorithms can significantly extend cycle-life, but after this only design and materials changes can effect substantive improvements. As discussed above, traditional IU and IUI charge algorithms are somewhat effective up to the point where the current draw for the oxygen cycle exceeds the finishing current level, which is almost always quite low (C_{50}–C_{100}). At this point, full recharge is impossible. Extending the charge to longer times and higher charge factors may be temporarily successful, but, after a few more cycles, this must be again increased or capacity 'walk-down' will occur. It was noted that it is more the rate of the finishing step that is of primary importance rather than the amount of overcharge. Thus, the target in optimizing cyclic charging algorithms is to complete the recharge as quickly as possible with a minimum of overcharge, as the latter tends to accelerate the creation of more void space, which further enhances the oxygen cycle.

This is shown conceptually in Fig. 9.21 [56]. As cycling progresses the percentage of charge for the oxygen cycle grows and there is a corresponding gradual increase in charge factor to account for this, slowly approaching the pre-set limit. When the current draw for oxygen recombination exceeds the overcharge limit (here, 10–20%), the discharge capacity must necessarily decline, as 100% charge return for active-material conversion is not being achieved (to the right of the vertical dotted line). If the overcharge limit is removed, there is a sharp increase in charge factor, as, in this region, the growth of the oxygen cycle is rapid due to the high separator void space. This will hold up the capacity for some time, but the excessive overcharge (most of which is being converted to heat) will destroy the battery, as in the region of thermal danger (Fig. 9.14) has now been entered.

In order to finish the charge rapidly (and, thus, minimize the time for the parasitic oxygen cycle to contribute to the charge factor), relatively high currents must be used, which can be damaging in terms of gassing water loss, grid corrosion, and heat build-up. Gassing and grid corrosion are minimized by keeping the charge factor as low as possible (1.10 or less) by using these high finishing currents. Nevertheless, this creates thermal management problems, as represented in Figs. 9.14 and 9.21.

Given the foregoing, a series of requirements for optimized charging of VRLA batteries can be formulated. It should be noted that this approach will be necessary earlier in life and more obviously effective with thin-plate products. Thick-plate cells,

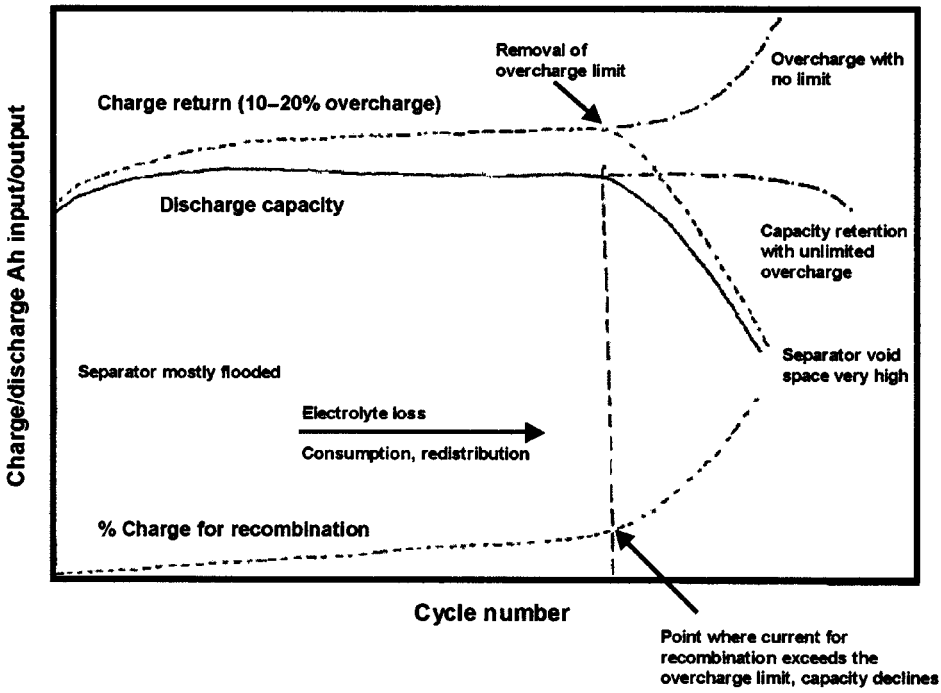

Fig. 9.21. Conceptual view of influence of oxygen cycle/recombination on cycle behaviour in VRLA batteries.

with their greater amounts of electrolyte per unit of plate surface area and larger plate spacings, will go many more cycles before this type of treatment is necessary. As current density is a key factor in all of this, it should be noted that thick-plate VRLA products can only accept relatively lower finishing currents than in the examples given below due to poorer charge-acceptance. This renders the treatment less effective, but this is offset by it being initiated at higher cycle numbers. Conditions for optimal charging, then, are as follows:

- current-limited CV or multi-step CC charge can be used to bring the battery to 80–100% SoC, depending upon the battery design and the charge rates available
- at this point, a finishing charge step is applied that is at a high enough current that the recharge is finished in a relatively short time; again, the finishing current will be dictated by the battery design (thin-plate designs can accommodate higher levels)
- this should be done with a charge factor of 1.05–1.10. The points of switching to the finishing step and charge termination are best done with current integration
- as the battery ages, it may be necessary to increase the magnitude of the finishing current to overcome the growing oxygen cycle (while still keeping the charge factor as low as possible); this can be done until heat build-up limits the viability of the recharge process.

This approach was developed using Optima 12-V/50-Ah and Hawker Genesis 12-V/38-Ah test batteries in an ALABC program [56,57]. The objective was to optimize cycle-life based upon the insights involved in Fig. 9.21. Initial attempts were based upon using high finishing currents, but with progressively larger amounts of overcharge. It was found that this accelerated the creation of additional void space and was self-defeating, in spite of temporary recoveries of discharge capacity with each increase. In addition, heat build-up towards the end of recharge eventually became excessive. This necessitated using lower finishing CC levels which, of course, resulted in higher charge factors, longer times for recharge and an acceleration of the creation of higher void volumes (which would call for higher finishing currents — an electrochemical 'Catch 22'!). In order to be able to use higher finishing currents (of the order of C_{10}–C_5, about an order of magnitude greater than for conventional IUI algorithms), an approach termed 'current-interrupt', or CI, was developed. This is simply a current-pulse technique with a period and duty cycle that resulted in better heat dissipation and liquid diffusion conditions during the finishing step. An additional benefit was realized in that hydrogen evolution during overcharge was virtually non-existent, as had been predicted previously [58]. The charge algorithm is shown conceptually in Fig. 9.22 for both CV and CC initial charge algorithms. A typical CI charge curve is given in Fig. 9.23, together with pressure measurements. In spite of achieving voltages in excess of 17 V during pulsing (no voltage limit is imposed), hydrogen evolution is minimal, as can be seen by the pressure decay to zero after charge is terminated, with any remaining oxygen being scavenged by the negative plate.

A similar algorithm was first developed for recovering and extending the cycle-lives of flooded maintenance-free and VRLA batteries [59,60], but its applicability was limited by the use of low-pulsed finishing currents (C_{50}–C_{100}), voltage limits and termination at a charge factor of 1.10. In the ALABC work, finishing currents were higher and charge voltages and charge factors were not limited (although charging was done in such a way as to minimize overcharge). Initially, switching from stepped-CC charging to the CI finish was done using trigger voltages, but the collapse of the shape of the voltage–time curve as the batteries aged, as shown in Fig. 9.19, dictated the use of Ah counting for switching. Otherwise, at some point the trigger voltage would not be reached during the last CC charge step and charging would continue indefinitely.

The result of using this approach is shown in Fig. 9.24, with a comparison to the standard Optima IUI charge algorithm described previously. It can be seen that the cycle-life to 80% of initial capacity is more than doubled and, perhaps more important, the loss of capacity using the CI algorithm is very gradual. Because this is a thin-plate product (1.0–1.2 mm) in a large size, the magnitude of the finishing current is limited and so overcharge levels increase sharply after $\sim$350 cycles. At about 750 cycles, this limits life due to heat build-up, with capacity still riding at the 50% level. Interestingly, in spite of the heavy overcharge levels for hundreds of cycles the weight loss ($\sim$0.15 g per cycle) and grid corrosion level (35% from chemical analysis) are relatively low. This illustrates the shift in the majority of the overcharge current from gassing and grid corrosion to the oxygen cycle as this type of VRLA battery ages in cyclic duty.

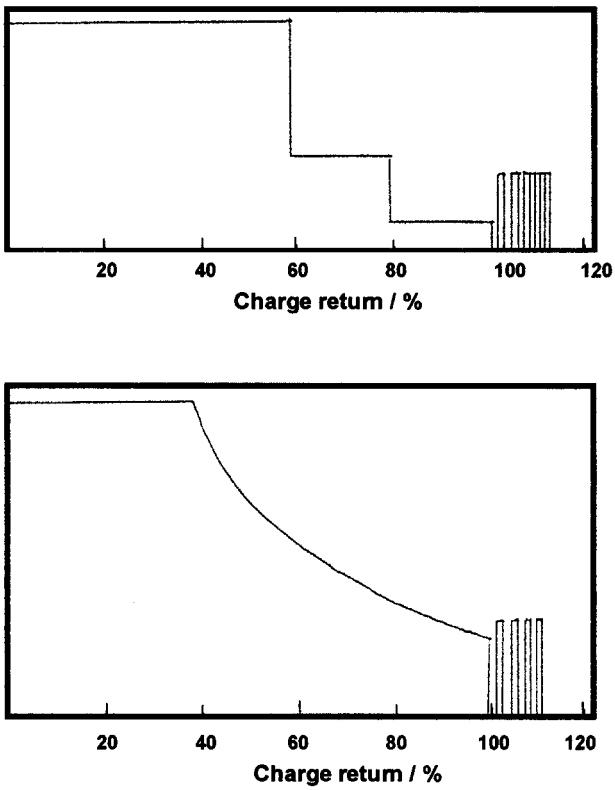

Fig. 9.22. Stepped CC (upper curve) and current-limited CV (lower curve) charge algorithms with a current-interrupt finish. CI can be initiated anywhere between 80 and 100% charge return. The *y*-axis is charge current in both cases.

While this cycling project did not achieve the goal of 1000 deep cycles, it should be noted that, in contrast to several other studies previously cited, these results are for continuous cycling (i.e., no conditioning cycles, save one) on a commercial 6-cell battery in a thin-plate design.

Based upon the thesis that longer cycle-life might be obtained by further minimizing overcharge, another algorithm was developed where the battery was given only ~97–99% charge return for 9 cycles and was then given a conditioning recharge with 20–25% overcharge every 10th cycle. This so-called 'partial-state-of-recharge', or PSoR, approach resulted in even higher cycle-lives and total Ah throughputs, as shown in Fig. 9.25. Again, weight loss and grid-corrosion levels were extremely low. This is an excellent result and could be applicable to real-world EV use, where partial recharges would be done on weekdays, with a full conditioning charge being done on the weekend.

The CI algorithm was also applied to a 288-V EV pack of Optima 12-V/50-Ah deep-cycling modules at the National Renewable Energy Laboratory [57]. This was an 80% DoD test with continuous cycling (i.e., no regular conditioning charges),

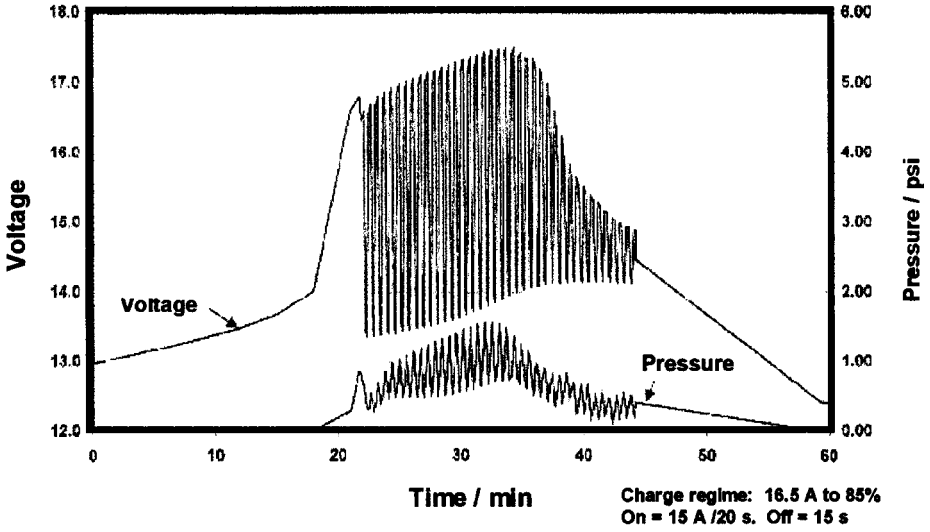

Fig. 9.23. Constant-current recharge with CI finish for 12-V/16-Ah VRLA battery at cycle number 326. Lower curve is internal battery pressure; note drop to zero psi when charge is terminated.

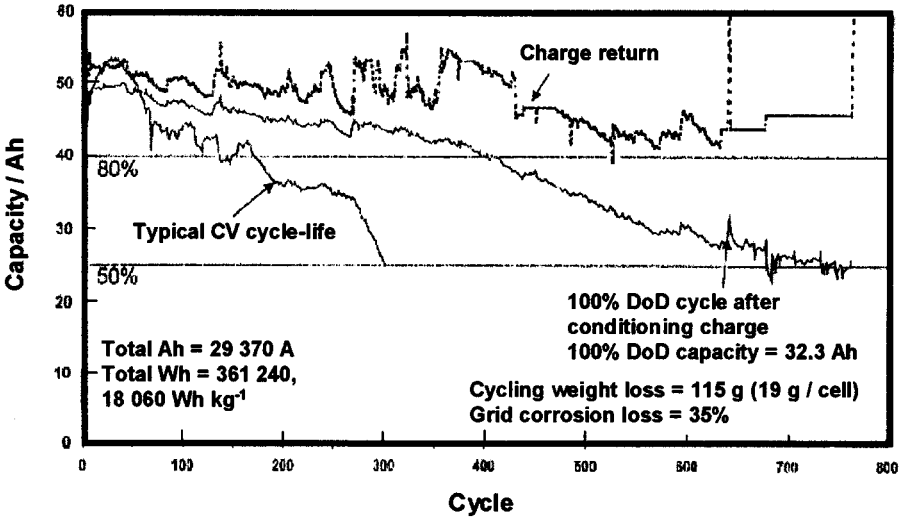

Fig. 9.24. Cycle *vs.* capacity plot for 12-V/50-Ah VRLA battery. Discharge is 25 A to 11.0 V (90% DoD). Charge is 200 A to 60% charge return, 50 A to 80%, 15 A to 100% with CI finishing charge; see Refs. [56,57] for details.

with discharges being terminated when the first module reached 10.5 V; defective modules were replaced as needed. The nominal 40-Ah discharge capacity was maintained until 600 cycles, as shown in Fig. 9.26, at which point the replacement of weak modules was discontinued. This was done with a charge factor of 1.10 or less to

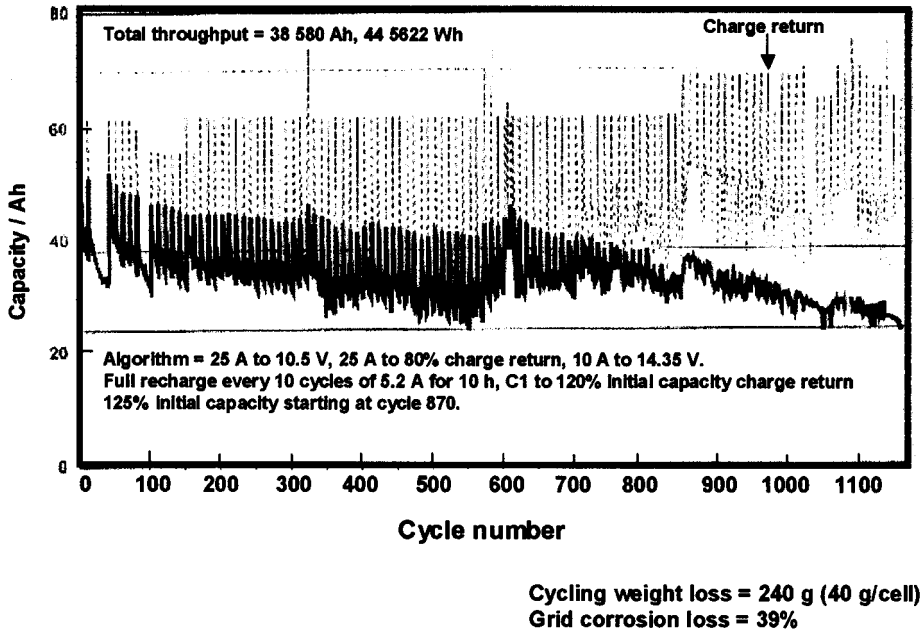

Fig. 9.25. Partial-state-of-recharge 100% DoD cycling of 12-V/50-Ah VRLA battery. Solid line is discharge capacity, dotted lines are charge return on conditioning cycles [55,56].

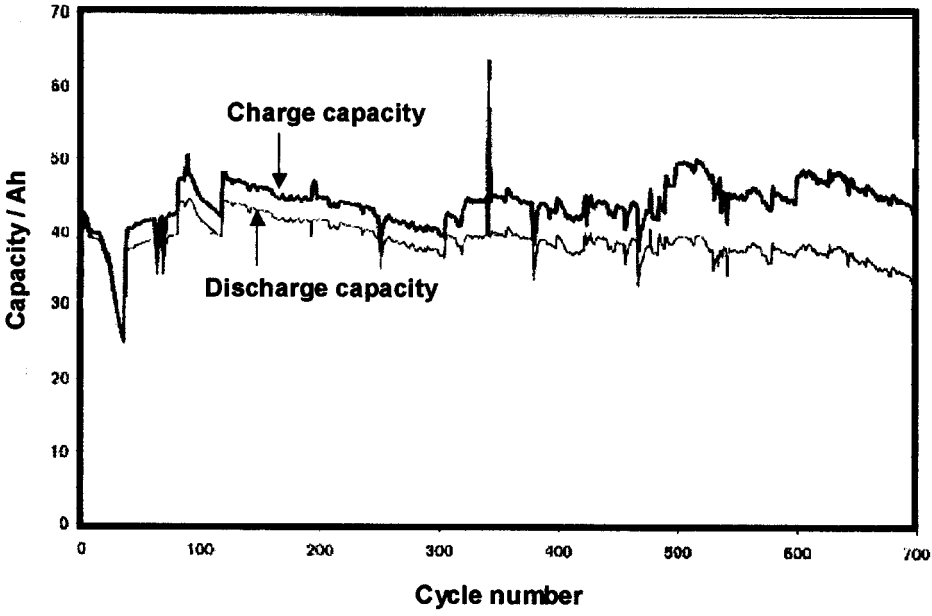

Fig. 9.26. Cycle vs. capacity plot for 288-V/50-Ah EV battery pack using CI finish [57].

500 cycles, at which point it had to be increased. Two of the original modules completed 1100 cycles to 50% of initial capacity.

Clearly, CI may not be a universal algorithm, but it would be interesting to see what cycle-lives could be achieved with this procedure on thicker-plate VRLA batteries, where the oxygen cycle is not as active as in the Optima and Genesis products. It should be noted that each product may require a unique approach, as design dictates maximum current levels and recharge times in VRLA products. This has been demonstrated in the Cominco ALABC work on fast charging of Optima (thin-plate) and Delphi (thick-plate) batteries [61].

9.4.3. Partial-state-of-charge cycling — an evolving algorithm

Due to the incorporation of VRLA products into such new applications as HEV and photovoltaics/wind/hydro-electric energy conversion, or RAPS (remote-area power sources), the development of cycling algorithms involving a relatively narrow SoC window has emerged. While it is beyond the scope of this review to cover this topic in great depth, a general overview will be presented.

Partial-state-of-charge cycling has an inherent advantage in that, within a fairly broad SoC window of ~20–80%, the battery is neither deep discharged nor put into overcharge under normal conditions of charge and discharge. From the standpoint of energy output, however, this approach is not attractive because only a fraction of the available energy is delivered on each cycle. This is counterbalanced by the fact that such cycling can result in very high cycle numbers for VRLA batteries, as first shown by GNB in a simulated photovoltaic test [62]. The PSoC duty cycle is demanded, however, in certain applications such as RAPS and HEV. In HEV applications, the battery is maintained at some nominal intermediate SoC and is irregularly cycled in both directions from this point. In RAPS, due to the vagaries of natural energy collection and an oversizing of the battery so that it is not routinely deep discharged, the battery is cycled over a large but variable SoC range. In HEV use, the battery serves a dual function of providing high-current pulses of energy for acceleration and hill climbing and taking up similar pulses during braking events (so-called 'regenerative braking', or 'regen'). This unusual duty cycle is shown conceptually in Fig. 9.27. In a more recent form of HEV use — the so-called 'mild hybrid', or 36/42-V battery — additional discharge functions of restarting the vehicle frequently and 'boosting' it up to some nominal speed can be incorporated [63].

All these applications are erratic in nature and some form of battery management is necessary to ensure that the proper SoC range is maintained. In RAPS, a low-rate version of PSoC cycling, charging is governed by the conversion of solar, wind, or hydro-electric energy to battery-stored electrical charge and, if the battery does not enter the overcharge region, the type of charging is not critical. This is likely to happen in some areas, however, so charge control is an issue. In the various forms of HEVs, charging is again dependent upon nominally uncontrolled events; in this case, braking periods where mechanical energy is converted to electrical through the motor/generator. Thus, in all cases, charging is not the

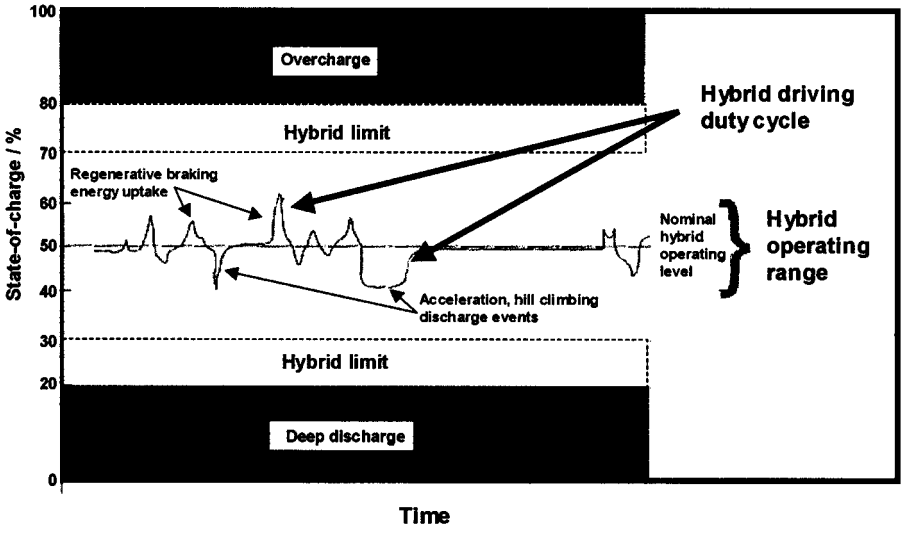

Fig. 9.27. Conceptual view of SoC variations for battery during HEV charge–discharge operation.

Table 9.3. Typical rates of discharge and charge and ranges of SoC for several different duty cycles

Duty	Float		Deep-cycle	Low-rate PSoC	High-rate PSoC	Automotive
Application	UPS	Telecom	EV	RAPS	HEV/36-V	12 V
Range of SoC	95–100[a]	95–100[a]	20–100	20–80	30–50, up to 70–90	70–80
Maximum normal rate for discharge[b]	4–5	C_8	4	0.2	15	10
Maximum normal rate for charge[b]	0.5	0.2	0.5	0.2	8–10	0.2

[a]With occasional deep discharges.
[b]In multiples of the 1-h rate.

same as that discussed for the more conventional standby and cyclic algorithms. Comparisons are made for several aspects in Table 9.3 [64]. In conventional float and deep-discharge use, the battery is maintained at or returned to a high SoC, 95–100%, periodically. Discharges can be partial (float) or complete (deep discharge) at low or high rates. Charge and recharge are always done in a controlled fashion to obtain maximum lifetime. SLI use can be viewed as a form of PSoC, but this is not really by design. Due to inefficiencies in alternator charging and low peak voltages most SLI batteries are maintained in a SoC range of ~70–90%; discharges are mostly very shallow but at high rates (although the power and energy demands

of modern vehicles are putting more of a discharge strain on the battery). Here, charging is somewhat controlled but not to the degree applied in float and deep-cycle use.

In RAPS, PSoC applications, charging times are largely uncontrolled and can be random, but the charging of the battery bank used to provide a.c. power is well regulated and can be either CV, CC, or a combination of both [65,66]. An example of a charge–discharge PSoC profile is shown in Fig. 9.28 [66]. Initially, the battery is taken from full charge down to ~20% SoC (Regime 1). There is then a long period of PSoC charge/discharge steps that are nominally between ~20 and 80% SoC (Regime 2). There is a gradual decline in the lower SoC, however, and periodically a thorough conditioning charge is carried out (Regime 3), returning the battery to ~100% SoC. Using this type of approach, it has been estimated that gelled-electrolyte batteries under RAPS conditions can deliver a useful lifetime of ~8 years [66].

High-rate PSoC operation is different in that the charge–discharge specific power levels are significantly higher and, thus, the SoC varies rapidly and somewhat unpredictably. There are several types of HEV duty cycles, and each of these can stress a VRLA battery in different ways [67]. Heavy, unbalanced charge or discharge use can take the battery to nominal SoC levels that can cause severe overcharge (high SoC) or overdischarge (low SoC), albeit normally for only short time periods. Thus, one of the greatest challenges in HEV operation is developing accurate SoC and state-of-health (SoH) algorithms.

In terms of charging and charge regulation, high-rate PSoC operation more or less 'dumps' charge into the battery at levels of ~1 kW per kg or more. Even though

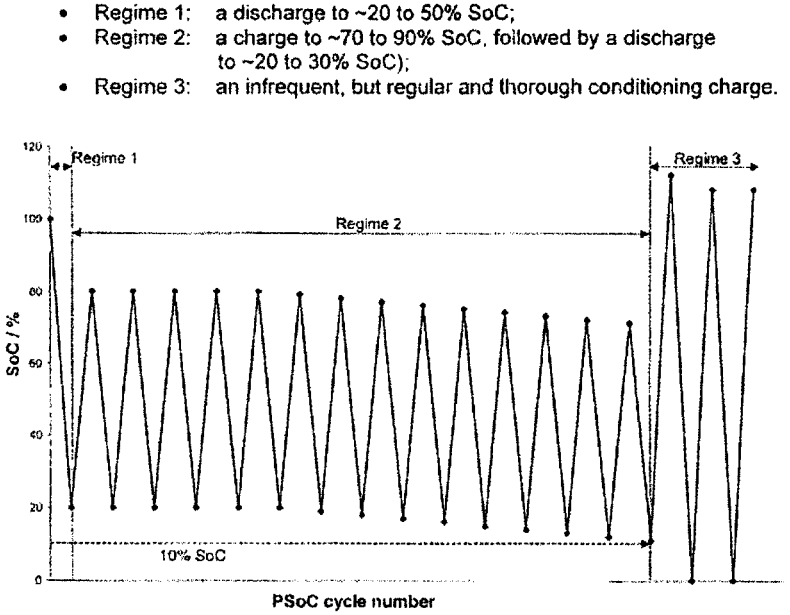

Fig. 9.28. Typical RAPS PSoC operating strategy [66].

the battery may be at a nominal SoC level of 50–60%, these charge pulses can drive it into the gassing region. While hydrogen evolution is probably not a serious issue [58], oxygen generation can result in additional sulfation of the negative plate beyond that created by the nominal 50–60% SoC. If this is not addressed and corrected by the management and control system, gradual deterioration of high-rate performance occurs.

Clearly, high-rate PSoC operation is a critical new application area for both 'hard' (144–288 V) and 'mild' (36-V) HEV batteries and the areas of SoC/SoH monitoring and control. Lifetimes in the hundreds of thousands of cycles (albeit only at 2–3% DoD) and improved charge-acceptance must all be addressed for VRLA batteries to function successfully in these new uses. The major issue is probably continuous functioning in a PSoC condition, which can involve the formation of irretrievable 'hard' sulfate. This can be overcome by periodic, conditioning full charges (an approach not favoured by automakers), additives in the PAM that will raise the overpotential for oxygen evolution and/or relief of mass-transport limitations local to the reaction sites in the PAM (thus improving its charge-acceptance) [64].

Another approach has recently been reported by Japan Storage Battery [68]. Using what appears to be ~ 2 wt.% of a special graphite in the NAM, it was reported that even though the negative plate may be at 50–60% SoC with considerable lead sulfate present, the graphite forms a conductive 'skeleton' that improves charge-acceptance significantly. Preliminary reports on this work were presented by Yuasa [69] and in several earlier presentations by JSB. Clearly, in order to improve the charge-acceptance of VRLA batteries radically, improvements in both positive- and negative-plate chemistries, along with thin-plate battery designs to minimize current densities, are necessary (see Chapter 17). It is likely that such improvements will also impact favourably on required cycle-lives in high-rate PSoC use, as failures often relate to heavy sulfation of the NAM and not fatal grid corrosion or dry-out. This is an exciting area of investigation, particularly for the development of 36/42-V VRLA products, which are necessary for the lead industry to retain the engine-start business that has been the province of lead–acid for decades.

9.5. Summary and Conclusions

Until the last decade, VRLA batteries were charged much like their flooded cousins. For float applications, CV charging was used almost exclusively (although the first AT&T SLC 96 telecom installations developed ~ 1980 used low-level CC). For cycling applications, charging was current-limited CV and, somewhat later, CV with a low-level CC finish (so-called IUI). It was well documented that, in long strings, VRLA cell voltages on both float and cyclic recharge showed significant variations and individual cells tended to 'wander' in voltage over a range of ~ 150 mV or more. Nevertheless, it was not until pioneering work by Atlung [38], Berndt [2,3], and Feder and Jones [21,22] that it became clear what was happening. It was not appreciated how strong the role of the oxygen cycle is in both float and cyclic charging until the mid 1990s. In earlier days, VRLA batteries were designed

to optimize the influence of the oxygen cycle and charge algorithms were overly conservative, based upon fears over early failure due to grid corrosion and/or electrolyte dry-out. In many instances, this resulted in very early failure due to undercharging. It now appears that, if the VRLA cell is not charged aggressively, the oxygen cycle depolarizes the negative plate to the point where some cells actually discharge on float.

Berndt and Teutsch [70] have shown that either electrode could partially discharge on float if the voltage is allowed to 'wander' in either direction under realistic conditions and with a variety of designs. There is a relatively small range of saturation where VRLA cell behaviour swings from acting like a flooded lead–acid product to being so resistant to polarization that full recharge is impossible (see Fig. 9.11). In float duty, as shown in Fig. 9.15, proper functioning of every cell in a series string or (worse) series–parallel array must operate in a narrow voltage window of 'ideal float voltages' for both plates to be properly polarized and fully charged at all times. From the variabilities inherent in most VRLA cell designs and manufacture, this is virtually impossible. Added to this is the general condition of decreasing saturation with age, which makes effective recharge or maintenance of proper float conditions untenable.

These two factors also affect cyclic charging, which is done at higher voltages than for float, but not voltages so high that uniform, complete polarization is achieved for all cells on every charge. This is demonstrated graphically in Fig. 9.29 [3] for a 6-cell VRLA battery early and late in cycle-life; a comparable variability is well documented in Tables 9.1 and 9.2 for float operation. Several significant points in Fig. 9.29 are worthy of comment. In the almost-new cells (cycle #17), the variability in cell voltages during CV charge is $\sim 200\,\text{mV}$; even during the final CC charge step the variability is $\sim 60\,\text{mV}$. When the battery is aged, the variability is significantly less but there is a general drop in voltages on charge, both during the CV and the finishing CC steps; in addition, the maximum temperature increases by some 14°C. All these factors are directly attributable to the growing influence of the oxygen cycle. The collapse in end-of-charge voltages is generic for VRLA batteries (Figs. 9.17 and 9.19) and has serious consequences for charging algorithms and termination methods late in battery life.

These conditions have resulted in a general shift away from CV charge algorithms to those employing high-voltage CV or CC charging. This is not surprising, as the electrochemical behaviour of a VRLA cell is closer to that of a Ni–Cd product than to a flooded lead–acid cell, particularly late in life. The Ni–Cd battery is actually simpler than the VRLA battery because there is no great change in saturation level throughout life. The initial saturation level in the Ni–Cd separator is very low relative to that in VRLA, so extreme charging measures need to be taken from the beginning of float or cycling lifetime since the oxygen cycle is well developed even initially in Ni–Cd products. It has been suggested that VRLA cells be floated using CC charging [71], similar to the above-mentioned AT&T SLC96 algorithm. As discussed previously, multi-step CC charging can result in excellent cycle-lives [5–7,31], and this approach has been strongly endorsed by at least one industry expert [72]. Even the IUI algorithm would be acceptable if the magnitude of the final current step were increased by a factor of 5–10, or even more late in life. This

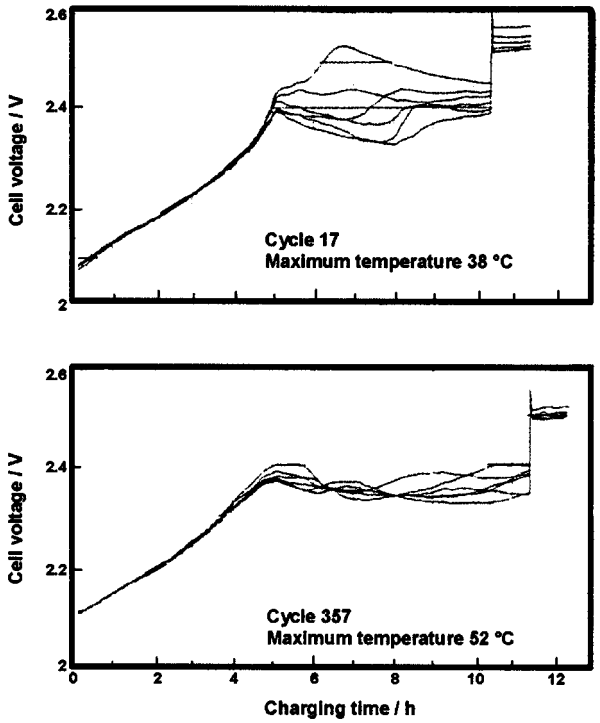

Fig. 9.29. Charging curves of six individual cells in a 24-V/440-Ah VRLA battery during IUI charge algorithm as shown in Fig. 6, solid lines [3].

eventually results in unacceptable thermal build-up, however, at which point recourse must be taken to pulsed charging approaches such as CI or PSoR [73].

For float charging, traditional CV or CC approaches will not work consistently unless all the cells in a string are perfectly balanced (which is virtually impossible); the 'knife edge' created by the oxygen cycle ensures early or mid-life failure due to extreme depolarization in some cells. The use of catalysts is a design approach that still remains to be fully validated, but it does look promising. For charging, the use of intermittent charging, IC, is recommended, but implementation of this will require a 'paradigm shift' in thinking of the standby industry to be widely accepted. The use of individual control for both charge and discharge is valid [74], but it adds considerable cost and complexity to a standby installation.

Non-traditional algorithms in cyclic charging are only part-effective; at some point, the oxygen cycle becomes so strong that it cannot be overcome without burning up the battery. What can be done at this point? It has been stated that oxygen recombination is clearly desirable to some extent, but it is becoming clear that only a moderate level of recombination may be optimal for these systems [75]. This opinion was published more than 10 years ago, and it has been found to be generally true.

For float charging, the use of gel technology, IC, catalysts and/or individual cell control should allow the realization of an inherent maximum operational lifetime in

the region of some 20 years. For cyclic applications, further advances must depend upon design and/or materials modifications. This must be done in the separator system and, possibly, in box and lid construction; the latter to allow higher levels of stack compression and vent pressures. Work on separator systems is targetted on maintenance of compression and development of a fine pore structure and/or high tortuosity in order to modify the influence of the oxygen cycle and, therefore, 'buy time' for the completion of recharge. Such an approach necessarily results in higher weight losses and more grid corrosion, but, from results such as those shown in Figs. 9.24 and 9.25, this compromise can be accommodated, at least for thin-plate VRLA products. In thicker-plate VRLA batteries, these effects are not seen as early in life, and it is possible that some flat-plate designs with plate thicknesses of 3–4 mm can realize deep-cycle lifetimes of 1500–2000.

References

1. K. Peters, A.I. Harrison, W.H. Durant, *Power Sources 2. Research and Development in Non-mechanical Electrochemical Power Sources*, Pergamon Press, New York, USA, 1970, pp. 1–16.
2. D. Berndt, *Proceedings of the 10th International Telecommunications Energy Conference*, San Diego, CA, USA, IEEE, 1988, pp. 89–96.
3. D. Berndt, *Maintenance-free Batteries*, Second Edition, Research Studies Press, Taunton, Somerset, England, UK, 1997, pp. 404–420.
4. Gates Energy Products Cyclon Battery Application Manual, 1982, pp. 24–27.
5. T. Ikeya, M. Iwasaki, S. Takagi, Y. Sugii, M. Yada, T. Sukabe, E. Kousaka, H. Tsuchiya, M. Kanetsuki, H. Nasu, M. Ono, H. Narisoko, Y. Mita, K. Nishiyama, K. Adachi, T. Iwachori, *J. Power Sources*, **69** (1997) 103–111.
6. T. Ikeya, N. Sawada, S. Takagi, J-I. Murakami, K. Kobayashi, T. Sakabe, E. Kousaka, H. Yoshioka, S. Kato, M. Yamashita, H. Narisoko, Y. Mita, K. Nishiyama, K. Adachi, K. Ishihara, *J. Power Sources*, **75** (1998) 101–107.
7. T. Ikeya, N. Sawada, S. Takagi, J-I. Murakami, K. Kobayashi, T. Sakabe, E. Kousaka, H. Yoshioka, S. Kato, M. Yamashita, H. Narisoko, Y. Mita, K. Nishiyama, K. Adachi, K. Ishihara, *J. Power Sources*, **91** (2000) 130–136.
8. Y. Guo, R. Groiss, H. Döring, J. Garche, *J. Electrochem. Soc.*, **146** (1999) 3949–3957.
9. L.T. Lam, H. Ozgun, O.V. Lim, J.A. Hamilton, L.H. Vu, D.G. Vella, D.A.J. Rand, *J. Power Sources*, **53** (1995) 215–228.
10. E.M. Valeriote, J. Nor, V.A. Ettel, *Proceedings of the Fifth International Lead-Acid Battery Seminar*, Vienna, VA, USA, 17–19 April 1991, pp. 93–122.
11. J.-P. Cun, J.-N. Fiorina, M. Fraisse, H. Mabboux, *Proceedings of the 19th International Telecommunications Energy Conference*, Melbourne, Australia, IEEE, 1997, pp. 389–396.
12. R. Brost, *Proceedings of the 15th Annual Battery Conference on Applications and Advances*, Long Beach, CA, USA, January 2000, pp. 243–248.
13. W.B. Gu, G.Q. Wang, C.Y. Wang, *Proceedings of the 16th Annual Battery Conference on Applications and Advances*, Long Beach, CA, USA, January 2001, pp. 181–186.
14. B. Culpin, J.A. Hayman, in: L.J. Pearce (Ed.), *Power Sources 11. Research and Development in Non-mechanical Electrochemical Power Sources*, International Power Sources Symposium Committee, Leatherhead, England, 1986, pp. 45–66.
15. European Advanced Lead-Acid Battery Consortium, Brite/Euram Project BE97–4085, The development of improved lead–acid batteries for electric vehicle service which are maintenance-free and fully recyclable, Final Report 1 January 1998 to 31 August 2001, Appendix IV, p. 50, Advanced Lead-Acid Battery Consortium, Research Triangle Park, NC, USA, 2001.
16. K. Peters, *J. Power Sources*, **42** (1993) 155–164.
17. B. Culpin, *J. Power Sources*, **53** (1995) 127–135.
18. D. Berndt, 5th ERA Battery Seminar and Exhibition, London, UK, April, 1988, Session 1, Paper 4.

19. R.F. Nelson, *Proceedings of the 12th International Telecommunications Energy Conference*, Orlando, FL, USA, IEEE, 1990, pp. 165–171.
20. R.F. Nelson, *Proceedings of the 4th International Lead-Acid Battery Seminar*, San Francisco, CA, USA, 25–27 April, 1990, pp. 31–60.
21. D.O. Feder, W.E.M. Jones, *Proceedings of the 18th International Telecommunications Energy Conference*, Boston, MA, USA, IEEE, 1996, pp. 184–192.
22. W.E.M. Jones, D.O. Feder, *Proceedings of the 18th International Telecommunications Energy Conference*, Boston, MA, USA, IEEE, 1996, pp. 358–366.
23. J. Jergl, B. Cole, S. Purcell, *Proceedings of the 18th International Telecommunications Energy Conference*, Boston, MA, USA, IEEE, 1996, pp. 351–357.
24. D. Berndt, *Proceedings of the 7th International Telecommunications Energy Conference*, Munich, Germany, IEEE, 1985, pp. 125–132.
25. R.F. Nelson, *Proceedings of the 11th International Telecommunications Energy Conference*, Florence, Italy, IEEE, 1989, Paper 12.6.
26. A. Cooper, *J. Power Sources*, **107** (2002) 245–272.
27. E. Nann, *J. Power Sources*, **33** (1991) 93–103.
28. R. Wagner, *Proceedings of the 11th International Lead Conference*, Venice, Italy, 24–27 May, 1993, Lead Development Association, London, UK, Paper 7.3.
29. D. Calasanzio, M. Caselli, D. Ghiotto, *J. Power Sources*, **53** (1995) 143–147.
30. M. Fernandez, F. Trinidad, *J. Power Sources*, **67** (1997) 125–133.
31. N. Hoshihara, *Proceedings of the 1st Advanced Automotive Battery Conference*, Las Vegas, NV, USA, 2001, Session 3, Paper No. 5.
32. K. Kordesch, *J. Electrochem. Soc.*, **113** (1972) p. 1053.
33. J.K. Nor, U.S. Patent 5,202,617 (1993).
34. E.M. Valeriote, T.G. Chang, D.M. Jochim, *Proceedings of the 9th Annual Battery Conference on Applications and Advances*, Long Beach, CA, USA, January 1994, pp. 33–38.
35. F.A. Fleming, P. Shumard, B. Dickinson, *J. Power Sources*, **78** (1999) 237–243.
36. R.F. Nelson, *J. Power Sources*, **73** (1998) 104–109.
37. P.T. Moseley, *J. Power Sources*, **95** (2001) 218–223.
38. S. Atlung, B. Zachau-Christiansen, *J. Power Sources*, **52** (1994) 201–209.
39. R.F. Nelson, Informal Presentation at the ALABC 3rd Members and Contractors Meeting, 27 March 1998, London, UK, 1998.
40. R.F. Nelson, ALABC Project B 7.1, Development of improved cycle-life by design of charge algorithms specifically aimed at VRLA batteries, Final Report, 1 August 1998 to 31 March 1999, Advanced Lead-Acid Battery Consortium, Research Triangle Park, NC, USA, 1999.
41. E. Meissner, *J. Power Sources*, **78** (1999) 99–114.
42. R.D. Prengaman, *Proceedings of the 4th International Lead-Acid Battery Seminar*, San Francisco, CA, USA, 25–27 April 1990, pp. 19–30.
43. A.G. Cannone, A.J. Salkind, F.A. Trumbore, *Proceedings of the 13th Annual Battery Conference on Applications and Advances*, Long Beach, CA, USA, January 1998, pp. 271–278.
44. T.G. Chang, D.M. Jochim, *J. Power Sources*, **91** (2000) 177–192.
45. R. Wagner, *J. Power Sources*, **53** (1995) 153–162.
46. B.A. Cole, M.A. Kepros, R.J. Schmitt, *Proceedings of the 19th International Telecommunications Energy Conference*, Melbourne, Australia, IEEE, 1997, pp. 221–229.
47. A.L. Ferreira, H.A. Lingscheidt, *J. Power Sources*, **67** (1997) 291–297.
48. S.S. Misra, T.M. Noveske, S.L. Mraz, A.J. Williamson, *J. Power Sources*, **95** (2001) 162–173.
49. D.P. Reid, I. Glasa, *Proceedings of the 6th International Telecommunications Energy Conference*, New Orleans, LA, USA, 1984, pp. 67–71.
50. E. Rossinot, C. Lefrou, F. Dalrad, J.-P. Cun, *J. Power Sources*, **101** (2001) 27–34.
51. R.F. Nelson, *Proceedings of the 13th Annual Battery Conference on Applications and Advances*, Long Beach, CA, USA, January 1998, pp. 291–295.
52. T. Sideras, S. Vasa-Sideris, E.K.L. Stefanakos, *Proceedings of the 21st International Telecommunications Energy Conference*, Copenhagen, Denmark, Holland, IEEE, 1999, Paper 6–3.
53. E. Nann, V. Toniazzo, U. Lambert, R. F. Nelson, ALABC Project S 1.2, Engineered separators for optimization of processing and performance in VRLA batteries, Final Report, 1 June 2000

to 31 December 2002, Advanced Lead-Acid Battery Consortium, Research Triangle Park, NC, USA, 2000.
54. A.L. Ferreira, *J. Power Sources*, **78** (1999) 41–45.
55. K. McGregor, S. Lau, H. Ozgun, C.G. Phyland, D.A.J. Rand, A.J. Urban, D.G. Vella, L.H. Vu ALABC Project S 1.1, VRLA Separator Essentials, Final Report, 1 July 2000 to 30 June 2002, Advanced Lead-Acid Battery Consortium, Research Triangle Park, NC, USA, 2000.
56. R.F. Nelson, E.D. Sexton, J.B. Olson, M. Keyser, A. Pesaran, *J. Power Sources*, **88** (2000) 44–52.
57. R.F. Nelson, J.B. Olson, E.D. Sexton, A.A. Pesaran, M.A. Keyser, ALABC Projects B 7.1 & 7.2, Development of improved cycle-life by design of charge algorithms specifically aimed at VRLA batteries, Final Report, 1 August 1998 to 31 March 2000, Advanced Lead-Acid Battery Consortium, Research Triangle Park, NC, USA, 2000.
58. D.K. Nowak, *J. Power Sources*, **40** (1992) 105–111.
59. R.A. Rider, R.M. Bendert, U.S. Patent 5,499,234, March 12 (1996).
60. J.L. Ayres, R.M. Bendert, D.A. Crouch, U.S. Patent 5,561,360 (1 October 1996).
61. K. Tomantschger, J. Sklarchuk, T.G. Chang, ALABC Project A001.3 Establishment of the distinction between the beneficial effects of optimum charge rate and the limitation of overcharge, Final Report, June 1997 to March 1999, Advanced Lead-Acid Battery Consortium, Research Triangle Park, NC, USA, 1999.
62. J. Szymborski, Final Report to Sandia Labs, 1982, personal communication.
63. R. Knorr, H.-M. Graf, P. Skotzek, Proceedings of the 1st Advanced Automotive Battery Conference, Las Vegas, NV, USA, February, 2001, Session 2, Paper No. 2.
64. P.T. Moseley, personal communication (Table 9.3 has been modified slightly by the author).
65. R. Wagner, D.U. Sauer, *J. Power Sources*, **95** (2001) 141–152.
66. R.H. Newnham, W.G.A. Baldsing, *J. Power Sources*, **107** (2002) 273–279.
67. R.F. Nelson, *J. Power Sources*, **91** (2000) 2–26.
68. T. Ohara, T. Noda, K. Hata, K. Yamanaka, K. Yamaguchi, M. Tsubota, *Proceedings of the 2nd Advanced Automotive Battery Conference*, Las Vegas, NV, USA, 2002, Session 4, Paper No. 1.
69. Y. Nakayama, *Proceedings of the 1st Advanced Automotive Battery Conference*, Las Vegas, NV, USA, 2001, Session 3, Paper No. 2.
70. D. Berndt, U. Teutsch, *J. Electrochem. Soc.*, **143** (1996) 790.
71. D. Calasanzio, M. Caselli, J. Mc Dowall, *Proceedings of the 16th International Telecommunications Energy Conference*, Vancouver, Canada, IEEE, 1994, pp. 176–180.
72. K. Peters, *J. Power Sources*, **59** (1996) 9–13.
73. E.D. Sexton, R.F. Nelson, J.B. Olson, *Proceedings of the 15th Annual Battery Conference on Applications and Advances*, Long Beach, CA, USA, January 2000, pp. 211–216.
74. H. Schmidt, C. Siedle, *Proceedings of the 15th International Telecommunications Energy Conference*, Paris, France, IEEE, 1993, pp. 146–151.
75. R.F. Nelson, in: T. Keilly and J. Baxter (Eds.), *Power Sources 13, Research and Development in Non-mechanical Electrochemical Power Sources, International Power Sources Symposium Committee*, Leatherhead, England, 1991, pp. 13–24.

This page intentionally left blank

Valve-Regulated Lead–Acid Batteries
D.A.J. Rand et al., editors

—CHAPTER 10—

BATTERY ENERGY-STORAGE SYSTEMS FOR POWER-SUPPLY NETWORKS

C.D. Parker and J. Garche

10.1. Introduction

This chapter discusses the application and benefits of large-scale energy-storage systems in electricity supply networks. The emphasis is on lead–acid battery energy-storage systems (BESSs), and especially on those that employ valve-regulated lead–acid (VRLA) batteries. Recent BESSs, dating from the early 1980s, for which descriptive information is reasonably available are reviewed. The extent of this information varies dramatically; some systems are defined by the most basic of parameters, i.e., energy and power capacities, while others are described in appreciable detail with the inclusion of performance data. The systems are categorized in terms of first-generation, transitional, or second-generation technology. Although not an exhaustive list, the BESSs described here are considered to provide a representative survey of the state-of-art. Battery issues *per se* are not discussed as these are examined in detail in other chapters of this book. In particular, the operation of VRLA batteries in stationary applications is reviewed in Chapter 13 [1].

10.2. A Historical Perspective

At the turn of the 20th century, the distribution of low-voltage, direct current (d.c.) electrical power within small, densely populated areas was the common practice. In such networks, BESSs were often used to provide peaking power and a short-term reserve. At that time, lead–acid batteries were likely the only practical option for energy storage. The emergence and maturing of alternating current (a.c.) systems allowed the transmission and distribution of high-voltage electrical power, which enabled delivery of more electricity over ever-larger areas. These developments also tended to circumvent the continued use of battery-supplied energy. Throughout the century, electric power producers and suppliers (electric utilities) also grew in size, and this extended the benefits of electric power to wider and more remote areas. With continued growth, these producers became neighbours that shared common boundaries. In the interest of system stability and reliability, adjoining utilities began to interconnect their systems, which led to the large utility networks that exist today.

Present networks are now highly interconnected at multiple locations, are well-instrumented, and are very complex. Power flows readily through the interconnections, and each utility typically generates at a level such that its power interchange with each neighbour sums to zero. Utilities often negotiate buy–sell agreements that are attractive to both or to multiple participants. Each utility also maintains a spinning reserve (there may be exceptions), i.e., generation that can be quickly brought on line. A specified level of spinning reserve, e.g., unloaded generation, which is synchronized and ready to serve additional demand, is usually a requirement imposed by some regulatory authority. Traditionally, spinning reserve was supplied by a generator that was 'spinning' in synchronization with the supply network in order to be quickly available. In recent years, however, the term 'rapid reserve' came into use because, with the advent of stored energy interconnected to the supply network via power electronics, the reserve resource does not necessarily 'spin'. Moreover, the stored energy resource interfaced via power electronics has a much faster response and, thus, has additional capabilities (see Section 10.4). The two terms, 'rapid reserve' and 'spinning reserve', represent similar functions and are sometimes used interchangeably. The following distinction may be useful. 'Spinning reserve' is unloaded generation that must 'spin' in synchronization with the network in order to be quickly available, e.g., hydro-powered generation. 'Rapid reserve' is an electrical power/energy resource that is not required to 'spin' in synchronization with the system and is available almost instantaneously (in milliseconds) [2], e.g., a BESS.

Also at the turn of the 20th century, the electronic processing of electrical energy, i.e., power electronics, was essentially a matter of controlling electronic conduction processes in gases and vacuums [3]. These rudimentary switching devices were followed by a succession of improved alternatives, e.g., grid-controlled rectifiers, magnetic amplifiers based on saturable-core magnetic reactors, and selenium rectifiers. The modern era of electronics began in 1948 at the Bell Telephone Laboratory with the invention of the transistor, which is a three-layer, two-junction, semiconductor device. In 1956, the same laboratory invented a four-layer, three-junction, triggering transistor, which is now known as a thyristor and also as a silicon controlled rectifier (SCR). The modern era of power electronics dates, perhaps, from the commercial introduction of the thyristor, or SCR, by the General Electric Company (GE) in 1958 [4]. This unidirectional power switch was followed by a host of other semiconductor-technology switches that have advanced power electronics to gigawatt power levels and to megahertz switching frequencies [3].

From a historical perspective, it is notable that power electronics is increasingly expanding opportunities to exploit the advantages inherent in high-voltage direct-current (HVDC) power transmission. These advantages include lower peak values of current and voltage for a given power capacity, reduced environmental impacts, reduced parasitic losses, and convenient volt–ampere reactive (VAR) control. Additionally, a HVDC link is often beneficial when interconnecting two asynchronous a.c. systems. Several examples of bi-directional interfaces between a.c. and d.c. systems at transmission voltages can be cited [5]. A recent system, perhaps indicative of the state-of-the-art, is a bi-directional, 1.4-GW, 250-kV, HVDC link between two 500-kV, 60-Hz transmission systems. The two HVAC

systems are on adjacent islands separated by 51 km of ocean, and the HVDC link is a submarine cable. This system was commissioned in June 2000, and there are plans to double its capacity by increasing the d.c. link voltage to 500 kV [6]. To date, utility interactive BESS systems have interfaced a.c. systems via primary distribution or lower voltage levels.

Through much of the 20th century, electric utility loads tended to be linear, i.e., drawing sinusoidal current from sinusoidal excitation. Typical commercial and industrial loads were, for example, furnaces and induction motors, which were powered directly from a.c. distribution without using switching controls such as adjustable speed drives. These loads were linear, slightly inductive, and unlikely to have a negative impact on power distribution. Throughout this era, power quality and reliability enhancement was largely limited to providing a spinning reserve, voltage regulation via autotransformers on long distribution lines, and power factor adjustment via distributed capacitor banks and synchronous condensers (at generating stations and sub-stations) — all linear interventions.

Since the early 1980s, many large energy-storage systems have been placed in routine, daily service to the benefit of either a host electrical utility or consumers with large, sensitive electrical loads. The storage systems have served numerous purposes including rapid (spinning) reserve, load levelling, peak shaving, voltage/frequency stabilization, VAR control, and facility upgrade deferrals (these terms are defined later in Section 10.4). The applications encompass a host of interventions such as the economic dispatch of stored energy and the enhancement of power quality and/or power reliability. In these roles, storage systems can be enormously valuable, but they are also expensive. The great majority of systems deployed has been BESS designs based on lead–acid technology. Computer-based, power-electronic control systems are creating a growing demand for reliable, high-quality electrical power that can be available via energy storage systems. This trend favours a growing number of BESS applications, but cost remains an issue.

10.3. Energy-Storage Technologies

In addition to lead–acid batteries (flooded and VRLA), there are other energy storage technologies that are suitable for utility- or large-scale applications. These include: (i) advanced batteries, e.g., redox-flow (vanadium, Regenesys), sodium–sulfur, zinc–bromine, lithium-ion; (ii) low- and high-speed electromechanical flywheels; (iii) superconducting magnetic energy storage (SMES); (iv) supercapacitors; (v) pumped-hydroelectric ('pumped-hydro') energy storage; (vi) compressed-air energy storage (CAES). Among these, pumped-hydro and CAES typically differ in scale (capacity) from the others; both are capable of high-power, high-energy (hours duration) discharges. They also differ in response times, taking multiple seconds to minutes to come on line from a standby or spinning-reserve status. Thus, they are not suitable for power-quality applications that require a more rapid response. Pumped-hydro and CAES also require special topological formations for implementation, i.e., upper and lower reservoirs for pumped-hydro, and aquifers or salt caverns for CAES. They are better suited for assignment as a

dispatchable energy resource for load levelling, for example, rather than as a distributed resource available from a standby status within milliseconds, i.e., a rapid-reserve resource. As a consequence, pumped-hydro and CAES energy-storage systems are only mentioned peripherally in this review.

An ideal energy-storage system is one that is well matched to its particular application, i.e., it would be scaled to meet the demands of the application. The most broadly applicable system would be capable of the following attributes:

- high power ratings (tens of MW)
- high energy-storage capacity (tens of MWh)
- separable power and energy ratings
- fast response times (ms)
- four-quadrant capability, i.e., watts and volt–ampere reactive (VAR) capability
- high turn-around efficiency
- low self-discharge
- black-start and island operating capability
- low investment and operating costs
- environmentally benign.

Energy-storage systems with lead–acid (flooded or VRLA) batteries as the storage component can have most of these attributes. On a given cycle, however, the energy available from a BESS is a function of the rate (power) at which it is withdrawn.

Lead–acid batteries, small (micro) SMES and low-speed flywheels are reasonably mature storage options, and all are suitable for some energy-storage applications. Among these several options, lead–acid batteries are the more mature. They are readily available from multiple, competing sources at listed prices, and many BESSs have established an impressive performance record (see Section 10.5). Low-speed flywheels and micro SMES systems are commercially available; multiple units are in service and price quotes are available. High-speed flywheels, large (mega) SMES, advanced batteries, and supercapacitors tend to be conceptual, prototype, or demonstration units. Pumped-hydro is a mature technology; many systems are in service and prices are quoted [7]. Only two large-scale CAES systems are in service, a 290-MW system in Huntorf, Germany and a 110-MW unit in McIntosh, Alabama, USA [8]. CAES is considered a commercially available technology, perhaps because the technology components are mature [7].

The power requirements of several energy-storage applications, together with the power capabilities of the several energy-storage options, are illustrated schematically in Fig. 10.1 along a common scale (abscissa) [9]. (The technology power ratings in Fig. 10.1 do not necessarily represent existing energy-storage systems. They are power ratings that are considered to be feasible based on the status of the technologies in 1996. Power ratings for pumped-hydro, for example, are not limited by technology. An example of a large-scale pumped-hydro facility is the Rocky Mountain facility near Atlanta, Georgia, USA, which is rated at 848 MW with a run-time of about 8 h [10].) From a power-rating perspective, the energy-storage systems rank, in descending order, as follows: batteries, SMES, flywheels, supercapacitors. A similar illustration which compares energy requirements and availability, in terms of

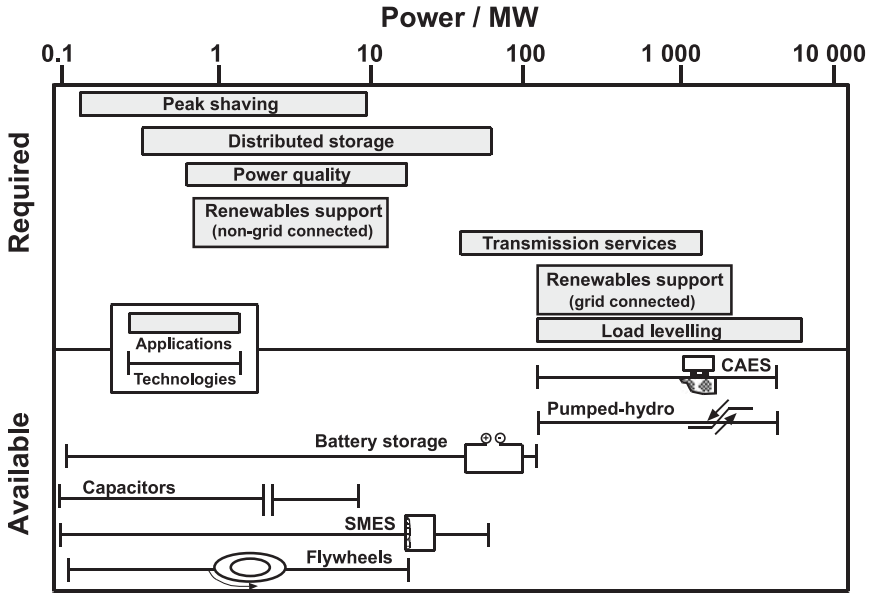

Fig. 10.1. Power requirements and capacities for energy-storage system applications and options [9].

discharge duration, is shown in Fig. 10.2 [9]. In this case, the descending-order ranking is: batteries (hours duration), flywheels, supercapacitors, SMES (seconds to minutes duration). These two illustrations indicate that BESS is suitable for a broad spectrum of applications. In terms of power requirements, SMES is a close competitor but is not well suited for applications that require long-duration (high-energy) discharges. These rankings are not absolute and are subject to change, because these technologies are still evolving. (Note: the high-power, high-energy capacities of pumped-hydro and CAES are also evident in Figs. 10.1 and 10.2, but these options are not generally suitable as distributed resources because of siting restrictions.)

The content of Figs. 10.1 and 10.2 is summarized in Fig. 10.3 by showing power as a function of discharge duration for both applications and energy-storage technologies. Supercapacitors, flywheels, and SMES are shown to be primarily useful for power-quality applications. Batteries are suitable for a broad spectrum of applications, and pumped-hydro and CAES are shown to be primarily useful for load levelling [9].

It is notable that, among these energy-storage technologies, only super-capacitors and SMES store energy directly as electricity. Batteries store energy in chemical form, and flywheels, pumped-hydro and CAES store energy in mechanical forms. For these latter four options, conversions are necessary both to charge the store from an electrical supply and to recover and use the stored energy as electricity.

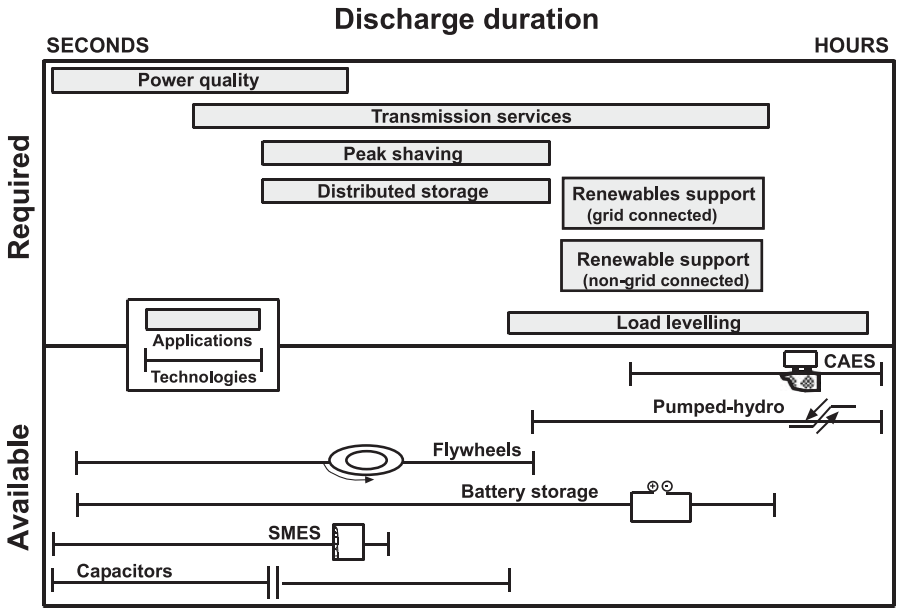

Fig. 10.2. Discharge duration (energy) requirements and capacities for energy-storage system applications and options [9].

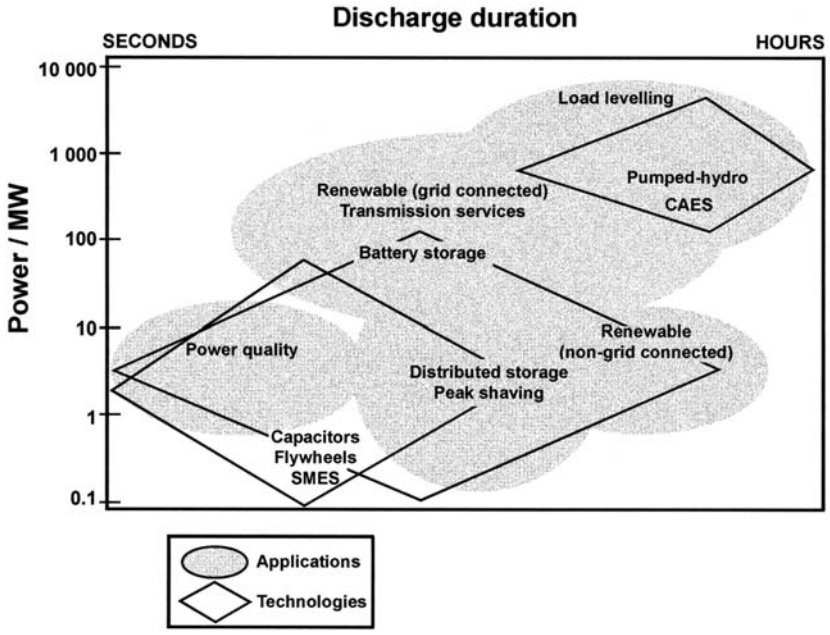

Fig. 10.3. Schematic illustration of power and duration (energy) requirements of energy-storage system applications and options [9].

10.3.1. Lead–acid (and advanced) batteries

Batteries store energy in chemical form in the active mass of electrochemical cells. In most batteries, e.g., lead–acid and nickel–cadmium, the active mass is integrated into the electrodes of the electrochemical cell, and the capacity and power are nearly proportional to the battery weight. In other electrochemical storage systems, e.g., zinc–bromine, and the vanadium systems (V^{2+}–V^{5+}) and the Regenesys (Na_2S_2–Br_2) redox flow systems, the active mass is in the electrolyte(s), which is stored externally and is pumped to the electrodes. In this case, the battery capacity (energy) can be changed independently of battery power by altering the size of the external storage tanks.

Batteries deliver d.c. when discharging and accept d.c. when charging. Thus, when used in a.c. systems, conversions between a.c. and d.c. are necessary in both directions. Among the several storage technologies, BESS is, perhaps, the most versatile because of its high specific power, acceptable specific energy, relatively low cost, and wide spectrum of applications. The response time of a BESS is typically about 4 ms.

10.3.2. Supercapacitors

Conventional capacitors store energy in the electric charge between two conducting plates that are separated by an insulating or dielectric material. The quantity of energy stored is given by:

$$W = CV^2/2 \tag{10.1}$$

where W is the energy in joules; C is the capacitance; V is the voltage across the plates. Capacitance, in turn, varies directly with the area of the plates and inversely with their separation, i.e.,

$$C = KA/d \tag{10.2}$$

where K is the dielectric constant of the material between the oppositely charged electrodes; A is the area of either of the charged plates; d is the separation between the charged plates. Supercapacitors differ from conventional capacitors in that they are 'electrolytic' rather than 'electrostatic' devices; they store energy at the interface between the ionic conducting electrolyte and the electronic conducting electrode (typically carbon), which forms an electrochemical double-layer. The carbon materials used have a very high surface area (up to $2000\,m^2\,g^{-1}$), and the electrode separation is of the order of a few angstroms. The voltage ratings of these supercapacitors are low, typically about 1.5 V for systems with aqueous electrolytes and about 3 V for systems with non-aqueous electrolytes. On the other hand, their specific energies can be thousands of times higher than conventional capacitors. In addition to the double-layer configuration, a redox configuration is also known. These redox capacitors, which are based mostly on ruthenium oxides, tend to be too expensive for most applications.

Compared with lead–acid batteries, the specific energies of supercapacitors are relatively low ($\sim 10\,\mathrm{Wh\,kg^{-1}}$). Nevertheless, they can be charged and discharged at very high rates (high-power capability) and can be cycled tens of thousands of times.

10.3.3. Flywheels

Flywheels store kinetic energy in the rotating mass of their rotors. The amount of energy stored is proportional to the mass of the flywheel and the square of its angular velocity. The latter is limited by the tensile strength of the rotor material. Lightweight materials allow higher speeds than heavy materials of the same tensile strength and, therefore, they can store more energy per unit weight and per unit volume. High-speed flywheels have rotors made of plastic reinforced with fibres of high tensile strength and sustain speeds up to 100,000 revolutions per minute (rpm). Low-speed flywheels have rotors made from steel of high tensile strength and are capable of only about 10,000 rpm.

Flywheels can deliver very high power, which is usually limited by the interfacing power electronics. The largest commercially available flywheels can supply about 1.6 MW for about 10 s, or about 4.5 kWh. They are often used in uninterruptible power supply (UPS) applications. Flywheels are much less costly than SMES and supercapacitors, and they compete with batteries in high-power, low-energy applications. The response time of a flywheel energy-storage system is of the order of a few milliseconds.

10.3.4. Superconducting magnetic energy storage

Superconducting magnetic energy storage (SMES) systems store energy in the magnetic field produced by current circulating through a superconducting coil. When cooled below its critical temperature (−269°C), the resistance of the superconducting coil drops to zero and, subsequently, the coil can conduct very high currents without electrical losses. (Note: critical temperatures vary among superconductors; the critical temperature of a superconducting coil that has been used in several SMES systems is –269°C.) The only losses in a SMES system are those associated with the refrigeration that is necessary to maintain the coil temperature below the critical value, and those in the power-conditioning circuitry, i.e., the non-superconducting components. The power available from a SMES system is limited only by the ratings of the power electronics. As with flywheels, the energy capacity of SMES systems is quite low, e.g., only a few kWh. The energy available from SMES is independent of the power level. The response time is also a function of the power electronics and is typically less than 4 ms. SMES systems are applicable where fast response, high-power, and low energy are needed, e.g., UPS and power-quality interventions.

10.4. Energy-storage Applications

Stores of energy that can be delivered as electricity on demand can resolve a host of power and energy issues that arise with electricity supply networks. These issues

encompass a wide spectrum of applications, which range from fast-response (milliseconds), high-power and short interventions (seconds-to-minutes) for enhancing power quality, to slow-response (seconds-to-minutes), high-energy and long interventions (minutes-to-hours) for improving economic despatch. These applications have been described in numerous publications. Two excellent examples are a Sandia National Laboratories (SNL) report [11] and a German publication that presents much information about BESS applications [12]. These documents identify power-supply network concerns that can be circumvented via a substitute or supplemental source of electricity and examine the ability of available and evolving energy-storage systems to alleviate such concerns. Contributors to the SNL report included an appreciable number of experts on the operation of utility and energy-storage systems. The SNL report is reasonably definitive in that, in many instances, parameter values (e.g., watts, durations, etc.) are quantified. These ranges of values are presented as order-of-magnitude estimates and have not necessarily been implemented in actual systems. Note that, the power rating of an energy-storage system is often the power rating of the power-conditioning electronics. The power-supply network concerns are discussed in the following sub-sections.

The following definitions may be helpful to readers unfamiliar with electricity-supply networks. In an a.c. system, the excitation voltage (V) is sinusoidal (i.e., the instantaneous voltage, $V_i = V_{max} \sin 2\pi ft$) and, in general, so is the current (amperes). If the load supplied is entirely resistive, the current (A) will be in-phase with the voltage and the power or watts (W) delivered to the load is the product VA (W = VA). If the load is entirely capacitive or entirely inductive, the current will lead the voltage by 90° or lag the voltage by 90°, respectively. In either case, power delivered to the load is zero. Fortunately, this circumstance is rarely, if ever, encountered. In most electricity-supply networks, the load is somewhat inductive and current lags voltage a few degrees, i.e., the power factor (see below) will be about 0.95. (Capacitors and inductors are called reactive loads and their reactance (impedance) is related to the excitation frequency, f, as follows: $X_l = 2\pi fL$ for inductors and $X_c = (2\pi fC)^{-1}$ for capacitors, where f is the excitation frequency, L is the inductance (in henrys) and C is the capacitance (in farads). The term $2\pi f$ is sometimes written as ω.)

It is instructive to represent power in an a.c. system via a 'phasor' diagram, as shown in Fig. 10.4. In this representation, the product VA, has a projection on the abscissa (real or power axis) and on the ordinate (quadrature, reactive power, or VAR axis), and the following relationships apply:

(i) VA is just that, the product of the root-mean-square values of V and A;
(ii) power (W) = VA × cosine θ (θ is the power-factor angle, i.e., the angular displacement between V and A, and cosine θ is the power factor);
(iii) reactive power, VARs = VA × sine θ.

Utilities need to keep the power factor near to unity, and they often purposely elect to draw leading current (e.g., via capacitors or synchronous condensers) to improve or maintain power factor at a value above ~0.95. Reactive power (VARs) is not real power, does no useful work, and does not spin a revenue meter.

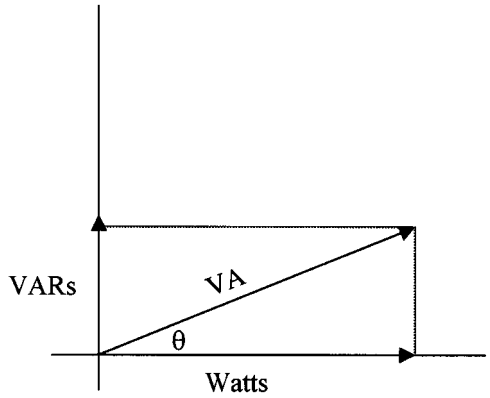

Fig. 10.4. A graphic illustration of relationships between VA, VARs, and Watts.

10.4.1. Rapid reserve (generation)

The above-mentioned SNL study [11] defines rapid reserve as 'generation capacity that a utility holds in reserve to meet National Energy Reliability Council (NERC) Policy 10 requirements to prevent interruption of service to customers in the event of a failure of an operating generation station'. The term rapid reserve is an acknowledgment that energy-storage systems meeting these requirements are not necessarily 'spinning'. Power-quality applications, for example, require a standby power source to be available within about 4 ms (about one-fourth of a 60-Hz cycle), whereas a traditional energy reserve that was 'spinning' was available within a few seconds at best (see Section 10.2). Power and duration requirements for an energy-storage system to provide rapid reserve are typically in the range of 10–100 MW for 10–100 min, respectively, for perhaps 10 times per year.

10.4.2. Area control and frequency responsive reserve (generation)

Area control is the ability of grid-connected utilities to prevent unplanned transfers of power between themselves and neighbouring utilities, while frequency responsive reserve is the ability of isolated utilities to respond instantaneously to frequency deviations. These applications, too, stem from NERC Policy 10 requirements [11]. Interconnected utilities must operate at the same frequency ('frequency control'), otherwise power will transfer between them. The remedy is for the offending utility to generate additional power. (Transfers of power among utilities can, however, be planned for and accommodated.) In the case of an isolated utility, e.g., an island utility, frequency deviations from the standard are a first indication of insufficient generation, i.e., excessive load. Remedies are either additional generation, perhaps from energy storage, or load shedding. Power requirements for these applications are in the range of 10–100 MW.

10.4.3. Commodity storage (generation)

Commodity storage is the capture of inexpensive off-peak power for (economic) dispatch during relatively expensive on-peak hours [11]. From a generation perspective, commodity storage also encompasses 'systems management' applications such as 'load levelling' (energy-cost savings), 'peak shaving' (demand-cost savings), and 'generation capacity deferral' [9]. The requirements of the energy-storage system are 1–100 MW for about 1–10 h, perhaps 100 times per year.

10.4.4. Transmission system stability (T&D)

Transmission system stability is required in order to keep all components on a transmission line in synchronization with each other and thus prevent system collapse [11]. Requirements are 1–100 MVA for 60–6000 ms, about 100 times per year.

10.4.5. Transmission voltage regulation (T&D)

Transmission voltage regulation is used to maintain the voltages at the generation and load ends of a transmission line within 5% of each other [11]. This involves supplying watts, and perhaps VARs, at selected locations to meet load demands. The requirements of the energy-storage system are 1–10 MVAR for 10–100 min. (Note: VAR is an acronym for volt–amperes reactive. In d.c. systems, voltage and current (amperes) are in-phase (VAR = 0) and power is defined as the product of volts and amperes, see Fig. 10.4 and associated text.)

10.4.6. Transmission facility deferral (T&D)

Transmission facility deferral refers to the ability of a utility to postpone installation of new transmission lines and transformers by supplementing the existing facilities with another resource [11], e.g., a BESS. In this application, BESSs function as fast-response sources of generation at selected locations. The requirements of the energy-storage are 0.1–1 MW for about 100 min, perhaps 100 times per year.

10.4.7. Distribution facility deferral (T&D)

Distribution facility deferral differs from transmission facility deferral only in that the storage resource is utilized along a distribution line (i.e., local, low-voltage, e.g., 23 kV, distribution) rather than along a transmission line (i.e., long-distance, high-voltage, e.g., 500 kV, 'bulk' distribution). The energy-storage system has to perform in essentially the same manner as that for transmission facility deferral, i.e., 0.1 to 1 MW for about 100 min, perhaps 100 times per year.

10.4.8. Renewable energy management (customer service)

Renewable energy management involves the application of storage systems to allow such energy to be available during periods of peak utility demand (coincident peak) and at a consistent level or rate [11]. The storage requirements are 0.01–100 MVA for 0.001–1000 min for hundreds of times per year.

10.4.9. Customer energy management (customer service)

Management of the demand on utility-sourced power by the dispatch of energy stored during off-peak or low-cost time periods is known as customer energy management [11]. This also encompasses 'peak shaving' and 'load levelling' (see commodity storage, Section 10.4.3), but from a customer perspective. The requirements of the energy-storage system are 0.01–10 MVA for 10–100 min for hundreds of episodes per year.

10.4.10. Power quality and reliability (customer service)

Energy-storage systems that circumvent voltage spikes, voltage sags, and power outages that last for a few cycles (less than one second to minutes) are helpful for customers with demands of less than 1 MW. The enhanced-quality power can reduce or prevent data loss and production disruptions [11]. There are BESSs that meet these requirements for customers with demands much greater than 1 MW, e.g., the BESS at Vernon, see Section 10.5.9.

10.5. Battery Energy-storage Systems

Many, perhaps most, of recent (since 1980), utility-scale BESSs are presented in Table 10.1. For each BESS, details are given of the location, rated capacity, principle applications, and date of installation. The more familiar systems, i.e., those for which descriptive information is reasonably available, are discussed below. In recent years, the lead–acid battery, energy-storage, and related industries have often been involved in acquisitions and other corporate structure changes such that name changes have taken place. The following discussion uses names that were appropriate when the BESSs came to public attention.

10.5.1. Elektrizitätswerk Hammermuehle, Germany

Hammermuehle is a small distributor of electric energy with a single customer that accounts for about 70% of its total load. The company purchases over 99% of its energy from a bulk power supplier and produces the remaining 1% via hydroelectric generation. The 400-kW, 400-kWh BESS at Hammermuehle has been used for peak shaving and the attendant reduction in demand charges. After 20 years of service (from 1980), this BESS was shut down in 2000 when the battery reached the end of its service life. The battery was not replaced and

Table 10.1. Recent (since 1980) large-scale BESSs.

BESS	Location	System capacity[a]	Applications[a]	Date[b]
Elektrizitätswerk	Hammermuehle, Germany	400 kW, 400 kWh	• Peak shaving	1980
BEWAG AG	Berlin, Germany	17 MW, 14 MWh	• Frequency control • Spinning reserve	1986
Kansai Power Co.	Tatsumi, Japan	1 MW, 4 MWh	• Multipurpose demonstration	1986
Hagen Batterie AG	Soest, Germany	500 kW, 7 MWh	• Load levelling	1986
Crescent EMC	Statesville, NC, USA	500 kW, 500 kWh	• Peak shaving	1987
Delco Remy Division, GM	Muncie, IN, USA	300 kW, 600 kWh	• Peak shaving	1987
Southern California Edison	Chino, CA, USA	10 MW, 40 MWh	• Multipurpose demonstration	1988
Vaal Reefs Exploration & Mining Co.	South Africa	4 MW, 7 MWh	• Peak shaving • Emergency power	1989
Johnson Controls, Inc.	Humboldt Foundry Milwaukee, WI, USA	300 kW, 600 kWh	• Peak shaving • Load levelling	1989
SDG&E	San Diego, CA, USA	200 kW, 400 kWh	• Peak shaving	1992
Pacific Gas & Electric (PM250)	San Ramon, CA, USA	250 kW, 167 kWh	• Power management	1993
Puerto Rico Electric Power Authority (PREPA)	San Juan, Puerto Rico	20 MW, 14 MWh	• Spinning reserve • Frequency control • Voltage regulation	1994
GNB Technologies	Vernon, CA, USA	3.5 MW, 3.5 MWh 2.45 MW,4.9 MWh 1.8 MW, 5.5 MWh	• Peak shaving • Spinning reserve • Environmental	1996
Metlakatla Power & Light	Metlakatla, AK, USA	1.3 MW, 1.3 MWh 915 kW, 1.83 MWh 700 kW, 2.1 MWh	• Utility stabilization • Power quality • Environmental	1997
Grid interactive, 1 MW solar plant with BESS	Herne, Germany	1.2 MW, 1.2 MWh	• Peak shaving • Power quality	1999
Grid interactive, 2 MW wind farm with BESS	Bochold, Germany	1.2 MW, 1.2 MWh	• Peak shaving • Power quality	1999
PQ2000	Homerville, GA (First commercial)	2 MW, 10 s	• Power quality • Standby power	1997

[a]Multiple entries under system capacity and applications for a BESS do not imply a correspondence between side-by-side entries.
[b]It is not always clear whether the reported date is for completion or commissioning of the BESS. Most are thought to be commissioning dates. The discussions that follow are more definitive about dates of events, when possible.

the BESS was taken out of service because the utility rate structure at that time reduced the potential for realizing cost savings. Nevertheless, the system is of particular interest because of its longevity.

The battery consisted of 114, tubular-positive cells, each with a C_4 capacity of 3200 Ah. In 1993, and again in 1995, the battery was capacity tested and exhibited a C_4 capacity of 98.8 and 94.8%, respectively. Thus, after 15-years of service, the battery appeared to be in very good condition and was expected to provide several additional years of peak-shaving service. Its longevity was likely due to the fact that the total energy throughput was relatively low, i.e., approximately 384 cycles after 12 years of operation [13].

10.5.2. BEWAG AG, Berlin, Germany

The BEWAG BESS facility was installed in 1986 to provide spinning reserve and frequency regulation for the isolated ('island') utility that served West Berlin. When placed in service, it was the largest lead–acid BESS in the world. It functioned for seven years, from the beginning of 1987 through to 1993. In December 1993, BEWAG was connected to the West European grid; this resolved the frequency deviation problem. Subsequently, the BESS continued to provide a spinning reserve until the end of the battery's service life, an additional two years. The battery's nine-year service life (1987 through most of 1995) was remarkable and there were virtually no problems. During the seven-year period that the system provided both frequency regulation and spinning reserve, the battery had a capacity or turnover of about 7000 times its nominal 14-MWh energy capacity, i.e., about 98 GWh.

The BEWAG battery consisted of 12 parallel strings, each with 590 cells ($= 7080$ cells). The cells were configured in 1416 modules, i.e., 5 cells per module. Each cell had a capacity of 1000 Ah at the C_5 rate; thus, the nominal battery capacity was 12,000 Ah or about 14 MWh (at 1180 V). The cells were made by Hagen and used flooded, copper-stretch-metal (CSM) technology, which featured enhanced negative-plate conductivity [14]. The CSM technology evolved, at least in part, as a response to the need to reduce the electrical resistance of the grids in large cells. In large (tall) cells, this resistance tends to be a greater percentage of the total internal resistance of the cell. Consequently, tall plates would not discharge uniformly, to the detriment of the cell. In CSM-technology, cells, the negative grids are copper plated with a thin layer of lead, and the positive plates are tubular. This design yields a more uniform current distribution in cells and, thus, better cell performance. A more detailed discussion of CSM technology is given in Chapter 13 [1], and also in Refs. [14,15]. Note that, the term OCSM also refers to a CSM-technology battery, a stationary battery; and so does the term OCSV, which is a 'sealed' or valve-regulated version [16].

The BEWAG battery was connected to a 30-kV distribution line via four parallelled converters. When providing frequency control, the converters were programmed to limit power flow to 8.5 MW. For spinning reserve, the power limit was increased to supply 17 MW [16].

10.5.3. Hagen Batterie AG, Soest, Germany

A 500-kW, 7-MWh BESS was placed in service at a Hagen industrial battery plant in Soest in 1986 to reduce energy cost by lowering energy demand and attendant demand charges via peak-shaving. The system was well instrumented and computer controlled such that utility-supplied power could be limited to a selected value. If the load exceeded the selected limit, the BESS supplied the excess demand. When the load demand fell below the selected limit, the system functioned to recharge the battery while continuing to limit the utility demand to the selected value. Typically, the battery began the week in a full state-of-charge (SoC). Each weekday, load demand would exceed the selected power limit, and the battery would supply the additional demand. When the load demand decreased below the selected utility-power limit, utility power was used to recharge the battery, but within the constraint of the utility-power limit. Thus, there was a daily, weekday cycle that would typically, but not necessarily, recharge the battery, but not always to a full SoC. Each weekend, when the load demand was typically low, the system would fully recharge the battery to 100% SoC. The computer control tracked the SoC of the battery and would, perhaps, alter the utility-power limit to prevent excessive battery discharges and, thus, optimize the performance of the system. Hagen used the BESS to maximize the energy purchased during off-peak periods and minimize the energy purchased during on-peak hours, to achieve appreciable savings in energy costs.

The 7-MWh battery consisted of two parallel strings, each of 200 cells with an individual capacity of 9000 Ah. The cells had tubular positive plates and copper negative grids [14,15]. An electrolyte agitation system prevented, or limited, acid stratification. The 400-V battery was connected to a 380-V bus within the plant via two parallel, 250-kW converters [16].

10.5.4. Crescent Electric Membership Corporation, Statesville, NC, USA

A 500-kW, 500-kWh BESS, located in Statesville, NC, has been used by Cresent EMC as a peak-shaving facility since July 1987 to reduce demand charges paid to their supplying utility, Duke Energy. Electric Membership Corporations (EMCs) are independent companies which, in general, distribute power in small towns and rural areas. The EMCs do not generate power, but purchase power from large, generating utilities such as Duke Energy. There are about 27 EMCs in North Carolina, and they have formed a state-wide organization, NCEMC, to purchase power collectively from the generating utilities. Crescent EMC recently merged with a neighboring EMC and is now known as Energy United EMC. The Crescent EMC designation is used here because the BESS located on their system has been identified with the company since 1987.

The BESS at Crescent EMC was originally installed for test purposes at the Battery Energy Storage Test (BEST) facility in New Jersey and underwent some cycling there, perhaps the equivalent of 200 cycles. At Crescent, it is cycled to reduce the demand whenever there is a possibility that Duke Energy will experience their

monthly peak load. This peak load establishes the demand charge for the entire month. Typically, the BESS is discharged for one hour (at 500 kW) on selected cold winter mornings and for three hours (at 200 kW) on selected hot summer afternoons, i.e., periods likely to correspond to Duke Energy's monthly peak. This strategy does not necessarily require daily discharges. For example, an exceptionally cold winter morning early in the month followed by days with mild temperatures can provide a respite, days when one can be confident that Duke Energy's load will not surpass the earlier monthly peak. On hot summer days, Duke Energy's peak-load is not as predictable and a three-hour discharge is selected to enhance the likelihood that Crescent will reduce their demand during Duke Energy's monthly peak load. The net result of this strategy is that the Crescent BESS is discharged about 75 times annually.

The battery consists of a single string of 324 cells configured six cells per module. These are flooded, deep-cycle cells with lead–antimony grids and were manufactured by GNB, Inc (now Exide). The battery is rated at 500, 300, and 200 kW at the $C_1/1$, $C_2/2$ and $C_3/3$ rates, respectively. When the battery was transferred to Crescent, its measured capacity was in excess of 2200 Ah. It was warranted at that time for 2000 cycles, or eight years, and has far exceeded that expectation.

The converter is a 12-pulse, line-commutated system rated at 500 kW with a three-phase, 480 Vac output. When charging the battery, current is initially limited to about 475 A. Subsequently, charging continues at a nominal, constant 755 Vdc until the current decreases to 30 A. At this point, a separate float charger continues the charging process. At full charge, the float current is about 3 A. Once fully charged, the battery remains on float charge for 48 h unless interrupted for a discharge cycle. If the fully charged battery is inactive for two weeks, the 48-h float charge is repeated [17].

After 15 years of service at Crescent, the BESS continues its peak-shaving duty although the battery capacity is somewhat diminished. There is not definite information on the total number of cycles that the battery has experienced. The automated system functions so routinely that Crescent tends 'to forget it is there'.

10.5.5. Southern California Edison, Chino, CA, USA

As of July 2003, the 10-MW, 40-MWh BESS installed by Southern California Edison (SCE) is believed to be the largest such facility ever assembled. It was located at the Chino sub-station, about 80 km east of Los Angeles. The project was initiated in August 1986, and the facility became operational in July 1988. The project was initiated by SCE, and the Electric Power Research Institute and the International Lead Zinc Research Organization participated by supplying the power-conditioning system and the lead for the batteries, respectively. The BESS was developed as a multi-purpose demonstration project and was used in a host of applications during its nine years as an experimental facility. It was de-commissioned in 1997 when the scheduled experimentation and demonstrations had been completed. The batteries were subsequently recycled. The following BESS

capabilities were demonstrated: peak shaving, load levelling, load following, spinning reserve, transmission and distribution facilities deferrals, frequency control (see below), voltage and VAR control, and black-start operations. The output of the BESS fed a 12.5-kV Chino distribution line that, in turn, fed a 69-kV line at the 230-kV sub-station. The interconnecting 69-kV/12.5-kV transformer operated at near rated capacity during peak hours at the time. In the early stages of service, a two-year test period established the following efficiencies: plant or BESS, round-trip (a.c. to a.c.) efficiency, 72%; battery efficiency, 81%; power-conditioner efficiency, 97%.

A somewhat unusual test project at Chino demonstrated the capacity of the BESS to damp low-frequency oscillations, which can affect the stability and limit the capacity of long transmission lines. SCE is part of the Western States Coordinating Council (WSCC), which consists of 14 western US states, British Columbia, and part of north-western Mexico. These regions are interconnected by a large power transmission system (the 'big O ring') that is generally heavily loaded (SCE imports about 40% of its energy from north-west USA and Arizona). Low-frequency oscillations (0.3–0.7 Hz) limited the power that could be transmitted via this system. Traditional power system stabilizers damp these oscillations by changing reactive power (VAR) output. The Chino BESS provided low-frequency damping and enhanced system stability by modulating its power output. The effectiveness of this service was restricted, however, by the limited power output of the BESS (10 MW).

The battery consisted of 8256 cells (six cells per module) configured in eight parallelled strings of 1032 cells each. The nominal battery voltage rating was 2000 V. The cells were Exide, GL-35 cells and featured compressed-air electrolyte agitation, flame arrestors, acid sampling tubes, thermocouple wells, stibine-arsine traps, and acid-level indicators. The cell capacity was 2600 Ah at the $C_4/4$ rate to 80% DoD. The battery rating was nominally 40 MWh. Cycle-life was warranted to be a minimum of 2000 cycles, which translated to a life of about eight years.

The power conditioner was an 18-pulse, stepped-wave, gate-turn-off thyristor (GTO) converter manufactured by GE. It was capable of four-quadrant operation, i.e., it was bi-directional and VAR capable. It was configured with three, six-pulse converters which were connected in series on the a.c. side and in parallel on the d.c. side. It was rated at 10 MW, and the input window voltage was rated 1750 Vdc to 2800 Vdc. A Westinghouse monitoring and control system provided the BESS with a highly automated supervisory control and data-acquisition capability [18,19].

10.5.6. Johnson Controls, Inc., Milwaukee, WI, USA

A 300-kW, 600-kWh BESS was developed by Johnson Controls as a turn-key, customer-side-of-the-meter demonstration project. It was placed in service at an in-house brass foundry with a base load of about 1.1 MW with 4 or 5 daily peaks to 1.5 to 1.6 MW. The peak loads corresponded to the melt cycles of two, inductively heated furnaces that were operated at the foundry. The BESS was used for peak

shaving and energy-usage redistribution. In the former service, the BESS reduced daily peak-demand charges. In the latter service, however, the associated cost savings were a more complex issue. Johnson Controls employed a control strategy together with the prevailing rate structure and on-peak charging, while still avoiding the higher peaks which corresponded to the furnace melt cycles, to converge to an optimum battery capacity. Thus, the peak demands of the foundry were reduced and the battery capacity was less than the capacity requirement when using off-peak charging. The net result also produced savings in energy costs. The battery DoD was limited to 80%. Of necessity, the operation of this BESS required an interactive, 'smart' controller.

The battery was assembled from VRLA modules of a gelled-electrolyte design, which had excellent deep-discharge capabilities. The modules had lead-coated copper terminals and bus bars, a status indicator that warned if the SoC dropped below 20%, and an internal air manifold for thermal management. The facility contained 64 modules connected in series to produce a 384-V, 1500-Ah battery.

The power-conditioning system was a self-commutated, dual-bridge, six-pulse design. The a.c. output was three-phase, 480 Vac. The BESS typically operated in a constant-power output mode. Charging of the battery was conducted initially at constant power and then finished at constant voltage [20].

10.5.7. Puerto Rico Electric Power Authority

In November 1994, a 20-MW, 14-MWh BESS began commercial operation at PREPA, an isolated island utility. The system provided rapid (spinning) reserve, frequency control, and voltage regulation. The successes of the Chino and BEWAG BESSs influenced the decision to build the PREPA BESS, and with the closure of the Chino facility, the PREPA BESS became the largest in the world. In October 1999, this BESS ceased operation because of numerous cell failures. Because the BESS was otherwise successful and seemingly highly valued by system operators during its five years of service, it was thought likely that PREPA would replace the battery, using different cells, and return the BESS to service and, perhaps, locate similar facilities elsewhere on the PREPA system. As of July 2003, however, the facility was still idle.

The PREPA BESS was a large facility selected by a public utility as the 'best' solution to a costly operating problem, i.e., insufficient spinning reserve and an attendant necessity to resort to load shedding to maintain system stability. The specifications and design were intended to meet the requirements of a commercial plant. No incentive funds or apparatus were involved in its construction.

The PREPA battery consisted of 6000 flooded cells arranged in six parallel strings of 1000 cells each. The rated cell capacities were 1280, 1680, and 2088 Ah at the $C_{0.5}/0.5$, $C_1/1$, and $C_3/3$ rates, respectively. The cells had the following features: flat, wrapped positive plates; flat negative plates; lead-calcium grids; automatic watering and airlift electrolyte agitation. The power-conditioning system was comprised of

two paralleled converters, which were manufactured by GE. Each converter was rated at 10 MVA and had three, 6-pulse GTO bridges (18-pulses) and a capacitor bank for harmonic filtering [2].

10.5.8. GNB Technologies, Vernon, CA, USA

The BESS at the GNB lead smelting and recycling center in Vernon is foremost a UPS system that serves an essential purpose at an environmentally sensitive facility. The recycling centre is located about 16 km south-east of downtown Los Angeles, and it recycles about ten million lead–acid batteries annually. A critically important part of the process is a recovery facility that prevents the escape of lead dust to the environment, which otherwise would be unacceptable both environmentally and economically. The area around the plant is closely monitored, and the owner, GNB (now Exide), would likely face penalties and punitive fines in the event of a single lead-emissions episode. The BESS also has sufficient capacity to be used daily in a peak-shaving role to reduce the power demand and the attendant demand charges of the centre.

Construction on the Vernon BESS began in January 1995 and commissioning tests were completed in November 1995. The BESS took up its UPS role in January 1996. In April 1996, the BESS also began operating periodically, three to six hours daily, in a peak-shaving role to reduce demand charges. By design, the BESS is depleted of about 50% of its capacity when peak shaving, and the remaining 50% capacity is held in reserve for the UPS role, i.e., to continue plant operations in the event of a power outage. It is a demand-side facility and provides an essential benefit on the consumer-side of the revenue meter.

The Vernon BESS was built as a turn-key facility by an established, credible, industrial alliance (GE–GNB) which, seemingly, was willing to quote, build, and warrant large-scale BESS facilities in the future. It is not clear that that is still the case.

The Vernon lead-recycling centre is powered via a three-phase, 4.16-kV feeder from the local utility. The total plant load is typically about 3.5 MVA, but it can peak to a maximum of 5 MVA. The critical loads, i.e., the loads that prevent lead-dust emissions, are about 2.1 MVA. Because of the utility energy-supply configuration, i.e., the critical loads are not isolated, the BESS is designed to carry the entire plant. In the event of an outage or other supply anomalies, the BESS will open the utility supply and carry the entire plant at up to 5 MVA for up to 10 s. During that period, it will shed all but the critical loads and then carry these at up to 3 MVA for about 1 h. Only about 20 min are required for an orderly, emissions-free shutdown of the critical loads. The BESS will either initiate such a plant shutdown or, if utility excitation returns, will synchronize with the utility and transition back to normal power. All these operations can occur automatically. In its peak-shaving role, the BESS battery, by design, has an additional reserve capacity to supply 500 kW for 3 h, or 1.5 MWh.

The battery consists of two parallel strings of GNB Absolyte IIP, type 100A99 VRLA modules of the absorptive glass-mat (AGM) design. These are configured as

three parallel cells per module (5000 Ah) with 378 modules per series string to give a nominal battery voltage of 756 V. The capacity is 3.5, 4.9, and 5.5 MWh at the $C_1/1$, $C_2/2$, and $C_3/3$ rates, respectively.

The power-conditioning system was built by GE and consists of paired, six-pulse converters that form a 12-pulse converter module, and three of these are paralleled to achieve the required power rating. The switches are GTO thyristors. The power conditioner incorporates harmonic filtering and provides for four-quadrant operation, i.e., the equipment is bi-directional and provides VAR control [21,22].

10.5.9. Metlakatla, AK, USA

Metlakatla is a small community on Annette Island, which is some 40 km from Ketchikan, Alaska. The island is relatively inaccessible, especially in the winter, and is usually reached by boat or float airplane. Metlakatla Power & Light (MP&L), a small, isolated utility, supplies the electricity needs of the island. The MP&L load consists of the Metlakatla community, several relatively small commercial loads and, until recently, a large sawmill. The load peaked at about 3.5 MW, and the sawmill load which was about one-third of the total, varied dramatically. The resources of MP&L consisted of about 4.0 MVA of hydroelectric generation and a large, 5.0-MVA/3.3-MW diesel generator. Typically, the hydro units could supply the load but could not respond rapidly enough to follow load fluctuations. As a consequence, MP&L operated the diesel generator, which was oversized to provide an adequate load-following rate, at about 1.0 MW to provide a suitable power dynamic range. Thus, the diesel supplied much of the required energy even though the pumped-hydro reservoirs frequently had to spill water. Moreover, the diesel operation was less efficient and required more maintenance than would have been the case with more favourable loading. Transporting and storing fuel for the diesel and the threat of fuel spills were also issues of concern, especially during the long Alaskan winters.

Studies showed that a BESS on the MP&L system could: (i) help stabilize and improve the power quality of the system, i.e., reduce voltage and frequency deviations; (ii) reduce reliance on the diesel generator, and thus realize attendant savings in fuel-related costs. Subsequently, the GE–GNB alliance (see Section 10.5.8) provided a suitable, 1.6-MVA (10 s)/1.0-MW (continuous) BESS, which was interconnected at a 12.47-kV sub-station. Construction began in April 1996, was completed in December 1996, and the BESS has been operational since February 1997. It provides a rapid (spinning) reserve, i.e., supplies instantaneous power when demand exceeds generation, and it accepts charge when there is excess power available from the hydroelectric generators. In this role, the BESS battery operates for long periods in a partial SoC. By design, it tends to oscillate or 'dither' between about 70 and 90% SoC, and equalization charges are scheduled only semi-annually. Moreover, the diesel generator typically stands idle for long periods of time.

The Metlakatla battery consists of a single string of GNB, Absolyte IIP, model 100A75 modules of the AGM design. Each module consists of three paralleled cells,

and 378 modules are connected in series to form the 756-V battery. The modules have capacities of 3600 and 2000 Ah at the $C_8/8$ and $C_{1.5}/1.5$ discharge rates, respectively. The battery is rated at 1.4, 1.8, and 2.1 MWh at the $C_1/1$, $C_2/2$, and $C_3/3$ rates, respectively. The battery has performed remarkably well. In September 2000, it was reported [23] that the total battery output had been 745,735 Ah or the equivalent of 295 cycles to 80% of the $C_8/8$ capacity, and the total charge returned was 751,468 Ah, which corresponds to only 0.77% overcharge.

In October 1999, GNB and Sandia National Laboratories (SNL) conducted a planned assessment of the battery. Four cells were removed for evaluation. The BESS monitoring system indicated that the battery was at about 78–81% SoC. The measured open-circuit voltages of the cells indicated they were at approximately 78.5% SoC. One cell was maintained in this status for subsequent chemical analysis, while others were subjected to a series of cycling tests, which included a range of discharge rates, overcharging, and equalization charging. The results were very encouraging and suggested that the cells had not been harmed by operating at a partial SoC for extended periods. Subsequent physical and chemical examinations of the electrodes, active materials, and other internal components of the cells were also encouraging. In summary, there were no anomalies, no sign of oxidation corrosion, positive grid corrosion was lower than expected, and there were no indicators of early degradation. It was concluded that the battery would likely exceed its projected design lifetime in this application. The battery is warranted for eight years.

The power-conditioning system (built by GE) is based on GTO thyristor technology and features rapid (4.2 ms) response and bi-directional four-quadrant operation (charge, discharge, and VAR capable), 12-pulse waveform (low distortion), and is self-commutating. It is rated at 1.6-MVA peak (10 s) and at 1-MW continuous power [23].

The sawmill on Annette Island ceased operation about June 2000 because of concern for the loss of trees. Nevertheless, the Metlakatla BESS is still used to stabilize the isolated, island utility. It is reasonable to assume that the BESS battery will last even longer than anticipated and, at the end of its life, will be replaced with a smaller battery.

10.5.10. Herne and Bochold, Germany

Recently, two very similar, multifunctional BESSs began operating in Germany. One BESS was installed in combination with a 1-MW solar plant in Herne, and the other was installed in combination with a 2-MW wind farm in Bochold. Otherwise, these two systems are essentially identical, i.e., the batteries and power conditioners are alike and the systems serve similar purposes. Both systems can store energy from their respective renewable generator and/or the utility grid. Their applications are peak shaving (see Section 10.4.3), UPS, and power quality (see Section 10.4.10). When peak shaving, these BESSs supply stored energy in parallel with the grid supply, and thus reduce the demand from the grid. As an UPS, the BESSs isolate and continue to supply the protected load in the event of a power disruption or

outage. The systems can affect power quality available to the load in several ways, e.g., drawing or supplying VARs to filter harmonics and momentary anomalies actively.

The batteries were assembled using Hagen, CSM-technology cells. The cells have established an excellent record of performance in a host of installations, including the BEWAG and Hagen Batterie, Soest facilities (see Sections 10.5.2 and 10.5.3). A reasonably detailed description of the batteries can be found in several publications [14,15], including Chapter 13 of this book [1]. Other features of the batteries at Herne and Bochold include provisions for automatic watering, electrolyte agitation, and temperature sensing. The cells are configured in three parallel strings of 272 cells (544 V) [15]. The resulting batteries are rated at 2.25 MWh at the 10-h rate (measured 1.47 MWh at the 1 h-rate).

10.5.11. PQ2000

The PQ2000 is a BESS that is designed to meet the growing market demand for high quality, reliable power for industrial and utility applications. It is primarily a rapid reserve resource that temporarily substitutes for the utility supply in the event of a power-line anomaly and, subsequently, returns the load to utility service excitation when the service returns to normal. Its capacity is scaleable, in 250-kVA increments, up to 2 MVA and 10 s duration [24]. This capacity enables the PQ2000 to protect a load from a great majority of the anomalies that defined the Computer and Business Equipment Manufacturers' Association (CBEMA) profile. (The CBEMA profile is a historic plot of episodes of voltage deviations from normal that resulted in computer equipment failures versus their duration. These data create a profile of voltage anomalies likely to disrupt microprocessor- or computer-controlled equipment.) In the event of an extended outage, steps would need to be taken to effect an orderly shutdown of the load or, alternatively, to transfer to a standby generator. It is notable that the developers of the PQ2000 (SNL, US Department of Energy (USDOE), AC Battery, Ominion Power Engineering Corporation, Electric Power Research Institute (EPRI), Pacific Gas & Electric (PG&E), and Oglethorpe Power Corporation) were recognized for its development with a 1997 R&D 100 Award from *R&D Magazine* in the USA [25].

The PQ2000 was designed as a modular BESS. It is housed in three containers that can be transported on a lowboy, flatbed trailer without requiring special permits and can be pad-mounted in an outdoor setting. The three containers house the PQ2000 module, the static switch (i.e., the interface module), and the isolation transformer. The PQ2000 module, which comprises the battery modules and power conditioners, features a roof-mounted ventilating and air-conditioning system for temperature control, and its modularity is designed to simplify maintenance. The PQ2000 is factory-assembled and tested prior to transporting to an installation site.

Modularity is taken a step further in that the battery is configured with up to eight, 250-kW lead–acid battery modules. Each of the PQ2000 modules contains its own inverter and charger, and each contains 48, 12-V batteries (nominally 576 V). When configured with a full complement of eight 250-kW battery modules, there are

384, 12-V batteries in the PQ2000 unit. The full-scale PQ2000 switches from standby to full operation in about one-quarter of a 60-Hz cycle (4.2 ms) and can supply 2 MW/2 MVA for 10 s. When the utility supply normalizes, load excitation is transferred back to the utility supply. If the disturbance is due to a recloser operation of the utility distribution-line, for example, the entire PQ2000 cycle will be completed in about 3 s. (Utilities use reclosers to open momentarily a feeder-line in the event of a fault on the line. Typically, the recloser is programmed to cycle about three times before it latches open and requires operator intervention.)

The batteries are Delco, Model 1150, 12-V units and use flooded, low-maintenance technology. In the PQ2000 application, the batteries are typically subjected to many, very shallow discharges and are quickly recharged using a proprietary algorithm. The power-conditioning inverters, one 250-kVA unit for each 250 kW battery module, feature insulated gate bipolar transistor (IGBT) switching technology. The utility interface is three-phase, 480 Vac [24].

The PQ2000 is commercially available. The first installation was at a lithography plant in Homerville, GA. The plant is served by the Slash Pine EMC, which, in turn, is supplied by Oglethorpe Power Corporation. The lithography plant was fed via a long transmission line in a region that experiences numerous lightning strikes, and the resulting power line disturbances plagued the plant's operations. This PQ2000 has been in service since about 1996. Since installation of the facility, downtime and spoilage have been reduced, productivity increased, and efficiency improved. There have been further PQ2000 installations in other locations.

There are two transportable versions of the PQ2000. An EPRI version, the TBESS, is a significantly modified version, which is nominally designed to provide 250 kW for about 40 min. An SNL version, the Transportable PQ2000, is essentially the PQ2000 permanently mounted and interconnected on a lowboy trailer, which can be coupled to a tractor and readily transported to most locations. The trailer remains with the PQ2000, and transportation to a different location involves disconnecting the wiring and coupling to a tractor. The SNL version was initially placed at a Virginia Power facility in Richmond for about two years. Currently, it is operating at a facility at the S&C Electric Company in Chicago.

10.6. Power Conversion

In the context of BESSs, a power-conditioning system (PCS) is required to interface the d.c. storage component with the balance of the system, e.g., other power sources and loads. A PCS typically includes power converters, filters, control circuits, and usually a transformer, which provides isolation between a.c. and d.c. systems, among other functions. There are many different power-conversion circuits, and PCSs often combine more than one. In BESSs, they typically convert d.c. power to a.c. power, and vice versa. They enable the battery to supply an a.c. load, which is often on a utility grid, and the grid often recharges the battery. In the event of a utility outage, for example, a PCS may isolate an a.c. load from the grid and continue to support it via battery-stored energy (a UPS application). Alternatively, a PCS may function to supplement the utility in the event of utility insufficiency (a rapid reserve

application), or to substitute for the utility in the event of a momentary or short-term power-line anomaly (power quality interventions). It may also deliver or draw reactive power (volt–amperes reactive (VARs)) to enhance voltage regulation.

Prior to the evolution of modern power electronics, power converters were typically rotary machines that combined motor and generator functions or, perhaps, glass-bulb, mercury-arc rectifiers. By contrast, modern converters depend on fast, high-power semiconductor switches and, consequently, are sometimes referred to as static (i.e., non-rotating) power converters. They date from the development of the SCR, a four-layer (pn:pn), three-junction semiconductor structure that functions like a rectifier with a third electrode or control terminal. When forward biased, the SCR remains in an off or non-conducting state until a momentary signal on the control terminal switches it to an 'on' or conducting state. A host of other semiconductor switches with different properties have followed the SCR. All are unidirectional switches that can be controlled to some extent, e.g., selectively turned on when forward biased and perhaps, but not necessarily, turned off independently of being reverse biased. This matrix of power switches is at the core of modern power electronics. Power electronics is based on rapid, repetitive, controlled, on–off switching of electric power. (Linear circuitry is not suitable for high-power applications because of power losses and the subsequent necessity of dissipating the attendant heat.) Increasing the number of switches equates to more waveform options of better quality. In utility networks, the waveform of interest is usually a three-phase sinusoid, and transformers are usually at the interface between the d.c. and a.c. systems. The transformers provide an essential isolation between these systems while concurrently providing other advantages, e.g., filtering and voltage-summing options, which may enhance the quality of the simulated waveforms.

10.6.1. Basic concepts

The purpose of this section is to introduce the basic concept of power conversion. Power conversion encompasses a wide range of applications, electronic components, circuit topologies, and related technical issues. An in-depth discussion of this technology is beyond the scope of this chapter and is best left to texts and papers authored by specialists in power electronics. Three instructive publications are an introduction to the technology by Bose [4], a technology review by Bose [26], and a Sandia National Labs overview report [27].

Power converter terminology can be confusing. Traditionally, a.c. to d.c. converters were referred to as rectifiers, d.c. to a.c. converters as inverters, d.c. to d.c. converters as choppers, a.c. to a.c. (at same frequency) as a.c. power controllers, and a.c. to a.c. (at different frequencies) as cyclo-converters [26]. Power electronic systems often combine multiple conversion processes and are often simply referred to as converters or power-conditioning systems.

A basic converter concept is shown in Fig. 10.5 [27]. As illustrated, the battery can supply an alternating, single-phase, square-wave voltage (current) to the load if the P and N switches are alternately closed and opened. The idealized load current and voltage waveforms would be rich in harmonics and, thus, a poor substitute for a

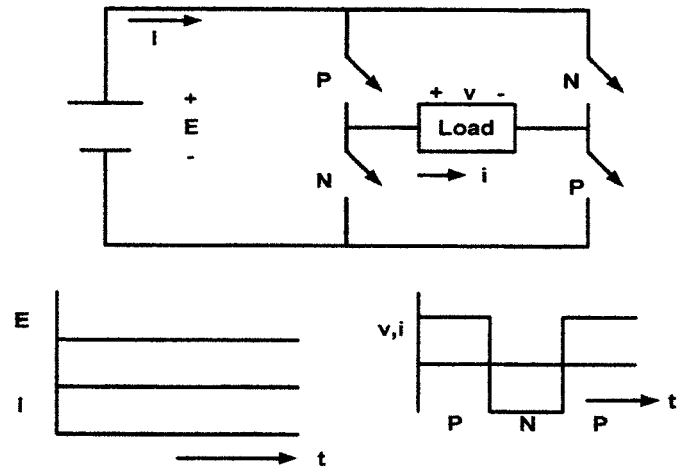

Fig. 10.5. Schematic illustration of basic converter concept.

utility distribution-line sinusoidal waveform. There are, however, remedies for this problem. For example, inserting a brief period when all switches are open between the P-on, N-off and N-on, P-off segments can reduce the harmonic content of the output a.c. waveform.

The load could be a utility distribution line coupled to the converter via a transformer. (Utilities would likely require transformer coupling to provide d.c.–a.c. isolation.) If that were the case, then the same topology could be used to charge the battery by opening and closing the P and N switch pairs at the appropriate times. In fact, if the switches were replaced by appropriately oriented diodes, the topology would be that of the familiar full-wave rectifier.

In many utility applications, the d.c. energy storage source would interface a 3-phase distribution line via a 3-phase power converter. A likely circuit configuration is illustrated in Fig. 10.6 [27]. Note that, the converter differs from the single-phase configuration in Fig. 10.5 in that a third 'leg' has been added, which requires two additional switches. The three outputs, a, b, and c, provide 3-phase power to a utility distribution line via a 3-phase transformer. The switching sequence and idealized transformer excitation waveforms are also included in Fig. 10.6. Each time-segment represents 60 electrical degrees, and the phase voltages shown are the battery voltages applied to the transformer primary windings. As suggested by the waveforms, the output of this configuration begins to approximate a 3-phase, sinusoidal excitation. The same converter, with the appropriate switch configuration, can subsequently recharge the battery from the utility distribution line (see Section 10.6.2). Each of the six switches would likely include a parallel diode or, perhaps, a parallel switch, which would enable the battery to supply and absorb VARs.

The preceding converters are called phase-controlled converters because the switches are turned on and off in a phase-controlled sequence. Further, the converter in Fig. 10.6 is a 6-pulse converter in that the excitation pattern to the three transformer nodes changes every 60 electrical degrees and a complete cycle of

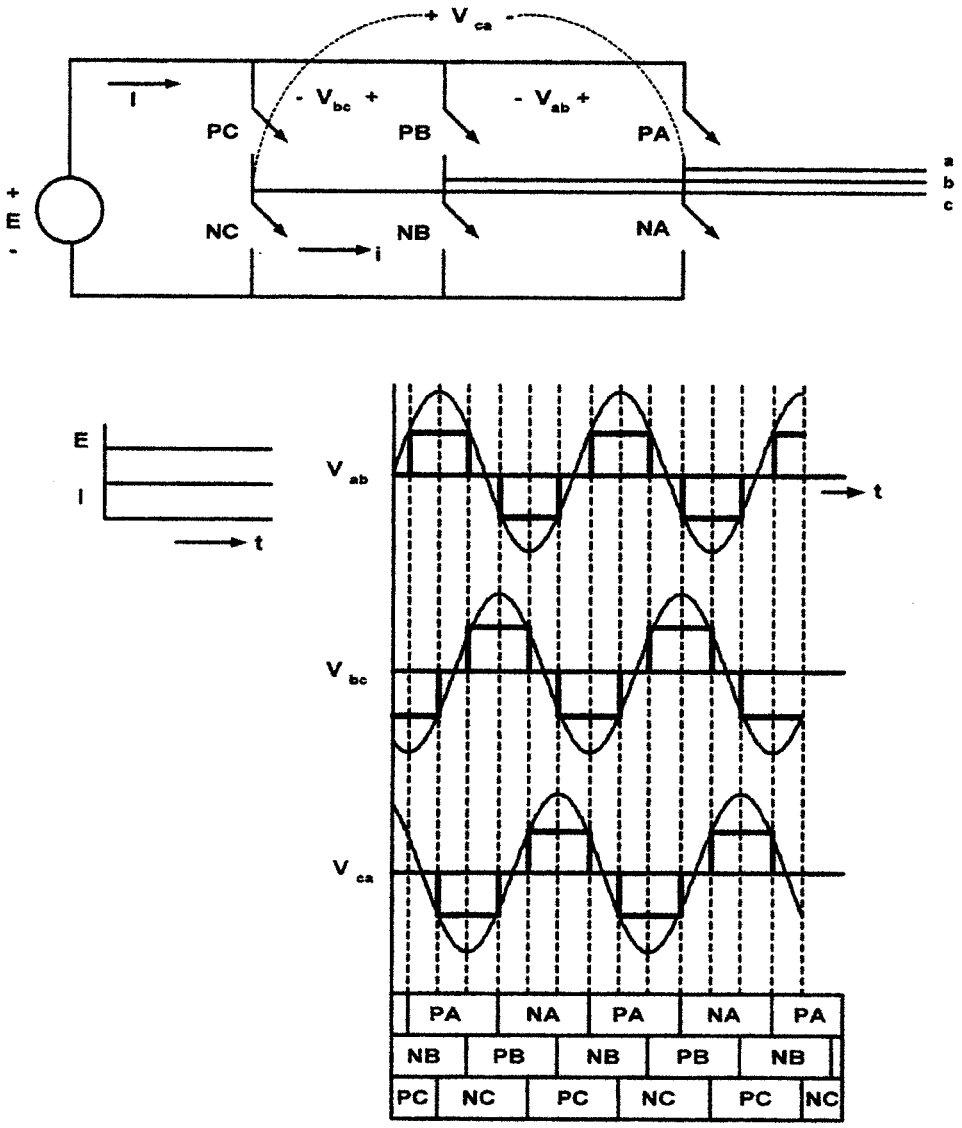

Fig. 10.6. Schematic illustration of basic 3-phase converter.

excitation is completed every 360 electrical degrees. Configurations with additional transformers and switches are often used to provide additional pulses, e.g., 12 or 18. Additional pulses eliminate additional lower harmonics, which equates to improved sinusoidal waveforms (higher harmonics (frequencies) are of a lower magnitude and are easier to filter.)

With the evolution of faster switches, e.g., metal-oxide-semiconductor field effect transistors (MOSFETs) and IGBTs, pulse-width-modulation (PWM) converters

became an option. Whereas the circuit topologies are very similar to the phase-controlled topologies; the switching is much faster and the result is a waveform simulation in which the on–off times of the switches are controlled to simulate a sinusoid. Each pulse, for example, may include an on-time and an off-time, which together define a constant period, and the on-time (or duty cycle), of the pulse would be the variable. The width of the on-time may be controlled to be proportional to the amplitude of a sinusoid at the desired output frequency. A principal advantage of PWM is that high-frequency pulses are much easier to filter than those of lower frequencies, and the resultant, filtered output waveform is improved.

10.6.2. Switch considerations

In modern power converters, the simple switches shown in Fig. 10.5 and 10.6 are, in reality, complex semiconductor devices that largely define the attributes of these converters. For the high-power applications frequently associated with converters that interface energy-storage systems with utility-scale loads, the most commonly used switches are SCRs, GTOs, bipolar junction transistors (BJTs), MOSFETs, and IGBTs. These are unidirectional switches that conduct current in only one direction, and all are controllable to some extent. The first two belong to the thyristor family, which is characterized by higher power, slower turn-on and turn-off, and less control flexibility; and the latter three belong to the transistor family, which is characterized by lower power, faster turn-on and turn-off, and more control flexibility. The thyristor-type switches require a momentary gate or on-signal to turn-on, after which they remain in a conducting state until forced to commutate or turn-off, which can be difficult to achieve. The transistor-type switches require a continuous gate (emitter) signal to remain in a conducting state, and they revert to a non-conducting state when that signal is removed. Depending on the application, it is usually necessary to use other components to compensate for certain limitations and to protect switches from large transients. With the concepts shown in Figs. 10.5 and 10.6, for example, each switch would require a parallel, or back diode to allow conduction in the reverse direction (from normal switch conduction) and, thus, enable battery charging and VAR compensation to occur. Converter switches are also frequently used with snubbers which reduce transient exposure, i.e., they limit dV/dt and dI/dt transients which otherwise could lead to undesired (and potentially catastrophic) switch closures. Switches are critically important in converter technology, and they continue to be the subject of much research and development.

10.6.3. Performance issues

Utility power distribution is intended to be a constant frequency (e.g., 60 Hz in North America), sinusoidal voltage source. Harmonic content is considered an undesirable distortion. The square-wave output of the simple converter illustrated in Fig. 10.5 would contain all of the odd harmonics, but the amplitude of each harmonic decreases as the harmonic number increases. The harmonic content of the

waveform supplied from either phase of the 3-phase converter of Fig. 10.6 would have less distortion; this waveform is a familiar one and is referred to as a 6-pulse output. In general, the more steps taken to simulate the desired sinusoid, the better the result, i.e., less distortion. Each of the three transformer nodes can be connected to either the positive or the negative d.c. terminal of the BESS. Thus, there are six possible connections, and the output waveform can be changed every 60 electrical degrees. If the d.c. excitation is applied to two different converters, one supplying a delta-connected transformer and the second a wye-connected transformer, the 30 electrical degree shift between the delta and wye configurations enables a doubling of the possible steps in the output wave form such that the simulation of the sinusoid is much improved; this provides twelve rather than six steps to approximate the sinusoid. (Note: wye- and delta-connections are two different ways to connect three-phase transformers to other components; to a user, the differences between the two types of connections are usually transparent.) In the latter case, the first harmonic in the waveform is the eleventh. It is evident that additional steps provide for a better approximation of a sinusoid. The converter used in the Chino BESS, for example, used nine single-phase transformers to generate an 18-pulse waveform, which simulated a 3-phase sinusoid whose lowest harmonic was the seventeenth [28].

Another approach to achieving good sinusoidal waveforms from d.c. storage is to use PWM, a simulation technique that varies the on-time of the power switches to simulate the sinusoid waveform. This simulation method requires additional switching, which increases switching-related losses but can also reduce harmonic distortion.

Most BESS applications require four-quadrant operation, i.e., the ability of the a.c. side to both absorb and deliver both VARs and watts. This capacity is provided by the back diodes that parallel the power switches and controls on the firing angles of the power switches.

10.7. Cost Considerations

Perhaps the best available cost estimates for the BESSs discussed in this chapter are those documented in a Sandia report [29]. The data, categorized in a standardized format, were requested from the appropriate utilities and suppliers. Because some suppliers were reluctant to reveal detailed costs and wished to maintain a degree of confidentiality, the costs were aggregated into three categories: the storage sub-system, the power-conversion sub-system (PCS), and the balance-of-plant (BoP). Some of the data were supplied in a percentage form.

Cost estimates for prototype, one-of-a-kind BESS systems of the type discussed in this chapter are often estimates that are not well documented. Demonstration projects, for example, may be funded via multiple sources and the cost estimates assembled somewhat after the fact. Peripheral costs such as site preparations, permitting, installations, etc., are sometimes overlooked. In other instances, unique circumstances not likely to reoccur can result in cost estimates that are not realistic. On the other hand, costs of new systems that are similar to existing or known systems (e.g., Vernon and Metlakatla) and especially systems that are replicated

Table 10.2. Costs of battery energy-storage systems[a,b]

BESS	Capacities	Cost of Sub-systems			Total costs		
		Storage	PCS	BoP	US$/kW	US$/kWh	US$(k)
Crescent[c]	500 kW, 500 kWh	41% US$ 518/kWh	40% US$ 506/kW	19%	1272	1272	636
Chino[d]	10 MW, 40 kWh	44% US$ 201/kWh	14% US$ 258/kW	42%	1823	456	18,234
SDG&E[e]	200 kW, 400 kWh	16% US$ 658/kWh	23% US$ 1855/kW	61%	8150	4075	1630
PREPA[f]	20 MW, 14 MWh	22% US$ 341/kWh	27% US$ 294/kW	51%	1102	1574	22,042
Vernon	3 MW, 4.5 MWh	32% US$ 305/kWh	19% US$ 275/kW	49%	1416	944	4250
Metlakatla	1 MW, 1.2 MWh	—	—	—	—	—	1200
PQ2000[g]	2 MW, 10 s	9%	65% US$ 316/kW	26%	495	—	899

[a]Data taken from Sandia reports [29]. Additional cost details for Crescent, Chino, SDG&E, PREPA, and Vernon are included in Appendix C of Ref. [29].
[b]Costs are in constant 1995 US$.
[c]Crescent BoP cost is exclusively the cost of a building (US$ 81,000) to house the BESS, the only cost incurred by Crescent.
[d]Chino BoP cost includes US$ 150K for load interface, US$ 3.8M for facility, and US$ 1.7M for services.
[e]The SDG&E BESS was a demonstration project that was over-engineered in many respects.
[f]PREPA is comparable with Chino, but was built six years later. The PREPA PCS is an improved version of the Chino PCS, and both were built by GE. BoP cost includes US$ 600K for load interface, US$ 1M for finance charges, US$ 4.7M for building the facility, and US$ 1.8M for services.
[g]The high discharge rate of the PQ2000 distorts the battery cost when specified in US$ per kWh. The PCS cost includes the converter and the static switch. The BoP cost includes delivery, installation, and start-up. Commercial maturity and economy-of-scale may have reduced the total cost below the given value.

(e.g., the PQ2000) will eventually benefit from economies-of-scale and familiarity. As a consequence, the costs listed in Table 10.2 should be viewed as approximations.

10.8. Concluding Remarks

The seventeen BESSs listed in Table 10.1 date from 1980 to the present. These systems encompass a wide range of capacities and a multitude of applications. They also reflect a maturing of BESS technology. Of the ten systems dating from 1980 through 1992, two are multipurpose demonstrations systems (Chino and Kansai Power). Three of these ten systems were operated by supply-side interest (Chino, Kansai Power and BEWAG), and the remaining seven by demand-side interest (including distributing utilities Crescent and Hammermuehle). Nine of the ten systems list some sub-set of multipurpose demonstration, peak shaving, and load levelling as applications. Only BEWAG, an 'island' utility, lists spinning (rapid)

reserve and frequency control as applications; these are typical, often urgent needs for such isolated utilities. The San Diego Gas & Electric (SDG&E) BESS provided peak shaving for a specific load, namely, a light-rail transportation system. This BESS, too, was a demonstration system and featured more recent technologies, e.g., VRLA (gel) battery modules and IGBT technology power conditioning. It demonstrated the technical viability of peak shaving the demand of the light-rail system, but it was not economically viable (at least partly because economic viability was not an original goal) and was shut down after a two-year demonstration period. Crescent has benefitted from the peak shaving of its BESS, but the facility was acquired under economic circumstances that are not likely to be available again.

The Pacific Gas & Electric (PG&E) system is also unique in that the PM250 was a prototype, power-management system and, perhaps, the forerunner of the PQ2000. PG&E was also a test site for the subsequent PQ2000 prototype.

The PREPA BESS can be viewed as a transitional system because it was selected by a utility to circumvent several system problems and funded without any outside incentive funds. The applications were characteristic of isolated or island utilities (note the similarities with BEWAG) and do not include peak shaving or load levelling. Its benefits were seemingly valued by PREPA. It will be interesting to see whether or not PREPA replaces the failed battery and returns the BESS to service.

The BESSs at Vernon and Metlakatla and the PQ2000 can be viewed as second-generation systems, or at least more mature systems. They are much smaller than BEWAG, Chino and PREPA, for example, and they tend to serve multiple, demand-side, power-quality related purposes. All three were produced by entities who assumed responsibility for the entire system, quoted a price, warranted system performance, and delivered a turn-key product. The Vernon BESS provides rapid (spinning) reserve, which initially continues the uninterrupted operation of the entire plant in the event of a power outage or disruption. Subsequently, the Vernon BESS will continue, if necessary, to power critical, environmentally sensitive loads until the outage or disruption goes away or a controlled shutdown is completed. Peak shaving at the Vernon site is a secondary application undertaken because the BESS has adequate capacity to provide an added benefit via peak shaving without compromising its primary purpose.

Metlakatla is another small, island utility in need of rapid reserve for utility stabilization and power-quality purposes. There are also environmental issues involved, i.e., fuel delivery and the stand-down of a diesel generator that would otherwise operate under difficult, inadvisable circumstances.

The PQ2000 is a commercially available BESS. Following its commercial introduction at Homerville, GA, additional units have been sold and placed in service. This is evidence of commercial maturity and economic viability. Note that its primary application is standby power (rapid reserve) for interventions in the interest of assuring power quality. In one sense, it is an industrial-scale UPS.

The Herne and Bochold BESSs in Germany interface renewable energy facilities (wind and solar) with storage to utility grids. They enhance power quality (reliability) by supplying stored energy in the event of an outage, and they enable stored, renewable energy to be used to peak-shave utility demand.

The cost data presented in Table 10.2 are interesting, but comparisons are difficult. Most of these systems are one-of-kind systems built for demonstration purposes and, in some instances, costs may have been a secondary issue. Chino and PREPA were large systems assembled from individual components. PREPA is the more expensive but was built six years later. The costs on a dollar per kW or kWh basis reflect the differences of their respective capacities. The BoP costs of the PREPA facility were much higher. Taking capacities into consideration, the SDG&E BESS was very expensive, perhaps unnecessarily so. The Metlakatla and Vernon systems differ in capacities, but are similar in many ways, e.g., similar components and built by the same entity. The costs of the Metlakatla BESS may reflect an economy based on experience and familiarity. The PQ2000 differs dramatically from the others; its future costs will likely reflect its growing market and commercial status.

It is notable that, of the 17 BESSs listed in Table 10.1, the majority employed flooded batteries. Only four are known to have used VRLA batteries, namely, the SDG&E, Johnson Controls, GNB-Vernon, and Metlakatla systems. The performance of the SDG&E (gel) and Johnson Controls (gel) batteries appears to be not well documented in the literature. The systems date from 1992 and 1989, respectively, and the SDG&E system was taken out of service about two years later. The BESS systems at Vernon and Metlakatla had AGM-type batteries. Both are still in service and seem to be performing well. These batteries date from 1996 and 1997, respectively.

References

1. R. Wagner, Chapter 13, this volume.
2. M. Farber-De Anda, J.D. Boyes, W. Torres, *Lessons Learned from the Puerto Rico Battery Energy Storage System*, *SAND99-2232*, *September 1999*, Sandia National Laboratories, Albuquerque, NM, USA.
3. J. Daan van Wyk, F.C. Lee, D. Boroyevich, *Proc. IEEE*, **89(6)** (2001) 799–801.
4. B.K. Bose, *Introduction to Power Electronics*, *Modern Power Electronics*, IEEE Press, Piscataway, NJ, USA, 1991.
5. G. Asplund, *Proc. PES Winter Meeting 2000*, IEEE, Vol. 4, pp. 2498–2503.
6. H. Akagi, *Proc. IEEE*, **89(6)** (2001) 976–983.
7. S.M. Schoenung, *Characteristics and Technologies for Long- vs. Short-term Energy Storage*, *SAND2001-0765*, *March 2001*, Sandia National Laboratories, Albuquerque, NM, USA.
8. P. Taylor, L. Johnson, K. Reichart, P. DiPietro, J. Phillip, P. Butler, *A Summary of the State of the Art of Superconducting Magnetic Energy Storage Systems*, *Flywheel Energy Storage Systems*, *and Compressed Air Energy Storage Systems*, *SAND99-1854*, *July 1999*, Sandia National Laboratories, Albuquerque, NM, USA.
9. C. Platt, P. Taylor, L. Charles, P. Butler, *Report on the Energy Storage Systems Program Executive Meetings Project*, *SAND97-2700*, *November 1997*, Sandia National Laboratories, Albuquerque, NM, USA.
10. J. Trujillo, *Experience With Air Gap Monitoring at the Rocky Mountain Pumped-Storage Hydroelectric Plant*, *User Conference on Machine Condition Monitoring*, *May 2001*, Orlando, FL, USA.
11. J.D. Boyes, *Energy Storage Systems Program Report for FY99*, *SAND2000-1317*, *June 2000*, Sandia National Laboratories, Albuquerque, NM, USA.
12. H.J. Haubrich (Ed.), *Batterie-Energiespeicher in der Elektrizitätsversorgung*, Aachen, Mainz, Germany, 1996.

13. P.W. Schneider, M. Leiers, H. Dominik, *Fifth International Conference*, *Batteries For Utility Energy Storage*, EPRI, NEDO, BEWAG, San Juan, Puerto Rico, July 1995.
14. R. Kiessling, *J. Power Sources*, **19** (1987) 147–150.
15. R. Wagner, M. Schroeder, T. Stephanblome, E. Handschin, *J. Power Sources*, **78** (1999) 156–163.
16. R. Wagner, *J. Power Sources*, **67** (1997) 163–172.
17. C.R. Zickefoose, *Third International Lead-Acid Battery Seminar*, EPRI, NEDO, BEWAG, Orlando, FL, USA, May 1989.
18. B. Bhargava, G. Dishaw, *Fifth International Conference*, *Batteries For Utility Energy Storage*, EPRI, NEDO, BEWAG, San Juan, PR, July, 1995.
19. G. Rodriguez, W. Spindler, D. Carr, *Third International Lead-Acid Battery Seminar*, EPRI, NEDO, BEWAG, Orlando, FL, USA, May 1989.
20. R. Hamann, R. Scarvaci, G. Brilmyer, *Third International Lead-Acid Battery Seminar*, EPRI, NEDO, BEWAG, Orlando, FL, USA, May 1989.
21. G.W. Hunt, *J. Power Sources*, **78** (1999) 171–175.
22. G.W. Hunt, C.B. John, *Conference Abstracts*, *Electric Energy Storage Applications and Technologies* (*EESAT*) *2000*, USA Department of Energy, SNL, IEEE Power Engineering Society, Energy Storage Association, Orlando, FL, USA, September 2000.
23. J. Szymborski, G.W. Hunt, R. Jungst, *Conference Abstracts*, *Electric Energy Storage Applications and Technologies* (*EESAT*) *2000*, USA Department of Energy, SNL, IEEE Power Engineering Society, Energy Storage Association, Orlando, FL, USA, September 2000.
24. G.P. Corey, *IEEE Aerospace and Electronic Systems Magazine*, IEEE, June 1996.
25. P. Butler, *Energy Storage Systems Program Report for FY97*, *SAND98-1733*, *August 1998*, Sandia National Laboratories, Albuquerque, NM, USA.
26. B.K. Bose, *Proc. IEEE*, **80(8)** (1992) 1303–1334.
27. S. Atcitty, S. Ranade, A. Gray-Fenne, *Summary of State-of-the-Art Power Conversion Systems for Energy Storage Applications*, *SAND98-2019*, *September 1998*, Sandia National Laboratories, Albuquerque, NM, USA.
28. L.H. Walker, *IEEE Transactions on Industrial Applications*, **26(1)** (1990) 63–72.
29. A. Akhil, S. Swaminathan, R. Sen, *Cost Analysis of Energy Storage Systems for Electric Utility Applications*, *SAND97-0443*, *February 1997*, Sandia National Laboratories, NM, USA.

Valve-Regulated Lead–Acid Batteries
D.A.J. Rand et al., editors

—CHAPTER 11—

VALVE-REGULATED LEAD–ACID BATTERIES IN AUTOMOTIVE APPLICATIONS — A VEHICLE MANUFACTURER'S PERSPECTIVE

R.D. Brost

11.1. Introduction

Electrochemical energy storage devices have been fundamental components of the automobile since their need was defined by Kettering's development of the electric ignition system in 1911 [1]. Despite the internal-combustion-engine's (ICEs) success over steam- and electrically powered vehicles at the turn of the century, the need for electrical energy storage has increased progressively up until the present time and shows no sign of abating, particularly given that electric brakes, steer-by-wire, electrified climate control, and all-electric traction drives are being contemplated by nearly all automobile manufacturers. Moreover, a significant portion (if not an outright majority) of options offered as customer-oriented features are electrical in nature; radios, CD players, passenger televisions, power points, cellular phones, vanity mirrors, electrically heated seats, electric doors, refrigerators, and a myriad of other devices have become influential marketing tools that many customers come to expect and depend on.

The need for improved energy storage devices to handle the increased load and capacity has followed the incremental usage of electric-powered devices on-board the automobile. Larger engines, higher crank speeds, a flourishing accessories market, and increasing customer expectation has motivated the industry to provide higher specific energy and longer service-life. The lead–acid battery has served this purpose well so far, given the simplicity, low cost, and high current capability. As the reliance of automobile operation on the battery increases, however, so do the demands on the technology. For example, the advantages of steer-by-wire are such that the widespread deployment of this technology is inevitable, and it is obvious to even the casual observer that a reliable energy source is an absolute necessity before this technology can be considered as appropriate for consumers. Other components such as on-board computers, lamps, ignition devices, and emissions-control devices also require a near-perfect power supply. An interruption of the energy source for any of these critical devices will compromise customer satisfaction and may lead to unacceptable social and economic costs.

The road to a new battery technology is a long and expensive one. Nevertheless, new technologies are coming to the forefront that could provide improved performance over the current flooded lead–acid technology. The battery technology landscape is changing very rapidly at this time, with advances in nickel–metal-hydride (Ni–MH) and lithium chemistries that could provide at least niche automotive markets for these devices. Although it would date this review to consider the current state of these emerging batteries in any kind of detail, it would be wise to consider these new technologies as alternatives to lead–acid chemistry that may eventually augment, or even supplant, some of the lead–acid market. This does not imply that these new technologies will appear as standard equipment anytime soon; the automotive industry cannot afford to adopt a new technology just for the sake of adopting a new technology since the expense of such a move would be great and the marketing advantage small for such a customer-transparent change. More appropriately, it should be remembered that the extent to which alternative batteries penetrate the automotive market is inversely related to the extent to which improvements are made in the lead–acid batteries. With the higher power and energy densities that are possible with valve-regulated lead–acid (VRLA) batteries, it is feasible that other favourable factors will yet champion VRLA as a best-choice energy storage device. Indeed, power and energy density are but two of the many considerations in battery selection, and it is the effectiveness of the overall performance that will likely provide a sustained future for the lead–acid battery.

11.1.1. Battery selection process

The battery selection process for automotive applications extends well beyond the conventional properties of capacity, power, safety, and cycle-life. Factors such as recycleability, manufacturability, commonality, ease of service, weight, temperature environment range, reliability, and of course, cost, are nearly equally important, so the selection process of automotive batteries becomes one of risk management where a poly-dimensional decision tree must be evaluated before a decision can be made. For example, the high power and long life of Ni–MH batteries can provide certain automotive advantages. These batteries, however, successful as they are in consumer electronics and other applications, have not seriously entered the automotive market on the wholesale scale that might be expected based on their bench performance. This can be attributed to many reasons, the most obvious being that of cost. Ni–MH batteries are on the order of US$ 1000 per kWh, compared with roughly US$ 30 per kWh for original equipment (OEM) automotive batteries. Even for the longer term, should cost become comparable, the prospect for Ni–MH chemistry to directly compete with lead–acid on a strictly energy basis is weak due to performance limitations at extremes of environmental conditions. Standard automotive operating temperatures, for example, range from –40 to $+70^{\circ}$C; few chemistries outside of lead–acid, and certainly not Ni–MH, are able to operate in this window without extraordinary means of support such as active thermal management. For these reasons Ni–MH will not likely be considered to be a drop-in replacement for lead–acid.

The presumption here is that within the context of the automotive industry, the ideal battery, with high energy, high capacity, perfect safety, low weight, low cost, six-sigma reliability, and 100% recycleability will likely never exist. The task of the design and release engineer becomes a balancing act to evaluate the benefits and risks for each of the possible technologies and how they fit to the potential application. Part of this decision matrix is to determine what the minimum capability of the technology is and how it relates to the project requirements; where it is clearly deficient, the engineer must eliminate the technology from the universe of choices. It is seen, for example, that Ni–MH fails as a direct replacement for lead–acid due to high cost and poor low-temperature performance. Likewise, lead–acid chemistry cannot be recommended in some hybrid applications, where high voltages, long life, and deep-cycling capability for 240,000 km (150,000 miles) are required.

In order to understand how an automotive battery selection is made, it is necessary first to understand the process involved in taking the product from concept to delivery. The decision matrix is a complex one that must deal with customer wants, governmental regulations, corporate standards, design realities, manufacturability, durability, costs, supplies, service, warranty, timing, and a multitude of other factors, any of which alone can de-rail an otherwise successful vehicle programme if inappropriately or incompletely handled. Overlaid on these imperatives are the staff and suppliers that must provide these services (Table 11.1). From the automotive manufacturing organization, these typically include an engineering director, his managers, corporate technical specialists, the manager's supervisors, and finally the supervisor's engineers and technicians. Engineers involved in battery selection have skill sets that collectively must include electrochemical, controls, thermal, mechanical, and electrical engineering. Frequently, a dedicated test engineer is also employed as part of the team, and generally one senior engineer is assigned as the lead for the project. He or she will coordinate the efforts of the other engineers and provide leadership for the product group, as well as act as a clearinghouse for deliverables and design reviews. This lead engineer is also legally responsible for product release. In parallel to core engineering, inputs from other engineering organizations that interface with the battery such as finance, purchasing, marketing, service, legal counsel, and administration are also required. From the suppliers organization, account managers, plant managers, engineering directors, product engineers, controls engineers, manufacturing engineers, test technicians, and line workers are assigned responsibilities related to a new product. All of these resources together, from directors to line-workers, play a role in the cascade from customer wants and needs to a final product. Moreover, the quality and success of the product will directly correlate to the quality and execution of the processes used.

The process from concept, to design, to product may be accomplished, a number of ways, but current professional practice uses systems engineering (Fig. 11.1), which is a method whereby requirements are cascaded to subtasks and then to a series of validations based on a methodical review of the design. It is a process that emphasizes engineering up-front, but in a cyclic way, which is internally and

Table 11.1. Roles and responsibilities in the automotive battery selection process.

Automotive manufacturer
Engineering Director
High level vehicle requirements
Provide budget
Provide headcount
Provide facilities
Participate in design reviews
Marketing
Customer needs cascaded
Finance
Procure funding for development activities
Manager
Recruit and manage allocated resources to meet vehicle requirements
Participate in design reviews
Sign-off on battery
Vehicle development timing plan — battery dates
Technical Specialists
Provide expertise
Analysis of problems
Purchasing
Global Terms acceptance/negotiations
Sourcing strategy
Sourcing RFQ package[a]
RFQ reviews and award source
Supervisor
Maintain contact with suppliers
Manage engineers
Develop workplan
Sourcing timing plan
Conduct design reviews
Development, DVP&R incremental facilities and funding identified[b]
Budget input/reconciliation
Lead Engineer
Requirements
Specification and prints
Identify suppliers responsible
Lead Engineer (continued)
Supplier on-site support plan
Power requirements
Voltage requirements
Open circuit voltage
Supplier capability assessment
Suppliers development timing plan
Suppliers manufacturing timing plan
Final specifications and print release
Supplier PV complete[c]
Production part numbers identified
Production print
Product specification
Service release
Supply warrant
Service part numbers identified
Service print
Service part specification
Production release
Establish tracking log of batteries in use
Production EDI in-place & functions[d]
Initial EDI forecast to actual capability
ln-plant battery maintenance (charging) requirements identified
Secondary supplier quality verification
PFMEA & Review[e]
Manufacturing process stack up studies
Process capability prove-out review
Audit of rejected parts quarantine process
SPC and other control methods management[f]
Data recording and retention
Shipping dunnage identified
Suppliers MSDS for module or other components[g]
Development parts schedule

Table 11.1. Continued.

Automotive manufacturer
Lead Engineer (continued)
Establish tracking log of batteries scrapped and disposition
Service part EDI in-place & functions
Service stock available
Service maintenance charging capability needed/in-place
Production part pick-up/ delivery (Ford transport) plan
Supplier production control contacts identified & Introduced to plant parts coordinator
Plant storage requirements
Establish recycling plan and recovery plan (service & EOL)
Battery Engineer (Electrochemical)
Capacity
Calendar life performance (if required)
Cycle-life testing
Charge algorithm
Control/sensor requirements
End of life/aging criteria
Design FMEA
Emissions (Gas/liquid)
Mechanical Engineer
Fastener identified
Weight/tolerances
Resistance to abrasion
Vibration requirements (x, y, & z)
Form factor/external dimensions — tolerance study
Terminal type
Torque requirements for connections requirements and analysis
Leakage Test
Case material
Conductive Land definition
Mechanical Engineer (continued)
Retention devices/surfaces
Resistance to solvents
Connector reconnections
Controls Engineer
provide controls logic and inputs
Electrical Engineer
Energy requirements
Programme operating duty/ drive cycle criteria
Cutoff voltage
Capacity variation range, sources of variation
Charge time
Discharge limits
Diagnostics requirements
Identify and review design parameters and critical characteristics/dimensions
Electrical performance simulation model
Develop DVP&R, and complete
Thermal Engineer
Temperature limits
Heat transfer model
Thermal performance analysis
Operating thermal range
Heat transfer characteristics
Thermal management interface
Test Engineer
Performance test
DVP plan execution[h]
Service
Service Part-shipping carton available
Service distribution plan and availability
Additional service tools identified and defined
Legal Counsel
Patent position cleared
Administration

Table 11.1. Continued.

Supplier organization	
Account Manager	*Process Controls Engineers* (continued)
Maintain interface with OEM	Equipment process capability
Concur on product volume	Critical parameters process controls defined and reviewed
Engineering Directors	Test equipment capability
Manufacturing plan including site selection	Review reaction plans for process failures
Concur with product strategy	Definition and agreement to supply Ford desired process information
Plant Managers	*Manufacturing Engineers*
Delivery schedule to demonstrate lead times	PFMEA
Product Engineers	Unique identifiers for modules (Barcode, date codes, etc.)
Product requirements	*Test Technicians*
Product design	Performance test
CFMEA[i]	Drop Test
DFMEA[j]	Altitude Test
Process Controls Engineers	Test results
Control plans and statistical support	*Line Workers*
Process capability studies	Support process capability studies
Production process, and control plan review	

[a] RFQ: Request For Quotation
[b] DVP&R: Design Verification Plan and Report
[c] PV: Process Validation
[d] EDI: Electronic Data Interchange
[e] PFMEA: Process Failure Modes and Effects Analysis
[f] SPC: Statistical Process Control
[g] MSDS: Material Safety Data Sheet
[h] DVP: Design Verification Plan
[i] CFMEA: Concept Failure Modes and Effect Analysis
[j] DFMEA: Design Failure Modes ans Effect Analysis.

externally consistent with the predecessor requirements. This process consists of three phases:

(i) requirements analysis, where requirements (customer, government, professional, and corporate) are collected, sorted, and translated into specific needs. Outputs consist of needs and wants
(ii) design phase, where alternatives are developed and evaluated using any of several design tools
(iii) verification stage, where it is shown through evidence that all requirements have been met.

Cyclic or reverse navigation is accepted as part of the process, but it is expected that most elements of the design will be determined and reviewed at

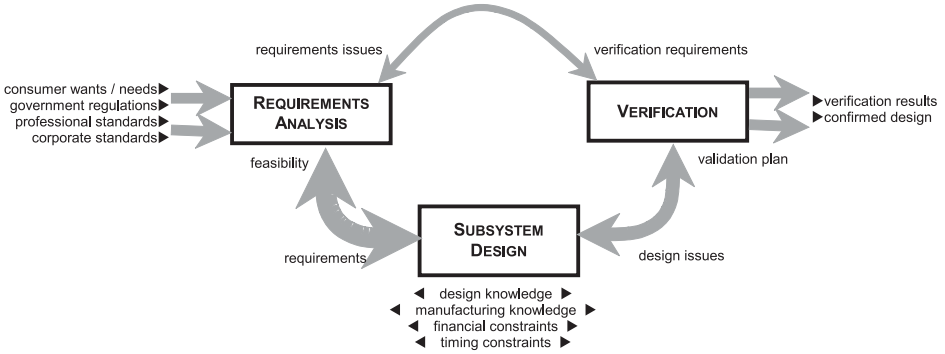

Fig. 11.1. System engineering approach thickness of the arrow proportional to flow of information.

an early stage such as the design phase where costs in both time and money are minimized.

Different organizations will have different means of cascading information from one step to the next, but generally they will take the form of prescribed documents that serve as points of controlled understanding between the phases of the engineering effort. For example, the vehicle programme may elect to post results of the Requirements Analysis in a Vehicle Design Specification, which is a document that contains vehicle-level specifications such as vehicle interface diagrams, duty cycles, and environment. The process of defining the vehicle level specifications is a long and important one that is key to the success of a quality vehicle line. All target metrics such as safety, package, dynamics, emissions, performance, NVH (noise, vibration, harshness), weight, customer life cycle, thermal needs, verification requirements, and cost targets will be identified within this document and in theory should be complete before substantial engineering efforts start.

The Subsystem Design phase is the point where individual component concepts begin to form in compliance with the cascaded requirements from the vehicle specifications. There are a number of ways to achieve this end, but a systematic method will include a description of the system relative to external features, how critical these functions are and the effects of failure, the means of identifying and dealing with failure, and how the actions are to be confirmed. Typical tools used to act on these needs are briefly described below.

11.1.2. Sub-system description

One method used to describe the subsystem and its interactions is the P-Diagram, which maps the interfaces by blocking out the signal, the noise factors, the control factors, and the response interfaces, see Fig. 11.2. The P-diagram relates each of these factors quantitatively where possible and to such a degree of completeness that

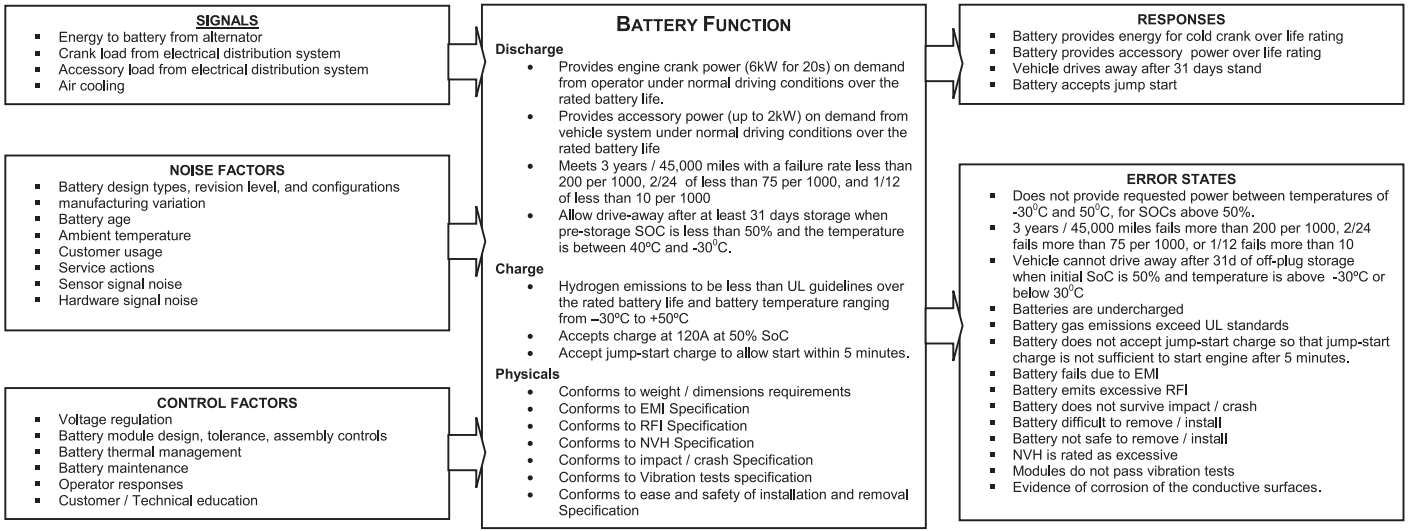

Fig. 11.2. Typical P-diagram describing start, lighting, ignition automotive battery function.

a casual observer from an unrelated discipline can understand all the effects that pertain to the performance. A test of completeness of the P-diagram is to be able to state that if a device existed that met all the needs in the function block, provided all the outputs in the response block, and had none of the problems described in the error states, then the device would meet all the technical requirements for that sub-component.

The P-diagram is a tool used to conceptualize the System Design Specification (SDS). The system specification establishes boundaries, describes the organization that is responsible for the requirements, and acts as a source definition of the essential requirements for the component. The system specification will also eventually link requirements to the design verification methods, which are tests that are designed to prove functionality.

The P-diagram format is only one method of function analysis, but it happens to provide a simple, but powerful, way to conceptualize the component function and the elements that affect the function. Block diagrams or process flow diagrams may be equally valid, provided that the result derives from an analysis of the vehicle design specifications, an examination of environmental and noise factors, and a clear understanding of the needed responses and how they may fail.

11.1.3. Initial design phase

The initial design phase requires a broad engineering knowledge of the scope and capabilities of the different technologies available that may meet the specific requirements described in the SDS. In the case of automotive energy storage, this may be as broad as knowledge of lithium-based chemistries, flywheel technology, or ultracapacitors. If the application is well known and characterized, it may take the form of detailed knowledge of available Battery Council International (BCI) sizes, cold-cranking amperes capability, and expected cycle-life.

With several alternatives in hand, a matrix should be designed to compare the alternatives on a common basis (Table 11.2). The battery function column of the matrix should derive from the P-diagram and it should be traceable to the SDS. For an advanced programme with high voltage, severe service, or extraordinary environmental needs, it is common to examine several battery technologies as well as, perhaps, several sizes and configurations.

11.1.4. Failure modes and effects analysis

The failure modes and effects analysis (FMEA) consists of several levels and may include a design FMEA (or DFMEA) and process FMEA (PFMEA). The FMEA is a before-the-event action, intended to capture potential failures before they become costly, and for this reason is an essential document prior to design sign-off. After the initial design phase, the design FMEA should be initiated and the attributes of the design requirements tested. It is well beyond the scope of this review to describe the FMEA process in its entirety, but it should be understood that it follows the sub-system description and initial design phase and is a precursor

Table 11.2. Typical decision matrix for automotive battery selection.

Requirement/option		A[a]	B	C	D	E
Discharge						
Provides 20 s of 6-kW engine crank power on demand from operator under normal driving conditions over the rated battery life.	−30°C					
	0°C					
	25°C					
	75°C					
Provides 2 kW accessory power on demand from vehicle system under normal driving conditions over the rated battery life	−30°C					
	0°C					
	25°C					
	75°C					
Meets 3 years/72,000 km (45,000 miles) with a failure rate less than 200 per 1000, 2/24 of less than 75 per 1000, and 1/12 of less than 10 per 1000						
Allow drive-away after at least 31 days storage when pre-storage SoC is less than 50% and the temperature is between 40°C and −30°C.	−30°C					
	25°C					
	40°C					
Charge						
Hydrogen emissions to be less than UL guidelines over the rated battery life and battery temperature ranging from −30°C to +50°C	−30°C					
	0°C					
	50°C					
Accepts charge at 120 A at 50% SoC	−30°C					
	25°C					
	40°C					
Accept jump-start charge to allow start within 5 min.	−30°C					
	0°C					
	40°C					
Physicals						
Conforms to weight/dimensions requirements						
Conforms to EMI specification[b]						
Conforms to RFI specification[c]						
Conforms to NVH specification						
Conforms to impact/crash specification						
Conforms to vibration tests specification						
Conforms to ease and safety of installation and removal specification						
Other						
CAFE/MAFE[d]						
Emissions						
Recyclability						
Manufacturability						
Cost						
Supplier capability						
Tooling costs						
Technology risk						
Strategic fit to product line						

[a]Columns A, B, C, D and E represent the data for alternative designs.
[b]EMI: Electromagnetic Interference.
[c]RFI: Radio Frequency Interference.
[d]CAFE: Corporate Average Fuel Economy, MAFE: Model Average Fuel Economy.

to design validation planning. A representation of an FMEA for an automotive battery is given in Table 11.3; completed documents may include several other columns such as actions, responsible parties, and may stretch to many tens of pages depending on the number of failure modes and interactions with other sub-systems.

11.1.5. Design validation plan

The design validation plan follows requirements and actions dictated from the design and process FMEAs. Without the FMEA in hand, it could be argued that the validation is, at best, incomplete since it is unlikely that the component specification team has unambiguously established what had to be tested (unless of course another process that achieves this result had been used).

While the resulting FMEA may not be perfect (and so the design validation plan may be incomplete), it forces a systematic way of thinking that encourages consideration and review of the technology and, for that reason, is considered an essential component of automotive engineering.

The following sections describe, in general terms, the requirements of the automotive industry for each of the critical performance metrics. Vehicle requirements will of course change from model to model and from year to year, so functional specifics, such as battery sizes or power, are not appropriate here. This list, however, should provide a starting checklist for anyone contemplating a particular battery for any of the header applications.

11.1.6. Future electric loads

A major driver for advanced batteries is from the ever-increasing electrical demands of the automobile. Some of the new high-power accessories under consideration include integrated starter-generators, emissions devices, steer-by-wire, brake-by-wire, electrified climate control, a.c. power taps, fast-clearing windshields, and convenience appliances such as refrigerators, microwave ovens, and vacuum cleaners. These are pulse loads from between 1 and 10 kW (and possibly higher) and will rely on the battery to provide occasional support.

In order to deliver this level of power efficiently, a voltage higher than the now-common 14-V bus is required. The standard is currently under negotiation, but it is expected that the voltage will settle at 36 V (or 42 V float) nominal. This standard is likely a practical maximum given that electrical safety rather than technology is the main consideration. A higher voltage is possible, but implementation of such a system would require extraordinary, and costly, safety features.

The voltage sag during operation of the vehicle is also important; in the case of a 36-V system, engine-on voltage cannot drop below 30 V without becoming a customer satisfaction issue as electrically powered devices such as blowers and lights are affected. Likewise, the voltage cannot drop below 21 V during an engine-start event without having an impact on vehicle electronics.

Table 11.3. Sample (partial only) DFMEA for automotive battery.

Item/function	Potential failure mode	Potential effect of failure	sev[a]	Potential cause/ mechanism of failure	Occur	Current design controls	Detect	RPN[a]
Provides engine crank power (6 kW for 20 s) on demand from operator under normal driving conditions over the rated battery life	Does not provide crank power	Engine will not start	8	Cell shorted	2	Process check for shorted cell	2	32
				Cell not constructed properly	3	Polarity/power check	2	48
				Cell not sufficiently large for application	2	Validation plan	2	32
				Cell worn out	6	Date code/dealer test	8	384
	Provides partial crank power	Engine will not start	8	Cell not sufficiently large for application	2	Validation plan	2	32
				Cell worn out	6	Date code/dealer test	8	384
	Insufficient crank power at low temperature	Engine will not start	8	Cell incorrect design for cold temperatures	2	Validation plan	2	32
				Cell worn out	6	Date code/dealer test	8	384
	Intermittent crank power	Engine starts intermittently	7					

Provides accessory power (up to 2 kW) on demand from vehicle system under normal driving conditions over the rated battery life	Does not provide accessory power	Accessories will not function at engine idle	8					
	Provides partial accessory power	Accessories will function but only with degraded function	7					
	No accessory power at low temperature	Accessories will not function at engine idle	8					
	Intermittent accessory power	Accessories will function intermittently	7					
Meets 3 years/ 72,000 km (45,000 miles) with a failure rate less than 200 per 1000, 2/24 of less than 75 per 1000, and 1/12 of less than 10 per 1000	Fails > 200 per 1000 at three years/ 72,000 km (45,000 miles)	Premature replacement/possible customer stranding	6					
	Fails > 75 per 1000 at 2/24		7					
	Fails > 10 per 1000 at 1/12		8					
Allow drive-away after at least 31 days storage when pre-storage SoC is less than 50% and the temperature is between 40°C and −30°C.	Does not allow drive-away after 31d stand		8					
	Allows drive-away with some assistance		7					

continued

Table 11.3. Continued.

Item/function	Potential failure mode	Potential effect of failure	sev[a]	Potential cause/ mechanism of failure	Occur	Current design controls	Detect	RPN[a]
Charge								
Hydrogen emissions to be less than UL[b] guidelines over the rated battery life and battery temperature ranging from −30°C to +50°C	Hydrogen emissions > UL guidelines at any time							
Accepts charge at 120 A at 50% SoC	Accepts charge at < 120 A, at 50%SoC							
	Intermittently accepts charge							
	Never accepts charge							

Accept jump-start charge to allow start within 5 min	Accepts jumpstart but requires > 5 min								
	Intermittently accepts jumpstart								
	Never accepts jumpstart								
Physicals									
Conforms to weight/ dimensions requirements	Does not conform to weight requirement								
	Does not conform to dimensions								
	Does not conform to dimensions but conforms to volume								
Conforms to EMI Specification	Does not conform to EMI specification								
	Some operation modes do not conform to EMI requirements								
Conforms to RFI Specification	Does not conform to RFI specification								
	Some operation modes do not conform to RFI requirements								

[a]sev = severity, RPN = Risk Priority Number. This is used in the Failure Modes and Effects Analysis process to rank failures in terms of their effect on a customer. RPN is calculated as the product of severity (1–10, 1 being no effect, 10 being a safety hazard), occurrence (1–10, 1 being less than 1 per 1.5 million, 10 being greater than 1 in 2 parts), and detectability (1–10, 1 being unable to detect, 10 being obvious to all). An RPN > 100 is usually (but not always) considered to be actionable.

[b]UL = Underwriters Laboratory.

Even after acceptance of a new higher voltage standard, there will, for some time, be a need for 14-V sources on a 42-V vehicle until electronics, switches, lamps, and other components complete the transition. This could be supplied through either a 42-V/14-V converter, a separate battery, or a low-voltage tap off the high-voltage battery. The latter alternative would imply additional equalization electronics if cells were charged in series.

11.1.7. Environmental

Any vehicle produced for today's market must address environmental concerns such as emissions, recycleability, and potential toxic contamination. Emissions cannot be toxic, corrosive, or otherwise hazardous. Emissions from batteries can be gaseous (by far the most common) or liquid (sometimes seen during overcharge events). Liquid emissions are often produced through evaporation and condensation or by entrainment of electrolyte in the battery exhaust gases. In flooded lead–acid systems, this condensate is usually acidic due to absorption of sulfur oxides that have a finite vapor pressure over the electrolyte and are emitted with the water vapor or water mist. In practice, VRLA batteries tend not to form a liquid condensate except through charger failure. In aqueous systems, the gaseous emission of concern is elemental hydrogen. By tradition, hydrogen emissions from aqueous batteries that could lead to explosive air mixtures have been an accepted risk mitigated by free movement of air around the battery and by customer education; but this latitude cannot be taken for granted in future batteries, particularly if the batteries are of large capacity, are assumed to accept charge at a high rate, or if they are packaged in a restricted space.

Underwriters Laboratory standards call for a maximum hydrogen concentration of 1% by volume (compared with a 4% lower flammability limit). The analysis of this situation requires knowledge of the air flow rates, maximum charge current, battery sizing, and thermal management strategy, all of which will be programme-specific. As battery packaging becomes less standard and batteries are mounted in the trunk, beneath seats, or in climate-controlled boxes, for example, hydrogen build-up becomes a concern. This is particularly so if the battery climate control exhausts air into the passenger cabin; the risk of gas build-up under that arrangement would be unacceptably high and, therefore, it would be difficult to justify this type of design under any circumstance.

Toxic gas emission must also be considered, although this is usually a low risk in aqueous systems if voltage regulation and venting operations are functioning properly. Nevertheless, concerns about toxic emissions carry over from arguments of hydrogen emissions; in this case, however, exhaust from the battery climate control directly to the passenger cabin is a very high risk and should never be considered acceptable.

Contamination arising through rupture of the battery case or wear-out should be considered. In the latter case, contamination risk is particularly significant for batteries that do not have a well-developed reclamation infrastructure. Unreclaimed

batteries are likely to be disposed of in landfills; for this reason, chemistries that include highly toxic elements such as cadmium are unlikely to gain wide commercial acceptance in North America in automotive applications. Although it could be said that there is a well-recognized health risk with exposure to lead, lead–acid chemistry has a clear advantage in terms of consumer familiarity and of reclamation, and inappropriate exposure is rare.

11.1.8. Cost

The automobile industry is a competitive one with consumer demand highly elastic. Pricing is a marketing tool that can determine, in large part, the success or failure of a vehicle line. An automobile may contain 15,000 parts, and, for this reason, everyone involved, from the release engineer to the chief programme engineer, carefully scrutinizes every cost increment.

Replacement parts for existing technologies must either demonstrate superior technology, which is marketable to the consumer such that the incremental cost can be recovered, or the cost of the replacement technology must be less than the original technology. For many of the new battery chemistries, cost is a considerable challenge since the materials and process costs are frequently greater than those of the incumbent lead–acid technology. Also the need for sophisticated controls is often greater, and volumes are such that an economic critical mass cannot be achieved for many years. The situation for VRLA is somewhat similar in that there is a somewhat higher cost for this technology. While there is little marketing advantage to VRLA, the economic justification may be easier to demonstrate if longer life and increased capacity are part of the vehicle requirements.

Pennies-per-component count given the number of components on the average automobile, and the cost of energy storage is certainly no exception. For this reason, lead–acid based chemistries hold a decided advantage over other non-traditional, but otherwise possible, electrochemistries. Flooded lead–acid, at US$ 30 per kWh for an OEM automotive battery, costs less by an order of magnitude than a Ni–MH or lithium equivalent on a first-cost basis. Some of the cost premium is mitigated by higher specific energy and longer operating life, however, the life cost of Ni–MH is at least equivalent to, and may be somewhat higher than, that of the lead–acid counterpart in most applications. The present economics for lithium-based batteries are similar to those of Ni–MH, but life tends to be closer to that of advanced lead–acid unless the capacity of the lithium cell is de-rated. Thus, the initial cost of the Ni–MH or lithium battery is expected to remain a barrier to widespread industry- and consumer-acceptance, given the highly competitive nature of the automobile industry.

This is not to say that price is the sole criterion by which batteries are selected in automotive applications; where benefit can be realized through either reduced weight, improved life, lower maintenance, less gassing, or increased reliability, the choice may be logically made to use VRLA in lieu of the flooded equivalent.

Likewise, there may be niche markets where Ni–MH, lithium, or some other technology holds a key advantage.

11.1.9. Reliability

Within the last few decades the automobile industry has undergone a revolution in overall vehicle reliability. With the large number of components and the number of potential failure modes, it has become necessary for a component to provide six-sigma (99.9999%) reliability over its operational life (now assumed to be ten years or 240,000 km/150,000 miles), in order to satisfy customer expectations. Current production automotive batteries do not perform to this standard of course, but it is expected that pressure will come to bear on the industry to perform to this level in years to come. In some respect this may be achievable; experience with the first generation Ni–MH traction battery cells in severe electric vehicle (EV) usage has demonstrated less than 25 ppm failures after three years of service [2]. In order to achieve this level of performance, however, a close partnership is essential between vehicle sub-systems as the life of the battery is intrinsically entwined with the engine, climate control, and battery charge systems.

Reliability is a key metric in the automobile industry; things gone wrong (TGW), incidents per thousand vehicles (IPTV), and things gone right (TGR) are commonly used measures of performance that directly correlate with customer satisfaction. As the indigenous North American and European industries reach the quality levels earned by Asian competitors, the bar is continually raised (or lowered, depending on the metric) so that 10-year service-life is now within reach of most automotive components. The remaining components, including the battery, are held under greater scrutiny and the pressure to improve life performance increases even as the demand for energy and power increases. While a 10-year lead–acid battery is likely to be a reality only many years in the future, a five to seven year battery will likely be an industry stipulation within the foreseeable future.

The most challenging application for batteries lies in high-voltage series-strings of cells, where open circuit failures can result in sudden failure of the system. Electric vehicles are a good example of this dependency, although high-voltage hybrids, and even 42-V systems, can be examined in this light. Based on system life distribution theory, the length of the string (described as N) is a key factor in determining the life of the battery pack:

$$\text{cumulative failure distribution} = 1 - \left[\text{reliability of single battery}\right]^{N} \quad (11.1)$$

Calculations show that reasonably high cell-reliability is not sufficient for high-voltage string operation; this factor is even significant just on increasing the string size from six cells to 18 cells. Where 98% reliability was sufficient to meet a 10% failure rate with six cells, a similar level of reliability for the 36-V battery will require 99.4% cell-reliability. For high-voltage (300 V) EV strings, this same failure rate would require 99.93% reliability. Looking at this another way, the current

failure rate of 12-V batteries of 10% would lead to 27% failure of the 36-V batteries and 93% of EV batteries over equivalent time periods. To achieve reasonably close to an automotive standard of 12 ppm failures, a six cell battery would require about 99.999% ('five nines' or 5*N*) cell reliability, an 18 cell battery will require about 6*N*, and a 150-cell EV battery will require 7*N* cell reliability.

Another feature that is becoming more of a concern in longer strings is the ability to match cell capacity as the product comes off the finishing line. For the very long strings used in EVs, it is generally recognized that battery module capacity must be well matched otherwise rechargeability becomes an issue. Experience shows that a capacity variation of more than 0.5% will lead to imbalance that will quickly degrade battery performance. The state-of-the-art of cell formation processes based on the Fauré process is barely capable of this precision without lengthy and expensive cell conditioning and screening. A variation of 5%, common today in automotive batteries, leads to a process capability (*C*p) of 0.04, far less than the generally accepted industry minimum *C*p of 1.33; in order to reach a *C*p of 1.33, variation would have to be less than 0.08% (see Fig. 11.3). Conventional lead–acid production processes are generally incapable of the precise mass control that is required to maintain mass to within 0.08% (less than 0.1 g on a 100 g plate). Plate manufacturing processes are noisy, from a controls standpoint, primarily due to poorly controlled oxidation, acid reactions, and formation. In light of this analysis, it is clear that the achievement of tight control of capacity is a stretch goal, but it is one that the industry will be tasked to accomplish in the years to come, particularly as battery voltage and the dependence on battery performance becomes more important.

The need for more precise manufacturing controls fits well with VRLA needs and requirements. The higher compression of the VRLA plate stack drives a need for improved plate-making quality. The question of saturation control early on in the process reduces the variation in formation and acid distribution, which in turn reduces variation in capacity.

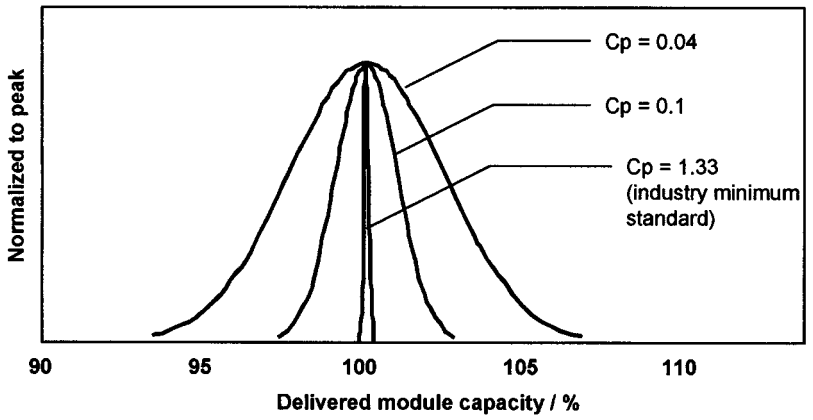

Fig. 11.3. Variation of battery capacity.

11.1.10. Safety

The relative safety of the lead–acid battery, with respect to other chemistries, becomes more appreciated as experience with the alternative chemistries increases. Battery safety consists of resistance to overcharge, over-discharge, accidental physical damage, short circuit behaviour, and fire exposure. In each of these situations, lead–acid operation is safe and a natural consequence of the material composition and design. Although most advanced batteries will pass puncture and crush tests, technologies such as Ni–MH and lithium require extensive and reliable charge controls to avoid thermal runaway. Short-circuit behaviour is also a problem, as the high rate of self-reaction may also lead to thermal runaway. Fire exposure tends to be more of an issue with advanced non-aqueous batteries, as high temperature often leads to electrolyte ejection and sometimes to ignition.

The VRLA battery has additional benefits over flooded designs. Spillage during operation and handling are known risks of batteries with free electrolyte, and the highly corrosive electrolyte may also be a physical risk to both the environment and personnel. The VRLA battery's adsorbed electrolyte greatly improves the resistance of the battery to this type of hazard, with no additional design safeguards required. During normal operation, the charge controls that VRLA batteries require also lead to substantially less explosive overcharge gas emissions, which may be a major benefit in the confined areas of heat-shielded battery boxes and containers.

11.1.11. Maintenance-free

The need for maintenance-free designs is clear-cut for longer strings, where access to the individual cells is often limited and may even require battery system disassembly. This type of procedure, if needed frequently, would be a major customer dissatisfier and a barrier to widespread acceptance of the technology. Proposals for automatic watering devices were once common, but such systems usually failed to pass reliability and practicality tests. This is not to say that watering flooded batteries is impossible; a watering procedure may hold promise for fleet applications where a dedicated staff and a service schedule that is conscientiously followed is possible, but such efforts must be factored into the costs of the technology.

Another maintenance issue that will become of greater concern with increasing string length is that of cell balance. Variation in cell capacity, described in previous sections, will drive a need for periodic balancing events. With slight differences in pack environment, differences between cell state-of-charge (SoC) will also gradually increase until performance is compromised; at the worst extreme, cell imbalance will lead to greatly shortened life as some cells become critically overcharged while others are undercharged. The VRLA recombination reaction is a simple way to correct cell imbalance during overcharge; done correctly, this may maintain balance with little life degradation. The frequency of the balancing operation in VRLA will depend on usage and pack design; in general, if open circuit voltage differences exceed 10 mV per cell ($\sim$ 5% SoC), equalization may be in order. This may be limited

to once every 10 × capacity throughput to eliminate equalization flags caused by cell variation.

Another means of cell balancing is via electronic devices that either shuttle charge between cells or selectively reduce the SoC of higher voltage cells. These devices are not necessarily specific to the chemistry, although in the case of those chemistries without natural non-destructive parasitic reactions (such as those with non-aqueous electrolyte); this electronic balancing may be essential. In practice, nearly all methods of electronic balancing show significant improvement in battery balance, from simple resistive elements that consume energy based on relative cell voltage to the more complex current-shuttling devices that use boost/buck converters to move fractional amounts of charge between cells as voltage differences are identified. Laboratory tests have shown that battery strings can function for much longer than usual without the need for equalization where such devices are installed and operational. The cost-to-benefit analysis of these devices is nebulous. As battery cell variability is reduced and the pack design improved so that cell differences are minimized, however, the need for such balancing becomes less. Until production variation approaches the 5*N* to 7*N* levels, however, such devices may play a role in providing low-maintenance and reliable battery packs, providing that they don't reduce quality through their own complexity and unreliability.

11.1.12. Weight savings

A common metric in vehicle design is the cost of weight reduction. This value spans all components and allows a common basis for decision-making. If a vehicle programme has a weight reduction target, the programme generally has the option of a number of actions that will reduce mass. An example of this is the choice of high-strength/low-density alloys for any of the other vehicle components. These advanced materials have a known cost-factor associated with their usage, which can be proportioned to the weight savings. A similar analysis can be conducted for a variety of battery types; a simplified analysis illustrating the method is shown in Table 11.4. With the assumptions in that example, it can be seen that VRLA can reduce mass economically, provided that other performance targets, like power, are met. Other features, such as additional controls and thermal management, must also be included in such a calculation.

11.2. VRLA in Automotive Applications

Automotive applications of batteries have developed well beyond the original crank requirement of Kettering and now include a continuum of function, from the basic crank and engine control modules all the way through hybrid and pure electric drive vehicles. Each of these applications has its own attributes and needs, so it is understandable that VRLA (or any battery technology) may be more suitable for one application than for another.

Table 11.4. Calculation of mass benefit of alternative battery chemistries.

	Flooded lead–acid	VRLA	Ni–MH	Lithium
Energy requirement (Wh)	800	800	800	800
Specific energy (Wh kg^{-1})	30	35	55	90
Mass (kg)	26.7	22.9	14.5	8.9
Mass reduction (kg)	(basis)	−3.8	−12.1	−17.8
Example cost (US$)	25	35	500	300
Cost increase (US$)	(basis)	10	475	275
Cost reduction (US$/kg)	(basis)	2.63	39.19	15.47

In considering the advantages of VRLA in automotive applications, this section briefly considers the general attributes of VRLA and then branches out to describe the specific features that are appropriate to the specific automotive application.

11.2.1. VRLA features of interest to the automotive industry

Maintenance-free. The maintenance-free requirement is assumed in most modern batteries, particularly in automotive applications where regular watering is not an accepted practice as it once was. In this respect, VRLA has a decided advantage over flooded lead–acid since design and controls presume that overcharge must be limited. Where overcharge is necessary for charge balance, the VRLA recombination process mitigates the material loss that would normally consume electrolyte in flooded designs.

Benign overcharge reactions. VRLA overcharge reactions result in waste heat (which can be dissipated into the vehicle environment) and some small amount of gaseous emission. This contrasts with the flooded lead–acid battery, which produces copious amounts of an explosive mixture of hydrogen and oxygen. Overcharge of non-lead chemistries such as Ni–MH can lead to thermal runaway if not well managed; similarly, overcharge of lithium can result in decomposition of the organic electrolyte and rupture of the cell.

Low gassing. The overcharge reactions of VRLA lead primarily to emissions of small amounts of hydrogen. On a properly managed battery (one with relatively sophisticated charging), VRLA will produce hydrogen at less than 0.06 ml/Ah over a 6 h charge; the reduced amount of hydrogen produced this way diminishes the hazard of an explosive hydrogen mixture and extends the life of the battery by reducing water-consuming reactions that lead to dry out.

Compatibility with chargers. Although VRLA responds well to a carefully managed charge process, it is possible to charge VRLA with a less complex (existing) voltage regulator that is slightly modified to recognize the different voltages

employed with the recombinant chemistry. From a vehicle electronic distribution perspective, this has considerable advantages since the fundamental controls used in flooded lead–acid can remain in place, only requiring minor re-calibration. In many cases, the changes to the voltage limit are clearly not optimized; but notwithstanding some life degradation, the VRLA will function at near capacity.

Special recharge. While VRLA can survive with only a very basic charge algorithm, the chemistry responds well to a controlled charge. The increasing sophistication of vehicle controls, the proliferation of control modules and the now ubiquitous communication networks allow a distributed controls architecture that can provide very precise energy and battery management. For example, a data acquisition module may sense voltage, temperature, and current values and convert them to digital signals that may be entered on the communications bus. A local or remote control module may then read the data stream and an algorithm may be applied to the data. An optimum instruction may then be sent to a controlled regulator, contactor, or other control device. In theory, this type of architecture could be applied to other advanced chemistries, but the need for high-speed reliable responses to emergency situations such as impending thermal runaway may not be compatible with the limitations of the communications bus, and a local module directly connected to the battery may be necessary to control those electro-chemistries.

Weight savings. A widely acknowledged weakness of lead–acid chemistry is the low practical specific energy. While theoretically a specific energy of $103\,\mathrm{Wh\,kg^{-1}}$ is possible, flooded automotive designs rarely see more than $30\,\mathrm{Wh\,kg^{-1}}$ by the time robust grids, straps, excess electrolyte, and cases are added. The starved-electrolyte design of VRLA tends to be somewhat better, at about $35\,\mathrm{Wh\,kg^{-1}}$, but this is still a poor performer relative to Ni–MH, at 60–$70\,\mathrm{Wh\,kg^{-1}}$, or lithium-ion, at over $100\,\mathrm{Wh\,kg^{-1}}$ (both exclusive of thermal management). It is important to note that weight is critical to the vehicle classification so that even marginal weight reductions are considered in vehicle estimates and may be a significant factor in the battery selection process.

Life. Battery life has been a contentious topic for a number of years and the upward creeping energy and power requirements have undoubtedly exacerbated the debate on this subject. The need for a longer-life battery follows the trend for ever-longer-lasting automotive components; with 160,000 km/100,000 mile sparkplugs and long-lasting synthetic oils on the near horizon, batteries may be one of the last bastions of three-year service items. This issue is all the more disconcerting as the size, and hence the expense, of batteries increases, particularly when massive EV batteries, costing in excess of the drive-train, become common, and life-cost reaches thousands of dollars per year.

VRLA has a definite advantage over flooded lead–acid in deep-cycling scenarios. Although direct comparisons are difficult, due to different active material limitations, utilization, and current densities, the chart given in Fig. 11.4 (and the correlation

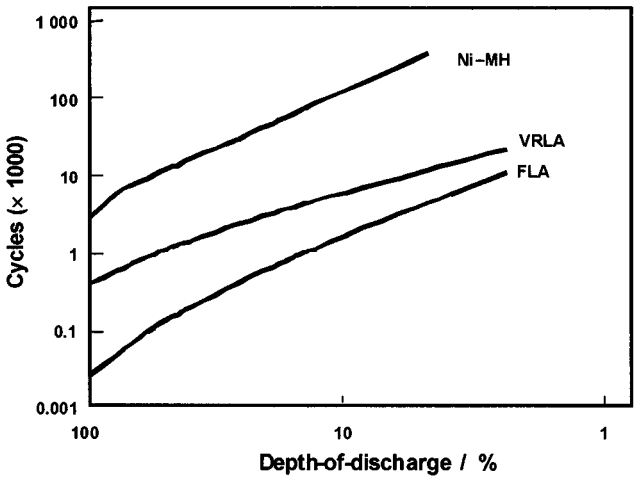

Fig. 11.4. Cycle-life dependence on DoD for flooded lead–acid, VRLA, and Ni–MH batteries. Based on nominally ambient cycling conditions, moderate rates of discharge (< 1*C* rate), short cell strings, and periodic full recharge; data from 12-V automotive, Ni–MH EV batteries, and VRLA EV batteries

Table 11.5. Correlation for battery cycle-life as a function of depth-of-discharge: $\Phi = A\ (e^{\Delta})^{B} + C\Delta^{D}$

	Flooded lead–acid	VRLA	Ni–MH
A	-1.462×10^{2}	-8.100×10^{2}	-1.071×10^{-5}
B	-7.042×10^{-1}	-2.169×10^{-1}	1.866×10
C	9.797×10	1.038×10^{3}	4.236×10^{3}
D	-1.286	-8.334×10^{-1}	-1.498

Where Φ = battery life and Δ = depth-of-discharge.
Based on nominally ambient cycling conditions, moderate rates of discharge (< 1C rate), short cell strings, and periodic full recharge; data from 12-V automotive, Ni–MH EV batteries, and VRLA EV batteries.

given in Table 11.5) is fairly typical of the relative improvement in cycle-life of VRLA as compared with flooded lead–acid. The chart also provides a comparison of VRLA life with that of Ni–MH chemistry.

Cost. Although VRLA is expected to settle at about 25% higher cost than flooded, there may be some applications where this cost increment is acceptable. High-capacity, deep-cycle applications are one case where low-cost automotive flooded batteries cannot usually match VRLA performance, but where alternative batteries that cost an order of magnitude more are not feasible. In this comparison, the lower cost of VRLA relative to Ni–MH or lithium batteries must be weighed against the higher mass and lower reliability of VRLA, but should the mass and life be within

range on a life cost basis, low initial cost will likely drive the technology decision to VRLA.

11.2.2. Continuum of electric drive

If only drive-related functions are considered, there are a number of states in which the automotive battery is active, ranging from maintaining on-board computers to providing all the energy required for electric drive. Five scenarios are mapped against function in Table 11.6 and sketched in Fig. 11.5. These are as follows.

- *Automotive*: functions that support the heat engine, such as cold crank (a 300 ms — 30 s burst of high power to start the engine) and engine controls.
- *ISA*: Integrated Starter Alternator (sometimes referred to as Integrated Starter Generator – ISG), which provides up to 12 kW of boost power, automotive functions, and accessory loads that allow the engine to stop when the vehicle stops.
- *Parallel hybrid*: provides up to 30 kW of boost power, plus ISA functions.

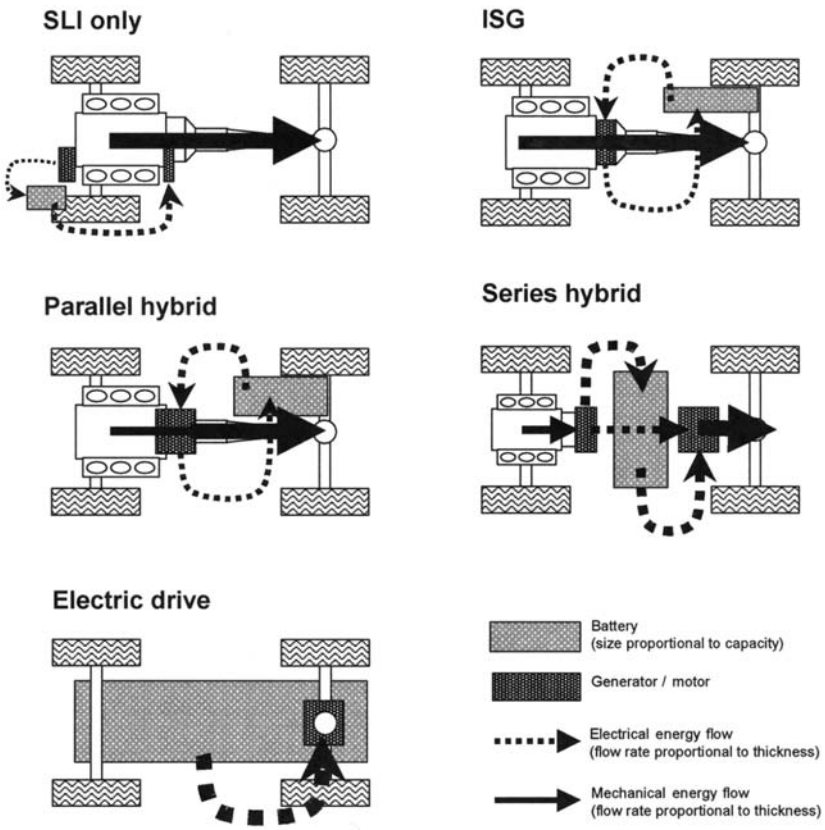

Fig. 11.5. Automotive electric-assist architectures.

Table 11.6. Energy requirements for automotive attribute.

Function	When applied	Time applied	Power needed	Automotive	Soft hybrid	Parallel hybrid	Series hybrid	Electric drive
Parasitic loads for on-board computers	all times	all times	0.3 W (discharge)	X	X	X	X	X
Accessory loads to support start function	key-on	during key-on	300–2000 W (discharge)	X	X	X	X	X
Cold crank	key-on	0.3–30 s	2–10 kW (discharge)	X	X	X	X	
Recharge from alternator	key on, when alternator power in excess of vehicle needs	10 s +	0.1–2.5 kW (charge)	X	X	X	X	
Provide boost to engine	from vehicle stop	5–10 s	(discharge)		5–12 kW	30 kW +	50 kW +	
Provide boost to engine	during drive	5–10 s	(discharge)			30 kW +	50 kW +	
Accept charge from drive-train	key on, when alternator power in excess of vehicle needs or during breaking	10 s	0–30 kW (charge)		10 kW	20 kW +	30 kW +	30 kW +
Provide electric-only drive function	Key on, engine off	5–30 s	5–60 kW (discharge)				X	
Provide drive function at all times	Key on	During drive (> 1 h)	90 kW (discharge)					90 kW

- *Series hybrid*: provides up to 50 kW of boost power.
- *Electric drive*: provides all drive power up to 90 kW.

It is also possible to define soft, mild, and full hybridization based on the degree of power-train electrification relative to the heat engine peak power; soft hybrids can be considered to contribute $< 10\%$ of peak ICE rating, mild hybrids contribute 10–25% of total drive-train energy, and full hybrids provide 25–50% of peak power [3].

11.3. Automotive Applications

11.3.1. 12-V automotive

Starter, lights, and ignition batteries currently make up the largest segment of lead–acid battery business. Lead–acid is a natural fit to this application; low cost, high power capability, excellent low-temperature performance, reasonable safety under nearly all circumstances, resistance to abuse, and long shelf life, have kept lead–acid the only plausible choice for this application. Moreover, the technology is mature and relatively robust, in part due to the substantial over-design that is currently an accepted cost of the technology. Unfortunately the low price and universal acceptance of the flooded lead–acid battery have insulated the current automotive battery designs from OEM insistence on substantial improvements; the low cost, approaching commodity levels, has in fact led to a certain level of complacency in the industry. This, plus a pricing strategy that offsets OEM cost relative to after-market sales, has led to a situation where there is relatively little motivation to enter into the large expense and risk involved in anything more than minor incremental improvements. These circumstances, however, will inevitably change. Standing expectations at the vehicle platform level for any component are that: (1) warranty claims will decrease, regardless of whether the costs of the reduction is borne by the supplier or the OEM, (2) weight will decrease without a decrease in function, and (3) costs will drop incrementally on a year-to-year basis.

For a mature technology, at commodity pricing, these goals may appear to be mutually unattainable. Nevertheless, the inefficiencies built into lead–acid technology today actually lay the basis for a successful propagation of lead-based technology into the decades ahead. For example, a commonly held view in design is that materials that under-perform cost twice: first as the extra materials that must be added to compensate for the weakness, second as the infrastructure that must be included to support the non-value added material. The counterpoint is that improvements in materials utilization are highly leveraged. For example, with respect to the flooded automotive battery, the extra grid lead, electrolyte, negative active mass, and positive active mass are all features that present substantial improvement opportunity through intelligent reductions. The actual specific energy of about $30\,\mathrm{Wh\,kg^{-1}}$ for most commercial products compares poorly to the theoretical maximum specific energy of $166\,\mathrm{Wh\,kg^{-1}}$ ($103\,\mathrm{Wh\,kg^{-1}}$ with 1.25 sp.gr. acid, $72\,\mathrm{Wh\,kg^{-1}}$ allowing automotive voltage ranges). Even worse is that to

Table 11.7. Estimate of effect of improvements on the specific energy of lead–acid batteries.

Utilization	Theoretical	Current	Improved
Energy required for 6 events × 5 kW for 6 s	50 Wh		
Reserve energy (at 25A)	100 Wh		
Energy required for 100 min reserve	500 Wh		
Active material utilization	100%	30%	50%
BASIS = 1 mol			
MWt_{PbO_2}	239 g		
MWt_{Pb}	207 g		
$m_{H_2SO_4}$	196 g		
m H_2SO_4 (1.25 to 1.10 sp.gr.)	1032 g		
Capacity	107 Wh	32.2 Wh	53.6 Wh
BASIS = 500 Wh			
m_{PbO_2}	1.12 kg	3.72 kg	2.23 kg
m_{Pb}	0.97 kg	3.22 kg	1.93 kg
$m_{H_2SO_4}$	4.81 kg	5.30 kg	4.81 kg
Grids	–	4.14 kg	3.04 kg
Top lead	–	0.91 kg	0.66 kg
Other	–	1.99 kg	1.46 kg
Total weight	6.90 kg	19.3 kg	14.1 kg
Specific energy	72.5 Wh kg^{-1}	25.9 Wh kg^{-1}	35.4 Wh kg^{-1}
Single start event DoD	1.1%	1.3%	1.1%

maintain a reasonable life, the battery must be shallow discharged so that the discharge required for engine start must be less than 1% of rated capacity. Should the efficiency of a 40 Wh kg^{-1} + battery be realized, the drop in weight alone would prove an appealing lure and competitive edge to the automotive industry. The reduction in the need for any of the materials used in lead–acid battery manufacture would thus directly improve the long-term marketability of the technology and may provide a strategic path that will enable lead–acid to compete successfully against newer technologies. Such a strategy would also directly improve the economics of the lead–acid battery; with less material purchased and a constant price, the financial picture for this technology is more favourable. As can be seen in Table 11.7 (charted Fig. 11.6), even a moderate increase in the utilization of the active materials will lead to substantial reduction in weight and hence cost.

The architecture of the 12-V automotive system is shown in Fig. 11.7. Within the battery system architecture fundamentally little has changed for many decades, with the possible exception that thermal management has become less straightforward and now requires additional components such as heat shields or boxes to help thermally isolate the battery from the engine.

11.3.1.1. Performance requirements. The automotive battery is typically installed within the engine compartment, which is, by all accounts, an abusive

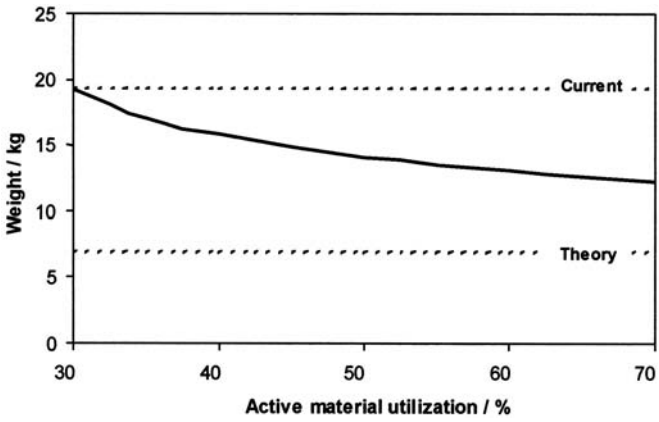

Fig. 11.6. Effect of material utilization on weight. Calculations assume a 100 min battery; theory value allows voltage to vary within automotive standards.

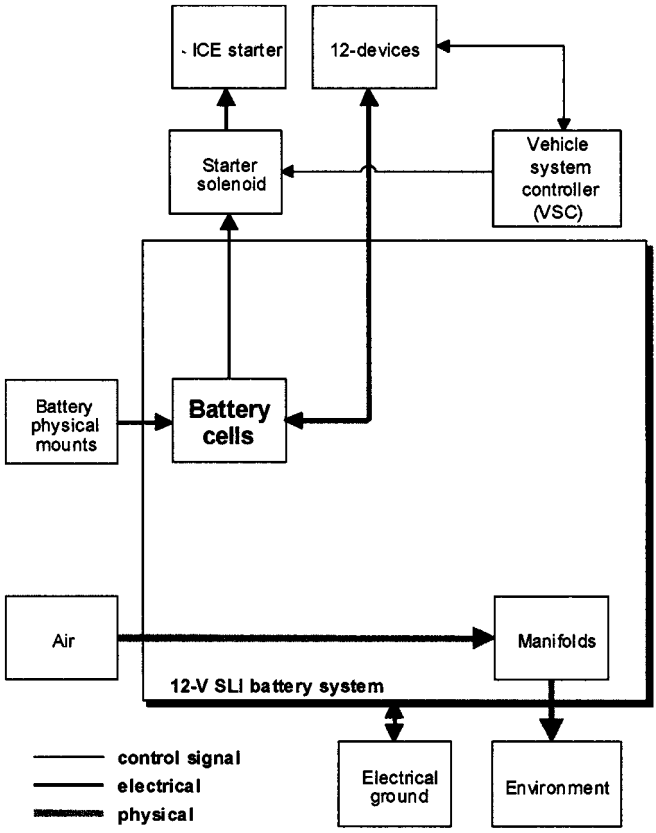

Fig. 11.7. Typical 12-V automotive battery architecture.

environment where temperatures can soar above 100°C. The situation is further aggravated by the increasing complexity of the engine such that additional heat-generating devices now take up space in the engine compartment, space that once contributed to cooling the battery environs. Some relief is given through ram-ducted air and battery receptacles designed to reduce the temperature experienced by the battery, but it is clear that the hotter engines seen today impose added stress on the battery.

The detailed specification for a candidate battery will depend on the vehicle type, engine size, and accessory loads, but generally the standard tests described in Table 11.8 will be required before battery selection. The tests, standards of pass/fail, and the number of replicates will be specified by the sourcing engineering centre of the vehicle programme. The spectrum of duty cycles for which a battery may be responsible is shown in Table 11.9; the standard tests specified in Table 11.8 are a means to estimate the performance of the candidate battery. It should be understood that these tests are bellwether and are designed to compare batteries on a common basis. A pass or fail on these specifications, however, may or may not be an indication of suitability in an application, since many factors outside the scope of this relatively narrow group of tests will determine the success of a battery design.

The actual process of sizing a battery so that an acceptably long and reliable life is realized will factor in many needs. The decision will ultimately rest, however, on the severity of the duty cycle and the expected response of the battery to that cycle. In the case of the automotive industry, it is a fallacy to assume that all vehicles have

Table 11.8. Standard automotive qualification tests.

Power	Capacity	Life
• High-rate discharge at 25°C	• Reserve capacity (25 A rate in min)	• Charge-acceptance • Vibration
• High-rate discharge at −30°C	• 30-day stand	• Vent leakage
• Cold-crank at −18°C		• Gassing rates • Life test (i.e., SAE J240A/B)

Table 11.9. Typical 12-V automotive duty cycle type and frequency.

Event	Power	Time	Voltage limits	Temperature	Cycles (10 y)[a]
Cold Crank	2–10 kW	< 5 s	> 7 V	−30 to +60°C	15 k
Idle	0–2 kW	< 120 s	> 10.5 V	0 to +50°C	250 k
Reserve	300 W	> 100 min	> 10.5 V	0 to +50°C	10
ICE charge	500 W–3 kW	< 120 s	< 16 V	0 to +50°C	250 k
31d stand[b]	0.3 W	31d/5 s	> 7 V, at 6 kW	25°C	25

[a] Over 10-year period.
[b] 31d = 31 days.

a similar duty cycle, and for that reason all applications at the outset should be considered unique, even between vehicles with similar features.

For an automotive battery, the five key functions that make up the duty cycle are:

(i) Engine start load and time

This is the power needed to overcome the friction, compression, and inertia of the engine to bring the engine rotation speed up sufficiently to fire the cylinders. The crank power will vary from engine to engine and with temperature, but it is generally in the kilowatt range.

(ii) Drive load/alternator capability

The drive load is the total power required to keep all appropriate accessories and controls energized at their required level. This will vary greatly, from several hundred watts in smaller vehicles to several thousand watts in modern, accessory-laden, premium vehicles. The alternator capability will vary with engine speed and normally will be oversized in anticipation of maximum demand. Any surplus output from the alternator will provide energy for the battery to recharge.

(iii) Idle loads and time at idle

While the vehicle is at idle (engine at minimum speed), most electrical loads are maintained. The low output of the alternator under these conditions, as shown in Fig. 11.8, means that the battery may need to boost voltage through discharge, and the burden on the battery may be substantial depending on the accessory load and the time at idle. For example, a 1-kW deficit for 5 min will discharge a 50-Ah battery by 13.9%, for which a flooded lead–acid would only survive 1000 cycles (cf., Fig. 11.4).

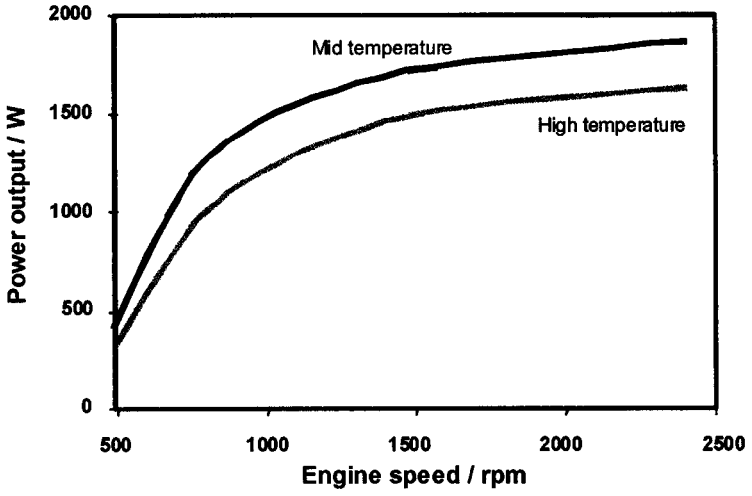

Fig. 11.8. Typical alternator output.

(iv) Engine stopped loads and time
These loads are normally rare, but they are essential and include engine-stopped conditions such as emergency flashers. Selected users such as police and municipal fleets, however, may require substantial drains on the automotive battery while the engine is off in order to power radios, computers, or other devices. In these applications, a greatly reduced flooded lead–acid battery life of about one year is the norm.

(v) Long-term storage (parasitic) temperatures and time
Vehicle on-board electronics consume small maintenance currents that will reduce SoC over time. This parasitic current is normally on the order of 20–30 mA at 12 V. Should the battery deeply discharge (say, during an extended airport park), there is a chance that the battery will not be of high enough SoC to crank the engine.

Of the five functions, only engine cold crank is an unambiguous power requirement and is the root of the first three tests described in Table 11.8. The opposite is true for the other four; the drive loads, idle loads, engine-stopped loads, and storage are all relatively low power needs that depend on capacity rather than high power. In this vein, it is interesting to note that the battery requirements range from very low parasitic currents (on the order of 25 mA) to hundreds of amperes during a cold crank event. Some of these requirements, such as engine start and long-term storage, are relatively well characterized and effects on a battery selection can be determined satisfactorily using standard tests (SAE or the equivalent). The remaining three features, however, will nearly always vary greatly from vehicle to vehicle and, unfortunately, may have a larger effect on battery life. For example, from the perspective of the battery, idle loads will usually surpass the output of the alternator, and the only reasonable way to maintain a reasonable SoC in the battery is to apply current during the drive sequence. Thus, in order to size a battery properly, it is necessary to have estimates of the alternator output during idle, the alternator output during drive, the accessory loads, and the times for each of these events. The following process should be performed.

(i) Determine the idle profile (time and frequency) for the vehicle
Casual examination of the matter will show that the frequency and length of idle time will vary from vehicle to vehicle, from driver to driver, and from trip to trip. Aside from some very specialized fleet service, there will therefore be a natural variation in when, and for how long, a vehicle stops (Fig. 11.9). Moreover, this distribution will vary with the vehicle type and usage patterns. For example, heavy-truck and police vehicles will likely see a shift in the curve to the right, while light service vehicles will see a shift to the left. It is normally the responsibility of the vehicle programme management to specify the targeted market, and hence the corresponding drive cycle.

(ii) Determine the alternator capability during vehicle idle
During idling it can be expected that the alternator will be producing charge to some extent, but generally this will be at a level insufficient to carry all of the idle loads.

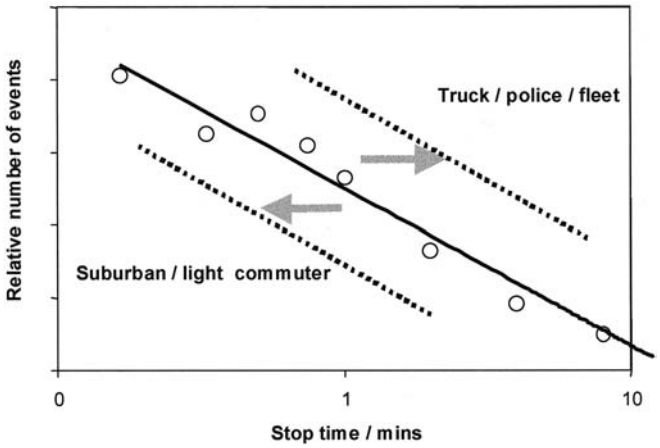

Fig. 11.9. Time and frequency of idle events in North American cars and light trucks, typical.

Since the load on the battery will be determined by this deficit, the alternator output curves and corresponding pulley speed are needed to size the battery.

(iii) Calculate the battery requirements in terms of capacity and life
From the idle information and the alternator power curve, a weighting should be done to equate the discharge cycle to standard life tests:

$$E_{\text{average}} = \frac{\sum(\text{event time})\left(P_{\text{loads}} - P_{\text{generator}}\right)}{n}$$
$$E_{\max} = \max(\text{event time})\left(P_{\text{loads}} - P_{\text{generator}}\right) \tag{11.2}$$

where E_{average} is the average energy per event time, $E_{\max}$ is the maximum energy required for the longest expected idle time, P_{loads} is the power needs for average loads, $P_{\text{alternator}}$ is the power available from the alternator during idle periods, and n is the number of events.

There are perhaps several ways to determine the life capability of a battery, but if the total amount of charge through the battery to end-of-life (EOL) is taken to be constant for an average depth-of-discharge (DoD) as in Fig. 11.10, then the life capability of the battery can be estimated, as shown in Table 11.10. The inputs and the result of this calculation underscore the importance of knowing the power required at various states of vehicle operation and the time of these events when considering batteries for a particular vehicle application.

(iv) Confirm that the alternator capability during drive is sufficient to provide positive net charge balance
At this point it is prudent to confirm that the alternator is capable of maintaining all the vehicle loads during a 95% drive profile. In the typical case described here, a constant load of 2 kW may be expected, which on a 12-V system is about 170 A.

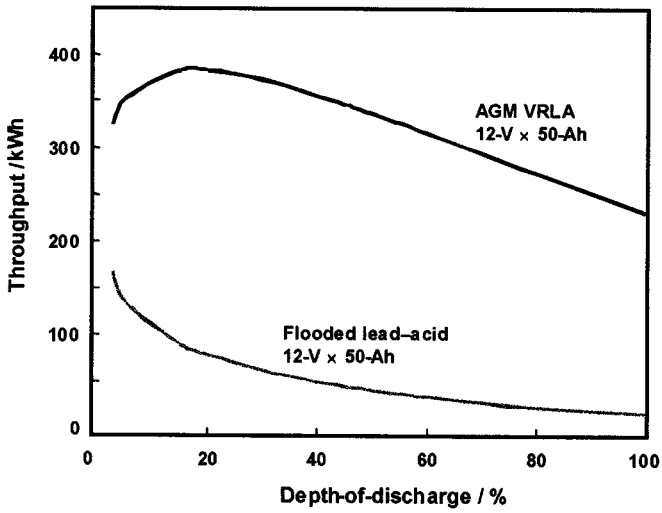

Fig. 11.10. Dependency of kWh throughput over life on DoD.

Table 11.10. Estimate of life for 12-V automotive battery.

Quantity	Value
Average time of event	60 s
Average current during idle	100 A
Energy per idle event	20 Wh
Battery makeup during idle	20%
Battery energy required per event	4 Wh
Energy per battery at reserve rate	500 Wh
Depth-of-discharge	0.8%
Cycles at depth-of-discharge	59 k cycles
Years, at 15 k events per year	3.96 y

The calculation is heavily dependent on the life curve (Fig. 11.10) and periodic checks should be made against this curve with the selected battery in the region of interest. As a general process, however, the size of reserve capacity can be assessed, provided that the battery meets all other performance specifications.

11.3.1.2. Controls and diagnostics for 12-V automotive batteries. Controls for automotive applications have been limited to simple voltage regulation based on temperature as measured at some location other than the battery, typically the engine-driven alternator. SoC, state-of-health (SoH), and previous history are not calculated or derived in this process. Furthermore, while voltage regulation is laudable, Fig. 11.11 shows that a 20°C temperature offset (easily conceivable when measuring temperature remotely) may result in a 600 mV charge error, which is certainly enough to compromise the charge strategy. This is somewhat mitigated by

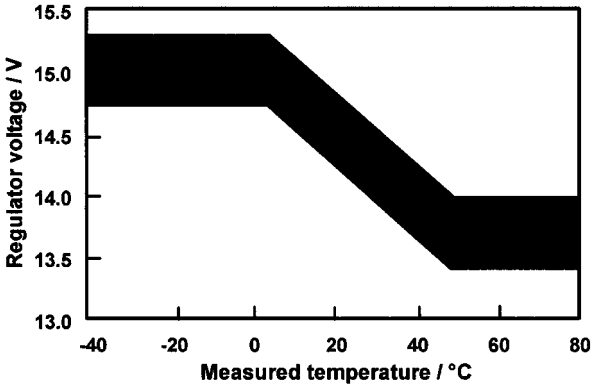

Fig. 11.11. Typical ranges of voltage regulation for automotive batteries.

the fact that the voltage response is quickly saturated at either end of the temperature range so that the voltage regulation quickly degenerates into a two-point control.

11.3.1.3. VRLA as a 12-V automotive battery. The trend in vehicles today is the ever-increasing idle loads; Table 11.11 is a listing of many of the present loads experienced by cars and light trucks, while Table 11.12 shows some of the features that are being considered by the industry and their relative impacts on the electric loads. It should be noted that the majority of these new electrical loads are active during engine idle, a state where the alternator is at a greatly reduced output and is already heavily dependent on the battery to maintain the system bus voltage. This points to an evolution of electrical loads that will skew the load distribution heavily to high reserve requirements during idle. This will greatly increase the demand on the battery through not only average power, but also by increasing DoD. Thus, the future, as described by automotive feature improvements, clearly points to an incremental but substantial gain in battery reserve. If ever-larger batteries with concomitant weight and costs are to be avoided, significant advances in battery technology must occur.

The VRLA battery has many of the traits needed to meet the above-described future requirement. Reduction of electrolyte, deeper discharge capability (reducing the need for active materials), and typically thinner grids all play to the needs of the next generation of automotive batteries. There are commercial VRLA designs that are renowned for their excellent power capability, but this is a consequence of the thin plate design that is encouraged by the needs of a VRLA battery in order to maintain connectivity between the separator and the grid. As batteries become sized for reserve capacity, however, the improved relative power will become less important.

It is well recognized that the architecture of the VRLA cell predisposes it to long cycle-life. The common failure modes for flooded automotive batteries are grid corrosion, lack of water, and damage to the positive plate [4]. Of these failure modes, VRLA may show some reduction in the extent of damage to the positive plate by

Table 11.11. Typical vehicle electrical loads.

Feature	Typical minimum power (W)	Typical maximum power (W)	Typical duty cycle (%)	Average minimum power (W)	Average maximum power (W)
Ignition and fueling	50	70	100	50	70
Blower speed 1	40	(50)	65	26	33
Blower speed 2	80	(120)	25	20	30
Blower speed 3	150	(200)	5	8	10
Blower speed 4	220	300	5	11	15
Heated rear screen	130	170	5	7	9
Heated front screen	500	670	2	10	13
Heated mirrors	20	30	2	0	1
Wiper speed 1	50	(60)	2	1	1
Wiper speed 2	80	100	1	0	1
Side lights	40	50	30	12	15
Dipped beam	100	(130)	20	20	26
Main beam	120	160	5	6	8
Fog front	90	120	2	2	2
Fog rear	30	40	2	1	1
Brakes	60	70	40	24	28
Radio	10	15	50	5	8
cd	10	(15)	50	5	8
Phone	10	15	50	5	8
Heated seats	90	120	3	3	4
Heater water pump	50	70	25	13	18
Cumulative power		2040		230	300
12 V current		170.0 A		19.0 A	25.5 A

Compare with Miller and Brost [3]: 1998 continuous plus intermittent loads 1200 W; 2005 continuous plus intermittent loads estimated at 2800 W.

Table 11.12. Proposed vehicle loads and their relative effect on electrical loads [7].

Drive loads	Effect	Idle loads	Effect
Electric all-wheel steering	+ + +	Electric powered air conditioning	+ + + +
Electronic valve activation	+ + +	Electric power point/appliances	+ + + +
Electric power steering	+ + +	Electrically heated catalytic converter	+ + +
Advanced powertrain control	+ + +	Supplemental instant heat	+ + +
Active suspension	+ + +	Electrochromic glass	+ +
Anti-lock braking	+ +	Zone adjustable climate control	+ +
Electronic fuel injection	+ +	Electric powered water pump	+ +
Electronic distributorless ignition	+ +	Memory seats	+
Traction control	+ +	Navigation aids	+
Electronic fuel injection	+ +	System and component diagnostics	+
Collision avoidance	+	Digital audio	+
Blind-spot sensors	+		

virtue of the compression that protects the plate from expansion. The largest life benefit, however, is reserved for deeper cycling activity that would normally result in positive material shed. Again, the plate stack compression that is necessary for a properly functioning VRLA battery has the added benefit that the plate structural integrity is preserved. Grid growth such as that seen in some high-temperature applications may likewise be reduced.

With the given deep cycle capability and possibly lighter mass, the challenge of the technology will be to offset the increase in cost of manufacturing by the decrease in cost of materials added, something that still requires some work and innovation but to which a mindset must be developed before VRLA is adopted for as widespread use as is the automotive battery. Regardless of the technology or innovation proposed, it is clear that there are substantial opportunities in mass-reduction and materials development that could, in theory, be tapped (Table 11.7). Undoubtedly these efforts will require proper examination of the roles and opportunities in grid alloy modifications, active material additives, optimization of separator types, and electrolyte composition improvements.

11.3.2. 42-V automotive

Through the 1900s to 1950, 6 V was the standard in nearly all automotive applications, but by 1960 nearly all automobiles had adopted the 12-V standard. This change was driven by better ignition performance, faster cranking speed for high compression engines, and a higher alternator output, which had reached 500 W by 1960 [5]. As automotive design in the 1950s showed, an increase in vehicle voltage follows increasing electrical complexity.

This evolution has continued to the present day. The alternator output for higher-end vehicles exceeds 2 kW, and if the increasing loads shown in Table 11.11 and Table 11.12 are indicative of the increasing customer expectations and their potential effects on the vehicle loads, ever-increasing power requirements can be expected. If it is accepted that the historical growth during the previous two decades of power-train electronics at 6% per year will be sustained, then it follows that, by 2020 the electrical generation capacity will exceed 10 kW in vehicles without electric propulsion and nearly 30 kW in vehicles with electric drive for propulsion [6]. While these levels of power need may be a number of years in the future, many of these features are near certainties. Unfortunately, increases in electrical power will have a detrimental effect on overall efficiency at the present voltage. At 5.8 kW (Fig. 11.12), for example, efficiency of the electrical distribution system falls to less than 65%; at 10 kW (Fig. 11.13), it is less than 40%. With energy efficiency being so critical, as measured through metrics such as the corporate average fuel economy (CAFE), the impact of this inefficiency on fuel economy ('mileage') will be significant at about 1 mile per gallon (0.43 km per litre) for every 750 W of loss [3]. Put another way, the automobile and consumer expectations have brought the 14-V electrical distribution system to its practical limit, and while the debate of what voltage to target is still not quite complete, within a decade a higher voltage standard is certain.

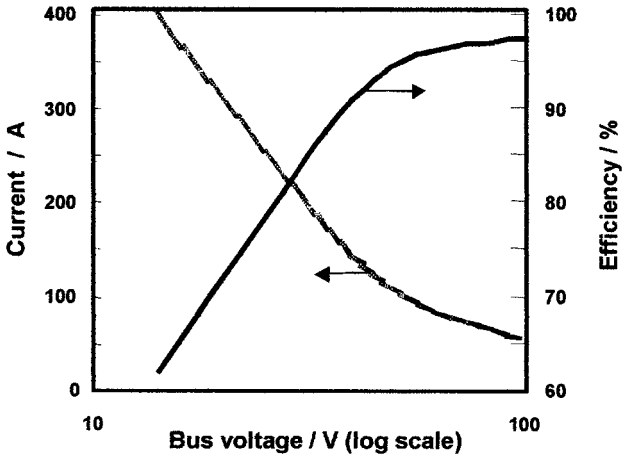

Fig. 11.12. Efficiency of current electrical distribution systems for 5.8 kW.

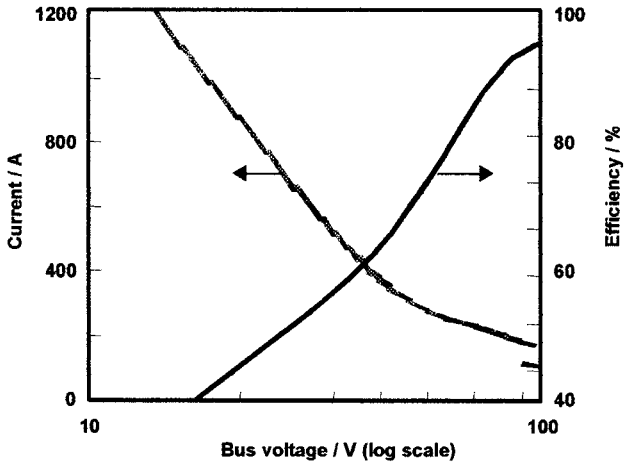

Fig. 11.13. Efficiency of current electrical distribution systems for 10-kW.

The architecture of the 36-/42-V system will probably contain a number of additional features over those of the current 12-/14-V systems, as suggested in Fig. 11.14. With the greater number of cells, some form of charge management and equalization will be needed to maintain the battery in functional condition. This will likely entail current sensors, temperature sensors, and one voltage sensor (although one voltage sense per six cells may be preferable), all communicating through the controller area network (CAN) or at least to a local controller. The higher voltage and power capability may also necessitate a fuse and contactor to isolate the battery quickly in case of an accidental hard short to chassis or during long stand times. Thermal management may yet be passive depending on the duty cycle

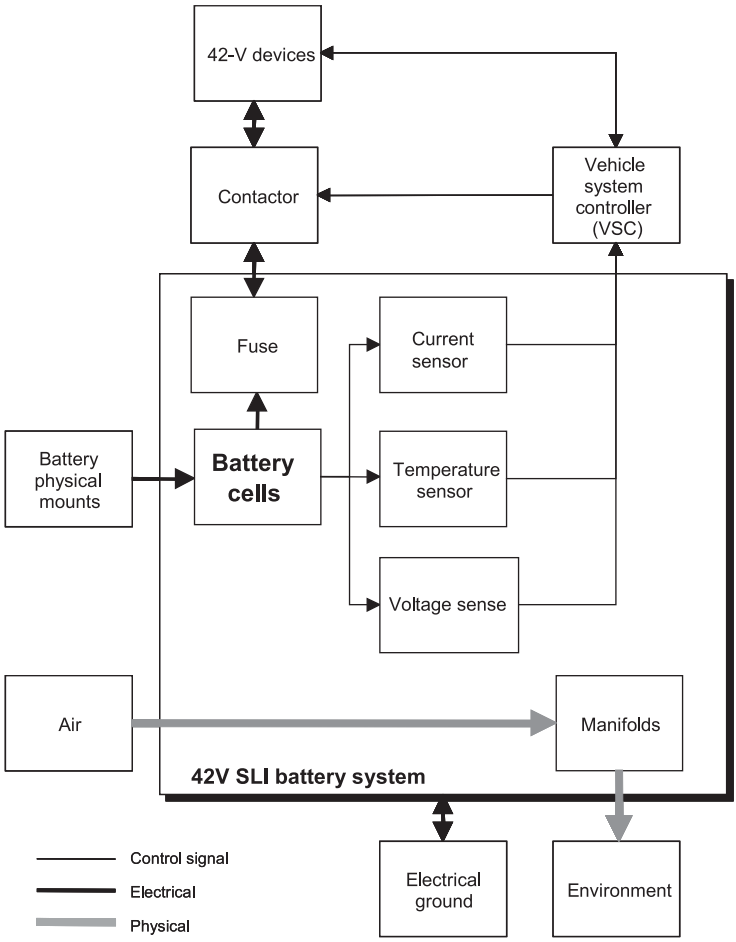

Fig. 11.14. Typical 42-V automotive hybrid battery architecture. Ground and communications to devices external to battery system not indicated.

and environment, but the escalating costs, temperatures, and duty cycles may pressure the establishment of some form of active thermal management such as a fan or a ram-air manifold.

11.3.2.1. General requirements. The cold crank power and parasitic drains on the 42-V automotive battery will both be close to comparable demands on the current 12-V battery. It is expected, however, that the idle loads and stopped vehicle energy requirements will increase with the evolution of the electric system accessories in the future (Table 11.12). Figure 11.12 shows that the higher the voltage, the better the electrical distribution system (EDS) efficiency. There are practical voltage limits dictated by safety standards, however, and it is commonly accepted that the danger

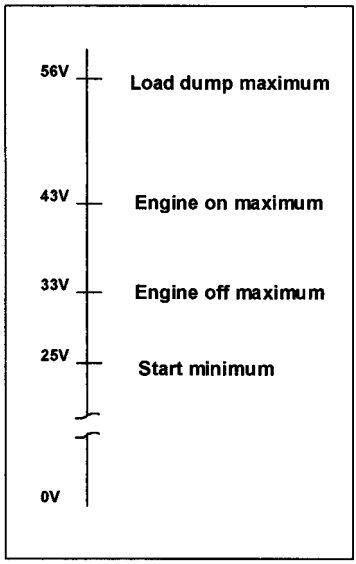

Fig. 11.15. 42-V PowerNet voltage ranges [11]. Start Minimum is the lower window of voltage acceptable to the vehicle system, Engine Off Minimum is the lower voltage acceptable to the vehicle system while the vehicle is in the key-on state (while the vehicle is within the scope of customer usage), Engine On Maximum is the maximum voltage while the engine is on and charging the battery, and Load Dump Maximum is the upper extent of voltage during surges due to loads coming on-line.

threshold for electrical shock is about 60 V. Voltages higher than this are certainly possible but not with exposed wire as seen with 12-V components, and considerable extra expense will be encountered to cover, for example, double insulation, ground fault sensing, and colour-coded cabling, to exceed this level safely [3]. The 42-V PowerNet voltage range (Fig. 11.15) is an attempt to capture a standard below the 60-V threshold.

The 42-V automotive battery is also likely to remain in the engine compartment, although this may change since the ohmic losses (i^2R) at higher voltage for the same power are less, thus allowing remote placement of the battery in a less hostile environment such as the cargo compartment (although this territory is often aggressively defended by the vehicle programme).

The type of connection will also play a role in the design of a 42-V battery. At the publishing date of this manuscript the standard connection had yet to be decided, but several options call for battery terminations to be close together in order to accommodate safety features that are active during disconnect of the battery. Battery designers will be faced with the options of building high-voltage batteries with high potential difference cells close together, providing insert-molded conductors, or cable, or poured lead straps to accomplish this feature. All these options have their problems. Extra conductor adds weight, expense, and complexity, while cells formed close together (side by side) open up the possibility of arcing when pinhole

Table 11.13. Typical 42-V automotive duty cycle type and frequency.

Event	Power	Time	Voltage limits	Temperature	Cycles (10y)
Cold Crank	6–10 kW	5 s	> 22 V	−30 to + 60°C	15 k
Idle	0–2 kW	120 s	> 32 V	0 to + 50°C	250 k
Reserve	300 W	> 100 min	> 32 V	0 to + 50°C	10
ICE charge	500 W–3 kW	120 s	< 50 V	0 to + 50°C	250 k
31d stand	0.3 W	31d/5 s	> 22 V, at 6 kW	25°C	25

Table 11.14. Proposed 42-V automotive battery message set.

Description	Message type	Source	Destination
Battery voltage	Sending	BMM	VC
Battery maximum voltage	Sending	BMM	VC
Battery minimum voltage	Sending	BMM	VC
Battery charge current request	Sending	BMM	VC
Battery source current available	Sending	BMM	VC
Battery sink current available	Sending	BMM	VC
Battery SoC	Sending	BMM	VC
Battery temperature	Sending	BMM	VC
Battery request for service	Sending	BMM	VC
Ambient temperature	Receiving	ECU	BMM

BMM: Battery Management Module
ECU: Engine Control Unit
VC: Vehicle Controller

defects occur with possible fire and explosion. Side by side cells may also suffer from thermal imbalance of centre cells, which will lead to charge problems and possibly premature failure. Typical requirements for a 42-V automotive battery are listed in Table 11.13.

11.3.2.2. Controls and diagnostics for 42-V automotive batteries. As a new product to the automotive industry, the 42-V automotive battery will be expected to deliver certain CAN-compatible messages to the vehicle system controller. A proposed message set for 42-V automotive applications which outlines some of these battery-related system variables is given in Table 11.14.

Future products such as CAN-controllable voltage regulators will allow more precise control of the voltage demands of the battery. Moreover, any temperature data available on the CAN network will be available at no extra cost. The temperature used to calculate the charge voltage can then be more representative of the battery; even ambient air may be a better indicator than the temperature of a device that emits its own waste heat and that is connected mechanically to the ICE.

Ultimately temperature measurement on the battery itself will provide the best data for voltage limit regulation, but this extra cost burden would have to be justified by proportionate warranty cost reduction.

The need for self-diagnosing components is a corporate directive for many automobile manufacturers and actions are underway to bring all components into compliance. Self-diagnosis is particularly appropriate to all service items, of which group the battery is without doubt a member. There have been a number of patents, proposals, and tests of diagnostic algorithms for automotive batteries based on polarization and historical data, but there has not as yet been a consensus regarding the nature or accuracy of such a parameter or group of parameters. Clearly, it would be in the best interest of any organization responsible for underwriting warranty to promote such a diagnostic, given that the vast majority of battery returns (by some estimates greater than 80%) are directly due to failure of some other component such as the voltage regulator or alternator. A reliable diagnostic would possibly reduce that amount by identifying a poorly maintained but otherwise healthy battery. The variable cost of the diagnostics algorithm could be minimal, given the proliferation of distributed microprocessors on current vehicles. This, plus the use of CAN standards, provides the opportunity to use existing controls hardware to support the diagnostics code; and with a modest investment in software, current sensors, and temperature sensors, this may be an economically feasible feature on future batteries.

11.3.2.3. VRLA as 42-V automotive battery. There are three aspects of 42-V operation that are pertinent to VRLA chemistry. The first and most obvious is the greater number of cells (18 rather than six). This is relevant since for a given energy, the cells in the 42-V system will have one-third the amount of electrode area. This would reduce the massively parallel systems that comprise most 12-V cell designs and will hence make them more sensitive to manufacturing or operational variation. Should there be more recombination in some cells than in others (due to, say, thermal gradients, material distribution, or dry-out), those cells would suffer and may fail prematurely. This predilection to imbalance is expected to be a chronic issue in the higher voltage designs. Symmetrical battery design and thermal management may be sufficient to maintain balance between the cells, but the greater number of cells coupled with the smaller surface area may lead to an effect that will require either electronic compensation through a charge-balancing circuit or periodic balancing through a prolonged overcharge step.

The second aspect, DoD, is also relevant to VRLA chemistry. It must be considered that battery capacity should be increased to supply loads not covered by alternator power. Alternatively, if these deficit periods and alternator output curves remain the same, battery capacity must increase to match DoD or total charge throughput in order to avoid premature failure of the battery. This cannot be totally taken up by battery mass, however, since mass is a critical cost in vehicle design and there is little interest in adding more. The ability of VRLA to survive deeper discharge cycles than the flooded equivalent (see Fig. 11.10) makes it a natural fit to these applications.

The third aspect is the apparent reduced ability of the VRLA battery to provide long service at higher temperatures. Under-hood temperatures have increased incrementally through engine design and reduction in air circulation patterns around the engine compartment. Some field and laboratory testing has shown VRLA to be somewhat inferior to flooded designs at high temperature, although some of this could be related to charging rates at high temperature. This aspect of VRLA chemistry will likely require additional research.

11.3.3. Soft hybrids

In the most basic sense, hybrid vehicle architecture: (a) allows a relatively small battery to augment the internal combustion power supplied to a drive-train and (b) allows the vehicle to recoup a portion of the vehicle's kinetic energy as electrical energy. In addition, common hybrid operating strategies provide non-idling (stop–start) performance, where accessory loads are maintained for at least several tens of seconds, and where fast, silent, and reliable engine restarts are expected. These functions are described in Table 11.15. It can be argued that the variants of hybrid vehicles are these functions taken to various degrees: soft hybrids are vehicles that provide the basic function of start–stop and regenerative braking ('regen') with some boost; the parallel hybrid provides start–stop, regen, with more substantial boost; and the series hybrid has start–stop and regen capability along with the ability to propel the vehicle at least short distances without the need of ICE augmentation. The soft hybrid is therefore the least energetic of the three hybrid architectures, but it is expected that the lower energy throughput will provide a much lower cost system while possibly maintaining most of the benefits of a hybrid vehicle. This, with the generally lower voltage of operation (< 50 V) makes the soft hybrid the most likely of all hybrid applications to implement lead–acid technology; in particular, the deep discharge tolerance of VRLA may give VRLA an advantage when judged against flooded lead–acid for resilience and Ni–MH for cost.

The architecture of the soft hybrid battery is described in Fig. 11.16. The contactor in this representation is denoted as outside the battery system, but it could be incorporated as part of the battery assembly. This representation also includes a battery controller within the battery assembly that may actually be physically located outside the battery box or even as shared space on another

Table 11.15. Soft hybrid system functions [9].

System function	Description
Alternator	Generate electrical power
Regenerative braking	Converts kinetic energy to electrical energy
Boost	Support the ICE with additional torque
Start–stop	Stop ICE at idle speed with rapid restart
Anti-jerk	Better driving with improved torque transient behaviour

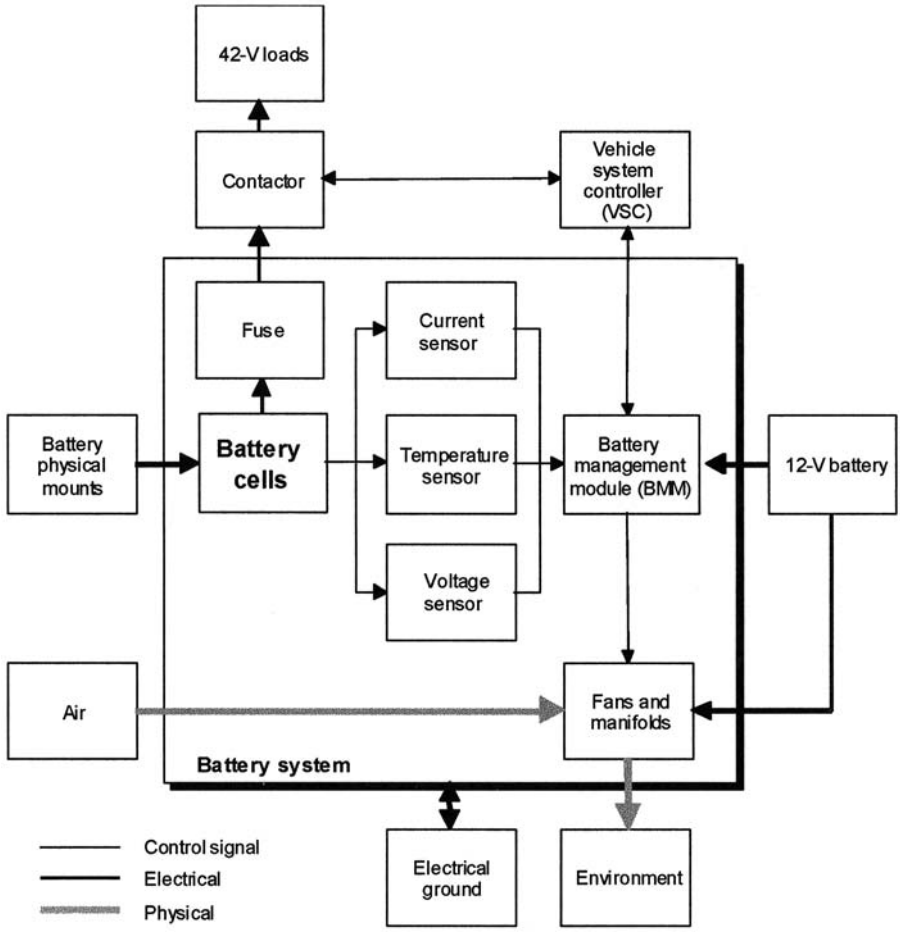

Fig. 11.16. Typical soft hybrid battery architecture.

controller on the CAN net. The higher energy and potential for very high rate discharges presses the need for a fuse and contactor in this system, as was the case for 42-V automotive batteries. The more aggressive duty cycle of the battery (up to 10 kW or an RMS current of over 100 A) will also necessitate some form of active thermal management (see notes below). In this respect, lead–acid chemistry may have an advantage since it is well known for ease of operation in hot environments relative to Ni–MH and lithium. It is also worth noting that this architecture uses a chassis ground and is not isolated. This feature may provide some cost and weight economy through cable length reduction (the cable between the negative lead and the alternator may be eliminated).

A 12-V battery power supply is also noted in Fig. 11.16; this may be eliminated in the future, provided that 42-V conversion of all other devices, including controllers, takes place.

11.3.3.1. General requirements. The hybrid battery design is recognized by vehicle programme managers as one of the key enablers of the hybrid system in total. While most battery engineers would automatically and enthusiastically agree with any sentiment that places the battery at the centre of the system, the greater electrification and the direct dependence on motive energy stored in the battery lend credibility to this argument. This focus brings with it some degree of leverage and priority during the process of claiming space aboard the vehicle, and with this latitude come improved form factors and thermal management opportunities. It is obvious to most that the conventional battery location under the hood is not suitable for a hybrid battery; size alone precludes this location, but the thermal management aspect is another, less obvious reason for isolation of the hybrid pack from the hot engine compartment.

High temperature is the traditional bane of secondary battery operation. This is particularly true in hybrid batteries, where the high pulse and average current densities over long drive periods can lead to high battery temperatures. The temperature rise is a natural consequence of the kinetics of non-reversible and secondary reactions. At some point, charge efficiency will suffer for most chemistries, and, in the case of Ni–MH or lithium, this situation may lead to thermal runaway and fire. Even with a high charge-efficiency and large-mass lead–acid battery, it can be calculated that the heat generation is substantial (Table 11.16). As can be seen, this problem becomes much worse for more aggressive duty cycles; at a 10-kW duty cycle, the battery would heat up by nearly 20°C within the first hour. If the initial temperature were 40°C, then, within an hour, the battery performance would have to be restricted until the battery cooled

Table 11.16. Calculation of heating rate for soft hybrid battery.

Basis: 18 cell flooded lead–acid, 70 Ah		6 kW	10 kW
Battery mass	m_b	68 kg	68 kg
Specific heat	C_{pb}	780 kJ kg^{-1} °C^{-1}	780 kJ kg^{-1} °C^{-1}
Battery specific heat	$C_b = m_b C_{pb}$	51 MJ °C^{-1}	51 MJ °C^{-1}
Charge time	t_c	10 s	10 s
Discharge time	t_d	8 s	8 s
Idle time	t_i	30 s	30 s
Current, charge	I_{ch}	143 A	237 A
Current, discharge	I_d	−175 A	−306 A
Average polarization, charge	η_c	3.7 V	4.5 V
Average polarization, discharge	η_d	−2.9 V	−4.4 V
Entropic/resistive heat loss	$P_l = (t_c i_c h_c + t_d i_d h_d)/(t_c + t_d + 2t_i)$	120 W	275 W
Heating rate (no heat rejected)	$P_{lt} = P_{lb}/C_b$	8.4°C h^{-1}	19.4°C h^{-1}

down. This would not be acceptable, and so the need for some form of thermal management is clear.

It should be recognized that the thermal management of hybrid batteries is key not only to function but also key to maintaining a reasonable life. Given the rough approximation that the free energy of the degradation reaction leading to battery failure is –50 kJ/mol and that there are no other secondary reactions, the following Arrhenius dependency on temperature can be obtained:

$$\begin{aligned} f &= \exp\left[\frac{E_a}{R}\left(\frac{1}{294}-\frac{1}{293}\right)\right] \\ &= \exp\left[\frac{-50{,}000}{8.314}\left(\frac{1}{294}-\frac{1}{293}\right)\right] \\ &= 1.07 \end{aligned} \tag{11.3}$$

or an $\sim 7\%$ increase in failure rate per degree Celsius, where f is the acceleration factor, E_a is the activation energy, and R is the gas constant. This suggests a two-fold increase in degradation rate for every 10°C increase in temperature, a factor to consider when weighing the cost/benefits of thermal management.

With hybrid vehicles, then, the option of active thermal management is often considered. Active thermal management may range from a simple plenum and small muffin-fan up to an evaporator system dedicated to battery cooling. The heat rejection needs can be roughly estimated from the discharge throughput (current multiplied by time) multiplied by the roundtrip efficiency. The roundtrip efficiency can be determined through a pulse technique, where equal charge and discharge power pulses of the same time and amplitude are sent through the battery starting at the high end of the expected operating SoC. If a reasonable time is allowed between the charge and discharge pulses, a realistic estimate of the open-circuit voltage (OCV) is possible and a good guess of the SoC is achievable.

Heating options may not be necessary since the typical high current density that the hybrid battery sees in normal operation provides enough self-heating to ensure that loss of function due to low temperature is rarely a terminal problem.

The size and weight allowance of the soft hybrid battery will vary, depending on the vehicle, duty cycle, and life requirement. Generally the expectation from the vehicle programme will be that a battery for soft hybrid duty will be somewhat larger and heavier than a standard automotive battery, but that the mass should be minimized. This is understandable since weight is a major factor in mileage; and since hybrid systems are generally meant to maximize fuel economy, it would be peculiar to improve fuel economy with a hybrid system on one hand and then degrade it with a heavy battery. Nelson described this effect [10]; where sub-optimum battery sizing occurs and where a high mass does not provide added benefit and where a low mass forces heavier use of the engine in regions of low efficiency (Fig. 11.17). This figure may be extended in other dimensions such as temperature, age, and duty cycle. The measured mass would of course depend on the technology. The higher energy and power density technologies such as lithium and nickel-based chemistry will result in a lower cell mass, but it should be considered when

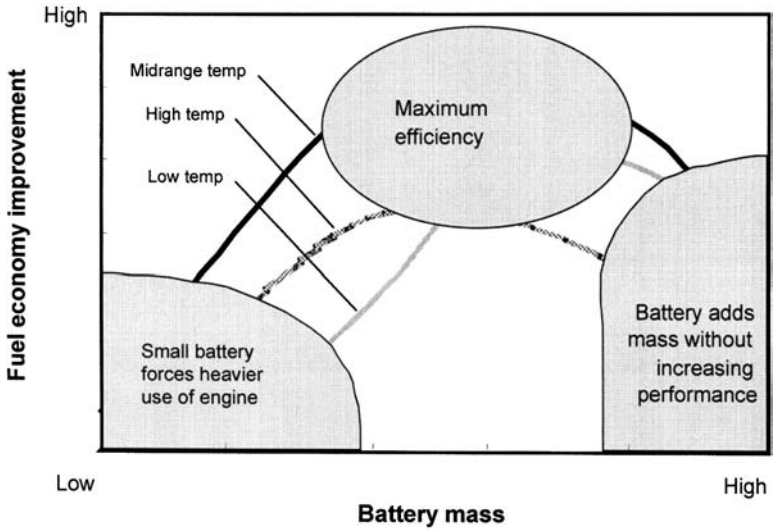

Fig. 11.17. Influence of battery mass on fuel consumption in a series hybrid electric vehicle [10].

calculating battery size that all components of the system, including thermal management and controllers, must be included. Also, if the thermal management of the battery places a cooling burden on the vehicle, this, too, should be included in the fuel economy estimates. In one extreme, for example, the energy recouped from regen braking could be expended by simply cooling the battery, a situation that is of little net benefit to overall fuel economy.

How the hybrid vehicle is used is an issue that will directly affect battery life and capabilities. For example, urban commuting will provide many opportunities for capture of regenerative braking power, while a metro-highway drive cycle will provide relatively few opportunities to improve mileage through regen capture. The highway strategy may, however, provide opportunity for boost. In either case the repeated cycles, whether charge or discharge, will stress the battery and thus limit life if events are not carefully controlled or prioritized.

When drive patterns force the battery through discharge/charge cycles, it should be possible to size any battery so that life goals can be achieved for the prescribed pattern. Factors to consider in this sizing of course weigh heavily on the charge-acceptance and power needs, but it is the occurrence of prolonged stop times, coupled with high static electrical loads in the vehicle, that contribute most to battery cycling and the consequent demand for higher energy batteries. Because of the entwining of the battery operation strategy with the vehicle energy management strategy, it is usually left to the vehicle system controller to manage engine start–stop events such that consecutive net loss of SoC does not accumulate to more than a reasonable DoD.

In one assessment of customer driving patterns in several North American cities, the duration of idle or vehicle-stopped periods was quantified with respect to the

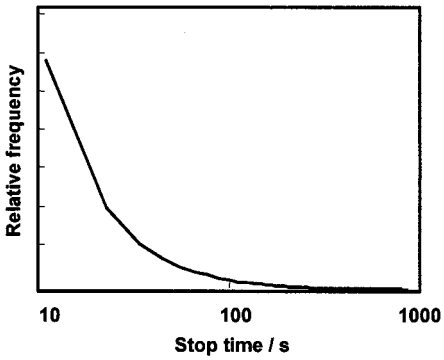

Fig. 11.18. Stop time frequency, average North American drive cycle.

Table 11.17. Estimate of battery life for soft hybrid.

Quantity	Value
Average time of event	10 s
Average power during idle	1500 W
Start energy	0.8 Wh
Boost time	5 s
Boost power	6000 s
Energy per idle event	9 Wh
Energy per battery at reserve rate	2520 Wh
Depth-of-discharge	0.53%
Cycles at depth-of-discharge	82,852
Years, at 25 k events per year	3.3 y

number of stop events (Fig. 11.18). The distribution of stops of course varies, but it was worthy to note that most stops were of 3 min or less, with the probability still non-zero above 10 min. If a weighted average time for stop events of 30 s and an average power or current is assumed, the life calculation of Table 11.10 can be revisited in Table 11.17. The values in Table 11.18 are typical for soft hybrid applications, although some applications may very well operate outside these ranges as a matter of operating strategy. Since soft hybrid strategies call only for augmentation of power rather than sole sufficiency, critical actions for the soft hybrid are limited to cold crank, reserve capacity, and 30-day stand, all of which parrot automotive operational requirements. Other functions are used for fuel economy improvement and so an inability to meet these functions will have a lower severity. As a consequence, the temperature range for these actions is somewhat reduced to the range at which improved fuel economy is significant (lower temperatures are expected to provide lower fuel economy due to increased use of climate control and the increased drag; higher temperatures can be expected to reduce fuel economy due to increased energy consumption of the climate control).

Table 11.18. Typical soft hybrid performance requirements.

Event	Power	Time	Voltage limits	Temperature	Cycles
Cold Crank	6–10 kW	5 s	> 22 V	−30 to + 60°C	15 k
Start	6–10 kW	0.5 s	> 32 V	0 to + 50°C	250 k
Boost	8–12 kW	10 s	> 32 V	0 to + 50°C	250 k
Idle	2–5 kW	120 s	> 32 V	0 to + 50°C	250 k
Regen braking	3–10 kW	10 s	< 50 V	0 to + 50°C	250 k
ICE charge	500 W–3 kW	120 s	< 50 V	0 to + 50°C	250 k
Reserve	300 W	> 100 min	> 32 V	0 to + 50°C	10
31d stand	0.3 W	31d/5 s	> 22 V, at 6 kW	25°C	25

Also note that the temperature range refers to battery temperature; as cold batteries are worked, the temperature increases substantially. This is particularly true at low temperature since polarization is highest and the efficiency is therefore lowest. Note that, the voltage limits in Table 11.18 are modified for the set of fuel economy actions so that boost, start, and idle do not result in any noticeable degradation of accessory performance such as light dimming or electronics fade.

11.3.3.2. Controls and diagnostics for soft hybrid batteries. The energy management viewpoint and additional functionality will logically make the controls for a soft hybrid more complex than those for the equivalent automotive battery. In addition, the deeper cycling hybrid battery leaves less leeway for error since the severity of non-function is significant. For example, braking may require some component of regen power acceptance by the battery; should this be understood by the energy management system to be available through a miscalculation when in reality it isn't, brake performance could be compromised. Likewise, a hot restart may be critical and the severity high in some traffic situations and so a non-functional battery is clearly not acceptable in this situation. A balance between the operating strategies of the battery and of the vehicle thus becomes a major concern, but maximum protection of the battery will likely defer to energy management.

Basic functional controls will include those in Table 11.19. Most of the values can be derived from a straightforward transfer function; but several, particularly those determining maximum charge current, discharge current, and state-of-charge, will require careful scrutiny of the definition, calculation, and error analysis.

The effective and safe use of batteries in enhanced electric function vehicles requires a more judicious use of the battery capability than is typically seen in present-day vehicles. For example, battery controls on most vehicles today consist of simple temperature-compensated voltage regulation. This has been sufficient since batteries are only infrequently discharged below high SoC, and, even when that does occur, the constant-voltage charge algorithm can rapidly replenish the battery. Moreover, the critical operation of the battery (engine crank) is at a vehicle-stopped state, which is relatively safe in case of function failure (a non-start condition is a customer dissatisfier, but does not directly endanger the operator). In contrast,

Table 11.19. Hybrid control message set.

Description	Message type	Source	Destination
Battery voltage	Sending	BMM	VC
Battery maximum voltage	Sending	BMM	VC
Battery minimum voltage	Sending	BMM	VC
Battery charge current request	Sending	BMM	VC
Battery source current available	Sending	BMM	VC
Battery sink current available	Sending	BMM	VC
Battery equalization current request	Sending	BMM	VC
Battery SoC	Sending	BMM	VC
Battery temperature	Sending	BMM	VC
Battery request for service	Sending	BMM	VC
Ambient temperature	Receiving	VC	BMM
Inverter input voltage	Receiving	VC	BMM
Inverter input current	Receiving	VC	BMM

battery management for deep-discharge batteries must be tied to the vehicle energy management strategy, since regen charge-acceptance, non-idle time, climate control, and other vehicle operations will all be logical inputs to the battery management algorithm. Where non-idle strategies are applied, it must also be assumed that engine start could be required anytime during the drive cycle. This would include periods where the vehicle is in a vulnerable situation such as at a controlled roadway intersection, where engine crank capability must be protected at all times. The ability to accept regen energy also points to advanced battery controls, since holding batteries at a lower SoC where charge-acceptance is sufficient is essential. Accurately calculating SoC under these conditions is not a trivial task for a non-100% coulombic efficient storage medium that ages and thereby changes, so innovative and sometimes complex algorithms are necessary. For these reasons, the advanced battery will require greater care in charge management and accurate knowledge of battery health, including SoC. Advances in vehicle communication networks will facilitate this need, but it should be recognized that particular attention must be paid to battery management, control, and diagnostics.

11.3.3.3. VRLA as a soft hybrid battery. Flooded lead–acid batteries have a number of strong points that favour use in soft hybrids such as robustness, a large thermal mass, and a conductive medium to remove the heat. Flooded lead–acid batteries are not considered contenders for soft hybrid applications, however, for the several reasons outlined below.

(i) The flooded lead–acid battery will not meet minimum service-life

The first reason is that, although the majority of cycles in the hybrid duty profile will be shallow, flooded lead–acid technology does not do well at deeper discharges, which would lead to poor life. To illustrate, whereas VRLA batteries yield optimum performance at about 20% DoD, Fig. 11.10 shows that the equivalent flooded

lead–acid battery will already be in steep capacity decline at that same DoD. Studies have shown that a car/light-truck can expect 12,000 stop events in excess of 100 s over a 10-year period. If this were the only duty for the battery, Fig. 11.4 indicates that at 3-kW idle load for the weighted period of time of 160 s, a 50-Ah flooded lead–acid battery would last no longer than 1.2 years, compared with 3.9 years for a VRLA equivalent.

(ii) Mass opportunities of VRLA are likely to be taken
The second concern is the mass of the flooded lead–acid battery. With weight being a key worry in almost all vehicle programmes, opportunities for mass reduction are encouraged and it could be presumed that a 10 kg reduction for VRLA over flooded lead–acid will be readily accepted.

(iii) Packaging flexibility is constrained when using flooded batteries
A third concern is the likelihood of spillage. Packaging the soft hybrid battery presents in itself certain challenges. Many solutions involve mounting the battery within the passenger compartment, but a flooded battery's free electrolyte may, in that case, be a chemical hazard in case of a crash. Although engineering could minimize the risk, it would reduce the packaging flexibility needed, particularly with such a large component.

For these reasons, it is expected that flooded lead–acid will not be seriously considered for many soft hybrid programmes. It is not yet clear, however, that VRLA is the best choice for the soft hybrid battery. There is much debate about this subject at this time, but much of the discussion centres on the life capability of VRLA. It is often assumed that the many deep discharges that are expected during hybrid battery life require a more advanced, high-rate battery chemistry and design such as Ni–MH. Indeed, that chemistry is for the most part well suited to this type of discharge with the exception of high- and low-temperature operation. Nevertheless, VRLA has demonstrated some capability to provide multiple deep discharges, and although a 250,000 cycle-life is probably outside the bounds of VRLA operation at any significant DoD, 80,000 cycles are not impossible if the battery is sized properly. Other compromises do exist with VRLA; specifically, the generally lower power and energy density of lead–acid relative to Ni–MH handicaps VRLA. There are a number of other factors, however, that reduce the appeal of Ni–MH such as space and mass efficiency degradation through the need for evaporator-based cooling of the Ni–MH batteries. Ni–MH batteries require temperatures to be no more than 60°C at any time and less than 40°C during operation to meet life targets. The thermal management to meet these conditions is substantial and may add 50% or more mass to the battery system in ducting, compressors, evaporators, and fans. The additional mass should be included in the mass of the battery system so that the apparent specific energy is reduced proportionally.

VRLA will also require cooling to some degree through fans and ductwork; to be consistent, this mass and cost should be factored into the energy density of VRLA.

Low temperature operation of Ni–MH. Ni–MH performance falls off steeply with temperature so that cells must be oversized for the application in order to meet

minimum performance in cold start. The additional size adds mass and cost and should be counted against the specific energy. Alternatively, a second battery such as lead–acid that is better suited to cold weather starts may be used for cold starts rather than increasing the size of the Ni–MH battery. In this case, the added mass of the second battery plus supporting devices such as a second starter motor should be accounted for.

High temperature operation of Ni–MH. The charge-acceptance of Ni–MH falls off quickly with temperature and imposes many restrictions on operation at high temperature. As discussed above, thermal management must be factored into the specific energy estimate for the system.

Engine-stopped cooling of Ni–MH. The need to cool batteries after an aggressive run continues for many minutes after the vehicle has shut down. This is particularly important for Ni–MH, where high temperatures may be detrimental to the life of the cells. One solution requires the cooling fans (but not the compressor) to be run during this time, however, automobile industry experience with fans running after key-off has not been good and many directives exist that prohibit or restrict fan operation after this time. This is a strategy question that may not be easily resolved.

Lead–acid, on the other hand, is reasonably stable at temperatures less than 70°C, and, unless the cells are being charged, occasional high temperature events have little effect on long-term life.

11.3.3.4. Low initial cost of VRLA. On a watt-hour life cost basis, it is estimated that the cost break point comes at a Ni–MH to VRLA cost of eleven to one; if nickel exceeds this amount, the life cost of VRLA is less than that of nickel. While the life cost will be a factor, the initial cost of a component may be a more significant notion in the valuation of a battery. Even with a smaller battery due to the better cycling ability of Ni–MH (some seven times smaller at the required DoD for each), it is estimated that the initial cost of VRLA will be only 20% of the initial cost of Ni–MH.

With these considerations of Ni–MH, the case for VRLA becomes somewhat stronger provided that at least a minimum standard of performance can be achieved. Reliability becomes an issue that must be addressed, as do any controls needed to maintain the battery in good condition.

11.3.4. Parallel–series hybrids

Typical hybrid architecture is shown in Fig. 11.19. Two features distinguish this architecture from the analogous soft hybrid. The first is the necessary inclusion of the contactor within the battery housing, which, as a high-voltage safety matter, must be under direct control of the battery management module (BMM). The second is the need for isolation from the chassis, given the inherent risk of high-voltage shock. The battery container must also be of a tamper-proof design and generally inaccessible to non-service people; because of the large size and aspect ratio of the battery, easy access by operators is rarely a problem, however.

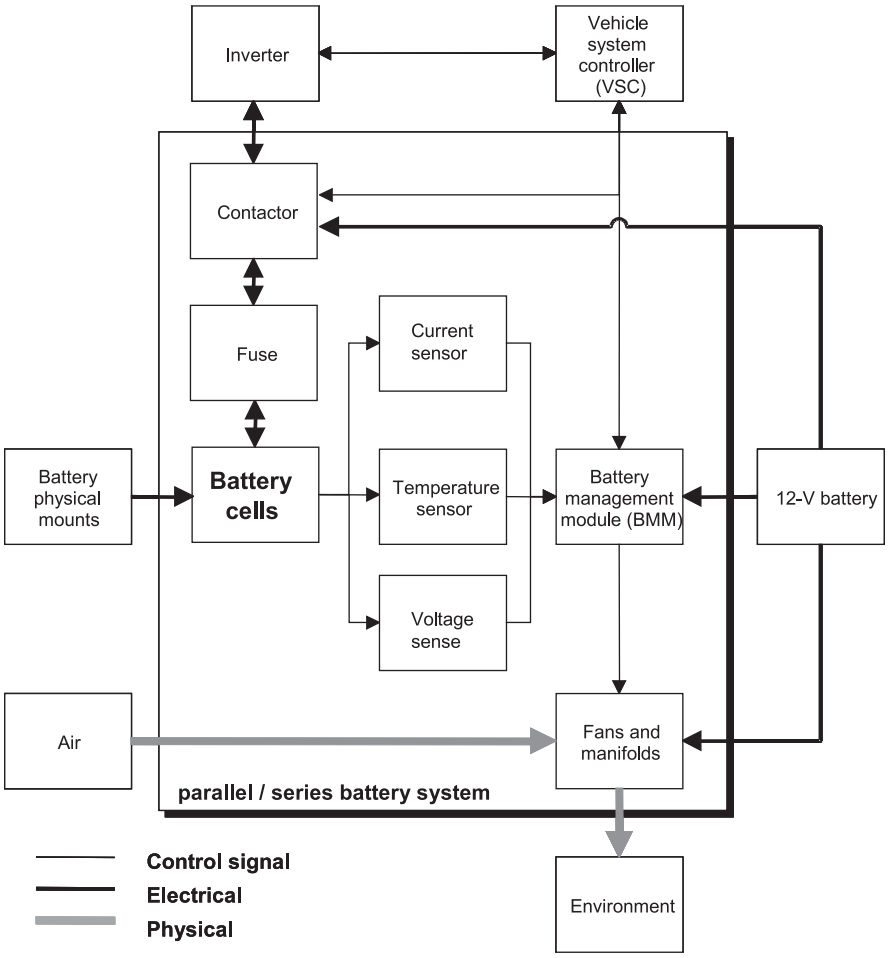

Fig. 11.19. Typical parallel–series hybrid battery architecture. Ground and communications to devices external to battery system not indicated.

From a purely battery perspective, the architecture of the series hybrid vehicle is similar to that of the parallel hybrid vehicle with the exception that power and energy requirements for a series hybrid may be as much as to provide full traction capability. The increased power and energy demands force a higher voltage; for example, 80 kW will optimize at about 300 V. Although the parallel hybrid vehicles and soft hybrid vehicles are similar conceptually (both being augmentation of the primary motive power from an ICE), parallel hybrid vehicles are different from soft hybrids on several clearly distinguishing points. The first is that the higher energy duty cycle of the hybrid architectures drives the need for a larger, higher-voltage battery. Figure 11.13 shows how rapidly the 10-kW efficiency can drop off for some

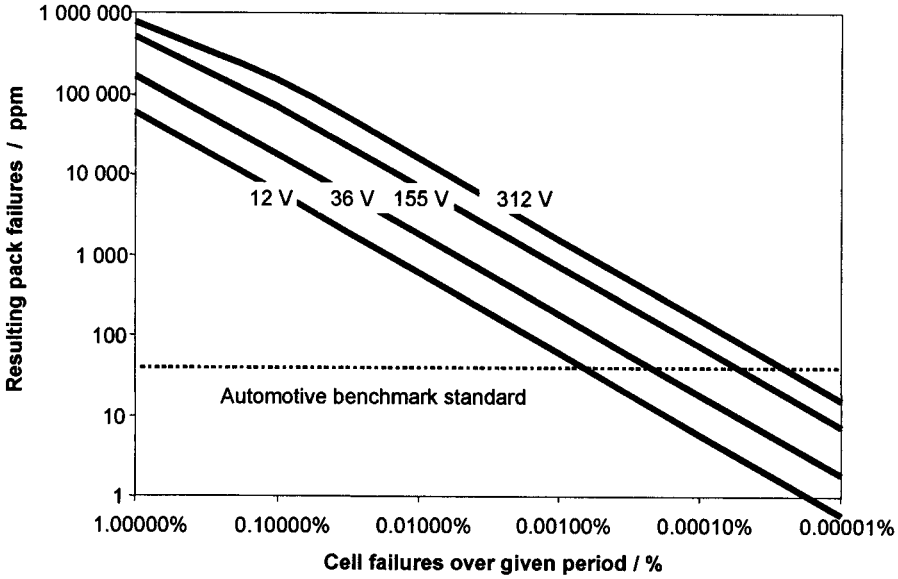

Fig. 11.20. Relation between cell reliability and vehicle failure rate.

lower-power sized systems and the fact that the most effective relief comes with an increase in bus voltage. For the 15–40 kW range, the optimum voltage range is between 125 and 175 V, all system components being considered.

This increase in voltage for either the parallel or series hybrid comes at some cost in terms of reliability of the battery. The increased number of cells in the higher-voltage battery will lead to lower overall quality for two reasons. First, the number of cells will increase in a series fashion. According to the data in Fig. 11.20, increasing the cell count from 18 to 72 for a parallel hybrid will require a four-fold improvement in quality to maintain the same level of pack reliability. Increasing the number of cells to 156 for a series hybrid will require a ten-fold improvement, or better. This is particularly of concern for VRLA since the quality performance for lead–acid is somewhat poor when compared with the currently accepted parts-per-million automotive standards scale. The second reason for reduced battery reliability is that the size of the cells will decrease, forcing either less parallel construction (fewer plates and connections) or thinner plates, which introduce new manufacturing techniques and problems.

The larger battery will tend to impose thermal management problems on the system, which will require more complex monitoring, controls and hardware to maintain. Larger temperature spreads may result in premature degradation or possible thermal runaway situations, and even small but chronic temperature differences will require more frequent equalization.

While the technological problems are recognizable, it is also important to note that, at the battery size that will produce an appropriate amount of energy, service due to lower quality will be readily cost-apparent to the customer and vehicle

Table 11.20. Parallel hybrid performance requirements.

Event	Power	Time	Voltage limits (approximate)	Temperature	Cycles (10 y)
Cold crank	6–10 kW	5 s	> 100 V	−30 to + 60°C	15 k
Start	6–10 kW	0.5 s	> 120 V	0 to + 50°C	250 k
Boost	15–40 kW	20 s	> 120 V	0 to + 50°C	250 k
Idle	2–5 kW	120 s	> 120 V	0 to + 50°C	250 k
Regen braking	10–25 kW	10 s	< 160 V	0 to + 50°C	250 k
ICE charge	10–25 kW	120 s	< 160 V	0 to + 50°C	250 k
31d stand	0.5 W	31d/5 s	> 100 V , at 6 kW	25°C	25

Table 11.21. Series hybrid performance requirements.

Event	Power	Time	Voltage limits (approximate)	Temperature	Cycles (10 y)
Cold Crank	4–10 kW	5 s	> 240 V	−30 to + 60°C	15 k
Start	4–10 kW	0.5 s	> 300 V	0 to + 50°C	250 k
Boost	40–80 kW	30 s	> 300 V	0 to + 50°C	250 k
Idle	3–5 kW	120 s	> 300 V	0 to + 50°C	250 k
Regen braking	10–40 kW	10 s	< 400 V	0 to + 50°C	250 k
ICE charge	10–25 kW	120 s	< 400 V	0 to + 50°C	250 k
31d stand	0.5 W	31d/5 s	> 240 V, at 6 kW	25°C	25

programme by way of costs of parts and labour. For this reason, lack of reliability will have substantial consequences.

11.3.4.1. General requirements. The attributes in Table 11.20 are typical for parallel hybrid applications, and the attributes in Table 11.21 are typical for series hybrid vehicles.

The range of power even within the same class of hybrid is remarkably wide, which will have a great effect on the battery sizing. The weight of the battery, regardless of the technology chosen, will impose many restrictions on the packaging and distribution on-board the vehicle. The size allowance for the battery will also vary greatly, but, as an order of scale, the Ni–MH, parallel hybrid battery is likely to be between 25 and 100 kg. The mass of a VRLA equivalent would be about an order of magnitude greater if a reasonable cycle-life is assumed. The situation with volume is no better and will vary depending on the thermal management. The equivalent series hybrid will be roughly double the size and weight of the parallel hybrid.

With its higher RMS power to mass ratio, the ohmic and entropic heating will be significant in hybrid batteries. As seen with the soft hybrid battery, a reasonable rate

of heat exchange will be needed to maintain the battery within the target temperature range. This implies at least a minimum of fan-forced air, and, in the case of Ni–MH, active cooling involving a local evaporator will be needed for service in nearly all conditions. This, of course, adds mass and cost, but experience has shown that such remedies are necessary more often than not.

The ten-year life requirement is expected to remain at about the same level as for other cars and light trucks, as are the temperature and time schedules.

The parallel hybrid vehicle will be somewhat more dependent on its battery than either a vehicle with only an automotive battery or a soft hybrid vehicle battery. In the latter case, after engine crank is complete, the battery takes on a secondary role where failure or partial function may lead to some customer inconvenience but at an acceptable severity. The soft hybrid boost and start–stop functions are not critical requirements, at least not to the point where they may be disabled should the system detect a sub-performing battery. This could happen with warning, but without the driver experiencing significant inconvenience. As electrification of the vehicle increases through participation in the traction system (as in higher power hybrid systems), a sub-performing battery will lead to unacceptable performance gaps that cannot be made up through alternative strategies. Although sufficient warning may be possible, the driver will almost certainly notice the decline in operation.

11.3.4.2. Controls and diagnostics for parallel–series hybrid vehicles. A typical set of control messages for hybrid vehicles is listed in Table 11.19. Although the variables are the same as those used in soft hybrids, the higher criticality of function implies that the calculated values, such as maximum source and sink currents, must be of even higher reliability if unexpected function fade or failure is to be avoided.

One value that may be of waning importance is battery SoC. SoC is strongly dependent on time and history, such that SoC by itself could be a misleading metric. This effect is worse as the RMS current density increases. For long, predictable discharges such as those seen in EVs, SoC is a reasonable indicator of battery capability, but when periodic, high-rate currents in excess of $50\,\mathrm{mA\,cm^{-2}}$ of electrode area (for lead–acid) are applied, concentration and utilization effects tend to distort the SoC. The hybrid cycle typically has a higher RMS current than most other battery application cycles and, therefore, easily falls into this class of discharge rates. Moreover, the SoC, although needed for internal computations, does not have an unambiguous use outside the battery box that isn't superseded in importance by the source current, sink current, and other diagnostics that are typically measured more reliably.

High-voltage safety considerations require that the architecture of parallel- and series-hybrid vehicles include an integral BMM such that the battery can be controlled from within the pack. This assumes that the battery will be of an advanced design, such as Ni–MH, where safety requires fast, reliable, and self-contained communication with the contactor and charger.

Diagnostics in function-critical components are one remedy in an inherently failure-prone series system. By improving the detectability of failure, the risk priority number (severity × occurrence × detectability) may be reduced to an acceptable

Table 11.22. Additional hybrid battery diagnostics.

Description	Message type	Source	Destination
Battery age	Sending	BMM	VC
Battery Ah throughput	Sending	BMM	VC
Number of low-voltage events	Sending	BMM	VC
Overcharge ratio	Sending	BMM	VC
Calculated impedance	Sending	BMM	VC
Estimated life available	Sending	BMM	VC
Battery condition (arbitrary scale)	Sending	BMM	VC

level. Given the importance of the battery to the hybrid drive, the diagnostics must be considered carefully.

A number of diagnostic conditions should be included in the control message set presented in Table 11.19. For detailed service, the message set in Table 11.19 may be expanded to include the diagnostic set described in Table 11.22. The algorithms for each of these values are expected to be proprietary given the commercial importance of the diagnostic; for example, an early or too conservative service request will increase warranty cost, while a non-sensitive diagnostic could cause customer inconvenience and additional, avoidable cost.

11.3.4.3. VRLA as a parallel–series hybrid battery. The high utilization of the hybrid battery predisposes sourcing to batteries that cycle extraordinarily well. Without question, flooded lead–acid batteries should not be considered, and despite a reasonable cycling ability, even VRLA is less than well suited for hybrid duty unless the VRLA battery is greatly oversized.

The cost dependency on a minimized cell size for Ni–MH and VRLA batteries is shown in Fig. 11.21. In these cases, VRLA is limited by life and Ni–MH is limited by power. At the energy levels required for parallel–series hybrid vehicles, it can be shown that the watt-hour life cost of Ni–MH would have to exceed 33 times that of VRLA, which is not the case even today with prototype batteries. The initial cost consideration that tipped the favour to VRLA for soft hybrids is far less impressive with parallel or series hybrids, since it can be further demonstrated that, even on an initial cost basis, VRLA is about 60% of the cost of the equivalent Ni–MH battery for the parallel–series application, well outside of the bounds where trade-off to initial cost could be considered.

VRLA use may not be appropriate for pure hybrids due to weight. Whereas a lower capacity battery (say, for soft hybrids) could propose an additional 50% weight premium in order to reduce cost without too many repercussions other than habitual objections from the programme management, this does not necessarily hold for a large mass battery where the overage could be many hundreds of kilograms. An example of this would be a 40 kW $\times$ 30 s battery for either a parallel or series hybrid. The Ni–MH battery reasonably sized for this service would weigh approximately

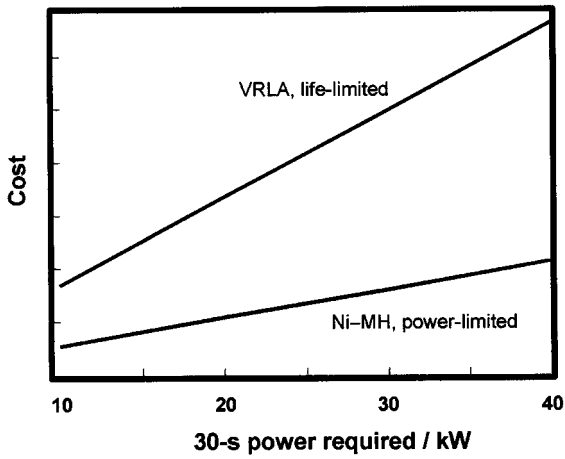

Fig. 11.21. Minimized life cost dependency on power for VRLA and Ni–MH batteries.

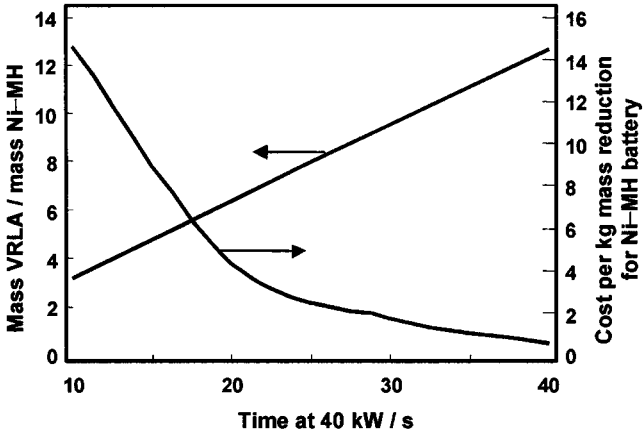

Fig. 11.22. Minimized cost dependency on time at power for hybrid batteries.

100 kg and would last about 10 years. A VRLA battery capable of 50 k cycles (about 2 years) at 40 kW × 30 s cycles would weigh about 1000 kg (very nearly an EV battery). The difference in cost per kilogram would be about US$ 1.70 per kg, which is a very competitive price for vehicle weight. In other words, the incremental cost for a Ni–MH solution would be very acceptable to the vehicle programme, particularly when the weight difference in the heavier battery will force the vehicle into a much higher weight class. It should be noted, however, that the shorter the discharge time the stronger the case for VRLA (see Fig. 11.22). This is a natural consequence of power limitations in the smaller Ni–MH battery and the cycle-life limitations of VRLA. If a 20 s high-power event is acceptable, then the weight ratio of VRLA to Ni–MH batteries drops to 6.3 and the initial basis mass reduction cost increases to US$ 4.40 per kg. Despite this 'improvement', it should be considered that the

weight difference is still in excess of 500 kg and is likely to be unacceptable to any programme on a purely cost basis.

This discussion highlights the importance of cycle-life to the success of a battery technology in hybrid vehicles. It is clear from numerous examples that thin-plate VRLA designs are sufficient for power in hybrid applications, but it is equally clear that, in order for VRLA to be a successful hybrid technology, substantial gains in cycle-life must be achieved. It is encouraging, though, that the numbers above will shift dramatically with even moderate improvements in the cycle-life relation as shown in Fig. 11.4. It is also worth noting that any benefit gained through operating at partial SoC is a legitimate extension of the life correlation, but only if the controls for this operating mode are feasible.

11.3.5. Electric vehicles

Pure electric propulsion systems have been in use throughout the 20th century; prior to 1910, EVs held a considerable fraction of the personal transportation market that did not wane until the advent of the electric start by Kettering. Electric drive vehicles at the turn of the century were considered to be the refined personal transportation of upper class women; women, because the crank start of the ICE at the time required a level of activity not considered appropriate, and upper class due the considerable cost of these early vehicles before the age of assembly lines. An often-unsaid attribute of these vehicles, however, was their reliability and robustness, generally better than the contemporary ICE equivalents.

The problems of electrical energy storage devices which still exist today were in fact responsible for the demise of the EV at the start of the century. By taking 12.3 kWh kg^{-1} as the theoretical energy-storage efficiency of gasoline, a conservative Carnot efficiency of 30%, and factoring some of the weight of the engine block, gasoline still produces at least two orders of magnitude more energy per unit weight than storage in lead–acid technology. With this perspective it should not be too much of a wonder why hydrocarbon storage of energy has eclipsed all but the smallest niches of a transportation industry.

Despite the present-day dominance of ICE vehicles, recent environmental initiatives have revived interest in electric drives. The interest started with California, New York, and other states and regions with urban centres greatly affected by automotive emissions. Despite a recent survey's findings that expressed the view that there will be a sizable market in the next several years for EVs, the recent sales trend for EVs has not supported this without further qualification. It is now clear that a successful EV must match the ICE vehicle, not only in terms of performance (except some concession to range), but also at no additional cost [11]. This is not to say that there have not been some niche successes; drivers and fleet owners of EVs are rediscovering some unexpected benefits of EVs with some sense of exploration; collateral attributes such as lower maintenance, near-silent operation, and high torque starts are all benefits that have surprised many converts to the technology. One example in particular is instant cabin heat in winter, which is a current reality in pure EVs but still a number of years in the future for ICE-based vehicles.

There of course have been some disappointments as well. Vehicle range for some long-range commuters has been problematic and variable with the weather, a natural consequence of battery behaviour. Large volumes that automakers have counted on to reduce costs have not materialized and so the manufacturing cost of the pure EVs has stubbornly held on at high levels that the public has not been willing to bridge.

Perhaps one of the more disappointing aspects of the manufacturing cost is the high cost of the battery, which has not seen much relief. In the last decade, lead–acid (including VRLA), nickel–cadmium, and Ni–MH were used with various degrees of success. Nickel–cadmium suffers from an environmental stigma due to the presence of cadmium, and although it was, on technical grounds, a success in Europe, it has not been considered for major fleets in North America. Ni–MH vehicles also had a very successful test trial but have been plagued by chronic high costs of the technology that has prevented widespread acceptance. Lead–acid costs are still higher than is considered to be acceptable, but interest in the vehicles is still moderately high even after three years of commercial and public sales. In this respect, it is worthwhile to consider successful cases of niche EVs such as plant forklifts, underground vehicles, and delivery trucks. In nearly all cases, quiet success has followed the use of common lead–acid batteries, despite their weight and relatively short lives.

The battery requirements of course follow the needs of the customer. Original electric-vehicle battery designs did not have the benefit of field studies to guide designs, however, and had some element of guesswork built into the assumptions. On the whole, however, most of the EV products hit home on functionality.

Ford's first public EV offering was a Ranger EV, a version of the production Ranger pickup truck. It was offered as two models, one having a 25 kWh, 312-V VRLA battery; and the other a 29 kWh, 312-V Ni–MH battery (see Fig. 11.23). The vehicle made few compromises to baseline ICE performance and included air conditioning, instant heat, ICE acceleration, and regular handling. Charge from 20 to 100% SoC required 8 h from a 6 kW wall charger that operated through a conductive connection. The lead–acid traction battery came with a 2-year full warranty with the third year pro-rated. Two driver-selected, forward-moving PRNDE settings were available. The first drive position ('D') gave full function performance, while the second position ('E') was an economy setting that increased coast-down regen capture and reduced maximum speed to 65 mph (105 kph).

The initial results from field studies after nine months of service were somewhat surprising. Figure 11.24 shows the moderately low range between charges on a Ranger EV, VRLA vehicle. These vehicles were sold or leased to several hundred customers ranging from large fleets to individual drivers for personal use. The average distance for this very mixed population was approximately 32 km/20 miles with a standard deviation of 10 km/6 miles. This fits well with the maximum design range of 80 km/50 miles such that 'three sigma' drivers could be covered, even in cooler weather.

In another study, a small Ranger EV fleet was driven over a fixed real-world course that included a 19 km/12 mile route of urban streets, suburban streets, and highway driving (Michigan), using both economy and drive PRNDE settings. Time, voltage, current, and temperature data were acquired continuously throughout the

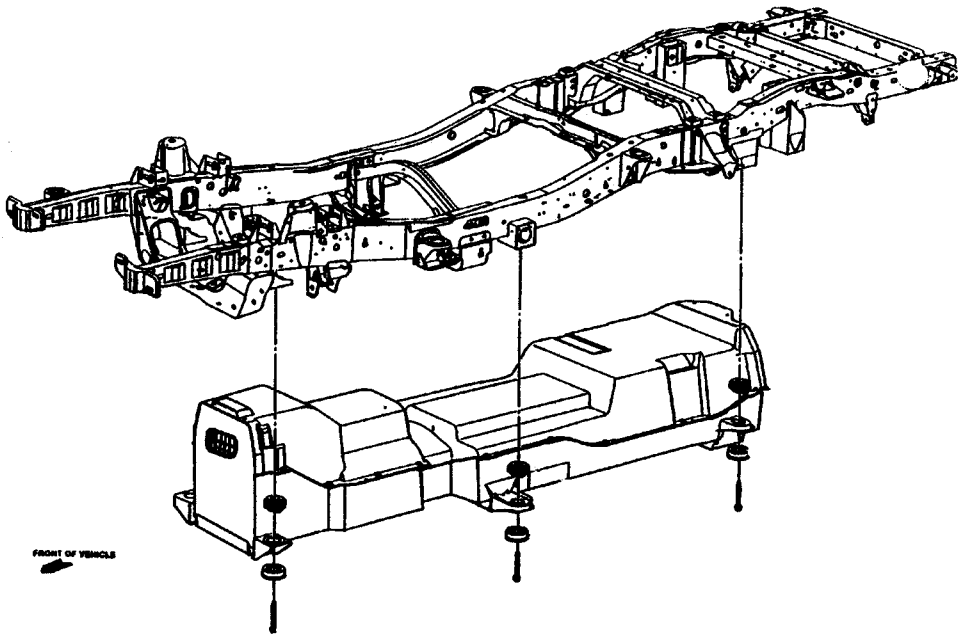

Fig. 11.23. EV battery pack.

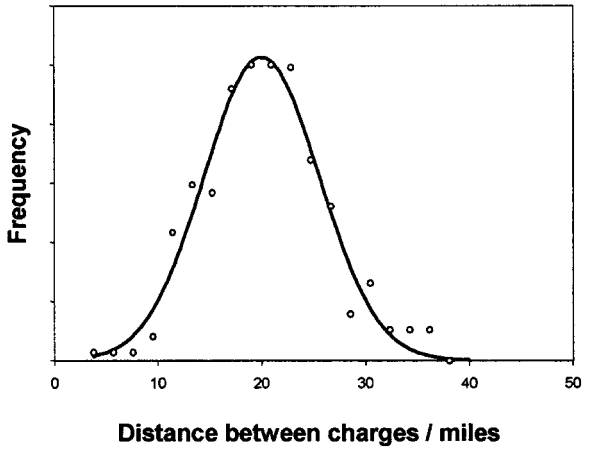

Fig. 11.24. Average drive distance between complete charges for US-based lead–acid UX168 fleet, February 1999 (binned data) [12].

drive sessions. The study was run through a one-year period using random volunteer drivers and instructions to use accessories such as climate control at will. The results, shown in Fig. 11.25, show the inherent scatter in energy consumption (particularly due to driver style), the effect of economy and drive settings on the PRNDE, and the effect of temperature on energy consumption. Of note is the conclusion that,

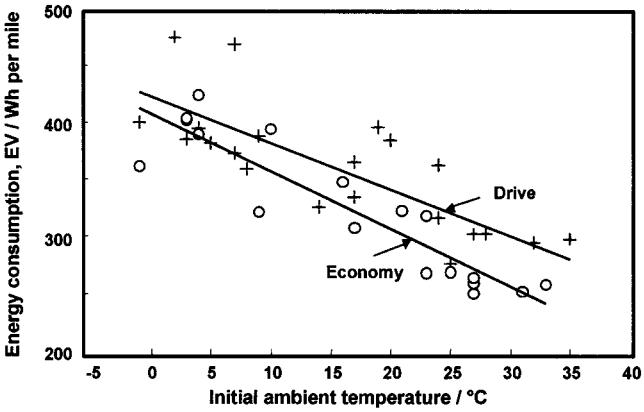

Fig. 11.25. Vehicle overall efficiency variation with temperature (suburban/highway/urban) for 1998 Ranger EV.

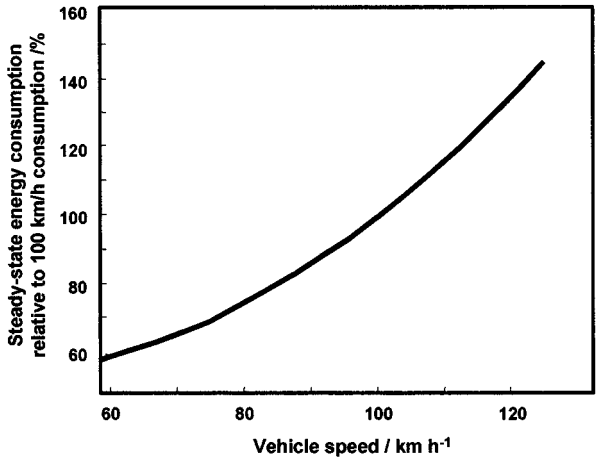

Fig. 11.26. Relative effect of steady state vehicle speed on energy consumption.

depending on any particular set of conditions, the energy consumption of the vehicle may nearly double with a proportionate decrease in range; moreover, this effect is independent of battery effects such as reduced capacity at low temperature.

The top speed of a vehicle duty cycle will also affect the energy consumption, as shown in the chart in Fig. 11.26. This value does not include start–stop inefficiencies or other loads such as climate control. Also note that this consumption rate is independent of battery capacity variation with average discharge current.

It should be recognized that pure EVs exist for a wide range of purposes, from neighbourhood electric runabouts, to full-function electric trucks such as the Ranger EV, and, because of this, the range of energy and voltage may vary greatly. One could roughly approximate small vehicles as consuming between 47 and 94 Wh per km (75 and 150 Wh per mile); mid-size vehicles up to 156 Wh per km (250 Wh per mile), and large vehicles (i.e., small trucks) up to about 250 Wh per km (400 Wh

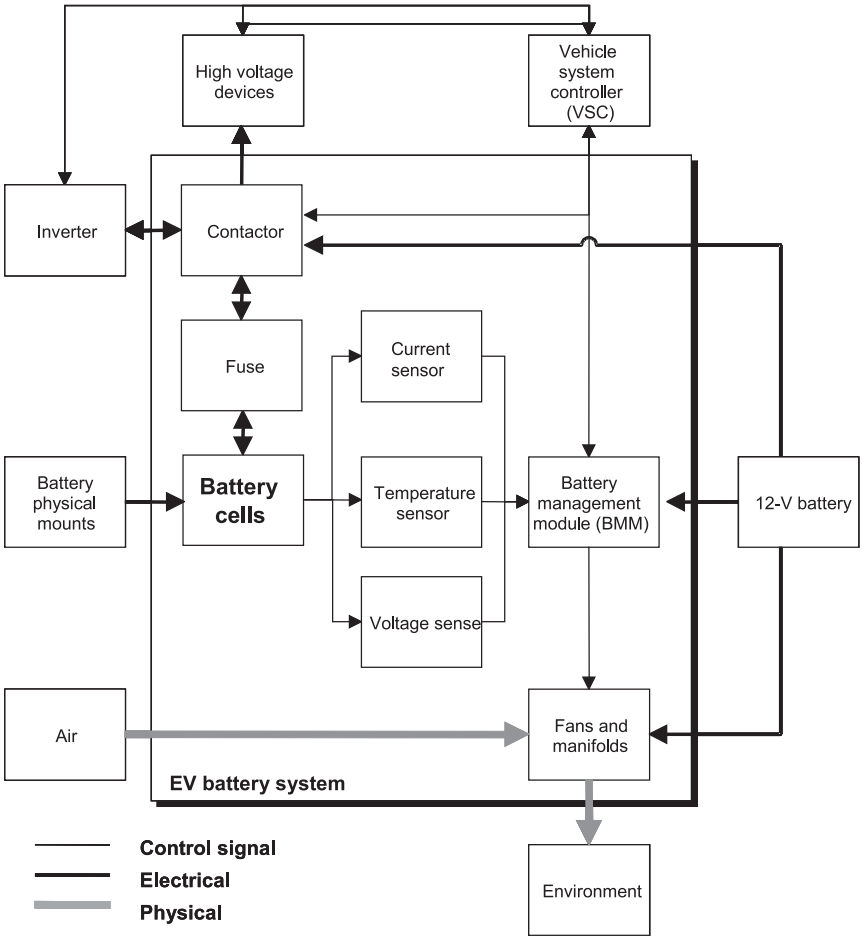

Fig. 11.27. Typical EV battery architecture. Ground and communications to devices external to battery system not indicated.

per mile). The size of the battery can be based on the expected range and a lower DoD, say 20%. For example, a 50-mile EV truck battery would be sized at approximately (50 mile)(400 Wh per mile)/(100 to 20%) = 25 kWh.

11.3.5.1. Performance requirements. Since efficiency in electronics is best maintained at high voltage, EV strings are normally in the 150–450 V range, although there are exceptions to this.

A typical EV architecture is shown in Fig. 11.27. This architecture is very similar to that for the hybrid battery packs, with the exception that there may be high voltage loads, such as climate control or heaters, that will power directly from the high voltage pack. Electric vehicles are also different from all other electric drives

in that it is assumed that the vehicle will be charged periodically from a stationary source, rather than from an ICE.

Access to stationary power also makes possible a battery heating strategy for cold-climate operation. This is important since the current density of the electric drive scenario will not provide the self-heating through ohmic and entropic means that would be seen in a hybrid drive schedule, so much longer operation at high discharge rates is necessary before appreciable temperature rise can occur. In addition, battery capacity is sensitive to temperature, so given the high severity of a low capacity battery in all-electric drive, reasonable efforts must be taken to ensure a reasonable capability in this respect. In usual heater arrangements, the incoming power can thus be directed as a.c. or inverted d.c. current to a series of resistive battery heaters interspersed throughout the pack. Alternatively, heated air may be used to heat the pack. In all heating scenarios, it is necessary to heat the pack slowly and evenly to avoid creating thermal gradients between cells; thermal gradients are not desired since thermal imbalance in excess of 5°C may lead to undercharge some cells and overcharge in others, thereby reducing battery life [13].

Some form of cooling is also necessary in an EV battery, although active cooling using a compressor/evaporator system is rare except for advanced batteries such as Ni–MH and lithium due to cost, complexity, and energy inefficiencies. Cooling through forced air is more common and is usually effective in most climates. Cooling, as heating, must be done isotropically (or at least symmetrically) to avoid creating thermal gradients.

With the addition of heaters and a stationary power supply, the performance of the battery no longer has to be assumed to meet conventional, –30°C drive requirements. Even if heaters are presumed, battery temperature may still see occasional low temperatures if the battery is left off-plug for 24 h or more, so a combination of customer education and pack insulation through design is needed to prevent that occurrence. For the more likely situation of a vehicle on a day-long stand (e.g., during the day after commuting to work in the morning), the battery system must be able to perform reasonably well at a reasonably low temperature (say, 0°C).

Cabin climate control is a substantial energy drain that may account for 25% or more of the energy consumption in an EV. The flexible nature of the electric systems allows a number of temperature control alternatives ranging from positive temperature coefficient heaters to heat pumps for heating and cooling.

High current density during regen and long charges lead to the possibility of hydrogen evolution in aqueous chemistries, although, for the most part, this concern is limited to vented chemistries such as flooded lead–acid. Vent fans in an enclosed pack are a simple way to reduce hydrogen concentration to below 1% by volume (25% of the lower flammability limit). If reasonable care is taken through temperature- and current-compensated voltage limits, vent fan air velocity can be minimal. In a large pack with sufficient air gaps to maintain a reasonable level of thermal management, this should not be a problem since hydrogen is well recognized for its high diffusion and dissipation rates. Alternatively, the gases may be manifolded and expelled outside of the pack area, but the added complexity and the possibility of tube disconnection during routine service (leading to injection of a

nearly pure hydrogen stream into an area of high voltage) are problems that require additional consideration before such a system is deployed to customers.

The SAE (Society of Automotive Engineers) and JEVS (Japan Electric Vehicle Society) has established a standard size for EV battery modules at L388(2) mm × W116(2) × H175(2) ((2) is the error allowed in the dimension), with a top-terminal configuration on the vertical longitudinal plane of symmetry [14]. In VRLA, this size provides a 12-V capacity of about 60 Ah; in Ni–MH, this provides 12-V capacity of about 100 Ah. The aspect ratio of this size allows flexible packaging and retention, and the weight of about 20 kg per module may be handled by a single service technician. The symmetric terminals also add to the versatility of inter-module connection.

Many consortia and publications have proposed a number of standard drives to evaluate battery performance. Schedules such as the Federal Urban Drive Schedule (FUDS), the Highway Fuel Economy Test (HWFET), and the Dynamic Stress Test (DST) are used as yardsticks of performance on a comparative basis. As metrics for fuel economy or other corporate standards, they may be appropriate; but these should not generally be used as the 'real-world' test of battery performance. Where performance is to be measured, it is recommended here that a Kochis Stress Test (KST) be used, which is a test philosophy that states that the maximum loads (charge and discharge) that will be used in the vehicle should be used to establish performance traits. This implies two points: (i) the test should be demonstrated and calibrated in a vehicle that is the intended application; (ii) if vehicle calibrations are changed, the effect on battery performance must be re-evaluated.

The most straightforward version of this test involves a hard acceleration to maximum speed, followed by hard braking at full regen to wheels stop, followed by a wait for 20s. This is repeated continuously until the battery is not capable of providing full power. Although this test may appear at first inspection to be overly aggressive, it is nevertheless appropriate on the basis that at some time, some fraction of the fleet will be exposed to such a cycle and it is wise to test this scenario.

The performance values in Table 11.23 are typical for a high-mass utility EV. No battery capacity values are provided since this will vary with the consumption and vehicle range expectations, which are the domain of the vehicle programme management.

Table 11.23. Performance requirements for a high mass utility EV.

Event	Power	Time	Voltage limits (approximate)	Temperature	Cycles (10y)
Drive	10–90 kW	> 5 s	> 250 V	0 to + 60°C	N/A
Idle	2–5 kW	> 120 s	> 200 V	0 to + 60°C	80 k
Regen. braking	10–60 kW	10 s	< 400 V	0 to + 60°C	80 k
31d stand	isolated	31d/5 s	> 250 V, at 25 kW	25°C	25
Charge	0–6 kW	< 8 h 20–100% SoC	< 400 V	0 to + 60°C	800

11.3.5.2. Controls and diagnostics for EVs. The capability of control of the EV battery is generally excellent. Typically high-speed CAN networks, extensive analogue-to-digital conversion, and an array of accurate current and temperature sensors present the opportunity for precise control of the traction battery. Voltage sense is usually available on the monobloc level, although temperature may not be quite so well surveyed. Since cells are in a series string a single sensor is all that is required for current, although the accuracy of this sensor is often critical for precise calculations.

The battery controls for EVs include direct command of discharge capability, charge requests, and maintenance charge requests. The charge algorithm should include checks for overcharge and undercharge, and should compensate voltage targets for temperature, current, and possibly history. The command set shown in Table 11.24 describes basic outputs of the control software.

Perhaps the most contentious and important value concerning the battery condition in EVs is the SoC calculation. SoC is used to determine maximum source and sink current, battery health estimates, and is one of the direct outputs to the customer information cluster. It should be understood that SoC can be interpreted to mean many things, but most definitions cast it as the ratio between the limiting active material available divided by the total active material available. As described above, the SoC for high-rate batteries (such as hybrids) may have little meaning. At the lower current densities used in EVs, however, it is reasonable to assume that the capacity is fairly stable, so in theory an accurate SoC gauge should be possible. Some of the methods used to calculate SoC (see also Chapter 8) are as follows:

(i) Amp-hour integration

In this method, current is integrated with respect to time and the SoC is calculated based on the ratio between the integrated current and an estimated capacity that may

Table 11.24. Electric vehicle control message set.

Description	Message type	Source	Destination
Battery voltage	Sending	BMM	VC
Battery maximum voltage	Sending	BMM	VC
Battery minimum voltage	Sending	BMM	VC
Battery charge current request	Sending	BMM	VC
Battery source current available	Sending	BMM	VC
Battery sink current available	Sending	BMM	VC
Battery equalization current request	Sending	BMM	VC
Battery SoC	Sending	BMM	VC
Battery temperature	Sending	BMM	VC
Battery request for service	Sending	BMM	VC
Battery condition (arbitrary scale)	Sending	BMM	VC
Ambient temperature	Receiving	VC	BMM
Vehicle state	Receiving	VC	BMM
Charger state	Receiving	VC	BMM

change with average current and temperature. The weakness of this technique lies in the sensitivity to error in current sensing and uncertainty in the estimated capacity, particularly in weak or failing cells, or if temperature is not representative of the battery internals. This technique also does not normally account for charge inefficiencies and so offsets develop quickly during cycling.

(ii) Look-up ('polarization') tables
Large, four-dimensional lookup tables map current, voltage, and temperature to SoC. This is one of the more robust and fastest solutions computationally, and it is accurate in that it responds to a weak cell by lowering that cell's SoC preferentially. The deficiency of this technique is the amount of calibration data required, the effects on accuracy with changes to the polarization table during normal aging, and the need to generate a new map for each battery type. This technique also does not work well during the latter phases of the charge process.

(iii) Neural network or fuzzy logic models
Computational intelligence is used to generate an algorithm that uses a matrix of weights with a series of inputs to derive an estimate of SoC. This method requires a minimum number of discrete data points, but it is possible through this technique to factor in the effects of age.

(iv) Active query method
Active query methods measure cell impedance, which is then correlated to SoC. The technique often superimposes an active signal (a low amplitude, characteristic high-frequency square or sinusoidal current pulse) onto the battery and then uses a transfer function on the response waveform to determine the ohmic polarization or a direct correlation to SoC. One permutation of this technique uses the voltage response to indigenous current spikes to map impedance in a similar way. This method provides reasonable results, but if hardware is involved it is often complex and expensive; even sensors will require a relatively high-speed data acquisition bus to minimize the slew between voltage and current.

Numerous battery charge management systems have been developed in recent years. These generally operate on the premise that the root of many of the problems in running a battery series string lies in the inability to charge individual cells to compensate for manufacturing and environmental variation. Over time, without equalization, these small differences will accumulate until the dissimilarity is sufficient to affect charge efficiency. Battery management systems impose selective currents (either charge, discharge, or both) at the cell or monobloc level in an attempt to balance the cells in the string. This can occur continuously, during charge, during discharge, or whenever the vehicle is in the key-on state. The initial results from most of these devices have been good to excellent, however, it has yet to be established that the benefits justify the added expense, complexity, and reduced system reliability (more components).

With the battery likely being the highest cost component of the EV, strategies to increase the life of the battery, improve the performance, or to effect minor repairs

are imperative. Equally, when the battery is truly incapable of meeting specification, it is important to be able to identify that pack for immediate replacement (better yet, with some reasonable warning that will provide some service response time before the pack is unsuitable for use). The need for accurate diagnostics is therefore linked to the ability to optimize battery life, and in so doing, to reduce life- and warranty-cost. The size and cost of the traction battery necessitates some level of service at the monobloc level.

It is evident that the high voltage attribute forces the need for special tools and training for service personnel, however, even trained service personnel will require guidance regarding monobloc replacement or the decision to replace the entire pack. As a matter of general practice it has been found that a small fraction (between 10 and 20%) of the pack monoblocs may be replaced before battery modules start to fail at such a rate that the replacement schedule is too great of a customer- and cost-burden. Once the pack has reached that point, it is often best to replace the pack.

The service technician requires unambiguous and fast guidance regarding what service action to undertake. The diagnosis must therefore be immediately available for download with one of the common service tools, since it is entirely outside the scope of service technicians to run more than very fast and rudimentary tests of the individual battery modules. This implies that the battery management module must have taken key information, processed the data, and stored the results well before the service call. Errors in this analysis could easily run to thousands of dollars even without pack replacement, so it is clear that the diagnostics algorithms and code must be both robust and reliable.

11.3.5.3. VRLA as an EV battery. The traction battery in EVs has long been identified as the key to commercial success of this product line; motors, transmissions, and silicon components can all attain reasonable economies of scale and technology, but the component which is the most resistant to cost-reduction is the battery. This is a critical point since batteries comprise approximately 20% of the total cost of lead–acid-powered vehicles and about 55% of the cost of Ni–MH vehicles (see Fig. 11.28) [2]. Therefore, batteries provide the best opportunity to reduce the overall cost of EVs. With the battery cost of advanced technologies such as Ni–MH greater than the vehicle cost, there is a clear need for a low-priced battery such as lead–acid can offer.

The cost of the VRLA battery must be measured over its life, and, to that extent, it is presently one of the more expensive transportation alternatives. In a North American scenario, by considering the cost-per-mile as compared with an ICE or a Ni–MH equivalent, electricity at US$ 0.05/kWh, fuel at US$ 1.50 per US gallon, and costs of new modules or ICE engines, it can be found that the life cost for lead–acid on a mileage basis is very high (Fig. 11.29) [2]. Most of the disadvantage relates to the cycle-life of lead–acid batteries. If a VRLA battery manages a 25,000 mile range before pack replacement, the total energy costs are US$ 0.19 per mile, excluding service. If this range increases to 35,000 miles, it will be roughly equivalent in operating cost to a Ni–MH battery at US$ 0.15 per mile. In order to match the operating cost of an ICE, however, it would take a range of 47,000 miles (75,000 km)

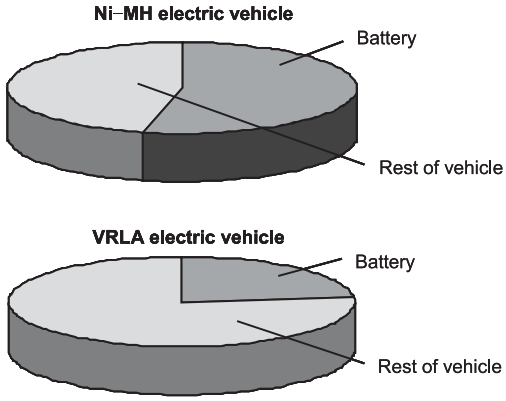

Fig. 11.28. Relative costs of traction batteries for VRLA and Ni–MH EVs.

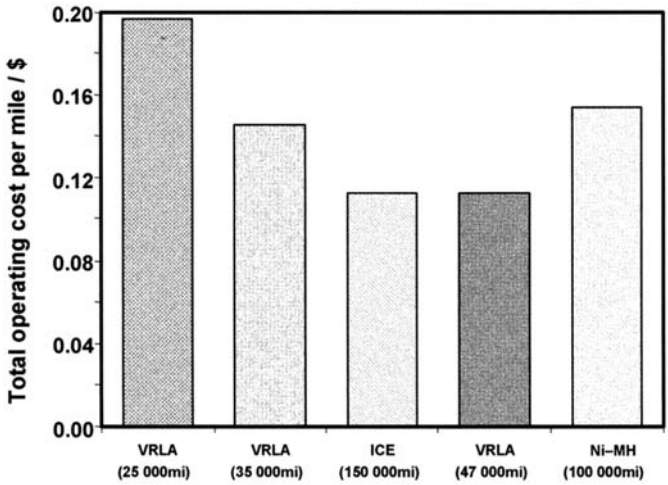

Fig. 11.29. Cost of operation of EVs.

before pack replacement to meet US$ 0.11 per mile. This is equivalent to 1500 deep-discharge cycles.

In other respects, though, VRLA shows perhaps the most promise. The robustness of the battery suits it for most climates, and, although weight is high, the Ranger EV has shown that performance and handling can match that of a comparable ICE. The no-maintenance aspect is an understated, but important, factor.

The downside of VRLA is the relatively low range and chronically high cost; although a VRLA vehicle with a range of 80–130 km (50–80 miles) is possible today, pressure to increase this range is expected. This can either be done by increasing the weight of the battery or by discovering new ways to improve the

utilization or cycling capability. Costs are tied to manufacturing processes, and as economies and improvements are made to the manufacturing line it is anticipated that some progress can be made on reducing customer cost.

11.4. Conclusions

As this chapter has described, the need for energy storage in automobiles will increase substantially over the years to come. The baseline technology, the 12-V flooded lead–acid battery, is not up to the task for several reasons, the most predominant being that the low voltage does not permit sufficiently efficient energy transfer. This will provide an opportunity for other technologies, including VRLA.

With the current state of VRLA battery technology, 42-V automotive and 42-V soft hybrid applications are likely successes, and even EVs will be based on lead–acid technology for some years to come. The weakness of VRLA arises in high-energy hybrid cycles that demand both high rates and many cycles; for this application, Ni–MH has a clear advantage. While VRLA carries with it many of the benefits of flooded lead–acid such as low cost, robustness, and safety, the attributes of low energy density and low cycle-life also follow. Of the two detractors, it has been seen that life is perhaps the more relevant, and that the cycle-life capability of VRLA is still a limiting factor in the widespread suitability of this technology. Positive results from work on VRLA life enhancement will no doubt directly improve the ability of VRLA to play a major role in the hybrid market as well.

References

1. C. Kettering, US Patents 1,150,523 and 1,171,055.
2. J. Wallace, *ALABC Fifth Members & Contractors Conference*, Nice, France, March 2000, Advanced Lead-Acid Battery Consortium, Research Triangle Park, NC, USA.
3. J. Miller and R. Brost, *Advanced Automotive Battery Conference*, Las Vegas, NV, USA, February 2001.
4. D. Linden, *Handbook of Batteries*, 2nd Edition 1995, McGraw-Hill, New York, p. 24.83.
5. G. Cameron, *The Battery Man*, **42 (12)** (2000) 14.
6. G. Cameron, *Sixth IEEE Workshop on Power Electronics in Transportation*, Novi, MI, USA, December 2000.
7. After J.R. Pierson, *The Battery Man*, **41 (2)** (1999) 20.
8. http://auto.mit.edu/consortium/.
9. After R. Knorr *The Battery Man*, **43 (5)** (2001) 64.
10. R.F. Nelson, *J. Power Sources*, **91** (2000) 2–26.
11. P.T. Moseley, *J. Power Sources*, **84** (1999) 237–242.
12. R. Brost, *15th Annual Battery Conference on Applications and Advances*, Long Beach, NY, USA, January 2000, pp. 243–248.
13. R. Brost, *13th Annual Battery Conference on Applications and Advances*, Long Beach, NY, USA, January 1998, pp. 25–29.
14. *J1797*, *Recommended Practice for Packaging of Electric Vehicle Battery Modules*, Society of Automotive Engineers, 1997.

Valve-Regulated Lead–Acid Batteries
D.A.J. Rand et al., editors

—CHAPTER 12—

VALVE-REGULATED LEAD–ACID BATTERIES IN AUTOMOTIVE APPLICATIONS — A BATTERY MANUFACTURER'S PERSPECTIVE

G. Richter and E. Meissner

12.1. Introduction

In common parlance, the term 'automotive battery' is usually taken to mean a battery on-board a road vehicle. The automotive battery in a vehicle for which the motive power is provided by a combustion engine is generally referred to as an SLI battery, from the basic electrical functions of starting (S), lighting (L), and ignition (I). All of the one billion or more motor vehicles in existence worldwide employ at least one such SLI battery. This battery provides the electric power for cranking the internal-combustion engine (ICE), buffers electrical energy within the main vehicle electrical power system during operation, provides electrical energy when the ICE is off — especially for lighting, and is recharged from an alternator driven by the ICE.

Today, the automotive battery preferred for the SLI function in cars is a flooded, 12-V design and comprises six lead–acid cells in a monobloc container. This battery is compatible with the vehicle electrical system that operates in the voltage range from about 12 to 14 V. Until around 1970, 6-V systems were also in use. In European trucks and buses on the other hand, it is common practice for two, 12-V batteries to be connected in series to achieve a nominal voltage of 24 V.

The dimensions of casings and types of connections for SLI batteries are standardized by EN (European Norm), JIS (Japanese Industrial Standards Committee), and the SAE (Society of Automotive Engineers) specifications. The electrical systems of all types of vehicle are generally designed around the energy content, the performance characteristics, and the terminal voltage of the batteries. Vehicle alternators provide about 14.3 V for charging 12-V, SLI batteries. Standardization results in universal compatibility; replacement batteries can be obtained anywhere in the world. Examples of battery designs that conform to EN standards for passenger cars and trucks are shown in Fig. 12.1 (a) and (b), respectively.

The function of the battery in a vehicle powered by an ICE is clear. In other types of vehicles, however, the function of the battery can be quite different. In the early days of motorized road transport, many vehicles were powered by electrical systems. The energy for the electric drive was provided from a storage battery, which, after

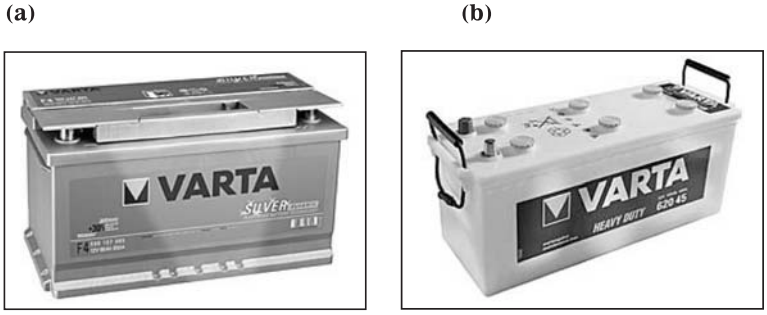

Fig. 12.1. State-of-the-art (a) 12-V automotive battery, (b) 12-V automotive truck battery according to European standard (EN); note, two batteries are connected in series in trucks.

discharge, was either recharged at a recharge station, when the vehicle was not in use, or was exchanged for a recharged battery. In other words, the electrical energy for vehicle propulsion was not generated on-board the vehicle but came from an immobile recharge station.

Today, a storage battery that is mainly used for propulsion of a vehicle and is recharged from an external energy source is referred to as a 'traction battery'. Typical applications are forklift trucks, automatically guided vehicles (AGVs) in modern production and logistics, and on-road electric vehicles (EVs).

Until recently, the distinction between 'traction' and 'automotive' batteries was sharp, because the classical SLI battery did not contribute to vehicle propulsion and the classical traction battery did not provide energy for cranking an ICE. The typical duty of a traction battery is characterized by deep cycles, starting from a full state-of-charge (SoC) to provide maximum driving range. By contrast, the operating mode of automotive batteries is characterized by a 'floating' operation in a medium-to-high SoC with shallow cycling, and full recharge and full discharge are seldom, if ever, required.

The situation is changing, however, now that hybrid electric vehicles (HEVs) have appeared on the scene. Early designs of HEVs were characterized by an independent installation of an electrical drive-train, in addition to the conventional ICE drive-train. This provided a dual-mode operation, namely, electric and emission-free power for driving in the city, and ICE power for long-distance journeys [1]. Battery recharge could be performed on-board and also at a recharge station (dual-mode, 'parallel hybrid'). With 'series hybrids', the vehicle is electrically propelled, the energy is provided by a generator driven by the ICE, and the battery is a buffering device between the electric motor and the generator (see Fig. 11.5, Chapter 5). A recharge station is not needed, and there is (theoretically) infinite electrical range if the ICE is operated when required. Different drive-train concepts of parallel and series hybrid vehicles are described in Ref. [2].

By means of clever combinations of mechanical drive-trains with appropriate gearing and clutches, a single electrical engine may operate for propulsion/acceleration assist of the ICE, for recuperation of braking energy, and for battery recharge. This would save both weight and cost. The battery may supply electrical

energy to the electric drive motor when needed to assist the ICE, e.g., for acceleration (ICE and electric drive in parallel), or to allow pure-electric driving downtown with the ICE switched off. Since a driving motor may also act as a generator, the mechanical energy of the moving vehicle can be recovered as electrical energy upon braking and stored in the battery to be used for the next acceleration [3,4].

The above considerations indicate that the distinction between traction batteries and automotive batteries will be less clear-cut in the future. The tasks, duties, and operating conditions of batteries in road vehicles will be diverse. Therefore, it may be useful to redefine what is meant by the term 'automotive battery'. In this chapter, this term is used for batteries in road vehicles that are: (i) not regularly recharged from an external electrical source but, rather, only from an on-board source, such as an ICE–alternator combination or a fuel cell, and are (ii) not designed for extended, full-electric vehicle propulsion (see, Fig. 12.2).

In the electrical power systems of present-day vehicles, the battery is absolutely passive. It is discharged whenever the current demand exceeds the current provided by the alternator, and it recharges when there is an excess of current from the alternator. The actual recharge voltage at the battery terminals depends on the alternator voltage and on the ohmic losses in the connections that arise from the current flowing to or from the battery or to other components. There is no control of the recharge current, however, and the SoC is a scarcely predictable function of electrical loads, driving conditions, alternator and regulator properties, and battery properties such as size, design, and temperature.

In advanced 'smart hybrid' designs, the drive modes (ICE only, electric only, both ICE and electric, battery recharge, braking by mechanical brakes or by

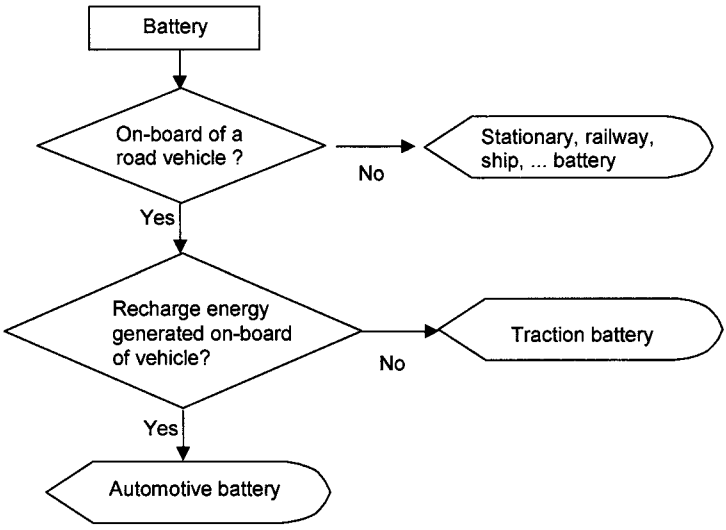

Fig. 12.2. Checklist for definition of the term 'automotive battery'.

recuperation, etc.) are not chosen by the driver but by an intelligent drive control system, which takes account of energy consumption, emissions, and battery status. This system keeps the battery SoC in an optimum operating window. The 'smart hybrid' vehicle with a relatively small electric motor and battery, which are usually used for vehicle propulsion only in combination with the ICE to accelerate cranking and to improve vehicle acceleration ('launch assist', 'boosting'), is sometimes called a 'mini hybrid', 'soft hybrid', or 'mild hybrid' [3–5].

In the future, the voltage of the vehicle electrical system is expected to increase in order to reduce ohmic losses in the electrical network and to allow for a higher efficiency of components. The introduction of a 42-V level is under discussion [6–11] as a compromise between an inadequate power supply on the one hand and a high voltage hazard on the other. Electrical machines of various designs may be used and may comprise both the alternator and the cranking function [12]. These include advanced, belt-driven designs of the established claw pole alternator type, flywheel designs with an additional clutch, and alternators mounted directly on the crankshaft. These latter, so-called 'crankshaft (starter)–alternators' or 'integrated starter–alternators', can be structured either as synchronous or as asynchronous machines, see several contributions in Refs. [9,11,13–14].

For ambitious soft hybrid and, especially, for HEV applications, a voltage significantly higher than 42-V will be needed [5,15,16]. The first series-production vehicle of this type is the Toyota *Prius*, of which production has exceeded 100,000 units since it was launched in 1997 [17,18].

In the future, the role of the ICE may be taken by a fuel cell that directly provides electrical energy for driving. This will not, however, remove the need for a battery, as a fuel cell is normally not able to operate as an electrolyzer. An electrical-storage device will still be required for recovery of braking energy as well as for peak power shaping and for supplying auxiliaries ('consumers') at stand still.

Today, flooded lead–acid batteries are used in SLI duty. Although installation of valve-regulated lead–acid (VRLA) batteries in series-production vehicles began as early as the late 1980s [19–22], penetration of the SLI market by VRLA batteries has, so far, been quite limited. VRLA batteries are primarily used only in motorcycles, some military applications and, recently, in niche-markets such as luxury cars, taxis, and agricultural vehicles.

VRLA batteries are either of the absorptive glass-mat (AGM) type, with a separator made from a highly porous glass-fibre mat filling the whole space between the electrodes and immobilizing the electrolyte, or of the gel type, with a more-or-less standard separator but having the electrolyte immobilized in a silica gel matrix. The resistance of gel batteries is usually significantly higher than the resistance of those with free electrolyte. Therefore, in automotive applications, which usually demand a high-power capability at a high voltage level and at low temperatures, AGM-type VRLA batteries are preferred. Gel-type automotive batteries are used only in niche applications, where the special properties of the gel concept are beneficial and neither high-power performance nor high voltage during cranking are essential. For descriptions of VRLA technologies see Chapter 1 and Refs. [23,24].

12.2. History of Automotive Batteries and Vehicle Electrical Systems

12.2.1. The beginning

At the beginning of the development of road vehicles powered by ICEs, there was no electrical function at all on-board the vehicle apart from fuel ignition. This latter was achieved by magneto ignition or, more reliably, by primary dry cells. Lighting of luxury cars electrically, by storage batteries, was soon added. It was not until 1912, however, that the first electrical starter motor was used in a series-production car. It was this replacement of the manual cranking lever by a battery-driven electrical starter motor that helped the combustion engine make the final breakthrough as the source of power for road vehicles. The electrical starter motor was incorporated into series-production automobiles worldwide almost immediately. The SLI concept penetrated the entire gasoline-powered vehicle industry within two or three years even though the first SLI battery, specially designed to provide both 24 V for cranking and 6 V for lighting and ignition, weighed as much as 30 kg [25].

The starter motor was a high-speed d.c. motor with a speed reduction ratio of about 50 : 1 to the crankshaft of the combustion engine, and this is the method still used today. Given that the start routine is very short, both the battery and starter motor have, over the years, undergone a complete optimization to obtain the best possible torque for the lowest possible manufacturing costs. As a result, no other system has yet gained a foothold in series-manufactured vehicles.

12.2.2. Development of vehicle electrical power systems and automotive batteries in 20th century

Further development of the vehicle electrical system was favoured by the fact that increasingly powerful alternators became available at ever-decreasing manufacturing costs. Also, the vehicle battery, which was repeatedly called upon to provide cold starting power, was required to deliver a minimum energy content at all times. This needed to be sufficient to cover electrical requirements even during periods when the power supply to auxiliaries was reduced because the alternator revolution rate was too low or the engine was at rest. These d.c. alternators (generators) suffered from low, or even zero, power output at low revolution rate, so the battery had to provide the electric power when the ICE was on idle. The limitations of d.c. alternators was not an issue, as for decades electrical ignition, lighting, and windscreen-wipers were the only consumers of electricity, and features like radio and electrically driven fans were limited to upper-class vehicles.

The automotive industry encountered a major electrical-energy bottleneck in the 1960s. This was caused by the rapid rise in the number of electrical auxiliaries that were installed in private vehicles. The industry responded by doubling the battery voltage to 12 V and introducing an adapted, 14-V, three-phase alternator as a replacement for the d.c. generator. The first high-power auxiliary, and the main driver for these changes, was the electrical window defroster.

The 12-V configuration has remained unchanged to the present day. For cars, 12-V, flat-plate, starter batteries with liquid electrolyte are produced throughout the world. The batteries are available with nominal capacities from approximately 25–110 Ah (20-h rate), and with cold-cranking (−18°C) currents from approximately 100–800 A (for 10 s, to a voltage of 7.5 V) according to the European (EN) Standard. The constant cold-cranking current test and the 20-h rate load, which represent vehicle lighting overnight, are idealized loads that should cover both ends of the typical battery load profile range. The ratio of cold-cranking amperes to nominal capacity is usually in the range of about 6–8. The voltage and current measured during the cranking of a high-end engine at ambient temperature are shown in Fig. 12.3. The engine is running within about 100 ms. Even at low temperature, a modern engine is running within a few seconds — or will not crank at all (Fig. 12.4).

Under low-temperature conditions, the battery will rarely achieve a full SoC. In fact, the specifications laid down in the various standards do not represent the duty the SLI battery has to serve in a modern automobile. For advanced vehicle electrical systems, which may be a motivation for new battery technologies like the VRLA, it is essential to know the expected operating condition in order to evaluate alternative energy-storage technologies.

In the USA, following the policy of the SAE, it is not the 20-h rate capacity but, rather, the reserve capacity (RC) that is used to characterize battery size. The RC is the capacity that can be discharged at a current of 25 A, i.e., it is not a specific characteristic.

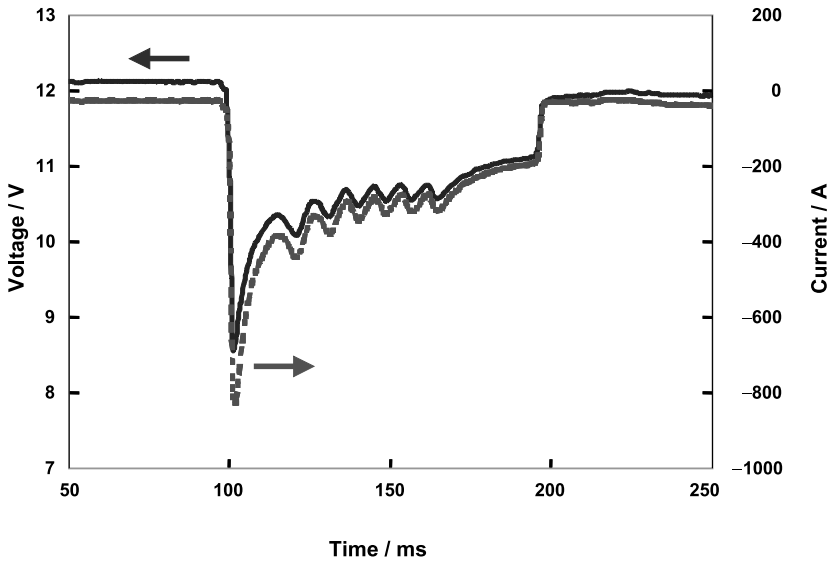

Fig. 12.3. Voltage and current measured during cranking of a high-end engine at ambient temperature.

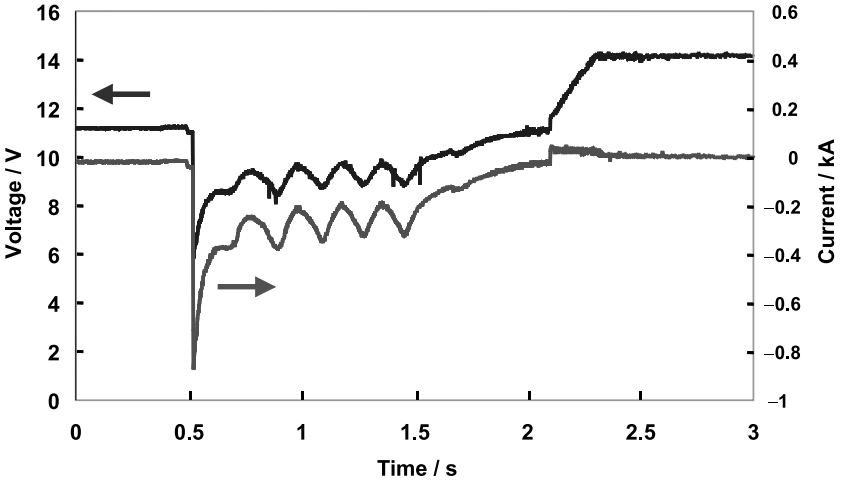

Fig. 12.4. Voltage and current measured during cranking of a 1.8-l diesel engine at −18°C.

A similar policy applies for motorcycles and for trucks, with smaller and higher battery capacity, respectively. Specific cold-cranking capability is less an issue for both these types of vehicle. Motorcycles are seldom used under conditions of extreme cold, and truck batteries are, in many cases, so high in capacity that even the low-temperature performance is sufficient for engine cranking.

Many changes within starter-battery technology have passed almost unnoticed by the public. In previous decades, topping up with water was a regular duty, as was checking engine oil level and tire pressure. Successive reductions of the antimony content in grid alloys has allowed reduced self-discharge rates and increasingly long service intervals between topping up with water. Hybrid batteries, with antimony-free negative grid alloys and low-antimony positive grid alloys, were an intermediate step. This type of battery, sometimes called 'low maintenance', was manufactured in the 1980s and 1990s. Today, an antimony-free positive grid alloy, which in most cases is a lead–calcium–tin or lead–calcium–tin–silver alloy [26], is mandated by many automotive manufacturers.

In order to minimize the parasitic reaction of water electrolysis, it is not sufficient to exclude antimony from the grid alloys; it is also necessary to use raw lead of higher purity than that previously employed for the active materials. As an increasingly high proportion of the global production of lead is being supplied for battery manufacture and the recycling rate of battery scrap is very high, more and more of the lead used in battery manufacturing is recycled material (see Chapter 15). Therefore, the avoidance of an accumulation of impurities, which can lead to greater evolution of hydrogen, is of increasing importance.

Completely antimony-free batteries represent the state-of-the-art in the original equipment (OEM) starter-battery business at the beginning of the 21st century. Accordingly, there is no longer any need for topping-up with water over the life of

the battery. SLI batteries are completely maintenance-free, and self-discharge is as low as 3% per month at ambient temperature, even at a high SoC. The result of minimal water decomposition and advanced lid design is that the evolution of gasses and acid spillage are no longer critical issues. Starter batteries with improved double lids may be tilted or even inverted for short periods without any acid leaking. The design of the double lid enables the electrolyte to return to the cell when the battery is turned back to its nominal position (Fig. 12.5).

For many decades, the discontinuous gravity casting of single electrode grids or pairs of electrode grids (double grids) was the dominant processing technology. Today, continuous processing is increasingly used in order to improve productivity and quality. Expanded-metal technology is dominant, but continuous casting and grid punching are also used (Fig. 12.6).

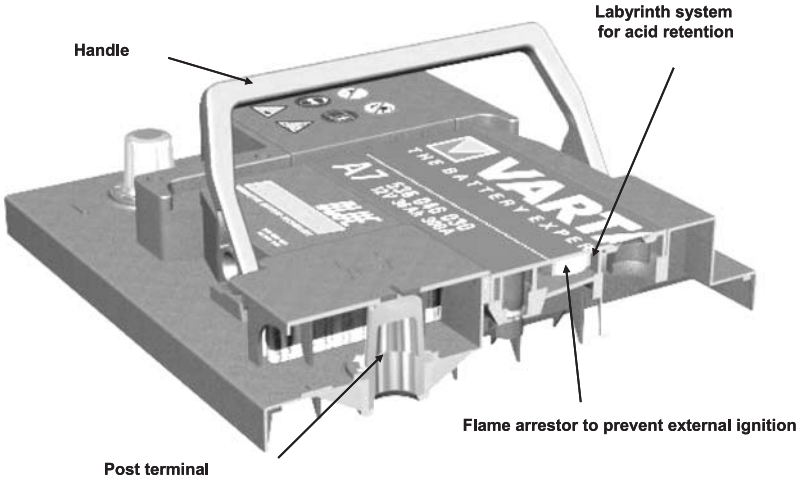

Fig. 12.5. Cross-sectional view of battery cover with labryrinth double lid and flame arrestor.

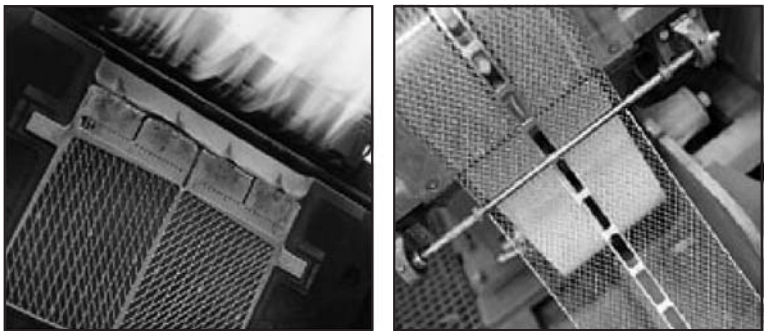

Fig. 12.6. (a) Gravity casting of lead–antimony grids (left) and lead–calcium expanded metal production (right).

Apart from grid manufacturing, the design of the grids has been a field of extensive improvement. To achieve higher voltage levels and uniform current distribution at high discharge rates, the arrangement, orientation, and size of grid wires, as well as the size and position of the grid lug, have to be optimized [27].

The potential distribution of a state-of-the-art plate with a near-centre lug is shown in Fig. 12.7. This position of the lug became possible when manufacturing was changed from tank formation of individual electrodes, which did not allow for that lug position for handling reasons, to container formation with the whole battery being formed after complete assembly.

Although hard-rubber containers had been used for many decades (Fig. 12.8), polypropylene (PP) containers and lids, manufactured by injection moulding, became standard from about the 1960s (Figs. 12.1, 12.5). Therefore, at the beginning of the 21st century, the standard SLI battery in a new car still uses the same

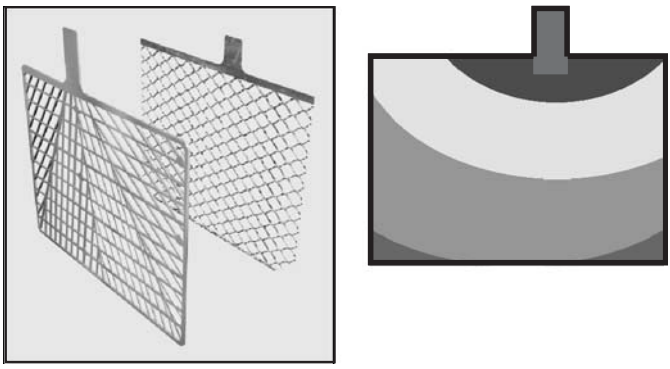

Fig. 12.7. (a) Gravity-cast grid with diagonal wires and centre lug for improved high-power performance (left); expanded-metal grid (right); (b) Potential distribution of a state-of-the-art plate with centre lug.

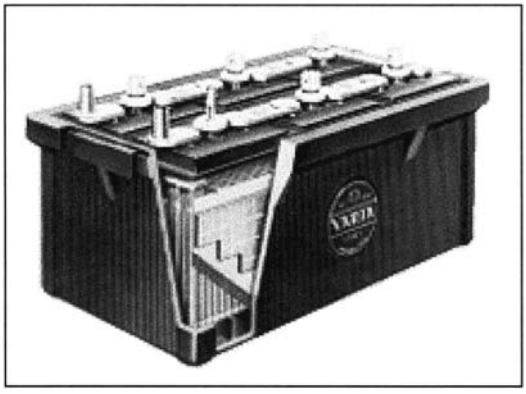

Fig. 12.8. Hard-rubber container with 'up and over' intercell connector.

electrochemical principles it would have used in 1912, and changes of the outer appearance during the last 50 years have been limited.

By contrast, a state-of-the-art SLI battery comprises improved materials for grids, containers, separators, etc., is produced by completely different processing technologies, needs no topping-up of water, is maintenance-free, shows lower self-discharge, provides longer service, is significantly lighter with the same electrical performance, provides higher cold-cranking power and capacity when compared on a weight basis, and is significantly lower in price (adjusted for inflation). From a vehicle perspective, there have already been significant changes with respect to duties and demands on the battery. Despite significant improvements in the power supply via improved characteristics and higher efficiency of the alternator, even at low and idle ICE speeds, the rapidly increasing demand for more and more electrical power on-board re-emerged as an issue in the 1990s.

Initially, difficulties were encountered with high-end vehicles that featured a multitude of electrical auxiliaries, particularly if only short daily distances were travelled in low ambient temperatures, e.g., in stop–start traffic. In such situations, discharged batteries were increasingly found to be the cause of inoperative vehicles. This was due to the decrease in idle speed, which was achieved via improvements in motor control electronics and yields fewer emissions and noise. Modern alternators are able to provide energy, even at such low rates of revolution, sufficient for standard demands but not for all the comfort components simultaneously.

Increasing problems are encountered with battery service-life, particularly if the electrolyte temperature is too high as a result of the location of the battery in the vehicle or because of climatic influences [28]. This is due, in part, to improved aerodynamic front-end designs, which reduce both space and wind turbulence under the hood, and to longer high-temperature operating intervals, which may result from traffic congestion. The correlation between battery duty life and climatic conditions is well established [29,30].

Another class of problems occurs when the cumulative energy throughput exceeds the critical value for lead–acid systems. For standard SLI batteries with a liquid electrolyte, this is about 100 times the nominal capacity (20-h rate) and is reached in a relatively short time. The increased energy throughput arises from an increasing number of electrical loads to which energy must be supplied when the engine is off or at idle. These quiescent loads include the clock, which has been present for 20 years, anti-theft equipment, tele de-lock, and the electronic engine controller, which is kept in a 'wake' mode for a period of time after the engine stops in order to provide a quick and environmentally friendly re-start. In the last case, especially, the use of VRLA 12-V starter batteries has the potential to achieve better performance than types with free electrolyte. Indeed, VRLA batteries have already yielded significant improvements in this function in worldwide fleet trials.

The standard SLI battery in a new car at the beginning of the 21st century is not only significantly different in design from that of earlier decades, but it must also: (i) comply with new duties and functions, including higher environmental temperatures, more cycling, and deeper discharge; (ii) guarantee higher reliability and lower self-discharge. Therefore, there are good technical reasons to introduce VRLA batteries, even in vehicles with conventional electrical systems. The

flooded SLI battery, with a global annual production of about 230 million, has evolved from a technical innovation to a commodity product during the course of the last century. An interval of change and evolution is also to be expected with VRLA batteries in the SLI application. Furthermore, the technical benefits of the VRLA battery must always be carefully balanced against cost. For an evolving technology like the VRLA battery, a comparison with standard (flooded) SLI batteries is especially difficult because of the significant improvements in the latter, as mentioned above.

12.2.3. Expected changes in vehicle electrical systems in next decade and corresponding demands on automotive batteries

Today, a significant portion of the fuel burned in an ICE vehicle is used to generate electrical energy for the various on-board electric components (about 1 l per 100 km, and even more in high-end cars) [31]. Inefficiency in the conversion of energy from fuel to electricity, some of which may be stored in the battery for a time, increases fuel consumption by about 0.15 l per 100 km to support a 100-W load, for example [6,32]. Reducing the electrical load by 100 W reduces fuel consumption by as much as a weight reduction of 50 kg, which demonstrates the great scope for optimization of the electrical power system for the reduction of fuel consumption and emissions and also provides the motivation to do so.

A completely new situation for the vehicle electrical system, and therefore for the battery, occurs if the predictions of energy suppliers and environmental scientists are taken into account [33,34]. According to them, fuel consumption levels for all newly approved vehicles are set to fall by the year 2015 to half of the present value of about 9 l per 100 km. At present, it can take between 5 and 10 years to move new technologies to the series-production stage, and the time taken to convert the entire range of models of an automotive group can also take from 5 to 10 years. There is, therefore, an urgent need for the technological development of these systems to be completed at an early date. This situation is particularly critical since halving the fuel consumption will only be possible if a number of very challenging technical measures are introduced simultaneously. The most important of these are:

- additional mechanical and thermodynamic measures such as direct gasoline injection; the introduction of low-friction, automatic, variable transmission control (VTC) or automatic switch gear (ASG); and the more frequent use of turbo chargers
- the automatic idling stop of the combustion engine when the vehicle is stationary or is coasting without any actual driving force
- the recovery of braking energy as electrical energy and making it available for other uses
- support for the combustion engine from the electric motor during starting (operation at low revolution rates), a condition when emissions are most severe
- the avoidance of throttle valve losses and optimum mixing in gasoline engines through electromagnetic valve actuation (EMVA).

Since the goal of reducing fuel consumption to desired levels can only be achieved by introducing the entire group of possible technical improvements, the following unavoidable demands are placed on energy production and energy storage in the vehicle electrical systems of the future:

(i) the introduction of a higher vehicle electrical system voltage (e.g., 42 V, using a nominal 36-V battery) [6,8,34];
(ii) the installation of significantly more powerful alternators and batteries that have greater cycle stability and feature the greatest possible performance in terms of current output and consumption [33];
(iii) sufficient energy-storage capacity and cycle stability to bridge the operating phases when the engine is off with a start–stop system [35].

VRLA-type batteries are not essential for the introduction of higher voltages in vehicle electric systems (point (i) above), but they do represent the best chance for lead–acid to attain the battery characteristics mentioned under points (ii) and (iii) [36,37]. Combining VRLA batteries with other energy-storage devices is also a possibility [38,39].

In parallel with this new class of load demands, the power required by more conventional loads increases, too. The power demand of a high-end vehicle increased from less than 500 W in the 1960s to more than 2 kW in 2000. For the next decade, automotive engineers predict a sharp electrical load increase to about 10 kW [40].

Predictions of power requirements for future vehicles vary considerably [7,40]. As several components are still under development, some reduction may be expected. The data in Table 12.1 may serve as a rough estimate. Most of these components are used only seasonally and/or for short periods of time (electric heating, windshield heating, and catalyst heating), but, unfortunately, most could possibly be required at the same time. Others, e.g., electric power steering and electro-hydraulic brakes,

Table 12.1. Power required by vehicle components.

Device	Maximum power (W)	Average power (W)
Electrical heating	~ 1000	depending on operation
Electric AC compressor	~ 2000–3000	~ 2000
Electrical power steering	~ 1000	~ 100
Electro-hydraulic brakes	~ 1400	~ 50
Electro-mechanical brakes	~ 2000	~ 200
Electric windshield heating	~ 1500	~ 120
Electro-magnetic valve actuation (depends on engine rpm)	~ 2400	~ 700
Electric catalyst heating	~ 2000	~ 20–40
Active chassis control	~ 4000	~ 150
Electric fuel pump	~ 450	~ 150
Electric fan for ICE cooling	~ 650	~ 50
Electric water pump	~ 400	~ 200

demand high transient power, but rather randomly and infrequently. On the other hand, electro-mechanical valve control, electro-magnetic valve actuation and active chassis control impose high-power transients on the electrical system continuously. As the alternator is not able to follow such fast electrical transients (and engineers are not willing to allow for torque feed-back to the engine crankshaft, which could generate loss of comfort to passengers), the battery has to buffer or smooth out these transients.

12.3. Design, Components, Manufacturing of Automotive Batteries

12.3.1. Components

The price of automotive batteries is virtually unaffected by the local economy and the level of industrialization, but, rather, corresponds to that of other vehicle wear parts, which are all at commodity levels. Over recent decades, even the nominal price has been decreasing in most countries; that is, including corrections for inflation, there has been an absolute annual price decrease of several percent per year. This decrease has only been possible through intensive and continuous improvements in productivity.

The low prices are made possible by the use of inexpensive, readily available, raw materials — primarily lead — that can be recovered from recycled accumulators almost limitlessly and with little effort worldwide (see Chapter 15).

The most common type of SLI battery comprises the following components:

- a multitude of lead-alloy grids, which keep the active mass in place and conduct current to the terminals
- the active mass, which is a mixture of sponge lead with additives in the negative plate and porous lead dioxide in the positive plate
- an electrolyte of dilute sulfuric acid, in which all the plates are immersed
- separators made of insulating porous polyethylene sheet material
- electrical connections, including the terminals, made of lead alloy
- the case, normally a heavy duty polypropylene box.

The average weight of a European SLI battery is about 15 kg, with a lead content of about 9 kg and a nominal capacity of about 60 Ah at 12 V.

12.3.2. Special designs/special applications

While differences in the outer appearance of SLI batteries are limited, the key properties are designed according to the demands of the vehicles in which they are to be installed. For passenger cars with diesel engines, the cold-cranking capability needs to be higher than for gasoline-fuelled engines. This is achieved by using a larger battery and by optimizing the design to meet this demand. With a higher number of thinner plates, a higher cold-cranking power is achieved. This holds for flooded as well as for VRLA batteries. For diesel engines, the additional cranking power needed can be achieved with a VRLA battery of smaller dimensions due to its

lower internal resistance. This may be a special benefit for packaging in small-size diesel vehicles, which are very popular in Europe due to their high fuel economy.

The service-life of a conventional flooded battery under the harsh operating scheme in taxis, i.e., extended periods of standstill with lights and other equipment switched on, is only 6–12 months in Europe. In high-temperature climates, this may be even shorter. Taxi operation generates much more cycling of the battery than is found for the same type of car in private use, and this results in a tremendous reduction in battery life. Field tests with AGM batteries have shown an extension of taxi-duty life by a factor of 2–3 over flooded batteries. Therefore, a major European manufacturer has equipped all new taxis with AGM batteries since 2001.

Trucks and buses require batteries that are robust with respect to vibration and shock. Robustness is achieved via thick plates and a special separator material with a layer of coarse glass-mat, which maintains the positive active-material in place. In many bus applications, good cycling performance is needed to supply all the electrical equipment. State-of-the-art commuter service and long-distance buses feature lights, air-conditioning, electric heaters, and refrigerators that must be supplied even when the ICE is on idle or off. The same is true of long-distance trucks. In many instances, drivers live on-board their vehicles, which must continuously supply power to electrical equipment such as refrigerators, mobile phones, CB transceivers, air-conditioners, and television sets. Delivery trucks, too, experience numerous standstill periods with electric loads (lights, mobile phone, tail lift, etc.) operative and with short driving periods in between. This results in high cycling duty and, often, a low average battery SoC. Most truck batteries are still manufactured with low-antimony positive grids (1.6–3.8 wt.% antimony) due to their superior cycling performance. The need for regular maintenance (water refilling) is more acceptable in professional applications than by private customers. Today, VRLA batteries (gel or AGM type) are used in only a few buses and trucks. In buses, hot ambient temperatures can be a problem when the battery is located near the ICE.

Experience with VRLA batteries in trucks and buses is not yet sufficient for a final verdict on their suitability in such applications. In the long-term, VRLA batteries may find a market share in industrial vehicles if the higher cost is compensated by savings in maintenance and by extended life. Furthermore, the rationale that supports VRLA battery use in passenger cars (higher power, more cycling, deeper discharge) may also hold in the long-term for trucks and, especially, for buses.

A specialized field of operation for maintenance-free batteries is military applications. Many vehicles are used very infrequently but should still be operable on short notice. Within European armies, a significant number of gel VRLA batteries are in use.

12.3.3. Plate arrangement — plate stacking and spiral winding

Automotive AGM batteries with a nominal voltage of 12 V (Fig. 12.9) have been on the market for several years [19–22]. While SLI batteries with free electrolyte are produced only with prismatic cells with a multiplicity of electrode plates, AGM

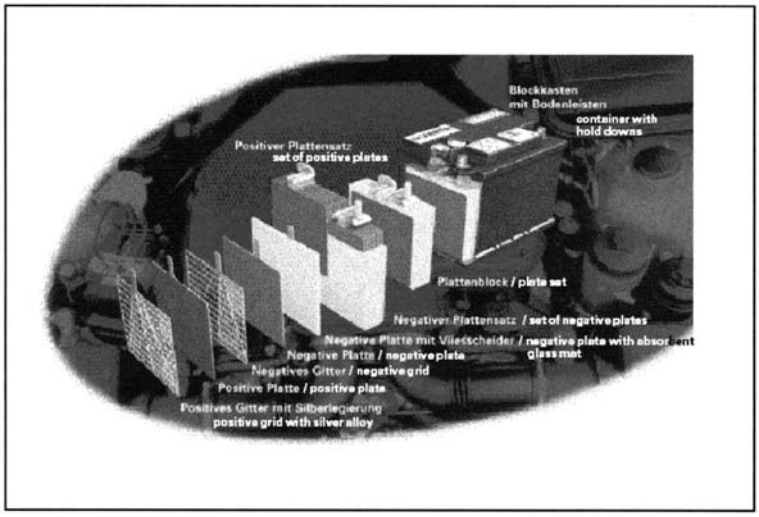

Fig. 12.9. AGM-type automotive battery; electrolyte immobilized in glass-fibre mat.

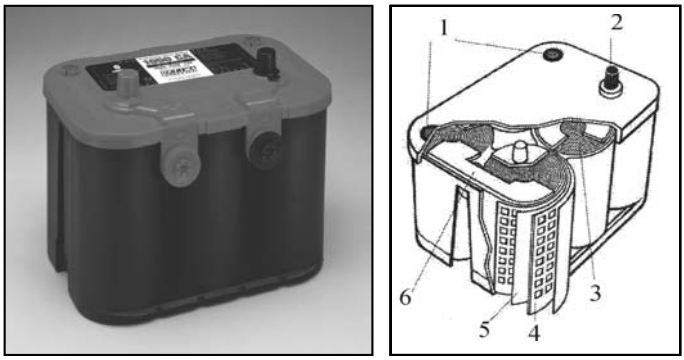

Fig. 12.10. 12-V AGM automotive battery with wound cells. (By courtesy of Optima Batteries, Inc.)

technology allows for both prismatic and spiral-wound cells. Whereas the AGM prismatic design retains most of the production processes used for flooded batteries and allows for either individual or continuous plate manufacturing, wound cells have only one electrode of each polarity, and a winding process replaces the stacking production step [21,36,41], see Fig. 12.10.

AGM cells with wound electrodes are claimed to have some technical benefits as compared with prismatic AGM designs. The wound arrangement of positive and negative electrodes with AGM separators between them maintains stack compression (for the benefits of compression, [42–47]) without load to the sleeves of the container walls. Softening of active material due to cycling is reduced, and

therefore cycle-life is improved. Furthermore, thinner electrode grids and electrodes can be used than with individual electrode stacks as less electrode stiffness is needed for winding than for plate stacking. This may allow higher specific power from wound cells.

Highly corrosion-resistant, antimony-free, lead alloys have been used successfully in the positive electrode grids of both single-plate and spiral-wound cells. Spiral-wound cells almost exclusively feature binary lead–tin alloys [36,41] whereas flat-plate electrodes use either lead–calcium alloys, with or without silver additive [26], or lead–tin alloys [48]. Binary lead–tin is known to be highly corrosion-resistant, but rather soft, which is a handicap for plate stacking in prismatic cells.

Prismatic cells contain electrode grids that are manufactured using gravity casting or the expanded-metal process. The dominant grid-manufacturing processes for spiral-wound cell electrodes include punching lead strip and continuous casting. At the present time, both prismatic and spiral-wound VRLA batteries are being evaluated and offered for use in automobiles, namely, 12-V versions for existing vehicles and 36-V units for future, 42-V PowerNet systems. It is obligatory that the dimensions of existing flooded batteries be maintained, especially those for existing vehicles and other 12-V applications. For the initial 42-V systems, vehicle manufacturers are also seeking to establish standard dimensions in order to facilitate packaging. Both 12-V (6 cell) and 36-V (18 cell) batteries must be arranged to make the best use of the available monobloc-container space.

While maintaining standard aspect ratios is not an issue for prismatic designs of VRLA battery, which can be manufactured in a wide range of dimensions, it does pose a fundamental problem for batteries with round cells. Cylindrical electrode coils have only two free parameters or dimensions, namely, height and diameter. Apart from the unavoidable volume loss between the cylindrical cells when they are arranged in rectangular-shaped space, there is further volume loss when cylindrical cells are arranged in the casing geometry standardized by JIS, SAE, or EN. The EN standard size L2 has been found to be particularly suitable for 12-V batteries that use spiral-wound technology as it minimizes unused space. Other EN sizes are less suitable. In the L5 size, for example, about 30% of the available space cannot be used by cylindrical cells. This is why VRLA batteries with cylindrical cells are not offered for all the standard sizes. For 36-V batteries, the EN sizes L5 (with an orthogonal arrangement of cylindrical cells) and L6 (with a hexagonal arrangement of cylindrical cells) are suitable for the 18 spiral-wound cells.

Conventional polypropylene is an appropriate container material for cylindrical VRLA cells because the necessary contact force for the glass-mat separator is supplied by the winding and maintained by a tensile force in the cell wall. Regardless of the nominal voltage, and therefore the number of cells, prismatic VRLA batteries require a reinforced plastic for the container and the lid to provide an AGM contact force and to keep the active-material compressed [42–44].

Valve designs used in stationary batteries have proven to be satisfactory for VRLA automotive batteries, and valves with an ethylene–propylene–diene polymethylene (EPDM, an artificial rubber) lip packing appear to be particularly well suited. Most European vehicle manufacturers demand a separate valve for each cell and, for all valve outlets, a joint gas-collecting duct with a flame arrestor

positioned before the exit point, to avoid explosions. It should not be possible for end users to remove the valves using commercially available tools.

As regards materials used for top lead and inter-cell connection, there are no differences between the two cell geometries. Lead–tin alloys are used, and a pre-tinning process is widely employed to achieve better lug integration.

Recipes for the positive and negative active masses are well known and are aimed at achieving a positive mass that is as porous as possible and a negative mass that can withstand the formation process, which can involve very high temperatures. The majority of separators are pure glass-mats, but present research is focusing on the use of synthetic fibre additives to make manufacturing simpler and cheaper.

Finally, it should be noted that the manufacturing methods differ only in terms of filling and formation. All manufacturers of VRLA batteries for ICE-powered vehicles are well aware that higher production tolerance requirements have to be met for VRLA batteries than for conventional SLI batteries with flooded electrolyte.

12.3.4. AGM and gel technology in vehicles

In motor vehicles, AGM is the dominant VRLA technology because of the demand for high power for cranking the ICE. This necessity likely precludes use of gel batteries, especially at low temperatures; the batteries have a higher resistance than flooded batteries and, especially, AGM batteries. Gel batteries comprise a porous (more or less standard) separator similar to that used in flooded batteries, and current flow and ion exchange are impeded by the volume (about 5% per volume) of the silica in the electrolyte. Furthermore, filling batteries with thin plates and short inter-plate spacings with gelled electrolyte is difficult. Therefore, high-power designs can be realized much more easily using flooded or AGM technologies, which have a significantly lower separator diaphragm resistance and can be produced with thinner electrodes.

The power-limiting attributes of gel batteries are even worse at low temperatures because the electrolyte shrinks and electrolyte contact to the active material in the plates is reduced. Thus, resistance is further increased and ion flow is further impeded. Accordingly, terminal voltage at a typical high discharge current is lower by 10–30% with gel batteries than with AGM batteries. As modern vehicles require current for creating torque in the starter motor to crank the ICE and also a sufficiently high voltage to operate the electronic motor control at the same time, the priority of this issue is high.

Gel batteries are best suited for applications where:

- cold cranking is not an issue for the vehicle, e.g., seasonal vehicles in agriculture and construction, vehicles with dual-battery systems
- the demand for energy storage is so high that a rather large battery is required and, as a consequence, the specific demand for cold cranking is relatively modest for the battery and its voltage is sufficiently high even under the anticipated load
- vibration is very harsh and the gelled electrolyte helps stabilize the active materials.

12.3.5. VRLA automotive 12-V batteries for standard vehicle electrical systems

Previous sections have described the most significant advantages of VRLA batteries, especially AGM batteries, and made clear that their costs are significantly higher than the costs of flooded batteries. The stiff competition within the automotive industry inevitably results in a highly rigid pricing policy; even small differences in the prices of supplied parts, especially when viewed in the light of large numbers of parts involved, require justification for using more expensive parts such as AGM batteries.

To complicate the situation even more, many of the properties of an AGM battery are already exhibited by modern, totally maintenance-free batteries with liquid electrolytes. This is particularly true for starter batteries as they are only expected to have a service-life of about 2000 h, which is considerably less than one-tenth of that which industrial battery manufacturers claim their products achieve when used in constant-voltage, float-charging applications. As a result, a VRLA battery will be used in vehicles with conventional electric power systems only if its advantages over a flooded battery are really needed. These include the following.

(i) *Vehicles with high cycling duty ($>0.1\,Ah\,km^{-1}$)*. These include taxis with a comprehensive array of electrical consumers. A similar requirement is exhibited by emergency vehicles such as ambulances and by motor homes, where cycling duty is of major importance due to extended engine-off periods with electric equipment in operation. Operating temperatures should, however, be moderate.

(ii) *Passenger vehicles with diesel engines*. These vehicles especially benefit from the use of VRLA batteries if the cold-cranking power of even the largest flooded battery that can fit into the available space is insufficient. AGM batteries may provide about 30% higher cold-cranking capability within the same volume, which facilitates and/or accelerates engine cranking; this attribute justifies the use of AGM batteries in recent European luxury cars with high-torque diesel engines.

(iii) *Vehicles with relatively long idle times*. In this case, there may be an attendant and significant probability of complete deep discharge of the electrical storage system. This is an issue with luxury sports cars and leisure vehicles. Because of their improved tolerance of accidental deep discharges, VRLA batteries may continue to operate satisfactorily even after such events. This is not meant to imply, however, that VRLA batteries should be operated continuously in a low SoC. Within a dual-battery system, a VRLA battery is an ideal partner for a separate starter battery that is installed for only cranking the engine and for no other purpose. With such a combination, mobility is guaranteed even if harsh misuse leads to complete discharge of the VRLA battery.

(iv) *Vehicles with batteries mounted within the passenger compartment*. The batteries can be used to power safety and convenience apparatus, and can be so located because VRLA technology will not leak electrolyte even if the container is broken.

These application scenarios exploit the high power density, the high cycling stability at moderate temperatures, and the advantageous behaviour in recovery from complete discharge that are provided by AGM technology. Such attributes justify the additional cost of AGM batteries.

Key features of AGM batteries, which have also been achieved in modern, high-end, flooded starter batteries, include:

(i) totally maintenance-free operation; most flooded batteries produced in Europe are made such that they cannot be topped-up with water;
(ii) high charge-acceptance, i.e., the ability to take up energy, particularly at low temperatures, at the charge voltage of approximately 14 V normally used in vehicle electrical systems; in this regard, there is little difference between flooded and VRLA batteries;
(iii) protection or safety against charge-gas (hydrogen) ignition; with both VRLA and modern, flooded lead–calcium batteries, this risk is currently all but non-existent;
(iv) high resistance against corrosion of the lead structure materials within the battery, which can bring the battery prematurely to the end of its service-life; today, similar grid materials are used for both antimony-free flooded and for VRLA batteries; at elevated ambient temperatures, VRLA batteries may be more prone to corrosion attack.

In summary, freedom from maintenance, high charge-acceptance, safety against hydrogen ignition, and corrosion resistance should no longer be regarded as drivers for choosing VRLA batteries over antimony-free flooded batteries, which are available at a lower cost. Nor is the notion of replacing a flooded battery with a smaller and/or lighter VRLA battery any longer realistic. An increasing number of key-off loads must be powered and, as a consequence, energy storage is becoming more important than cranking power, except in small vehicles with high-power diesel engines.

12.3.6. 36-V VRLA automotive batteries for 42-V PowerNets

As the architecture and components of the 42-V automotive PowerNet and the demands placed on the system are still in an embryonic stage of development, forecasts of the types of battery required are still very vague. This is due to technical as well as cost issues of advanced systems [35].

The three following directions, however, may be regarded as already relatively certain.

(i) For cost reasons, the automotive industry will do everything possible to the vehicle and to the battery/batteries to achieve success with the lead–acid system, as this will exploit the familiar technology and experience that has been achieved with the 12-V vehicle electrical system. Other electrochemical systems, e.g., nickel–metal-hydride (Ni–MH), lithium-ion, etc., will be accepted only if features or attributes are required which are beyond the capability of the lead–acid system.

(ii) Initially, a VRLA battery will be used because the change to 42-V systems will introduce vehicle applications that comprise substantial cycling of the energy-storage system.
(iii) There are expected to be applications in future vehicles, which cannot be covered by lead–acid batteries. Other electrochemical systems will eventually find their place in road vehicles.

More detailed considerations of capacity, design, and the connection system, for example, are still preliminary. A battery with an energy content of approximately 1 kWh (i.e., 36 V, 27 Ah at the 20-h rate) is required in higher classes of vehicles, and such a battery with prismatic cells can be housed in an EN, L5 container. The weight of such a battery is about 28 kg; thus, its specific energy is about $35\,\mathrm{Wh\,kg^{-1}}$. The power level of a 36-V VRLA battery in an L5 container at 20°C and 100% SoC exceeds 10 kW ($\sim$ 300 A) over 10 s at a voltage well above 30 V, which is the proposed lower voltage limit for the 42-V PowerNet when the vehicle is in operation. At 28 kg, 10 kW equates to a specific discharge power of approximately $350\,\mathrm{W\,kg^{-1}}$. At −18°C, a current of 300 A can be drawn for 60 s. At −25°C, the specific cold-cranking power exceeds $300\,\mathrm{W\,kg^{-1}}$ at a voltage well above 30 V [39], and at 80% SoC, the discharge power still exceeds 7.5 kW for short periods of time. Various designs for 36-V, VRLA automotive batteries (e.g., see Fig. 12.11) have been proposed [36–37,39,49,50].

The design of the future connection system for batteries in the 42-V system is not yet defined. The interests of vehicle manufacturers (cost, quantities), manufacturers of wiring harnesses and plug-in connectors (integration of proprietary mechanical systems) and the battery industry (manufacturing costs and resistance to corrosion) have yet to be consolidated. Some guidance can be drawn from safety requirements proposed by international committees and standards bodies. [35]. The risks of short-circuits and arcing, especially when loads are disconnected, are of much greater concern with 36-V than with 12-V systems [51]. The results of very intensive studies show that plug-in connector designs are currently competitive with stud bolts in screw or clamp technology [50], which can also be designed to meet

Fig. 12.11. (a) 36-V AGM automotive battery in EN container size L5 (= DIN H8). (b) High-performance 36-V/27-Ah AGM automotive battery with 2 × 9 cell arrangement in L5 container according to EN. (By courtesy of VARTA.)

the technical and safety-relevant requirements that have been specified [39]. From the perspective of manufacturers of lead–acid batteries, any design has to facilitate a reliable connection of the internal 'acid environment' to the external user environment. With this challenge in mind, a technique for welding lead sleeves with lead bolts has proven particularly advantageous in many applications of lead–acid batteries in recent decades, and this might be transferred to 36-V battery applications.

Many questions about 36-V, VRLA batteries remain yet unanswered, e.g., production reliability, need for individual-cell charge control in the 18-cell string, and the anticipated heat build-up during intensive cycling operation. Battery technology, however, is not expected to impede the introduction of the 42-V PowerNet — a marked contrast to the plans to introduce EVs as a mass-product in the 1970s and 1990s.

12.4. The VRLA Battery in Automotive Applications and its Interaction with the Vehicle

12.4.1. VRLA batteries in present vehicle electric systems

By the beginning of the 21st century, a limited number of passenger cars were already using AGM batteries. These cars were in the upper performance and price segment, including both sports cars and limousines. Such batteries also perform well in taxi fleets, in buses, and in delivery trucks. Another suitable application segment has been in agriculture and construction vehicles, since these have a very seasonal duty and also require high robustness against vibration.

The main benefits of AGM batteries in present-day automotive applications, as compared with flooded battery designs with the same outer dimensions, are: (i) higher power capability; (ii) improved cycling capability, e.g., as in taxis; (iii) vibration resistance via compression of the active materials; (iv) fewer problems with a wide SoC operation range (reduced acid stratification); (v) a leak-proof, spillage-free, no-gassing design that allows for more flexible mounting, including in the passenger compartment. These strengths of AGM batteries are already being exploited in the current, standard-vehicle electrical power system, which is illustrated in Fig. 12.12. Similar power systems are common to passenger cars, trucks, buses, and to specialty vehicles in agriculture and construction. These systems comprise an alternator (driven by the ICE) as the only source of electrical energy and various consumers as energy sinks. Some of the latter are under the control of the driver (switched) and others are not (operating continuously). The battery is an energy-storage device for buffering between the changing supply and demand for energy.

The alternator of today is a claw-pole machine [52], which is driven by the crank shaft via a belt. The current available from the alternator depends on its speed of rotation, i.e., on driving conditions, and on its temperature. When the engine is on idle, the available current is about 60% of the maximum current at higher speed (note, the current level may vary according to alternator design). The thermal

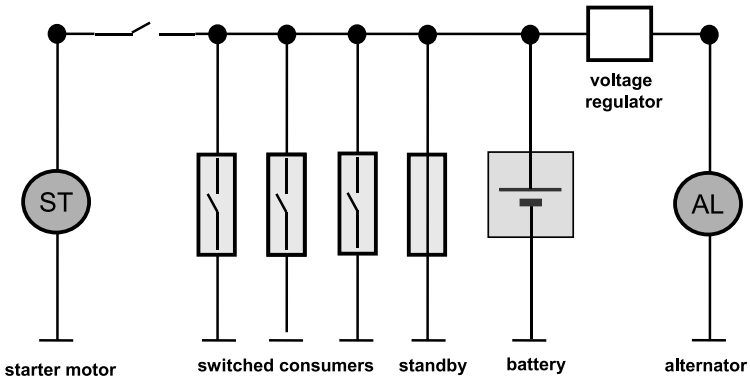

Fig. 12.12. Schematic of a present vehicle electric system.

properties of copper and the magnets are such that a hot alternator cannot provide as much current as a cold one. The controller regulates the alternator voltage at about 13.8–15 V in order to protect lamps, electronics, and the battery in those instances when the current capability exceeds the needs of the electric consumers [52]. When the alternator cannot provide sufficient energy, however, the shortfall is provided by the battery and the system voltage drops to the discharge voltage of the battery. Therefore, the voltage level in the electrical system is not constant, but varies between the regulator voltage and a lower value, typically about 11 V. These values depend on the layout of the system (size of alternator, battery, type and number of loads) and battery properties (SoC, temperature, age).

At high loads such as cranking the ICE, the battery voltage may drop much further, typically into the range of 8–10 V, or even lower at low temperatures (see Figs. 12.3 and 12.4). In this architecture, the battery is a completely passive, unregulated component [38]. The battery discharges when the energy demand exceeds the alternator output, regardless of whether or not the battery can provide all of the shortfall. The battery can recharge when the energy production by the alternator exceeds the demand by the consumers, provided its circumstances are such that it can accept the charge.

A measured voltage vs. current profile is given in Fig. 12.13 and the situation is illustrated schematically in Fig. 12.14. A hysteresis-like behaviour is observed as the SLI battery is alternately discharged and recharged. The voltage level and the duration of the periods of discharge and recharge, respectively, depend on the operating conditions as well as on the layout of the system and the battery properties. It is clear that an AGM battery, which can sustain more energy throughput than other lead–acid batteries, will provide longer duty time, but only if energy throughput limits the life, as is the case with taxis and other vehicles in frequent traffic jams. There is a particular advantage if the battery is operated regularly at low SoCs and/or with wide changes of SoC, since acid stratification is reduced by electrolyte immobilization in the AGM battery.

On the other hand, vehicles that generate little energy throughput due to their system layout, support a limited number of loads and operate at high

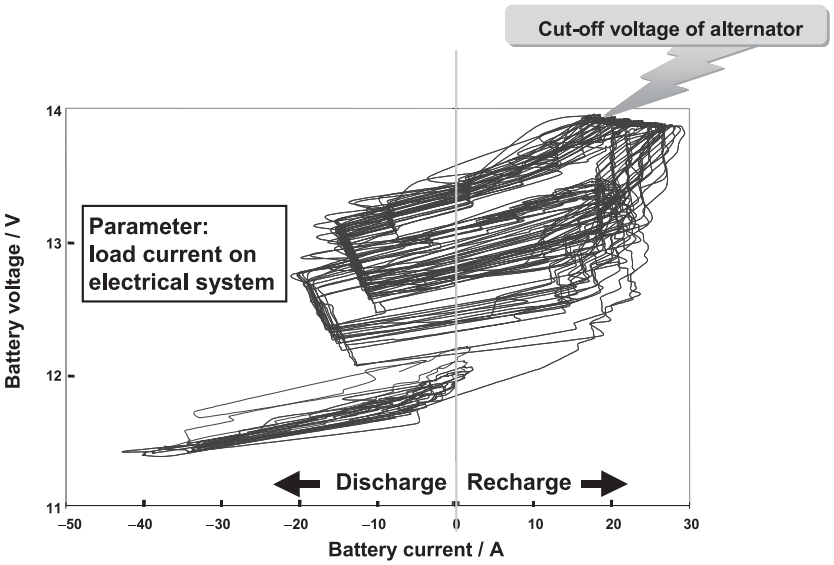

Fig. 12.13. Voltage–current profile of automotive battery when vehicle is operated.

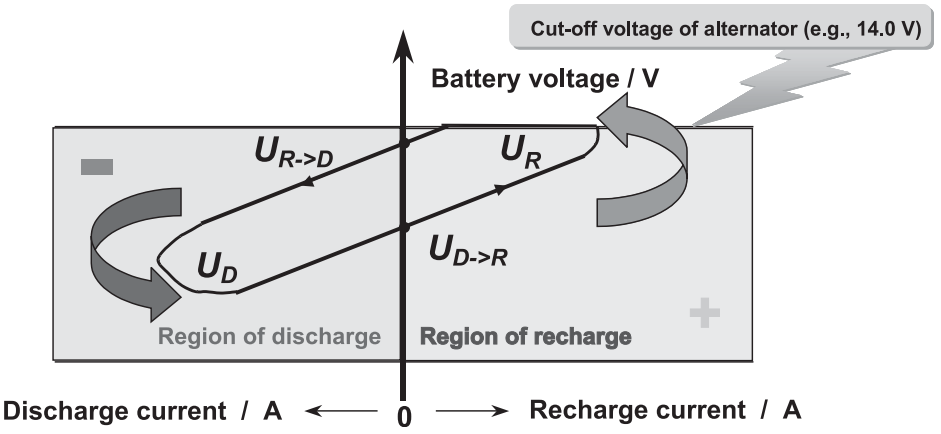

Fig. 12.14. Schematic of voltage vs. current profile from drive cycle (hysteresis-like behaviour).

engine-revolution rates and will gain little from the installation of an AGM battery. Moreover, if battery temperatures are likely to be very high, a VRLA battery installation cannot be recommended. Therefore, a decision to install an AGM battery has to be made with careful consideration of the advantages and disadvantages, and this may result in different decisions for applications that differ significantly in only one parameter.

12.4.2. VRLA batteries in vehicles with new components and new operating strategies

Technological developments in the automotive industry and their consequences for the vehicle electrical system, and especially for the battery, are proceeding rather quickly. The overall electrical demand in vehicles is going to increase due to: (i) new technical features; (ii) the demand for fuel economy without loss of comfort for the customer; (iii) the demand for higher reliability of the electrical supply to safety-relevant devices (x-by-wire); (iv) the potential to reduce production and operational costs. All these factors will introduce additional, and more demanding, electrical consumers.

The vehicle electrical architecture is undergoing an evolutionary change. Dual-battery systems, dual-voltage (14-V/42-V) systems [53,54], high-voltage systems, starter/alternator integration, recuperation and boosting, etc., (which may be realized independently or in combination) are all under discussion as a means to improve the efficiency of production, distribution, control, and storage of electrical energy in the vehicle. New battery designs with performance patterns to meet the requirements of the new architectures are needed, and some of the new demands may exceed the capabilities of lead–acid batteries [55,56,38]. Single- and dual-battery systems offer a wide variety of capabilities when combined with intelligent means to maintain the batteries in an appropriate operational window. These intelligent means and detection of battery SoC and state-of-health (SoH) become more essential as new types of duties require batteries with high specific power and high specific energy. The function of the battery changes from that of a passive component to that of a pivotal unit, which must be monitored, supervised, and managed in order to maintain vehicle functionality and safety.

The technical demands on the battery resulting from the above innovations are manifold. For example:

- new cranking technologies accelerate the combustion engine from standstill to idle speed within some hundreds of milliseconds [13,57], and thereby reduce both exhaust and noise emissions; this requires very high discharge power from the battery and the situation may be aggravated if, simultaneously, other high-power loads, e.g., an electrically heated catalyst, must be powered
- increased energy demands during engine-off and engine-idle periods require high battery capacity and, if these situations occur often, also high battery cycle-life
- as energy taken from the battery during such periods has to be recharged quickly to provide a repeatable function, a good recharge capability is required
- high reliability for cranking and for providing energy to safety-relevant components may be provided by redundancy from multi-battery architectures and/or battery monitoring and management [38,54].

Demands on the battery are even greater when a start/idle-stop function or even a boost/recuperation function is implemented in the vehicle. Periodically, much electrical energy must be provided during standstill, to crank the engine, and even to assist during vehicle acceleration (‘launch assist’). The energy given up has to be

recharged as rapidly as possible, and very high recharge power must be accepted in order to recover braking energy. The motivations for the introduction of such features are fuel savings and the reduction of emissions.

The development of vehicle electrical systems operating at a nominal 42 V and its standardization with ISO is underway. A working group of the European Vehicle Electric System Architecture Forum has prepared a draft standard for this new voltage level [58]. The 42-V level was chosen as a compromise between the demand for an increased voltage to achieve higher efficiency in electrical and electronic components and the exclusion of safety hazards, even under extreme operational conditions like load dump, etc. The term '42-V PowerNet', or simply 'PowerNet', is now established worldwide [9,11,59].

The nominal and limiting voltage values, as shown in Table 12.2 and Fig. 12.15, have been chosen to be both compatible with the lead–acid battery system and with technical improvements that exceed the present standard. The PowerNet shall be more than just a tripling of present voltage levels. The specified voltage range refers to any point in the electrical system, i.e., the voltage shall not exceed the quoted values at any point in the electrical circuit. This means that the voltage at the battery must be higher at discharge and lower upon recharge than the limiting voltages to accommodate ohmic losses. Full functionality of the PowerNet components shall be provided within an operating window from 30 to 48 V, RMS. During cranking, the relevant components shall operate even at 21 V. For less than 70 ms, the voltage may be in the range $18\,V < U < 21\,V$. AGM technology offers significant improvements over the standard SLI battery to meet these demands, as explained above in Sections 12.3.5 and 12.4.1. Nevertheless, despite significant improvements in cycle-life, the integral energy throughput of AGM batteries of standard size (i.e., $\sim$ 500–1000 Wh) is limited to some hundreds of kWh. This compares favourably with flooded SLI designs, but may not be sufficient for start–stop systems when the start–stop function is used extensively.

Table 12.2. Voltages in the 42-V PowerNet [58,59].

Code	Operating voltage			Minimum operating voltage $U_{op,min}$ (V)	Operating conditions for equipment/ components
	Working voltage of PowerNet U_{PN} (V)	Maximum operating voltage $U_{op,max}$ (V)	Effective value of maximum operating voltage $U_{eff\text{-}op,max}$ (V)		
L	42	50[a]	48	21[b]	Full functionality during starting
M	42	50[a]	48	30	Full functionality with engine off
N	42	50[a]	48	30	Full functionality with engine on

[a] Including ripple.
[b] Plus starting profile.

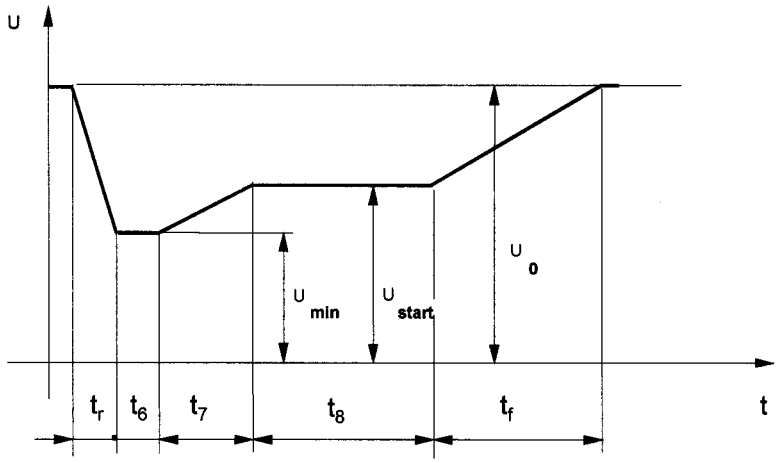

Voltage profile of starting pulse

U_{min} (V)	U_{start} (V)	t_r (ms)	t_6 (ms)	t_7 (ms)	t_8 (ms)	t_f (ms)
18	21	5	15	50	500 to 20000	100

Fig. 12.15. Profile of starting pulse for 42-V PowerNet (extraction from Draft Standard submitted to ISO).

A start–stop system is an operating strategy for the ICE vehicle that switches off the ICE when the vehicle is stationary and no propelling power is needed. The ICE is cranked automatically when the driver pushes the accelerator pedal. With this strategy, ICE idle-speed running, which is a very inefficient operating mode, is significantly reduced. Depending on the philosophy employed, switching off is done either automatically (via the vehicle-management system) or manually. While conservative strategies allow for engine-off only when the vehicle is stationary, a more fuel-efficient strategy may be to switch the engine off also when the vehicle is 'sailing', i.e., is moving but does not need propulsion power.

From the point of view of the battery, it is not the cranking of the engine at the end of the stop phase (some kW for some tenths of a second, i.e., $\ll 1$ kWs of energy) that is most challenging, but the electrical power to supply all the electrical equipment during the stationary phase, which requires a large throughput of charge, as demonstrated by the following rough estimation. If the vehicle were to draw only about 500 W at standstill (a power level which may be much higher under harsh conditions, e.g., when an air-conditioning unit is also to be driven in the engine-off mode), a standard-sized AGM battery may last 300–600 h (i.e., a lifetime energy throughput of 150–300 kWh) in a stop-mode, at most. If a stop were to last about 1 min (i.e., 8.3 Wh) and there were 1–2 such stops (say 10 Wh) per km of driving, the

battery would be worn out after 15,000 (minimum for 0.5-kWh battery) to 60,000 km (maximum for 1-kWh battery) of driving. This may be sufficient for customers with limited downtown driving (although for such drivers start–stop concepts offer less benefit) but not for courier and delivery services (where the start–stop approach may deliver considerable cost savings).

In the case of Ni–MH batteries, which can be cycled about 5000 times their nominal capacity at 80% DoD and more than 15,000 times their nominal capacity with shallow cycling [55,56,60–63], may be an appropriate choice. In the future, lithium-ion batteries may also enter the automotive market. Their high specific energy, which exceeds that of lead–acid systems by about a factor of three at medium discharge rates, would allow air-conditioning to be operated even in the engine-off mode. The calendar-life of lithium-ion batteries under automotive operating conditions, however, still needs to be improved, and there must be a reduction in cost to an acceptable level for such batteries.

This broad overview of start–idle–stop systems shows that the demarcation between the use of AGM batteries and the use of other electrochemical storage systems in future vehicle electrical systems with high cycling duty is not yet clear. There will be no either/or situation, but several battery systems have advantages and disadvantages and will exist side-by-side. What is unclear today is the portion of the overall automotive market each will cover.

Changes to the architecture of the vehicle electric power system are expected to proceed in an evolutionary rather than a revolutionary manner. It is the intention of the automotive industry and its suppliers that the 42-V PowerNet [9,11] will be available for technical situations which require very high power demands. Due to cost considerations as well as to uncertainties with respect to the availability and reliability of newly designed components [35], modifications will be introduced stepwise only when really needed. This process is expected to last many years. Therefore, the long-term solutions to the problems of increased vehicle electric power demand, the implications for battery design and manufacturing, and the possible intermediate steps have all to be considered carefully by the battery industry.

Increase of the vehicle electrical system voltage to the level of the 42-V PowerNet is not the only direction of present development. Several of the new vehicle functions, especially those aiming at improved reliability and comfort, can be achieved already using the existing 14-V electrical system.

A dual-battery system [38,64] may guarantee the capability to crank the combustion engine and to maintain the mobility of the vehicle, even in extreme operating scenarios and in the case of failure or misuse of the power-supply system. Two different batteries, specialized for high discharge power (cranking) and high energy storage and cycling (energy), respectively, are combined with a control unit to keep the SoC of the starting battery high. Furthermore, the control unit manages irregular situations in a fashion designed to make maximum use of the redundancy provided by the dual-battery concept.

An example of an electrical system layout that is used in a European high-end sports car launched in 2001 is shown in Fig. 12.16. A cycling AGM battery, directly connected to the consumer harness and to the alternator, buffers electric energy, as

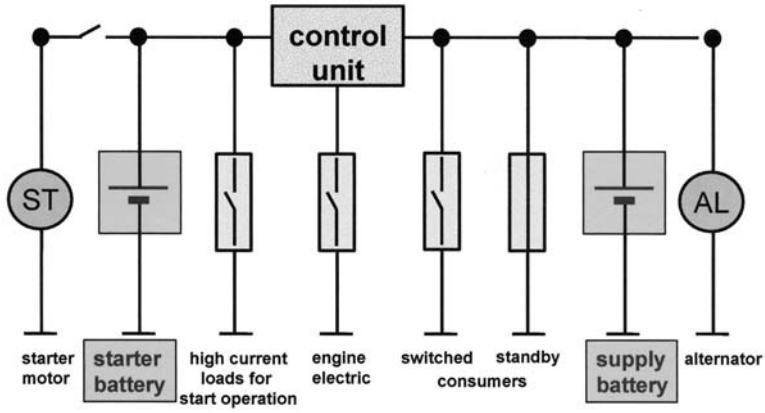

Fig. 12.16. Dual-battery system: electrical system layout.

in conventional vehicles, and a power-optimized battery (POB) is provided solely for the cranking operation. This battery is recharged with priority via the control unit from the alternator (or from the AGM battery) via a d.c.–d.c. converter. As the d.c.–d.c. converter is used only for this purpose, its voltage can be controlled according to the needs of the battery. Thus, elevated recharge voltages can be applied without compromising other electrical components such as headlights, etc., and recharge can be terminated when a sufficient SoC is achieved, in order to avoid overcharge. This intelligent recharge strategy considers both battery temperature and duration of recharge (for details on this strategy and on the POB see Ref. [38]).

This dual-battery approach provides a fully charged cranking battery in order to guarantee mobility, even when the energy battery is down due to over-discharge or failure. Under other circumstances, the control unit can be by-passed, and energy can be supplied from the starting battery to the electrical harness when necessary to keep other functions of the vehicle operable after cranking is successfully accomplished.

This is one example of a dual-battery design. High mobility, i.e., high reliability for cranking is, however, not the only goal that can be achieved with a dual-battery design. Some of the other reasons for using such designs are listed in Table 12.3, i.e.,

- for cranking reliability, one battery (best a small high-power type) is always kept at a high SoC; the other battery may be a high-cycle and/or a high-energy type, as determined by other demands
- in the case of extreme needs for cranking power, two batteries may be paralleled for cranking; the types chosen may be optimized for other demands, but should not be too different
- for the supply of systems which require very high reliability, e.g., electrical power braking and steering, a second battery may provide cover in case of failure; the specification of the fall-back battery depends on the demands of this application

Table 12.3. Motivations for dual battery systems [38].

Goal of dual battery system	Strategy to achieve goal	Battery 1 (B1)	Battery 2 (B2)
Mobility — high cranking reliability	Always high SoC/ no quiescent load to B1	High power; high SoC	High cycle and energy
Very high cranking power	B1 and B2 in parallel for cranking	Standard (high energy or high power)	Standard (high cycle)
Redundancy for high reliability	Fall-back for bridging in case of failure	Standard or high power	Standard or high cycle
Weight saving	Two extreme specialty designs	Ultra power	High cycle
Reliable supply for electrically heated catalyst	Cycle proof battery always in high SoC	Standard (high power)	Standard (high cycle)

- for saving weight, two extremely specialized battery designs may be used, but this configuration requires careful management
- for reliable operation of an electrically heated catalyst, a cycling battery should be maintained at a high SoC (the electrical heating of catalysts is becoming redundant due to improved designs of catalyst system and advanced strategies for engine operation).

Of course, multiple goals can be achieved simultaneously via a dual-battery system of appropriate design. To take full advantage of the two independent batteries, the control unit must be able to recharge each battery independently. Additionally, the control unit should incorporate a sophisticated switching strategy to conduct energy flow even in extreme situations (e.g., high quiescent loads due to consumer defects, battery defects, extended traffic jam in cold or hot climate, etc.).

Due to the barrier of increased cost that confronts the introduction of any new system, the time-scale for volume production of vehicles with 42-V systems is still uncertain. Nevertheless, once the 42-V PowerNet is introduced into a vehicle, manufacturers will convert many functions to the new voltage level when the relevant components are available at low cost, even if the higher voltage is not essential for the function in question. Dual-voltage (14-V/42-V) systems, with a separate battery at each of the two voltage levels, are under discussion for the intervening period [54].

Whatever may be the final design of the vehicle electrical system: (i) more electrical power will be required on-board than is needed today, even when the vehicle is stationary; (ii) alternators will be chosen for the average, rather than the maximum, power demand. Therefore, the battery will have to provide essential power at a

greater level than it provides today. In addition, for systems that require a highly reliable power supply, the battery will have to serve as a fall-back power source in case the alternator does not provide sufficient (or any) power. Therefore, battery monitoring and management will become higher priorities in order to maintain the battery in a good operational range, to check its actual state, and to predict its capability in the near future. Again, this is true not only for the 42-V PowerNet, but is already required for advanced vehicle electrical systems that operate at the 14-V level. The battery will be challenged via many demands, and some of these will be conflicting, namely: (i) more power and energy, but less weight and volume; (ii) more energy together with longer cycle-life; (iii) better transient damping; (iv) a wider operating temperature range.

12.4.3. State-detection and management of VRLA batteries

As battery performance depends on temperature, SoC, and SoH, it is essential to measure or estimate these properties to guarantee full functionality of the electrically powered components, for triggering means to keep the battery in its best operational window, and for early detection of limited battery functionality. Battery monitoring provides for optimum use of the capability of a battery, guarantees the power supply to high-reliability devices, and provides guidance for replacement strategies. Furthermore, monitoring the actual SoC allows for electrical power management, which may include both reducing demand by limiting operation of luxury applications and increasing power generation by appropriate control of the alternator, e.g., via idle speed and automatic gearbox control [65]. Strategies for the determination of SoC and SoH have to be chosen according to the operational goals, which include expected duty-cycle scenarios and acceptable error tolerances. Various approaches are under development, including those with and without sensing of battery current. Most probably, to predict short-term and even long-term battery performance, a combination of several methods is needed to assure sufficient reliability (for a definition of SoC and SoH, see Ref. [38]). This subject is discussed further in Chapter 8. Battery monitoring and estimation of SoC and SoH without using special sensors within the battery, i.e., only from observations of the voltage–current behaviour and temperature, can be achieved more easily with AGM batteries than with flooded counterparts. This is because the problem of vertical inhomogeneity of electrolyte and electrodes is reduced in VRLA batteries. On the other hand, VRLA batteries are more sensitive to high temperatures than flooded batteries because their starved-electrolyte design makes any water loss, via evaporation, grid corrosion or electrolysis, more critical. This issue has to be considered in the design of the packaging of the car; battery positions near high-temperature components (engine, catalyst, etc.) must be avoided.

The electrical self-heating of the battery is minimal in standard vehicle electric power systems. The moderate, mean power throughput limits heat generated via ohmic losses. In evolving electrical systems, with harsh, high-rate, cycling operations, especially those with start–stop and boost/recuperation duty, self-heating is significant. Consider, for example, start–stop operation with a 600-W electrical

discharge load in stop mode and with the total duration of operating and stop periods unchanged. This type of operation would generate an average power loss of 100 W, if a total recharge–discharge efficiency of 84% is assumed. A lead–acid battery of 1-kW capacity has a heat capacity of about $7\,\mathrm{Wh\,K^{-1}}$, i.e., after 1 h of continuous operation, the battery temperature would increase by 14 K if no heat transfer to the environment were possible. This heating is not a special feature of VRLA batteries and their oxygen cycle but, rather, a consequence of new duties of the battery, and it shows the necessity for consideration of the thermal needs of the battery (see also Chapter 1, Section 1.4).

12.5. Performance Data

Immobilization of the electrolyte in an AGM battery allows for higher electrode surfaces and lower current densities. This is because the electrode plate can be made taller as no top-space is needed for a reserve of electrolyte to compensate for water loss. Together with the relatively low separator resistance of the AGM as compared with standard polyethylene separators for flooded SLI batteries, this provides a higher voltage at a high rate of discharge. In other words, a higher specific cold-cranking power (both $\mathrm{W\,kg^{-1}}$ and $\mathrm{W\,l^{-1}}$) is available with an AGM battery as compared with standard 12-V SLI batteries in an identical container (see Table 12.4). On the other hand, since there is no free electrolyte, the specific utilization of the active materials is usually lower (starved-electrolyte design), which causes a reduction of specific energy ($\mathrm{Wh\,kg^{-1}}$) at low discharge rates, although the energy density ($\mathrm{Wh\,l^{-1}}$) is about the same. With increasing discharge rates, the lower internal resistance of the AGM design helps to reduce this drawback. Such batteries offer superior power density ($\mathrm{W\,l^{-1}}$) compared with flooded types. Finally, it should be noted that gel VRLA batteries provide less energy density than prismatic AGM and flooded batteries.

12.6. Outlook

Today, there is a much larger variety of battery designs available for selection in automotive applications than some years ago. Besides standard SLI batteries with flooded electrolyte, there are derivatives of flooded prismatic lead–acid batteries such as the POB (Power Optimized Battery) [38], as well as AGM batteries in prismatic and spiral wound designs [19,21,22,36,41,66–68]. The ultimate high-power design with thin-film electrodes was realized with thin metal foil (TMF) [21,36,66,68], and this design can provide very high power for short periods of time, which is exactly what is required for rapid starting concepts, e.g., crankshaft starter/alternators [13]. Prototypes of batteries for the 42-V PowerNet have also been produced with standard outer dimensions to allow for integration into the vehicle, which avoids packaging problems [37,39].

No further radical design improvements of VRLA batteries for automotive applications are foreseen at present (but, see Chapter 17). Any improvements which were achieved with flooded lead–acid systems in the past will be adapted to the

Table 12.4. Specifications of batteries in L5 containers according to the EN, i.e., about 1 kWh of energy content (unless mentioned otherwise).

	Flooded 12 V[a]	AGM 12 V[b] prismatic	AGM 12 V[c] wound	AGM 12 V[d] 'Inspira'	Gel 12 V[e] prismatic	AGM 36 V[f] prismatic
Specific energy (Wh kg^{-1}) 20 h, 20°C, $U_{min} = 10/30$ V	46	39	35	22	34	35
Energy density (Wh l^{-1}) 20 h, 20°C, $U_{min} = 10/30$ V	95	95	70	40	71	81
Specific discharge power (W kg^{-1})[g] 100% SoC; −18°C; 10 s > 7.5/22V	215 (EN)	235 (EN)	315 (CCA 750A BCI)	~1500	155 (EN)	290 (EN)
Power density (W l^{-1}) 100% SoC; 18°C; 10 s > 7.5/22 V	445 (EN)	570 (EN)	630 (CCA 750A BCI)	~2700	325 (EN)	670 (EN)
Cycles (times nominal capacity) at ~ 20% DoD[h]	~ 100	> 300	~ 50 ('deep cycles' (BCI))	5300	> 640 (to < 60% initial capacity)	> 300

[a]Standard European automotive.
[b]For example, as manufactured by VARTA Automotive, www.varta-automotive.com.
[c]Optima Batteries, Inc., Red Top 34 (50 Ah, approx. L3 container/design is not available in L5 container), cf. www.optimabatteries.com, accessed 14.03.2002 [36].
[d]Johnson Controls, Inc., 12 V/2.5 Ah [21,36] calculated from data of [66], similar design.
[e]Exide Europe, Type G60 (12 V/60 Ah, L4 container/design is not available in L5 container); from prospectus Exide-Gel, dated 01.06.2000.
[f]VARTA Batteries, 36 V/27 Ah [39], see Section 12.3.6, this Chapter.
[g]Discharge power calculated from specified EN/CCA current, multiplied by threshold voltage (7.5, V etc.).
[h]Cycle-life calculated as integral throughput of charge for cycles to 20% DoD, until capacity < 50% of initial (unless mentioned otherwise; cycle numbers should not be compared in this case).

VRLA battery, which indicates that further progress towards the required quality in material, processing, and cost is likely to proceed through a sequence of small steps.

The energy throughput, i.e., cycling of the batteries, will certainly gain in importance. The dissolution–precipitation reaction of the lead–acid system, however, remains a significant limitation to both its cycle-life and its recharge performance, especially at low temperatures. In particular, it is noted that:

(i) structural information is lost upon cycling because the morphology of both electrodes changes during operation (which may induce failure modes such as softening, shedding, mossing, dendrite growth, and premature capacity loss [69]);
(ii) the dissolution rate of lead sulfate limits recharge at high rates, especially at low temperatures;
(iii) the sulfuric acid electrolyte is involved in the main reactions, and depletion problems appear at high discharge rates.

These shortcomings hold for all lead–acid batteries, either with flooded or with immobilized electrolytes, and either in prismatic or in spirally wound designs. The VRLA battery design may reduce, but cannot eliminate, the cycle-life handicap. On the other hand, the strengths of the lead–acid system are its excellent high-rate discharge capability, high reliability, and robustness. The low cost in both manufacturing and recycling must be emphasized, as lead–acid batteries are manufactured mainly from a single, low-cost metallic raw material.

Nickel–metal-hydride batteries of both prismatic and cylindrical cell designs are now available for automotive use. In 2003, the fleet of hybrid vehicles with Ni–MH batteries is more than 100,000 world-wide, most of these are in Japan. This can be considered as a significant and reliable fleet test that demonstrates the maturity of this battery system for automotive use [70].

While these hybrid vehicles are operating at voltages of 100–300 V, Ni–MH batteries may also be considered for 42-V PowerNets due to their excellent cycling performance, which is currently more than ten times better than that of the most advanced lead–acid systems. To avoid packaging problems and to facilitate integration into the vehicle, Ni–MH battery prototypes for the 42-V PowerNet have been produced with the standard outer dimensions [39].

Lithium-ion [71–73] and lithium-ion polymer batteries [74] are commodity products in consumer applications, but are not yet ready for use in the harsh automotive environment. Although in an advanced state of development, the batteries are not expected to be ready for mass production for use in automotive applications in the near future. If limitations in calendar life at elevated temperature can be overcome and production costs can be lowered to an acceptable level, the lithium-ion battery may become a serious competitor to both AGM lead–acid and Ni–MH batteries, as the lithium-ion system combines the strengths of both these battery systems.

Supercapacitors [75,76] and fuel cells [77,78] have also been proposed for road vehicles, but are not expected to be widely used in the present decade. As an auxiliary power unit (APU), a fuel cell could replace the alternator for the generation of electrical energy. The motivation for this change would be higher overall efficiency,

which may reach 30–40% in fuel-cell systems. The efficiency chain of the ICE–alternator combination, which strongly depends on speed and load profile, seldom exceeds 20% under optimum conditions and is about 10% on average. Fuel cells will only prove practical, however, if appropriate fuels are available (or reformed from suitable precursors) on-board. Furthermore, a fuel cell cannot make use of regenerative power during braking. For recuperation technology, the energy from the alternator has to be stored somewhere, most probably in a battery.

Changes in vehicle electric system architecture have immediate consequences for the performance profile expected from the battery. More specialized battery designs will be needed. Multiple batteries will be combined to meet demands and battery state detection will help to keep the battery in its best operational window to assure a sufficient power supply for critical components in all vehicle operational conditions.

Above all, cost is the ruling criterion in the automotive industry. Therefore, the lead–acid battery occupies a good position as the likely workhorse for automobiles of the future, especially for those with standard and semi-advanced electrical concepts. The handicaps of the lead–acid system may be overcome by using: (i) dual (and multiple) battery architectures which comprise lead–acid specialty batteries of different designs that are optimized for different purposes; (ii) electronic equipment for the control of energy flow. The VRLA battery concept widens the design range, especially with respect to increased cycle-life and energy throughput. With respect to advanced vehicle electrical systems, the lead–acid battery faces a serious challenge. Standard designs will have a chance of acceptance only in combination with other types of battery in dual- and multi-battery architectures. Redundancy can, however, be provided by any reliable energy-storage system. A combination of a VRLA energy-storage unit with a small Ni–MH battery, designed just for throughput of moderate amounts of energy but very frequently at high power rates, is a very attractive possibility [38,39].

In summary, the VRLA battery will claim a significant portion of the future automotive battery market. Due to cost considerations, conventional designs will also continue to be used. On the other hand, since lead–acid technology is limited in some applications, other electrochemical systems will also gain a share of the market.

References

1. F.-J. Paefgen, M. Lehna, *ATZ Automobiltechnische Zeitschrift*, **99(6)** (1997).
2. H. Wallentowitz, J.-W. Biermann, R. Bady, C. Renner, *VDI Berichte*, **1459** (1999) 49–71 (VDI Verlag, Düsseldorf, Germany, 1999).
3. H. Toshihiro, in: A. Krappel (Ed.) and 30 co-authors, *Kurbelwellenstartergenerator (KSG) — Basis für zukünftige Fahrzeugkonzepte*, 2nd Edition, Expert-Verlag, Renningen-Malmsheim, Germany, 2000, pp. 107–119. (Note, papers were presented at the conferences on *Kurbelwellen-Startergenerator (KSG) — Basis für künftige Fahrzeugkonzepte*, 16–17 June 1999, Munich, Germany, and 19–20 October 1999, Essen, Germany.)
4. R. Erikson, in: A. Krappel (Ed.) and 30 co-authors, *Kurbelwellen-Startergenerator (KSG) — Basis für zukünftige Fahrzeugkonzepte*, 2nd Edition., Expert-Verlag, Renningen-Malmsheim, Germany 2000, pp. 120–133. (Note, papers were presented at the conferences on *Kurbelwellen-Startergenerator (KSG) — Basis für künftige Fahrzeugkonzepte*, 16–17 June 1999, Munich, Germany, and 19–20 October 1999, Essen, Germany.)

5. T. Teratani, K. Kuramochi, S. Nakamura, in: A. Graf (Ed.), *The New Automotive 42-V PowerNet — Preparing for Mass Production*, Expert-Verlag, Renningen-Malmsheim, Germany, 2001, pp. 29–47; *Proceedings of the 2nd International Congress on 42-V PowerNet*, 24–25 April 2001, Ludwigsburg, Germany.
6. J.G. Kassakian, H.C. Wolf, J.M. Miller, J.J. Hurton, *Proc. IEEE Workshop on Power Electronics for Transportation*, Dearborn, MI, USA, October 24–25, 1996, p. 3; and *IEEE Spectrum*, August 1996, p. 22.
7. J. Kassakian, *VDI Berichte*, **1287** (1996) 35–47 (VDI Verlag, Düsseldorf, Germany 1996).
8. J. Kassakian, *VDI Berichte*, **1415** (1998) 21–33 (VDI Verlag, Düsseldorf, Germany 1998).
9. A. Graf (Ed.), *Proceedings of the 1st International Congress 42-V PowerNet: the First Solutions*, 28–29 September 1999, Villach, Austria (organized by Haus der Technik, Essen, Germany).
10. H.-D. Hartmann, in: A. Graf (Ed.), *Proceedings of the 1st International Congress 42-V PowerNet: the first solutions*, 28–29 September 1999, Villach, Austria (organized by Haus der Technik, Essen, Germany).
11. A. Graf (Ed.), *The New Automotive 42-V PowerNet — Preparing for Mass Production*, Expert-Verlag, Renningen-Malmsheim, Germany, 2001; *Proceedings of the 2nd International Congress on 42-V PowerNet*, 24–25 April 2001, Ludwigsburg, Germany (organized by Haus der Technik, Essen, Germany).
12. P. Adamis, R. Miersch, in: H. Schaefer (Ed.) and 32 co-authors, *Integrierter Starter-Generator (ISG)*, Expert-Verlag, Renningen-Malmsheim, Germany, 2001; *Proceedings of the Congress 'Integrated Starter Generator'*, 5–6 December 2000, Munich, Germany (organized by Haus der Technik, Essen, Germany).
13. A. Krappel (Ed.) and 30 co-authors, *Kurbelwellenstartergenerator (KSG) — Basis für zukünftige Fahrzeugkonzepte*, 2nd Edition, Expert-Verlag, Renningen-Malmsheim, Germany, 2000 (Note, the papers were presented at the conferences on *Kurbelwellen-Startergenerator (KSG) — Basis für künftige Fahrzeugkonzepte*, 16–17 June 1999, Munich, Germany, and 19–20 October 1999, Essen, Germany.) (organized by Haus der Technik, Essen, Germany).
14. H. Schaefer (Ed.) and 32 co-authors, *Integrierter Starter-Generator (ISG)*, Expert-Verlag, Renningen-Malmsheim, Germany, 2001; *Proceedings of the Congress 'Integrated Starter Generator'*, 5–6 December 2000, Munich, Germany (organized by Haus der Technik, Essen, Germany).
15. W. Buschhaus, L.R. Brandenburg, R.M. Stuntz, *Proceedings of 15th Electric Vehicle Symposium EVS-15*, 1–3 October 1998, Brussels, Belgium, pp. 3–4.
16. W. Buschhaus, A.K. Jaura, M.A. Tamor, *VDI Berichte* **1459** (1999) 123 (VDI Verlag, Düsseldorf, Germany, 1999).
17. S. Sasaki, *Proceedings of 14th Electric Vehicle Symposium EVS-14*, 15–17 December 1997, Orlando, FL, USA, 1997.
18. G. Killmann, T. Yeagashi, K. Hirose, T. Takaoka, *VDI Berichte*, **1459** (1999) 109–121 (VDI Verlag, Düsseldorf, Germany, 1999).
19. K. Takahashi, H. Yasuda, H. Hasegawa, S. Horie, K. Kanetsuki, *J. Power Sources*, **53** (1995) 137–141.
20. S. Fouache, J.P. Douady, G. Fossati, C. Pascon, *J. Power Sources*, **67** (1997) 15–26.
21. J.R. Pierson, J.P. Zagrodnik, R.T. Johnson, *J. Power Sources*, **67** (1997) 7–14.
22. J. Höcker, G. Richter, *VDI Berichte*, **1418** (1998) 223–239 (VDI Verlag, Düsseldorf, Germany, 1998).
23. D. Berndt, *Maintenance-free Batteries*, John Wiley & Sons, New York, 2nd Edition, 1997.
24. D. Berndt, *J. Power Sources*, **100** (2001) 29–46.
25. R.H. Schallenberg, *Bottled Energy*, American Philosophical Soc., Philadelphia, PA, USA, 1982.
26. R.D. Prengaman, *J. Power Sources*, **95** (2001) 224–233.
27. E. Meissner, *J. Power Sources*, **42** (1993) 103–118.
28. J.R. Pierson, R.T. Johnson, *J. Power Sources*, **42** (1993) 237–246.
29. J.H. Hoover, D.P. Boden, *J. Power Sources*, **33** (1991) 257–273.
30. G. Richter, H.-G. Burghoff, *J. Power Sources*, **53** (1995) 343–350.
31. R. Schoettle, D. Schramm, *VDI Berichte*, **1287** (1996) 295–318 (VDI Verlag, Düsseldorf, Germany, 1996).

32. K. Bolenz, *Aachener Kolloquium Fahrzeug- und Motorentechnik*, *Proceedings of Conference by Aachen Technical University*, Aachen, Germany, October 1991, pp. 667–684.
33. K. Bolenz, W. Schleuter, *Proceedings of SAE 1994 Convergence Conf.*, p. 355.
34. J.M. Miller, D. Goel, D. Kaminski, H.-P. Schoener, T.M. Jahns, *Proceedings of SAE 1998 Convergence Conf.*
35. T. Keim, *2nd Advanced Automotive Battery Conference*, Las Vegas, NV, USA, 4–7 February, 2002.
36. R.G. Gruenstern, J.R. Pierson, R.A. Rizzo, *J. Power Sources*, **95** (2001) 38–42.
37. C. Kuper, E. Nann, *2nd Advanced Automotive Battery Conference*, 4–7 February 2002, Las Vegas, NV, USA, 2002.
38. E. Meissner, G. Richter, *J. Power Sources*, **95** (2001) 13–23.
39. C. Rosenkranz, J. Kuempers, G. Richter, *2nd Advanced Automotive Battery Conference*, 4–7 February 2002, Las Vegas, NV, USA, 2002.
40. R. Schoettle, G. Threin, *VDI Berichte*, **1547** (2000) pp. 449–458 (VDI Verlag, Düsseldorf, Germany, 2000).
41. F. Trinidad, F. Saez, J. Valenciano, *J. Power Sources*, **95** (2001) 24–37.
42. M. Calabek, K. Micka, P. Baca, P. Krivak, L. Sacha, *J. Power Sources*, **78** (1999) 94–98.
43. M. Perrin, H. Döring, K. Ihmels, A. Weiss, E. Vogel, R. Wagner, *J. Power Sources*, **95** (2001) 85–96.
44. M. Calabek, K. Micka, P. Baca, P. Krivak, *J. Power Sources*, **95** (2001) 97–107.
45. A.F. Hollenkamp, K.K. Constanti, M.J. Koop, K. McGregor, *ALABC Project AMC-003. Advanced Lead–Acid Batteries for Electric Vehicles: Examination of Premature Capacity Loss. Final Report: April 1993–March 1995*, Advanced Lead–Acid Battery Consortium, Research Triangle Park, NC, USA, 1995.
46. K.K. Constanti, A.F. Hollenkamp, M.J. Koop, K. McGregor, *J. Power Sources*, **55** (1995) 269–275.
47. A.F. Hollenkamp, R.H. Newnham, *J. Power Sources*, **67** (1997) 27–32.
48. W.A. O'Brien, R.B. Stickel, G.J. May, *J. Power Sources*, **67** (1997) 151–155.
49. M.-L. Soria, *2nd Advanced Automotive Battery Conference*, 4–7 February 2002, Las Vegas, NV, USA, 2002.
50. W. Tajika, *2nd Advanced Automotive Battery Conference*, 4–7 February 2002, Las Vegas, NV, USA, 2002.
51. E. Herzmannseder, J. Zuercher, in: A. Graf (Ed.), *The New Automotive 42-V PowerNet — Preparing for Mass Production*, Expert-Verlag, Renningen-Malmsheim, 2001, pp. 173–185; *Proceedings of the 2nd International Congress on 42-V PowerNet*, 24–25 April 2001, Ludwigsburg, Germany, p. 173.
52. Bosch, *Kraftfahrtechnisches Handbuch*, 23rd Edition, Vieweg, Braunschweig, Germany, 1999.
53. S. Mueller, X. Pfab, *Proceedings of SAE 1998 Convergence Conference*, October 1998.
54. R. Schöttle, H. Bischof, in: A. Krappel (Ed.) and 30 co-authors, *Kurbelwellenstartergenerator (KSG) — Basis für zukünftige Fahrzeugkonzepte*, 2nd Edition, Expert-Verlag, Renningen-Malmsheim, Germany, 2000, pp. 237–256. (Note, the papers were presented at the conferences on *Kurbelwellen-Startergenerator (KSG) — Basis für künftige Fahrzeugkonzepte*, 16–17 June 1999, Munich, Germany, and 19–20 October 1999, Essen, Germany.)
55. E. Meissner, G. Richter, D. Übermeier, *1st International Congress 42-V PowerNet: the first solutions*, 28–29 September 1999, Villach, Austria (organized by Haus der Technik, Essen, Germany).
56. U. Koehler, E. Meissner, G. Richter, *1999 Vehicle Electronics Conference*, 9–10 June 1999, Coventry, UK (organized by ERA Technology, Ltd., Leatherhead, UK).
57. G. Richter, in: H. Schaefer (Ed.) and 32 co-authors, *Integrierter Starter-Generator (ISG)*, Expert-Verlag, Renningen-Malmsheim, Germany, 2001, pp. 213–227.
58. Working Group Standardisation of Forum Bordnetzarchitektur/Vehicle Electric System Architecture Forum; see ref. [59] and www.sci-worx.de. For Forum Bordnetzarchitektur, see K. Ehlers, *VDI Berichte*, **1287** (1996) 203–218 (VDI-Verlag, Düsseldorf, Germany, 1996).
59. K. Ehlers, H.-D. Hartmann, E. Meissner, *J. Power Sources*, **95** (2001) 43–57.
60. G. Richter, E. Meissner, in: A. Krappel (Ed.) and 30 co-authors, *Kurbelwellenstartergenerator (KSG) — Basis für zukünftige Fahrzeugkonzepte*, 2nd Edition, Expert-Verlag, Renningen-Malmsheim, Germany, 2000, pp. 167–193. (Note, papers were presented at the conferences on *Kurbelwellen-Startergenerator (KSG) — Basis für künftige Fahrzeugkonzepte*, 16–17 June 1999, Munich, Germany, and 19–20 October 1999, Essen, Germany.)

61. U. Koehler, M. Ullrich, *Proceedings of 16th Electric Vehicle Symposium EVS-16*, Beijing, China, 13–16 October, 1999.
62. U. Koehler, J. Kuempers, E. Meissner, *1st Annual Advanced Automotive Battery Conference*, 5–8 February 2001, Las Vegas, NV, USA, 2001.
63. U. Koehler, J. Kuempers, M. Ullrich, *J. Power Sources*, **105** (2002) 139–144.
64. J.P. Douady, C. Pascon, A. Dugast, G. Fossati, *J. Power Sources*, **53** (1995) 367–375.
65. A.-M. Kreipp, M. Zuber, P. Duba, Q. Sterner, *42 V Systems and Development by Simulation*, in: A. Graf (Ed.), *The New Automotive 42-V PowerNet — Preparing for Mass Production*, Expert-Verlag, Renningen-Malmsheim, Germany, 2001, pp. 1–28; and A.-M. Kreipp, E. Lodowicks, R. Regler, M. Zuber, *VDI Berichte*, **1646** (2001) 495–498 (VDI Verlag, Düsseldorf, Germany, 2001).
66. R.C. Bhardwaj, *J. Power Sources*, **78** (1999) 130–138.
67. R. Friedrich, G. Richter, *J. Power Sources*, **78** (1999) 4–11.
68. T. Juergens, R.F. Nelson, *J. Power Sources*, **53** (1995) 201–205.
69. E. Meissner, *J. Power Sources*, **78** (1999) 99–114.
70. A. Taniguchi, N. Fujioka, M. Ikoma, A. Ohta, *J. Power Sources*, **100** (2001) 117–124.
71. J. Kuempers, *Proceedings of 18th Electric Vehicle Symposium EVS-18*, 20–24 October 2001, Berlin, Germany, 2001.
72. L. D'Ussel, G. Chagnon, C. Chanson, *Proceedings of Electric Vehicle Symposium EVS-18*, 20–24 October, Berlin, Germany, 2001.
73. N. Terada, T. Yanagi, S. Arai, M. Yoshikawa, K. Ohta, N. Nakajima, A. Yanai, N. Arai, *J. Power Sources*, **100** (2001) 80–92.
74. B. Scrosati, F. Croce, S. Panero, *J. Power Sources*, **100** (2001) 93–100.
75. Y. Matsuda, B. Barnett (Eds.), *Advanced Capacitors Part I: Japan*, *J. Power Sources*, **60** (1996) 137–253.
76. A. Burke, *J. Power Sources*, **91** (2000) 37–50; and *1st Annual Advanced Automotive Battery Conference*, 5–8 February 2001, Las Vegas, NV, USA, 2001.
77. J.M. Ogden, M.M. Steinbugler, T.G. Kreutz, *J. Power Sources*, **79** (1999) 143–168.
78. D.G. Lovering (Ed.), *Proceedings of the Sixth Grove Fuel Cell Symposium*, 13–16 September 1999, London, UK; *J. Power Sources*, **86** (2000) 1–577.

This page intentionally left blank

Valve-Regulated Lead–Acid Batteries
D.A.J. Rand et al., editors

—CHAPTER 13—

VALVE-REGULATED LEAD–ACID BATTERIES FOR TELECOMMUNICATIONS AND UPS APPLICATIONS

R. Wagner

13.1. Introduction

Lead–acid batteries have been used for more than 130 years in many different applications including automotive and various traction duties and also telecommunication systems and uninterruptible power supplies (UPS). The last two groups constitute the major part of the so-called stationary battery sector, and the lead–acid battery has proved to be a very reliable system for these applications.

Although the lead–acid battery has a relatively low specific energy in comparison with alternative electrochemical storage systems, it remains the world's most important secondary power source. This is due to the fact that it is not sufficient to consider specific energy alone. In the final analysis, it is the combination of specific energy, life, and cost that is usually decisive in battery selection for industrial use. Further, attributes such as specific power, reliability, availability of raw materials, and the possibility of recycling are also important. Taking all these factors into consideration, the lead–acid battery provides a good compromise and, therefore, is expected to remain the most important electrochemical storage system for a long time. This is especially true for stationary applications where the high weight of lead is not so important. For such applications, the volumetric energy density has a higher priority than gravimetric energy density (specific energy) and, therefore, the lead–acid battery is a suitable choice.

This chapter provides an overview of stationary battery applications and presents the different battery types that are currently used, focusing especially on valve-regulated designs. Batteries with capacities of up to about 200 Ah usually have flat positive plates; for higher capacities, tubular designs are also used.

Lead–acid batteries were first used in stationary, stand-by applications more than 130 years ago [1]. For a long period of time, only flooded lead–acid batteries were used. Nowadays, UPS and telecommunications applications use valve-regulated batteries. Large, utility-scale applications such as load levelling continue to use flooded batteries, but it seems that, increasingly, valve-regulated batteries are chosen even for these applications.

During stand-by service, the battery should be maintained in a completely charged state by applying a float voltage that is slightly higher than the battery open-circuit

voltage and that provides the energy for all the side reactions in the battery. These reactions are, in general, grid corrosion and oxygen evolution on the positive plate and hydrogen evolution and, in the case of valve-regulated batteries, recombination of oxygen at the negative plate. The choice of the optimum float voltage at different temperatures is an important factor in maintaining valve-regulated lead–acid batteries in a healthy state. This issue is discussed further in a subsequent section.

13.2. Features of VRLA Technology

Among the many advances in lead–acid battery technology, (e.g., increases in energy density and cycle-life, reductions of self-discharge, automation of manufacture leading to reduced production costs, etc.), the development and introduction of the gas-recombination technology is probably one of the most important. These gas-recombinant batteries, i.e., valve-regulated lead–acid (VRLA) batteries, make possible the use of lead–acid batteries in applications where flooded batteries cannot be used due to risk of acid spillage.

There are additional advantages with recombination batteries. For example, topping up with water is not necessary over the whole life of the battery, and the battery can be designed to survive a 30-day short-circuit test and, after recharge, have virtually the same capacity as before the test. Due to a marked reduction in water decomposition, there is only a small release of hydrogen gas and a low rate of self-discharge. Many studies of VRLA batteries have been published in recent years; some examples are given as Refs. [2–14] (see also Chapter 1).

In VRLA batteries, the electrolyte is immobilised by an absorptive glass-mat (AGM batteries) or by a gelling agent (gel batteries). Immobilization of the electrolyte makes the recombination process possible; oxygen produced at the positive plate, especially during charging, can migrate to the negative plate where it reacts (recombines) to form water (see Chapter 1). As this reaction reduces the amount of hydrogen gas evolved at the negative plate, there is a marked reduction in the amounts of hydrogen and oxygen that leave the cell. Nevertheless, the amount of gas released is not exactly zero and the term ‘sealed battery’, which is sometimes used, should not lead to the assumption that there is no gas release at all.

The two technologies, gel and AGM, have many similarities, but there are also some differences. For example, it is well known that for tall cells in a vertical position, only gel cells can be used; otherwise, acid stratification cannot be avoided. There are some fairly tall AGM cells on the market, but these are intended for use only in a horizontal position in order to avoid the acid stratification problem. For short cells, both gel and AGM designs are possible without restriction on cell orientation. Often, AGM is used when high power is requested whereas gel is especially useful to achieve a long lifetime.

13.2.1 Positive-grid corrosion

In general, VRLA batteries use lead alloys that are virtually free of antimony. This is because antimony is released from the positive grid by corrosion and migrates to the

negative plate where it lowers the hydrogen overvoltage. As a result, there is an increase in hydrogen evolution and, consequently, higher self-discharge and more water loss.

Nowadays, most battery manufacturers prefer to use lead–calcium alloys. Calcium acts as a grid-hardening agent. There is also some tin (up to 1%, sometimes more) in the alloy. This improves the casting process and helps to avoid problems at the grid/active-material interface of the positive plate (see Chapter 2).

There is a substantial difference between the corrosion behaviour of lead–calcium–tin and lead–antimony alloys. Tests reveal that antimony-containing alloys generally exhibits a higher corrosion rate, and that the rate decreases with decreasing antimony content. This type of corrosion, which is typical for antimony alloys, is an intragranular process with a quite regular corrosion front over the whole area. In the case of lead–calcium alloys, well-cast samples undergo low corrosion rates, but, if the grids are not properly cast, there can be heavy intergranular corrosion. This type of corrosion is not uniform but penetrates deeply into some parts of the grid and causes tremendous grid growth.

As positive grid corrosion is an important influence on the expected lifetime of standby batteries, there have been many investigations of the parameters that influence the corrosion rate. It has been established that many parameters influence grid corrosion and growth. The most important are: (i) alloy composition; (ii) grid design; (iii) casting conditions; (iv) positive active material; (v) impurities that accelerate corrosion; (vi) battery temperature; and (vii) potential of the positive plate.

Many investigations have been made of the influence of alloy composition on the corrosion stability of positive grids in VRLA batteries [15–26]. In practice, it has been found that lowering the calcium content reduces the corrosion rate. Unfortunately, since a lower calcium content results in slower grid hardening, a compromise is often necessary. A calcium content is used that is sufficiently high to allow handling of the grids during plate processing but sufficiently low (in general, markedly below 0.1%) to avoid severe corrosion. In general, this compromise imposes a rather small acceptable range of calcium content.

Of course, the influence of the other variables mentioned above has also to be taken into consideration. It turns out that a relatively high calcium content (up to about 0.09%) can be tolerated if all other conditions are favourable. Conversely, unfavourable variables (items (ii) to (vii) above) can cause high corrosion rates even with a much lower calcium content.

The influence of grid design on the casting process and on corrosion behaviour is often underestimated. Particularly for applications where high discharge currents are needed, there has been a tendency to modify the grid structure so as to reduce its electrical resistance. The necessary calculations can be performed quite readily (and with high accuracy) using computers, and the results are grid-structure designs with markedly reduced electrical resistance. Unfortunately, it is not as easy to cast grids to have a minimal electrical resistance, and attempts to do this can result in higher corrosion rates. Therefore, changes in the grid structure have to be performed carefully with due consideration of possible casting and corrosion problems.

The casting process involves many variables that influence the quality of the grids and, therefore, the corrosion behaviour. These variables include for example, the

grid/mould design, the temperature of the pot of molten alloy and the mould, the speed of casting, the cooling rate, and the pressure in the case of pressure casting. In general, pressure casting is used for tubular plates and, provided that all other variables are reasonably favourable, produces lead–calcium–tin grids with very low corrosion rates. Even after several years in use, the spines of grids produced in this way exhibit only a very thin corrosion layer. Corrosion of lead–calcium–tin tubular grids has seldom been the cause of the failure of VRLA batteries.

Gravity casting of grids is usually employed for the manufacture of flat positive plates. Flat positive lead–calcium–tin grids are more sensitive and more prone to corrosion than tubular grids. Nevertheless, it must be pointed out that even for batteries with flat positive plates, corrosion has been only one of the limiting factors during standby applications.

An example of the influence of alloy composition and casting conditions on grid corrosion is given in Fig. 13.1. During this accelerated corrosion test of gravity-cast, lead–calcium–tin grids in sulfuric acid (60°C, 1.26 specific gravity, 1.85 V constant potential against SHE), the grids were taken out of the electrolyte every 3 weeks. They were washed and dried without removal of the corrosion layer, and their weight was determined. In all experiments, there were small increases in weight during the first weeks due to the oxidation of some of the grid material. The decreases in weight during the latter weeks of the tests can be explained by the shedding of oxidised material during the progressive oxidation.

Normally, good corrosion stability gives only a small increase of weight in the beginning of cycling, and shedding starts quite late, whereas poor corrosion stability gives a higher increase of weight in the beginning followed by a more rapid decrease of weight due to shedding. It can be seen from Fig. 13.1 that an improvement of the alloy with respect to calcium and tin contents gives a slightly better corrosion stability, but the influence of casting conditions is more pronounced.

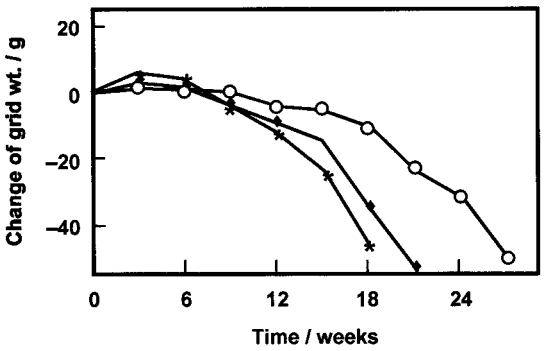

Fig. 13.1. Accelerated corrosion test of gravity-cast, lead–calcium–tin grids in sulfuric acid (60°C, 1.26 specific gravity, 1.85 V constant potential against SHE). Change of grid weight measured every 3 weeks without removal of corrosion layer: (*) standard alloy/standard casting; (△) improved (in terms of calcium and tin content) alloy/standard casting; (○) improved (in terms of calcium and tin content) alloy/improved casting.

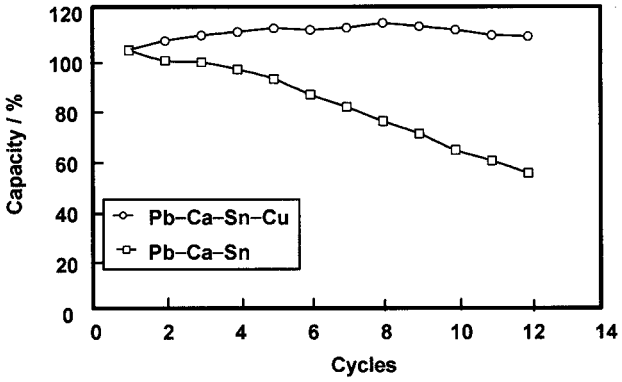

Fig. 13.2. Accelerated overcharge test of gel batteries (A400 type) with and without copper as a grain refiner for the positive alloy.

The addition of copper as a grain-refining material can improve markedly the corrosion resistance of the positive grids. Figure 13.2 gives the results of an accelerated test on gel, A400 monobloc batteries by overcharge with 2.40 V per cell at 45°C. The battery without grain refiner had a marked capacity loss after 12 test cycles, and a tear-down analysis showed significant positive grid corrosion. Conversely, the battery with copper addition to the positive alloy behaved much better, with capacity stable and still above 100% after 12 test cycles. Tear down analysis of this battery showed a much lower corrosion rate.

It is not easy to understand completely the influence of the positive active mass on grid corrosion, although much has been published about this subject [27–30]. There must be an influence, however, because the results of corrosion tests are different for bare and pasted grids. The influence of the mass may be due to an increase in the pH near the grid surface at the end of discharge, which is due, in turn, to a limited diffusion capability of the electrolyte in the pores of the mass. Another factor may be the stress on the grid due to volume changes of the mass during charge and discharge. It must also be considered that some parts of the grid are in very close contact with the mass such that no electrolyte can reach these parts. The active mass can accelerate or slow down grid corrosion, but in either case it must not be ignored. Thus, the results of corrosion tests with well-prepared lead samples in the laboratory can be quite different from the results obtained with batteries.

Impurities that accelerate the grid corrosion rate (e.g., organic acids or chlorine components) are well known, and there is, in general, no difference between the behaviour witnessed in flooded cells and in valve-regulated cells. Normally, impurities can be excluded rather easily. By comparison with flooded cells, valve-regulated cells have the advantage that topping up of water is not required and, therefore, impurities cannot be introduced into the cell during use. Battery manufacturers, of course, must be careful to avoid introducing contamination or impurities during fabrication. This is important because of accelerated corrosion of grids and because there is a marked influence of some impurities on both self-discharge and hydrogen evolution.

The features discussed so far are, in general, the responsibility of the battery manufacturer. Beyond these, incorrect use or abuse of valve-regulated batteries is also an important determinant of grid corrosion. The most pertinent factors are temperature and charging voltage or, more correctly, the potential of the positive plate. The influence of temperature is often described by the general rule that a higher temperature results in a higher corrosion rate. This is valid for both flooded and VRLA batteries. For standby service, the expected lifetime is often specified for a temperature of 20°C, which implies a recommendation to keep the battery around 20°C in order to obtain maximum endurance.

Although reasonably self-evident, it is emphasised here that battery temperature and not the temperature of the environment is the relevant factor. If battery temperatures appreciably above 20°C cannot be avoided, then it is necessary to adjust the charging voltage, according to the instructions of the battery manufacturer, in order to avoid a serious reduction in service-life. Regulation of charging voltage may also be necessary if the battery temperature is appreciably below 20°C.

A typical malpractice is to place batteries as close together as possible in order to save space. As batteries produce some heat, even on float, tight packing of batteries can produce a situation whereby the heat emission (a combination of heat radiation and heat transportation by air convection around the battery) is smaller than the heat produced so that the battery temperature increases (see Chapter 1). Ignoring the heat produced by batteries can give a marked reduction in service-life due to accelerated grid corrosion, even if the temperature does not reach a level such that drying out or thermal runaway takes place. Although this is also valid for flooded cells, the situation described can be more dangerous for valve-regulated batteries because, during float, nearly all the electrical energy input is used for the oxygen recombination process and is completely transformed into heat.

The influence of charging voltage on the corrosion behaviour of positive grids has been reported widely. A discussion about the special situation in valve-regulated batteries can be found in [6,31–33]. The corrosion rate does not depend only on the charging voltage but also on the oxygen recombination efficiency. The latter influences the charging current and, therefore, the potential of the positive plate, which is the determining factor for corrosion.

The polarization of the positive electrode at different cell voltages for flooded, gel, and AGM cells is shown in Fig. 13.3. For a flooded cell, it is assumed that the overvoltage of the positive and the negative plate is nearly the same. In the case of gel and AGM cells, one example is given of a high and one of a low oxygen recombination efficiency. It is emphasised that this is only a schematic representation of the behaviour. In reality, the situation may be more complicated [6]. Adapting the charging voltage to acid density, and vice versa, is very important [33].

13.2.2 Improvement of service-life

Drying out is mostly connected with a too severe charging regime, often in combination with high cell temperature. The best way to circumvent this problem

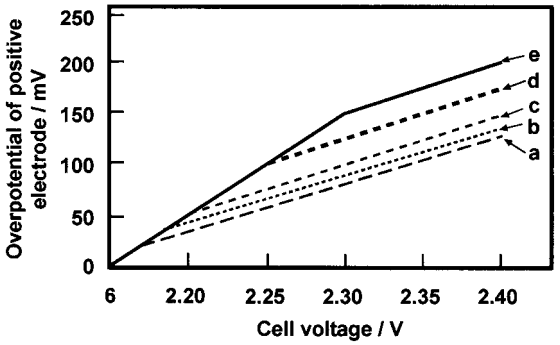

Fig. 13.3. Schematic of positive electrode polarization of flooded, gel, and AGM cells (assumed specific gravity: 1.30). (a) flooded cell; (b) gel, new cell; (c) AGM, low recombination efficiency; (d) gel, after prolonged periods of use; (e) AGM, high recombination efficiency.

is to prevent extreme situations in battery operation. This means, for example, the avoidance of charging at a too high rate, especially after deep discharge and at high battery temperatures. In cases where very high temperatures are a potential threat, the use of special cooling systems might be required. In general, drying out reduces the capacity of the cell and, finally, limits its life. Drying out also increases the oxygen recombination efficiency, and this can be a severe problem in UPS applications where excessive recombination efficiency can increase the temperature of the battery dramatically. The so-called 'thermal runaway' effect, which can be exhibited by VRLA batteries in UPS service, arises as a consequence of these phenomena.

The best way to avoid dry out and runaway is to remember that, during float charging, the battery produces some heat and, therefore, avoid packing batteries closely together. It is much better to provide a spacing of at least 10 mm between adjacent batteries. Keeping batteries at such a distance normally allows an effective dissipation of the heat.

As discussed in more detail below, a high charging voltage is helpful for reducing charging time and avoiding sulfation. Nevertheless, it must be remembered that, under this condition, a higher current flows through the cell, which promotes the risk of thermal runaway and dry out. Therefore, a higher charging voltage should only be allowed for a restricted period after discharge. A charger that automatically reduces the charging voltage to the float voltage after a given period of time would be an appropriate way to circumvent this problem.

The best way to avoid thermal runaway is to monitor battery temperature and to change the float voltage or current automatically, according to the measured temperature. It is strongly recommended that the measured battery temperature and not the room temperature be used for controlling the float voltage or the float current. In the case of AGM batteries, it is also important to have good control of the degree of saturation of the separator. It is well known that too low a level of saturation will result in a very high oxygen recombination efficiency and in high currents, even at quite moderate float voltages.

The fact that, with the same float voltage, quite dissimilar currents can flow through an AGM cell, as determined by the oxygen recombination efficiency, has been discussed previously [6]. The situation in a gel battery is different at the beginning of life when the recombination efficiency is always rather low. After some water loss, however, the recombination efficiency in these batteries will increase also. If too much water is lost (dry out), the recombination efficiency of gel batteries can be quite high.

Papers published over the past few years have described the benefits of gas recombination catalysts in VRLA cells [34–36]. The insertion of a catalyst into the headspace of a cell can assist the combination of a significant amount of hydrogen that would otherwise escape and constitute water loss. It is claimed that such catalysts not only reduce water loss but can also balance float charging of VRLA batteries. There remains some uncertainty, however, about the reliability and service-life of such catalysts.

A pressure-release valve with a high opening pressure could be helpful in reducing water loss, but the benefit of such a device is not sufficient to offset other problems that must be faced with high pressures in the cell. In general, a pressure between 100 and 200 mbar seems to be a good compromise to avoid excessive loss of water. Problems with negative plates can arise when the pressure release valve does not close correctly after opening. Oxygen can then enter the cell, and this causes oxidation of the negative mass, which is manifested as sulfation of the negative plate during storage of the battery. Failure of the valve to close properly can also contribute to the risk of dry out during battery use.

Another important factor affecting service-life is the choice of technique for welding and cast-on-strap (COS) operations. It is well known that welding of lead–calcium alloys is not an easy task and, therefore, special techniques have to be used to obtain a good bond between the lug and the top bar. If COS is used, good cleaning of the surface of the lug (i.e., a proper fluxing process) is necessary to achieve a good bond. This precaution is important for both positive and negative plate groups. In order to avoid any problem of corrosive attack in the lug/top-bar region of the negative plate, it is advisable to avoid the use of antimony, as this metal is particularly deleterious in this critical area.

A short circuit inside the battery virtually always results in a failure. Formerly, there were sometimes short-circuits through the separator from the growth of lead needles, especially if the battery had been deep-discharged. Nowadays, this is no longer a severe problem, because the addition of special ingredients to the electrolyte (in general, sulfate salts), effectively prevent the growth of lead needles and there is no longer any risk of a short-circuit through the separator.

In order to increase volumetric energy density, plate dimensions have been progressively extended. Often, the plates are standing directly on the bottom of the case, because a ‘mud space’ is no longer needed in valve-regulated batteries. If glass-mats are used as single sheets, there is always a latent danger of short-circuits at the bottom of the cell. Enveloping at least one of the two polarities of the plate (either the positives or the negatives) by glass-mats is a good way to circumvent this problem. In cases where the plate dimensions have been extended to extreme values, the dimensions of the glass-mats may not exceed by much those of the plates and,

during assembly of the cell, the glass-mats have to be positioned quite carefully in order to avoid short-circuits at the sides or the tops of the plates.

The behaviour of valve-regulated batteries during float operation is influenced by many parameters and is rather complex [14]. A mathematical model has been developed [37] that describes the effects of kinetic cell parameters, float voltage/current, and temperature on electrode potentials and rates of electrode reactions. In flooded batteries, the main side reactions are grid corrosion and oxygen evolution on the positive side and hydrogen evolution on the negative side. In valve-regulated batteries, the recombination process, i.e., oxygen reduction at the negative plate, must also be considered. The mathematical model, in combination with experimentation, has shown clearly that discharge of the active material can occur under unfavourable conditions during float duty.

When recombination efficiency is high, oxygen evolution will be virtually balanced by oxygen reduction, and it follows that the hydrogen evolution current at the negative plate must be approximately equal to the grid corrosion current at the positive plate in order to avoid any discharge of the electrodes. If the grid corrosion rate is too high in comparison with the hydrogen evolution rate, the positive plate will be slowly discharged, resulting in some sulfation of the positive plate. On the other hand, if the hydrogen evolution rate is too high in comparison with the grid corrosion, the negative plate will be slowly discharged and sulfated. Therefore, the choice of a proper float voltage and the right temperature compensation has a significant influence on maintaining the positive and negative plates in a completely charged state. In particular, too high a reduction of float voltage at higher temperature can result in sulfation problems of the battery.

An improved temperature compensation of the float-charge voltage for gel batteries has recently been proposed [38]. Important elements of this scheme are that, in comparison with past practice, the float voltage is reduced less at higher temperatures, and there is a range of temperatures within which no compensation of the float voltage is necessary. For a type A400, gel battery, Fig. 13.4 shows how the float and equalisation-charge voltages should be changed for different

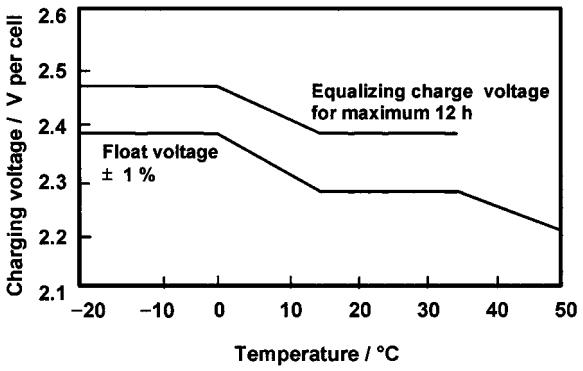

Fig. 13.4. Float and equalisation charge voltages at different temperatures for type A400, gel batteries.

temperatures. The equalisation charge is used to bring all the cells of a string to a complete state-of-charge. This higher voltage charge, however, should be limited to a period of no more than 12 h.

In some cases, AGM batteries used under float operation suffer from sulfation of the negative plate. It has been established that, in order to avoid sulfation of the negative plates, impurities that reduce the hydrogen overvoltage at the negative plate must be kept to a sufficiently low level [39]. The worst situation with regard to the health of the negative plate is a very corrosion-resistant positive grid and a high concentration of deleterious impurities in the battery.

Float operation with an occasional discharge is the standard service of standby batteries. In some cases, however, the application includes more discharges than usual, and this means that some cycling performance is also needed. The result of an 80% DoD cycle test with 6-V, 240-Ah gel batteries is shown in Fig. 13.5. Every 50 cycles there was a capacity test. It can be seen that there is a rather long time period where the capacity is rather stable around 100%. After about 600 cycles the capacity decreased steadily, reaching the 80% level after 800 cycles. This result is typical for gel batteries with flat positive plates. In general, gel batteries have a rather good cycle-life.

The cycle performance of AGM batteries has been improved significantly in recent years [7,11]. At the beginning of the development of AGM batteries for cycling applications, there were severe problems with acid stratification. By improving the design of such batteries, it has become possible to avoid the acid stratification phenomenon almost completely. A key factor was to impose a sufficiently high stack pressure and to choose the right degree of saturation of the separator. For tall-plate AGM designs, however, acid stratification can only be overcome by placing the cells in a horizontal position.

Some decades ago, when lead–acid batteries with positive lead–calcium grids without antimony were first placed on the market, there was a major disaster in terms of very poor cycle-life. Investigation of the phenomenon revealed that the cause of the failure was the formation of a barrier layer of lead sulfate between the

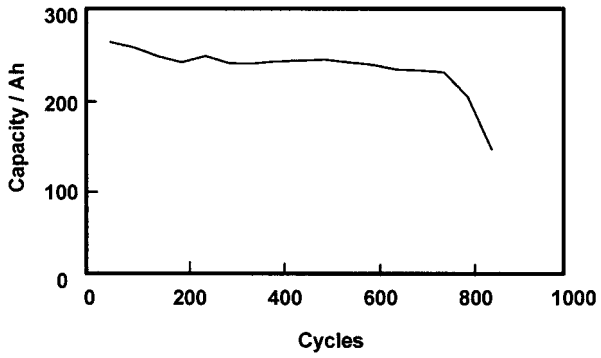

Fig. 13.5. Cycle test (cycling to 80% DoD) with a 6-V, 240-Ah gel battery. Capacity test every 50 cycles.

positive grid and the active material. Since this occurred more easily when antimony was excluded from the battery, it was called the 'antimony-free effect'. Following this unfortunate experience with the early lead–calcium batteries, the antimony-free effect and the influence of grid alloy composition on the behaviour of the positive plate during charging and discharging has been the subject of many investigations and much research activity [40–46] (see also Chapters 1 and 2).

An important result of these studies was the discovery that a lack of antimony has not only an effect on the grid/positive-material interface, but also on the whole crystalline structure of the positive active mass [43] and on the so-called mass softening process. Nowadays deleterious effects that are promoted by using grids without antimony are collectively termed 'premature capacity loss' (PCL). There has been much research effort worldwide to overcome the PCL problem [47].

It appears that softening of the positive material is a more severe problem than the development of barrier layers. As a result of much research activity (e.g., improvement of the curing process, the paste formulation and the alloy composition, especially the tin content and the use of additives), it seems that barrier layers no longer have a marked effect on the life of valve-regulated batteries, even when the battery is used for applications which include some cycling. This finding conflicts with the original idea that lead–acid batteries without antimony fail principally through the formation of lead sulfate barrier layers at the positive grid/mass interface.

Softening of the positive material can easily be distinguished from sulfation, as the former failure does not produce any reduction of acid density in the cell. This is because the soft mass consists predominantly of lead dioxide, and the content of lead sulfate is generally quite low. Softening of the mass occurs because PbO_2 particles lose contact with each other, so that parts of the active mass become electrically isolated and cannot participate any longer in the discharge process. Therefore, batteries with softening of the positive mass have the nominal open-circuit voltage (OCV), but a lower available capacity. Softening always starts from the outer part of the plate and subsequently progresses into the inner parts as the number of cycles increases. It has been shown that the decrease in capacity during the latter stages of cycling is directly associated with increasing amounts of softened material [7].

The cause of softening of the positive mass has been the subject of many investigations during the last few years. In some papers, the so-called 'Kugelhaufen' theory has been formulated to provide an explanation for the degradation of the positive mass [43,48–51]. This theory uses a model in which the positive active mass is considered to be a network of agglomerates of spherical particles with narrow contact zones. It would appear that this is a good approach towards describing the changes in the crystalline structure of the positive mass that take place during charge and discharge. For a complete understanding of the softening phenomenon, however, there might be the problem that, in reality, the active mass consists not only of spherical particles with smooth surfaces, but there is also a marked microstructure on the surface of the particles and much of the material can take the form of needle-shaped crystallites.

A second theory considers the active mass to be a mixture of crystalline parts and gel parts [45,52,53] (see also Chapter 3). It is assumed that there is a significant

portion of hydrogen in the mass of the gel zones and that changes in these gel zones during cycling could be the cause of the loss in contact between the particles of lead dioxide. The influence of hydrated zones and of the so-called X-ray 'amorphous' material on the behaviour of the positive active mass during cycling has been discussed [54–58] (see also Chapter 3). Recently there was a detailed investigation of the change of the microstructure of lead dioxide during charge–discharge cycling [59].

Although both theories allow a better understanding of the degradation of the positive active mass during cycling, even today it is not completely clear which parameters are the most important in avoiding softening, or at least in slowing down the softening process. Often it is found that softening is promoted by high discharge rates, but the effect sometimes happens even when rather small discharge currents are used. In general, however, it is true that high discharge pulses accelerate the softening process. There are several parameters that strongly influence the speed of softening. These parameters include the design of the battery, the plate processing, the type of application, and the charging regime. There have recently been studies of the influence of different charge regimes [49,50] (see Chapter 9). The influence of paste density and processing, focusing especially on curing and formation, has also been investigated in detail [60,61].

Sulfation of the positive mass is often caused by a charging regime that does not match well the application of the battery. There are some battery applications that require a duty that is intermediate between standby service, with only a few discharges during the whole life of the battery, and a cycling duty with an extensive discharge nearly every day. Often there is only a small margin between overcharging, which results in water loss and eventual dry out, and undercharging which produces sulfation of the positive mass [6–8].

The operational characteristics of valve-regulated batteries configured in parallel strings have been studied. Data, presented recently, have shown that parallel-configured battery strings can be satisfactorily operated under a wide range of discharge and recharge conditions [62]. Parallel strings share the current required by the load on discharge and recover the energy delivered on recharge in proportion to the nominal capacity available in each of the battery strings.

13.3. Gel Batteries

Gelling is another way to immobilise the electrolyte (see also Chapters 6 and 7). The gelling agent is, in general, a silica with a very high surface area of $200\,m^2\,g^{-1}$ or more. The primary particles are extremely small but, in the cell, they form a three-dimensional network structure. The gel structure and the different stages of the gelling process are illustrated in Fig. 13.6. Before filling, the gel is a highly dispersed mixture of electrolyte with silica, and it is possible to maintain it at a low level of viscosity by stirring with a suitable agitator. The primary particles, which had already been transformed into small aggregates during the production of the silica, form agglomerated aggregates, but the mixture still behaves as a liquid system, which can be filled into the cell quite easily. Afterwards, when there is no longer any

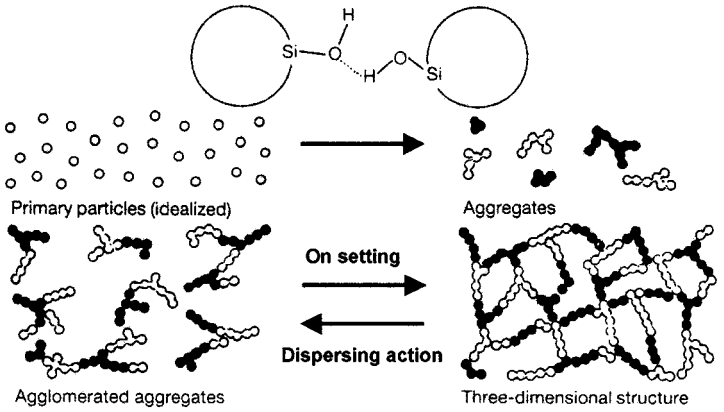

Fig. 13.6. Illustration of gel-structure development.

dispersing action, the silica forms a three-dimensional structure, and the mixture stiffens to form a firm gel. A more detailed discussion about the silica structure and the gel ageing effects is given in Ref. [63].

It is an important feature of this gel structure that acid stratification can be avoided even in the case of large cells with tall plates standing in the vertical position. Acid stratification is a well-known problem for flooded batteries where either some overcharge, resulting in strong gassing, or an electrolyte agitation system must be used to re-mix the electrolyte. Gel batteries do not suffer from acid stratification to any significant degree.

For gel batteries, both tubular and flat positive plates are used. Gel cells with tall plates often have the tubular positives design although there are some with flat positives. Gel cells with small plates, in general, have flat positives, however, a few exceptions will have tubular positives. In comparison with the AGM design, gel batteries have a markedly higher internal electric resistance. This is a clear disadvantage for all high-power applications.

The advantages of the gel design are that it provides a very long service-life and has an extremely high reliability, even under extreme conditions (for example, higher temperatures or deep discharge periods). Another advantage is that gel batteries can be stored for a rather long time (up to two years) at room temperature without any charging. This is due to the very low rate of self-discharge and to the excellent recharge behaviour. It is well known that, normally, recharging batteries after two years storage is rather difficult; with gel batteries, this is not a problem.

Gel batteries are sometimes produced with phosphoric acid added to the electrolyte and sometimes without. Phosphoric acid is not generally used for standby applications; it is mainly used for applications, which includes some cycling. Investigations of the effect of phosphoric acid, especially with regard to an improvement in cycle-life, can be found in the literature [64–70]. According to the results of these investigations, there is an adsorption of phosphoric acid on to the lead dioxide surface, which modifies crystal growth. It has also been pointed out that

phosphoric acid hinders the formation of an insulating film between the positive active mass and the grid.

The most important application of gel technology is in the telecommunications market. As already discussed, this is mainly due to the very high reliability of gel batteries. Also, the float current of gel batteries is, in general, relatively low and does not increase too much with temperature, which is very helpful for avoiding the risk of a thermal runaway. Gel batteries are also used when the standby operation includes a significant amount of discharge–recharge cycling.

Sonnenschein was the first company to introduce gel battery technology to the market successfully. They started in 1958 with rather small batteries for flashlights. Since that time, this technology has steadily replaced the conventional, flooded lead–acid battery in various applications [38,71,72]. Phosphoric acid addition for cycling was first introduced in 1965. Larger gel batteries with tubular positive plates were developed for stationary applications in 1978. More recently, gel batteries have been produced for starter and traction applications, and thick, flat positive plates were added for telecommunications applications.

Gel batteries with higher capacities normally have tubular plates. For such batteries, the capacity range is generally between 200 and 3000 Ah. A special characteristic of these batteries is extremely high reliability and very long service-life. Kramm and Kretzschmar [71,73] investigated the use of such gel batteries for standby applications, and especially for the influence of temperature and charge voltage on the endurance of the batteries. The results of these investigations show clearly that a remarkably long life can be achieved with standard gel batteries of the OPzV design (lead negative grid). The expected life of one type of gel battery during float operation is shown as a function of temperature in Fig. 13.7. As this type of battery has been on the market for some decades, there is much experience available from the field proving that the real service-life at around 20°C is between 15 and 18 years.

Since the electrolyte is immobilised as a gel, the cells can also be placed in the horizontal position without any risk of acid leakage. A 48-V, 1000-Ah, lead–acid battery with gel cells, positioned horizontally for a telecommunications application, is shown in Fig. 13.8.

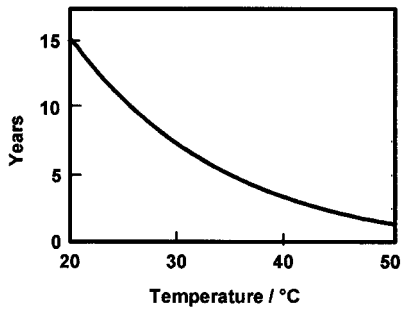

Fig. 13.7. Life of stationary, gel batteries (OPzV (A600) type) during float operation at different temperatures.

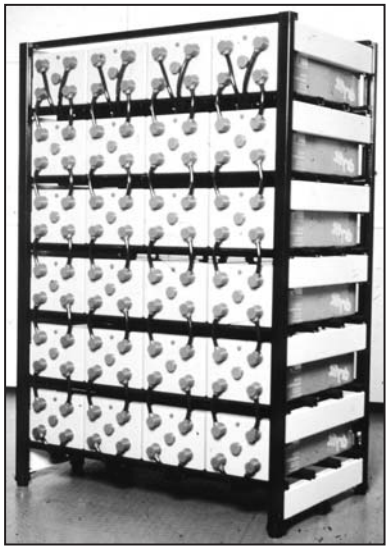

Fig. 13.8. Stationary, 48-V, 1000-Ah battery with OPzV, A600-type gel cells for telecommunications application in a horizontal position.

Gel batteries are also produced in 6-V and 12-V monoblocs with capacities between 5 and 180 Ah. These are also mainly used for telecommunications applications. They have flat positive plates, and provide a service-life of more than 12 years. The results of an accelerated life test of 12-V, 16-Ah batteries at 40°C and a float voltage of 2.22-V per cell are shown in Fig. 13.9. It can be seen that the capacity decreased below the 80% level after about 35 months and reached 50% after about 40 months. This equates to an expected life of more than 12 years at 20°C. The influence of discharge rate and temperature on the available capacity is shown in Fig. 13.10. Most of the applications of this battery-type require discharge currents between 1 and 4 times the 10-h discharge rate. Therefore, this battery-type has been optimized to a high energy density for discharge times between 10 and 2 h.

There are some applications where, after a discharge, only a short time interval is available to bring the battery back to a relatively high state-of-charge. It is well known that lead–acid batteries, in general, can be charged quite fast after a discharge, as long as the SoC is below about 70–80%. Beyond this point, however, charging becomes steadily more difficult, and, for the last few percent, a much longer time is needed. This is true for flooded, gel, and AGM batteries.

The recharge time of a gel battery to different states-of-charge (50, 70, and 90%) after a complete discharge (100% DoD), for different initial charge currents and a voltage limit of 2.40-V per cell, is shown in Fig. 13.11. It can be seen that, with an initial charge current of 10 times the 20-h discharge rate, a state-of-charge of 70% can be reached after about 2 h, and after 4 h the state-of-charge is 90%. Although high-power AGM batteries can be recharged even faster, Fig. 13.11 shows clearly that, for gel batteries too, fast charging is possible.

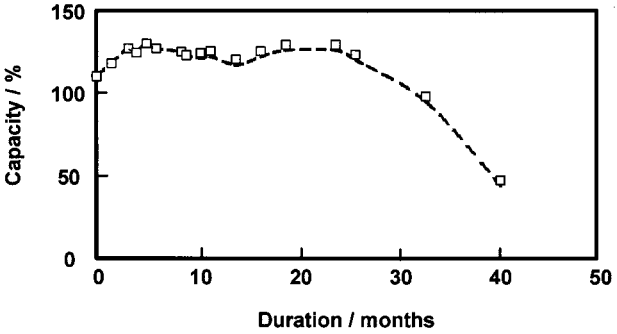

Fig. 13.9. Accelerated lifetime test at 40°C of gel batteries (A400-type) with a float voltage of 2.22 V per cell.

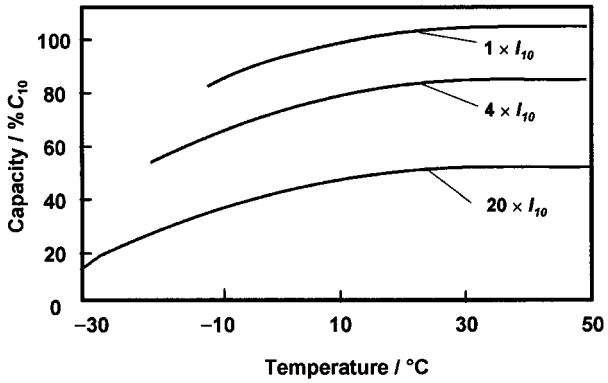

Fig. 13.10. Capacity of a dryfit battery (A400-type) at different discharge rates and temperatures. I_{10} is the discharge current for a uniform, 10-h discharge.

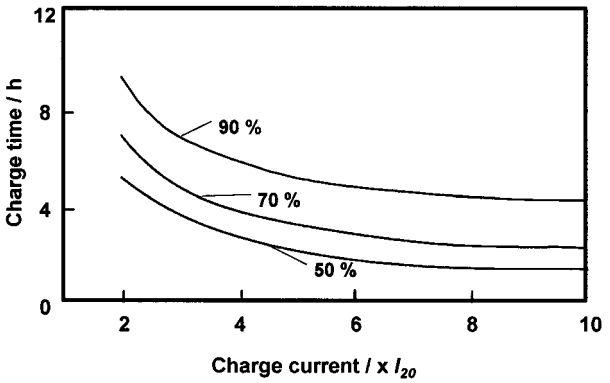

Fig. 13.11. Charging time of a dryfit battery (A500-type) to return to a certain SoC after a complete discharge (100% DoD), at a charge-voltage limit of 2.40 V per cell for different initial currents. (I_{20} is the discharge current for a uniform 20-h discharge.)

It must be realised, however, that the charge voltage limit of 2.40 V per cell is significantly higher than the float voltage. This is possible for gel batteries as well as for AGM without any service-life reduction, as long as the time period for that higher charge voltage is limited and the charge voltage returns to the float level soon. Therefore, it is important to adhere to the maximum voltage and time period specified by the battery manufacturer for such fast charging procedures.

13.4. AGM Batteries

In AGM batteries, the electrolyte is immobilised in glass-mat separators with a very high porosity of more than 90%; a typical value is 93% (see also Chapters 6 and 7). The glass fibres are rather fine and, therefore, the absorption capability is high. The medium pore size of the glass-mat is around a few μm. A picture of a typical glass-mat separator with fine and coarse fibres is shown in Fig. 13.12. The interweaving glass fibres can be seen clearly.

As fine fibres are much more expensive than coarser ones, a compromise is often adopted in which a blend of, for example, one-third fine fibres and two-thirds coarse fibres is used. The decision about the proportion of fine fibres is much influenced by the mechanical properties demanded of the separator as well as by other parameters, e.g., wicking ability and mean pore size. Investigations of batteries with different amounts of fine fibres in the separator have shown that a higher portion of fine fibres is helpful in reducing acid stratification and extending service-life. Glass mats with 100% fine fibres are seldom used due to the high cost of such material. For extreme conditions where a standard blend of fine and coarse fibres is inadequate, however, the use of 100% fine fibres, or of a blend with a high proportion of fine fibres, is a good option.

In recent years, the AGM separator has become the focus of much attention (see Chapters 6 and 7), and attributes such as compressibility and resilience have

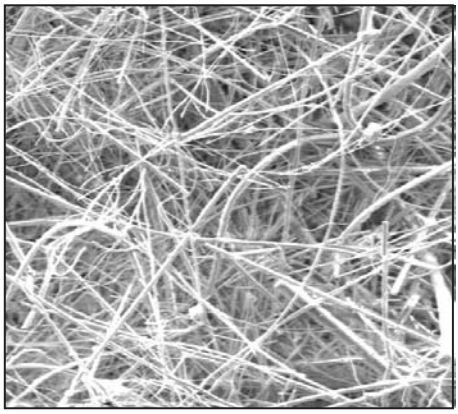

Fig. 13.12. SEM picture of an AGM separator, magnification of 500. (Fibres range in diameter between approximately 0.5 and 5 microns.

been thoroughly investigated [74,75]. For AGM batteries, in general, glass-mat separators are used which are made from 100% glass fibres. Some synthetic fibre reinforcement can be employed in order to improve the strength of the separator [76]. Although the 100% glass fibre version has some advantages, the mechanical properties are relatively poor, and this can be a disadvantage during plate group processing and for avoiding short circuits inside the battery. As a compromise, sometimes a few percent of organic fibres are added to achieve an AGM separator with better mechanical behaviour without losing too much of the performance of the 100% pure glass version.

For AGM batteries, in general, flat positive plates are used. The high porosity and the pore structure of the separator result in an extremely low electrical resistance, which makes AGM most suitable at high discharge rates. Indeed, tests with AGM and gel batteries have shown clearly that the higher the discharge rate the better is AGM in comparison with gel. Thus, for most of the applications where high power performance is needed, AGM is used rather than the gel design. For some applications, however, those with extreme conditions such as high temperatures or deep discharges, gel can be the better choice even if the power demand is high.

AGM batteries can be optimized either for life and energy density or for power. The discharge curves of a long-life, 12-V, 80-Ah AGM battery with an expected lifetime of 12 years at 20°C are shown in Fig. 13.13. It can be seen that, even with a current of 120 A, the discharged capacity is about 35 Ah. The discharge time is more than 17 min and the voltage is at a relatively high level for a quite long time. This is a typical characteristic of high-power, AGM batteries.

This battery type is available as 6 or 12-V monoblocs with a capacity range between 30 and 180 Ah at the 10-h discharge rate, and as 2-V cells with capacities between 200 and 500 Ah. It is used for telecommunications systems as well as for all applications where long service-life, high energy density, and medium to high discharge power are needed.

A special group of batteries has an unusual front terminal design. These are long-length, short-width batteries with both terminals at the front of the battery rather than one at each end. This makes the installation of the battery, and especially the

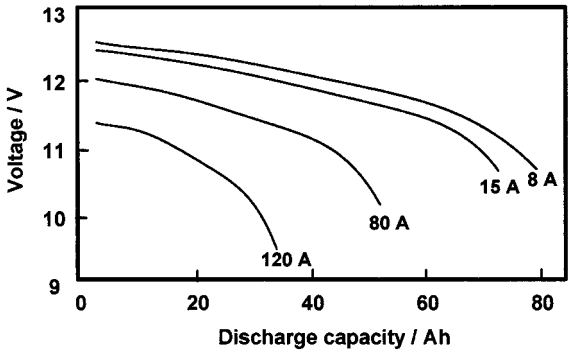

Fig. 13.13. Discharge curves of a 12-V, 80-Ah AGM battery (Marathon-type) at 20°C.

connection of the individual monoblocs in racks or cabinets for telecommunications applications, much easier. A picture of such a front-terminal, 12-V, 100-Ah battery is shown in Fig. 13.14. Such front terminal batteries are used nowadays in telecommunications systems.

An accelerated life-time test, at a temperature of 55°C and a float-voltage of 2.27 V per cell on 12-V, 50-Ah, front-terminal AGM batteries, confirms the expected life of 12 years at 20°C. At intervals of about two months, capacity was checked at the 10-h discharge rate, and the test results are shown in Fig. 13.15. During more than 300 days the capacity remained at a high level and rather stable. Afterwards, the capacity decreased significantly, and the test was stopped after 380 days when the capacity had dropped to 70% of the nominal value. The float life at 55°C is, therefore, 1 year, and this equates to a life of 12 years for a float operation at 20°C.

AGM batteries designed to provide very high power ($180\,W\,l^{-1}$ at the 15-min discharge rate) may offer a life of 10 years and are produced as 6 and 12-V units with capacities between 60 and 180 Ah. Such batteries are often used for applications

Fig. 13.14. 12-V, 100-Ah AGM battery (Marathon-type) with front terminals for telecommunications applications.

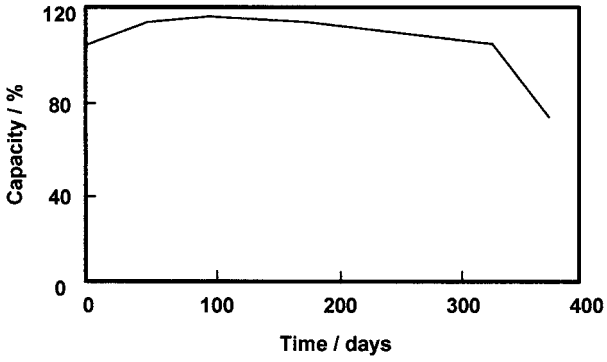

Fig. 13.15. Accelerated lifetime test of 12-V, 50-Ah front-terminal batteries (Marathon-type) at 55°C with a float voltage of 2.27 V per cell.

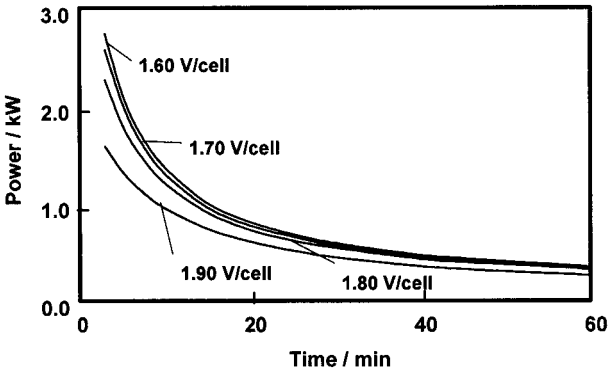

Fig. 13.16. Discharge power per cell of a 40-Ah, AGM battery (Sprinter-type) for discharge time periods between 3 and 60 min at different cut-off voltages between 1.60 and 1.90 V per cell.

with discharge times below 1 h and down to about 5 min. The power per cell of one of these batteries with a nominal capacity of 40 Ah at the 10-h rate, is shown in Fig. 13.16 for discharge time periods between 3 and 60 min at different cut-off voltages between 1.60 and 1.90 V per cell. It can be seen that the power available from one cell is more than 2000 W for a discharge time of 5 min.

A second group of very high power batteries includes 12-V units with capacities between 5 and 85 Ah. These batteries have been optimized to a power density of $200\,W\,l^{-1}$ at the 15-min discharge rate. The typical application is UPS. Due to the optimization towards extremely high power, however, the expected life is significantly shorter than for the 10-year battery.

All the AGM batteries discussed here are designed to accommodate a short circuit. This means, they can survive a 30-day short circuit and, after recharge, have virtually the same capacity as before the test. This is also true for the gel battery-types described earlier.

In addition to high-power performance, AGM batteries also have good charge acceptance. The charge behaviour of a 12-V, 60-Ah, AGM battery during current-limited, constant-voltage charging (14.4 V, limited to 100 A) is shown in Fig. 13.17. The battery was initially discharged to 100% DoD. It can be seen that the battery accepted the 100 A for more than 20 min. More than 50% of the total capacity was recharged during this time period. After 1 h, the charge current had reduced markedly, and the battery was recharged to about 90% of capacity. It is important to realise that high-power, AGM batteries can be recharged very quickly to about 50% SoC, then relatively fast to 80–90% SoC. For the last few percent of charge restoration, however, a significantly longer time is needed.

The charge behaviour shown in Fig. 13.17 was measured with AGM batteries with medium plate thickness. The trend is to reduce the plate thickness in order to achieve even higher power performance. This will further improve the charge acceptance of the battery.

The temperature inside an AGM battery increases during fast charging [77,78]. Tests have shown a significant increase in the temperature although, normally, this

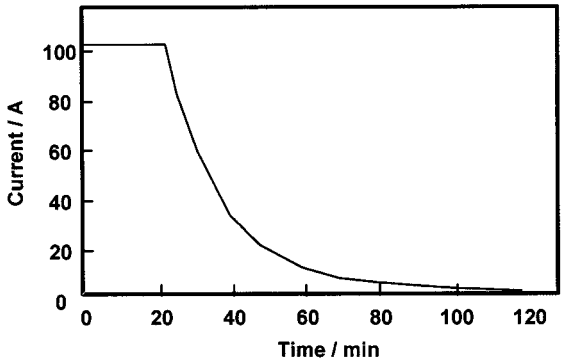

Fig. 13.17. Fast-charging characteristics of a 12-V, 65-Ah AGM battery with current limit of 100 A and voltage of 14.40 V.

increase remains within tolerable limits. Thus, fast charging is an acceptable way to restore the battery quickly after a discharge. Under certain conditions, however, charge-control based on the battery temperature is also needed. When both temperature and charge voltage are controlled, the life of AGM batteries will not be reduced by fast charging [11].

13.5. Large Batteries for Stationary Applications

Stationary batteries with tubular positive plates are commercially available as 2-V units with capacities up to some thousands of ampere-hours. Batteries with such high capacities often have tall plates. A general rule is that, the taller the plates, the greater is the ratio of grid electrical resistance to the total, internal resistance of the cell. As a result, plates taller than about 50 cm undergo a lower depth-of-discharge (DoD) at the bottom of the cell. The large voltage drop down the grid reduces the available energy of the battery and also increases heat generation in the cell. In order to improve this situation, a novel cell with a 'Copper-Stretch-Metal' (CSM) grid design was developed and placed on the market more than a decade ago [79–81].

CSM cells have the same weight and volume as a standard cell, but copper is used instead of lead as the negative-grid material. Actually, the grid is an expanded copper structure covered with a thin layer of lead. On the positive side of the cell, tubular plates are used. The influence of copper as the grid material of the negative plate on the discharge and charge behaviour of the cell has been estimated by using a theoretical model [82,83]. In this model, the cell is considered as a network of vertical and horizontal resistances. A comparison of cells with plates of the same height (555 mm) shows the CSM cell internal resistance to be about 17% lower than that of the standard cell. Due to the lower resistance of the negative plate, the CSM design displays a markedly more uniform current distribution between the top and the bottom of the cell [84]. Experimental investigations of the current distribution in CSM and standard cells have confirmed the predictions obtained from the theoretical model.

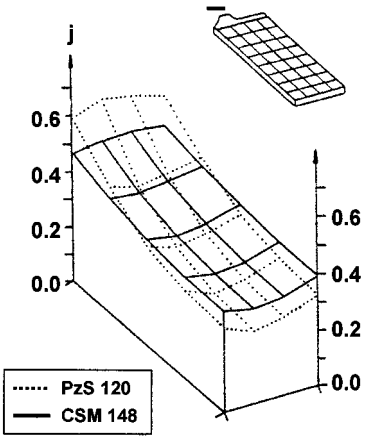

Fig. 13.18. Local current-density distribution of standard (OPzS) and CSM cells with the same plate height at a discharge rate of $2 \times I_5$. I_5 is the discharge current for a uniform 5-h discharge.

The current-density distribution in standard and CSM cells with the same plate height (555 mm) are illustrated in Fig. 13.18 at the beginning of a $2 \times I_5$ discharge where I_5 is the current at the 5-h rate. At the top of the plates, there is a much higher current density with the standard cell than with the CSM. Conversely, near the bottom of the plates, the CSM cell has a higher current density than the standard cell. This means the current distribution is more uniform in CSM plates. The difference in local current density also means a difference in the local DoD of the plate. Therefore, the standard plate has a significantly different mass utilisation between the top and the bottom areas, especially at high discharge rates; the mass utilisation at the top is relatively high, while at the bottom there are mass reserves that cannot be used.

As the electrical conductivity of copper is much higher than that of lead, less grid material is required in CSM cells. This provides an option of having more active mass and electrolyte in the cell which, in turn, results in an increase in both volumetric energy-density and power density. It is important to realise that the use of copper instead of lead for the negative grid is not only a benefit during discharge, but also provides a greatly improved charge acceptance with better energy efficiency. CSM cells (flooded type for traction applications) and OCSM cells (flooded type for stationary applications) should be used whenever cells with tall plates are required, to provide medium or high discharge power and high-energy efficiency [79–81].

Discharge curves for a 1380-Ah, OCSM cell, at constant-power discharges of 1.47 kW and 2.94 kW are shown in Fig. 13.19. This figure also shows the discharge curves of an OPzS cell (flooded, lead negative grid) with the same weight and size and at the same discharge rates. The much better performance of the OCSM design can be seen clearly in each case.

OCSM cells with tubular positive plates and copper negative grids have been used successfully for various stationary applications. In 1986, for example, a

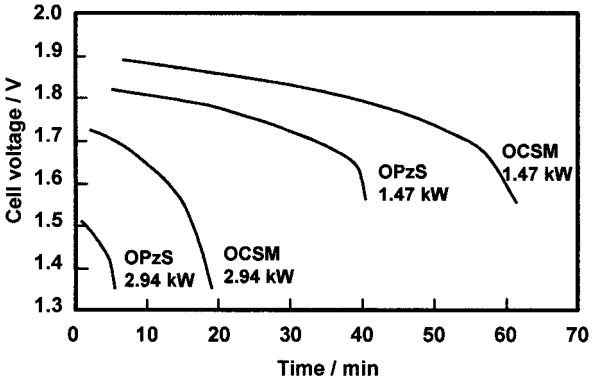

Fig. 13.19. Discharge curves of 1380-Ah, OCSM (stationary-type) cells in comparison with standard (OPzS) cells at high discharge rates with constant power of 1.47 kW and 2.94 kW.

17-MW/14-MWh battery was installed at BEWAG in Berlin. At that time, the battery was the largest in the world [85,86]. Designed to strengthen Berlin's 'island-utility' system, it was used from the beginning of 1987 for frequency regulation and spinning reserve (see also Chapter 10).

In 1995, the BEWAG battery reached the end of its service-life. During its time in service, the 14-MWh battery storage system operated successfully with virtually no problems [87]. This was a very remarkable result, as the operating conditions were severe. The battery had a capacity turnover of some 7000 times the nominal capacity, and the total energy turnover was about 100 GWh.

Originally, BEWAG planned to install four more battery storage systems of the same size in the Berlin electricity grid. Due to the political changes in Eastern Europe, however, Berlin ceased to be an 'island utility,' and plans for further battery storage systems were abandoned. It should be noted, however, that a battery design such as that used at BEWAG could be of considerable interest for other 'island systems' around the world.

Large OCSM batteries are also suitable for other utility applications. Recently, the concept of a multifunctional energy storage system, which is useful to improve the utilisation of regenerative energies, has been evaluated [88]. This system includes three different functions: (i) uninterruptible power supply (UPS), (ii) improvement of power quality, and (iii) peak load assists via the use of regenerating power sources, with surplus energy from periods of low demand stored in a battery for peak-load periods (see Chapter 10).

Two multifunctional energy storage systems, each with a 1.2-MWh lead–acid battery, were installed recently in Germany. There is one system in combination with a solar plant and another one in combination with a wind farm. The batteries consist of OCSM cells with the standard design, but modified according to the special demand of a multifunctional application.

In the future, there will be an increasing market for large lead–acid batteries, especially as there is a growing demand for high-quality power arising from the

sensitivity of many operating systems to the perturbations of electric grids. Flooded batteries can be used for such utility applications, but the valve-regulated type is an option where floor-space is limited. A careful design of these batteries is necessary, however, in order to avoid potential difficulties such as temperature inhomogeneity.

The use of the CSM technology for large valve-regulated batteries can result in high-power, lead–acid batteries, which have all the advantages of the valve-regulated design. To date, copper negative grids have only been used in gel cells, as copper is most useful with tall plates and, in such designs, gel is preferred over AGM. An investigation of the combination of copper negative grids and gel technology established that this combination gives high-power, maintenance-free batteries without any risk of copper dissolution [89]. The results of this investigation agree well with field experience with this type of battery. During more than 10 years in different stationary applications, no noticeable amounts of copper have been found either in the electrolyte or on the negative active mass surface.

Besides higher power, such cells have also better charge acceptance. The charging times for different initial charging currents to return a standard gel cell, OPzV (lead negative grid), and a gel cell with copper grids, OCSV, to 100% of the discharged capacity are shown in Fig. 13.20. It can be seen that the use of copper grids reduces markedly the charging time, due to the better charge acceptance of the OCSV cells.

The CSM design brings benefits to the performance of VRLA cells and flooded cells. OCSV cells have already been used successfully in a large, 500-kWh battery in a stationary application [72]. The use of such cells in batteries with even higher energy, up to some MWh, is the next step in the application of the technology.

Experience with a large, 1.4-MWh, AGM battery in a stationary application was reported recently [90]. The battery was installed in the island village of Metlakatla, Alaska in 1997 in order to stabilise the island's power grid by supplying instantaneous power to the grid and absorbing excess power from the grid. The battery consists of 2-V, 3600-Ah, AGM modules; each module consists of 3 individual cells connected in parallel. The cells are operating in a horizontal position to avoid any problem with acid stratification. The success of this system is described in some detail in Chapter 10.

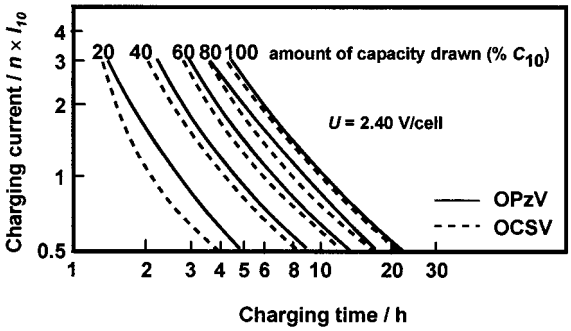

Fig. 13.20. Charging time and initial charging current to return a standard (OPzV) and a CSM gel (OCSV) battery to 100% of discharged capacity after discharge to different depths-of-discharge.

In summary, it seems that there is a rapidly increasing market for large batteries in a variety of utility applications. So far, this has mainly been a market for flooded batteries, but it is likely that the valve-regulated battery can replace the flooded battery in utility applications in the same way that it has replaced them in UPS and telecommunications applications.

13.6. Future Trends in Stand-by Batteries

For UPS applications, there has been a clear trend to shorter discharge times and higher discharge rates. The discharge time required is often between 5 and 15 min, and a high-power supply during this time interim is the only discharge performance the customer expects from the battery. Currently available technology provides $200\,W\,l^{-1}$ at the 15-min rate, however, $220\,W\,l^{-1}$ is a target that is not unrealistic, and prototypes to achieve this have already been produced. Thinner positive and negative plates have to be used in order to pack more couples into a given cell volume. This implies the use of thinner grids. In order to maintain the service-life of the battery in this application, the corrosion rate must be sufficiently low.

For telecommunications applications, there is also a trend to higher energy and power density. In this application, however, the most important discharge time is around a few hours. In future, this application will also require high reliability and a long service-life, sometimes under extreme conditions. This has to be achieved with a reduced grid thickness, when higher energy and power densities are also needed. In the case of telecommunications applications, there is also an increasing demand for batteries with the front-terminal design.

Thus, the general trend towards higher volumetric power and energy densities, in combination with a long service-life, requires thinner grids with low corrosion rates. This can be achieved with the conventional batteries by improving positive grid alloys and other parameters that influence the corrosion behaviour. There are more options, however, when advanced battery designs are used.

13.6.1 Continuous plate-processing

For standby batteries, the standard grid manufacturing technology has been book-mould casting for flat plates and pressure casting for tubular plates. The production of starter batteries, however, has already moved to more advanced grid production techniques such as expanded-metal or continuous casting. These techniques have made it possible to manufacture plates continuously with an automated process line. A view of part of an expanded-metal grid ribbon, such as is used for plate production for starter batteries, is shown in Fig. 13.21. Due to the positive experience gained with this technology, it can be expected that it will progressively replace the traditional grid casting in starter-battery plants.

At the beginning of the development of the expanded-metal technology, there were severe problems with the corrosion rate of the positive grids. By using improved alloys and a special rolling process for the strip, however, this problem has been effectively eliminated. Expanded positive grids with lead–calcium–tin alloys no longer suffer from the corrosion problems that formerly reduced the expected life of

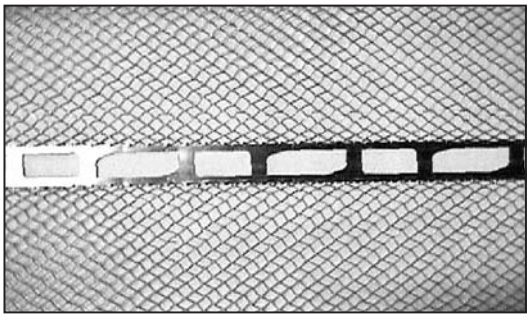

Fig. 13.21. Expanded-metal grid ribbon used for continuous plate production of automotive batteries.

batteries under typical automotive applications [91]. Initially, expanded-metal grids were used with the flooded battery design, however, there has recently been developed an AGM battery with expanded positive and negative grids for automotive applications [92].

There is no reason, in principle, why continuous plate processing, such as the expanded-grid technology, cannot be used also for standby batteries. Of course, the standby application is significantly different from automobile duty, and battery-life expectation also is different. The main issues are the corrosion and possible growth of the positive grids, the bonding of the positive active mass to the grid and the avoidance of short circuits.

Further improvements of the alloys and the grid-manufacturing techniques, as well as of the complete plate fabrication process, could make it possible to extend the life of batteries with expanded-metal grids so much that they would be a good alternative to the traditional book-mould cast grids, at least for some standby battery applications. A detailed discussion of the metallurgy and performance of cast and rolled lead alloys for battery grids is given by Prengaman [93–95] and in Chapter 2.

Another alternative route to continuous plate processing is the continuous grid casting process where the molten lead or lead alloy is fed to a casting shoe sliding on a rotating drum. The method is restricted to rather thin grids because, otherwise, the amount of lead in the cavities of the rotating drum surface cannot be cooled fast enough. If the so-called 'Concast' process is used with lead–calcium–tin alloys for negative-grid production, in general, no problems occur. The positive grids, however, suffer significantly from grid corrosion and growth.

A way to overcome this problem is to use a special rolling process just after the continuous casting. By using such a 'Conroll' process, the problem of grid corrosion seems to disappear completely. Mass-adhesion is another issue, however, and this is much influenced by the special, two-dimensional structure of such grids, which is significantly different from the three-dimensional structure of book-mould cast or expanded-metal grids. There has been some investigation about how to overcome the mass-adhesion problem by special plate processing, but up to now it is not clear whether lead–calcium–tin 'Conroll' grids can be a practical alternative to the standard grid technologies.

A second way to overcome the corrosion problems of 'Concast' positive grids is the use of either pure lead or a lead-tin alloy. The disadvantage is the well-known fact that such grids, without any calcium, are very soft. Therefore, significant problems can occur during plate processing as well as during assembling of the battery. The corrosion rate of the positive grid can be much reduced. Besides any handling difficulty, however, there is still the problem of achieving a sufficient positive-mass adhesion, and this makes good plate processing a necessity.

Another way to produce grids continuously is by the punching of lead sheets. This brings the disadvantage that a relatively large proportion of the original lead sheet forms scrap and has to be remelted. This method, however, does allow the production of relatively thin grids from pure lead and these have a very low corrosion rate. There is, again, a handling problem due to the softness of the calcium-free grids, but the good corrosion resistance makes the punching technique quite attractive for high-power, standby batteries with thin plates.

13.6.2 Spiral technology

Apart from the traditional design of AGM batteries with flat plates, there is also the option to make cylindrical cells with spiral electrodes and AGM separators. A key point is that the spiral design and the tightly wound layers of a lead–tin grid make it possible to keep the separator under high compression. This is very useful in helping to achieve a long life and a good performance of the battery. The thin-electrode design provides an active mass surface that is significantly larger than in conventional, flat-plate, batteries. This reduces the internal electrical resistance and provides exceptionally high power [96]. A picture of a 12-V, spiral battery with a capacity of 50 Ah is shown in Fig. 13.22.

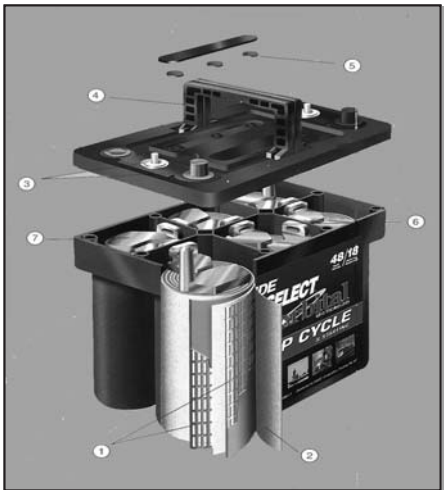

Fig. 13.22. AGM spiral battery for automotive applications.

This design was developed recently as an automotive starter battery. It has very high gravimetric energy and power densities, both of which are important factors for automotive applications. Related to the volume, the energy and power densities are lower due to the cylindrical shape of the cells, which results in some volume that cannot be used for the electrochemical elements. As the volumetric energy and power densities are more important than the weight of the battery for many of the standby applications, this might not be the best approach for standby service. As this design has a relatively high specific energy, however, even though not all the volume is used, it could be an interesting alternative for at least some standby applications in future.

13.6.3 Advanced separators

A clear disadvantage of the AGM separator is that it does not provide sufficient restraint to prevent positive active mass expansion. This is due to the fact that the glass-mat is compressible. The use of a very high stack pressure is limited by the mechanical properties of the glass fibres, which cannot withstand high pressures. There can also be a lack of resilience of the glass-mat. Therefore, positive active mass expansion, which may occur during discharge–charge cycling, cannot be avoided completely with the AGM design.

A material with similar properties to a glass-mat separator, but which is much less compressible, would be a good alternative. Recently, an acid jellifying separator (AJS) that consisted of an ultrahigh molecular weight polyethylene with a certain amount of silica inside the pores was tested [97,98]. The mean pore size of the AJS was 0.2 μm and, therefore, was much smaller than that of AGM, which is typically a few μm. The porosity of the AJS was above 80%, but is lower than that of glass-mat separators, which is above 90%. The porosity of the AJS seems to be high enough, however, to absorb a sufficient amount of electrolyte between the plates so that this design could be used in a valve-regulated battery.

Indeed, an AJS has a behaviour between that of gel and AGM separators and might become a third way to immobilise the electrolyte in valve-regulated batteries. The compressibility of the material is much lower than that of a glass-mat. The thickness reduction in an AJS and an AGM separator with increasing stack pressure is shown in Fig. 13.23. Also included is a similar curve for an AJS separator after 467 cycles in a battery. As the AJS is nearly incompressible, active mass expansion is precluded, and this can be a clear advantage for some applications, especially those that include cycling. Although the main application seems to be related to cycling, such a material could also be suitable for certain standby applications.

13.7. Conclusions

Lead–acid batteries will continue to have, by far, the major share of the standby battery market, due to their outstanding specific-energy, life and cost characteristics. It is expected that there will be a significant growth of the standby battery market during the next few years. Most standby batteries already have the valve-regulated

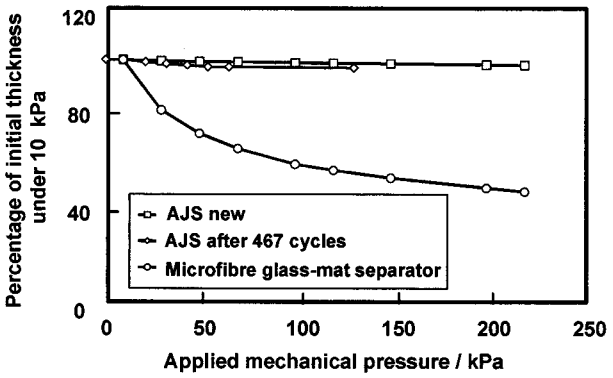

Fig. 13.23. Reduction of AJS and AGM separator thickness with increasing stack pressure.

design. For UPS applications, there is a clear tendency to a higher power requirement with a discharge time of only a few minutes. Therefore, improvement of the high-power performance, without a reduction of life and/or reliability, has become the most important objective of battery development for standby applications.

References

1. H. Bode, *Lead–acid Batteries*, Wiley-Interscience, New York, 1977.
2. R.F. Nelson, *J. Power Sources*, **31** (1990) 3.
3. H. Tuphorn, *J. Power Sources*, **31** (1990) 57.
4. D. Berndt, *Maintenance-Free Batteries*, Research Studies Press, Taunton, Somerset, UK, 1993.
5. G. Baudo, *Proceedings of the 11th International Lead Conference*, Venice, Italy, 1993, Lead Development Association, London, UK, Paper 7.1.
6. R. Wagner, *Proceedings of the 11th International Lead Conference*, Venice, Italy, 1993, Lead Development Association, London, UK, Paper 7.3.
7. R. Wagner, *J. Power Sources*, **53** (1995) 153.
8. R. Wagner, D.U. Sauer, *J. Power Sources*, **95** (2001) 141.
9. B. Culpin, *J. Power Sources*, **53** (1995) 127.
10. K. Takahashi, H. Yasuda, H. Hasegawa, S. Horie, K. Kanetsuki, *J. Power Sources*, **53** (1995) 137.
11. R. Wagner, W. Bögel, J.-P. Büchel, *Proceedings of the 29th International Symposium on Automotive Technology and Automation*, Florence, Italy, 1996, pp. 57–66.
12. M. Calabek, K. Micka, P. Baca, P. Krivak, L. Sacha, *J. Power Sources*, **78** (1990) 94.
13. F.A. Fleming, P. Shumard, B. Dickinson, *J. Power Sources*, **78** (1999) 237.
14. D. Berndt, *J. Power Sources*, **95** (2001) 2.
15. A.M. Howart, E. Willihnganz, *Electrochem. Technol.*, **6** (1968) 370.
16. W. Sharfenberger, S. Henkel, *Z. Metallk.*, **64** (1973) 478.
17. G.W. Mao, J.G. Larson, P. Rao, *J. Electrochem. Soc.*, **120** (1973) 11.
18. M.V. Rose, J.A. Young, *Proceedings of the 5th International Lead Conference*, Paris, France, 1974, Lead Development Association, London, UK, pp. 37–52.
19. J. Perkins, G.R. Edwards, *J. Mat. Sci.*, **10** (1975) 136.
20. R.D. Prengaman, *Proceedings Electrochemical Society*, Fall Meet., Las Vegas, NV, USA, 1976, pp. 31–33.
21. E.M.L. Valeriote, *J. Electrochem. Soc.*, **128** (1981) 1423.

22. N.E. Bagshaw, in L. J. Pearce (Ed.), *Power Sources 11. Research and Development in Non-mechanical Electrochemical Power Sources*, International Power Sources Symposium Committee, Leatherhead, England, 1989, 113.
23. R.D. Prengaman, *J. Power Sources*, **33** (1991) 13.
24. H. Giess, *J. Power Sources*, **53** (1995) 31.
25. L. Albert, A. Goguelin, E. Jullian, *J. Power Sources*, **78** (1999) 23.
26. S. Fouache, A. Chabrol, G. Fossati, M. Bassini, M.J. Sainz, L. Atkins, *J. Power Sources*, **78** (1999) 12.
27. A.C. Simon, S.M.Caulder, *J. Electrochem. Soc.*, **121** (1974) 531.
28. S. Feliu, E. Otero, J.A. Gonzalez, *J. Power Sources*, **3** (1978) 145.
29. G. Papazov, T. Rogachev, D. Pavlov, J. Garche, K. Wiesener, *J. Power Sources*, **6** (1981) 15.
30. J. Garche, *J. Power Sources*, **53** (1995) 85.
31. W.B. Brecht, D.O. Feder, J.M. McAndrews, A.J. Williamson, *Proceedings of the 10th International Telecommunications Energy Conference*, San Diego, CA, IEEE, 1988, pp. 124–131.
32. M.E. Fiorino, F.J. Vaccaro, R.E. Landwehrle, *Proceedings of the 10th International Telecommunications Energy Conference*, San Diego, CA, IEEE, 1988, pp. 114–118.
33. W.B. Brecht, N.F. O'Leary, *Proceedings of the 10th International Telecommunications Energy Conference*, San Diego, CA, IEEE, 1988, pp. 35–42.
34. W.E.M. Jones, D.O. Feder, *Proceedings of the 18th International Telecommunications Energy Conference*, Boston, MA, USA, IEEE, 1996, pp. 184–192.
35. D. Berndt, W.E.M. Jones, *Proceedings of the 20th International Telecommunications Energy Conference*, San Francisco, CA, USA, IEEE, 1998, pp. 443–451.
36. S.S. Misra, T.M. Noveske, S.L. Mraz, A.J. Williamson, *J. Power Sources*, **95** (2001) 162.
37. D. Berndt, U. Teutsch, *J. Electrochem. Soc.*, **143** (1996) 790.
38. F. Kramm, *Proceedings of the 20th International Telecommunications Energy Conference*, San Francisco, CA, USA , IEEE, 1998, pp. 161–165.
39. F.A. Fleming, L. Gao, P.R. Shumard, R. Evans, R. Kurian, *Proceedings of the 21st International Telecommunications Energy Conference*, Copenhagen, Denmark, IEEE, 1999, Paper 3–3.
40. J. Burbank, *J. Electrochem. Soc.*, **111** (1964) 1112.
41. H. Giess, in K.R. Bullock, D. Pavlov (Eds.), *Advances in Lead–acid Batteries*, The Electrochemical Society, Pennington, NJ, USA, 1984, pp. 241–251.
42. T.G. Chang, in K.R. Bullock, D. Pavlov (Eds.), *Advances in Lead–acid Batteries*, The Electrochemical Society, Pennington, NJ, USA, 1984, pp. 86–97.
43. A. Winsel, E. Voss, U. Hullmeine, *J. Power Sources*, **30** (1990) 209.
44. A.F. Hollenkamp, *J. Power Sources*, **36** (1991) 567.
45. D. Pavlov, A. Dakhouche, T. Rogachev, *J. Power Sources*, **42** (1993) 71.
46. M. Kosai, S. Yasukawa, S. Osumi, M. Tsubota, *J. Power Sources*, **67** (1997) 43.
47. P.T. Moseley, *J. Power Sources*, **88** (2000) 71.
48. U. Hullmeine, A. Winsel, E. Voss, *J. Power Sources*, **25** (1989) 27.
49. E. Meissner, E. Voss, *J. Power Sources*, **33** (1991) 231.
50. E. Meissner, *J. Power Sources*, **46** (1993) 231.
51. E. Bashtavelova, A. Winsel, *J. Power Sources*, **46** (1993) 219.
52. D. Pavlov, I. Balkanov, T. Halachev, P. Rachev, *J. Electrochem. Soc.*, **136** (1989) 3189.
53. D. Pavlov, *J. Electrochem. Soc.*, **139** (1992) 3075.
54. S.M. Caulder, J.S. Murday, A.C. Simon, *J. Electrochem. Soc.*, **120** (1973) 1515.
55. A.C. Simon, S.M. Caulder, in D.H. Collins (Ed.), *Power Sources 5. Research and Development in Non-mechanical Electrochemical Power Sources*, Academic Press, London, UK, 1975, pp. 109–122.
56. J.P. Pohl, H. Rickert, in D.H. Collins (Ed.), *Power Sources 5. Research and Development in Non-mechanical Electrochemical Power Sources*, Academic Press, London, UK, 1975, pp. 15–22.
57. K. Harris, R.J. Hill, D.A.J. Rand, *J. Electrochem. Soc.*, **131** (1984) 474.
58. J. Yamashita, Y. Matsumaru, *J. Appl. Electrochem.*, **18** (1988) 595.
59. I.M. Steele, J.J. Pluth, J.W. Richardson, *J. Power Sources*, **95** (2001) 79.
60. R. Wagner, P. Scharf, *Proceedings of the 30th International Symposium on Automotive Technology and Automation*, Florence, Italy, 1997, pp. 135–142.
61. I. Dreier, F. Saez, P. Scharf, R. Wagner, *J. Power Sources*, **85** (2000) 117.

62. B.A. Cole, R.J. Schmitt, J. Szymborski, *Proceedings of the 20th International Telecommunications Energy Conference*, San Francisco, CA, USA, IEEE, 1998, pp. 356–363.
63. F. Kramm, H. Nieppraschk, *Proceedings of the 21st International Telecommunications Energy Conference*, Copenhagen, Denmark, IEEE, 1999, Paper 6–2.
64. K. Eberts, in D.H. Collins (Ed.), *Power Sources 2. Research and Development in Non-mechanical Electrochemical Power Sources*, Pergamon Press, Oxford, UK, 1970, pp. 69–92.
65. S. Sternberg, A. Mateescu, V. Branzoi, L. Apatenau, *Electrochim. Acta*, **32** (1967) 349.
66. K. Bullock, D.H. McClelland, *J. Electrochem. Soc.*, **124** (1977) 1478.
67. K. Bullock, *J. Electrochem. Soc.*, **126** (1979) 360.
68. K. Bullock, *J. Electrochem. Soc.*, **126** (1979) 1848.
69. G.A. Morris, P.J. Mitchell, N.A. Hampson, D.I. Dyson, *Power Sources, 12. Research and Development in Non-mechanical Electrochemical Power Sources*, International Power Sources Symposium Committee, Leatherhead, UK, 1989, pp. 61–76.
70. E. Meissner, *J. Power Sources*, **67** (1997) 135.
71. F. Kramm, H. Kretzschmar, *Proceedings of the 18th International Telecommunications Energy Conference*, Boston, MA, USA, IEEE, 1996, pp. 193–197.
72. R. Wagner, *J. Power Sources*, **67** (1997) 163.
73. F. Kramm, *Proceedings of the 19th International Telecommunications Energy Conference*, Melbourne, Australia IEEE, 1997, pp. 25–28.
74. G.C. Zguris, *J. Power Sources*, **67** (1997) 307.
75. C. Pendry, *J. Power Sources*, **78** (1999) 54.
76. R. Simarro, *J. Power Sources*, **78** (1999) 65.
77. H. Giess, *Proceedings of the 22nd International Telecommunications Energy Conference*, Phoenix, AZ, USA IEEE, 2000, pp. 749–754.
78. P. Häring, H.Giess, *J. Power Sources*, **95** (2001) 153.
79. R. Kießling, *J. Power Sources*, **19** (1987) 147.
80. R. Wagner, in H. Kahlen (Ed.) *Batterien*, Vulkan, Essen, Germany, 1992.
81. R. Wagner, *VDI Berichte*, **1058** (1993) 131.
82. J. Euler, W. Nonnenmacher, *Electrochim. Acta*, **2** (1960) 268.
83. J. Euler, L. Horn, *Electrochim. Acta*, **10** (1965) 1057.
84. J. Meiwes, *Electrotech. Zeitung*, **8** (1986) 3.
85. H. Dominik, G.K. Krämer, B. Voigt, *Proceedings of the 21st Intersociety Energy Conversion and Engineering Conference (IECEC)* San Diego, CA, USA, 1986, pp. 1028–1033.
86. R. Kießling, *J. Power Sources*, **19** (1987) 227.
87. K.G. Krämer, *Proceedings of the 5th International Conference on Batteries for Energy Storage*, Puerto Rico, 1995.
88. R. Wagner, M. Schroeder, T. Stephanblome, E. Handschin, *J. Power Sources*, **78** (1999) 156.
89. R. Wagner, *J. Electrochem. Soc.*, **143** (1996) 139.
90. J. Szymborski, G. Hunt, A. Tsagalis, R. Jungst, *Proceedings of the 22nd International Telecommunications Energy Conference*, Phoenix, AZ, USA IEEE, 2000, pp. 484–492.
91. M.D. Achtermann, M.E. Greenlee, *J. Power Sources*, **33** (1991) 87.
92. S. Fouache, J.P. Douady, G. Fossati, C. Pascon, *J. Power Sources*, **67** (1997) 15.
93. R.D. Prengaman, *J. Power Sources*, **67** (1997) 267.
94. R.D. Prengaman, *J. Power Sources*, **78** (1999) 123.
95. R.D. Prengaman, *J. Power Sources*, **95** (2001) 224.
96. F. Trinidad, F. Saez, J. Valenciano, *J. Power Sources*, **95** (2001) 24.
97. W. Böhnstedt, *J. Power Sources*, **78** (1999) 35.
98. M. Perrin, H. Döring, K. Ihmels, A. Weiss, E. Vogel, R. Wagner, *J. Power Sources*, **95** (2001) 85.

This page intentionally left blank

Valve-Regulated Lead–Acid Batteries
D.A.J. Rand et al., editors

—CHAPTER 14—

REMOTE-AREA POWER-SUPPLY (RAPS) SYSTEMS AND THE VALVE-REGULATED LEAD–ACID BATTERY

R.H. Newnham

14.1. The Need for Remote-area Power-supply Systems

Over two billion people who live in developing countries do not have access to an adequate electricity supply [1–4], see Fig. 14.1. Generally, this is the result of: (i) the isolated and fragmented geography of many of the countries (the Philippines, for instance, consists of over 7000 islands); (ii) the high cost of installing and maintaining large-scale electrification networks [5]. Where mains grids have been established, the power supply is frequently unreliable and of poor quality. Further, the upgrading and extension of a grid can often be beyond the financial capabilities of a country. Many developing nations have abundant renewable energy from the sun and/or wind. Hence, the wide-scale deployment of remote-area power-supply (RAPS) systems that incorporate renewable energy can be a cost-effective alternative to large-scale mains grids [6]. RAPS systems are also used in areas where an electricity network exists but where a stand-alone power system is more cost-effective than grid extension. A good example of this is freeway lighting, where the installation of a RAPS system can avoid the expensive process of running power cables underground.

14.2. RAPS System Components

As their name suggests, RAPS systems are expected to operate reliably in a variety of inhospitable environments. They can be confronted with the searing heat of the desert, the stifling humidity of the rainforests, or the intense cold of the tundra. The facilities may even be sited on oceans or atop mountains. The systems service a diverse range of applications with widely different levels of energy consumption, such as: (i) houses and villages; (ii) electric fences; (iii) community dwellings and services; (iv) sign lighting; (v) telecommunications; (vi) water pumping; (vii) emergency lighting; (viii) cathodic protection; (ix) lighting beacons; (x) vaccine refrigerators.

RAPS systems capable of supplying continuous power must have either a diesel generator in constant operation and/or a battery bank. If renewable energy is abundant, RAPS systems can also include a photovoltaic (PV) array, a wind generator, and/or a hydro-generator. An inverter to convert direct current (d.c.) to

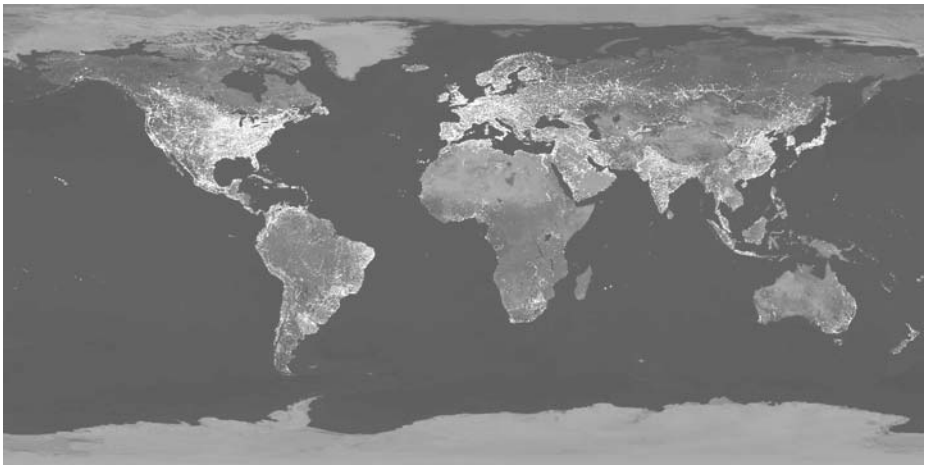

Fig. 14.1. Composite satellite photograph showing those areas of the world with electricity and those without (the dark areas have no power) [1].

alternating current (a.c.) is also a common item. Further, all RAPS systems must have a control strategy and associated equipment to manage the power flow and to allow the system to operate at an acceptable level of efficiency. Basic RAPS componentry is summarized in the Sections 14.2.1–14.2.7.

14.2.1. Battery bank

To date, three different types of rechargeable batteries have been employed for energy storage in RAPS facilities, namely, nickel–cadmium, nickel–iron, and lead–acid. Nickel–cadmium units give excellent service lives and have a high resistance to abuse, but are disadvantaged through low charging efficiency, high cost, appreciable self-discharge, and excessive water consumption (vented design only). The use of cadmium also introduces environmental problems; several countries have already enforced strict regulations for its safe disposal. The application of nickel–iron batteries in RAPS systems has been favoured in many eastern block countries. Again, these batteries suffer from low charging efficiency, high self-discharge, and high water consumption. By contrast, the lead–acid battery has gained wide-scale acceptance in RAPS applications and is still the most efficient and cost-effective option for the majority of situations — it is approximately one-quarter the price of its nickel-based counterparts. Moreover, in most countries, there is an effective infrastructure for the distribution, servicing, and recycling of lead–acid batteries.

Other battery systems that have been suggested for use in RAPS facilities include zinc–bromine [7], vanadium redox [8], and aluminium–air [9]. It is considered unlikely, however, that these systems will be used in mainstream RAPS applications as their cost is still significantly higher than that of lead–acid alternatives, and their long-term reliability has yet to be proven.

In terms of life-cycle costs, batteries are usually the most expensive component of a RAPS system and, therefore, it is advantageous to minimize the required capacity. The battery should, however, be sized to supply a significant portion of the anticipated daily load in the absence of diesel- or PV-generated power, e.g., from 20 to 50%. This would allow the diesel to remain idle for much of the day and to operate under relatively constant, high-load conditions for only a few hours each day. Further, the battery should be sized such that the daily depth-of-discharge (DoD) is limited in the interest of enhancing battery cycle-life. (The cycle-life of a battery is affected by several factors which include DoD, temperature, and charging procedure.)

14.2.2. Diesel generator

Diesel generators are the energy source for many RAPS systems. Such units consist of an internal combustion engine (fuelled by diesel oil) and an alternator that produces a.c. power. Generators that deliver d.c. power have also been used, but they are no longer common as they are not as efficient as their a.c. counterparts. Petrol generators can also be employed for RAPS duty, but they have greater maintenance requirements and are more expensive to operate.

To obtain the best possible fuel efficiency from small (< 12 kW) diesel generators, as well as to minimize maintenance requirements, it is important to maintain the load factor above 60–70%. This means that such generators should be operated at no less than 60–70% of their maximum power output. Larger generators can be operated at a somewhat lower rating, i.e., around 40–50% of their maximum power output.

14.2.3. Photovoltaic array

A PV ('solar') cell converts energy from the sun directly into electricity. A group of such cells (usually 36) connected in series and environmentally protected via a backing and covering is referred to as a PV panel, or a PV module. When a number of these panels are connected together, the assembly is known as a PV array. Generally, PV modules have an operating voltage of 12 V and power outputs that range from 25 to 75 W. The panels can be arranged in series and/or in parallel to provide the required operating voltage and current. To obtain performance at optimum efficiency, the modules must be correctly oriented with respect to the sun.

Maximum power-point trackers can be included in PV-based facilities to increase system efficiency. These devices are basically d.c. to d.c. converters and are placed between the PV array and its load. The concept is based on the principle that maximum power is obtained at a particular array voltage, which varies with insolation and array temperature. The procedure is to monitor the power output to the load and, periodically (typically every 15 s), to adjust the array voltage so as to maintain the power close to its maximum value. It is common for increases in efficiency of 10–15% to be realized in systems that are capable of producing from 3 to 5 kWh per day.

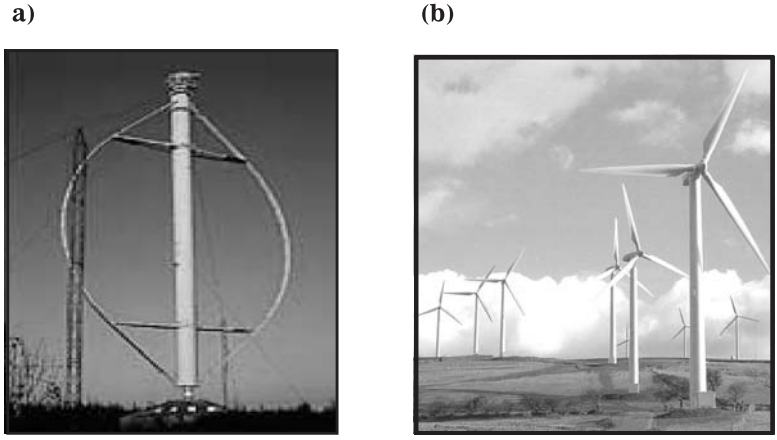

Fig. 14.2. (a) Vertical-axis and (b) horizontal-axis wind turbines.

14.2.4. Wind generator

There are two main designs of wind generators, namely, vertical-axis (Fig. 14.2 (a)) and horizontal-axis (Fig. 14.2 (b)) machines. The former technology is more suited to high-wind conditions and has the advantage of being serviceable from the ground. Horizontal-axis turbines are, however, more efficient at lower wind speeds and are more widely accepted and used. These machines are available in two configurations. One version has the turbine blades on the upwind side of the generator and tower, while the other has the blades situated downwind.

Modern wind generators are capable of delivering $>500\,\mathrm{kW}$ and incorporate sophisticated power electronics that allow the generation of electricity over a range of rotor speeds. Recent advances have resulted in significant increases in efficiency. At average wind speeds above $6\,\mathrm{m\,s^{-1}}$, the electricity produced by these machines is comparable in cost with that supplied by power-stations burning fossil fuels. In most situations, RAPS sites do not have such large power requirements. Hence, smaller wind turbines (0.25–10 kW) are common.

The location of the wind generator is critical if it is to provide satisfactory performance. Indeed, the positioning is more important than in the case of PV arrays, as considerable variations in wind speed can occur from one site to another, particularly in mountainous and wooded areas. An acceptable site should be free of obstructions such as trees, hills, buildings, and other wind generators. Ideally, the wind speed at prospective locations should be monitored for a period of up to 2 years to ensure that the wind regime is both sufficient and reliable.

14.2.5. Hydro-generator

Hydro-generators can provide a continuous supply of energy, given a reasonably consistent supply of water from a nearby stream or river. In practice, however,

hydro-based RAPS facilities for domestic use often have small battery banks to provide additional power during peak periods, i.e., for load levelling or peak shaving. Smaller turbines commonly produce 10–30 kWh per day and, once installed, require minimal maintenance. Although the capital cost of a hydro-generator can be high, such facilities can produce energy more cheaply than can a PV array. This is because the price per installed kW from hydro-generators decreases with increasing system size. For example, upgrading a 1-kW turbine to a 2-kW unit may only increase the initial capital cost of the system by 30%.

14.2.6. Inverter

Inverters are employed to convert d.c. drawn from battery banks to a.c. The ideal inverter should possess the following performance characteristics and features.

- Provide an output waveform of suitable quality, i.e., a low-distortion sine-wave (see below).
- Have an efficiency of greater than 90%, when operating between about 20 and 100% of the nominal load.
- Possess a standby mode, i.e., during periods of low load, the inverter switches to a low power consumption state.
- Have an automatic or demand start, i.e., the inverter should switch immediately from standby to full supply mode when required.
- Contain circuitry to minimize radio-frequency interference to sensitive equipment, e.g., television, hi-fi, and computers.
- Possess accurate voltage regulation to ensure that the output voltage remains within specification.
- Have protection against the insertion of a d.c. signal into the output.
- Provide an overvoltage limit to protect the inverter if the battery voltage should rise above the normal level.
- Have high current and/or temperature protection.
- Disconnect on excessively high d.c. voltage to input.
- Be completely protected from overload and short-circuits.

Traditionally, inverters installed in RAPS systems have been based on either square-wave or modified square-wave technology. Although such units are relatively crude and offer a poor approximation of the a.c. sine wave, they are inexpensive and, hence, still find application in small RAPS systems. Such inverters can, however, give rise to background noise in hi-fi equipment, as well as cause operational problems with: (i) electric motors; (ii) fluorescent lights; (iii) radios; (iv) televisions; (v) microwave ovens; (vi) computers.

Modern inverters installed in RAPS systems are called ‘sine-wave inverters’ and, as this name suggests, produce sine-wave outputs. The devices produce high-quality, low-distortion power and can be used to operate even the most sensitive of electrical equipment. Sine-wave inverters are very efficient ($> 95\%$) and have proven to be rugged and reliable. Bidirectional sine-wave inverters are also available. These devices also act as battery chargers, have inputs for renewable energy generators,

and can synchronize with any a.c. signal (i.e., the power outputs from external a.c. sources and the inverter are additive). They are microprocessor-controlled and utilize advanced charge–discharge algorithms to optimize system operation.

14.2.7. Control system

An effective control system is required both to ensure that the RAPS facility operates at an acceptable efficiency and to guarantee the longevity of components. Control systems vary significantly in complexity. The simplest control devices are those that regulate small PV–battery systems (i.e., one 12-V battery and one PV panel). Such control units may impose only: (i) a top-of-charge voltage (ToCV); (ii) a low-voltage disconnect set point; (iii) a load reconnect voltage. There are two common designs for these controllers or regulators, i.e., either shunt or series type. These designs can be further sub-divided into either 'linear' or 'switching' types. The linear type provides a 'true' constant-voltage charging regime, whereas the switching type involves 'interrupting' or 'chopping' the PV current. Although switching strategies possess the advantage of not having to dissipate energy through the production of heat, they do have a charging hysteresis. This can lead to a 'quasi' partial-state-of-charge (PSoC) cycling of the battery, rather than to constant-voltage duty. The preferred option for small-scale controllers is to use pulse-width-modulation. This technique employs switching at very high frequency and, as a result, produces less charging hysteresis.

For medium-to-large RAPS facilities that have multi-energy inputs, more sophisticated control strategies are employed. Microprocessor-based units that record and utilize many different parameters (such as those used in bidirectional inverter–battery hybrid systems, see Section 14.2.6) offer the most accurate control. These devices can monitor/calculate variables such as battery voltages, string currents, battery temperatures, ambient temperatures, battery bank state-of-charge (SoC), and battery overcharge delivered. Such devices are recommended for use with all RAPS systems that use VRLA batteries, as the latter require carefully controlled charging in order to deliver a satisfactory performance.

14.3. RAPS System Design

Many different configurations are possible for RAPS systems. Various factors are used to determine a suitable system design for a given facility. These include: (i) power and energy required; (ii) availability of renewable energy; (iii) cost of generator operation and system maintenance; (iv) site accessibility; (v) available finance. The basic layout of most RAPS systems is shown in Fig. 14.3 and consists of an energy-generation facility, a controller, and a load. Most, but not all, RAPS systems include an energy-storage component. The energy input to the system from renewable (PV, wind, or hydro) or non-renewable (fossil fuels) sources is directed by the controller to the energy-storage facility, and/or to the load. This control device can vary in complexity, as dictated by the intricacy and sophistication of the RAPS

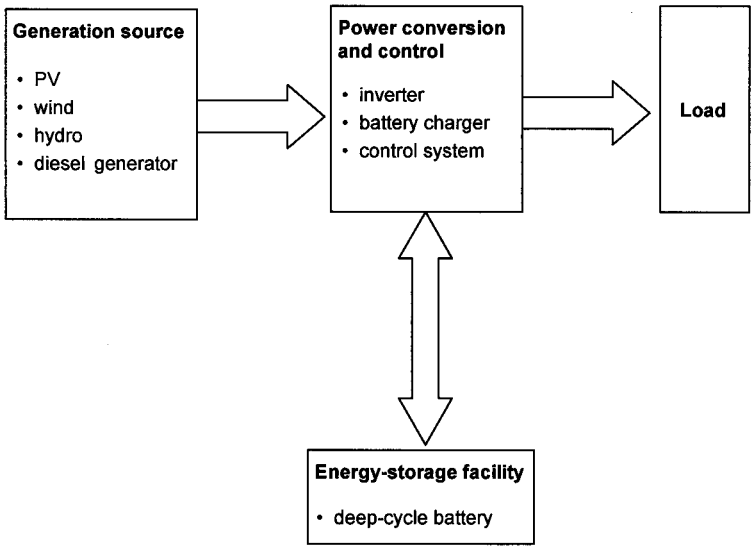

Fig. 14.3. Schematic diagram of basic design for RAPS systems.

system. Sophisticated systems may have several independent energy sources, a large battery bank, an inverter, a battery charger, and a control unit.

The traditional configuration of RAPS systems incorporates a diesel generator that operates through a simple control system. More recently, the cost of fossil fuels has increased significantly while the cost of renewable energy technologies has fallen. In some cases, these changes have caused renewable-energy-based systems to become cost-competitive with fossil-fuel-based systems [10]. Attention has therefore focused on the development of more sophisticated RAPS designs that incorporate one or more renewable energy sources and operate via improved load-management strategies.

RAPS systems can be divided into two basic types, i.e., one that provides d.c. power and one that provides a.c. power. These configurations are described in more detail in Sections 14.3.1. and 14.3.2. There are also some RAPS systems that provide both a.c. and d.c. outputs.

14.3.1. Direct-current RAPS systems

The simplest, and often the most energy-efficient and cost-effective, RAPS systems are those based on d.c. Such facilities are especially suitable for powering lighting and small d.c. appliances in households with low energy demands. The most common configuration consists of a PV array, a battery, and a controller (designated design 'A', Table 14.1). With this design, energy from the PV array is transferred directly to the battery (note, in some instances, controllers have been excluded, but this approach generally requires a larger battery). A typical system may comprise a 75-W PV panel, a 12-V, 100-Ah battery, and a control unit. Such a facility is capable

of producing 200–500 Wh per day and could power a television (d.c.) and up to three lights for 3–5 h per day.

14.3.2. Alternating-current RAPS systems

Systems based on a.c. are usually recommended for sites with moderate-to-large loads. Generally, such facilities are not as energy-efficient as their d.c.-based counterparts, but they utilize standard wiring, switches and lights, and are capable of powering numerous a.c. appliances. The following design configurations are commonly used for a.c.-based systems.

Stand-alone diesel generators have been a popular choice in the past and can still be cost-effective given the following: (i) the load curve is relatively constant, i.e., the load factor of the diesel is kept above 50–70% (below this, the efficiency of the generator decreases markedly and maintenance costs increase, see Section 14.2.2); (ii) diesel fuel is reasonably priced; (iii) the expense incurred in connecting individual homes to a central generating unit is acceptable (for communities only). Unfortunately, most houses or villages have high peak to base-load ratios. Hence, since the diesel generator must be sized to accommodate peak-power demands, extended periods of operation at low load/efficiency often occur.

RAPS systems that incorporate a component of renewable energy generally require battery energy-storage. Examples of such systems, together with their application and associated service, are summarized in Table 14.1.

Design B: a renewable energy source, a battery, a controller, and an inverter. The renewable energy can be derived from a PV array and/or a wind generator and/or a hydro-generator. A PV–battery–inverter system is a common option in areas where insolation is plentiful. The capacity of such systems usually ranges from 0.5 to 2 kWh per day. Often, these systems provide a.c. power for household appliances as well as d.c. power for efficient lighting. For sites where the energy required is significantly higher than 2 kWh per day, design B becomes less attractive due to the relatively-high capital cost of the PV panels, unless the facility is remote and diesel fuel is expensive. An alternative is a wind-based system. Modern wind generators require minimal maintenance; typically, routine service is performed every 5 years. Also, the cost of power per installed kW decreases significantly with increasing size of the wind turbine. Hence, for sites that have acceptable wind regimes (average $> 6\,m^{-1}$), wind-powered configurations start to become cost-effective as the daily load exceeds 2–3 kWh per day. As wind generators generally produce a.c., a battery charger is required for these systems. Hydro-generators can also be used to power such facilities, but this option has not been applied widely as it requires an adjacent, regular flow of water and has a somewhat high capital cost.

Design C: a diesel generator, a battery, a controller, and an inverter. Such a configuration is useful in systems where high peak/base-load ratios are experienced (i.e., the majority of applications). This option is commonly used for sites with energy requirements that exceed 2 kWh per day, provided site access is adequate and maintenance and diesel fuel costs are reasonable. As the battery and inverter component can supply the load independently, operation of the diesel generator can

be deferred until high-load conditions arise. This results in an increase in system efficiency relative to that obtained from a stand-alone generator. Also, the use of a bidirectional inverter allows large peak loads to be serviced, as the battery and the generator can provide power concurrently.

Design D: renewable energy (wind, solar, or hydro) in combination with available-on-demand energy from a diesel generator. Generally, this configuration is used at sites that have relatively high energy requirements, i.e., greater than 2 kWh per day.

PV–battery–inverter systems (B1) are usually not cost-competitive with diesel–battery–inverter counterparts (C, D) for sites with energy requirements in excess of 2 kWh per day, unless poor site access results in high diesel-fuel and maintenance costs. The viability of designs B2, B3, C and D for use as village/community power systems is, however, dependent on reasonable power-distribution costs. If these costs are too high, then designs A and B1 may become preferable. Wind–battery–inverter facilities are generally less-expensive than solar-powered configurations

Table 14.1. Design options for RAPS systems.

Design	System	Service
Isolated homes with low energy consumption: 0.2–0.5 kWh per day		
A	• PV array • battery bank • controller	• d.c. lighting • limited number of d.c. appliances
Isolated homes with moderate energy consumption: 0.5–2 kWh per day		
B1	• PV array • battery bank • controller • small square-wave inverter	• d.c. lighting • moderate number of a.c. appliances
Small villages or isolated homes with energy consumption: > 2 kWh per day		
B2	• wind generator • battery bank • controller • inverter	• moderate to large number of a.c. appliances (viable when diesel operation is expensive)
B3	• PV array and/or wind generator • battery bank • interactive inverter	• multiple a.c. appliances (for situations where diesel generator operation is not feasible)
C	• diesel generator • battery bank • bidirectional inverter	• multiple a.c. appliances (cost-effective when diesel fuel and maintenance expenses are reasonable)
D	• PV array and/or wind generator and/or hydro-generator • battery bank • diesel generator • bidirectional inverter	• multiple a.c. appliances (useful when costs of diesel operation are high but not prohibitive; also used when continuity of supply is important)

for the daily supply of 2–3 or more kWh, provided that there is an acceptable wind regime.

14.4. VRLA Batteries for RAPS Systems

Traditionally, flooded lead–acid batteries have been the technology of choice for use in RAPS systems. During the last 10 years, however, there has been a considerable shift towards VRLA batteries. The main driver for this change is the low maintenance requirement of the latter technology. This and other important issues are discussed in the following sections.

14.4.1. Advantages

Flooded batteries operated in RAPS systems require water maintenance on a regular basis. Unfortunately, it is not uncommon for owner/operators to neglect this tedious task. This situation can affect the performance of the system and can ultimately result in premature failure of the batteries. Problems can also arise if the water used for 'topping up' contains excessive amounts of impurities. For example, the presence of chloride ion leads to enhanced corrosion of the positive grids [11]. Also, some RAPS systems are located in areas where access is very difficult, e.g., microwave repeater stations on the tops of mountains. Hence, the cost of maintaining flooded batteries can be very high.

VRLA batteries do not require water maintenance throughout their lifetime because the oxygen produced at the positive plates during charging is reduced to water at the negative plates. This 'recombination' reaction is promoted by incorporating the following design features in the batteries: (i) the positive-to-negative stoichiometric ratio of active material is kept close to unity, thus the positive plate starts to gas before the negative plate with the result that the oxygen liberated diffuses to the negative, where it reacts with metallic lead and sulfuric acid to form lead sulfate and water; (ii) antimony is not generally employed in the grid alloys; (iii) a non-flooded electrolyte system is used, this facilitates diffusion of oxygen from the positive to the negative plates; (iv) the battery is sealed and operates under pressure in order to assist the rate of oxygen recombination.

The handling and transport of VRLA batteries are simpler than those of their flooded counterparts. This is important as many RAPS systems are transported long distances before being installed at their operational sites. VRLA batteries are sealed, and acid spillage will not occur unless the battery case is ruptured. Even then, only a small amount of acid can escape from the battery because the electrolyte is immobilized. This feature is especially beneficial when batteries are being carried over rough terrain, particularly in developing countries. Also, the low risk of acid leakage often allows VRLA batteries to be conveyed as non-hazardous cargo by both air and sea. By contrast, flooded units are always classified as hazardous freight. This latter category requires special packaging and results in additional shipping costs.

Almost all RAPS facilities that use flooded batteries have a dedicated battery room. The majority of these rooms are fitted with special ventilation systems to remove both hydrogen and acid mist, which can result in explosions and in corrosion of metal surfaces (e.g., battery holders, posts, connectors, nearby equipment), respectively. As VRLA batteries emit negligible quantities of sulfuric acid and hydrogen gas under normal operating conditions, ventilation requirements are less stringent. Moreover, given the reduced risks of corrosion and explosion, all the RAPS components can be housed in single enclosure, together with sensitive electronic equipment and, if required, a diesel generator. This lowers both the capital cost and the maintenance requirements of the facility.

The use of VRLA batteries in RAPS systems is also very attractive where space is limited and/or real estate is expensive. The batteries can generally be operated on their sides and can be stacked together closely in racks as access is not required for water maintenance. This can result in a 50% decrease in both the footprint and the volume taken up by the battery bank.

Electrolyte stratification has been responsible for the failure of many flooded battery banks. In simple terms, this phenomenon can be defined as a build-up of higher strength acid at the bottom of the battery. Stratification occurs because sulfuric acid has a higher density than water and, when formed during the charging process, will sink to the bottom of the battery container. Such behaviour results in a decrease in battery capacity due to uneven utilization of the active material [12]. Moreover, if the resulting concentration gradient is allowed to remain for extended periods, premature failure of the battery can occur.

Electrolyte stratification in flooded batteries has traditionally been removed by providing significant levels of overcharge — often, up to 15% of additional overcharge is required to remove electrolyte concentration gradients via gas-bubble stirring. VRLA batteries suffer less from stratification and are not subjected to this deliberate overcharge. The AGM design can, however, experience some stratification [13–15] unless care is taken in cell design and manufacture. For example, the use of glass-mat of poor quality, plate heights ≥ 15 cm, and inaccurate acid-filling techniques can all increase the likelihood of stratification in AGM batteries. Gel versions of VRLA batteries experience negligible electrolyte stratification during operation and, therefore, do not suffer from stratification-related failures [16]. Therefore, gel batteries is the preferred type of VRLA for RAPS applications.

The reduced tendency of VRLA batteries to exhibit stratification (and, the consequent reduced need for overcharge), can represent a benefit in terms of a decrease in both positive-grid corrosion and charging time. This acts to increase the life of the RAPS system components and also improves the efficiency of the system, especially when a diesel generator is included.

14.4.2. Disadvantages

A major complication with the use of VRLA batteries in RAPS systems is that careful control of both charge and discharge is required to achieve maximum battery life. This is best accomplished by using microprocessor-based devices that can

manage the batteries by means of advanced charging strategies (see Section 14.4.6). If sufficient control is not provided, premature failure can occur via any of several mechanisms, e.g., corrosion, electrolyte dry-out, thermal runaway, undercharge [17–23].

In RAPS battery banks that comprise strings of either VRLA or flooded batteries, there is a tendency for the capacity of individual cells to become unequal, i.e., some cells slowly decrease in capacity relative to others. In extreme situations, cells can be driven into reversal during over-discharge. This behaviour can be exacerbated by: (i) large differences in initial cell SoC; (ii) variable product quality, e.g., uneven pasting of plates; (iii) very long strings; (iv) deep and continuous cycling; (v) inadequate charging. VRLA batteries are more susceptible to this phenomenon because of the possibility of variations in recombination efficiencies. The use of microprocess control combined with carefully developed charging algorithms can, however, reduce major imbalances in cell capacities to a negligible level.

A further operational disadvantage of VRLA batteries is that the relative density of the electrolyte cannot be measured unless the battery is disassembled. Hence, voltage and current data are the only parameters that can be used to evaluate the condition of the batteries during operation. In addition, VRLA batteries are not available in a dry-charged condition. As a consequence, they have a shelf-life of only two years. (Note, dry-charged, flooded batteries if sealed airtight can have a shelf-life of >5 years.)

14.4.3. Failure modes

The failures of VRLA batteries can generally be classified as either 'catastrophic' or 'progressive.'

Catastrophic failure is characterized by a sudden decrease in charge–discharge performance and generally occurs as a result of poor manufacturing processes. Examples of these are faulty welding (both plate-to-busbar and intercell), inadequate seals between lid and case, and contamination of the electrolyte. Battery damage, such as cracked cases and crushed cell groups can also result in rapid catastrophic failure. Thermal runaway (see below) can also cause immediate failure, but this is usually related to a poorly controlled charging incident, and/or a high rate of oxygen recombination as a result of electrolyte dry-out.

Progressive failure of lead–acid batteries is characterized by a gradual decrease in battery performance. Such deterioration can arise as a result of subtle variations in battery construction and/or design. Examples include the contamination of lead and leady oxide used in battery plates, inadequate curing or forming procedures, the use of separator materials of poor quality, and inadequate plate thickness and/or compression. Progressive failure can also be induced by unfavourable operating conditions. RAPS batteries are especially susceptible to this type of deterioration as they often encounter abusive conditions such as overcharging, undercharging, temperature extremes (e.g., in desert and polar regions), and heavy-duty cycling. Advanced management strategies and hardware can minimize the damage associated with the more extreme conditions. As a consequence, batteries tend to experience

failure modes that are specific to particular types of RAPS service rather than to particular environments. Failure modes are therefore discussed here in terms of specific duty.

14.4.3.1. Overcharging. It is normal for VRLA batteries to lose some water from the electrolyte during cycling. This process results in an increase in the number and size of the oxygen pathways between the positive and negative plates and, thereby, improves the efficiency of oxygen recombination within the battery and decreases the subsequent rate of water loss. If overcharge of the battery is excessive, however, water loss can continue to be appreciable and can eventually reach a critical value (often quoted as 10% of that initially available) at which the electrical resistance of the battery increases and its performance is impaired. Water loss can also occur by diffusion through the battery case and lid, but this is not usually significant in well-designed VRLA RAPS batteries for which these components are usually thicker than for flooded types of battery.

Undue water loss also increases the likelihood of thermal runaway. This phenomenon can be defined as an increase in battery temperature due to uncontrolled recombination between oxygen and the negative plates. Gel batteries are less susceptible to thermal runaway than AGM units because they have lower internal heat generation (due to lower float currents) and higher heat transfer. Both technologies, however, become more susceptible to thermal runaway with ageing, especially AGM versions. Excessive recombination also reduces the operating efficiency of the battery (i.e., the battery requires more overcharge to achieve a fully charged state) and, in turn, decreases the efficiency of the entire RAPS system.

The delivery of too much overcharge can also result in damage to the positive active-material [24]. It has been suggested that the vigorous evolution and movement of gas as a result of this process can disrupt the internal structure of the active material. The related decrease in performance has been explained in terms of a loss of electrical conductivity within the positive plate due to progressive expansion of the active mass.

Excessive overcharge can accelerate the corrosion of positive grids. If corrosion reaches a critical value (usually around 40–50% of the total grid lead, depending upon battery design), conductivity through the grid|corrosion-layer|active-material regions can decrease to a level whereby battery performance is compromised. The corrosion process also consumes water from the electrolyte and, in some cases, the water loss can equal or even exceed that caused by the venting of oxygen and hydrogen [25]. It is worth noting that the lead–tin alloys which are typically used for the positive grids of VRLA RAPS batteries do not tolerate the same level of corrosion as the lead–antimony grids employed in flooded batteries. This behaviour, however, is more than compensated by the lower overcharge used. VRLA batteries are generally subjected to a charge return of only 103–105%, compared with 110–115% for flooded designs.

Extensive corrosion can also result in unwanted grid growth. This situation can promote a loss of contact between the grid and the active material and, in severe

cases, can give rise to the development of short-circuits. The incidence and severity of grid growth is determined by the creep resistance and tensile strength of the alloy used, and the extent and morphology of the corrosion product.

14.4.3.2. Undercharging. Undercharging is a common cause of failure of VRLA batteries operated in RAPS systems. Traditionally, manufacturers have recommended conservative charging regimes in order to minimize the likelihood of overcharge and related electrolyte dry-out (see above). Such strategies usually involve a low-to-moderate ToCV, e.g., 2.3–2.4 V per cell). Whilst this approach is satisfactory for shallow cycling, the time required to charge a battery fully following a deep discharge can often exceed the time available (see above) and charging may remain incomplete.

VRLA batteries that have been undercharged in RAPS systems often experience an accumulation and growth of lead sulfate crystals in the active material, i.e., the formation of so-called 'hard sulfate'. This phenomenon occurs in both the positive and negative plates, especially at the bottom of the latter. The hard sulfate forms as a result of continued recrystallization of the initial discharge product, via so-called 'Ostwald ripening'. The sulfate is difficult to recharge as it has a lower surface area than 'normal' lead sulfate. Also, the reduced surface area means that charging current densities are higher and, as a result, the voltage during charging rises prematurely. The net result is that, for a given ToCV, less charge is returned to a sulfated battery than to a non-sulfated battery. Such a reduction in charge return further exacerbates under-charging problems (note, hard sulfate in VRLA RAPS batteries can often be removed by means of an extended constant-current recharge, but this procedure will increase the rate of electrolyte dry-out).

A further problem that can arise from the undercharging of VRLA batteries in RAPS applications is the formation of dendrites that cause short-circuits between plates of opposite polarity, i.e., so-called 'leading through' [18]. If the relative density of the electrolyte reaches very low levels, e.g., as a result of over-discharge or prolonged stand on open-circuit in the discharged condition, the pH can increase and give rise to soluble species that promote the growth of dendrites from the plates. AGM batteries are more susceptible to this failure mechanism than gel counterparts, as penetration of the dendrites is more likely to occur through an AGM separator than through the traditional, microporous-based separators used in gel designs. Another problem faced by VRLA batteries operated at low SoC for extended periods of time is increased corrosion of the positive grids and posts (note, the corrosion rate reaches a maximum at low acid strengths [20]). An investigation conducted by Garche *et al.* [19], however, has demonstrated that gel batteries are not particularly prone to this problem. It was found that a gel battery could deliver $\sim$90% of its nominal capacity after standing at 33% SoC for over five years (note, the battery was given a capacity test every four months).

In extreme cases of undercharge, batteries can experience 'cell reversal'. This condition results in positive material being converted to negative material, and negative material to positive material, and can arise when cells in a series string develop appreciably different capacities. Cell reversal damages the active

material of both positive and negative plates. Hence, cells that have already undergone reversal have a reduced capacity and are more likely to suffer a repeat of this failure mode.

14.4.3.3. Temperature extremes. The most common failure modes of VRLA batteries operated under high-temperature RAPS duty are corrosion of the positive grids and electrolyte dry-out. Thermal runaway can also occur in older batteries, mainly during long, constant-voltage recharges, although this mode of failure is not common. Possible damage as a result of high-temperature operation can be minimized by careful design of both the operating system and the battery.

It is important that the control system in RAPS facilities be able to decrease and increase the ToCV as the battery temperature increases and decreases, respectively. This procedure, called 'temperature compensation', is required to minimize both corrosion and water loss at high temperatures, and undercharging at low temperatures. Typically, the ToCV is decreased and increased by 4 mV per cell for each °C change above or below 25°C, respectively. (Note, this procedure is especially important at temperature extremes, i.e., above 40°C and below 10°C.) Battery temperature is usually measured by means of a probe attached to the battery. Preferably, the probe should be fixed to a side of the battery that is parallel with the face of the plates. It should also be held against the battery case with a piece of closed-pore foam. In applications where discharge and charge rates are low and diurnal temperature swings are small, the ambient temperature can be used as a basis for the compensation.

The reliability of VRLA batteries under high-temperature operation can be improved markedly through careful cell design. It is recommended that flat-plate designs have thick positive grids and tubular varieties have large diameter spines. The batteries should also have electrolyte of moderate relative density (it should be noted that whilst this latter feature will reduce the corrosion of positive grids, it will also decrease battery capacity). Batteries with a large content of electrolyte are also favoured, as more water can then be lost before electrolyte dry-out affects performance. Gel batteries typically contain 20% more acid than AGM counterparts and are therefore preferred for high-temperature RAPS duty. A further recommendation for high-temperature applications is to design batteries with positive-grid alloys of high corrosion resistance, provided that the required balance between the corrosion current at the positive grids and the self-discharge current at the negative plates is maintained.

Some RAPS facilities are located in Arctic and Antarctic regions where the dark season can last for several months and the temperature can drop below −50°C. Obviously, batteries installed in PV-powered RAPS systems in these regions can experience low SoCs at sub-zero temperatures for extended periods of time. As might be expected, the two main failure modes of batteries operated under such duty are sulfation of the active material and freezing of the electrolyte [26]. The latter mode is particularly prevalent when the battery is in a discharged state. This is because the temperature at which sulfuric acid freezes increases with decreasing relative density. (Note, it is quite unusual for a fully charged battery to experience this problem.)

Freezing of the electrolyte can result in over-compression of the plate group and in short-circuits; in extreme cases, it can rupture the battery case.

14.4.3.4. Deep-cycle operation. Flooded batteries operated in RAPS systems under deep-cycle conditions usually experience softening and shedding of the positive active-material [14,21–23]. Shedding is much less of a problem in VRLA batteries due to the use of an immobilized electrolyte. On the other hand, softening of positive active-material often causes an appreciable loss of capacity. The degradation is caused by volume changes during discharge and charge — it is well known that positive active-material expands during discharge and contracts during charge [24]. The increase during discharge is caused by the conversion of lead dioxide to the more voluminous lead sulfate. During charge, the plate material contracts as lead dioxide is re-formed. After extended deep cycling, the expansion of the active material can exceed the degree of contraction, so that a net expansion occurs. The progressive expansion involves a decrease in the packing density of the positive material, which, in turn, directly affects the bulk conductivity and reduces greatly the extent to which the plate can be discharged.

14.4.4. Preferred design features

A common reason for the premature failure of batteries in RAPS systems has been the use of poor quality, or inappropriately designed, batteries. Battery choice is usually determined by economic constraints. Unfortunately, the cheaper the battery, the poorer is the performance. It should also be recognized that some system suppliers lack a fundamental understanding of the lead–acid battery.

In general, using purpose-built VRLA batteries in RAPS systems instead of generic units will significantly extend the time between battery replacements. The decision to employ purpose-built batteries should be carefully considered, however, as they are considerably more expensive. The lifetime cost of the battery bank should be calculated and should include expected cycle-life, transport charges, installation, and disposal. For example, if the batteries are to be located on a mountain and access is by helicopter, the battery with the longest life (and, most likely, the highest cost) is usually the most cost-effective choice. On the other hand, a less-expensive battery (albeit with a lower cycle-life) may be more cost-effective in systems situated closer to cities where the costs of installation and eventual disposal are much lower. The following simple guidelines should be followed in selecting an appropriate battery for a given RAPS system.

14.4.4.1. Purpose-built batteries. Gel batteries with either tubular plates or thick, flat plates (≥ 5 mm) are recommended when a long cycle-life is required. Both designs have a high level of resistance to positive-plate degradation, and can tolerate high levels of positive-grid corrosion.

Many manufacturers around the world offer tubular-plate gel batteries for heavy-duty RAPS operations. As the name suggests, the batteries have tubes that contain the plate material. This design is employed only for the positive plates, as these are

more susceptible to damage under deep-cycle conditions than the negative plates. The positive active-material is held under high compression in a gauntlet and this generally provides a long service-life under deep-discharge conditions.

Flat-plate, gel batteries should have their positive plates wrapped vertically with a thin sheet of glass-mat, and should have microporous separators inserted between the two plate polarities. Alternatively, a layer of glass-mat may be bonded to the separators. This absorbent material faces the positive plate, i.e., the ribbed side of the separator should be in contact with the negative plate (enveloped separation is not required for this plate as it experiences very little shedding of active material). Flat-plate batteries should also be designed to accommodate reasonable levels of grid growth. This may include protective sheets between the top of the plate group and the busbars, caps on the top of the positive plates, and/or 'hung' positive plates (i.e., the positive plates are suspended by the busbars and held together by plate-group compression, thereby allowing for growth downwards).

The grids of both flat-plate and tubular batteries should not contain antimony or any other additive that may decrease the hydrogen overpotential of the negative electrode. Indeed, it is recommended that ultra-pure lead be used to manufacture both the grids and the active material in order to avoid the possibility of excessive self-discharge at either the positive or the negative plates.

The batteries should be able to deliver at least 1600 discharge cycles to 80% DoD (5-h rate at 25°C; failure when capacity $< 75\%$ of nominal). Also, the self-discharge of the batteries should not exceed 3% of the rated C_5 capacity per month (at 25°C).

If batteries are to be operated at elevated temperatures for extended periods, the relative density of the electrolyte should be decreased appropriately (generally to between 1.260 and 1.240). For low-temperature applications, batteries should have a large volume of electrolyte of high relative density to minimize the likelihood of freezing, and compressible separators and/or spacers that can absorb expansion should freezing and related expansion occur. The gel battery is considered to be the most appropriate VRLA technology for this task, as it can be constructed with an excess of acid. It also uses microporous separators, which should reduce the likelihood of short-circuits if the electrolyte were to freeze and expand.

In applications where the DoD is shallow ($\sim 20\%$) and the ambient temperature is moderate (< 35°C), AGM batteries can be used. These should, however, have short plates (below 20 cm in height), and/or be operated with their plate-groups in a horizontal orientation to avoid stratification. (Note, operating the batteries in this orientation should be verified by the manufacturer to ensure that the warranty is not rendered invalid.)

14.4.4.2. Lower-cost batteries. For applications that do not require both a long cycle-life and a high level of reliability under extreme conditions, less expensive, standard flat-plate, gel batteries can prove cost-effective. These batteries typically provide 800 cycles to 75% DoD, which is half that of the purpose-built designs. This reduction in cycle-life is primarily related to the use of less robust positive plates (typically 3-mm thick) and less attention to detail in the general construction of the

battery. Generally, the batteries are also produced in much larger numbers, which provides a greater economy-of-scale.

14.4.5. Recent developments

There have been a small number of reports published recently that describe the development of purpose-built batteries for RAPS systems. A VRLA battery for use in PV power systems has been described by Shiomi *et al.* [27]. The negative plates contain a high level of carbon, but the particle size and concentration of the additive are not described. The recommended level of carbon is simply given as 'ten times normal levels'. The type of VRLA battery used in the experiments is also unclear. Batteries with and without the additional carbon were operated under simulated PV duty for extended periods. Increasing the carbon by ten-fold was found to extend the cycle-life of the batteries from 400 to 1000 cycles. This improvement was attributed to the formation of a conductive network of carbon around the peripheries of lead sulfate crystals. The subsequent increase in conductivity was claimed to improve the rechargeability of the negative plates and, thereby, to suppress the accumulation of lead sulfate.

A flat-plate, gel battery has also been specifically designed for RAPS duty, especially in high-temperature applications [23]. The battery has thick positive plates (5.5 mm), has a large reservoir of moderate strength acid, and is constructed using an ultra-pure form of lead [28] that endows the battery with a high charging efficiency. It is claimed that the battery can provide over 1100 cycles to 100% DoD (3-h rate, 25°C) before the capacity decreases to 75% of the nominal value.

A more recent publication [29] describes a battery that has been developed for use in PV power systems. This battery differs from conventional AGM and gel types in that it contains a unique form of silica-containing electrolyte. Little detail is given on this material (termed granular silica), although it is presumed to be a highly porous form of precipitated silica. The electrolyte is packed both between the plates and around the cell groups, and it is claimed that this approach applies high compression to these components and minimizes deterioration of the active material. The negative plates contain a high concentration of carbon to improve their rechargeability (see above).

14.4.6. Advanced operating strategies

Effective control systems and strategies are required in order to obtain acceptable operating efficiencies from RAPS systems. Good system management also improves the longevity of both battery banks and diesel generators.

The simplest controllers used in RAPS systems are those that regulate small PV–battery–controller systems. Such units may impose only: (i) a ToCV limit; (ii) a low-voltage disconnect set-point; (iii) a load reconnect voltage value. Often, such units are of poor design, do not deliver the required reliability and have voltage set-points that are inappropriately/incorrectly adjusted. For large RAPS facilities that have multi-energy inputs, more sophisticated control strategies are required.

Microprocessor-based units that record and utilize many different parameters offer the most accurate control and are recommended for RAPS facilities that operate with VRLA batteries. These devices can monitor/calculate variables such as battery voltages, string currents, battery temperatures, ambient temperatures, battery bank SoC, and overcharge delivered. Advanced controllers should also be fully programmable to allow for any combination of constant-voltage, constant-current, and constant-power charging. Further, as it is common for loads at RAPS sites to be underestimated and/or to increase with time, management systems of RAPS facilities should be able to allow for increases in system capacity, via the addition of further energy generation and/or battery storage.

Traditional charging procedures employed for VRLA battery banks in RAPS systems have generally been based on algorithms that have been formulated for flooded systems, but with a reduced ToCV limit (i.e., typically 2.3–2.4 V per cell for VRLA compared with 2.5–2.6 V per cell for flooded). The strategies usually comprised an initial constant-current charge which is followed by a period at constant voltage. As mentioned earlier, undercharging is a potential problem in RAPS systems that employ low ToCV limits and, where practical, a periodic boost charge has often been provided.

Shortcomings associated with the use of constant-current–constant-voltage strategies become obvious when the time required to charge VRLA batteries fully from a low SoC is considered — this time can exceed 24 h for new units. Obviously, most RAPS systems are unable to provide such extended charge times, especially PV-based facilities.

Many of the problems related to constant-voltage charging can be avoided by completing the charging process with a period of constant current, i.e., a so-called constant-current–constant-voltage–constant-current charge. This approach can deliver an accurate level of overcharge and, thereby, reduces the possibility of excessive dry-out and corrosion. A variation to this approach is to use a constant current until recombination has commenced (i.e., $\sim$2.45–2.5 V per cell), then charge at a lower value of constant current until a preset voltage change (dV/dt) has been reached (see Chapter 9). Obviously, both these strategies require a reliable charge return and, therefore, are best suited for use in systems that incorporate a diesel generator. The strategies can still be used in PV-only RAPS systems, but a more sophisticated control strategy is required to ensure that the batteries receive a regular full recharge.

An operating strategy that is gaining favour in the RAPS community is called partial-state-of-charge operation. It is useful for batteries that are resistant to electrolyte stratification (e.g., gel designs), and operates the battery below a full SoC for extended periods of time between full recharges (Fig. 14.4). PSoC operation significantly decreases the overcharge delivered to the battery compared with traditional operating algorithms and, as a consequence, reduces electrolyte dry-out, corrosion of the positive grids, and other related damage to the positive active-material during charge. The strategy can also be used with flooded batteries, provided that they are fitted with a system to circumvent acid stratification.

In one study [30], a gel battery retained over 90% of its original capacity after performing 5500 PSoC cycles between 40 and 70% SoC, with a full recharge every

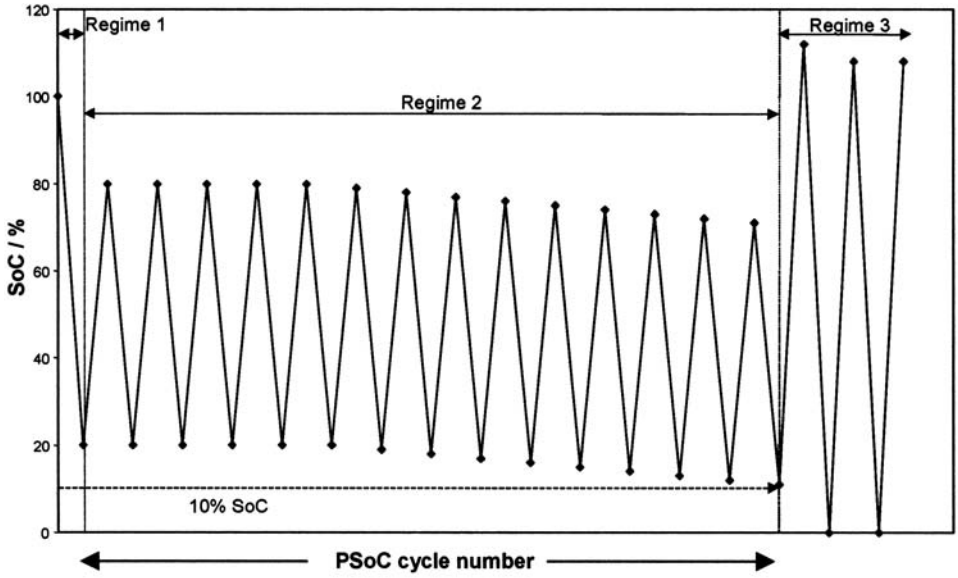

Fig. 14.4. Schematic representation of PSoC operating procedure.

84 PSoC cycles. The Ah throughput of the battery was equivalent to 1500 cycles at 100% DoD, which was approximately three times that predicted by the manufacturer. Also, the total overcharge delivered to the battery was below 101%, and this gave a charge efficiency of above 99%. Another investigation [29] reported data for a novel form of gel battery operated between 60 and 90% SoC. The capacity of the battery was still greater than 80% of the nominal value after 6000 cycles.

Series strings of VRLA batteries operated under PSoC operation require a full recovery charge on a semi-regular basis in order to maintain capacity and correct imbalances between both negative and positive plate-groups and cells. The regularity of this recharge may vary from weeks to months; if it is not provided, sulfation of active material and related capacity loss may occur. The required frequency, time, and intensity of the recovery procedure depends on the cycling history of the battery. For example, batteries charged at low rates experience less gassing and have a superior charging efficiency than those operated at high rates. Hence, the former are less likely to develop plate and/or cell imbalances and, as a result, will require less frequent recovery than the latter.

The charging efficiency of VRLA batteries also decreases with increasing SoC. For instance, a unit operated within a PSoC window of 30–70% SoC will provide a superior charge efficiency than a battery cycled between 50 and 90% SoC. As a consequence, a battery operated under the 50–90% regime would require a more frequent recovery than a unit cycled between 30 and 70% SoC.

The practical benefits of PSoC operation are being demonstrated in a project based in Peru that was instigated in 1997 by the government of Peru, the International Lead Zinc Research Organization (ILZRO), the Solar Energy

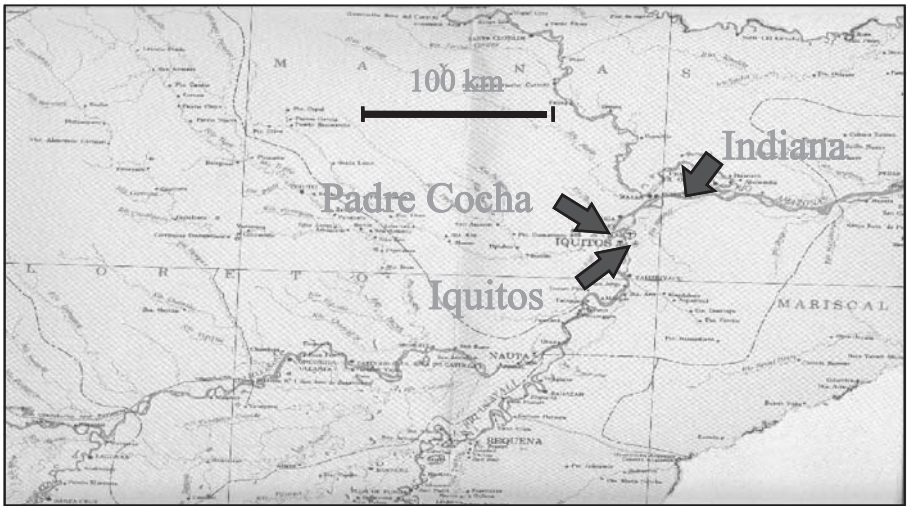

Fig. 14.5. Location of RAPS sites at Padre Cocha and Indiana in Peru.

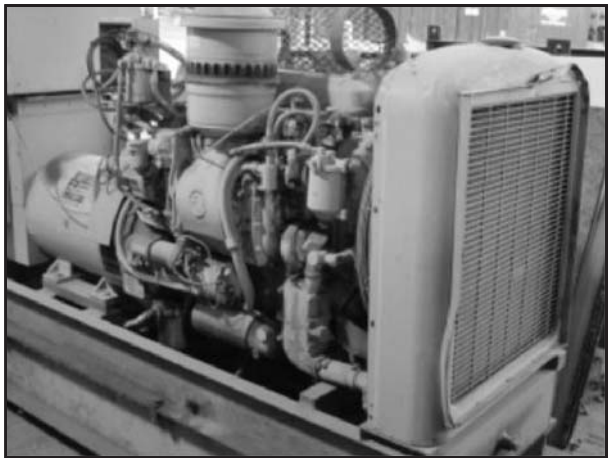

Fig. 14.6. Typical diesel generator used in RAPS systems.

Industries Association (SEIA), and several international companies and research groups. The initiative involves the installation and demonstration of a series of RAPS facilities in the Amazon region. Funding has come from the United Nations Development Program, as well as from other national and international energy, environmental and developmental organizations and agencies. Initially, RAPS systems are being installed in two villages, namely, Padre Cocha and Indiana (Fig. 14.5). The facilities comprise diesel generators (Fig. 14.6), a PV array (Fig. 14.7), and a VRLA battery bank (Fig. 14.8); the facilities are operated and monitored remotely. The PV array provides between 30 and 35% of the energy generated for the system

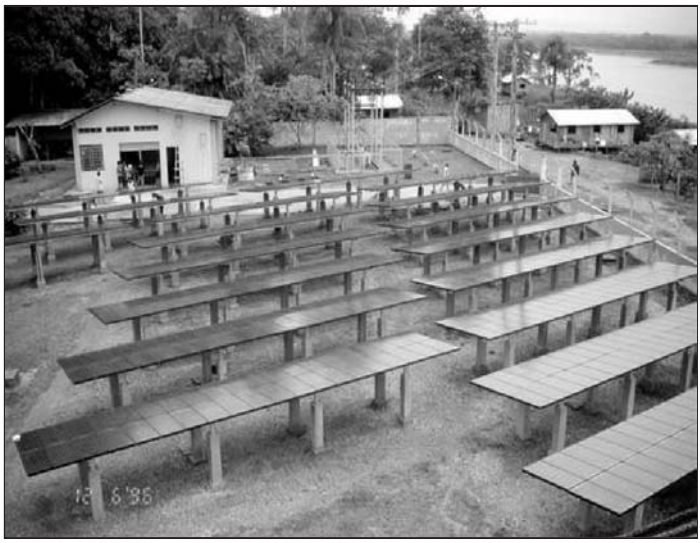

Fig. 14.7. Photovoltaic array located at Padre Cocha in Peru.

Fig. 14.8. VRLA batteries that will be installed in the Peru RAPS sites.

daily; the remainder is generated by the diesel generator. The villages will thus be provided with 24-h electric power for the first time (Fig. 14.9). The batteries chosen for the project are of the gel design and have been specially designed for high-temperature RAPS applications [23]. The units are operated using algorithms specifically designed for the project by CSIRO in Australia. The algorithms are based on PSoC operation and have been proven in the laboratory under simulated

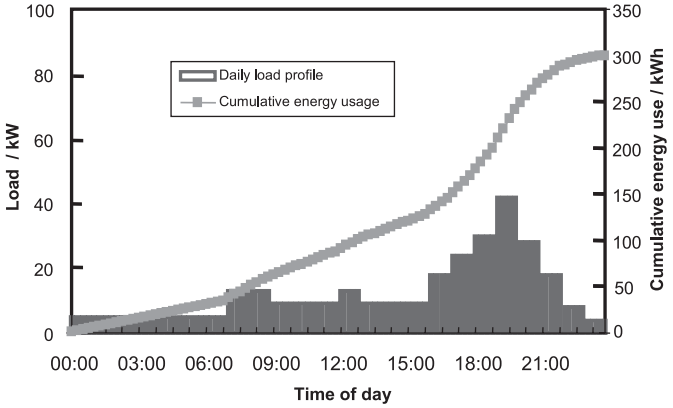

Fig. 14.9. Typical load data for RAPS site at Padre Cocha in Peru.

RAPS conditions. They will be fine-tuned in the field via feedback provided by a satellite data-link. This strategy is expected to extend battery life to eight years and reduce diesel run-time. Thus, system efficiency will be improved and fuel consumption and its related pollution will be decreased.

References

1. C. Mayhew, R. Simmon, NASA/GSFC, NOAA, NGDC, DMSP Digital Archive.
2. K.V. Ramani, *Finesse Workshop for Financing of Energy Services for Small-scale Energy Users*, Kuala Lumpur, Malaysia, 1991, p. 37.
3. Philippines Market Study Team, *Finesse Workshop for Financing of Energy Services for Small-scale Energy Users*, Kuala Lumpur, Malaysia, 1991, p. 27.
4. H. Hofling, W. Gocht, K. Knecht, B. Schleich, F. Diederich (Eds.), *Proceedings of the International Seminar on Strategies and Measures for the Dissemination of Solar Energy Systems in Rural Areas of South East Asia*, Manila, Philippines, 1989, p. 107.
5. C.S. Heruela, W. Gocht, K. Knecht, B. Schleich, F. Diederich (eds.), *Proceedings of the International Seminar on Strategies and Measures for the Dissemination of Solar Energy Systems in Rural Areas of South East Asia*, Manila, Philippines, 1989, p. 216.
6. M. Watt, E. Hart, A. Langworthy, *J. Power Sources*, **16** (1985) 205–232.
7. P. Singh, B. Jonshagen, *J. Power Sources*, **35** (1991) 405–410.
8. J.M. Hawkins, T. Robbins, *Proceedings of the 21st International Telecommunications Energy Conference*, Copenhagen, Denmark, IEEE, 1999, p. 27.
9. T.A. Dougherty, A.P. Karpinski, V. Alminauskas, J. Billingsley, J. Stannard, W. Halliop, *Proceedings of Power Sources Conference*, **37** (1996) 13.
10. M. Stevens, *Proceedings Remote-area Power-supplies and Renewable Energy Applications Conference*, Townsville, Queensland, Australia, 1993, Electricity Supply Authority of Australia, 1993, p. 17.
11. R.H. Newnham, A.F. Hollenkamp, D.A.J. Rand, *J. Power Sources*, **53** (1995) 215–228.
12. G.W. Vinal, *Storage Batteries*, Wiley, New York, 1955.
13. W.G.A. Baldsing, R.D. Bramley, R.H. Newnham, C. Power, *Lead–acid Batteries for Remote-area Energy Storage, ERDC Project No. 1525 — Final Report, February 1993*, CSIRO Division of Mineral Products, Port Melbourne, Australia, Commun. MPC/M-379, 208 pp.
14. K. Higashimoto, A. Miura, T. Hayakawa, A. Komaki, *Prog. Batteries Sol. Cells*, **8** (1989) 268–270.
15. Y. Nakayama, T. Nagayasu, K. Kishimoto, Y. Kasai, *Yuasa Jiho*, **71** (1991) 46.
16. H. Tuphorn, *Rev. Gen. Electr.*, **3** (1990) 45.

17. R.H. Newnham, *J. Power Sources*, **52** (1994) 149–153.
18. B. Culpin, D.A.J. Rand, *J. Power Sources*, **36** (1991) 415–438.
19. J. Garche, A. Jossen, H. Doring, *J. Power Sources*, **67** (1997) 201–212.
20. J. Garche, A. Jossen, H. Doring, in: A. Attewell, T. Keily (Eds.), *Power Sources 15*, *Research and Development in Non-mechanical Electrical Power Sources*, International Power Sources Symposium Committee, Leatherhead, England, 1995, pp. 199–219.
21. M. Whitehead, *Batteries International*, **5** (1990) 30–31.
22. A. Brunia, D. Schmal, H.P.W. Fransen, R.J.C. van Zolingen, *Report for Netherlands Organisation for Energy and Environment (NOVEM)*, Institute for Environmental Sciences, Netherlands, 1992, 101 pp.
23. R.H. Newnham, W.G.A. Baldsing, *J. Power Sources*, **66** (1997) 27–39.
24. A.F. Hollenkamp, R.H. Newnham, *J. Power Sources*, **67** (1997) 27–32.
25. D.A.J. Rand, L.S. Holden, G.J. May, R.H. Newnham, K. Peters, *J. Power Sources*, **59** (1996) 191–197.
26. O. Ikkala, A. Nieminen, *J. Power Sources*, **31** (1990) 321–327.
27. M. Shiomi, T. Funato, K. Nakamura, K. Takahashi, M. Tsubota, *J. Power Sources*, **64** (1997) 147–152.
28. L.T. Lam, N.P. Haigh, C.G. Phyland, N.C. Wilson, D.G. Vella, L.H. Vu, D.A.J. Rand, *Proceedings of the 20th International Telecommunications Energy Conference*, San Francisco, CA, USA , IEEE, 1998, pp. 452–460.
29. M. Adachi, Y. Okada, M. Shiomi, M. Tsubota, *GS News Technical Report*, **57** (1) (1998) 10.
30. R.H. Newnham, W.G.A. Baldsing, *J. Power Sources*, **59** (1996) 137–141.

Valve-Regulated Lead–Acid Batteries
D.A.J. Rand et al., editors

—CHAPTER 15—

RECOVERY AND RECYCLING OF LEAD–ACID BATTERIES

M.W. Stevenson

15.1. Introduction

The recycling of lead–acid batteries has been an established practice since the introduction of the battery in the late 1800s. Of course, other processes that involve the remelting of lead have been known for over 2000 years. Thanks to its ease of recycling and subsequent refining, lead has become one of the most recycled metals. Spent batteries are now a vital source of lead units in the smelting industry, with over 60% of the world's supply of lead sourced from secondary processing. Without recycling, lead would become an expensive commodity, and the threat from alternative battery systems would be much more significant.

Total recovery and recycling of the lead–acid battery is relatively straightforward, as batteries are easily retrieved from most of the automotive and industrial applications in which they are used. Recovery of the lead and other components from the battery is uncomplicated because batteries are easily broken and divided into their various fractions. If a suitable combination of materials is chosen during design and construction of the battery, almost complete recovery and re-use of materials is possible at the expense of only a relatively modest amount of energy [1].

Although lead has been classified for many years as a hazardous product, the main driver behind the recycling of lead–acid batteries is the value of lead as a tradeable commodity. Lead and its products form part of the scrap-metal family (with aluminium, zinc, and copper and its alloys) that has been the focus of scrap-metal merchants for many years. Throughout the world, efficient scrap networks and channels exist to supply the recycler with raw materials such as aluminium cans, copper wire, and lead–acid batteries.

Early secondary battery smelting was carried out in small-scale operations, often by the scrap-metal merchants themselves. Whilst most of the small operations have now been phased out in Western countries via either closure or consolidation, small-scale smelting practices still exist in many Asian countries, e.g., India, China and Indonesia. Even in these countries, where recycle rates are very high, price is the driving influence on the scrap-metal industry. This applies no less to the recovery of lead.

The dynamics of the secondary-lead industry are quite different from those of the primary-lead industry. For many years, battery scrap has been the sole domain of

the secondary smelters, with the primary smelters relying on mine concentrates as their major feed. Differences between these two feeds, particularly the presence of lead sulfate in battery scrap and the subsequent recovery methods, have led to a differentiation between primary and secondary lead. The varying recycling methods employed throughout the world, ranging from clay-lined, 44-gallon drums in India to the latest pyrometallurgical and hydrometallurgical methods available elsewhere, will do little to change this distinction in the near term.

As a result of the increasing role of maintenance-free and valve-regulated lead–acid (VRLA) batteries in automobile and industrial applications, demand will increasingly be placed on the secondary industry to produce lead and alloys of higher purity to meet the tighter specifications for these batteries. Furthermore, as the design of the battery and the materials used in its construction change, and the number of battery sizes increases, challenges will confront the secondary industry as it strives to provide lead of the required quality at no added cost.

This chapter presents a brief outline of the recovery and processing of spent batteries, the basic smelting and refining principles of lead, and some of the hurdles that the secondary sector will face in meeting the challenge of building a better battery.

15.2. Battery Collection and Processing

It has been common practice for many years to collect and recycle spent lead–acid batteries because of their value as a major source of lead units. This has led to highly developed operations whereby batteries are collected, sorted, and delivered to the secondary smelter for recovery of the lead and other materials of value.

15.2.1. Battery collection

It is the value of lead as a commodity rather than solely environmental considerations that dictates recycling rates for batteries, particularly in developing countries. As living standards increase, the economic incentive to collect spent batteries decreases. The role of governments has been to support recycling efforts via environment legislation. In many western countries, recycling schemes and directives have been introduced to maintain the high recycle rate of the battery and to ensure that it is collected, transported, and recovered in an environmentally sound manner. Some countries in the European Union have been at the forefront of regulations to control the collection and treatment of batteries [2,3], as follows.

- Italy. The consortium, COBAT, was created in 1988 with the responsibility for collection and marketing of used batteries, the re-treatment of collected batteries if market economics are not effective, and the research and development for cleaner recycling of spent batteries. The consortium comprises secondary lead smelters, battery manufacturers, scrap merchants, and battery retailers. The customer pays a fee on each battery, and this is used to fund COBAT.
- Denmark. In 1996, Denmark had set a target of 99.9% collection and recovery of lead–acid batteries. A fee is imposed on all importers and producers of lead

batteries, and all retailers are obliged to take back used batteries free of charge. Legislation has been enacted by the Danish government to ban the use of lead, but temporary exemptions have been granted for a list of applications, and this includes the lead–acid battery.

- Germany. The German government has attempted a comprehensive approach to cover all types of batteries. An obligation is placed on the consumer to return spent batteries to the retailer or scrap merchant. A levy of €10 is placed on all batteries purchased without the return of a similar spent battery, and there is an obligation on retailers to accept all batteries returned by consumers. The retailer/merchant is also required to report annual statistics on the sales/returns balance to the authorities.

Many other western countries have implemented similar formal collection schemes to produce an efficient and environmentally focused recovery chain, thereby maintaining recycle rates of greater than 90%. Spent batteries move quickly from the end user to the secondary smelter via a single collection agency. Tight regulations apply to the handling and delivery of the product. For example, it is not permitted to drain the acid from the battery until it is delivered as a whole unit to the smelter. Interfering or tampering with the battery is prohibited by most regulations.

Other countries, particularly in the developing world, have high recycle rates (often approaching 100%), but rely on informal collection routes and environmentally unsound treatment of the spent battery before it reaches the smelter. Collection of the battery usually starts with the scrap collector and passes through a maze of battery reconditioners, scrap merchants, and traders. The final product delivered to the smelter can often be a hessian bag of broken battery pieces. During its journey, the battery is drained of acid, plastic is stripped, and the metallic components are removed and melted. Whilst there may be regulations and laws governing the correct handling and disposing of batteries, these are infrequently followed in many developing countries.

The high recycle rate in developing countries is supported by the scrap prices, which, even in western terms, are very high. In China, spent automotive batteries are purchased for US$ 270–300 per tonne, compared with an equivalent of US$ 80–90 per tonne in Europe and US$ 60–80 in Australia. This creates a strong demand for all types of lead–acid batteries, including small 6-V and 12-V VRLA batteries. Western countries are still devising collection schemes to recover batteries of this size, which is a challenging task due to their low per-unit value and wide dispersion.

15.2.2. Battery processing

Once received at a secondary smelter, a lead–acid battery undergoes several processing stages to recover and treat the various component parts. In most modern plants, automatic battery breakers are used to process and recover these parts. There are many variations to battery-breaking operations throughout the world, although the outputs obtained from each operation are similar, namely, battery pastes, metallic fractions, acid, plastic components.

Fig. 15.1. Typical battery-breaker from Battery Recycling Industries. Conveyor belt in foreground is for small VRLA batteries that bypass the trommel, which is in the background.

Two manufacturers of processing equipment are Engitech Impianti CX [4] and Battery Recycling Industries (formerly MA Industries) (Fig. 15.1). These companies supply whole battery-breaking operations or selected machinery for parts of the process, as required by the smelter. Smelters often build auxiliary equipment for their own operations, because battery feedstock, product recovery or furnace feed requirements may demand different equipment from that available off-the-shelf.

Before being processed, the batteries are drained of their free acid, and this is pumped to a separate plant. In most plants, the acid is neutralized with either calcium or sodium hydroxide:

$$H_2SO_4 + Ca(OH)_2 \rightarrow CaSO_4 + 2H_2O \tag{15.1}$$

$$H_2SO_4 + 2NaOH \rightarrow Na_2SO_4 + 2H_2O \tag{15.2}$$

The gypsum produced in reaction (15.1) is disposed of at a secured landfill site whilst the water, often required to be slightly alkaline, is sent to a sewer. For processes using sodium hydroxide, depending upon the environmental requirements, the sodium sulfate is sent to a sewer or recovered as a solid, via an evaporator/crystallization process, and sold for uses such as household detergent. Other plants have found outlets for the dilute acid in areas such as alkali waste neutralization.

The first major battery-breaking step is the dismantling or breaking of the battery to gain access to the lead units. There are numerous ways to do this, but the most common approach is via a hammer mill or roller crushers. The fragmented product is fed to a sink/float or hydrodynamic separator where the fractions are sorted. In the basic sink/float cell, the plastic fractions are floated off and removed to the plastics recovery section whilst the lead-bearing portions of metallics and compounds sink to the bottom and are removed via conveyors or other means, for further

classification into metallic and oxide fractions. The hydrodynamic separator works in a similar mode, although the plastic fractions, e.g., polypropylene, are separated at an earlier stage.

Other processes exist where the top of the battery is removed by saw and the battery plates extracted via a trommel. The plates and separators are then dried and are charged directly to the furnace. The case, top-lead and other residual lead are recovered via hammer mill and classification. This process, referred to as plate extraction, is mainly used for rotary furnaces utilizing the soda–iron system (see Section 15.3).

The lead units are separated by various classifiers, screens, and filters into two fractions: lead paste and the metallic fragments. The metallic fraction, consisting of grids, terminals, and straps, is a valued feed in secondary operations, as it requires little processing and often bypasses the smelter to be directly melted in the refinery.

The recovered lead paste is a mixture of the positive (lead dioxide) and negative (lead sulfate) active materials, small metallic fractions from the grid and other materials that have been added to the battery paste such as carbon black, expanders, and reinforcing fibres. A typical range of components in recovered battery paste is given in Table 15.1.

Due to the pyrometallurgical and hydrometallurgical difficulties associated with recovering lead from lead sulfate, the paste must undergo a desulfurization process to remove the unwanted sulfate ion. The paste, which is dark brown due to its content of lead dioxide, is pumped as a slurry into reaction tanks where sodium carbonate is added (see also Chapter 16). The resultant reaction allows the conversion of the sulfate present in the slurry to lead carbonate via the following reaction:

$$PbSO_4 + Na_2CO_3 \rightarrow PbCO_3 + Na_2SO_4 \tag{15.3}$$

Alternatively, the slurry containing lead sulfate may be treated with sodium hydroxide rather than sodium carbonate to produce lead oxide via:

$$PbSO_4 + 2NaOH \rightarrow PbO + Na_2SO_4 + H_2O \tag{15.4}$$

Each of the above processes offers some advantages over the other, in terms of sulfate conversion, solubility of additives, or formation of unwanted insoluble salts. The smelter will select the process most suitable according to circumstances.

Table 15.1. Typical composition of components in battery paste.

Material	wt.%
Lead sulfate	55–60
Lead dioxide	30–35
Metallic lead	1–4
Others	5–10

The desulfurized slurry from both processes is pumped to a filter press. Soluble sodium sulfate and carbonate/hydroxide (depending on the reagent used) are removed through a series of backwashing and rinsing cycles. The solid product, once dried, is ready to be charged to the furnace whilst the soluble sodium sulfate is either disposed of via the plant's effluent system or is reclaimed as a solid product, similar to that in the caustic soda/acid neutralization process outlined above.

In the plastics recovery section, the polypropylene is separated from other plastics and products such as PVC separators, ebonite cases, labels, rope handles, etc., via a series of classifiers and hydro-cyclones. The polypropylene pieces or chips are cleaned, washed, and separated from any remaining paste and dust. Once the material has been shredded to smaller fragments, the plastic is a valuable by-product of battery recycling. Plastic cleaning and processing methods are so effective that heavy metal contamination in the final polypropylene product is very low. The final product can be used in household goods such as washing machines, vacuum cleaners, and dishwasher parts, or in products for the automotive industry [5].

The waste plastic material separated from the polypropylene is either sent to the smelter to use as a reducing agent in the furnace or disposed of in a secure landfill.

15.3. Recovery and Refining

Two methods exist for the recovery of lead from battery paste, grid material, and other lead components; pyrometallurgical and hydrometallurgical. Pyrometallurgical systems, commonly referred to as smelting, are the dominant methods used in the recovery of both primary and secondary lead throughout the world, with only a very small tonnage recovered by various hydrometallurgical methods. Electrolytic methods are used in refining some of the resultant lead bullion metal from smelting operations, although pyrometallurgy remains the dominant overall process for refining. Electrolytic refineries are commonly found in China, Japan, and Korea.

Just as there are minor operational variances from plant to plant in the separation and recovery of lead-bearing units, so it is for lead smelting and refining operations. Although smelters appear to have varying operations with the differing furnace types, the overall basic chemical reactions are the same, as outlined below.

15.3.1. Pyrometallurgical methods

Smelting is a process whereby metals, such as lead, iron, or copper, are recovered from a feedstock by the chemical reduction of their compounds. These reactions occur in various processes and take place at temperatures up to 1400°C in some lead blast furnaces, and to over 1800°C in iron blast furnaces. Various types of furnace are utilized worldwide for the smelting lead. These include the blast, reverberatory and Isasmelt/Ausmelt technologies [6] (see also Chapter 16), and the QSL [7] and Kivcet [8] processes. Not all secondary lead producers use modern technology such

Fig. 15.2. Coal-fired reverberatory furnace processing battery scrap in China still in operation today.

as the Isasmelt/Ausmelt process. For example, 1800s technology is still widely employed in developing countries. The coal-fired reverberatory furnace shown in Fig. 15.2 is one of many types of older smelting technology still in use throughout Asia and Africa today.

Although each smelter may have a distinctive mode of operation, all smelters produce similar outputs, viz: lead bullion, slag and, in some cases, a complex sulfide matte or speiss. Depending upon the operational parameters of the process, such as the fluxes and reagents used, the unrefined lead bullion contains varying amounts of impurities. These include valuable elements such as gold, silver, copper, and other, sometimes unwanted, elements like antimony, cadmium, and arsenic. In smelting processes where impurities such as antimony, tin, and arsenic are encouraged to enter a slag/matte phase, the resultant lead bullion is termed 'soft'. The antimony content is around 0.1–0.5 wt.%; other metallic elements ('impurities') are present in only trace amounts. By contrast, 'hard' lead bullion is produced in other processes where all the impurity elements report to the lead bullion to leave a depleted slag for disposal. Levels of over 1.5 wt.% antimony are found in 'hard' lead bullion. (The slag/matte recovered in the 'soft' bullion process is typically re-smelted in a blast furnace to recover the impurity elements. The resulting material often contains over 8 wt.% antimony and is used for blending in the production of various lead alloys.) Both types of bullion require further refining, which is outlined in detail below.

Until recently, in many countries around the world, the recycling of battery scrap and residues was only carried out by secondary producers. This is now changing as primary smelters, who formerly handled only concentrates, are adapting their plants to handle battery scrap and other residues. This change has been prompted by a number of factors, particularly the financial viability of smelters and the need to maintain a continuous supply of concentrate/lead units to the smelter.

Previously, primary lead producers would not process battery scrap and residues due to a number of problems encountered in the plant, as follows.

- The presence of chlorides from the PVC separators in the battery posed significant problems with the larger, integrated lead smelters who recovered other metals such as silver, copper, and zinc. Chlorides have serious implications for the recovery of these other elements. They reduce the life of the refractory lining of the furnace and affect the sinter quality. These difficulties have largely abated with the shift to polyethylene separators.
- Primary plants were not geared up to handle varying product mixes or low tonnage material through the sintering and feed operations to the blast furnace.
- Given the low level of valuable elements in battery scrap — most notably silver — it was often a financial disadvantage for major primary smelters to treat battery material in preference to a concentrate that may contain over 1000 grams of silver per tonne of lead.
- Difficulties in treating and smelting the lead sulfate contained in the lead paste.

The treatment of incoming sulfur units in the feed is the major difference between the operations of primary and secondary plants, as the form and concentration of sulfur is quite different in the two cases. Most concentrate feed used by primary smelters is a lead sulfide, generally galena, which contains from 10 to 20 wt.% sulfur according to the quality of the concentrate. This material must be processed via a sintering plant or by other methods such as the QSL or Isasmelt processes, where the concentrate is oxidized via the following reaction to produce a material that is suitable for smelting in the furnace:

$$2PbS + 3O_2 \rightarrow 2PbO + 2SO_2 \tag{15.5}$$

This reaction is exothermic, and the heat evolved is utilized in the sintering plant to agglomerate the lead oxide and added fluxes, such as limestone and silica, into a porous lumpy mass (sinter) suitable for feeding to the furnace. Sulfur levels are quite critical in maintaining the dynamics and throughput of a sinter plant.

By contrast, the lead sulfate contained in battery scrap does not oxidize like lead sulfide and can hinder the reactions in the sintering operation. In fact, lead sulfate passes unchanged through the sintering process and delivers unwanted sulfur to the furnace where, via various reactions, the lead is finally recovered.

To overcome the problem of processing lead sulfate, two smelting regimes have been adopted across the world for secondary lead smelting. These two processes are loosely termed in the industry the 'silicate' and 'soda–iron slag' systems. The major difference between the two systems is the smelting chemistry used to treat lead sulfate. The soda–iron smelting method operates within the sulfide system by means of an unusual 'oxidation-reduction' reaction, whilst the silicate slag system is oxide-based after the battery paste has been pre-treated, as outlined in Section 15.2. There are other smelting methods used, but they are generally derivatives of one or the other of the above systems.

In production terms, the silicate system dominates throughout the world; it accounts for over 90% of the four million tonnes per annum of the secondary lead

market. The system is generally adopted for the larger furnaces such as the blast/reverberatory types, with outputs that range from 30,000 to 140,000 t per annum, although rotary and other furnace types also utilize this slag system. The soda–iron system is generally used in conjunction with the short-barrelled rotary furnace (see Fig. 15.3 later). This type of furnace, whilst very adaptable to different scrap types, has a relatively small tonnage output of around 8000 to 15,000 t per annum.

The silicate slag system is utilized extensively in the recovery of secondary lead. It is also the most widely used pyrometallurgical system for the smelting and recovery of other important metals, particularly iron, copper, and zinc. The system is employed in many types of furnace and in a variety of smelting practices, but in each case where it is used in the production of lead, the end-products are a silicate-based slag and lead bullion. Unlike the soda–iron system, there are also many variations in the composition of the silicate slag. Depending on the operational parameters of the individual smelter, the slag can contain appreciable amounts of calcium, iron and aluminium oxides. These produce complex silicate materials such as kirschsteinite ($CaFeSiO_4$) and hardystonite ($Ca_2FeSi_2O_7$) [9].

Lead smelting using the silicate system is usually carried out between 950 and 1400°C, depending on the type of furnace and the slag composition required. Charge materials to the furnace generally include the following.

- Lead-bearing residues. These materials consist of pre-treated battery paste and scrap, dusts, wastes, etc., and make up the major portion of the charge.
- Reductant. Generally, coke or coal is used, but charcoal can be substituted. Ebonite from hard rubber batteries was previously used, mainly as a disposal route, but is now phased out following the decline in the use of the material as a battery case. Some processes smelt whole batteries and employ the polypropylene cases and separators as the reducing agent.
- Slag formers or fluxes. Silica, iron oxides, and other minerals are naturally present in the concentrate feed of primary smelters. In the case of the secondary lead furnace, however, such materials must be added. Sand, limestone, and iron are common additives. In recent times, due to the use of AGM separators in VRLA batteries, silicate levels are increasing in the lead feed.
- Viscosity- (or slag-) modifiers. In some furnaces that operate at relatively low temperatures, borates or sodium-containing compounds are added to decrease the viscosity of the slag. These work by modifying the silicate structures.
- Foam-depressants. Iron and other additives are often added to help reduce foaming in the furnace. Foaming occurs when the charge is too rich in metal or in the early smelting stages when carbon dioxide evolution occurs [10].

The lead-bearing residues are generally lead oxides, although carbonates may be present in the pre-treated battery paste, depending on the de-sulfurization process used. Any lead carbonate present in the paste will quickly decompose once the temperature increases above 315°C. The material converts to lead oxide (reaction (15.6)), i.e.,

$$PbCO_3 + \{heat\} \rightarrow PbO + CO_2 \qquad (15.6)$$

The thermodynamic driving force for the reduction of the lead oxide is the same as that for iron, copper, and other metal oxides, i.e., metal oxide is reduced by carbon to release metal and carbon dioxide:

$$2PbO + C \rightarrow 2Pb + CO_2 \tag{15.7}$$

Other metal oxides in the lead feed, particularly the alloying elements in the parts and grid fractions, also undergo reduction during the smelting process. Each element is deported at a different stage to yield different end-products for either further refining or disposal, as follows.

- Antimony, arsenic, and tin. Depending on the process used, the operator can place the majority of these elements either in the bullion metal or in the slag. In most cases, the elements are recovered in the bullion and subsequently used to produce alloys, although there will always be some metal loss to the slag fraction. Antimony and arsenic trioxides can be found in the fume.
- Copper, bismuth, and silver. The major portion of these elements reports to the lead bullion, although minor trace levels, particularly of copper and bismuth, can be found in the slag.
- Selenium and cadmium. As furnace temperatures increase, selenium and cadmium volatilize and report to the fume (note, the boiling points of selenium and cadmium are 685 and 765°C, respectively). No appreciable quantities of these elements are found in the lead bullion, although cadmium levels can be found in the slag.
- Calcium and aluminium. These elements return to their oxide state and report to the slag. They are not found in the bullion in their metallic state.

Once the smelting cycle is complete, most processes allow for the separate tapping of the bullion lead and the slag. The bullion lead is subsequently transferred to the refinery for processing and refining, whilst the slag is tapped into a form ready for disposal or re-treatment. This can involve water quenching into granules or casting directly to large blocks, which simultaneously allows any metallic lead caught in the viscous slag to settle out and to be reclaimed. Slag that does not contain any valued elements, such as antimony or tin, is termed 'spent slag' and is discarded according to relevant government requirements.

Environmental and legislative considerations increasingly influence the disposal of products such as spent slag. For example, silicate slags are being widely substituted for soda-iron slags, as residual elements are permanently immobilized in the silicate structure, whereas they can be leached out of the soda–iron slag.

As previously mentioned, secondary smelting operations include many variations of furnace design, operating conditions, and type of feed. Some of these differences include the following.

- Two-stage smelting. Often the large secondary smelters use a two-stage process to smelt battery scrap. With a limited amount of reduction in the first stage, a 'soft' lead and a high antimonial slag are produced. This process is usually carried out in a reverberatory furnace with capacities exceeding

50,000 t per annum. In the second reduction stage, the antimony slag is reduced to produce high antimonial lead bullion and a silicate slag. Blast, rotary, or electric arc furnaces are used for the second smelt stage. One major advantage of this method arises in the refinery where it is easier to process the soft lead, as fewer chemicals are needed. This process is common in the USA and in Japan.

- Smelting battery components. Companies with smaller furnaces, such as the rotary, are able to batch-process different lead residues from battery-breaking operations and other sources. Materials with high metallic content, such as battery grids and parts, are smelted/melted separately from materials that contain battery paste. This may require a change in the amount of reduction agents and fluxes required, but it can result in a cost saving for the smelter.
- Production of matte. A few secondary smelters form a matte, a high sulfide material generally containing arsenic, to remove unwanted elements. This process is common in primary smelting.
- Direct feed of whole batteries. Some processes allow the direct charging of whole batteries to the furnace. This process uses the polypropylene cases, separators, and other plastic materials as the reducing agent in the furnace rather than coke or coal. Some smelters use the cases intermittently, as dictated by the plastic sale price with respect to the cost of coke or coal.

The soda–iron slag regime is based around the sulfide reaction series. There are very few applications in the metal recovery and smelting industry using a sulfide reaction. The only smelting operation of note is the reduction of antimony sulfide by iron to claim metallic antimony.

For lead sulfate, the system proceeds in two stages. First, sulfate is converted to lead sulfide by the addition of a reductant such as coke or coal, as shown in reaction (15.8). Second, the lead sulfide is converted to metallic lead in the presence of iron, with the formation of iron sulfide via reaction (15.9). The iron is generally in the form of waste turnings or chips.

$$PbSO_4 + 2C \rightarrow PbS + 2CO_2 \tag{15.8}$$

$$PbS + Fe \rightarrow Pb + FeS \tag{15.9}$$

To complete the process, sodium carbonate, which is added as the fluxing agent, combines with the iron sulfide to produce the soda–iron slag, as shown in reaction (15.10). (Although often referred to as a slag, the product is in fact a matte, due to its high sulfur content.) The reactions of the process, particularly the slag formation, have been simplified here, but detailed information on the system has been outlined by Queneau [11].

$$2PbSO_4 + Na_2CO_3 + Fe + 9C \rightarrow 2Pb + FeS \cdot Na_2S + 9CO + CO_2 \tag{15.10}$$

The two major benefits of the soda–iron slag are its low melting point and its ability to capture virtually all of the sulfur present in the battery scrap. The lowest melting point for the slag is at the eutectic point, 36 wt.% FeS at 640°C. The system does exhibit a large range of low melting points, particularly between 25 and 75 wt.% FeS, where the highest temperature is 695°C at 73 wt.% FeS. These temperatures are well below the melting point of the various silicate slags that can range to over 1200°C. Around 98% of the sulfur charged to the furnace in the battery scrap is captured by the slag. The remaining 2% is usually found in the fume collected by a baghouse or other dust collection devices. Due to low levels in sulfur stack emission, no auxiliary equipment, such as acid plants or scrubber is required.

The slag system combined with the short-barrelled rotary furnace, as shown in Fig. 15.3, has appealed over the years to the small secondary lead producer. Such an operation offers the following benefits.

- Simplistic operation. No complex equipment is needed in the operation of a plant. The rotary furnace requires little maintenance compared with other smelting operations.
- Feed pre-treatment. Battery scrap does not have to be pre-treated as in the case for the silicate system. Residues and other material can be fed directly into the furnace in almost any size or form.
- Flexibility. The furnace is operated in batch mode, so the operator has the ability to use other feeds which include concentrates. The furnace can be shut down or started up with relative ease and speed.

Lead-smelting operations based on the soda–iron system still exist in Australia, South-East Asia, Europe, and Central America despite the fact that the system is prone to environmental problems. First, sodium compounds present in the slag are somewhat soluble and can thereby produce a caustic effluent and leave the iron and other compounds behind as a fine powder. Second, due to un-reacted coke and iron particles found in the slag under certain conditions, the slag can spontaneously combust. Secure landfills are required in most countries for the storage of the slag,

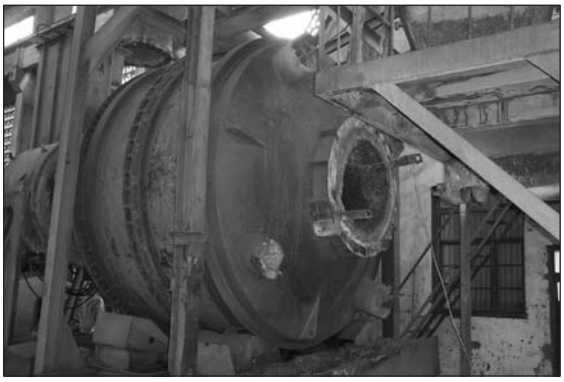

Fig. 15.3. Short-barrelled rotary furnace undergoing maintenance. Note, fume hood and ductwork has been removed.

but in most cases, these are becoming expensive and governments are prohibiting products such as the soda–iron slag.

15.3.2. Hydrometallurgical methods

Although substantial work has been carried out on the recovery of lead from battery residues by electrolytic means, no system has been adopted for large-scale commercial operations. Companies such as Engitech Impianti in Italy and RSR in the USA have patents on electrolytic systems, whilst a European consortium, led by Tecnicas Reunidas in Spain, has developed the chloride-based PLACID and PLINT lead recovery processes.

Electrolytic processes can potentially produce lead of greater purity than secondary pyrometallurgical routes, without passing through a conventional smelting and refinery process, and they have fewer waste products. The disadvantage of this type of operation is the high cost of electricity and/or other consumables that are needed to yield a metal that is often priced at below US$ 500 per tonne.

In all of the above processes, pre-treatment of the battery paste is required so that compounds, such as lead sulfate and lead dioxide, can be accessed by electrolytic methods. Short summaries of the three processes are given below.

- Engitech process. This technology uses a leaching solution of fluoroboric acid and lead fluoroborate. The desulfurized battery paste (Section 15.2.) is added to a reactor with the leaching solution. The solution is heated and stirred, and metal is recovered via an electrolytic cell.
- RSR EW process [12]. This process uses fluorosilicic acid as the leaching solution. To convert the desulfurized paste to a form that is accessible by the solution, the paste is dried and then heated to convert the lead carbonate and lead dioxide to lead oxide. Graphite anodes coated with lead dioxide are used for electrowinning the lead.
- PLACID/PLINT process [13,14]. The PLACID process (see also Chapter 16) is based on the electrowinning of lead from a chloride solution in a cell where the cathode and anode are separated by a semipermeable membrane. Lead oxide and lead dioxide are converted to soluble lead chloride, whilst lead sulfate is converted in a hot brine circuit. The sulfate ion is removed as gypsum after the addition of lime. The PLINT process is an advanced adaptation of the PLACID process and operates in parallel with a pyrometallurgical route that smelts the metallic lead fractions from the battery.

These technologies may prove to be of importance in the future, as environmental regulations become tighter and place more emphasis on cleaner processes and minimizing hazardous waste arisings.

15.3.3. Refining and alloying of lead

Once bullion lead has been recovered via the various primary and secondary smelting operations, it must undergo a refining process to remove impurities. Bullion

Table 15.2. Sample analysis (wt.%) of primary and secondary bullion lead.

Element	Primary	Secondary
Silver	0.25	0.002
Bismuth	0.17	0.022
Copper	0.27	0.03
Antimony	0.45	1.2
Arsenic	0.02	0.05
Cobalt	0.0004	< 0.0001
Tellurium	0.005	0.0005
Sulfur	0.01	0.01
Selenium	0.002	< 0.0001
Gold	0.003	< 0.0001
Nickel	< 0.0002	0.002
Iron	< 0.0001	< 0.0001
Manganese	< 0.0001	< 0.0001
Tin	< 0.0002	0.08
Cadmium	< 0.0001	< 0.0001
Zinc	< 0.0002	< 0.0002

lead, as such, cannot be used for any part of the lead–acid battery due to the high levels of impurities.

Analyses of bullion lead from primary and secondary sources are given in Table 15.2. The data show that the main impurities found in secondary lead are the major constituents of the lead alloys used in the construction of the battery, namely, antimony, tin, arsenic, and copper, whilst minor contaminants include nickel, cadmium, sulfur, bismuth, and silver.

Analysis of primary lead reveals higher impurity levels, particularly for valuable elements such as silver and gold. The removal and recovery of these elements is an important and valuable process in primary smelting.

Two methods of lead refining — the 'fire refining' pyrometallurgical and electrolytic methods — are well established throughout the world. The choice of method depends on the impurity content of the bullion (particularly for primary operations) and on important economic considerations.

15.3.3.1. Fire refining. Fire refining is the most common technique used in the refining of both primary and secondary lead throughout the world. The method involves five major stages for processing primary lead, but only two or three for secondary lead. This is due to the different level of impurities, particularly silver and bismuth, as shown in Table 15.2. The refining process is generally a batch operation, although there are some larger primary smelters that run the process in a continuous mode. Each stage of the process is carried out in steel kettles that hold the molten metal at varying temperatures. The capacity of these kettles ranges from 10 to 400 t. Typical secondary operations employ kettles of between 25 and 150 t capacity, as determined by the size of the plant. Primary smelters dedicate one

or two kettles to each stage of the refining, whilst secondary smelters often use a single kettle for the whole process.

In primary refining, all lead bullion must pass through the refinery for the valuable elements to be recovered [15]. Elements such as antimony, arsenic, tin, and copper must be removed first to gain access to metals such as silver, gold, and finally, depending on the level in bullion, bismuth. The final product from the refinery is usually 99.97 or 99.99% lead, as dictated by market requirements. The removal of copper, the first part of the process, is usually performed in two stages: first, by casting lead bullion to a copper-drossing kettle and cooling; second, by sulfur additions to a sulfur-drossing kettle. The operation of the copper-drossing kettle is essentially one of cooling the incoming hot bullion at around 700°C, which causes the lead to reject copper in the form of copper sulfide crystals. This material floats to the top of the molten lead and, depending on the operational temperatures and processing requirements, is either liquefied to a copper matte or collected as a powdery dross. The cooled bullion, which contains about 0.06 wt.% copper, is pumped to the next kettle for subsequent sulfur treatment. This involves stirring elemental sulfur into the kettle at around 330°C. A phase rich in Cu_2S is produced, rises to the surface as a black dross, and is removed. The process reduces the copper level in bullion to around 0.005 wt.% and removes small amounts of other elements such as arsenic, sulfur, iron, and tin. Iron pyrites, or a mixture of iron pyrites and sulfur, may be substituted for the sulfur in the interests of greater safety.

The next stage in refining is the softening process in which arsenic, antimony, tin, and other elements are removed by oxidation into a lead-oxide-rich slag. This is done by injecting oxygen or oxygen-enriched air into a kettle held at around 600°C. The resulting softened metal contains around 0.003 wt.% arsenic, 0.04 wt.% antimony, and less than 0.001 wt.% tin. The accompanying fluid slag contains around 4–8 wt.% antimony, and 1–4 wt.% arsenic, according to the efficiency of the process. The slag is tapped off, solidified, and treated separately in a rotary furnace with charcoal to produce high antimony–arsenic bullion. The recovered bullion is often used as feedstock in the production of antimonial alloys.

Silver and gold are removed in the next stage, termed the Parkes, or the de-silverizing, process. In this process, softened bullion is cooled in the kettle to reduce the concentration of dissolved oxygen, often aided by small additions of zinc. The lead is then reheated to 650°C, and more zinc is added until the lead becomes saturated. Upon cooling the lead to near its freezing point, a zinc crust rich in silver and gold is ejected from the lead and floats to the surface. The crust is removed from the lead, although in some plants, recirculation of crusts low in silver is practised to increase the silver content of the final crust. The silver content in the lead bullion is reduced to around 2–8 ppm, whilst the crust, containing around 20 wt.% silver, is sent to the precious metals refinery for extraction of the silver and gold.

The last part of the de-silverizing process is the removal of excess zinc from the lead bullion. This can be achieved in numerous ways, such as chlorination and oxidation, but the accepted practice by major primary smelters is vacuum distillation of the zinc from the bullion. The zinc-rich lead is heated to 600°C, and a vacuum is applied. Zinc distils from the lead and deposits in a solid crystalline state on a

water-cooled condenser where it is recovered and re-used in the de-silverizing process. Over 90% of the zinc is recovered, leaving approximately 0.05 wt.% in the lead bullion. To remove the last traces of zinc, the lead is treated with molten caustic soda to reduce the final level to below 1 ppm.

The next stage of primary lead refining is the removal of bismuth. De-bismuthizing is a similar operation to the removal of silver, with calcium–magnesium metal replacing zinc as the additive. On cooling of the kettle to around 350°C, a calcium/magnesium bismuthide crust forms on the surface and reduces the bismuth levels in lead to below 0.005 wt.%. The crust is removed and upgraded by centrifuging to separate lead metal from the bismuthide, which is recovered for its bismuth content. The procedure is known as the Kroll–Betterton process [16].

The last stage of the process is the final caustic clean, which removes any trace impurity of elements such as antimony, calcium, magnesium, and zinc that may have passed through from the previous processes. The metal is pumped from the de-bismuthizing area to the final kettles where it is held at about 500°C. Caustic soda is added and stirred into the lead for about one hour. Samples are taken at regular intervals to ensure that the product meets the required lead specifications. Once the lead is in specification, it is cast in the required shape and either sold to the market or used internally for production of calcium and antimonial alloys.

Refining secondary lead is not as complex as refining primary lead. The low levels of bismuth and silver contained in the product, as shown in Table 15.2, are generally below the specification limits required for most lead alloys and do not require removal. As mentioned above, the processes to remove these elements from lead are quite complex and there are no economic incentives to recover them, as the levels are far too low.

Unlike primary lead refineries, secondary producers can operate in a true batch mode by using one pot to refine and alloy the lead to the required specification. A typical secondary refinery is shown in Fig. 15.4. Depending upon the alloy

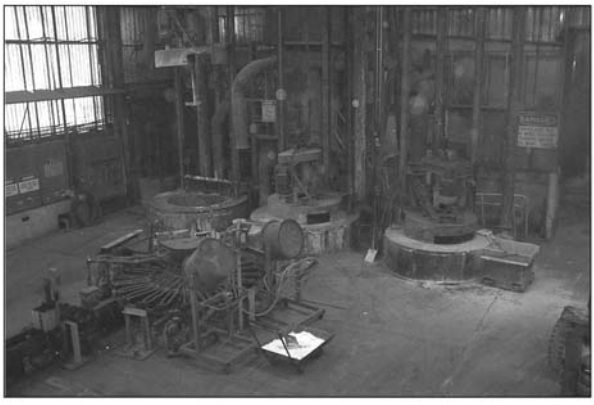

Fig. 15.4. Typical secondary refinery set-up with three kettles and a rotary casting machine. Each kettle has a capacity of 40 t.

specification and requirements, the secondary producer will select the refining operation most appropriate for the batch. For example, in the production of antimonial alloys, secondary smelting operations benefit from the antimony contained in the bullion lead. After simple drossing operations to 'clean' the lead by lowering the level of impurities, lead bullion is available for alloying almost immediately. The major removal steps for the relevant elements are as follows.

- Copper. For most antimonial alloys, this element does not have to be removed as alloys often specify the element. In calcium and soft-lead alloys, it is removed by the addition of sulfur (or iron pyrites/sulfur) to the bullion lead, as in the sulfur drossing process in primary refining.
- Nickel. Although not an alloying element, nickel enters the lead stream through the addition of nickel–cadmium battery scrap (unintentional and/or intentional) or stainless-steel parts to the furnace. It is removed from lead by the addition of caustic soda at the solidus point of the alloy.
- Antimony, arsenic, tin, and sulfur. Two methods of reducing/removing these elements from lead are available. The choice depends on the final level required in lead product. If the elements are to be removed from the bullion, the softening process is used. Alternatively, to reduce these elements to a specified level, caustic soda and/or sodium nitrate is stirred into the kettle held at about 500°C. This latter method is commonly referred to as the Harris process.

Due to the bypassing of some of the refining stages, secondary lead alloys can have an elevated level of impurities, particularly in antimonial alloys.

15.3.3.2. Electrolytic refining. Lead of very high purity can be produced from the electrolytic process. Most electrolytic refineries utilize the Betts process [17]. In this process, lead bullion is cast into anodes and placed in an electrolytic cell which contains an electrolyte of fluorosilicic acid and lead fluorosilicate. The cathode is a thin sheet of high-purity lead referred to as the 'starter sheet'. Lead is deposited on the cathode while the impurities form an adherent, but porous, slime layer on the anode. The slimes are collected for recovery and refining as they contain valuable impurities such as silver, gold, copper, and bismuth.

The resultant cathodes must undergo a further refining step as small levels of tin and antimony can often be deposited along with the lead. These elements are removed by oxygen softening and/or caustic drossing from the remelted cathodes. To limit the level of cathode contamination, some lead refineries apply partial softening to the lead bullion before the anodes are cast.

To close the recycling loop, the majority of the production from secondary lead producers returns to the battery manufacturer as alloys and soft lead. At present, secondary producers experience no problems in achieving the purity requirements for most automotive battery alloys, particularly those that are antimony-based. The increased purity requirement in VRLA batteries will, however, make the refining stages more critical.

Secondary producers often employ the same kettles for alloy formation as are used in the refining process. This is because the equipment needed to alloy certain elements is common to both processes. High-speed stirring and correct fume

extraction is a requirement when alloying volatile elements such as selenium, arsenic, and calcium. It is important that these elements are alloyed into the molten lead as quickly as possible. Selenium and arsenic will fume on contact with the molten lead, whilst calcium can oxidize vigorously on the surface of the metal. High melt losses can occur with inefficient alloying of these elements, and costly re-alloying is often required.

Alloying elements such as copper, silver, and antimony have a much higher melting point than lead and thus require continuous agitation, or stirring, in the kettle to promote dissolution. Tin, on the other hand, has a lower melting point and is the easiest element to alloy with lead.

15.4. Challenges Facing the Secondary Lead Industry

As the markets for VRLA batteries continue to expand, higher demands will be placed upon the quality of the raw materials used in the manufacture of such batteries. It has been well documented that raw materials of high quality, i.e., lead, alloys, acid, and separators, are essential in order to guarantee battery performance [18]. There will also be a responsibility to recycle the VRLA battery in an as environmentally sound and efficient manner as now occurs with conventional flooded batteries.

To process the many different sizes and types of VRLA batteries and to meet new and more stringent lead specifications, secondary smelters may be required to modify parts of their operation. A further issue is the development of alloy technology that involves the widespread introduction of silver and other elements. The problems in processing, smelting, and refining that may occur as a result of these changes are not insurmountable, but they may cause the production of high-quality lead under the present cost structure to become more difficult. Likely changes to smelters which will arise from an increasing feed of VRLA batteries and changes in alloy technology are outlined below.

15.4.1. Processing and recovery

In most breaking and recovery systems, little change will be necessary to accommodate the processing of VRLA batteries, as they can be easily fed directly to the hammer mill. (Note, this includes small 6-V and 12-V batteries.) Problems are most likely to occur in the plate-extraction process, where the tightly packed cells in the VRLA battery will be difficult to remove from their case. The increasing throughput of lead units passing to the hammer-mill/classifier section will require plant upgrades to handle the excess material.

The major challenge to all recovery systems will be the increasing level of other plastic types in the feed material. Materials such as ABS (acrylonitrile butadiene styrene) are being used in VRLA battery cases, due to their toughness and rigidity relative to traditional polypropylene. For the recycler, this means that the valuable polypropylene tonnage will fall with a reciprocal increase in plastic types that cannot be recycled. This material will have to be disposed of, as ABS and

similar plastics are not favoured as reductants in the furnace due to their structure; the presence of complex polymer structures composed of benzene-type moieties is seen as undesirable, as they can decompose to form hazardous chemicals in the waste gas stream.

Increased usage of other materials, such as silica compounds from AGM separators, can in fact benefit the secondary smelter. Larger amounts of the separator will help those smelters who use the silicate slag system, as less secondary silicate feed (sand) will be needed.

15.4.2. Refining

In smelting and refining terms, the general lead feed from spent VRLA batteries is excellent, as impurities are low and the resultant lead bullion requires minimal refining. Unfortunately, during the battery recovery operation, VRLA batteries are mixed with other battery types. This results in contamination of the lead bullion with elements such as antimony, copper, and silver. These elements are also present in unrefined primary lead, but as Section 15.3 outlines, they are 'stripped out' and recovered. They can re-enter the lead stream as added alloying constituents or as impurities in furnace feed material. With increasing production of VRLA batteries, demands will be placed on the secondary lead producer to provide high-purity alloys and soft lead, and therefore the elements (impurities) must be removed again. Clearly, the dynamics of removal of impurities from the secondary bullion will tend to change. Some of the problems associated with this change are outlined below.

15.4.3. Silver

With the recent introduction of various calcium–tin–silver alloys [19–22] for use in automotive batteries, silver levels are rapidly increasing in recycled lead streams. Although silver-containing lead alloys have been made for many years, their overall tonnage has been small and therefore the alloys have had little impact on recycling. Now, with widespread use of these alloys, silver levels are approaching the upper limits of many specifications [23]. The rising level of silver in recycled lead in the USA over the past eight years is shown in Fig. 15.5.

It has been reported that silver decreases the rate of oxidation of lead, particularly in the Barton-pot process [25], by up to 10%. In the active materials, silver increases oxygen evolution (at the positive plate) more than it does to hydrogen evolution (at the negative plate). The promotion of gassing by silver, however, does not appear to be as serious a problem as was once thought, at least for materials with silver contents up to 0.01 wt.% [25].

The difficulty for secondary plants is that, whilst the de-silverizing process (outlined in Section 15.3) can be used for the removal of low levels of silver in secondary lead bullion (i.e., up to 0.01 wt.%), the same amount of zinc must be added as for primary bullion that contains up to 0.5 wt.% silver. With this method, silver cannot be removed economically from recycled lead, as the cost of zinc alone

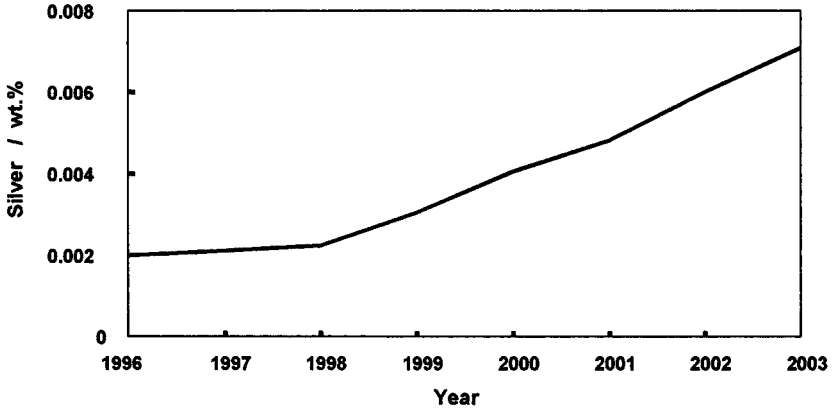

Fig. 15.5. Silver content of pure lead from RSR plants, USA [24].

far outweighs the value of the silver recovered. At present, there is no economical way of removing silver from secondary bullion.

15.4.4. Antimony

Antimonial alloys have been the mainstay of the battery industry for many years; they constitute the major alloy group for the grids, straps, and terminals. Although the level of antimony in alloys has been gradually reduced via alloy improvements and modifications in battery technology, the alloys are still widely used. Secondary smelting operations have benefitted because the bullion lead often contained up to 2 wt.% antimony. With simple chemical drossing operations to 'clean' the lead by lowering the level of impurities, the bullion can be rapidly turned into alloys of the composition required for the manufacture of flooded batteries.

The problem facing all smelters is that there is a continuous occurrence of antimony in their lead streams, at a time when there is a rapidly declining demand for the element. Declining sales of the alloy, which coincide with increasing use of soft-lead-based alloys, will result in antimony effectively becoming a major contaminant that requires removal. Whilst it is relatively easy for secondary refiners to remove antimony from the bullion, the antimony-rich residue from the process may have to be stockpiled. The residue, which contains around 80 to 90 wt.% lead, effectively ties up lead units and can have a major cost impact on the refinery.

15.4.5. Catalyst elements

A recent development for the VRLA battery is the inclusion of a precious-metal catalyst which, it is claimed, reduces water loss and increases battery life [26,27]. Gasses produced from the battery are recombined into water rather than passing through the vent and exiting the cell. The catalyst used is palladium-based and designed to fit into custom-made vents for the battery.

Platinum-group metals are rarely found in primary lead smelting and, if present, report to the lead bullion along with gold and silver. They are removed from the bullion using the de-silverizing process. In the secondary recycling stream, if catalyst-containing batteries are smelted, the precious metals will also report to the lead bullion. As no de-silverizing steps take place for secondary bullion, the palladium and other metals remain in lead.

Although the level maybe very small in the first instance, it will build-up over time as more material is recycled. The problem may lie undetected, as there are very few primary or secondary lead companies in the world that analyse for elements such as platinum and palladium. The elements are somewhat difficult to determine quantitatively with conventional analytical equipment, but they may aggravate gassing problems.

15.4.6. Other elements

An element that is now increasing in some secondary lead streams is bismuth. Bismuth has been a 'stable impurity' for many years, with levels that range from less than 0.001 to 0.025 wt.% in both primary and secondary lead.

In recent years, bismuth has been added to high-purity lead at levels of between 0.05 and 0.06 wt.% for oxide production. Unlike antimony and silver, however, bismuth has been found to be beneficial in a number of aspects of battery production. For example, extensive studies carried out by CSIRO [28–30] and Pasminco [31,32] have clearly demonstrated that this element imparts many advantages to VRLA batteries. Other research from China has reported no adverse effect of bismuth on grid alloys when added at levels below 0.1 wt.%.

Tin is also added to lead for its beneficial properties, especially in the case of alloys. It provides two main advantages: (i) in battery production it aids the castability of the grid and strap; (ii) it suppresses the PCL-1 effect in maintenance-free and VRLA batteries (see Chapter 2). Tin levels are increasing in battery scrap, but over 80% is lost to the slag during smelting. The remaining level is quickly removed during refining, generally through the addition of caustic soda. Unfortunately, although tin is a valuable element, there is presently no practical recycling circuit or recovery method for its reclamation.

In summary, the lead–acid battery can meet the ever-increasing demands for higher performance, but this presents major challenges to lead producers. The prime requirement is to supply a growing battery market with lead of higher purity than previously specified. This is not an impossible hurdle to overcome, but it will require a focused effort — particularly in the secondary lead area.

References

1. H.H. Kellogg, *J. Metals*, **28** (12) (1976) 29–32.
2. A. Franckaerts, *Proceedings Lead 97 Conference*, Salzburg, Austria, 22–25 September 1997, pp. 59–64.
3. E.C. Bied-Charreton, *Proceedings Lead 97 Conference*, Salzburg, Austria, 22–25 September 1997, pp. 399–405.

4. R.M. Reynolds, P.E. Hudson, E.K. Hudson, *Lead-Zinc '90*, The Minerals, Metals and Materials Society, 1990, pp. 1001–1022.
5. G. Martin, A. Siegmund, *Recycling of Metals and Engineering Materials*, The Minerals, Metals and Materials Society, 2000, pp. 93–101.
6. K.R. Robilliard, *International Symposium on Injection in Process Metallurgy*, The Minerals, Metals and Materials Society, 1991, pp. 181–198.
7. M.J. Walker, *Lead–Zinc '90*, The Minerals, Metals and Materials Society, 1990, pp. 919–932.
8. T.R.A. Davey, *Lead–Zinc '80*, The Minerals, Metals and Materials Society, 1980, pp. 48–65.
9. C.J. Beyke, *Process Mineralogy XIII*, The Minerals, Metals and Materials Society, 1995, pp. 275–284.
10. D. Eby, *Lead–Zinc '90*, The Minerals, Metals and Materials Society, 1990, pp. 825–840.
11. P.B. Queneau, *International Symposium on Primary and Secondary Lead Processing*, The Metallurgical Society of CIM, 1989, pp. 145–178.
12. R.D. Prengaman, H. McDonald, *Lead–Zinc '90*, The Minerals, Metals and Materials Society, 1990, pp. 1045–1076.
13. G. Diaz, C. Frias, L.M. Abrantes, A. Aldaz, K. van Deelen, R. Couchino, *Third International Symposium on Recycling of Metals and Engineering Materials*, The Minerals, Metals and Materials Society, 1995, pp. 843–856.
14. D. Andrews, A. Raychaudhuri, C. Frias, *J. Power Sources*, **88** (2000) 124–129.
15. G. Saint, J.E. Legg, M. Pizzey, *Australian Mining and Metallurgy*, Sir Maurice Mawby Memorial Volume, 1993, pp. 559–563.
16. J.D. Iley, D.A. Ward, *Advances in Extractive Metallurgy* 1977, Institute of Mining and Metallurgy, London, UK, 1977.
17. A. Bowen, *Handbook of Extractive Metallurgy*, Eleventh Edition, Shakespeare Head Press, Pty. Ltd., Sydney, Australia, 1959.
18. F.A. Fleming, L. Gao, P.R. Shumard, R. Evans, R. Kurian, *Proceedings of the 21st International Telecommunications Energy Conference*, Copenhagen, Denmark, IEEE, 1999, paper 3–3.
19. J. Bauer, C. Standke-Thiemann, A. Tonnessen, US Patent No. 6,210,837 (2001).
20. D.J. Knauer, US Patent No. 6,114,067 (2000).
21. P. Rao, T.F. Uhlemann, US Patent No. 5,691,087 (2000).
22. P. Rao, T.F. Uhlemann, J. Larson, S.R. Larsen, US Patent No. 5,434,025 (1995).
23. M.W. Stevenson, J.E. Manders, S. Eckfeld, R.D. Prengaman, *J. Power Sources*, **107** (2002) 146–154.
24. R.D. Prengaman, IBMA Meeting, Chicago, Illinois, USA, 1999, p. 18.
25. D.AJ. Rand, D.P. Boden, C.S. Lakshmi, R.F. Nelson, R.D. Prengaman, *J. Power Sources*, **107** (2002) 288–290.
26. W.E.M Jones, H.A. Vanasse, C.E. Sabotta, J.E. Clapper, E.F. Price, *Proceedings of the 20th International Telecommunications Energy Conference*, San Francisco, CA, USA, IEEE, 1998, pp. 461–469.
27. W.E.M Jones, *Proceedings of the 22nd International Telecommunications Energy Conference*, Phoenix, USA, IEEE, 2000, pp. 447–452.
28. L.T. Lam, N.P. Haigh, O.V. Lim, D.A.J. Rand, J.E. Manders, *J. Power Sources*, **78** (1999) 139–146.
29. L.T. Lam, O.V. Lim, N.P. Haigh, D.A.J. Rand, J.E. Manders, D.M. Rice, *J. Power Sources*, **73** (1998) 36–46.
30. L.T. Lam, N.P. Haigh, C.G. Phyland, N.C. Wilson, D.G. Vella, L.H. Vu, D.A.J. Rand, J.E. Manders, C.S. Lakshmi, *Proceedings of the 20th International Telecommunications Energy Conference*, San Francisco, CA, USA, IEEE, 1998, pp. 452–460.
31. J.E. Manders, L.T. Lam, R. De Marco, J.D. Douglas, R. Pillig, D.A.J. Rand, *J. Power Sources*, **48** (1994) 113–128.
32. M.W. Stevenson, C.S. Lakshmi, J.E. Manders, L.T. Lam, *J. Power Sources*, **95** (2001) 264–270.

Valve-Regulated Lead–Acid Batteries
D.A.J. Rand et al., editors

—CHAPTER 16—

ENVIRONMENTAL ASPECTS OF RECYCLING VALVE-REGULATED LEAD–ACID BATTERIES

C.J. Boreiko and B. Wilson

16.1. Introduction

Recent technological developments have enhanced the performance characteristics of the lead–acid battery. As a result, continued use of lead–acid batteries is foreseen, and expansion of battery markets is anticipated, as societal demands increase for cost-efficient energy-storage systems. Although the technical performance of evolving valve-regulated lead–acid (VRLA) battery technology will be critical to ensure stable markets, future patterns of battery utilization will also be evaluated in accordance with life-cycle criteria that seek to ensure the long-term compatibility of products with precepts of sustainable development and sustainable consumption. Lead–acid batteries must be amenable to production and use, as well as to recycling in a fashion that preserves the safety and well-being of workers, the general population, and the environment.

Assessments of the environmental and health impacts of the battery industry have usually been conducted in countries with intensive battery usage associated with large vehicle fleets. Moreover, assessment outcomes have been determined by emissions for a restricted range of toxic substances such as lead. With the adoption of principles for sustainable development, these areas of focus will change. The ultimate acceptance of battery production and use will not be determined by industry's compliance with regional regulatory frameworks, such as those that exist in the USA or the European Union. Rather, industry's performance will be evaluated on a global basis and will increasingly take into consideration the performance of the industry in developing countries. Furthermore, future evaluations will entail more holistic life-cycle analyses that assess the ramifications of technology and material selection decisions upon multiple environmental impact indicators. Although emissions of lead will continue to be of concern, increased importance will be assigned to the re-use and utilization of all components of the battery. Energy requirements, greenhouse gas emissions, and release of other undesirable pollutants will further be considered.

This chapter provides a review of life-cycle issues that are likely to be important for lead–acid battery production and recycling. Issues specific to VRLA technology are noted, as are generic considerations associated with other lead–acid battery

technologies. Given the globalization of the industry, challenges faced by developing countries are highlighted, and note is taken of measures that might be pursued by industry, national governments, and inter-governmental organizations so as to ensure the environmentally sound management of battery production, use, and recycling.

16.2. Justification for Recycling

Encouragement of lead–acid battery recycling has focused upon recycling as a means of limiting environmental dispersion of lead. The recycling of lead–acid batteries, however, is to be encouraged for many reasons. Battery production entails the use of materials that are ultimately finite in their supply, and proper management of these material resources is required to ensure their availability for future generations. The environmental release of all the materials within a battery can also be curtailed through recycling. Indirect emissions, such as those associated with electricity consumption, also tend to be lower for reclaimed materials. Finally, as lead–acid battery consumption increases in developing countries, the establishment of recycling infrastructures will contribute to economic growth and stability. Social and economic benefits can provide significant incentives for recycling in developing countries.

The ideal closed loop for lead–acid batteries (Fig. 16.1) would be: (i) lead bullion production; (ii) battery manufacture; (iii) recovery and recycling of the battery materials. The components of used lead–acid batteries (ULAB), in whatever form, are all recyclable [1]. The battery itself, however, does nothing to close the recycling loop if it is not collected and delivered to a recycler for processing. It is therefore essential that governments and battery manufacturers ensure that used batteries enter the loop by creating an infrastructure that will encourage, promote, and facilitate environmentally sound recycling. There are many benefits from recycling batteries, as follows.

(i) *Saves natural resources*. Recycling ULAB and manufacturing new batteries from secondary lead instead of primary material conserves land resources and reduces the need to mine for more minerals.

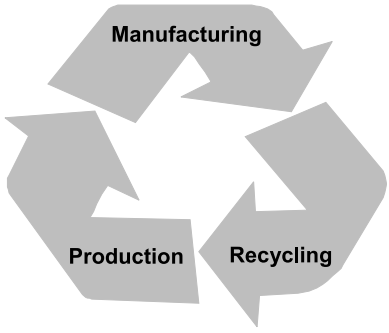

Fig. 16.1. Optimized closed loop for recycling.

(ii) *Saves energy*. Four-times less energy is required to produce a tonne of secondary lead [2] than a tonne of primary lead [3], and so it follows that less energy is required to make a new battery from recycled materials. As confirmed by a recent life-cycle inventory, production of a tonne of secondary lead bullion requires one-fourth the energy needed to produce a tonne of primary lead [4].

(iii) *Reduces emissions*. Secondary lead production has lower emissions of lead and sulfur dioxide. Greater energy efficiency means that secondary lead production is characterized by lower emissions of greenhouse gases.

(iv) *Saves landfill space*. For those cases where ULAB are recycled, instead of being disposed of into dump sites, landfill space is conserved. Secondary production generates smaller volumes of waste than primary production.

(v) *Saves money and creates jobs* [5]. The infrastructure required to source, collect, sort, store, transport, and recycle ULAB creates more jobs than disposal to landfill sites or waste incinerators. In the long-term, recycling is frequently the least expensive waste-management option for cities and towns.

16.3. Recycling Rates

From an industry perspective, lead–acid batteries are an environmental success story — in most OECD countries, 96% of all battery lead is recycled [6]. Compared with the usual 'flagship' recycled products, such as glass bottles at only 38%, aluminum cans at nearly 64%, and newsprint at about 68%, lead–acid batteries are the leaders in the field (see Fig. 16.2). ULAB have topped the list of the most highly recycled consumer products for over a decade.

16.4. Collection of Used VRLA Batteries

There are many ways that ULAB can be collected. By far the most efficient is through the battery retailer, distributor, or leasing agent [7]. Either a discount is given against the purchase price of a new battery, provided that the customer returns

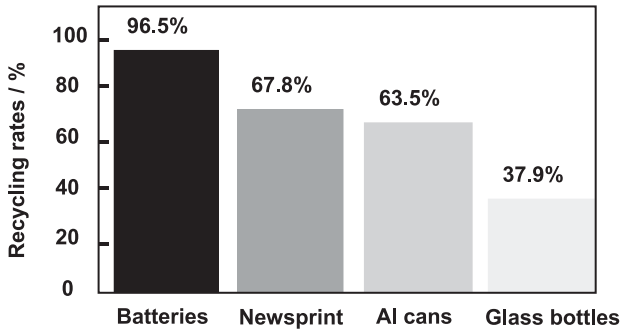

Fig. 16.2. Comparative recycling rates.

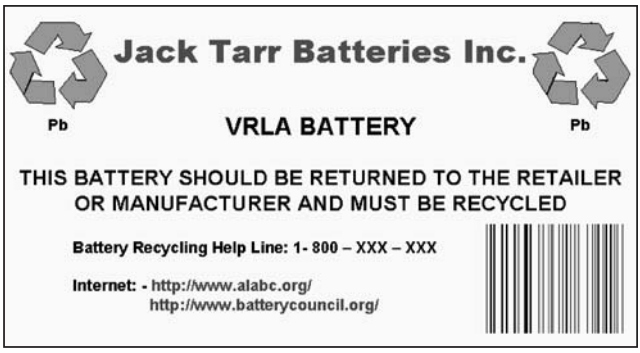

Fig. 16.3. An example of a recycling label for a new VRLA battery.

the used battery, or the lease is renewed at agreed preferential rates. In some countries, a deposit has to be paid when a new battery is purchased or leased and is only refunded to the customer when the battery is returned to the retailer or leasing agent for recycling.

Prior to leaving the manufacturing plant, all lead–acid batteries should be labelled (Fig. 16.3) in accordance with prevailing national and international [8] regulations and with the international recycling symbol ISO 7000–1135, better known as the Moebius loop. Furthermore, there should be instructions for the recycling of the battery or a point of contact clearly displayed when it is at the end of its useful life. Each label should state, 'lead–acid battery', 'Pb' or the words 'LEAD', 'RETURN and RECYCLE'. If possible, the label should also have a bar code which contains information about the place of manufacture, the date of production, the battery type, and its components.

Collection systems must be open to all sources of lead–acid batteries. For example, garages and repair shops may remove batteries from wrecked vehicles. It is important to establish a network of all businesses that might recover a battery so that there are clear instructions for delivery to the approved nearest recycler of secondary lead.

Technical guidelines for the environmentally sound management of lead–acid battery wastes [9] were adopted by the technical working group of the Basel Convention in May 2002, and were approved by the Conference of the Parties (COP) in December 2002. Section 3.2 of the guidelines deals with collecting ULAB and advocates that:

(i) the only way to implement a successful lead–acid battery recycling programme is to install an appropriate and efficient collection system and infrastructure;
(ii) the most spontaneous process of ULAB collection occurs through a dual system of distribution and collection when manufacturers, retailers, wholesalers, service stations, and other retailing points provide new batteries to users and retain the used ones to be sent to recycling plants; such a scheme is sustainable because it is based on the economic value associated with the lead-content of the ULAB;

(iii) control measures must be implemented at collection points in order to minimize the risk of accidents that may cause personal injury or environmental contamination, e.g., batteries should not be drained at collection points. The drainage of battery electrolyte poses threats to human health and the environment because it contains high lead levels and is highly acidic;
(iv) accordingly, used batteries should be stored in a secure compound to minimize the risk of accidental spillage and to permit damaged or leaking batteries to be contained; storage should be under cover on a flat, even, and impermeable surface; but if stored on asphalt or concrete, the surface should be coated with an acid-resistant epoxy, fibreglass, or plastic coating;
(v) although VRLA batteries are sealed and have an immobilized electrolyte that reduces the risks of electrolyte spillage, they should be stored in an upright position to minimize risk of leaking from vent holes or cracks.

All returned batteries should be inspected and tested electrically to determine whether they could be recharged and re-used. This practice ensures that any batteries still charged are identified, to reduce the risk of sparking during transit. In some countries, it may be feasible to return usable batteries to the market without the need for recycling.

Wherever used batteries are stored, it is important to ensure that there is:

- water to wash down the storage area and any batteries that are leaking
- drainage to an isolated sump to contain any spillage of electrolyte
- personal protective equipment (PPE), such as neoprene gloves, safety glasses, steel-capped safety boots/shoes, dust masks, overalls, and a first-aid kit with eye-wash water bottles; it is also strongly recommended that an emergency safety shower be installed close to the working areas.

16.5. Transport of Used VRLA Batteries

Section 3.3 of the Basel Convention Guidelines covers the safe transportation of ULAB [9]. The same recommended practices apply to used VRLA batteries. Used VRLA batteries must be considered as hazardous waste when making arrangements to either return them to the manufacturer or to transport them to the recycler. The main risk is that associated with battery electrolyte that may leak from a battery in transit.

It is important to package the ULAB in a manner that renders the battery easy to transport while reducing the risk of any movement during transit, to avoid damaging the battery case. Battery manufacturers may provide a suitable cage or packing case to return a used battery. In most instances, however, it will be necessary to pack the battery prior to delivery to the recycler. If possible, batteries should be stacked on to wooden pallets or skids. A sheet of corrugated, heavy-duty cardboard should be placed between each layer of batteries to reduce movement, to absorb any electrolyte that might leak, and to prevent any parts protruding from the top of a battery from puncturing the plastic case of the battery stored above. A sheet of corrugated, heavy-duty cardboard is also placed on top of the final layer.

The whole stack should be shrink-wrapped in plastic as tightly as possible to minimize any movement during transit. When storing the packed batteries prior to transportation or shipment, the layers of pallets should not be stacked more than two high. As a further precaution, the guidelines recommend that ULAB be transported in a sealed, shock-resistant container that will not leak electrolyte.

The vehicle used to transport the used battery must be correctly identified following international conventions and local legislation. The appropriate symbols and colors should be used to identify the fact that corrosive, hazardous waste is being transported. A complete Material Safety Data Sheet (MSDS) should also be visible, either attached to the side of the used battery stack or inside the transport vehicle. Appendix 1 contains a sample MSDS sheet, for illustration purposes only.

Due regard must be given to the safety of those transporting used batteries and anyone who may assist in the event of an accident. Each vehicle should have equipment necessary to combat simple spillage or leakage problems, and there should be personal protective equipment available. The appropriate authorities and emergency services should be notified of the transport route and, wherever possible, a route should be chosen that minimizes the risk of possible accidents and avoids populated areas.

Due care must also be taken to ensure that vehicles delivering batteries to a recycler do not leave the plant contaminated with lead dust. It is important, therefore, to ensure that all vehicles leaving a secondary lead recycler pass through a wash bay (Fig. 16.4) with high pressure water sprays that wash the underside of the vehicle, the tires, both sides and the rear, the cab and the top. All the wash water should be allowed to settle in an interceptor pit to permit the large particulates to settle before being pumped to the water treatment plant to remove contaminants.

Fig. 16.4. Truck wheel wash at the Met-Mex Peñoles plant in Torreon. (By courtesy of Met-Mex Peñoles S.A. Mexico.)

16.6. Recycling Process

Modern secondary plants take in whole ULAB batteries and break them in a mechanical hammer-mill. The broken battery pieces are usually gravity separated in a series of water-filled tanks with slow-moving classifier belts to promote the capture of the battery paste. In this way, battery electrolyte is contained within the recycling process, and the acidic component can then be treated in one of the five ways [10]:

- neutralized, and the resulting effluent treated to meet clean water standards and then released into the public sewer/sanitary system or a local aquatic system
- converted to powdered sodium sulfate for use in glass and textile manufacturing, or as a filler or stabilizer in laundry detergent
- converted to agricultural fertilizer using ammonia in a purpose-built plant
- converted to gypsum for use in the production of cement, or by the construction industry in the manufacture of fibreboard
- recovered, treated, and restored to be used as a battery electrolyte [11].

It is important to achieve maximum separation of the plastics from furnace materials, such as the oxides and grid metal, to minimize the risk of dioxin formation during the smelting process.

Washed and dried polypropylene pieces are sent to a plastic recycler, where the chips are melted [12] and extruded to produce plastic pellets for use in the manufacture of battery cases and other plastic components. Great care must be taken to ensure that the mechanical breaker cleans the polypropylene chips free of any residual oxide, because subsequent handling of the chips by operating personnel, especially at the plastic recycling plant, can result in significant levels of lead exposure. Should the wash sprays on the breaker fail to remove all traces of battery paste, consideration should be given to further washing with a dilute sodium hydroxide solution.

As many used VRLA batteries will contain gelled electrolyte, it is essential that particular attention be paid to the threat of sulfur dioxide emissions. In conventional flooded batteries, most sulfuric acid is removed during the breaking phase of the process. Residual sulfur entrained in the paste as sulfate can be removed by either high pressure or vacuum filtration. If the battery paste containing sulfur compounds is charged into a furnace, removal of sulfur dioxide gas from the combustion exhaust gases can occur in a scrubbing tower.

Increased retention of electrolyte in VRLA batteries of the gel design will increase the sulfur content of the furnace charge material. The cost of desulfurization will increase accordingly, as more lime will be required to neutralize the acidic gases in a scrubbing tower. Alternative means of neutralizing acidic gases in the scrubbing tower, without increasing the extraction of limestone, can be sought. For example, fly ash from power stations can be used as an alkaline reactant to remove sulfur dioxide and thereby eliminate the need for precipitators and further limestone purchases. If the amount of sulfur removed increases, then the range of by-products produced for sale may also need to be extended to ensure that none of the 'waste'

from the desulfurization process is dumped. Saleable products [13] include the following:

- sulfur can be substituted for Portland cement and water to act as a binding agent to produce a durable, acid-resistant concrete
- sulfur can be used in protective coatings to improve the resistance of conventional building materials to chemical attack and other stresses
- fabrics can be impregnated with sulfur and additive materials to produce flexible or rigid lining materials
- sulfur compounds can be used as an asphalt extender, or can be used as an asphalt replacement that totally eliminates the need for asphalt
- utilization of a pozzolanic stabilization reaction process, where lime-based reagent is added to scrubber sludge and fly ash, creates a mineral product suitable for roadway base course.

Another option for secondary smelters is to desulfurize the battery paste prior to smelting. Chemical desulfurization, however, is dependent on physical mixing conditions and temperature. Chemical desulfurization is achieved by adding a concentrated sodium carbonate solution to an agitated mix of battery paste sludge to convert the lead sulfates to lead carbonates. Complete conversion of lead sulfate to lead carbonate eliminates sulfur in the furnace feed material and sulfur dioxide in the exhaust gases. Complete desulfurization is, however, rarely achieved under normal industrial conditions.

The basic desulfurization equation [14] for the conversion of lead sulfate to lead carbonate is:

$$PbSO_4(\text{in paste}) + Na_2CO_3(\text{aq.}) \rightarrow PbCO_3(\text{solid}) + Na_2SO_4(\text{aq.}) \qquad (16.1)$$

In the industrial process, the pH range for desulfurization is 8–8.5, and the temperature is usually 35–40°C. As the reaction progresses and lead carbonate is produced, the paste mix becomes increasingly viscous and difficult to stir. It is

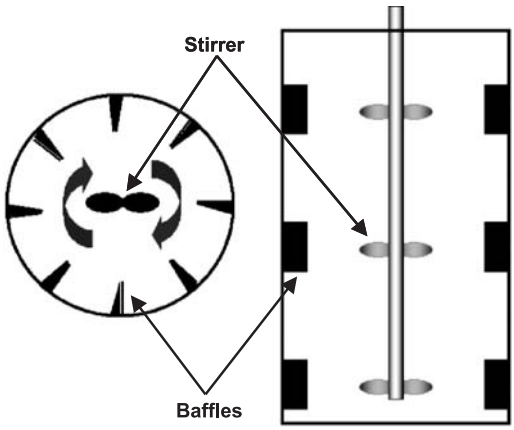

Fig. 16.5. Optimal design for a desulfurization mixing vessel.

important to maintain agitation in the reaction vessel (Fig. 16.5) to encourage the reaction of sodium carbonate with lead sulfate and to complete desulfurization. If agitation is not vigorous, the reaction will stall and much of the lead sulfate will remain suspended in the mix. Any suspended, gelled-electrolyte in the mix is also unlikely to react under such conditions and could find its way into the furnace.

Reaction conditions can be improved, even if agitation cannot be increased, by re-circulating the paste mix through the transfer pump [15] and back into the reaction vessel several times in order to mix the reagents in the pump. Alternatively, a second or even third mixer blade can be added to the mixer shaft to create a stronger vortex. Additional baffles, or even larger baffles, can be added to the sides of the reaction vessel to increase turbulence. Careful consideration of the design of the mixing vessel is important. While most plants use wide vessels for mixing, it might be better, especially if three stirrers are fitted to the mixing shaft, to have a long narrow vessel. Such a vessel would also make the turbulent effect of the side baffles in the vessel much more efficient. So that 'eddies' do not form behind the baffles and reduce mixing, the baffles should be solid and should slope away from the direction of the mix.

Other options to ensure desulfurization of the paste can be considered, namely:

(i) raising the temperature for desulfurization to between 50 and 54°C; higher temperatures have been adopted by some US secondary lead plants to overcome the low solubility of sodium carbonate and is accompanied with higher agitation rates as the reaction is much quicker;
(ii) using a 50% sodium hydroxide (NaOH) solution; this option may provide the following advantages:

- the NaOH content is nearly stoichiometric because the concentration of 50% NaOH solutions is normally within 1% of its nominal value; commercial soda ash, on the other hand, is usually no more than 93% pure and has sodium chloride, a desulfurization reaction inhibitor, as one of the main impurities;
- the absence of chloride ions eliminates the need to purge the desulfurization process periodically
- solid insoluble salts are not formed
- the NaOH desulfurization process precipitates a hydrated lead oxide ($3PbO{\cdot}H_2O$) that is about 12% lighter than the corresponding carbonate, which thereby slightly reduces the viscosity of the desulfurization mix.

The desulfurized paste should then be filtered in a press, and dried prior to charging to a furnace.

The grid metallics should be stored and recovered separately from the battery paste so that metals from the alloys in the battery grids do not contaminate the relatively pure lead paste, which is ideal for producing soft lead. Alloys used to manufacture VRLA batteries do not contain either antimony or arsenic, and this means that the potential hazard of stibine (antimony hydride, SbH_3) and arsine (arsenic hydride, AsH_3) formation during the storage of the metallics is removed. Many automotive batteries with antimonial and arsenical alloys are still in use,

however, and it may not be until 2030 that the last of these alloys passes through a recycler and the potential danger of toxic gas formation is eliminated. Accordingly, care must still be taken to store grid metallics in a dry environment.

16.7. Recycling Options

There are many ways of recycling used batteries, but consideration should be given to choosing the method that is most environmentally friendly. If simply disposed of into a landfill site, or recycled in a manner that produces a toxic and leachable residue that is sent to landfill for disposal, then the process is polluting and serious contamination may ensue. Increasingly, industry is producing 'inert' slags, that are non-hazardous and that can be considered as a 'clean' product.

One example of such a process is 'Green Slag' [16] technology for Rotary Furnaces developed by the Mexican-based Lead Metal Technologies (LMT) and adopted by Enertec in Mexico and secondary lead smelters in Canada, Venezuela, and Brazil. This technology requires the installation of specialized auxiliary equipment and computer-controlled software for charge preparation to blend secondary feed materials and refinery by-products carefully. The residue produced is inert and complies with the stringent USA EPA Toxic Characteristic Leaching Procedure (TCLP), which is an analytical method that simulates sanitary landfill contaminant leaching in waste samples. Based upon concentrations of the TCLP constituents and guidelines, the solid waste samples can be deemed hazardous or non-hazardous.

Another example is Boliden's Kaldo Process [17], also based on a rotary design, in which the furnace is angled so that the burner flame can be directed on to the liquid bath (Fig. 16.6). The Kaldo Furnace was primarily developed for smelting lead concentrates (sulfides or carbonates), but it can also be used for processing secondary materials such as batteries, for smelting by-products, and for refining drosses. The lead oxides and sulfates are smelted by mixing fluxes and a reducing agent, such as coke breeze, in the furnace, followed by smelting with an oxygen–fuel burner.

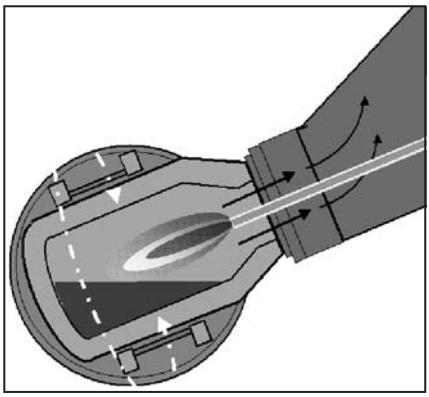

Fig. 16.6. Boliden's Kaldo furnace.

The tilting technology of the Kaldo furnace incorporates oxygen flame enrichment to reduce smelting cycle times and to lower the back pressure on the furnace. This allows a significant reduction in ventilation requirements. These energy-saving benefits contribute to the overall environmental performance of the process. The technology can be scaled to suit the expected material throughput, and it has eliminated the use of soda-based fluxes, so that an inert stable slag that passes the TCLP test is produced.

The energy efficiency of traditional rotary furnaces can be improved by blanking off the end of the furnace opposite the burner and by forcing the hot gases from the burner back towards the furnace door. This effectively achieves a double pass (Fig. 16.7). As the heat from the burner flame is forced back from the end of the drum towards the door, more heat is applied to the refractories than would have been possible with a single-pass burner. In turn, refractories pass additional heat contained in the bricks into the smelting mix as the drum rotates and the bricks pass under the liquid bath. A swing-door ventilation duct directs the furnace exhaust gases upwards from the mouth of the furnace and into a hygiene hood, which thereby reduces the risk of fugitive emissions. The combination of exhaust gas and hygiene ducting also lowers electrical and maintenance costs with respect to those associated with more traditional dual-flue designs.

Other technologies, for example the IsaSmelt [18] and Ausmelt [19] processes developed by CSIRO in Australia, produce inert, stable, non-leachable residues, i.e., a fayalite slag (Fe_2SiO_4) rather than a soda or soda–matte slag. These processes also overcome other environmental problems, such as dioxin and furan formation [20] following the breakdown of any old PVC separators that have contaminated the feedstock. With the CSIRO technology, the formation of dioxins and furan is avoided by lance post-combustion of process gases at temperatures in excess of 1300°C followed by rapid cooling. The resulting levels of dioxins and furans are well below $0.1\,ng\,m^{-3}$. Dioxin and furan formation would be prevented in traditional

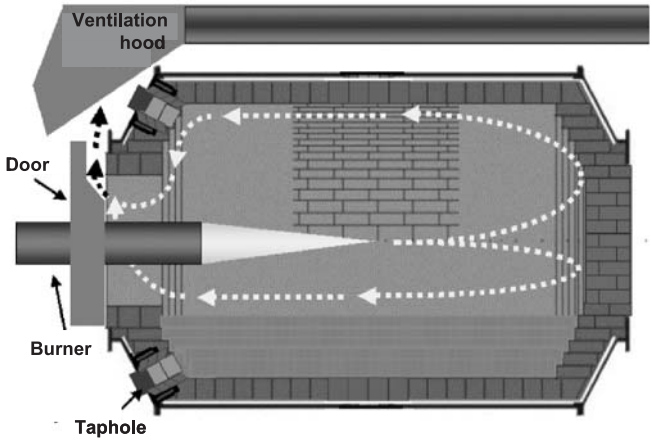

Fig. 16.7. Rotary furnace with double pass burner configuration.

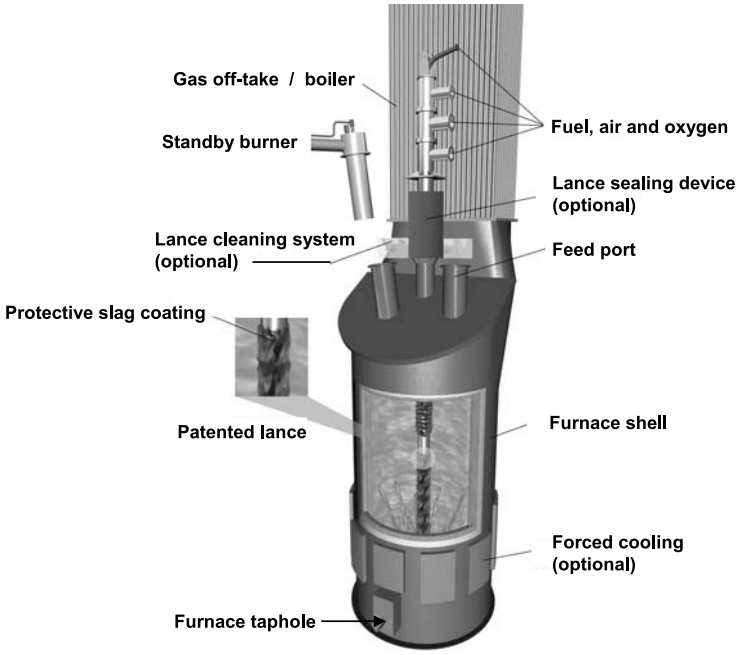

Fig. 16.8. IsaSmelt/Ausmelt furnace technology.

blast, reverberatory, and rotary furnaces by utilizing an afterburner positioned in the flue system close to the furnace exhaust. In addition, these processes are energy efficient because heat is delivered below the surface of the melt and directly into the liquid bath of the smelting chamber (Fig. 16.8).

Nevertheless, both hazardous and inert residues are solid wastes and require landfill. Dumping solid waste to landfill, even non-hazardous clean wastes, is not sustainable and is not entirely 'green'. An ideal 'green' technology is one that consumes all materials involved in the production process to produce only re-useable or new products, without generating solid waste that requires disposal to landfill. Such smelters can be found in Trail, British Columbia, Canada at the Cominco lead and zinc primary smelter and in Malaysia in Kuala Lumpur at the Metal Reclamation primary and secondary lead smelter [21].

Hydrometallurgical recycling processes are gaining interest amongst the environmental community as an alternative to pyrometallurgical secondary smelting. Indeed, the European Community funded a project in the mid 1990s at the Technicas Reunidas Company in Spain, to develop a sustainable hydrometallurgical secondary lead process called the PLACID Process [22] (Fig. 16.9). Following conventional battery-breaking, battery paste is leached in dilute hydrochloric acid in a brine solution to dissolve the lead oxides and sulfates. Sulfate contamination is removed with lime in a carefully controlled manner to precipitate a commercial form of gypsum, which is then removed by filtration. Lead powder is then injected into the leachate to precipitate metallic impurities such as Cu, Bi, Sn, Ag, As, and Sb.

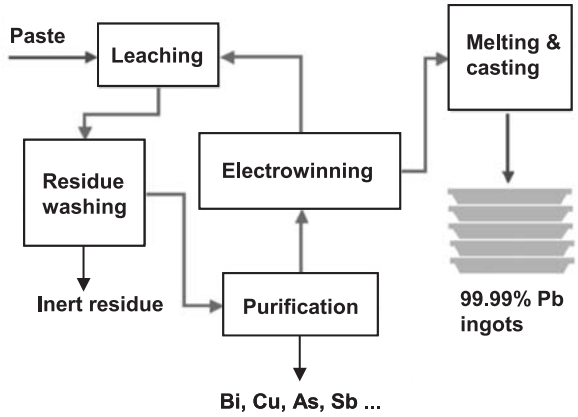

Fig. 16.9. The PLACID process.

The electrolyte for the two electrodes in the PLACID electrolytic cell is different and is separated by a membrane that is permeable only to protons (H^+). On the cathode, lead chloride is stripped of its lead atom to leave chloride ions which, in turn, combine with protons passing through the membrane from the anode to reproduce hydrochloric acid. The latter is returned to the leaching bath for re-use. The electrolysis deposits lead as dendrites (spongy form of lead). The dendrites are shaken off the cathode, collected, and removed from the bath on a semi-submersed conveyor belt. The dendrites are pressed to expel excess electrolyte, and form platelets of pure lead that can be melted in a conventional refining kettle and cast into ingots of 99.99% purity.

The environmental benefits of the PLACID hydrometallurgical process are:

- there are no liquid effluent discharges and the hydrochloric acid used in the initial leaching process is regenerated and re-used
- the process produces half the amount of solid residues compared with conventional pyrometallurgical recycling, and the residue is a saleable commercial grade of lead-free gypsum, which is suitable for sale to the cement and construction industries
- sulfurous or greenhouse gases, such as carbon dioxide, are not directly produced
- any lead dust or drosses collected during the recycling process can be recycled through the leaching process
- lead-contaminated residues from pyrometallurgical recovery operations and contaminated soils from abandoned mine sites and disused lead smelters can be treated using the PLACID process and the lead content removed.

The PLACID hydrometallurgical process provides the benefit of minimal occupational lead exposure because there are no lead emissions or any lead dust from by-products or residues.

16.8. Monitoring and Controlling Emissions

Monitoring and controlling air quality during the recycling of batteries is critical so as to reduce point-source emissions to the atmosphere. Operations should be monitored where lead exposure is likely to be high, in order to guide occupational health programmes.

Modern industry practice can be extremely effective in limiting lead emissions from recycling facilities. Facility emissions have been a cause of historic concern, with speculation that increased use of lead–acid batteries in electric and/or hybrid electric vehicles might result in unacceptable levels of lead contamination. For example, Lave *et al*. [23] estimated that emissions to water and air associated with primary lead production, secondary lead production, and battery production were 4, 2, and 1%, respectively, of the total amount of lead processed. In contrast, Socolow and Thomas [24] estimated that secondary smelting and refining were associated with system losses of up to only 0.01% of material processed.

Reasons for differences in estimates of industry performance are varied. High estimates of emissions are typically related to the use of estimates of emission factors for lead smelters that were derived prior to the development of modern technologies for the control of air and water pollution. Emission estimates will also differ with respect to the fate that is presumed for lead contained in different waste streams. For example, lead within slags or other process wastes is usually managed so as to prohibit undesirable levels of environmental contamination. In the absence of waste-management practices, high levels of environmental dispersion might result.

A life-cycle inventory analysis [4] has examined the performance of lead production and battery manufacturing facilities in North America. This study collected data descriptive of industrial emissions in the base year of 1995–1996. The mass flows indicated that the estimates offered by Socolow and Thomas [24] are indeed characteristic of the industry. Secondary lead production was associated with losses to air and water of the order of 0.009%. Lead losses during battery production amounted to 0.002% of material processed. These estimates are some three orders of magnitude lower than those made by Lave *et al*. [23]. Levels of lead release continue to decrease with improvements in technology and operating practice.

Occupational health concerns exist in multiple phases of recycling. Breaking of batteries in the secondary industry has the potential to generate a lead-contaminated acid mist during the sawing or crushing of whole batteries. The battery crusher must therefore be hooded and ventilated to prevent mist from escaping into work areas. Operators working in the breaking area should be equipped with respirators fitted with the appropriate filters for protection against acid mist.

Smelters operate more efficiently if the furnace charge can be prepared and blended prior to charging. Charge-preparation beds, or mixing sheds, will generate lead dust, so consideration should be given for enclosing such areas and restricting access. Vehicles operating in these areas should be fitted with air-conditioned cabs. Drivers delivering materials must not be allowed to leave their vehicles.

Lead emissions can occur during furnace charging, smelting, and tapping. The greatest emissions are encountered when ‘red’ hot molten metal is drained from a

furnace. Refining lead bullion in the secondary circuit can also generate lead emissions. Casting of the final product can further generate a low level of lead emissions, as can any dross removed during the casting process.

The lead-in-air concentration of workplace areas should be measured in accordance with an appropriate national or internationally recognized procedure. Measurements are required often, at least every three months. Employees should be advised of the likely levels of exposure in the workplace and the precautions necessary to minimize the risk of lead exposure.

16.9. Engineering Control in the Workplace

Occupational exposure to lead and other toxic substances can be problematic at the multiple stages of the recycling process. Although much attention has been paid to exposure reduction via ventilation controls or PPE, basic process design is also important. Process modifications may be feasible to eliminate or reduce the generation of emissions, for example:

- blend dusty materials in enclosed facilities using water as needed to reduce dust levels
- lower pot temperatures to decrease the rate of dross formation and the surface generation of dust
- tap furnace metal either into moulds/pots under a ventilated shroud or directly into a bath of covered and ventilated molten lead between 310 and 350°C to minimize fugitive emissions
- modify plant layout to minimize movement and reduce the amount of materials handled.

Exposure can be reduced if machines are used to perform high-exposure tasks, which would thus permit employees to be removed from the area. This is especially useful during the furnace-tapping phase when close proximity to slag and melt taps can result in high personal exposure. Many companies have automated the tapping operation so that it is controlled remotely from an air-conditioned environment.

Efforts should be made to enclose any emission source to the greatest extent feasible. Because enclosures are seldom air-tight, however, a negative draft exhaust system should be applied to the enclosure. One of the most common ways to control emissions is to provide local exhaust ventilation at the source of emission generation. Capturing emissions at the source reduces the potential for emissions to disperse into the air and prevents occupational exposure created by the re-entrainment of surface dust contaminants. The capture velocity of an exhaust hood must be sufficiently great to prevent fumes or dust from escaping the airflow into the hood. The airflow must, in turn, have sufficient velocity to carry fume and dust particles into the hood and to overcome the disrupting effect of cross-drafts and other random air movements. The velocity required to accomplish this will vary from application to application, but in general, 100–150 $\mathrm{m\,min^{-1}}$ is used as the benchmark.

A number of other housekeeping measures can be effective. These include:

- where engineering controls are provided to minimize or contain lead emissions, inspections and maintenance regimes must be established at service intervals that are either recommended by the manufacturer or comply with statutory regulations; an up-to-date record of all inspections and engineering maintenance work must be kept
- efforts should be made to wash-down areas with water and keep areas damp, especially the working surfaces; operator training, prudent work practices, and good housekeeping are key elements in minimizing lead exposure when operating mobile equipment
- local exhaust ventilation and clean-air stations with positive filtered air can be provided so that employees can retreat to the stations when they are not needed in the process areas
- respiratory protection is important and should be available to any employee; such equipment can be of the mask type or the filtered-air hood; if sulfur is present carbon filter combinations should be made available
- belt wipes should be added to all tail pulley systems; conveyors should be subject to regular cleaning, and skirting should be placed at the head of any belt-drive system; this is especially important for battery-breaking equipment, because engineers will be working on the equipment when it is dry
- it is also important to make efforts to contain dust-emitting processes in one enclosed building and to separate one operation from another so that there is no cross-contamination in the event of fugitive emissions.

16.10. Process Emission Controls

Furnace gases and lead fumes, together with drossing dusts, must be captured and contained. There are a variety of methods to do this, but the most effective are filtration plants.

Fabric collectors remove particles by straining, diffusion, and electrostatic charge. The fabric may be constructed of any fibrous material, either natural or man-made, and may be spun into a yarn and woven or felted by needling, impacting, or bonding. The best modern bag is made of Teflon in a form that will capture sub-micron particles, but this material has a high initial cost. Regardless of construction, the fabric presents a porous mass through which gas is passed unidirectionally such that the dust particles are retained on the dirty side and the clean gas passes through. A non-woven or felted fabric is more efficient than a woven fabric of identical weight, because the void areas (pores) in the non-woven fabric are smaller. A specific type of fabric can be made more efficient by using smaller fibre diameters, by using a greater weight of fibre per unit area, or by packing the fibres more tightly. For non-woven construction, the use of finer needles for felting also improves efficiency.

An alternative to the filter bag is an electrostatic precipitator. In these baghouses, an electric field at high potential is established between discharge and collecting electrodes. The discharge electrode has a small cross-sectional area (e.g., a wire or piece of flat stock), while the collection electrode is large in surface area (e.g., a plate).

The gases to be cleaned pass through the electric field between the electrodes. At a critical voltage, gas ionization takes place at or near the surface of the discharge electrode. Ions which have the same polarity as the discharge electrode attach themselves to neutral particles in the gas stream as they flow through the precipitator. These charged particles are then attracted to a collecting surface where the dust particles give up their charge. The captured particles can then be easily removed by washing, vibration, or gravity.

Chamber or spray-tower collectors consist of a round or rectangular chamber into which water is introduced by spray nozzles. The principal mechanism for air cleaning is impaction of dust particles on the liquid droplets created by the nozzles. These droplets are separated from the air stream by a centrifugal force or impingement on water eliminators. Wet-centrifugal collectors comprise a large portion of the commercially available wet-collector designs. This design utilizes centrifugal force to accelerate dust particles and impinge them upon a wetted collector surface.

Wet-dynamic precipitators are a combination of fan and dust collector. Dust particles in a contaminated air stream impinge upon rotating fan blades that are moistened with water from aerosol spray nozzles. The dust particles impinge upon the water droplets and are trapped, along with the water, by a metal cone while the cleaned air makes a turn of 180°C and escapes from the front of the specially shaped impeller blades. Contaminated effluent from the water cone goes to the water and sludge outlet and the cleaned air goes to an outlet section which contains a water-elimination device. The orifice type of wet collector design has the air flowing through the collector and in contact with a sheet of water in a restrictive passage.

As a further stage to ensure the removal of any small particles of dust, flue gas can be directed to a Venturi-type dust collector. At both the inlet and the outlet of this type of collector, dust is covered by condensate through adiabatic expansion and collected by sprayed water that is circulated via tanks installed at the inlet and the outlet, respectively. This system is also a useful preparation for the removal of traces of sulfur dioxide by passing the gases through an absorber tower where the sulfur oxides are removed by contact with circulating water that is sprayed into the tower.

Many plants still employ cyclone dust-collectors (Figs. 16.10 and 16.11), either as a first-stage separator for the heavier dust particles or in series to achieve a high level of separation, prior to entry into a baghouse filtration plant for a final treatment before release to atmosphere. The operation of a cyclone is very simple, but effective. Contaminated air enters the cyclone at a high velocity and, under its own momentum, is spun around the cone in a circular motion that throws particles against the cone wall. As the cone narrows, large particles spin into the hopper where the dust can then be discharged into a container through a valve in the base. Smaller particles, typically less than 10 μm, will run back up through the centre of the cyclone and discharge through the outlet for further treatment.

16.11. Emission Testing and Analysis

The effectiveness of control measures should be assessed by all of the following methodologies: (i) static atmospheric monitoring; (ii) personal lead-in-air monitoring

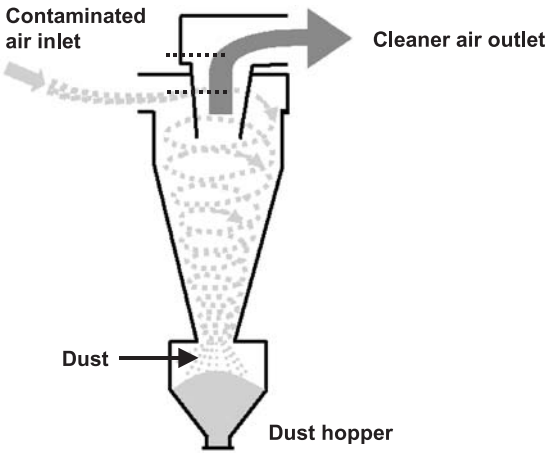

Fig. 16.10. Cyclone dust separator.

Fig. 16.11. Cyclones in series at the Baterias de El Salvador plant in San Salvador. (By courtesy of Baterias de El Salvador S.A.) [26].

(in the breathing zone of the employee); (iii) biological monitoring of employees in lead-risk jobs. When persons are liable to receive significant exposure to lead in workplace air, the employer must ensure that the concentration of lead-in-air is measured in accordance with a suitable national, regional, or international

Table 16.1. Sampling air in the workplace.

Type of Sampler	Characteristic and purpose
Static perimeter	Located on the boundary limits of the operations
Personal monitoring	Located on the employee and the test proceeds as he/she undertakes his/her duties; the test measures the level of occupational exposure at the place of work
Static process	Located close to those operations most likely to produce lead fumes or dusts; typically used to monitor efficacy of emission controls
Static urban/rural	Located outside the plant and close to places that may be of concern to the public; typical locations would be a farm, local housing estates, hospital, school, or nursery

procedure. Emission testing and analysis can take a number of forms, but it is generally important to test for particulates, sulfur dioxide, and visible emissions.

Air samples of the workplace should be taken using calibrated sampling pumps with cassettes that contain either mixed cellulose ester (MCE) or polyvinyl chloride (PVC) filters. There may be a number of country-specific statutory sampling requirements. The guide shown in Table 16.1 provides an overview of the effectiveness of control measures.

Secondary operations may also be required to test for hydrocarbons and dioxins in the furnace off-gasses. The engineering maintenance department should pay particular attention to any baghouse leaks using opacity tests or baghouse leak detectors. In-line organic or sulfur dioxide testing equipment is available but will not function consistently unless installed downstream of the baghouse or dust-collection control equipment. After any new installation or modification to the lead process, it is recommended that a determination of lead-in-air values be made as soon as possible and that the sampling covers the lead exposures of a representative number of employees who are likely to be those most exposed to airborne leaded dust.

While it is essential to comply with national emission limits for any lead industry, it is also important to set internal company standards, and these should cover three sources: (i) process emissions; (ii) fugitive sources of emissions; (iii) fugitive dust sources. Before any monitoring takes place, a clear strategy should be agreed with all concerned so that everyone understands that it is in the interests of employees and the local community that all workers cooperate with the program. Those implementing the strategy should be aware of all the lead processes at the workplace including: (i) equipment used for transporting and processing lead-containing materials; (ii) the composition of lead-containing materials; (iii) process details, e.g., smelting regimes, temperatures, and cycle times; (iv) the range of operational tasks in the process and maintenance areas. Sufficient samples, whether from static or personal sources, should be taken during routine monitoring to identify any major changes in exposure levels. Any abnormal results, whether low or high, should be carefully investigated by trained personnel in order to establish the reasons for the

abnormality. If the results are higher than expected, it is important to ensure that the employees concerned are protected adequately until any further controls needed are introduced. Group sampling and observation is the most efficient and effective monitoring method, because comparisons can be made between employees and rogue results are easily identified and eliminated. When such procedures are carried out, however, it is important that results are carefully analyzed to make certain that they are valid for all the individuals who make up the group.

The statutory requirements of many national standards for occupational health monitoring require results to be reported as a time-weighted average, normally based on an 8-h working day. As personal sampling rarely lasts more than 4 h, it is important to take into account the full range of operations carried out, particularly those at the beginning or end of the work period where there might be significant lead exposure. Any monitoring strategy should therefore require monitoring times to vary throughout the shift so that, over the course of a year, workers in all the various stages of the recycling process are sampled.

Fugitive emissions and fugitive dusts can be measured with a personal monitor or high-volume filter equipment when studying internal emission sources. Working methods and personal practices are, however, the most important factors that affect occupational lead exposure, and all personnel involved in lead operations must be trained adequately in lead abatement strategies and informed of the results of observations and monitoring, whether a cause for concern or not.

16.12. Biological Monitoring

Monitoring of lead-in-blood levels is critical to ensure worker safety. Although many regulatory agencies require monitoring of, and limits to, lead levels in air, it is the level of lead in the employee's blood that is the determinant of whether or not a risk of adverse health effects exists. The sampling of blood, preferably by venipuncture, and analysis for lead concentration is the most commonly accepted index of exposure in the occupational setting, where exposure via air and ingestion constitute the primary routes of exposure. Dermal absorption of inorganic lead through unbroken skin is considered to be minimal. The relationship between blood-lead and air-lead has been the subject of much study. In general, the relationship is curvilinear in nature. This is to say, the impact of a given air-lead level upon blood-lead will vary as a function of intensity of exposure. In general, a given unit of lead-in-air will produce a greater increase of blood-lead in an individual with a low blood-lead level as opposed to one with a high blood-lead level. Thus, estimates of the relationship between blood-lead and air-lead suggest that there is an increase between 0.02 and 0.08 $\mu g\,dl^{-1}$ of lead-in-blood for each $\mu g\,m^{-3}$ of lead-in-air, as dictated by a person's lead-in-blood level.

The relationship between air-lead and blood-lead in the occupational setting will also vary as a function of the particle-size distribution and chemical speciation of the lead contained within occupational aerosols [25]. The uptake of inhaled lead varies as a function of the area of the respiratory tract in which it deposits. Deposition patterns within the lung, in turn, will vary as a function of particle size. Very fine

particulate matter (less than approximately 5 μm in diameter) will deposit in the deep lung. Material that deposits in this section of the lung is taken up into the body with very high efficiency. Particulate matter that deposits in the upper airways or in the nose and throat exhibits much different behaviour. Head and throat deposition is followed very rapidly by swallowing and transport of material to the gastrointestinal tract. Upper airway deposition is followed by mucociliary clearance, which similarly transports deposited particles into the gastrointestinal tract. The uptake efficiency of lead from the gastrointestinal tract is much lower than uptake from the lung and is typically of the order of 5–10% of the amount ingested. Furthermore, whereas uptake from the deep lung is very high and independent of chemical speciation of the aerosol, the uptake of material from the gastrointestinal tract will vary as a function of chemical speciation. In general, soluble forms of lead (e.g., the sulfate) will be taken up with higher efficiency than insoluble forms (e.g., lead metal).

The lead-containing aerosols in many work environments are quite coarse; approximately 90% of the particles have a diameter equal to or larger than 10 μm. Thus, upper airway deposition, followed by clearance to the gastrointestinal tract, is to be expected in many work environments. The particle-size characteristics of any aerosol, however, will potentially have extreme variability and will vary in a site-specific fashion as a function of both process-specific and general work environment conditions. This variability imparts yet further uncertainty into the anticipated impact that a given amount of lead-in-air will exert upon increased blood-lead levels in workers. The nature and extent of engineering controls employed at a facility will also impact upon the particle-size characteristics of workplace air. Engineering controls will dramatically lower the total amount of lead-in-air but tend to have highest capture efficiency for larger particle sizes. Engineering controls can thus yield workplace aerosols with very fine particle sizes that are capable of deep lung penetration and deposition. Therefore, from a practical standpoint, it is not possible to infer direct proportionality between reductions in air-lead that result from engineering controls with decreased exposure risk. A ten-fold reduction of lead-in-air will not yield a ten-fold reduction of lead exposure risk if the lead removed from occupational air is predominantly large particulate matter taken up into the body with low efficiency, to leave behind fine particulate matter taken up with high efficiency. In the extreme, an aerosol with very fine particulates will increase blood-lead levels by about $2\,\mu g\,dl^{-1}$ for every $\mu g\,m^{-3}$ of lead-in-air.

The actual level of exposure experienced in the occupational setting will also vary as a function of industrial hygiene practices. Ingestion of lead via frequent hand to mouth activity, inadequate industrial hygiene, smoking, or eating in the workplace can all produce significant increases in blood-lead. Thus, proper control of lead exposure in the workplace requires both that adequate safeguards are maintained to limit inhalation exposure and that industrial hygiene programmes are in place to limit exposure through ingestion.

The precise guidelines to be followed for the monitoring of lead-in-blood will vary as a function of regional regulatory requirements. In any workplace, it is important to establish a starting point for the exposure of a new employee. Accordingly, an exposure baseline should be obtained before any worker commences an activity that involves potential contact with lead or any of its compounds. Workers should then

be tested at regular intervals, with the frequency of testing increasing as a function of exposure intensity. Thus, a worker may be tested every month upon first exposure to lead and/or if blood-lead levels are in excess of a value such as 20 or $25\,\mu g\,dl^{-1}$. Some employers will also increase the frequency of monitoring for a given employee if there has been an increase in blood-lead of $10\,\mu g\,dl^{-1}$ between tests. Should lead-in-blood levels remain low, typically below $25\,\mu g\,dl^{-1}$, the frequency of testing will often be decreased.

All biological monitoring results are generally shared with employees and a full explanation of the meaning of any lead-in-blood level is presented. Such a practice is a very important part of any strategy for reducing lead risk. This is especially true for adverse trends, and only by discussing a person's work schedules and tasks, and then checking these activities with any personal background lead-in-air monitoring and the levels of respiratory protection or the ventilation afforded to the employee, can conclusions be drawn and recommendations for reducing exposure be agreed and implemented. This counselling aspect of the risk-management process is being increasingly recognized by the secondary lead industry as an essential component of a medical surveillance programme. Moreover in 2003, the US Department of Labor's Occupational Safety & Health Administration (OSHA) introduced an 'e-tool' [26] for secondary producers that describes ways to reduce lead exposure to employees in lead smelter plants. This internet-based resource specifically targets the following operations: raw materials processing, smelting, refining, casting, environmental controls, maintenance. There are helpful diagrams which highlight potential exposure sources, as well as useful suggestions for either reducing the levels of lead exposure through an engineering solution or a change in working practice. Employers should also review test results for all workers by job, department, section, process, and shift in order to help identify jobs or work areas where there is a pattern of problems which are associated with elevated lead exposure.

A detailed review of the toxicology of lead is beyond the scope of this discussion. Comprehensive reviews of lead toxicology have been prepared by the International Programme for Chemical Safety [25] and others. Long-term, high-level exposure to lead has been documented to have adverse effects on the kidneys, the formation of red blood cells, the nervous system, and fertility. More moderate levels of lead exposure have been associated with adverse effects upon neuropsychological function and reproduction. Outside the occupational setting, the impact of greatest concern is usually the ability of excess lead exposure to impact upon child development.

16.13. Respiratory Protection

Whilst every effort should be made to minimize the risk of lead emissions during the recycling process, it is prudent to ensure that operating personnel are suitably equipped with the appropriate respirators in the event of fugitive emissions or ventilation system failure. Personnel working in hot-metal areas should wear an airstream helmet (Fig. 16.12), because it also provides a full face mask to protect against metal and slag splashes. Airstream helmets have a battery-powered motor

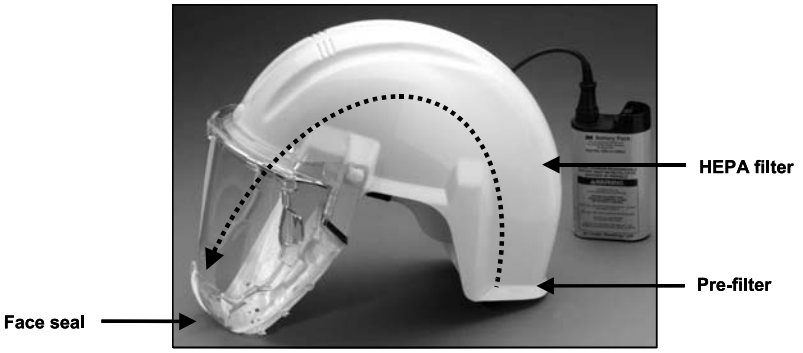

Fig. 16.12. A 3M HEPA airstream helmet. (By courtesy of 3M Company, Inc.)

and fan located in the helmet shell that draws contaminated air through a pre-filter at the base of the helmet. Air from the fan then passes through a high-efficiency particulate air (HEPA) filter and over the user's head. The filtered air is directed down over the user's forehead and provides a pleasant, cooling airflow over the entire facial area. The air is expelled at the bottom and periphery of the disposable face seal.

For operators working in the battery-breaking or desulfurization processes, the standard HEPA filter will not afford protection against the chemical mists that can be given off during operations. In such situations, and others where a specific toxic gas threatens the well-being of workers, the most efficient method for ensuring safe working is to use a battery-powered motorized filter pack, such as the 3M Breathe Easy with interchangeable filters (Fig. 16.13). In this device, a turbo motor draws ambient air through a filter–cartridge–canister system and supplies filtered air through the breathing tube to the headpiece. The turbo unit can be paired with a number of conventional masks and airstream helmets that are designed to fit the breathing tube to form a complete filtration system. The fan-assisted flow of cool filtered air makes breathing easier, and thus eliminates the fatigue caused by the effort of inhaling through filters during many hours of work.

Maintenance and engineering work inside baghouses and filtration systems requires specialized equipment and airline breathing apparatus supplied with filtered air from an external or self-contained supply (Fig. 16.14), such as a gas bottle. Face masks and personal filter systems are not designed to cope with the extreme exposure that is likely to occur when inspecting or maintaining filtration equipment. It is very important to choose a mask with an external supply nozzle and its own filter so that when the external supply is disconnected the wearer will be able to breathe filtered air. Such respirators are designed to be worn in an air or water shower, and any operator working in extreme conditions must continue to wear the face mask until all contaminated clothing has been removed, placed in a suitable bag, and he/she has washed off any dust in the shower. Only then should the mask be removed, and the operator should wash again. The mask must be placed in a suitable bag to be decontaminated.

Fig. 16.13. The 3M BreatheEasy. (By courtesy of 3M Company, Inc.)

Fig. 16.14. 3M airline supplied breathing apparatus. (By courtesy of 3M Company, Inc.)

For those personnel working in 'low risk' areas, the use of a paper 'comfort mask' should be strongly discouraged. These masks do not provide a good seal around the mouth and nose and do not conform to the standards required for protection from lead-in-air. As a minimum standard, only those 'paper' masks specifically designed for particulates and welding (with neoprene face seals and adjustable nose clips)

Fig. 16.15. 3M-8511 N95 particulate respirator. (By courtesy of 3M Company, Inc.)

should be used. In addition to a neoprene face seal, such respirators feature an exhaust valve to keep the inside of the respirator as dry as possible (Fig. 16.15).

16.14. Employees' Amenities

In addition to the supply of personal protective equipment and the maintenance of plant hygiene control systems, it is essential to ensure that:

- cleaning regimes are in place in all the operating areas
- employees are provided with clean working clothes every day
- there is a clean area to drink and eat meals
- hot showers are available so that employees can wash at the end of the working day and whenever they are contaminated with lead dust during the course of their work.

The design of a changing room in a secondary lead-plant or battery manufacturing facility, together with washing facilities and eating areas, should address the principles set out in the Sections 16.14.1–16.14.3 [27].

16.14.1. Location

The changing room should be sited on the perimeter of the secondary lead plant so that access to the 'leaded' area is only possible through a lead-free area. All amenities for employees working in the leaded areas should be located in the same building as the changing rooms. Workers will thus be in close proximity to work clothing, safety equipment, washing facilities, and the canteen or eating area.

16.14.2. Segregation

The clean and plant changing rooms should be segregated, with access from the clean side to the plant side through a corridor that passes the plant clothing and safety store. Works personnel should leave all their own clothes, including underwear, in their designated clean lockers. The lockers should have coded locks so that there is no need to take keys into the plant. There should be access to a bathroom and lavatory from the clean changing room.

Access to the plant from the clean locker room should be via a corridor with a one-way restaurant door so that once an employee passes through the door, he/she cannot go back into the clean area without passing through the washroom. The corridor should take the works personnel past the clothing store where they can collect clean overalls and/or any necessary safety equipment. As personnel enter the corridor they should place simple disposable or washable sandals or socks on their feet for hygiene purposes. These socks or sandals are discarded at the end of the shift or placed in the wash-bin. When works personnel have changed into their works clothing and are wearing the appropriate safety equipment, they should leave the changing room by the only exit to the plant.

16.14.3. Containment

At the end of the shift, or when it is time for a meal break, plant personnel should enter the only entrance to the locker room. Outside the entrance, there should be ample boot cleaners. These can be electric-powered vacuum brush cleaners, although upturned wet brushes in standing water will suffice. After cleaning their boots, employees should enter the lobby area of the locker room and remove their boots. Then all contaminated works clothing should be removed and placed in a 'used-clothing bin' located in the lobby of the changing room. This should be a sealed bin with an envelope slot facing the entrance to the plant so that contaminated clothing can be pushed into the bin without creating any lead-laden dust. The 'used-clothing bin' can have more than one slot if segregation of the various items of clothing is required. Furthermore, water-soluble bags can be used to line the bins so that full bags can be placed straight into the washing machines, and so avoid exposure risks to the amenity and laundry attendants. The contents of the bag need never be handled. The bag dissolves totally into a bio-degradable solution in hot water at over 60°C.

Works personnel should proceed to the shower and washroom area through another one-way door, so that they cannot return to the plant room from the shower area. Ideally, the design should be such that operators must pass through automatic showers. Thus, all workers have to shower as they leave the plant. Lavatories, soap dispensers, and clean towels should be available in the shower room. 'Clean' plant personnel can then exit the washroom and return to the clean changing room through another one-way door. Personnel can change back into their clean clothes and either leave the plant at the end of their shift or go to the canteen.

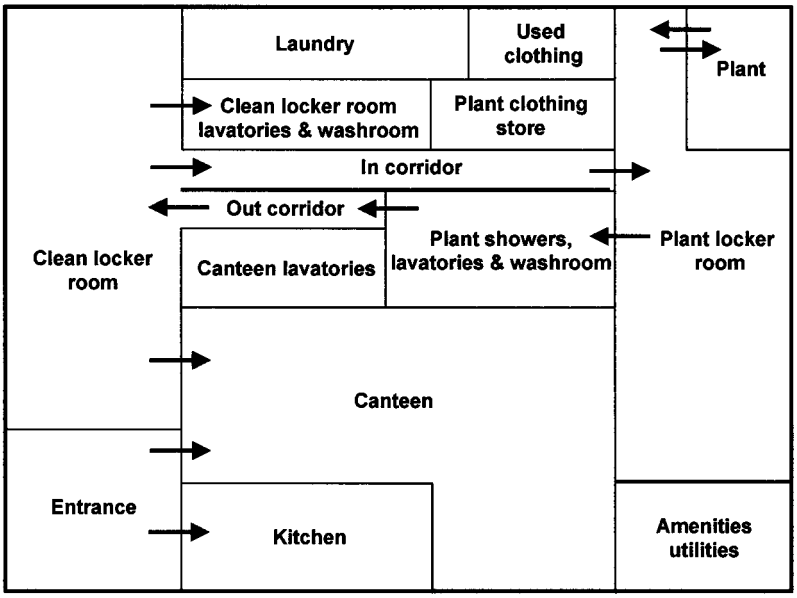

Fig. 16.16. Typical design for a lead plant change room and canteen.

One strategy and design for a changing room is shown in Fig. 16.16. This layout minimizes the risk of lead exposure. There are, however, a number of additional points to bear in mind:

- the whole washroom, canteen, and changing facility should be air-conditioned; the air pressure in the locker room should be less than that outside so that lead dust does not enter the clean areas
- as plant personnel should not carry money into work areas, clean drinking water must be freely available in the plant
- safety equipment must be returned to the safety store at the end of each shift for cleaning
- smoking should be banned; if not, plant personnel will undermine the segregation strategy if they take cigarettes into the plant and then return to the clean areas with them; hand-to-mouth contact during smoking will also increase lead ingestion
- access to and from the canteen and laundry must be carefully planned in order to maintain the highest level of segregation
- similar facilities should be provided for both men and women if both sexes work in the plant.

16.15. Effluent Control

Liquid waste from a secondary lead plant will normally be acidic, extremely corrosive, and toxic due to the presence of heavy metals. These properties will render

the effluent a hazard to plants and wildlife. The management of contaminated effluent is further complicated because lead is soluble in both acid and alkaline solutions. Lead dissolved in liquid effluent and fine lead dust particles suspended in the liquid are difficult to remove. Inadequate collection and containment of contaminated process water and excess surface water will permit the effluent to drain into either the municipal sanitary/sewage systems or into local streams and waterways. Percolation into surrounding soil can also occur.

To determine the most cost-effective process for water treatment, sources of contaminated water should be analyzed to determine whether there should be a centralized scheme, or whether effluent from some sources, for example the truck wash, should be treated separately. To ensure that effluent treatment complies with national standards, it is essential to test both surface and process water at each treatment stage, as well as prior to release.

Whilst some tests might be site-specific, depending on the complexity of other operations on a site, it is essential to analyze for: (i) suspended lead; (ii) dissolved lead; (iii) pH; (iv) other metals such as antimony, copper, arsenic, cadmium, and mercury; (v) oil, grease, and dissolved salts, particularly if the process requires the use of caustic soda or other reagents that produce soluble metal salts.

The following guidelines provide the basis for the control of contaminated liquid effluent:

- ensure that there are adequate collection and containment facilities on site for both process and surface water
- for those plants at risk of flooding during heavy rains, ensure that the water-treatment plant is not only above ground, but also above the level of likely flooding; in addition, ensure that there are channels and barriers around the perimeter of the plant to direct floodwaters away from the process areas
- segregate the process and surface effluent to ensure that relatively uncontaminated surface water does not have to pass unnecessarily through the entire water treatment plant prior to discharge
- allow time for the small and fine particles suspended in the effluent to settle in a lagoon or intermediate storage tank, and test the waste water to determine the appropriate treatment
- every effort should be made either to utilize or to re-circulate the treated water and thereby reduce the amount of waste water discharged to the environment and the quantity of fresh water required for topping-up the process.

In order to benefit from the potential cost savings of segregating process water from surface water, it is essential that the plant working areas be kept as clean and lead-free as possible. It is also far easier to remove one or two contaminants at a time than to treat a 'cocktail' of liquid effluent. Therefore, the system for the collection of waste water should be designed so that different waste streams can be segregated and treated separately, as needed.

Contaminated surface water and process effluent should always drain to sealed lagoons, concrete bunkers, or storage tanks to allow solids to settle prior to any treatment. An exception might be a lagoon adjacent to a battery breaker, where it may be preferable to agitate the effluent to maintain the lead oxides and sulfates

in suspension so that, when the water is returned to the gravity-separation stage of the process, they can be removed in the settlement tanks of the oxide separation conveyors. Two or three smaller lagoons are usually easier to manage than one large lagoon. For example, three lagoons could be managed so that one would be filling with waste water, a second would be settling prior to treatment or being filtered and chemically treated, and the third would either be discharging or being used to top-up the process water.

Settlement and/or filtration are usually all that is required for most of the rainwater and the water collected from a vehicle wheel wash prior to re-circulation or discharge. Much of the waste process water will, however, require a period to allow suspended solids to separate and also chemical treatment prior to discharge to the environment.

With recycling in mind, consideration should be given to utilizing any waste battery acid. Filtered battery acid can be recovered and, following chemical treatment, re-used in new batteries. Neutralization of the battery acid with, for example, ammonia or magnesium salts can produce valuable crop fertilizers. Neutralization with calcium salts, such as lime, will produce 'gypsum' that can be used in the manufacture of cement and plaster board. Neutralization with sodium salts will produce an inert filler — sodium sulfate — which is often used by the manufacturers of washing powder. Filtered, recovered battery acid can also be used in the water-treatment plant during some of the specific chemical-treatment processes to neutralize the effluent after precipitation of heavy metals (e.g., cadmium at pH 11, see Fig. 16.17, below).

Water is essential to many of the processes in the secondary lead industry, and as clean water becomes an increasingly expensive commodity, it makes economic sense wherever possible to collect rainwater from surface water drains and to top-up process water requirements 'free of charge'. The sound management of surface water

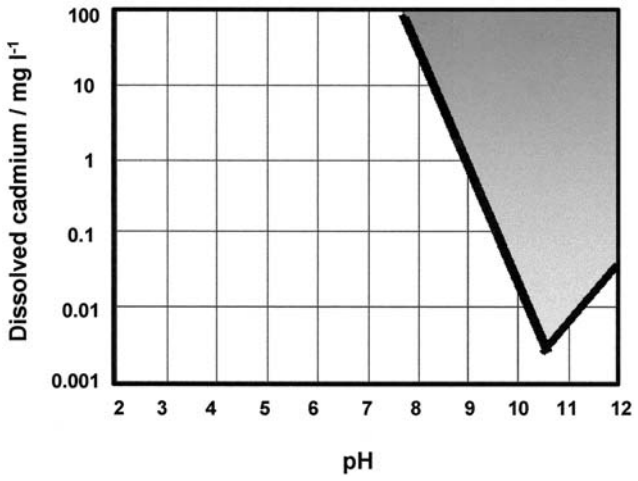

Fig. 16.17. Theoretical solubility of cadmium hydroxide vs. pH [28].

will also ensure that, in the unlikely event of a major chemical or toxic metal spillage, the surface water drainage system will isolate any environmentally unfriendly spill on the site. Accordingly, a closed-loop system for process water provides ideal environmental control and maximizes recycling.

Once the segregated waste water has been collected, the operators should: (i) remove the suspended solids by filtration or settlement; (ii) chemically treat the waste water to remove any heavy metals; (iii) adjust the pH to between 7 and 9. Whilst it is prudent to analyze the solids captured by the filtration process, in the vast majority of instances this portion of the waste effluent can be returned to the process feedstock for reprocessing.

Any metallic contaminants remaining in the effluent after filtration will be in solution. The most effective treatment methodology to remove the unwanted metals is precipitation as insoluble hydroxides [28] by careful pH adjustment of the effluent, followed by mechanical removal of the solid metallic salt. The effectiveness of this treatment method varies according to the concentration of the dissolved metal and the pH of the effluent. The most common approach is to add sodium hydroxide solution to the effluent in a suitable mixing vessel, in order to react with metal ions to form solid metal hydroxides that will precipitate. By way of example, the theoretical solubility of cadmium hydroxide as a function of pH is shown in Fig. 16.17. The *y*-axis represents the concentration of dissolved cadmium on a logarithmic scale from 0.001 to 100 $mg\,l^{-1}$. The shaded region of the chart shows the concentration levels and pH values for metal precipitation. For any conditions outside this region, cadmium will be in a solution and its removal by precipitation will not be possible. Therefore, adjusting the pH from, for example, an acidic value, as would be expected after the battery breaking, to an alkaline value between 10.5 and 11, will cause most of the cadmium to precipitate from solution. As virtually all the contaminant metals found in the effluent of a secondary lead plant display similar characteristics, albeit at different pH values, the various metals can be precipitated selectively.

The particle size of the precipitated metallic hydroxides is very small and precipitation by gravity would take a very long time, as would separation through a filter medium. In practice therefore, precipitation is accelerated by the addition of iron salts or organic polymers (coagulants). These salts and polymers attach themselves to the small, metal hydroxide particles, and thereby effectively increase the size of the 'solid' particles to form a flocculent that considerably increases the rate of settlement to between 1.5 and 3 h, as determined by the size and shape of the precipitation vessel. Very often, when a 'cocktail' of metal contaminants is present, discharge standards can be met if the pH is raised to a value of between 9 and 10, where non-ferrous metal contaminants will precipitate to values below 10 $mg\,l^{-1}$, as shown in Fig. 16.17 for cadmium. The effluent is filtered to remove any precipitate that has not settled, then the pH is adjusted to 7 in a holding tank and the effluent is sampled to check that the liquid meets the discharge standards. The precipitate can be returned to the process if any of the metals can be used as alloys; if not, the 'sludge' may be sold to a specialist metals smelter for further treatment.

Any waste water that cannot be recycled may be allowed to evaporate — a most economical method of disposal in a hot climate. In cooler climates, and particularly where industrial effluent discharge limits are extremely difficult to meet, evaporation

of excess effluent using the waste heat from the furnace is also an option. In those cases where compliance with effluent discharge standards remains difficult to achieve consistently, it may be necessary to install an in-line de-ionization unit, specific to the contaminants to be removed, prior to the final discharge point.

Finally, discharge points to any fresh water river, and the rates of discharge, should be determined with care, so that large volumes of oxygen-deficient water are not released into the aquatic environment to the detriment of native aquatic life and the river's ecosystem.

16.16. International Conventions and Protocols

16.16.1. Basel Convention

The Basel Convention on the Control of Trans-boundary Movements of Hazardous Wastes and their Disposal was adopted in 1989 and entered into force on 5 May 1992. The trans-boundary shipment of used VRLA batteries must comply with all relevant terms and commitments made by the Conference of Parties, especially as lead–acid batteries are classified as a hazardous waste.

The fundamental provisions of the Basel Convention seek to impose a 'prior informed consent' (PIC) regime on waste trading, even for those wastes which are destined for recovery or recycling. Designated 'authorizing agencies', labelling forms, and packaging and transportation safety standards are all specified by the convention.

The Convention contains the following specific trade provisions:

(i) any sovereign nation may ban waste imports, and all members are required to respect such bans by prohibiting waste exports to those countries;
(ii) if a country does not specifically prohibit a category of waste covered by the Convention, parties must still prohibit exports of such waste to that country unless it gives consent in writing to the specific import;
(iii) parties must prevent the export of hazardous waste if there is 'reason to believe' the waste will not be managed in an environmentally sound manner;
(iv) waste exporting to Antarctica is prohibited, so any VRLA batteries sent to Antarctica must not be left there at the end-of-life;
(v) parties cannot engage in waste trade, either importing or exporting, with states that are not parties to the Convention; Article 11, however, permits parties to trade with non-parties if they have entered into a bilateral or multilateral agreement or arrangements outside the Basel Convention that satisfy certain environmental safeguards and conditions; in particular, and as far as used VRLA batteries are concerned, such agreements or arrangements must not derogate from the environmentally sound management of hazardous wastes, as required by the Convention; such agreements must stipulate provisions that are no less environmentally sound than those provided for under the terms of the Convention.

Implicit under the terms set out in provision (iii), used VRLA batteries must only be shipped to a secondary lead plant known to recycle ULAB in an environmentally

sound manner (ESM). From a practical point of view, verification of ESM is not always an easy matter, so it is advisable to check for one or more of the following where applicable:

- valid government-issued operating license or permit to recycle ULAB
- current ISO 14001 certification for ESM
- recent national clean production awards, e.g., the Mexican SEMARNAP 'Clean Industry Award' La Secretaría de Medio Ambiente, Recursos Naturales y Pesca.

The Bamako Convention of 1990 [29] goes further than the Basel Convention and bans any waste imports into Africa and has been signed by all African nations.

In summary, the environmental management of materials involved in the manufacture, use, and recycling of VRLA batteries can be responsibly controlled. In fact, this is already true in many instances. Assessments of the need for further tightening of operating procedures for VRLA recycleable materials will undoubtedly be based upon a sound evaluation of the most reliable data available, and will be guided by the principles of environmentally sound management and sustainable development.

Appendix 1

Note: This material is presented for illustration purposes only and should not be regarded as a substitute for a manufacturer-supplied MSDS sheet.

Material Safety Data Sheet — Valve-Regulated Lead–Acid Battery

1. Identification of Waste Materials and the Company

Product	Used valve-regulated lead–acid battery
Product name	Jack Tarr automotive battery
Importer	The Best Recycling Company
Technical/Emergency support	Telephone numbers

2. Composition/Information about the Materials in Transit

Main components	Lead, lead sulfate, sulfuric acid (20%)
Other components	Polypropylene

3. Hazard Identification

Lead–acid battery	Electrical hazard if short circuited. Battery can produce high current if positive and negative terminals are short-circuited, which can result in sparks leading to fire hazard. Maximum voltage per battery/pack ___V.
Constituents	Lead and lead alloys toxic if ingested. Sulfuric acid — corrosive. If the battery case is broken acid leaks can damage skin and eyes on contact. Damage will also occur if in contact with materials and clothing.

4. First-aid measures

Sulfuric acid	Skin contact — flush with water, seek medical assistance if contact area is large or blisters form. Eye contact — flush with plenty of water until medical assistance is provided. Ingestion — flush mouth with water — give patient milk or sodium bicarbonate solution until medical assistance arrives.

5. Fire-fighting measures

	In the event of fire, keep containers cool by spraying with water. The plastic components may release toxic fumes, advisable to wear breathing apparatus.

6. Accidental release measures

Damaged batteries	Use goggles, rubber gloves, and protective clothing to prevent direct contact with hazardous substances. Have eyewash bottle and clean water available. Put any damaged items into a plastic acid proof container and identify as a corrosive hazard. Dilute any spillage with clean water and neutralize with sodium bicarbonate.

7. Handling and storage

Precautions	Store in cool dry conditions out of direct sunlight. When packed for transport the terminals should always be protected from short circuit. Do not store with items that could cause short circuit. Prevent sparks and naked flames in the vicinity. Wear protective footwear — the batteries are very heavy.

8. Exposure control and personal protection

Precautions	Do not remove any VRLA batteries from the packing or the containers. Wear neoprene gloves when handling the packed batteries or any of the containers with VRLA batteries. Wear protective footwear — the batteries are heavy.

9. Physical and chemical properties

Lead–acid battery	Sealed and will not spill, but some liable to leak if the cases are cracked.	
Lead	Appearance:	Solid
	Colour:	Silver-grey metal
	Odour	None
	Flammability:	None
	Density:	11.34
	Solubility:	None
	Melting Point:°C (Boiling)	327.4°C
Lead sulfate	Appearance:	Powder
	Colour:	White
	Odour:	None
	Flammability:	None
	Density:	6.29
	Solubility:(15°C)	$40\,mg\,l^{-1}$
	Melting Point:°C	1087
Lead dioxide	Appearance:	
	(compressed as solid)	Powder
	Colour:	Brown
	Odour:	None
	Flammability:	None
	Density:	9.4
	Solubility:	None
	Melting Point:(Decomp.)	290°C
Sulfuric acid	Appearance:	Liquid
	Colour:	Colourless
	Odour:	Acidic
	Flammability:	None
	Density:	1.3 approx.
	Solubility:	100%
	Boiling Point:	114°C approx.
Plastics	Appearance:	Solid
	Colour:	Various
	Odour:	None
	Flashpoint:	400°C
	Density:	$0.9–2.6\,g\,cm^{-3}$ at 25°C
	Solubility:	None
	Softening point:	95°C

10. Stability and reactivity

Lead	Oxidizes (If battery case split and lead is exposed)
Sulfuric acid	Corrosive
Plastic	Combustible

11. Toxicology

Lead and lead compounds	Toxic if ingested — seek medical help. Carcinogenic in animals. Can cause

	reproductive, developmental, hematological, renal, or neurological disorders.
Sulfuric acid	Corrosive and irritant.

12. Environmental

Valve-regulated lead–acid battery	Do not dispose of battery in household/domestic waste. Return complete battery for recycling. Under no circumstances incinerate.

13. Recycling

Lead–acid battery	Local regulations apply — consult Environment Agency for nearest recycling ULAB collection centre.

14. Transport Regulations

Lead–acid battery	Local/National/International regulations apply.

References

1. *Hawker Batteries Technical Manual for Standby Batteries*, Hawker Energy Products, UK, July 1999, p. 13.
2. C.L. Kusik, C.B. Kenahan, *Energy Use Patterns for Metals Recycling, Information Circular 8781*, US Department of the Interior, Bureau of Mines, Washington DC, USA, 1978.
3. P. Chapman, F. Roberts, *Metal Resources and Energy*, Butterworths Press, London, 1983, p. 138.
4. *ILZRO Project LEH-8, Ecobalance, Inc., Life Cycle Inventory Analysis of a Lead-Acid Battery, Final Report, November 1998*, International Lead Zinc Research Organization, Inc., Research Triangle Park, NC, USA, 1998.
5. N. Seldman, *Recycling Sector has 30-year Record of Impressive Growth*, Institute for Local Self-Reliance (ILSR), Media Release, January 2002. http://www.ilsr.org/recycling/recyclingma.htm
6. G.R. Smith, *1998 National Recycling Rate Study*, Battery Council International, Chicago, IL, USA, December 1998, p. 6.
7. *Handbook on the Implementation of EC Environmental Legislation*, 91/157/EEC49, The Batteries Directive, 1999. http://europa.eu.int/comm/environment/enlarg/handbook/intro.pdf
8. *EU Directive on Batteries and Accumulators*, *98/101/EC*, December 22, 1998.
9. United Nations Environment Programme, *Technical Guidelines for the Environmentally Sound Management of Waste Lead–acid Batteries*, *UNEP Press Release UNEP/CHW.6/22*, December 2002, Section 3.3, p. 14. http://www.unep.ch
10. B. Wilson, *Proc. Basel Convention Technical Working Group Workshop for the Environmentally Sound Management of Used Lead–acid Batteries in Central America and the Caribbean*, Trinidad, May 2001, p. 9. http://www.ilmc.org/Workshops/Basel/Trinidad/Presentations/English/leadacid/9.html.
11. R. Leiby, M. Bricker, *Proc. 1995 International Symposium on Recycling of Metals and Engineered Materials: Recycling Symposium*, Point Clear, AL, USA, 1995.
12. M. Stout, *Proc. 1995 International Symposium on Recycling of Metals and Engineered Materials: Recycling Symposium*, Point Clear, AL, USA, 1995.
13. M. Campbell, W. Glenn, *Profit from Pollution Prevention*, Pollution Probe Foundation, 12 Madison Avenue, Toronto, Canada M5R2S 1, 1982.
14. S. Morocutti, M. Olper, Engitec Impianti S.p.A., *Proc. 1995 International Symposium on Recycling of Metals and Engineered Materials: Recycling Symposium*, Point Clear, AL, USA, 1995.

15. B. Wilson, *UNCTAD /ILMC Project Report*, *A Review of the Environmental and Occupational Impact of Philippine Recyclers Inc. at the Bulacan site Republic of the Philippines*, *1997 to 2000*, International Lead Zinc Research Organization, Inc., Research Triangle Park, NC, USA, 2002.
16. F. Lima, *Lead Metal Technologies*, *Green Slag for Secondary Lead Rotary Furnaces*, Monterrey, Mexico, 1993.
17. L. Hedlund, *Proc. TMS International Symposium on Recycling of Metals and Engineered Materials: Recycling Symposium*, Point Clear, AL, USA, 1995.
18. R.B.M. Brew, C.R. Fountain, J. Pritchard, *Proc. 10th International Lead Conference*, Nice, France, 1991, pp. 170–181.
19. J.S. Robert, J. Sofra, S.P. Hughes, *Proc. GDMB European Metallurgical Conference*, 18–21 September, 2001, Friedrichshafen, Germany, Volume 1 (2001), pp. 281–294.
20. *'Ausmelt Dioxins and Furans'*, internal communication with selected parts published in J. Floyd, T.C. Hughes, R.A. Hughes, *Proc. MINPREX 2000, International Congress on Mineral Processing and Extractive Metallurgy*, Melbourne, Australia, 11–13 September 2000, pp. 43–48.
21. B. Wilson, *Proc. Asia Solid and Hazardous Waste Management Conference*, Kuala Lumpur, Malaysia, November 2001, pp. 142–152.
22. D. Martín, G. Díaz, *Proc. ILZSG Conference on Recycling Lead and Zinc — The Challenge of the 1990s*, Rome, Italy, 1991, pp. 315–336.
23. L.B. Lave, C.T. Hendrickson, F.C. McMichael, *Science*, **268** (1995) 993–995.
24. R. Socolow, V. Thomas, *J. Ind. Ecology*, **1** (1997) 13–36.
25. *Environmental Health Criteria 165 — Inorganic Lead,* International Programme on Chemical Safety, World Health Organization, Geneva, Switzerland, 1995.
26. http://www.osha-slc.gov/SLTC/etools/leadsmelter/index.html
27. *ILMC Tool Box Series, 1.4 The Design of Lead Plant Changing Rooms and Washing Facilities*, *2003*, International Lead Zinc Research Organization Inc., Research Triangle Park, NC, USA. http://www.ilmc.org/toolbox/1.4/
28. D.M. Ayres, A.P. Davis, P.M. Gietka, A Manual, http://www.erc.umd.edu/TES/techtips/PMG%20metal%20precip%20man.pdf
29. *Organization of African Unity: Bamako Convention on the Ban of the Import into Africa and the Control of Trans-boundary Movement and Management of Hazardous Wastes within Africa*, Addis Ababa, Ethiopia, Organization of African Unity, 1991.

Valve-Regulated Lead–Acid Batteries
D.A.J. Rand et al., editors

—CHAPTER 17—

THE NEXT GREAT CHALLENGE FOR VALVE-REGULATED LEAD–ACID BATTERIES: HIGH-RATE PARTIAL-STATE-OF-CHARGE DUTY IN NEW-GENERATION ROAD VEHICLES

A. Cooper, L.T. Lam, P.T. Moseley, and D.A.J. Rand

17.1. Future Automobile Electrical Systems

Over the past three decades, the development of the valve-regulated lead–acid (VRLA) battery from its flooded electrolyte precursor has involved considerable research and technological effort — in managing the oxygen cycle, in grid alloy and separator designs, and in optimization of charge strategies. As a result of this work, VRLA batteries are now well-established, reliable devices for the storage of electrical energy in stationary applications. At the start of the 21st century, however, a new challenge is in view that is likely to prompt a further wave of development of the system.

It is now expected that the familiar 12-V battery/14-V alternator system in automobiles will, progressively, be supplanted by alternative electrical configurations. The motivation for this change springs from the pressure for reduced vehicle emissions — which relates directly to an increase in fuel economy. In California, for example, well over half of the atmospheric pollution emanates from the road transportation sector, and the need to find practical ways to abate such pollution is mirrored in many other regions of the world.

There is much debate over which of the possible electrical configurations for new-generation road vehicles will predominate. At least eight distinct options have been proposed, as listed in Table 17.1 [1,2]. The first four configurations in the list are intended to provide the electrical power that is necessary for an increasing range of electrical ancillaries. It should be noted that configurations 3–6 employ a 36-V battery together with a 42-V alternator, and are commonly referred to as 42-V PowerNets. Configurations 5 and 6, as well as 7 and 8, make use of both electric and internal-combustion engine (ICE) propulsion; these vehicles are generically termed 'hybrid electric vehicles', or more briefly 'HEVs'. Clearly, it would appear that at present there is no unequivocal classification of each of the various types of new-generation vehicle. The eight options given in Table 17.1 range from the dual 12-V battery systems, through a variety of designs in which the vehicle makes use of increasing electrical functionality, to a plug-in hybrid which would provide

Table 17.1. Possible configurations of electrical systems for new-generation vehicles [1].

1.	12-V dual-battery to power ancillaries
2.	12-V dual-battery for stop–start (and regenerative braking)
3.	42-V 'upscale' SLI battery for starting, lighting, ignition, and to power ancillaries[a]
4.	42-V with stop–start[a]
5.	42-V with launch-assist ('soft' hybrid)[a]
6.	42-V with some power-assist ('mild' hybrid)[a]
7.	High-voltage power-assist ('full' hybrid)
8.	Hybrid with electric range at full power ('plug-in' hybrid)

[a]System with 36-V battery and 42-V alternator.

the vehicle with a substantial range of electric-only drive; further details of the candidate configurations are given in Chapters 11 and 12. One sector appears to be already established, namely, high-voltage power-assist vehicles. Following the tentative introduction of such HEVs to the market place in late 1999, total sales passed the 100,000 mark before the end of 2002. All these vehicles employ nickel–metal-hydride batteries because, when the vehicles were designed, it was thought that lead–acid products were unable to cope with the required duty cycle for an adequate life.

Vehicles which do not fall within the hybrid classification will retain a conventional ICE architecture, but will require batteries (12 V or higher voltage) that are capable of accepting and delivering much greater power than is possible with standard automotive batteries in order to meet the demands of vehicle design engineers. The time required for this change to be completed is unclear. Nevertheless, it should be noted that the first vehicle with a 36-V battery, the Toyota *Crown*, was launched in Japan in October 2001.

17.2. The Challenge of High-rate Partial-state-of-charge (HRPSoC) Duty

Obviously, a battery can only be acceptable in any given application if it is capable of delivering an adequate service-life. As indicated in Table 17.2, the life-limiting processes (failure modes) for the conventional SLI battery (first a 6-V unit, then a 12-V unit) are well known, and the reliability of the battery has been progressively improved to keep pace with advancements in automobile design over the better part of a century.

When attention focused on pure-electric vehicles (EVs) at the beginning of the 1990s, it was clear that the VRLA battery could not deliver the desired service-life. Within a decade, however, the industry, supported by the extensive research programme mounted by the Advanced Lead-Acid Battery Consortium (ALABC), had made the necessary investment in research and development to achieve a ten-fold increase in deep-cycle life. The VRLA battery was then able to compete with alternative chemistries (e.g., nickel–cadmium, nickel–metal-hydride, lithium-ion) as an acceptable power source for EVs.

Table 17.2. Typical duty and performance characteristics for VRLA batteries in different categories of present and new-generation vehicles.

Parameter	Application		
	SLI, 12-V	Electric vehicle	42-V PowerNet, HEV
Duty	High-rate start	Deep-cycle	High-rate PSoC
State-of-charge	85–90%	20–100%	42-V PowerNet: 70–90% HEV: 60–70%[b]
Maximum normal discharge[a]	$10C_1$	$4C_1$	$15C_1$
Maximum normal charge[a]	$0.5C_1$	$0.5C_1$	$8C_1$
Failure modes	Corrosion, shedding	PCL 1, PCL 2 (see Chapter 9)	Under-charge and sulfation of negative plates

[a] In multiples of 1-h rate.
[b] This is the normal operating range for the Honda *Insight*, but the battery management system of this vehicle will allow a wider range of operation between 30 and 80% state-of-charge if so required by the driving pattern.

In all eight of the electrical systems that have been proposed for new-generation vehicles (Table 17.1), the batteries will be required to operate in a manner which is quite unlike the duty experienced by present 12-V automotive types (i.e., starting, lighting, and ignition — 'SLI' types). In general, the battery will have to supply significant amounts of electrical energy for on-board electrical functions and, in several of the systems, will have to accommodate charge returned via 'regenerative braking' as part of the scheme to save fuel. Under such duty, the battery will have to operate continuously at a partial-state-of-charge (PSoC) and accept charge at extremely high rates. In addition, high-rate discharge is necessary for engine cranking and power-assist. Overall, the battery is said to undergo high-rate partial-state-of-charge duty, or more briefly 'HRPSoC duty'. An example of such duty is shown in Fig. 17.1 [3]. The anticipated marked shift in the function of the battery in new-generation vehicles and the limitations to its life performance are summarized in Table 17.2.

Clearly, the lead–acid community now faces a change in the market which promises to be more far-reaching than was the introduction of modern EVs. Operation over a reduced range of depth-of-discharge, as required by the new automobile protocols, might be expected to lead to a longer cycle-life than in the case of the deep-discharge duty employed for EVs (see Fig. 17.2). This advantage is more than offset, however, by a challenge to the charge efficiency of the negative plate. Normally, this charge efficiency is high until charging is almost complete, so that operation in a PSoC mode ought to be favourable. It appears, however, that at the very high rates of charge experienced in HEVs (see Table 17.2), the charge efficiency is diminished, even when the plate is not at a full state-of-charge.

Lacking a construction which is purpose-designed for HRPSoC duty, VRLA batteries typically lose at least 50% of their initial capacity after operating in

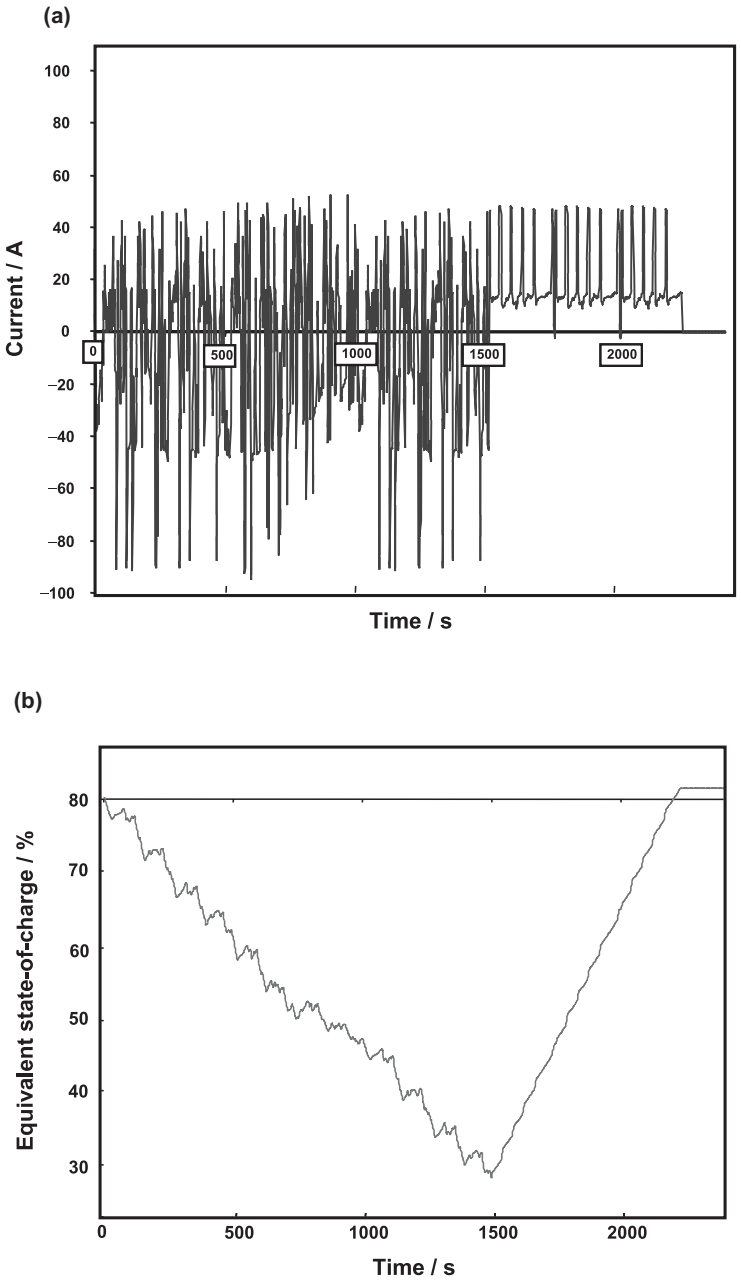

Fig. 17.1. (a) Composite test cycle compiled from current measurements on the battery in a Honda *Insight* running round Millbrook test track in UK. Arduous driving for 1500 s followed by sequence of regenerative braking events; discharges reach around $15C_1$ and charges $8C_1$. (b) Capacity removed and restored during test cycle in (a). Short-term changes in state-of-charge involve ~4% of total capacity; overall range covered is nearly 50% of total capacity (removed in 25 min, i.e., at a rate of $1.2C_1$, and restored in 12.5 min, i.e., at a rate of $2.4C_1$).

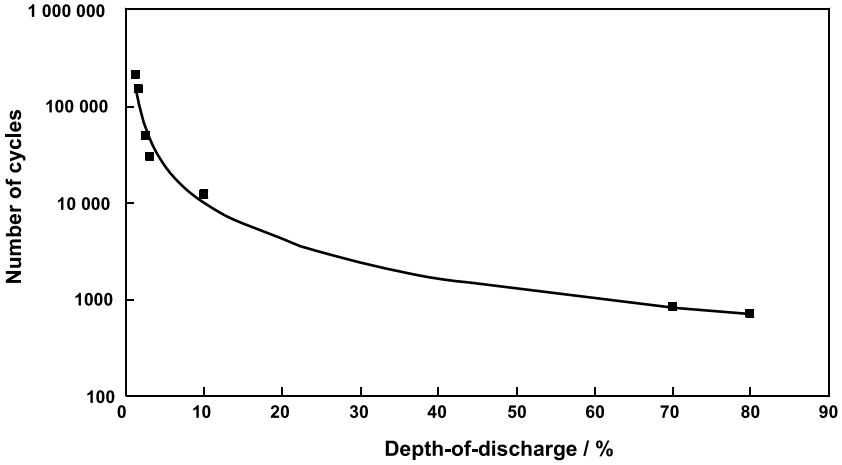

Fig. 17.2. Variation of cycle-life with depth-of-discharge of a spiral-wound VRLA battery (Courtesy of Exide Technologies).

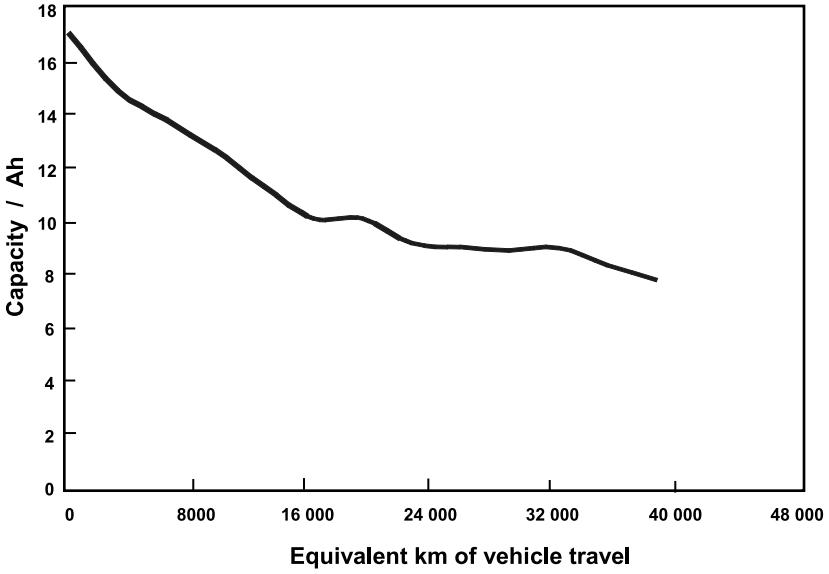

Fig. 17.3. Change in capacity of standard VRLA battery under simulated HEV duty. Charge and discharge limited to $2C_1$ [4].

a simulated HEV mode for an equivalent service-life of around 32,000 km, as demonstrated by the example given in Fig. 17.3 [4]. This loss of capacity has been attributed to a progressive build-up of lead sulfate on the negative plate, especially at the bottom. Since the battery is not brought to a full state-of-charge in PSoC duty (see, for example, Fig. 17.1(b)), there is no routine method available to remove this lead sulfate [5,6].

17.3. Mechanism of Lead Sulfate Accumulation During HRPSoC Duty

Recent investigations conducted by CSIRO [7,8] have provided the following explanation for the mechanism of lead sulfate accumulation in negative plates during HRPSoC duty.

The discharge and charge processes at the negative plate can be expressed by reactions (17.1)–(17.4), shown in Fig. 17.4. During discharge, the conversion of sponge lead to lead sulfate proceeds via two steps. First, the sponge lead at the negative plate reacts with HSO_4^- to form Pb^{2+}, SO_4^{2-} and H^+, i.e., the so-called 'dissolution process', reaction (17.1). Then, the Pb^{2+} combines with SO_4^{2-} to form $PbSO_4$, i.e., the so-called 'deposition process' or 'precipitation process', reaction (17.2). The first step is an electrochemical reaction and thus involves electron transfer. Such transfer of electrons takes place only on the conductive sites, i.e., on fresh lead. The rate of the electrochemical reaction is therefore dependent not only on the diffusion of HSO_4^- species, but also on the effective surface-area of the sponge lead. On the other hand, the second step is a chemical reaction and proceeds at a rate which is acid-dependent. The solubility of lead sulfate does not increase with increase in sulfuric acid concentration [9]. Rather, it reaches a maximum value at 10 wt.% sulfuric acid (1.07 rel. dens.), and then decreases rapidly with further increase in concentration (Fig. 17.5). Thus, the Pb^{2+} will precipitate as lead sulfate at concentrations above the solubility curve. Clearly, for a given concentration of Pb^{2+} above $\sim 1\,mgl^{-1}$, the deposition (or precipitation) of Pb^{2+} to lead sulfate will be faster at plate locations which experience high concentrations of acid.

During the initial stages of the discharge of a fully charged negative plate, electron transfer can take place at any location because the entire plate is conductive. Accordingly, the discharge process (both dissolution and deposition steps) occurs both on the surfaces and in the interior of the plate. Nevertheless, the reaction in the

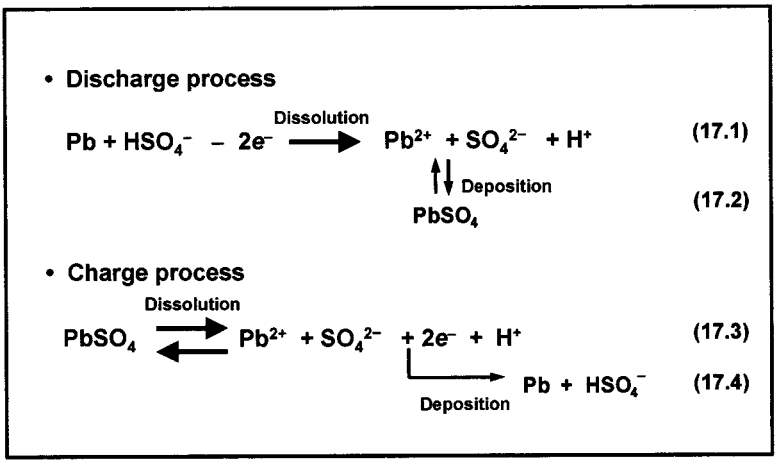

Fig. 17.4. Discharge and charge reactions at the negative plate of a lead–acid cell.

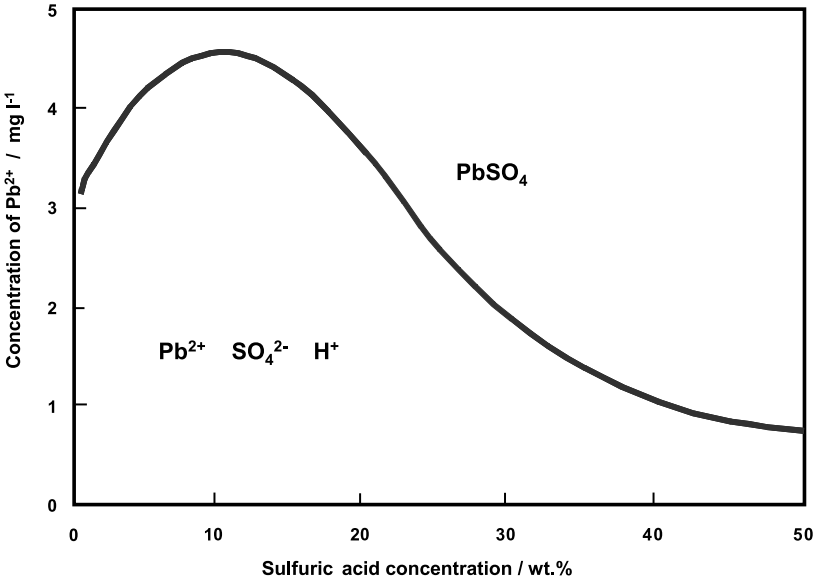

Fig. 17.5. Solubility of lead sulfate in sulfuric acid as function of acid concentration [9].

interior of the plate will soon slow down and/or stop, while that at the surfaces of the plate will continue. This is because less acid is now available in the interior.

The depth to which lead sulfate penetrates is dependent on the rate of discharge, as well as on the density and surface area of the plate. Paste density is the key factor in providing the macropores which are necessary for the transport of solution and ionic species to and from the reaction sites within the interior of the plate, while surface area provides sites for the current-generating electrochemical reaction. For the same paste density and surface area, the extent to which lead sulfate can penetrate is determined by the discharge rate.

Under low-rate discharge (i.e., $< 0.4C_1$), the dissolution rate of Pb^{2+} from each lead crystal is slow and, therefore, the accompanying consumption of HSO_4^- in the interior of the plate is likely to be counterbalanced by the diffusion of HSO_4^- from the bulk of the electrolyte. Furthermore, the subsequent deposition of Pb^{2+} to $PbSO_4$ (reaction (17.2)) also occurs slowly due to the low supersaturation of Pb^{2+} in the vicinity of each parent lead crystal. (Note that, the deposition rate of $PbSO_4$ is proportional to the degree of supersaturation of Pb^{2+} in the sulfuric acid solution, i.e., the higher the supersaturation, the faster is the deposition rate.) Since the rate of deposition is slow, newly formed $PbSO_4$ tends to precipitate preferentially on the already-deposited $PbSO_4$ crystals, i.e., growth rate > nucleation rate. Consequently, the deposited lead sulfate will continue to grow to various sizes of discontinuous crystals, both on the surface and in the interior of the negative plate. This form of lead sulfate is particularly desirable on the surface of the plate, as it provides an open structure that facilitates the ingress of HSO_4^- ions. Therefore, the discharge process can proceed deep into the interior of the plate.

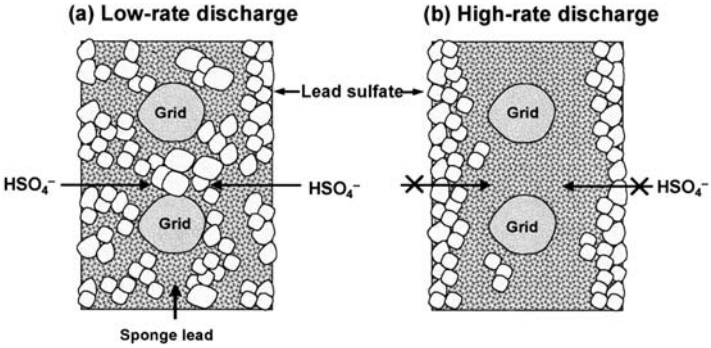

Fig. 17.6. Schematic representation of the distribution of lead sulfate in a negative plate subjected to (a) low-rate discharge or (b) high-rate discharge.

Accordingly, the lead sulfate develops evenly throughout the cross-section of the negative plate, as shown schematically in Fig. 17.6(a).

The formation of lead sulfate is quite different under high-rate discharge, e.g., under cranking-current ($\sim 18C_1$) conditions. The electrochemical reaction, i.e., reaction (17.1), Fig. 17.4 now proceeds so rapidly that the diffusion rate of HSO_4^- cannot catch up with the consumption rate. Consequently, lead sulfate forms mainly on the surface of the plate. Moreover, high-rate discharge generates a very high supersaturation of Pb^{2+} in the vicinity of each parent lead crystal. The lead sulfate will therefore precipitate rapidly on any available surface, irrespective of whether this be sponge lead or already-deposited lead sulfate, i.e., nucleation rate > growth rate. Thus, a compact layer of tiny lead sulfate crystals will develop on the surface of the plate. This will reduce the effective surface-area for electron transfer and will also hinder the diffusion of HSO_4^- into the interior of the plate (Fig. 17.6(b)). Under such conditions, the discharge reaction cannot proceed into the interior, but stops at the surface of the plate and at the walls of the pores.

During charging, the conversion of lead sulfate to sponge lead also proceeds via two reactions, namely, dissolution and deposition. Nevertheless, the nature of each of these reactions differs from that of the corresponding discharge reactions. Dissolution is now the chemical reaction, while the subsequent deposition is the electrochemical reaction. The lead sulfate first dissociates to Pb^{2+} and SO_4^{2-} ions (reaction (17.3), Fig. 17.4). The Pb^{2+} then receives two electrons and reduces to lead (reaction (17.4), Fig. 17.4). Simultaneously, SO_4^{2-} combines with H^+ to form HSO_4^-. The electrons flow to the active sites in the negative-plate material via the grid members because the electrical resistance of the grid metal is much smaller than that of the discharged material. In addition to the reduction of Pb^{2+} to lead, there is the competing reaction of hydrogen evolution. Usually, hydrogen evolution only takes place near the end of charging for the following reasons: (i) most of the $PbSO_4$ has been converted to lead and, correspondingly, the sulfuric acid concentration, i.e., the H^+ concentration, has increased; (ii) further dissolution of $PbSO_4$ to Pb^{2+} and SO_4^{2-} is slow. Having said this, hydrogen can also be involved during the early stages of the charging process, if the dissolution of $PbSO_4$ is hindered (*v.i.*).

Having described the basic chemistry of the discharge–charge process, it is now appropriate to consider charging of the negative plate after it has been deeply discharged at a low rate. As discussed above, lead sulfate is formed throughout the entire cross-section of the plate and the relative density of the acid after discharge is low because of the high utilization of the active material. The dissolution of $PbSO_4$ to form Pb^{2+} and SO_4^{2-} increases at low acid concentrations (see Fig. 17.5). Thus, the subsequent reduction of Pb^{2+} to sponge lead can take place smoothly before the evolution of hydrogen. With an overcharge of ~10%, the plate can be brought to a fully charged state without any difficulty. This is also true when the plate is subjected to low-rate PSoC cycling with equal amounts of charge input and charge output. In such duty, the state-of-charge of the negative plate decreases with cycling, but can be brought to 100% after the application of an equalization charge.

By contrast, charging of the negative plate after deep discharge at a high rate is difficult. Since high-rate discharge cannot proceed into the interior of the plate, but stops at the surface, the utilization of the active material is low. Consequently, the relative density of the acid after discharge is still at a high level and this decreases the dissolution of $PbSO_4$ (see Fig. 17.5). The lower concentration of Pb^{2+} will then impede the subsequent electrochemical reaction and, during the early stages of charging, will cause the negative-plate potential to become more negative to such extent that hydrogen can start to evolve. Furthermore, as mentioned above, the electrons flow from the grid members towards the surfaces of the plate. These electrons will reduce some hydrogen ions to hydrogen gas before reaching the lead sulfate layer, as shown schematically in (Fig. 17.7). Thus, complete conversion of lead sulfate at the plate surface cannot be achieved, even with an overcharge of 10%, because of the combined effects of the early evolution of hydrogen and the oxygen-recombination reaction (see Chapter 1). In addition, the overcharge factor will

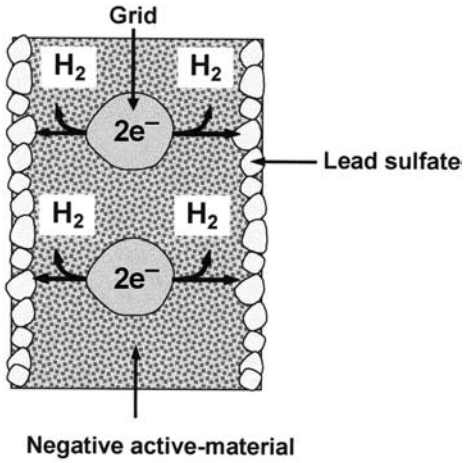

Fig. 17.7. Schematic representation of the charging process of a negative plate after high-rate discharge.

increase with cycling because progressive water loss will dry-out the separator, increase the amount of oxygen reaching the plate, and hence will enhance the level of oxygen recombination. Thus, lead sulfate will accumulate on the surface of the negative plate and, eventually, the battery will be unable to provide sufficient power for engine cranking.

Experimental verification of the concentration of lead sulfate near the surfaces of a negative plate under simulated HRPSoC (HEV) duty is shown in Fig. 17.8 [10]. The data also confirm that, at this stage, the top-of-charge potential for the plate exceeds that at which hydrogen is evolved. It should be noted that in this test both charge and discharge are conducted at the $2C_1$ rate. In actual HEV duty, however, the rates will be much higher and the resulting effect on battery performance may be more serious.

In summary, the lead–acid battery developed over decades for SLI duty must be modified significantly in order to provide the power capability demanded by future automobile electrical systems, and to be able to sustain this function for an adequate service-life. The key objective is to overcome the processes that give

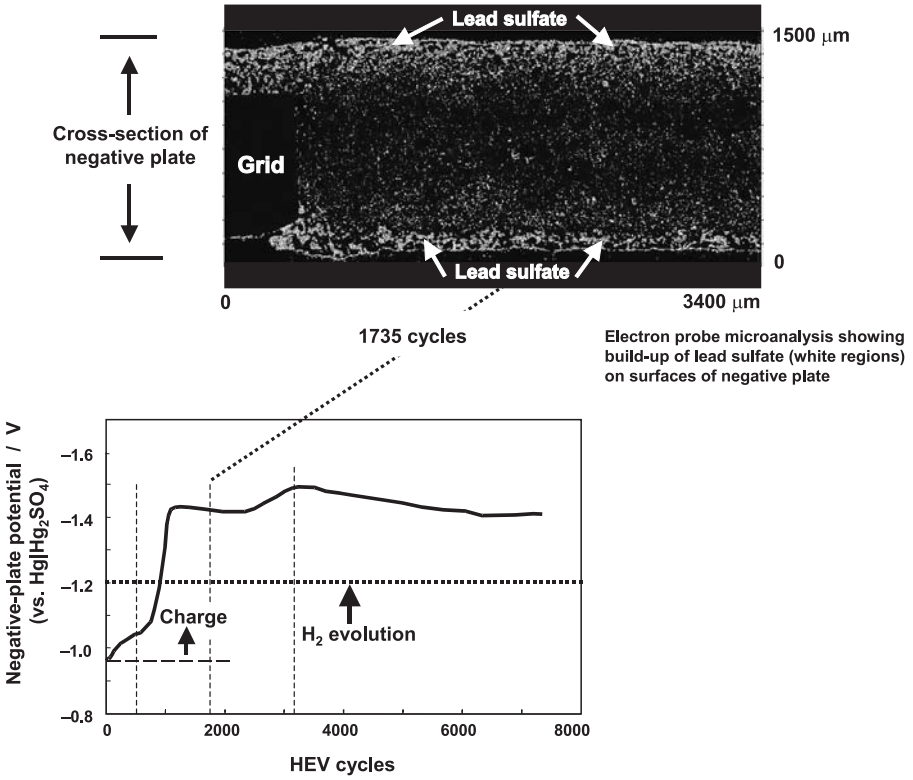

Fig. 17.8. Build-up of lead sulfate and concomitant evolution of hydrogen in negative plates after 1735 cycles of simulated HRPSoC duty (battery initially discharged at C_1 rate to 50% state-of-charge; duty cycle: charge and discharge at $2C_1 = 3\%$ state-of-charge) [10].

rise to the accumulation of sulfate on the negative plate in HRPSoC duty. In effect, this requires controlling the secondary reactions of hydrogen evolution and oxygen recombination through modifications to the design of the negative plate as well as to the morphology and composition of its active material. The establishment of a mathematical model for the VRLA battery operating in HRPSoC regimes would be a valuable asset in predicting performance characteristics and in helping with detailed design adjustments. In formulating a sound model of the processes taking place in HRPSoC duty, it will be important to establish experimentally how the current at high-rate charging splits between the main charging reaction and the secondary (parasitic) reactions.

17.4. Controlling Secondary Reactions During High-rate Charge

The following lines of on-going research show considerable promise for extending the life of VRLA batteries in HRPSoC service.

17.4.1. Trace element control

Small amounts of trace elements can cause major changes in the overpotentials at positive and negative plates and thus can alter the rates at which the gassing reactions proceed. A thorough study undertaken by CSIRO in Australia [11] has found that elements not required by the fundamental stoichiometry of the cell reaction can influence gas evolution — either individually, or in combination when subtle synergistic effects can occur. For example, early indications show that zinc has a strong ability to suppress hydrogen gassing at the negative plate, and that a combination of antimony and iron can suppress the oxygen-gassing effect of some transition metals at the positive plate.

17.4.2. Separator design

As pointed out in the preceding reviews of separator function and separator materials (Chapters 6 and 7, respectively) and of charging strategies (Chapter 9), the separator plays a crucial role in VRLA cells. Provision of a separator with the appropriate microstructure can constrain the rate of oxygen arrival at the negative plate and thus restrict the suppression of the plate potential caused by the oxygen-recombination reaction.

17.4.3. Carbon inventory

The active material on the positive plate generally presents a surface area which is significantly greater than that of the negative plate. This manifests itself as a difference in the flux of electrons to the reaction sites on the two plates. If the surface available at the negative plate can be extended, then the influence of the unequal dependence on diffusion in negative and positive plates can be reduced.

Interestingly, as shown in Fig. 5.9 in Chapter 5, an increase in the quantity of carbon in the negative active-material can extend battery life under HEV duty to a significant extent. Moreover, these early results, again from CSIRO [12], have indicated that the form of the selected carbon is of critical importance. Graphite particles, evidently with a plate-like form well-suited to inter-particle contact, produce far better results than carbon black employed in the same weight fraction. Elsewhere, Meissner [13] has found that acicular conducting particles are far more effective in increasing the conductivity of a resistive medium than equi-axed powders, by a factor of up to 1000 as dictated by the aspect ratio of the particles. The influence of plate-shaped particles was not reported but, by analogy with the case of acicular materials, it would seem that any departure from the spherical shape would be beneficial, so that the result presented in Fig. 5.9, Chapter 5 is not unexpected.

17.5. Grid Design for HRPSoC Duty

At the extraordinarily high power levels demanded in HRPSoC duty (see Table 17.2), consideration must also be given to optimizing the current-collection function of the grid. It is well established that the performance of lead–acid batteries can be adversely affected by a non-uniform distribution of current over the plates as a result of ohmic losses [14]. This effect becomes more pronounced the higher is the rate (of charge and discharge) and the larger is the plate [15,16]. At the highest rates, the voltage drop down the grid causes an inhomogeneous utilization of the active material (that near the current take-off 'tab' is worked harder than that further away) and increases the heat generated in the cell. Non-uniform distribution of current can be ameliorated by increasing the electrical conductivity of the grid, as shown in Fig. 13.18, Chapter 13.

More recently, research conducted at CSIRO [17] has demonstrated that the addition of a second current take-off tab, symmetrically placed opposite the first, will bring considerable benefit in terms of improved performance from VRLA cells subjected to HRPSoC duty. The current passing through each tab is half that which would pass through a single take-off and the extra connection also acts as an additional heat-sink. Both these features safeguard against the development of high operating temperatures within the cells and result in more uniform utilization of the plate active-materials. These benefits, in turn, translate into improved power capability and longer cycle-life. For example, in an initial demonstration under simulated HEV duty at ambient temperature (24°C), a 'dual-tab' battery provided 8800 cycles and remained at a steady temperature of 38 ± 2°C, whereas a commercial (single-tab) battery sustained only 6900 cycles and reached a temperature of 65°C, see Fig. 17.9.

The patented dual-tab concept [18] has been applied effectively to the spiral-wound design of VRLA in a project funded jointly by the UK government and the ALABC to develop HEV batteries [3]. The design of the cell used in this demonstration is shown in Fig. 17.10(a), where the positive and negative connections can be seen projecting from each end of the unit. The performance of this cell has been compared with that of the conventional, single-tab cell from which it was

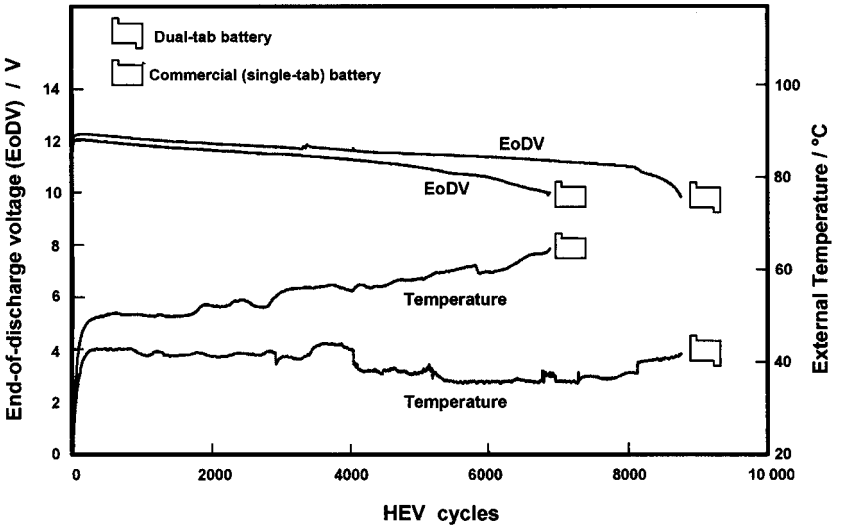

Fig. 17.9. Performance of dual-tab and commercial (single-tab) batteries under simulated HEV cycling (charge and discharge at $2C_1$) [17].

derived. Each cell design was deployed in an 18-cell, 36-V battery (Fig. 17.10(b) shows the dual-tab version), and the resulting batteries were subjected to the simulated HEV cycle shown in Fig. 17.1(a). During this test, the battery state-of-charge was run down to 30% from an initial value of 80%, and then returned to 80%. (Note, this is an accelerated schedule and is more demanding than that expected in HEV duty, i.e., 40–60% state-of-charge, see Table 17.1.) A battery of conventional cells was unable to complete even one pass through the cycle (Fig. 17.11(a)). By contrast, the dual-tab counterpart completed the cycle with less voltage fluctuation (Fig. 17.11(b)) and, moreover, went on to sustain 65 consecutive cycles before failure (Fig. 17.11(c)). When a 36-V dual-tab battery was subjected to the same demanding procedure, but with conditioning charging after every 10 cycles, 291 of these very tough cycles were completed before the battery failed to deliver full power.

The above remarkable demonstration results from the fact that the plate has been designed to avoid heterogeneous current distribution of the type shown in Fig. 13.18, Chapter 13. Such research has provided strong evidence that a radical re-design of VRLA batteries is necessary for the technology to make a significant contribution to the growing HEV share of the automotive sector. Further benefits may accrue from the use of a battery management system that is also being developed in the above ALABC project [3]. The approach being taken is to manage each 2-V cell separately and to add one extra cell to each set of 18 cells. This will allow charge to be moved around the pack in order to provide a systematic conditioning process, as and when necessary, even while the battery is on load.

Provided that the remarkable benefits associated with the dual-tab design in HRPSoC duty can be attributed to a reduction in ohmic losses [14,15], then it can be anticipated that a similar performance improvement could be achieved by a

(a)

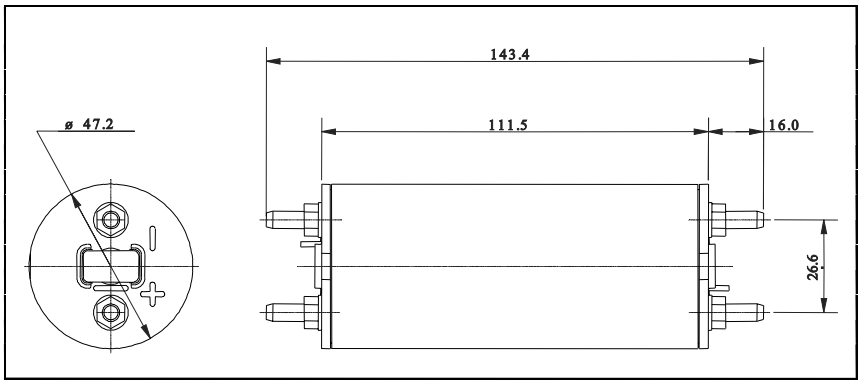

(b)

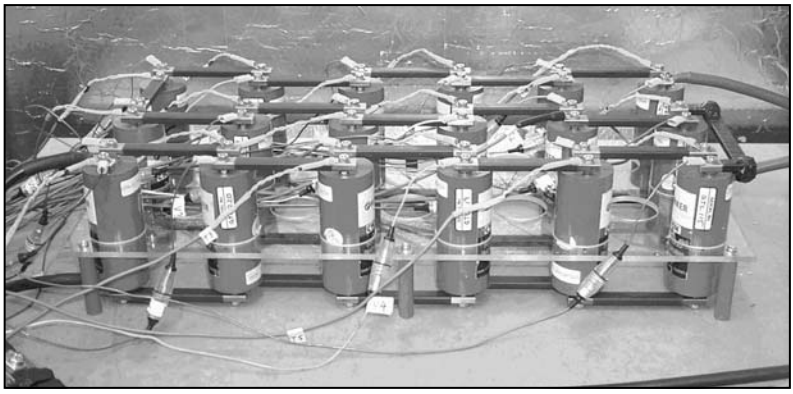

Fig. 17.10. (a) Spiral-wound cell with dual tabs; (b) 36-V battery, composed of spiral-wound dual-tab cells, on test.

number of other approaches to grid design. These include: (i) altering the aspect ratio of the grid so as to minimize the distance of the tab from the remote corners of the plate (i.e., avoid tall, narrow plates); (ii) increasing the thickness of the appropriate grid wires to reduce the maximum resistance down (across) the grid; (iii) using copper-cored wires of greater electrical conductivity (feasible in the negative plate).

17.6. The Role of Plate Thickness

In the past, high power has usually been required over a wide range of depth-of-discharge so that very thin plates (high overall surface-area) have been

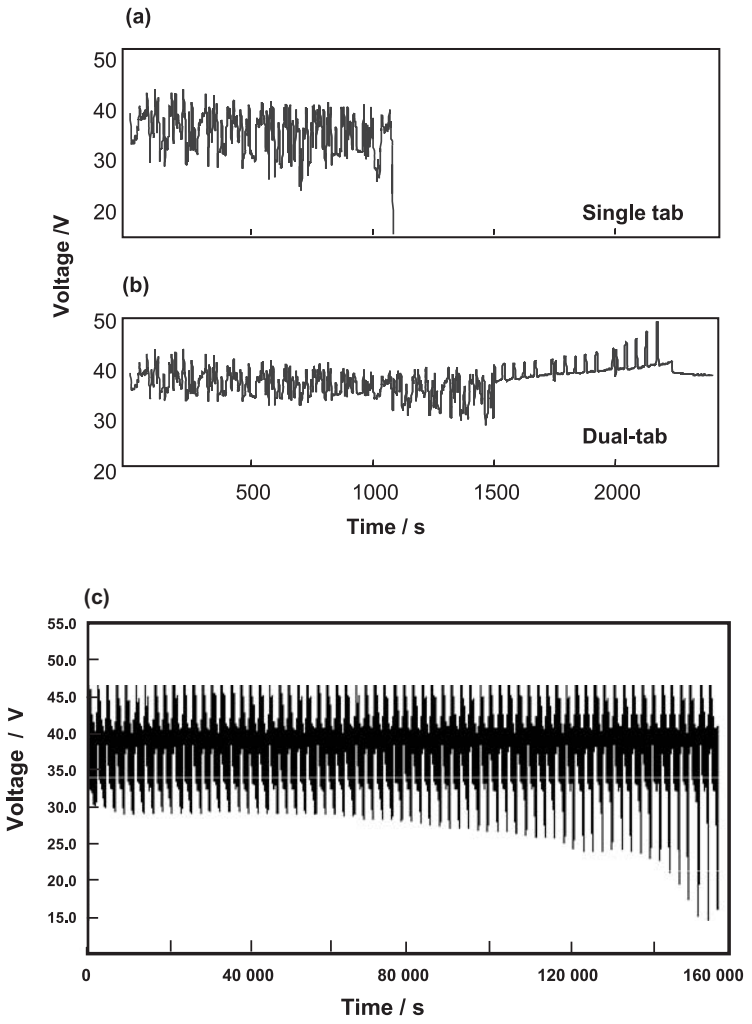

Fig. 17.11. Tests based on HEV battery protocol shown in Fig. 17.1(a). Test starts with battery at 80% state-of-charge and 40°C. (a) Conventional (single tab) battery fails to complete one test; (b) dual-tab battery completes the test and exhibits a more stable voltage [3]; (c) voltage versus time for dual-tab battery through 65 simulated HEV cycles — equivalent to continuous driving for 44 h without rest or conditioning [3].

used. In HEV duty, however, those charges and discharges that are demanded at the highest rates only draw upon a small fraction of the battery's capacity (see Fig. 17.1(a), (b)). This capacity can be supplied by using only the acid from within the plate (in pores, and perhaps supported by inert porous media which act as local reservoirs). High rates can be sustained for small ranges of state-of-charge because the necessary diffusion path lengths are short. Evidence has recently emerged [19] to suggest that such high-rate capacity could be supplied more readily

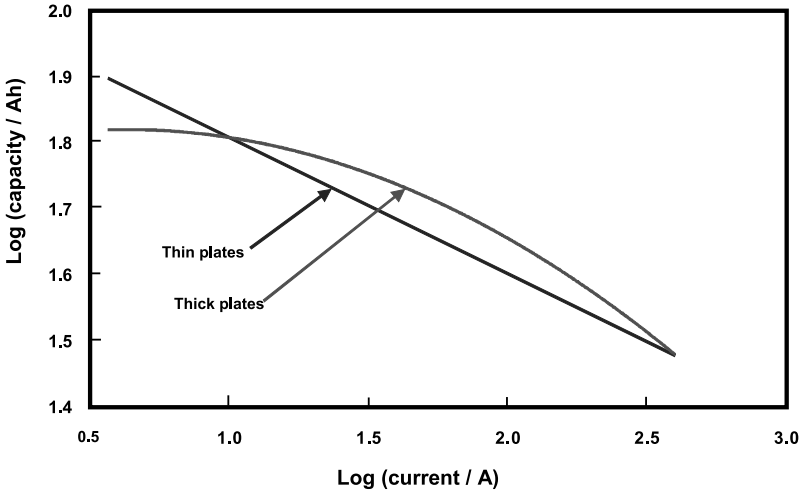

Fig. 17.12. Double logarithmic (Peukert) plot of capacities of battery with thin plates (positive 1.7 mm, negative 1.35 mm, 30% of available acid contained within plates) and battery with thick plates (positive 4.0 mm, negative 2.2 mm, 50% of available acid contained within plates) over a range of discharge currents. Both batteries have a nominal capacity of 70 Ah [18].

by thick plates than by thin ones. This new study has shown that, at discharge rates between approximately C_5 and $6C_1$, the capacities available from batteries with thick plates are greater than those available from batteries with thin plates (Fig. 17.12). Evidently, thicker plates, which contain more acid, are able to support high-rate discharges by using only acid within the pores of the active material. Avoiding the need to draw on acid diffusing from outside the plate appears to favour high-rate discharge.

As the lead–acid battery industry comes to grips with the novel circumstances of HRPSoC duty, there appears to be scope for a fresh approach to plate design, perhaps supported by the provision of more porosity within the plates to accommodate more 'local' acid.

17.7. Concluding Remarks

In batteries for either 36-/42-V automobiles or HEVs, the cells in the strings will have to be matched better than in the past, and also assembled and managed in such a way that they will not tend to become unbalanced.

All of the future vehicle concepts listed in Table 17.1 call upon increased electrical capacity and power compared with today's conventional automobiles. The battery requirements of these future vehicles will not be met by present lead–acid products. Adjustments to the grid design and to the surface area and conductivity of the negative active-mass, as well as the deployment of elements capable of reducing the proclivity of the cell to evolve gas (especially hydrogen) during charging, all show

promise in advancing the capability of the VRLA battery to cope with the rigorous duties that are envisaged.

It remains to be seen whether the benefits that can be gleaned from these design adjustments, when employed together, will prove to be sufficient to provide a satisfactory life for VRLA batteries in new-generation road vehicles. If this is indeed achieved, then the rewards, particularly in terms of reduced battery costs for such vehicles, will be enormous.

References

1. M. Anderman, *Proceedings of Third International Advanced Automotive Battery Conference*, 10–13 June 2003, Nice, France, 2003, Section 1, Paper 1.
2. M. Anderman, *J. Power Sources* (2003), in press.
3. A. Cooper, *ALABC Project 'Rholab', Reliable, highly optimized lead–acid battery*, Quarterly Reports 1 September 2000 to December 2002, Advanced Lead-Acid Battery Consortium, Research Triangle Park, NC, USA, 2003.
4. B. Dickinson, AeroVironment, Inc., Monrovia, CA, USA, personal communication, 2003.
5. B. Culpin, D.A.J. Rand, J. Power Sources, **36** (1991) 415–438.
6. M. Shiomi, T. Funato, K. Nakamura, K. Takahashi, M. Tsubota, *J. Power Sources*, **64** (1997) 147–152.
7. L.T. Lam, N.P. Haigh, C.G. Phyland, T.D. Huynh, D.A.J. Rand, *ALABC Project C2.0, Novel technique to ensure battery reliability in 42-V PowerNets for new-generation automobiles*, Extended report, January to April 2003, Advanced Lead-Acid Battery Consortium, Research Triangle Park, NC, USA, 2003.
8. L.T. Lam, C.G. Phyland, N.P. Haigh, D.A.J. Rand, U.S. Provisional Patent Application 60/444, 559 (2003).
9. H. Bode, *Lead–Acid Batteries*, John Wiley & Sons, Inc., New York, USA, 1997, p. 27.
10. A.F. Hollenkamp, W.G.A. Baldsing, S. Lau, O.V. Lim, R.H. Newnham, D.A.J. Rand, J.M. Rosalie, D.G. Vella, L.H. Vu, *ALABC Project N1.2, Overcoming negative-plate capacity loss in VRLA batteries cycled under partial-state-of-charge duty*, Final Report, July 2000 to June 2002, Advanced Lead-Acid Battery Consortium, Research Triangle Park, NC, USA, 2002.
11. L.T. Lam, H. Ceylan, N.P. Haigh, T. Lwin, C.G. Phyland, D.A.J. Rand, D.G. Vella, *ALABC Project N3.1, Influence of residual elements on the oxygen- and/or hydrogen-gassing rates of lead–acid batteries*, Final Report, July 2000 to June 2002, Advanced Lead-Acid Battery Consortium, Research Triangle Park, NC, USA, 2002.
12. R.H. Newnham, W.G.A. Baldsing, A.F. Hollenkamp, O.V. Lim, C.G. Phyland, D.A.J. Rand, J.M. Rosalie, D.G. Vella, ALABC Project C/N1.1, *Advancement of valve-regulated lead–acid battery technology for hybrid-electric and electric vehicles*, Final Report, July 2000 to June 2002, Advanced Lead-Acid Battery Consortium, Research Triangle Park, NC, USA, 2002.
13. E. Meissner, *Brite/Euram Project BE7297, Task 1, Effect of electronically conducting additives to the positive active material on high-rate performance of lead–acid batteries*, Final Report, 1 January 1994 to 31 December 1997, Advanced Lead-Acid Battery Consortium, Research Triangle Park, NC, USA, 1998.
14. P. Král, P. Krivák, P. Bača, M. Calábek, K. Mička, *J. Power Sources*, **105** (2002) 35–97.
15. M. Calábek, K. Mička, P. Bača, P. Krivák, *J. Power Sources*, **85** (2000) 145–148.
16. R. Wagner, Chapter 13 of this book.
17. L.T. Lam, R.H. Newnham, H. Ozgun, F.A. Fleming, *J. Power Sources*, **88** (2000) 92–97.
18. F.A. Fleming, R.H. Newnham, U.S. Patent 6,555,265 (April 29, 2003).
19. E. Nann, B. Wagner, V. Toniazzo, U. Lambert, R.F. Nelson, *ALABC Project S1.2, Engineered separators for optimization of processing and performance in VRLA batteries*, Final Report, 1 June 2000 to 31 December 2002, Advanced Lead-Acid Battery Consortium, Research Triangle Park, NC, USA, 2002.

This page intentionally left blank

SUBJECT INDEX

This page intentionally left blank